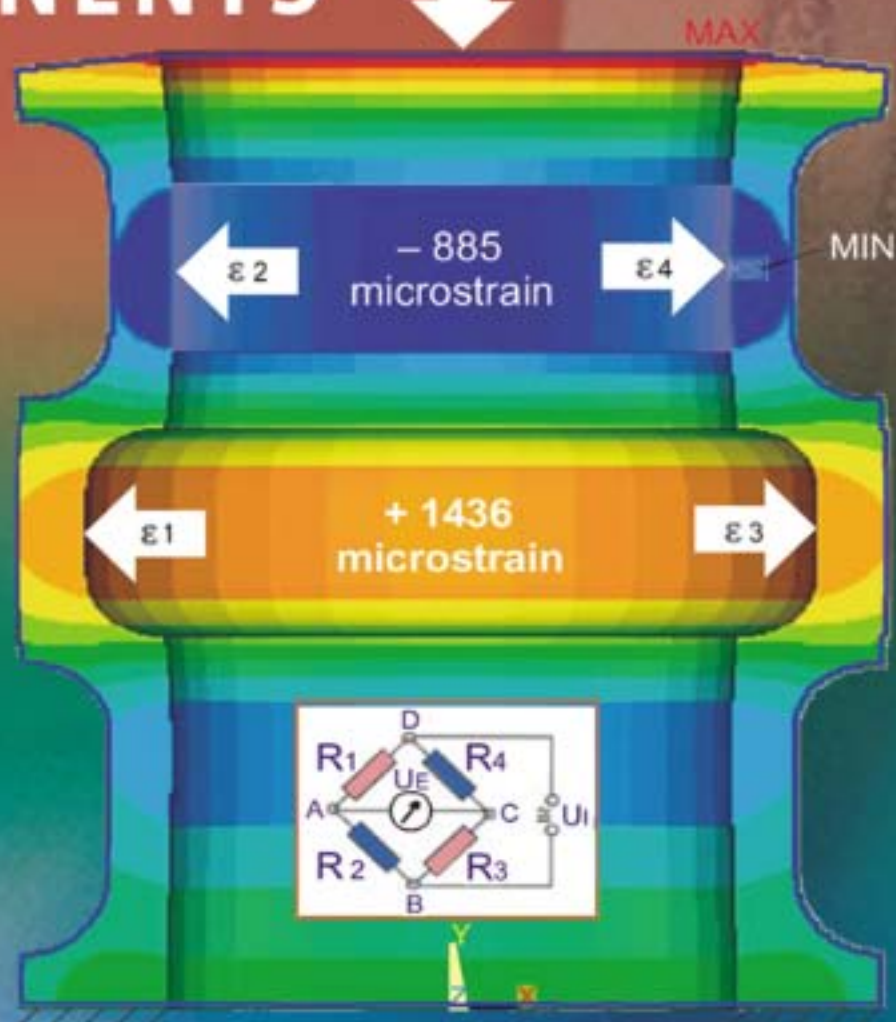


Dan Mihai Ștefănescu

Handbook of Force Transducers

PRINCIPLES
AND
COMPONENTS

$F = 1 \text{ MN}$



Springer

Handbook of Force Transducers

Dan Mihai Ștefănescu

Handbook of Force Transducers

Principles and Components

Author

Dr. Eng. Dan Mihai Ștefănescu
Romanian Measurement Society
Bd. Iuliu Maniu 71, Bloc 4, Scara 1,
Apt. 15, Sector 6, Bucharest-061088,
Romania
E-mail: stefidanro@yahoo.com

ISBN 978-3-642-18295-2

e-ISBN 978-3-642-18296-9

DOI 10.1007/978-3-642-18296-9

Library of Congress Control Number: 2011922617

© 2011 Springer-Verlag Berlin Heidelberg

This work is subject to copyright. All rights are reserved, whether the whole or part of the material is concerned, specifically the rights of translation, reprinting, reuse of illustrations, recitation, broadcasting, reproduction on microfilm or in any other way, and storage in data banks. Duplication of this publication or parts thereof is permitted only under the provisions of the German Copyright Law of September 9, 1965, in its current version, and permission for use must always be obtained from Springer. Violations are liable to prosecution under the German Copyright Law.

The use of general descriptive names, registered names, trademarks, etc. in this publication does not imply, even in the absence of a specific statement, that such names are exempt from the relevant protective laws and regulations and therefore free for general use.

Typesetting: Data supplied by the author

Cover Design: Kirchner, Erich

Printed on acid-free paper

9 8 7 6 5 4 3 2 1

springer.com

I should like to offer my grateful acknowledgements to all those
who have helped me in this considerable undertaking,
especially to my mentor, Dr. Aurel Millea.

Dr. Dan Mihai Ștefănescu

Chamfort: Among the gifts given to us by Mother Nature
the force of reasoning is the first one.

Moliere: Love is the most potent force in the universe.

StefiDanRo: To everybody I love and cherish!

Mihai Eminescu, Romanian national poet (1850 – 1889):
Only by a continuous reading your brain will become
a limitless laboratory of ideas and images.

ACKNOWLEDGEMENTS

My parents	Dumitru (1913–1967) and Viorica Ștefănescu (1916–1991)
Teachers	Emil Giurgiu (Mathematics), Georgeta Nicolov (Physics) and Rodica Gruia (English)
Professors	Mihai Drăgănescu (Electronic Devices), Constantin Iliescu (Electrical Measurements), Mariana Beliș (Electronic Measurements), Roman Stere (Electronic Instrumentation), Alexandru Spătaru, Alexandru Popovici (Information Theory), D.R. Mocanu, Costică Atanasiu, Nicolae Iliescu and Ioan Constantinescu (Experimental Stress Analysis), Brândușa Pantelimon (Sensors and Transducers) and Aurel Millea (Metrology and Instrumentation)
Laboratory heads	Eudoxie Procopovici and Gheorghe Bădescu (National Institute for Aerospace Research), Gheorghe Buzdugan and Mihail Buga (“Politehnica” University of Bucharest, Strength of Materials)
Tensometric help	Gheorghe Bănoiu, Radu Enache, Constantin Stoian
FEM assistance	Adriana and Marin Sandu, Paul Bârsănescu, Eugen Ghita and Laurențiu Niculcea (România), Thomas Allgeier (Germany), H.H. Shin, Jakal Lee and Sam-Yong Woo (South Korea)
PhD dissertation cum laude	<i>Methods for increasing the sensitivity of strain gauge force transducers</i> – Promoter Prof. Dr. Ing. Aurel Millea, P.U.B.
NATO grant with	Prof. P.P.L. Regtien, Twente University, Enschede, Netherlands
Brain Pool with	Dae-Im Kang, Korean Research Institute of Standards + Science
R+D cooperation	Chisheng Chang, Industrial Technology Research Institute, Center for Measurement Standards, Taiwan, R.O.C.
Translation	Lavinia Boșilcă, Rodica Lazăr, Mircea Radeș, Petre Răzvan and (from German language) Traian Demetrescu
PC consultancy	Alexandru (born 1980) and Florian Ștefănescu (born 1983)
Typesetting	Veronica Ștefănescu (married 1974) and Marina Ghemuleț
Drawings	Maria Petric and Angelica Niculescu (manual drawings), Lia Dolga and Ecaterina Prună (computer graphic design)

Logistic support	Cornel Oprișiu, Ion Nilă and Valentin Butoescu (INCAS), Valentin Silivestru and Victor Beșleagă (COMOTI), Ion Fuiorea (STRAERO) and Răsvan Stănescu (BISNET)
Springer Science + Business Media	Thomas Ditzinger (Senior Editor), Jessica Wengrzik and Holger Schäpe (Engineering Editorial), Erich Kirchner (cover design) and Barbara Schmidt-Loeffler (copyright)
Scientific Publishing Services	Abbas Manthiri Mohammad and Suguna Ramalingam (Book Data Processing Team, Chennai, India)

Permissions to reproduce copyrighted materials:

Joan Anuels and Natalie David (Elsevier), James Dimond and Jill Membrey (Institute of Physics, London), Gerald Gerlach and Jacqueline Hansson (IEEE), Leo van Biesen, Tamás Kemény and Karolina Havrilla (IMEKO), Isabell Henking (Sensor + Test conferences, Nürnberg)

Wolfgang Bittner and Helga Rosenzweig (VDI / VDE), Manfred Kochsiek and Amritlal Sawla (PTB, Germany), Baljit Sidhu (NPL, United Kingdom), Velda Wong (Institute of Measurement and Control, London), Jacob Fraden (American Institute of Physics), Eileen LaManca (American Physical Society)

Richard Jones (John Wiley & Sons, Inc.), Bettina Loycke (Wiley – VCH Verlag), Jan-Kees van Oord (Brill / Martinus Nijhoff Publishers), Kevin Danahy (Artech House Publishers), Gabriele Josiger (Carl Hanser Verlag Munich)

Manfred Kreuzer and Klaus Bathe (Hottinger Baldwin Messtechnik), David Cohen and Carla Leguia (Honeywell), Marti Spalding (Vishay Micro-Measurements), Roland Nater (Mettler – Toledo), Stephan Weyhe (Sartorius), Scott Wayne (Analog Devices), Raymond Sepe (Electro Standards Laboratories), Tony Ingham (Sensor Technology Ltd), Will Delsman (NK Technologies), Antonin Platil (Czech Technical University, Faculty of Electrical Engineering, Department of Measurement)

Sergey Yurish (www.sensorsportal.com – IFSA), Jim Pierson (www.sensorland.com), Melanie Martella (www.sensorsmag.com)

I did the rest, and I did my best!

DMS

IN LIEU OF PREFACE

This book is dedicated to the **force transducers**, a wide category of measuring means that can frequently be encountered in a large variety of measurement systems, from the simplest ones to others of great complexity and sophistication.

Generally speaking, any measuring system implies three categories of devices: (a) transducers (or sensors), which are the direct recipients of the information from the object under measurement, (b) intermediate processors, performing various conversions / signal processing / reshaping actions, and (c) output devices, whose role is the transmission of the measurement result(s) in an adequate form to the end user. Among these, the class of transducers is always of a major interest, since they are the only that strongly depend on the input quantities (measurands).

On the other hand, in a book addressed to transducers the other two classes of elements – intermediate converters and output devices – can not be omitted or neglected. More generally, it is necessary to start with a structured body of concepts and **principles**. However, it is not enough to treat them simply as functional blocs of **components**, they must be analyzed and designed on the basis of their physical environment and their modeling should be based on their **characteristics**. Finally, when presenting measurement and instrumentation devices, design concepts and ideas of knowledge engineering and problem solving (i.e. **applications**) ought to be also added.

The first two above-mentioned parts – *principles and components* – are the object of this first volume of the “*Handbook of Force Transducers*”, while the subsequent two parts – *characteristics and applications* – will be treated in a later volume.

* * * * *

Force is a physical quantity of a ubiquitous presence in the world and its measurement represents a multidisciplinary task. When treating this subject, one can finally arrive at a basic philosophical dilemma: *synthesis* of all that has been achieved in the past (Platon, Kant) or *analysis* of new development directions (Aristotle, Hegel). We decided to adopt the wisest middle way. Antinomies often occur in the world of physics and mathematics: Leibniz searched for algorithms, as general as possible, for describing the phenomena, while Newton had in view solving a number of concrete physical problems. Nowadays, just the spectacular combination of basic and applied research has led to the development of some unique force transducers, intended for specific cases, as well as of universal models, employed in a wide range of industrial processes.

Newton's "spiritus subtilis" has surpassed the mechanistic model of the elastic medium and "transdisciplinarity" dominates today the sphere of engineering, an example being the synergetic mixture called "mechatronics", obviously under its evolved, computerized variant. There exists a tendency to suggestively concentrate most visual information in the form of images, graphic representations and figures, confirming the Chinese saying: "A good picture values more than a thousand of words."

* * * * *

During the work on the handbook, I strived to learn as much as I could from my great teachers and professors, like the Academicians Radu Voinea (in mechanics) and Remus Răduleț (in electricity) or the humanist Tudor Vianu – an "artist" in the interpenetration of all knowledge fields and permanent open-ness towards everything new, an ambassador of the Romanian universality. They helped me uniting under a global vision the mechanical-gravitational and the electromagnetic forces, at both micro (intra-atomic) and macro (cosmic) scale.

I thank all colleagues and friends, from all over the world, who helped me with vivid discussions and high quality written documents, and first of all my mentor and promoter, **Prof. Dr. Ing. Aurel Millea**, who supported and assisted me by all means and ways. My parents would have been proud of this notable feat, my sister and my wife are amazed of being able to achieve such a hard work and my sons and their descendants will enjoy the richness of the content of this first Handbook in the field of Force Transducers.

Last but not least, I gratefully underline the efficient co-operation under "astral" auspices between the author born in Bucharest in the Researcher's Day and the global and open-minded Springer Senior Editor of the Success Secret's Day, **Dr. Thomas Ditzinger** from Heidelberg, Germany.

* * * * *

After defining the proper terminology (strain gauge sensor as an input transducer but force transducer as a complex measuring device), Part I introduces the basic "*Principles and Methods of Force Measurement*", according to classification into a **dozen** (apostolic figure!) of **force transducers types**, namely: resistive, inductive, capacitive, piezoelectric, electromagnetic, electrodynamic, magnetoelastic, galvanomagnetic (Hall effect), vibrating wires, (micro)resonators, acoustic and gyroscopic. Two special chapters refer to force balance techniques and to combined methods in force measurement, respectively.



Part II discusses the “*Strain Gauge Force Transducers Components*”. The functional scheme of an electric force measurement chain is brought out in principle, having in view the physical parameters linear transformations that succeed one other and the passage from the classical force transducer to the digital / intelligent one, with the incorporation of three subsystems (sensors, electromechanics and informatics).

The basic properties of the associated Wheatstone bridge, best suited to the parametrical transducers, are mentioned too, together with the appropriate electronic circuits for strain gauged force transducers (SGFTs).

The specific stages (comparative analysis, modeling, simulation, implementation, testing) were focused on the elastic element (abbreviated EE), which is the “heart” of the force transducer and basically determines its performance. A **12-type elastic element classification / hierarchization** is proposed (stretched / compressed column or tube, bending beam, bending and /or torsion shaft, middle bent bar with fixed ends, shear beam, bending ring (and “glasses”), bent yoke and frame, diaphragm / membrane, axial-stressed torus, axisymmetrical and voluminous EE), thoroughly analyzing the optimum location possibilities of the strain gauges.

In order to choose a certain elastic element, several criteria shall be considered, even if contradictory (range, sensitivity, space requirements, dynamic behavior, cost, etc.), that can make the option difficult. Having a postdoctoral NATO grant within the Department of Measurement and Instrumentation, Twente University of Enschede, The Netherlands, the author has initiated activities in the view of creating a scientific database for force transducers, along with an expert program to be used in the design and optimization of the transducers elastic elements.

Although there is a tendency to replace prototype testing by computer simulation, the experimental procedures are still vital not only for understanding the physical phenomena but also for the certification and validation of theoretical results. In this respect the continuous improving of force transducers within the measuring system is still an important issue in research-development and engineering practice all over the world. The final chapter is dedicated to the digital and intelligent force transducers.

* * * * *

A lot of tests were carried out by the author at various didactic stages (student scientific circle, diploma work, Master and PhD dissertations, associate lecturer, postdoctoral grant) and technical levels (engineer, senior researcher, head of Metrology and Instrumentation Department) in the Strength of Materials and Transducers laboratories of the “Politehnica” University of Bucharest and,

respectively, in the Measurement Techniques laboratory of the National Institute for Aerospace Research “Elie Carafoli” in Bucharest.

Latest results of his activity as visiting scientist and invited researcher within Force Measurement and Evaluation Laboratory of the South Korean Research Institute of Standards and Science (KRISS), and, respectively, in the Center for Measurement Standards (Metrology) in Taiwan, R.O.C. are included.

This proposed handbook fills a gap in the field of Force Measurement, both experts and newcomers, no matter of their particular interest, finding a lot of useful and valuable subjects in the specific area of **Force Transducers**; in fact, it is the first specialized monograph in this inter- and multidisciplinary field, and a real “tour de force”.

Dan Ștef

București, România
5 Ianuarie 2011



The author at the IMEKO World Congress in Rio de Janeiro, Brazil, September 2006

CONTENTS

PART I: PRINCIPLES AND METHODS OF FORCE MEASUREMENT

1 INTRODUCTION TO FORCE MEASUREMENT.....	3
1.1 Various Approaches to Force Transduction	3
1.2 Newton – Measurement Unit of Force	6
1.3 Mechanical Measurements of Forces & Tribology	8
1.4 Force Transducers Other than Electrical	10
1.5 Terminology: Sensors or Transducers?	13
1.6 Force Measurement Systems	16
REFERENCES	20
2 ELECTRICAL METHODS OF FORCE MEASUREMENT	23
2.1 Energetical Aspects in Force Transduction.....	24
2.2 Examples of Force Measurement in Thermal Processes	27
2.3 Typical Requirements for Force Transducers	29
2.4 Force Transducers (FTs) Classifications.....	30
2.4.1 First Attempts of Force Transducers Systematization.....	30
2.4.2 German FT Classifications.....	32
2.4.3 Dutch FT Classifications.....	34
2.4.4 English FT Classifications	35
2.5 Nonconventional Types of Force Transducers.....	37
2.5.1 Electrodynamical Force Transducers	37
2.5.2 Galvanomagnetic Force Transducers (Based on Hall Effect)	37
2.5.3 Acoustic Force Transducers (SAWs).....	38
2.6 An Enlarged Classification of Force Transducers.....	40
REFERENCES	44
3 RESISTIVE FORCE TRANSDUCERS.....	49
3.1 Resistive Force Transducers Types.....	50
3.2 Potentiometers.....	52
3.3 Pretensioned Wires	53
3.4 Strain Gauges	54
3.5 Piezoresistive Sensors	56
3.5.1 Silicon Devices.....	57
3.5.2 Carbon Film Coatings and Carbon Nanotubes (CNTs).....	59

3.6	Force Sensing Resistors (FSRs)	62
3.7	Force Sensing Resistive Networks	65
	REFERENCES	68
4	INDUCTIVE FORCE TRANSDUCERS	73
4.1	LVDT (Linear Variable Differential Transformer)	74
4.2	Variable Reluctance Transducers	78
4.3	Mutual Inductance Variation Force Transducers.....	79
4.4	Inductive Eddy Current Transducer.....	81
4.5	Biparametric Inductive Force Transducers.....	81
4.5.1	Biparametric LR	81
4.5.2	Biparametric LC	82
	REFERENCES	85
5	CAPACITIVE FORCE TRANSDUCERS	87
5.1	Capacitive Force Transducers Classification.....	87
5.2	Capacitive Force Transducers (CFTs) with Plates.....	88
5.2.1	CFT with Variable Thickness of the Dielectric Pad	88
5.2.2	CFT with Variable Distance between Plates	90
5.2.3	CFT with Plates Arranged under a Certain Angle	91
5.3	Multiple Plates Capacitive Force Transducers	92
5.4	Interdigitated and Matrix of Capacitive Sensors	94
5.4.1	CFT with Interdigitated Electrodes.....	94
5.4.2	CFT Using a Matrix of Capacitive Sensing Elements	96
5.5	Cylindrical Capacitive Force Transducers.....	97
5.6	Applications Based on Electrostatic Forces.....	100
5.6.1	Electrostatic Force Balances.....	100
5.6.2	Other Applications of Electrostatic Forces for the Measurement of Mechanical Quantities	102
5.7	Electronic Circuits for Capacitive Transducers	103
	REFERENCES	105
6	PIEZOELECTRIC FORCE TRANSDUCERS (PZFTs).....	109
6.1	Piezoelectric Materials	110
6.1.1	Quartz Crystals	110
6.1.2	Sensors with Organic Polymers.....	111
6.1.3	Solid State Devices.....	113
6.2	Unidirectional Piezoelectric Force Transducers	114
6.3	Tridirectional Piezoelectric Force Transducers	117
6.4	Piezoelectric Bimorph as Force Transducer	120
6.5	Electronic Circuits for Piezo Force Transducers	123
6.6	Complex Applications with Piezoelectric Devices.....	125
	REFERENCES	126

7	ELECTROMAGNETIC FORCE TRANSDUCERS.....	131
7.1	Classification	131
7.2	Magneto-resistive Force Transducers	135
7.3	Force Measurements in Magnetic Field.....	138
7.3.1	Resistive Force Transducers in Magnetic Field.....	139
7.3.2	Capacitive Force Transducers in Magnetic Field	140
7.3.3	Pressure Transducers Based on Magnetic Higher-Order Harmonic Fields	141
7.4	Electromagnetic Weighing by Force Compensation	142
7.5	Electromagnetic Devices for Small Forces.....	144
7.5.1	Electromagnetic Probes for Micro- and Nano-force Measurements	144
7.5.2	Magnetic Flux Quantum as a Sub-pico-newton Weight	146
7.5.3	Casimir Forces and Levitation Pressures Measurement	148
	REFERENCES	149
8	ELECTRODYNAMIC FORCE TRANSDUCERS	153
8.1	Electrodynamic Force Compensation Principle.....	155
8.2	Load Cells with Electrodynamic Feedback	156
8.3	Electrodynamic Force Compensation Balances.....	157
8.3.1	Hydrodynamic Gravimetric Balance	157
8.3.2	Electrodynamic Vacuum Microbalance.....	158
8.3.3	Electrodynamic Devices for Small Particles Experiments.....	159
8.4	Micromechanical Testers with Moving Coils.....	160
8.5	Multifunctional Transducers with Moving Coils.....	161
	REFERENCES	163
9	MAGNETOELASTIC FORCE TRANSDUCERS.....	165
9.1	The Magnetostrictive Principle.....	166
9.2	Classification of Magnetoelastic FTs	168
9.3	Axial Magnetoelastic Force Transducers	170
9.3.1	Magnetostrictive Strips and Bars	170
9.3.2	Magnetostrictive Amorphous Wires	172
9.4	Frame-Shaped Magnetoelastic Force Transducers	173
9.5	Tubular Magnetoelastic Force Transducers.....	174
9.6	Circular Magnetoelastic Force Transducers	176
9.7	Block-Shaped Magnetoelastic Force Transducers.....	178
9.8	Magnetoelastic Shafts for Torque Transducers	180
9.9	Magnetoelastic FTs Electronic Circuitry	181
	REFERENCES	183
10	GALVANOMAGNETIC FORCE TRANSDUCERS.....	185
10.1	Hall Effect and Its Applications	186
10.2	Force Transducers Based on the Hall Effect.....	189

10.2.1	Hall Effect in Geotechnical Engineering	189
10.2.2	Medical Applications with Hall Sensors	190
10.3	Hall Devices for Other Mechanical Quantities	191
10.3.1	Displacement and Position Measurements Using Hall Sensors	191
10.3.2	Weighing Based on Hall Devices	192
10.3.3	Pressure and Flow Measurements by Means of Hall Sensors	193
10.3.4	Shock Measurements Using Hall Devices	194
10.3.5	Penetration Velocity and Rotational Speed Measured with Hall Sensors	195
10.4	Galvanomagnetic FTs in Complex Measurement Chains	196
10.4.1	Combined Measurands in Galvanomagnetic Force Transducers	196
10.4.2	Triaxial Galvanomagnetic Force Transducers	198
10.5	Other Electromagnetic Principles in Force Measurement	199
	REFERENCES	200
11	VIBRATING-WIRE FORCE TRANSDUCERS	203
11.1	Vibrating Wire as Force Measurement Principle	203
11.2	VWFTs' Structures and Characteristics	206
11.3	Electronic Circuits for VWTs	209
11.3.1	Vibrating-Wire Excitation Methods	209
11.3.2	Measuring Circuits for Vibrating-Wire Transducers	211
11.3.3	Digital Weighing Based on Vibrating-Wire Transducers	211
11.3.4	Virtual Musical Instruments Investigated by Means of VWFTs	212
11.4	Different Types of Vibrating-Wire Transducers	213
11.5	VWTs' Applications for Other Physical Quantities	217
11.5.1	Viscometers and Densimeters	217
11.5.2	"Piezometers" (for Underground Water Pressure)	219
11.5.3	Tiltmeters / Inclinometers and Slope Indicators	220
11.6	VWTs' Progress and Their Extended Utilization	220
	REFERENCES	223
12	RESONATOR FORCE TRANSDUCERS	227
12.1	Resonator Principle in Force Measurement	228
12.2	Materials for Resonators and Their Q-Factors	230
12.2.1	Quartz Resonators for Force Transducers	231
12.2.2	Silicon Resonators for Force Transducers	232
12.3	Various Shapes of Resonators	235
12.3.1	Resonating Beams for Force Transducers	235
12.3.2	Resonating Diaphragms / Membranes for Force / Pressure Transducers	237
12.3.3	Resonating Tubes for Force Transducers	238

12.4	Single Beam (Micro)Resonators	238
12.5	Double Beam (Micro)Resonators	240
12.5.1	Classical Double-Ended Tuning Forks (DETFs)	240
12.5.2	Modern Solutions for DETF Resonators.....	242
12.6	Metallic Triple Beam Resonators (MTBRs).....	244
12.6.1	Force Transducers with MTBRs	244
12.6.2	Torque Transducers with MTBRs.....	246
	REFERENCES	247
13	ACOUSTIC FORCE TRANSDUCERS	251
13.1	Interdigital Transducers (IDTs)	252
13.2	Acoustic Emission and Waveguides.....	254
13.2.1	Acoustic Emission Applications	254
13.2.2	Acoustic Waveguides Applications	254
13.3	Ultrasound Force Transducers	256
13.3.1	Industrial Applications of Ultrasound Force Transducers	256
13.3.2	Ultrasound Force Transducers for Food and Farmacology.....	259
13.3.3	Medical Applications of Ultrasound Force Transducers	260
13.4	Acoustic Radiation Force Transducers	261
13.4.1	Acoustic Radiation Force Transducers in Medicine	261
13.4.2	Acoustic Radiation Force Transducers in Metrology	262
13.5	Surface Acoustic Wave (SAW) Transducers.....	264
13.5.1	SAW Force Transducers	265
13.5.2	SAW Torque Transducers	266
13.5.3	SAW Pressure Transducers	267
13.5.4	SAW Fluidic Transducers.....	267
13.6	SAW Electronic Circuits	268
	REFERENCES	272
14	GYROSCOPIC FORCE TRANSDUCERS	275
14.1	The Gyroscopic Principle in Force Measurement	275
14.2	Conventional Gyroscopic Force Transducers	277
14.3	Types of Micro-Gyroscopic Force Transducers	279
14.3.1	Inertial Gyroscopes	279
14.3.2	Piezoelectric Gyroscopes.....	281
14.3.3	Resonator / Vibrating Gyroscopes.....	282
14.3.4	Acoustic (and SAW) Gyroscopes	284
14.3.5	Coriolis Force Transducers in Medical Applications.....	285
14.4	Optical Gyroscopes.....	286
14.4.1	Fiber Optic Gyroscopes (FOGs)	286
14.4.2	Laser Gyroscopes.....	288
14.4.3	MOEMS (Micro-Opto-Electro-Mechanical System) Gyroscope.....	288
14.5	A Topical Review of Gyroscopes.....	288
	REFERENCES	290

15	FORCE BALANCE TECHNIQUES	293
15.1	Force Balance Principle Applied to Transducers.....	294
15.2	Electromagnetic Force Compensation (EMFC).....	297
15.3	Electrostatic Force Compensation	299
15.4	Optical Devices Based on Force Feedback.....	302
	REFERENCES	304
16	MIXED METHODS IN FORCE MEASUREMENTS.....	307
16.1	Force Transducers Using Advanced Electronics	308
16.2	Cantilever Beams for Various Force Transducers	310
16.3	CNTs for Measuring Mechanical Quantities	312
16.4	Combined Methods of Force Transduction	316
16.4.1	Force Transducers in Medical Instruments.....	316
16.4.2	EMAT (Electro-Magnetic Acoustic Transducer) and Lorentz Force.....	318
16.4.3	Multitransducer Equipment	320
16.4.4	Force Transducers Involving Optical Techniques	321
	REFERENCES	324
 PART II: FORCE TRANSDUCERS COMPONENTS		
17	THE FORCE MEASUREMENT CHAIN.....	331
17.1	Force Measurement Chain Components	331
17.2	Strain Gauge Sensing.....	334
17.3	Strain Gauges Signal Conditioning.....	337
17.4	Strain Gauges Signal Processing.....	340
17.5	Data Presentation for Force Transducers	343
	REFERENCES	345
18	WHEATSTONE BRIDGE – THE BASIC CIRCUIT FOR STRAIN GAUGE FORCE TRANSDUCERS	347
18.1	Wheatstone Bridge – General Presentation.....	347
18.2	Wheatstone Bridge – Fundamental Properties	348
18.3	Bridge Compensation and Adjusting Resistors.....	350
18.4	Supply Possibilities for Wheatstone Bridges	352
18.5	Different Applications with Measuring Bridges	353
18.6	Further Connections for Wheatstone Bridges	356
	REFERENCES	358
19	STRAIN GAUGES ELECTRONIC CIRCUITS	361
19.1	Signal Conditioning for Force Transducers	361
19.2	Signal Conditioners.....	362
19.2.1	Pre- and Post-Conditioning.....	362
19.2.2	High-Gain Signal Conditioning	363
19.2.3	“QuantumX” Universal Conditioner.....	363

19.3	Analog-to-Digital Converters	365
19.3.1	Different Conversions to Frequency	365
19.3.2	Resistance-to-Time Converter	365
19.3.3	Sigma-Delta Converter	366
19.4	Bridge Oscillators	367
19.4.1	Wien Bridge Based Oscillator	367
19.4.2	Wheatstone Bridge Based Oscillator	368
19.5	AC Generators	369
19.5.1	Sine Wave Generator	369
19.5.2	Saw-Tooth Wave Generator	369
19.5.3	Rectangular Wave Generator	370
19.6	Strain Gauged Force Transducers Connected to PC	371
19.6.1	Direct Resistance Change Measurement	371
19.6.2	Strain Gauge Bridge Signal Processing	371
	REFERENCES	373
20	CLASSIFICATION OF ELASTIC ELEMENTS	375
20.1	Elastic Elements Loading Modes	375
20.2	Examples of Elastic Elements Classifications	378
20.3	Comprehensive Classification of Elastic Elements	381
	REFERENCES	387
21	STRETCHED / COMPRESSED COLUMNS	389
21.1	Classical Columns	389
21.2	Optimized Columns	394
21.3	Increasing Sensitivity for Columnar Transducers	394
21.4	Complex Structures Composed by Bars / Columns	395
21.5	Dynamic Testing for Cylindrical Transducers	396
	REFERENCES	397
22	STRETCHED / COMPRESSED TUBES	399
22.1	Classical Tubes	399
22.2	Concentric Tubes	403
22.3	Profiled Tubes	404
22.4	Tubes with Holes or Slots	408
22.5	Tubular Structures under Complex Loading	410
	REFERENCES	411
23	BENT LAMELLA (CANTILEVER BEAMS)	415
23.1	Various Applications with Cantilever Beams	415
23.2	Cantilever Beams for Lower Forces	419
23.3	(Bio)Chemical Cantilevers	424
23.4	Several Shapes of Cantilever Beams	428
23.5	Cantilever Beams in Multicomponent FTs	431
	REFERENCES	434

24	BENT AND/OR TORSION SHAFTS.....	437
24.1	Bending of Cantilever Tube or Cylinder.....	437
24.2	Rotating Shafts.....	439
24.3	Complex Loaded Shafts.....	441
	REFERENCES	443
25	MIDDLE BENT BARS WITH FIXED ENDS.....	445
25.1	Examples of Middle Bent Bars with Fixed Ends.....	445
25.2	Slotted Structures for Middle Bent Bars with Fixed Ends.....	448
25.3	Dynamic Applications of Double Ended Beams.....	450
25.4	Various Models of Four-Spoke Wheels.....	452
	REFERENCES	455
26	SHEARING STRAINED ELASTIC ELEMENTS.....	457
26.1	'I'-Profiles Subjected to Shearing.....	459
26.2	Load Measuring Pins / Bolts.....	460
26.3	Hollow Discs / Wheels.....	462
26.4	S (Z) Shaped Elastic Elements.....	464
26.5	Helix Load Cells.....	465
	REFERENCES	466
27	BENT YOKES AND FRAMES.....	469
27.1	Various Shapes of Bent Yokes and Frames.....	471
27.2	Force-Measuring Clamps.....	474
	REFERENCES	475
28	BENT RINGS AND "GLASSES".....	477
28.1	Various Shapes of Bent Rings.....	477
28.1.1	Circular Rings.....	477
28.1.2	"Square" Rings.....	480
28.1.3	Hexagonal Rings.....	481
28.1.4	Octagonal Rings.....	481
28.1.5	Other Shapes of Bent Rings.....	482
28.2	"Glasses"-Shaped Elastic Structures.....	484
28.3	Multiple "Glasses"-Shaped Elastic Elements.....	490
	REFERENCES	491
29	BENT MEMBRANES.....	495
29.1	Various Types of Bent Membranes.....	495
29.2	Circular Membranes.....	500
29.3	Square Membranes.....	505
29.4	Membranes with Various Shapes of Apertures.....	509
29.5	Other Shapes of Membranes.....	511
	REFERENCES	514

30	COMPLEX LOADED TORUS	517
30.1	Torus as Elastic Element for Force Transducers	517
30.2	Toroidal Elastic Elements in Special Applications	520
	REFERENCES	522
31	AXISYMMETRIC ELASTIC ELEMENTS	523
31.1	Various Axisymmetric EEs for Force Transducers.....	523
31.2	Axisymmetrical EEs for Very Large Force Transducers	528
31.3	N-Shaped Axisymmetric Elastic Elements	534
	REFERENCES	537
32	VOLUMETRIC ELASTIC ELEMENTS	539
32.1	Spheres.....	539
32.2	Cubes	542
32.2.1	Full Cubes	542
32.2.2	Cubic Blocks with Slots	543
32.3	Complex Bodies with Oblique Slots.....	547
	REFERENCES	548
33	COMPLEX, COMPOSED AND COMBINED ELASTIC STRUCTURES	549
33.1	Complex Elastic Structures.....	550
33.1.1	Plane Complex Structures	550
33.1.2	Spatial Complex Structures	552
33.2	Composed Elastic Structures	554
33.3	Combined Elastic Structures.....	558
33.3.1	Plane Combinations of Elastic Elements.....	558
33.3.2	Axisymmetric Combinations of Elastic Elements.....	559
33.3.3	Spatial Combinations of Elastic Elements	560
	REFERENCES	562
34	ELASTIC ELEMENTS SELECTION CRITERIA	563
34.1	Elastic Elements (EEs) Evaluation Criteria	565
34.2	Elastic Elements Comparative Analysis	566
34.3	EE Selection for Specific Applications.....	569
34.3.1	From Single- to Multi-component Force Transducers	569
34.3.2	Force Transducers in Mechatronics	570
34.3.3	EEs for Very Large Forces.....	571
34.4	Elastic Elements Automatic Selection	572
	REFERENCES	574

35 DIGITAL AND INTELLIGENT FORCE TRANSDUCERS.....	577
35.1 Evolution from Analog to Digital	577
35.2 Automatic Recognition of Force Transducers	579
35.3 Force Transducers in Dynamic Regime	581
35.4 Intelligent (Smart) Force Transducers	582
35.5 Further Prospects: Materials, Technologies, Ideas.....	583
35.5.1 Smart Materials and Structures.....	583
35.5.2 Intelligent Design and Smart Technology	584
35.5.3 Neuro-Fuzzy Concepts	585
35.6 Updated Force Transducers + Data Communication.....	585
35.6.1 Dual Output Force Transducers	585
35.6.2 Data Display and Communication.....	587
REFERENCES	589
 ANNEX 1. Rules for Strain Gauges Placement on the Elastic Elements of Force Transducers.....	 591
 ANNEX 2. The Newton's Apple Tree in Korea	 595
 INDEX	 597

ABBREVIATIONS AND ACRONYMS

- a-C: amorphous carbon
ABB: Asea Brown Boveri Ltd.
ABS: anti-lock braking system
AC/DC: alternating current / direct current
ACD: active compression-decompression
AD: Analog Devices
ADC: analog-to-digital converter
AE: acoustic emission
AFM: atomic force microscopy
AGC: automatic gain control
AIP: American Institute of Physics
AIST: Advanced Industrial Science and Technology (Japan)
AMC: Automatică – Management – Calculatoare series, Editura Tehnică, București, România
AMR: anisotropic magneto-resistance
ANFIS: adaptive neuro-fuzzy inference system
ANOVA: ANalysis Of VAriance
API: application program interface
APMF: Asia-Pacific Mass & Force Symposium
APS: American Physical Society
ARES: advanced rheometric expansion system
ARFI: acoustic radiation force impulse
ASIC: application-specific integrated circuit
ASME: American Society of Mechanical Engineers
ASSP: analog sensor signal processing
BEV: Bundesamt für Eich- und Vermessungswesen – (Austrian) Federal Office for Metrology and Surveying
BIPM: International Bureau of Weights and Measures (at Sevres, France)
BLH: (US) Baldwin Lima Hamilton Corporation
BSSM: British Society of Strain Measurement
CAD/CAE: computer-aided design / engineering
CAN: controller area network
CAOS: computer-aided optimization of shapes
CCD: charge coupled device (camera)
ccw: counter-clockwise
CD: compact disk
CEI/IEC: International Electrotechnical Commission
CENAM: CEntro NAcional de Metrología (Mexico)
CEM: Centro Español de Metrología
CFD: computational fluid dynamics
CFRP: carbon fibers reinforced polymer
CFT: capacitive force transducer
CIM: computer integrated manufacturing
CMM: coordinate measuring machine
CMOS: complementary metal-oxide semiconductor
CMR: common mode rejection

CMS: Center for Measurement Standards (Taiwanese Metrology)
 CMT: connect & measure transducer
 cMUT: capacitive micromachined ultrasonic transducer
 CNC: computer numerical control
 CNT: carbon nano-tube
 CPR: cardio-pulmonary resuscitation
 CPU: central processor unit
 CRC: Chemical Rubber Company Press
 CRT: cathode ray tube
 CVD: chemical vapor deposition
 CVG: Coriolis vibratory gyroscope
 cw: clockwise

DAC: digital-to-analog converter
 DAQ: data acquisition system
 DBMS: data-base management system
 DEP: di-electro-phoresis
 DETF: double-ended tuning fork
 DFM: dynamic force microscopy
 DLC: diamond-like carbon
 DLCC: digital load cell companion (TedeA)
 DMM: digital multi-meter
 DMS: Dehnungs-meß-streifen (German), i.e. resistive strain gauges
 DoF: degrees of freedom
 DRF: direct radiation force
 DSP: digital signal processing
 DSSP: digital sensor signal processing
 DTC: discharge time constant
 DUT: device under test
 DVD: digital video disk
 DVM: digital volt-meter
 DVRT: differential variable reluctance transducer
 DWCNT double-walled carbon nano-tube

EAL: European Accreditation Laboratory
 ECFS: electrically controlled force and stiffness

ECR: electron cyclotron resonance
 EDF: electro-dynamic field
 EDL: extensor digitorum longus (muscle)
 EDM: electro-discharge machining
 EE: elastic element
 EEPROM: electronically erasable programmable read-only memory
 EFB: electrostatic force balance (NIST)
 EFPI: extrinsic Fabry-Perot interferometer
 EIS: electrochemical impedance spectroscopy
 em: electro-magnetic
 EMAT: electro-magnetic acoustic transducer
 emf: electro-motive force
 EMFC: electro-magnetic force compensation
 EMFi: electro-mechanical film (electret)
 EMFR: electro-magnetic force restoration
 EMG: electro(cardio)myography
 EMI: electro-magnetic interference
 EN: European norm / standard
 EP: European patent
 EPM: embedded piezoresistive microcantilever
 ESA: experimental stress analysis
 ESD: electro-static discharge
 ETA: electro-thermal actuator

FBAR: thin-film bulk acoustic-wave resonator
 fc-AFM: force controlled Atomic Force Microscopy
 FDM: frequency division multiplexed
 FEA: finite element analysis
 FEM: finite element method
 FET: field-effect transistor
 FFT: fast Fourier transform (analyzer)
 FIB: focused ion beam
 FIT: fast intelligent transducer

- FM: frequency modulated
 fMRI: functional magnetic resonance imaging
 FOG: fiber optic gyroscope
 FOLPS: fiber-optic-linked pressure sensing
 FPGA: field programmable gate array
 FPR: Fabry-Perot resonator
 FRAS: force recording and analysis system
 FRT: force rebalanced transducer
 fsd: full scale deflection / deviation
 FSM: force standard machine
 fso: full scale output
 FSR: force sensing resistor
 FSW: friction stir welding
 FT: force transducer
- GMR: giant magneto-resistance
 GNSS: global navigation satellite system
 GPIB: general purpose interface board
 GUI: graphical user interface
- HBM: Hottinger Baldwin Measurements (US)
 HBM: Hottinger Baldwin Messtechnik (D)
 HCI: human computer interface
 HF: high frequency
 HG: Hall generator
 HIFU: high intensity focused ultrasound
 HP: Hewlett-Packard
 HPF: high-pass filter
 HTS: high-temperature superconductor
- IBM: International Business Machines Corporation
 IC: integrated circuit
 ICP: integrated circuit piezoelectric
 ICT: information and communications technology
 IDE: inter-digital electrode
 IDL: intelligent digital loadcell
- IDT: inter-digital transducer
 IDWS: intelligent dispersive weighing system
 IEEE: Institution of Electronics and Electrical Engineers
 IEEJ: Institute of Electric Engineers in Japan
 IEN: Industrial Engineering News magazine
 IFAC: International Federation of Automatic Control
 IFSA: International Frequency Sensor Association
 IFT: implantable force transducer
 I²C: intelligent interface controller
 IMAGES: interactive microcomputer analysis of general elastic structures
 IMC: Institute of Measurement and Control (UK)
 IMEKO: International MEasurement COnfederation
 IMOG: interferential micro-optic gyroscope
 IMT: Institute for Microtechnologies, Bucharest
 IMU: inertial measurement unit
 INCAS: National Institute for AeroSpace Research “Elie Carafoli”, Bucharest (RO)
 INM: (Rom) National Institute of Metrology
 INMETRO: Instituto Nacional de METROlogia, Normalização e Qualidade Industrial (Brazil)
 INRIM: Istituto Nazionale di Ricerca Metrologica (Italy)
 INS: inertial navigation system
 I/O: input / output
 IOP: Institute of Physics – London
 IPMC: ionic polymer-metal composite
 IR: infra-red
 ISA: Instrument Society of America
 ISE: ion-selective electrode
 ISFET: ion sensitive field-effect transistor

ISiT: Fraunhofer Institute for Silicon Technology, Berlin

ISMCR: International Symposium on Measurement and Control in Robotics

ISO: International Standards Organization

IST: Instituto Superior Técnico, Lisbon, Portugal

ISWC: International Symposium on Wearable Computers

ISWM: International Society of Weighing and Measurement

JSAE : Japan Society of Automotive Engineers

KPFM: Kelvin probe force microscopy

KRISS: Korean Research Institute of Standards and Science

LAN: local area network

LCD: liquid crystal display

LDI: laser Doppler interferometer

LDV: laser Doppler vibrometer

LED: light emitting diode

LINAC: LINear ACcelerator

LMSG: liquid metal strain gauge

LNE: Laboratoire National de Métrologie et d'Essais (France)

LPA: Laboratory for Process Automation, Saarland (D)

LPF: low-pass filter

LSI: large-scale integration

LVDT: linear variable differential transformer

MAW: magnetostrictive amorphous wires

MCDM: multi criteria decision making

MDL: magnetostrictive delay line

MEG: magneto-encephalo-graphic (recording)

MEMS: micro electro-mechanical system

MESA: Institute for Nanotechnology, University of Twente Enschede (NL)

MESFET: metal-semiconductor field-effect transistor

MFM: magnetic force microscopy

μ C: micro-controller

μ CP: micro-contact printing

MI: magneto-inductive

MIFS: mutual inductance force sensor

MIS: metal-insulator-semiconductor

MIT: Massachusetts Institute of Technology

MM: Micro-Measurements (Vishay)

MMIC: mixed-mode integrated circuit

MOEMS: micro-opto-electro-mechanical system

MOS: metal-oxide semiconductor

MRF: magneto-rheological fluid

MRFM: magnetic resonance force microscopy

MRG: micro rate gyroscope

MRI: magnetic resonance imaging

MTBR: metallic triple-beam resonator

MUSic: multi-sensor interface circuit

MWCNT: multi-walled carbon nanotube

MZI: Mach-Zehnder interferometer

NASA: (US) National Aeronautics and Space Administration

NASTRAN: NAsa STRuctural ANalysis

NCP: nanoscale contact pressure

NDT: non-destructive test(ing)

NEMS: nano-electro-mechanical system

NFC: nano force calibrator (KRISS)

NI: National Instruments – Test & Measurement

NIM: National Institute of Metrology (China)

NIST: (US) National Institute of Standards & Technology

NL: non-linearity

- NMRG: nuclear magnetic resonance gyroscope
- NPL: National Physical Laboratory (British Metrology)
- NRAM: nonvolatile random access memory
- NT: nano-technology
- NTC: negative temperature coefficient
- NW: nano-wire
- OA: operational amplifier (op-amp)
- OEM: original equipment manufacturer
- OIFS: optical interference force sensor
- OIML: International Organization of Legal Metrology
- ONERA: Office National d'Etudes et de Recherches Aérospatiales (France)
- PC: personal computer
- PCB: printed circuit board
- PDF: portable document format
- PDMS: poly di-methyl siloxane
- PDO: process data object
- PEM: phase exiation modulator
- PEM: photo-elastic material
- PFM: piezoresponse force microscopy
- PGA: programmable gain amplifier
- PID: proportional integral derivative (controller)
- PIN: positive intrinsic negative (diode)
- PLC: programmable logic controller
- PLib: parts library
- PLL: phase-locked loop
- PLV: pulsed laser vaporization
- PME: precision measurement equipment
- PMN: plumbum / lead magnesium niobate
- POWER: Professional Organization of Worldbest Engineering Resources (Korea)
- PPB: parallel plate beam
- PPF: plasma-polymerized films
- ppm: parts per million
- PPR: pivot-plate resonator
- PSD: position-sensitive detector
- PSD: power spectral density
- PSK: phase shift keying
- PSL: pressure sensitive lock
- PSR: phase-sensitive rectifier
- PTB: Physikalisch Technische Bundesanstalt (German Metrology)
- PTC: positive temperature coefficient
- PUB: "Politehnica" University of Bucharest (RO)
- PVDF: poly-vinylidene fluoride
- PVG: precision voltage generator
- PZFT: piezoelectric force transducer
- PZT: piezoceramic transformer
- PZT: plumbum / lead zirconate titanate
- PWM: pulsed wave modulation
- QCM: quartz-crystal microbalance
- QEMS: quantum electro-mechanical system
- QHE: quantum Hall effect
- QMB: quartz microbalance
- QSPI: queued serial peripheral interface
- QTC: quantum tunneling composite
- QXR: quartz crystal resonator
- RF: radio-frequency
- RFB: radiation force balance
- RFI: radio frequency interference
- RLG: ring laser gyroscope
- RMOG: resonant micro-optic gyroscope
- rms: root mean square
- rpm: rotations per minute
- RTD: research and technological development
- RTG: resistance-to-ground (isolation)
- SAPOP: structural analysis program and optimization procedure
- SAW: surface acoustic wave

SCADA: surveillance, control and data acquisition
 SCR: stress concentration region
 SDA: scratch drive actuator
 SDC: symmetric differential capacitor
 SDI: Systron Donner Inertial (company)
 SDO: service data object
 SEM: scanning electron microscopy
 SEM: (US) Society for Experimental Mechanics
 SFA: surface-force apparatus
 SFM: scanning force microscopy
 SFT: smart force transducer
 SG: strain gauge
 SGFT: strain gauged force transducer
 Si: silicon
 SI: International System of (Measurement) Units
 SLD: super luminescent diode
 SMA: shape memory alloy
 SNOM: scanning near-field optical microscope
 SNR: signal-to-noise ratio
 SOI: silicon-on-isolator
 SOS: silicon-on-sapphire
 SPC: smart pre-concentrator
 SPE: spectral photoelastic effect
 SPI: serial peripheral interface
 SPIE: Society of Photo-optical Instrumentation Engineers
 SPM: scanning probe microscopy
 SQUID: superconducting quantum interference device
 SRB: solid rocket booster
 SRM: Societatea Română de Măsurări (Romanian Measurement Society)
 SSC: superconducting super collider (particle accelerator in Nuclear Physics)
 SSP: smart signal processor
 STEP: STandard for the Exchange of Product model data
 STM: scanning tunneling microscopy
 SWCNT: single-wall carbon nano-tube

T-ID: transducer identification
 TCP/IP: transmission control protocol / Internet protocol
 TEDS: transducer electronic data-sheet
 TEM: transverse electro-magnetic (wave)
 TEM: transmission electron microscopy
 Terfenol: TERbium FE (iron) NOL (Naval Ordnance Laboratory)
 TFT: thin-film transistors
 TI: Texas Instruments
 TNO: Toegepast Natuurwetenschappelijk Onderzoek – Applied Scientific Research (NL)
 TRPS: tenso-resistive pressure sensor
 TSLC: torsional sensing load cell (Helix)
 TTL: transistor transistor logic
 TU: technical university
 TUE: Twente University of Enschede (NL)
 TUT: Tampere University of Technology (FIN)
 TÜV: Technischer Überwachungs-verein – German Technical Monitoring Association
 TVSG: transverse voltage strain gauge (Hall effect)
 TWCNT: triple-walled carbon nano-tube
 UFDC: universal frequency-to-digital converter
 UHF: ultra-high frequency
 UME: Ulusal Metroloji Enstitüsü (Turkish Metrology)
 USB: universal serial bus
 USW: ultrasound standing wave
 UT: ultrasonic test(ing)
 UV: ultra-violet
 VCCS: voltage-controlled current source
 VCO: voltage-controlled oscillator

VCSEL: vertical-cavity surface-emitting laser
VDI/VDE: Verein Deutscher Ingenieure / Elektrotechniker
VEE: visual engineering environment
VFI: Der Versuchs- und Forschungsingenieur (technical journal)
VGA: variable gain amplifier
VHDL: visual hardware design language
VHF: very-high frequency
VIM: International Vocabulary of Metrology
VLSI: very-large-scale integration
VMF: variable message format
VPG: Vishay Precision Group Inc.

VNIIM: "D.I. Mendeleev" All-Russian Institute for Metrology
VSG: vibrating structure gyroscope
VTS: vector touch sensor
VWFT: vibrating-wire force transducer
VWT: vibrating-wire transducer

WAN: wide area network
WELMEC: West-European Legal Metrology Cooperation
WIM: weigh(ing)-in-motion
WSFL: wavelength-swept fiber laser
WTEC: World Technology Evaluation Center, Baltimore, MD
www: world wide web

PART I

PRINCIPLES AND METHODS OF FORCE MEASUREMENT

Galileo: We must measure all that can be measured and we must make measurable all that isn't yet done.

Horatio: There is a measure in all.

Protagoras: Man is the measure of all things.

Carlyle: Force is the measure of any value.

Chapter 1

INTRODUCTION TO FORCE MEASUREMENT

1.1. VARIOUS APPROACHES TO FORCE TRANSDUCTION

Our sense of touch is a primary means of interaction with environment. If we have to create interfaces that can communicate force information [1.1], a wide range of sizes is conceivable, capable of generating and sensing time-varying forces at a single point or a distributed array of points on a surface (Table 1.1).

On a relatively small scale, a single-point force transducer can be as simple as a push button that senses or generates fingertip forces, while distributed-force input/output devices are active surfaces, which can generate and/or sense distributed forces, e.g. a meter-size force display would be capable of reproducing a large three-dimensional topographical terrain map that could be felt with two hands. On a middle scale, the “Phantom” invention is a general-purpose single-point haptic interface that allows the user to feel virtual 3D objects using a single finger. A proper measurement principle and a good mechanism design are crucial aspects of accurate force transducers. No doubt, force transduction is an essential element of user-friendly environments.

Table 1.1 Range of possible human-technology interfaces concerning force information

Relative density	Force I/O devices:				
Highly distribution	Tactile display	Braille display	Deformable keyboard	Player piano	Adaptive structures (vehicles, buildings)
Single point	Active push button	Computer mouse	“The phantom”	Robot arms	Entertainment theater rides
Scale [m]	10^{-3}	10^{-2}	10^{-1}	10^0	10^1

Professor Jacob Israelachvili
Engineering Department
University of California
at Santa Barbara

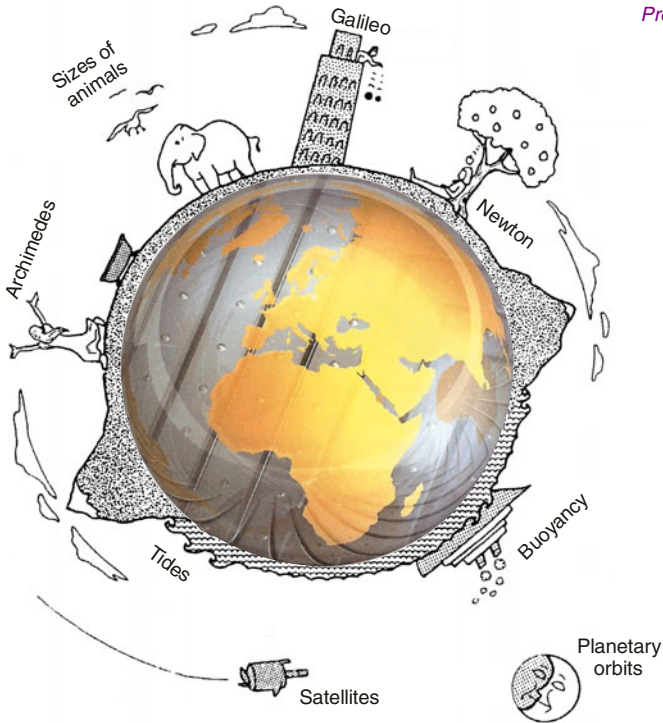


Fig. 1.1 Gravitational and intermolecular forces on Earth (globe inserted from [1.2])

There are four types of interaction forces in nature [1.3]:

- *strong* and *weak interactions* that act between neutrons, protons, electrons and other elementary particles. They have a very short range of action, less than 10^{-2} pm, and belong to the domain of nuclear and high-energy physics.
- *electromagnetic* and *gravitational interactions* acting between atoms and molecules. These forces are effective over a much larger range of distances, from subatomic to practically infinite distance, and are consequently the forces that govern the behavior of everyday things.

Electromagnetic forces – the source of all intermolecular interactions – determine the properties of solids, liquids and gases, as well as the behavior of particles in solutions, chemical reactions and biological structures. Gravitational forces account for cosmological phenomena, and, when acting together with intermolecular ones, determine the animals and trees maximum size (Fig. 1.1).

NOTE. This chapter is treated in an unconventional manner, in many cases, going from particular examples to general assertions. Author has considered more adequate here this unusual approach.

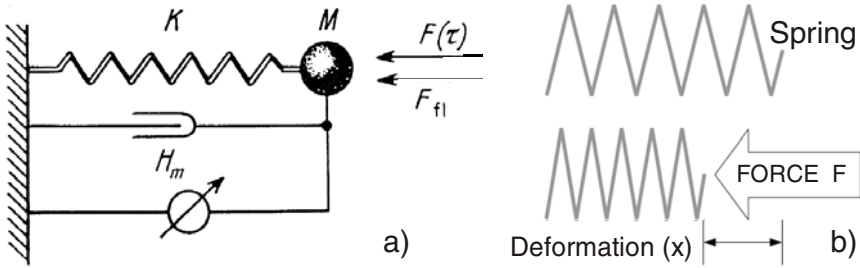


Fig. 1.2 a) Physical model for small forces influence on the resonant frequency of a mechanical oscillator. b) Force measurement through the displacement of a linear spring

A simple model of mechanical oscillator (Fig. 1.2a), with mass M (sometimes called inertance), damping factor H_m and spring constant K , is subjected to an external force $F(\tau)$, which can be a sinusoidal train or a single impulse, and a fluctuating force F_{fl} [1.4]. Assuming an ideal instrument for measuring as small as desired mechanical movements under the applied forces, the criterion is that the change due to the external force exceeds the effect of fluctuational force with a chosen level of confidence which depends on the statistical errors of the first and second order. For highly precise measurement of small forces one can find quartz-fiber torsion balance, electrostatic balance and smart gravimeter (Goodkind & Warburton). The latter uses a superconducting sphere levitated approximately to zero weight by a persistent magnetic field, then balanced by electrostatic sensing and levitating plates, and measuring changes in gravitational field of one part in a billion [1.5].

Besides these physical experiments, here is an engineering concept on force measurement: When a mechanical force is applied to an elastic element, it strains until the generated stress balances that produced by the applied force [1.6]. Conforming Hooke's Law: The relative change in dimension, i.e. strain ϵ , is proportional to the stress σ produced by the applied force on a nonmobile body, in the region below its elastic limit. Considering that *stress* and *strain* share the same Latin root word "*stringere*", it is not surprising that their meanings are closely related [D. Lineback, *Etymology of Stress and Strain*, In: *Experimental Stress Analysis Notebook*, Issue 18, p. 6, Measurements Group, Inc., Raleigh, NC, Febr. 1992].

Force can also be measured by compressing or extending a spring (Fig. 1.2b), using a simple instrument based on the Hooke's Law:

$$F = K \cdot x \quad (1.1)$$

where F is the applied force, K the spring constant and x the spring deformation.

It becomes a simple measurement of distance which is linearly related to force within the spring elastic range. In other words: *Strain ϵ , the relative change in dimensions, is proportional to stress σ produced by the applied force F through the elastic (Young's) modulus E .*

Why measure force? [1.7] Accurate force measurements are required in many applications, among them:

- strength of materials, quality control and safety test,
- weighing vehicles, tanks, bins, hoppers, ladles, products, animals and so on,
- structural integrity of aircraft components and civil engineering structures,
- determining when a missile has developed sufficient thrust to take off,
- automated industrial processes: control roll pressure on bar steel, paper, etc.

Biological systems are also sensitive to mechanical forces and react to them. The book [1.8] shows how the physical forces affect the human biology and (patho)physiology.

This handbook approaches the Force measurand and its associated physical quantities, proposing a dozen of measurement principles (presented in the First Part of this volume) and being information-oriented in a wide range of technical and human applications (to be continued in another volume).

1.2. NEWTON – MEASUREMENT UNIT OF FORCE

Force is everywhere, and is connected with many other mechanical quantities such as torque, pressure, acceleration. In the SI system of measurement units the Force is placed atop of a complicated hierarchic scheme [1.9], suggestively represented by a tree (Fig. 1.3). A selected list of basic mechanical measurands [1.10] is added.

It is a conventional practice to express any measurable physical quantity as a numerical value associated with a unit of measure. The international system of units (known as SI) is coherent, meaning that there are no conversion factors in mathematical expressions linking a base unit with a derived unit, widely accepted as the standard for (inter)national trade, science and engineering.

The unit of force is derived from a fundamental quantity, mass, whose unit is the *kilogram* (kg). The kilogram itself is still defined by means of an artifact: the mass of a platinum-iridium cylinder, kept at BIPM (International Bureau of Weights and Measures) at Sevres, near Paris, France (1889). The unit of force is the *newton* (N). By the definition adopted in 1901, at the general Conference on Weights and Measures, the *newton* is the force required to give a one-kilogram mass an acceleration of one meter per second squared. Remember the Second Law of Sir Isaac Newton (1642-1727): *An unbalanced force F acting on a body will cause that body to accelerate in the force direction with acceleration a inversely proportional to the mass m of the body:*

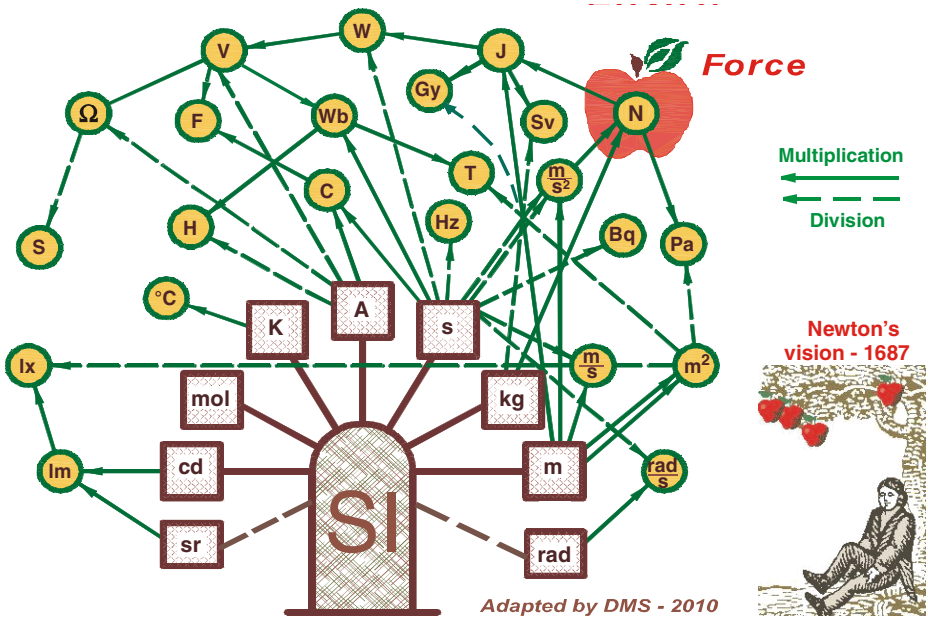


Fig. 1.3 SI tree (conf. Bulletin OIML 95, Juin 1984) and basic mechanical measurands:

- Acceleration – Acoustic energy – Angular velocity or acceleration –
- Compliance – Constant of gravitational attraction – Deflection –
- Deformation (strain) – Density – Displacement – Efficiency – Elasticity –
- Flow rate (mass or volumetric) – Frequency – FORCE (simple or complex) –
- Friction – Hardness – Impulse – Kinetic energy – Mass – Mobility –
- Moment of force (pitch, roll and yaw) – Moment of inertia –
- Momentum {i.e. velocity times mass} – Power – Pressure –
- Reynolds number – Rotational speed – Roughness – Shape – Shock –
- Sound level – Stiffness – Tension (stress) – Thickness – Torque –
- Vibration – Viscosity – Wavelength – Weight – Work – Young’s modulus

$$a = \frac{F}{m} \tag{1.2}$$

Force is a vector quantity, with both direction and magnitude, a measure of the interaction between bodies. Although the definition of force unit is based on free body acceleration, most force measurements are made on bodies in equilibrium, and therefore are measures of forces within a structure.

At the end of the previous century (and millennium), i.e. 1998, the classical range of forces covered is from approximately 10^{-12} to 10^9 newtons, and those forces may be static or dynamic, single or multi-axis, concentrated to a spot or distributed over a relatively large area.

Nowadays the lower limit is pushed to the order of piconewton (or even lower): A micromachined force transducer made by Sandia National Labs [1.11] is able to measure forces as small as 1 pN.

From the metrological point of view, the easiest way to determine categories of application is to use accuracy criteria [1.12] as follows:

- A. Universal force transducers,
- B. Transducers as force measuring devices in material testing machines,
- C. Transducers for the verification of materials testing machines,
- D. Force comparison standards.

1.3. MECHANICAL MEASUREMENTS OF FORCES & TRIBOLOGY

The direct force measurement of the fist at fairs is made with the help of mechanical devices: the punch applied to a boxing bag causes an arch to be released and, directly related to the applied force, a trolley ascends a vertical track, producing sound and light effects, thus attracting more spectators to try out their power. In industrial applications a primary mechanical conversion can be made within lever or spring systems [1.13]. Two mechanical dynamometers for evaluating the micromotors braking systems [1.14] are shown in Figure 1.4.

The loading column is one of the simplest elastic devices (1D), i.e. a metal cylinder subjected to a force along its axis [1.15]. The cylinder length is directly measured by a dial gauge, and force estimation can be made by interpolating between the lengths measured for previously applied known forces. The proving ring has a similar functionality except that the elastic element is a circular ring (2D), and the deformation under the applied force is usually measured across the inside horizontal diameter. Finally, another mechanical method for force measurement utilizes spherical balls as a cheap way to estimate the applied force by the remanent deformation magnitude (Fig. 1.5a); they are 3D devices for measuring forces with complicated statistic analyses and high degree of approximation [1.16].

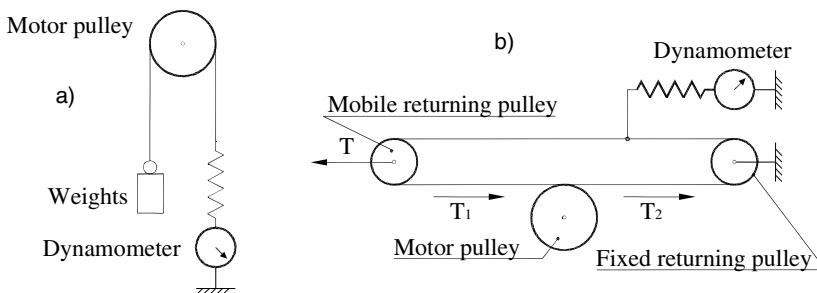


Fig. 1.4 Simple (a) and differential (b) braking systems evaluated by dynamometers

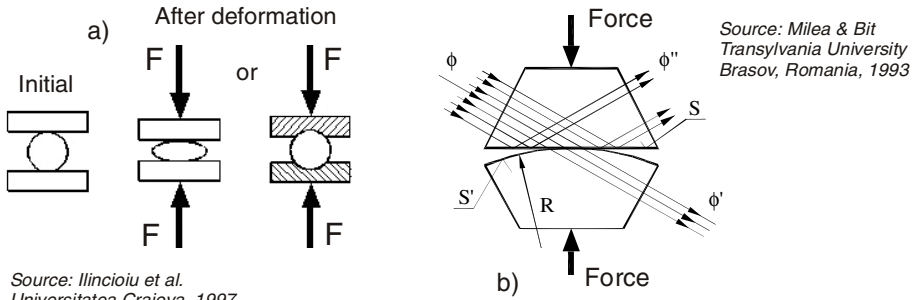
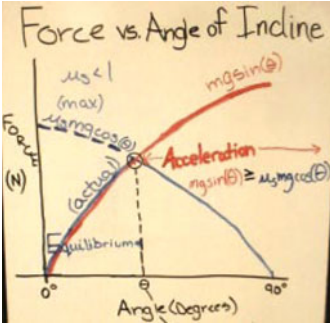


Fig. 1.5 a) Force mechanical indicators based on plastic deformations (measuring the diameter of the aplatized ball) or on the “prints” left into the plates as in hardness testing machine. b) Force measurement method by means of elasto-optical contact.

The elasto-optical contact properties of two surfaces (reflection and refraction of a light ray at the separation level between two transparent bodies) can be also used in the field of force measurement. An original apparatus based upon the mechano-optical modulation of a light wave through an elasto-optical contact is depicted in [1.17]. A plane prism with its surface S' , is continuously approached to the surface S on which the total reflection takes place. From a certain distance between the two surfaces, S and S' , a light ray through S' will appear while the reflected light ray intensity will diminish (Fig. 1.5b). If the surface S' is convex (radius R) and the both bodies in contact are pushed by the force F , then S and S' will have an elastic deformation, their contact area depending on the force F . This way, the transmitted light flux ϕ' increases, while the reflected flux ϕ'' diminishes proportionally under the applied force F .

Friction is the force that opposes the (tendency toward) relative motion of two surfaces in contact. It is not a fundamental force, as it is made up of electromagnetic forces between atoms. Work [1.18] presents some student experiments to use Vernier dual-range force transducers set at the ± 10 N range to measure the magnitude of the force parallel to the surface of a dynamics track acting on low-friction dynamics carts (mass = 0.500 ± 0.005 kg) as a function of the angle of inclination of the tracks (Fig. 1.6).

In a friction testing apparatus [1.19], a stationary contact lens was loaded against a linear reciprocating glass plate. The friction force transducer consisted of a counter-balanced slender beam with mounted strain gauges (SGs). The tribological behavior of dental materials and hard tooth tissues is analyzed in a special device which simulates oral kinematic conditions and the cyclic loading during masticatory process by an adjustable oscillating movement [1.20]. The dental tribometer has two SG full bridges for the measurement of loading and friction forces, by which the friction coefficient is determined.



Angle	Necessary force to move an object
0° (horizontal surface)	Maxim
Equilibrium (on inclined plane)	The static frictional force adjusts its magnitude just to balance the magnitude of an applied force up to a value at which sliding begins.
90°	0 (free fall)

Source: E.P. Wyrembeck
 The Physics Teacher,
 Vol. 43, p. 110, 2005.

Fig. 1.6 Diagram of friction force versus angle of track incline for dynamic carts

Sliding friction levels in molecularly thin layers can be measured experimentally by means of the quartz-crystal microbalance (QCM) technique [1.21]. Both solid and liquid monolayers of the adsorbed films are well-described by the “viscous friction” law:

$$F = -\eta \cdot v_a = -\frac{m}{\tau} \cdot v_a \tag{1.3}$$

where: F is the friction force, η – the friction coefficient, v_a – the average film sliding speed and m – the mass of the adsorbed film. The slip time, τ , which is inversely proportional to the friction level, is a characteristic time for the average adsorbate sliding speed to decrease to $1/e$ of its original sliding speed v .

At present the force is almost exclusively measured by electric methods. The mechanical dynamometers [1.22] are not in current use unless in conjunction with laser installations. The evolution process is from the “hybrid” systems, in which standard mechanical scales are adapted to produce electronic rated outputs, towards the highly integrated computerized mechatronic systems. Moreover, the calibration, as well as the sensitivity on the whole, refers to the relationship between the output and input signals of the weighing system.

1.4. FORCE TRANSDUCERS OTHER THAN ELECTRICAL

A hydrostatic force transducer to measure the compression and tension forces in one direction is depicted in [1.23]. It consists of two components (part A and part B) that behave like a piston and a cylinder (Fig. 1.7a). The pressure in the fluid trapped between A and B is measured by a pressure transducer. A standard face seal prevents fluid leakage. The clamping force is applied by tightening the screws. The more the screws are tightened, the greater preloading force that can be generated in the fluid. If load F is a tension force,

the fluid pressure decreases from the initial preload value. If load F is a compression force, the fluid pressure increases. This force transducer is well-suited for measuring large but slowly varying forces.

The hydraulic load cell (Fig. 1.7b) is a device filled with a liquid (usually oil) which has a preload pressure. Application of the force to the loading member increases the fluid pressure which is measured by a pressure transducer or displayed on a pressure gauge dial via a Bourdon tube.

The operating principles of the pneumatic load cell (Fig. 1.7c) are similar to those of the hydraulic load cell. The force is applied to one side of a piston or a diaphragm of flexible material and balanced by pneumatic pressure on the other side. This counteracting pressure is proportional to the force and is displayed on a pressure dial.

Improved hydraulic and pneumatic actuators comprise PDMS (polydimethylsiloxane) lipseals which prevent the driving fluid leaking to the outside, without introducing friction, and offer superior power and force densities [1.24]. The prototype actuators have an outside diameter of 1.5 mm, and are able to generate forces of 1.2 N at a supply pressure of 1.6 MPa.

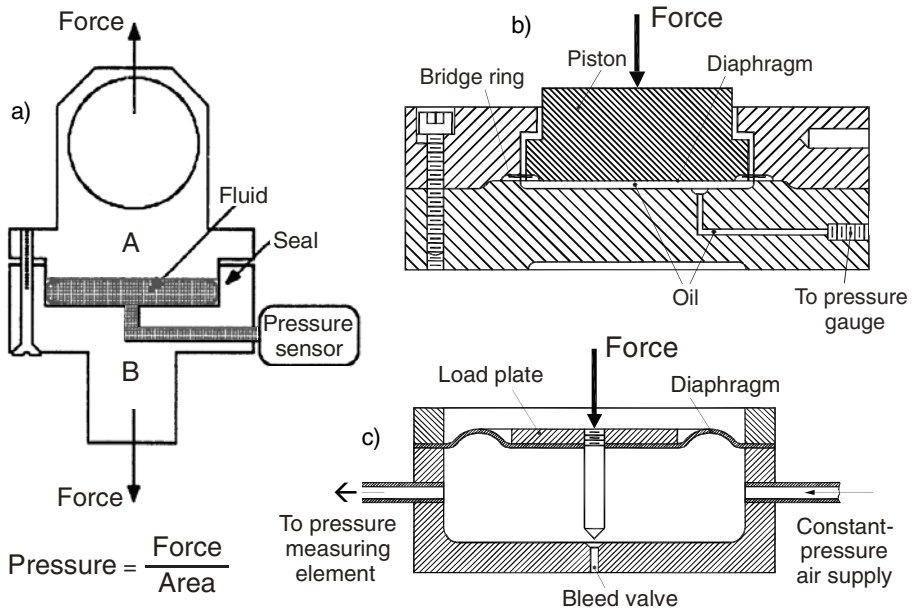


Fig. 1.7 Schematic of the hydrostatic force sensor configuration (a). Sections through a hydraulic (b) and, respectively, a pneumatic load cell (c), after T.G. Beckwith and N.L. Buck, *Mechanical Measurements*, Addison-Wesley Longman Publishing, 1961.

A ring-type hydraulic load cell characteristic feature is its annular design of the measuring piston which offers wider range of applications: 0 to 200 N up to 0 to 2.5 MN [1.25].

A special cylinder with an additional piston is primary composed of a cylinder body, from which it evolves, sunk into a pressurized fluid [1.26]. The lower surface is a little bigger than the superior one due to the piston rod steerage. In the lower part of the cylinder body there is a reception piston from which its loading, through an elastic membrane, produces a hydrostatic pressure for the working fluid, equal to the two different surfaces of the piston. Because the two surfaces are different, the forces from the two faces of the piston are different too. The spring positioned inside the cylinder is solicited by a sensible force lighter than the force applied to the reception piston.

BEV Austria has developed an automatic dead load machine to determine low value forces up to 10 N [1.27]. To realize force-steps of 1 μ N, a modified Sartorius balance has been connected through a specially designed hydrostatic force transducer to the suspension system of the weights. The “force” between the balance and suspension is adjusted by the buoyancy of a floating body (a small double cylinder with a motor inside for changing the cylinder volume).

A weigh-in-motion (WIM) transducer based on a hydraulic system is proposed in [1.28]. A hydraulic system is considered to be advantageous because it will be robust and relatively cheap. This transducer will be suitable to be built into roads and will determine the weight of passing trucks. The oil filled chamber is deformable only on its upper wall; the lateral walls are thought to be rigid. Under the action of the force F , the volume of the chamber changes by V . This change of the volume produces a change of its inside pressure. The idea of the hydraulic system is based on the discrimination of very fast pressure peaks from slowly varying pressures due to temperature changes. A simple orifice, acting as a low pass filter and a differential pressure measurement perform this discrimination.

A computerized, feedback-controlled, portable, battery-powered, hydraulic dynamometer which can be used in normal, reduced-g, and zero-g environments is described in [1.29]. The relevance of the proposed equipment for NASA lies in its ability to evaluate astronaut strength and endurance levels as well as to design and follow appropriate exercise protocols in all gravitational environments. The force and position transducers provide the analog input signals. The acquired data can be stored on computer for later evaluation and for use in conjunction with other medical or physiological assessments in the continual effort to identify and counter the deconditioning caused by micro-gravitational conditions.

Typical ranges for hydraulic force transducers are 500 N ... 5 MN, and for pneumatic force transducers: 10 N ... 500 kN.

1.5. TERMINOLOGY: SENSORS OR TRANSDUCERS?

The words “*sensor*” and “*transducer*” are both widely used in the description of measurement systems. The former is popular in the USA whereas the latter is more often used in Europe. The word *sensor* is derived from the Latin *sentire*, meaning “to perceive” while *transducer* is from *transducere* meaning “to lead across.” Here are some specific differences:

- i) Paul Regtien, Enschede, the Netherlands, 1992 [1.30]: Since most physical measurement quantities are nonelectric, they should first be converted into an electrical form in order to allow electronic processing. This conversion is called *transduction* and is performed by a transducer or sensor. In this book a *sensor* is considered as the smallest technical unit in which data conversion from the nonelectric to the electric domain takes place. A *transducer* is a unit containing the *sensor*, wiring connections and part of the signal processing if so desired, all put together in a casing. In general, the transducer is separate from the main instrument and can be connected to the latter by a special cable. The sensor or input transducer connects the measuring system to the measurement object; it is the input port of the system through which the information enters the instrument.
- ii) Dan Mihai Ștefănescu, Bucharest, Romania, 1999 [1.31]: If force is the measurand then the device that is converting it into an electric signal is called a *force transducer*. In accordance with the international metrology terminology, the item that measurand directly influences is called *sensor* (detector, or “capteur” in French); and the transducer is the device that enables the correspondence between input and output, in compliance with a specific law. Sensor is the primary sensitive element that enables a first conversion of the measured value applied at input (for instance, the strain gauge applied on the elastic element); the *transducer* is the assembly in which the *sensor* is mechanically installed and electrically connected; a microprocessor for data processing can be also included. In Mechatronics / Robotics the sensor detects the environment, while the transducer delivers the control signals to the main operation unit.
- iii) Henrik Pedersen, Aalborg, Denmark, 2006 [1.32]: *Sensor* is a device that responds to a physical stimulus, such as thermal energy (...) or pressure, by producing a signal, usually electrical. *Transducer* is a device for converting energy from one form to another for the purpose of measurement of a physical quantity or for information transfer.

And then a little philosophical extension, including other terms. Jacob Fraden [1.33]: A *sensor* is a *translator* of a generally nonelectrical value into an electrical value. Dave LePine (Oakville, CT) in *Sensors Magazine Online*: The term *transmitter* should be used for any device that sends information over a distance, regardless of whether it is a sensor, transducer, both, or neither.

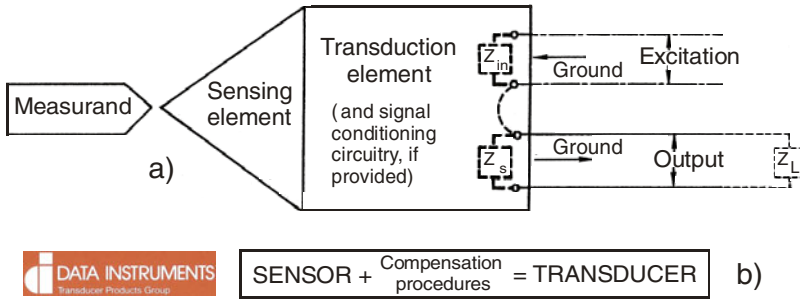


Fig. 1.8 American vision of sensor and transducer positions within the measurement system: a) Norton [1.34], b) Data Instruments [1.35]

Finally, the American perception is illustrated by two equivalent diagrams in Figure 1.8. So, the measurement process consists of sensing with specificity by means of a “sensing element” and then transforming it into another form by a “transduction element” [1.36]. The sensor-transduction element combination will hence forth be referred to as the “transducer.”

The term commonly used in industry “*weighing or load cell*” is equivalent to the more scientific formula “*force transducer.*” Measurement transducer and instrument transducer are redundant. The term *device* is from time to time used in order to replace the word *transducer*, avoiding repetition.

There are some examples of imprecise combination of these terms:

- *Force transducers* and *load cells* [1.37], but load cell is only for weighing, a first member of a force measuring system, while force transducer has a more general utility.
- *Force transducers* and *strain gauges*, referring to implanted strain gauge force transducers successfully used to measure “real-time” gastrointestinal contractility in guinea pigs or postoperative rejection in porcine small bowel transplantation [1.38]. These strain gauges, laparotomy-implanted, are low-impedance, low-level sensors, they are not force transducers!

Note: Avoid a mistake of “translation”: to include a transducer inside a sensor!

Force Sensing is a more general term, as it is found in commercial databases [1.39], representing the mode of operation, not the measuring means which could be: mechanical dynamometer, web tension indicator, weigh module, laboratory balance, impact hammer for modal analysis, load cell or force transducer.

Transducers may generally be divided into two classes [1.40]:

- *Sensors*, which monitor a measurement system, and
- *Actuators*, which produce the display (observable output: LED, LCD, etc.) or initiate some action (e.g. moving coil) in a measurement system.

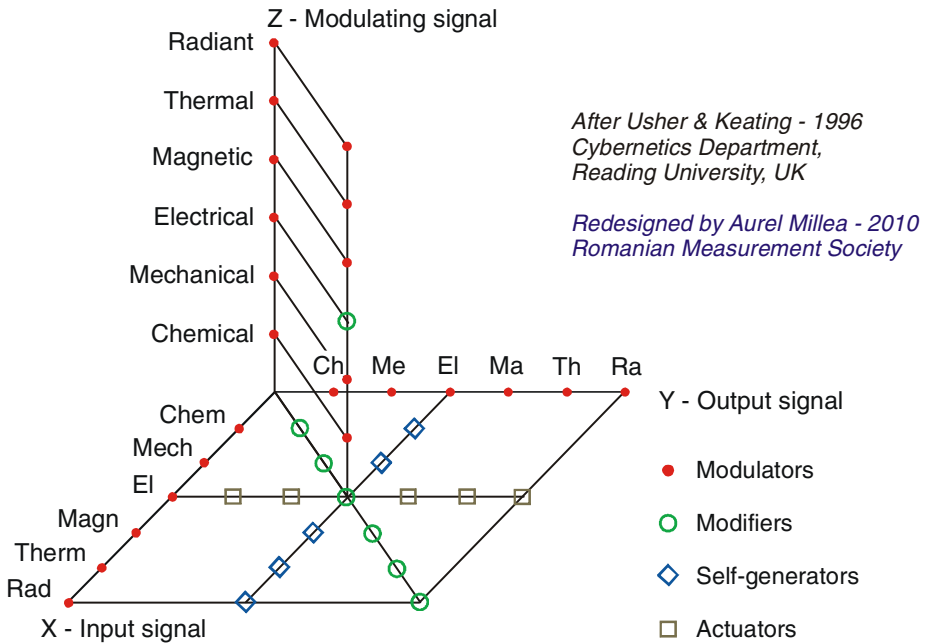


Fig. 1.9 A 3D representation of transducers’ cube with its “electrical heart”

Reversible transducers can operate as sensors or as actuators, but not as both simultaneously! An interesting three-dimensional representation of the transducers’ cube (Fig. 1.9) was proposed by Middelhoek and Noorlag in 1981 and developed by Usher and Keating in [1.41]. The primary energy input to the system is represented along the X-axis and the energy output along the Y-axis. Self-generating transducers therefore lie in the X-Y plane. With the six forms of energy represented on the axes there are 36 combinations, of which six are modifiers (having the same form of energy at both input and output). In general, the word “signal” better expresses such conversions than “energy”.

Four categories of transducers are shown in this 3D representation:

- *self-generators* input transducers, the most important are five (having electrical output), shown as rhombs;
- *actuators* – the most important (having electrical input) are shown as squares;
- six *modifiers* (in which electronic signal is converted, processed and modified) are represented as small circles;
- *modulators* – represented by points in 3D space, the Z-component being the modulating (signal) input. There are evidently 216 modulators in all; the most important are those for which both input and output energy are electrical, of which there are five (shown by dots on the central vertical line).

Self-generating transducers are also known as “active” transducers [1.42], e.g. piezoelectric, while the modulating ones are called “passive”, in which an energy flow supplied by an energy source is modulated by the measurand, e.g. carrier frequency amplifier conditioning a strain gauged force transducer.

Tom Imerito, Science Communications, Pittsburgh concludes about force measurement terminology [1.43]: A *sensor detects* a nonelectrical force, a *transducer converts* it into electrical signal, and an *actuator performs* a mechanical action. Just how each of those things gets done is a matter of intelligence, imagination and innovation on the part of smart designers.

1.6. FORCE MEASUREMENT SYSTEMS

Force transducers can be divided into another two classes:

- *qualitative* or *threshold* devices, their output signals indicating when force magnitude exceeds a predetermined level, e.g. a computer keyboard where a key makes a contact only if it is sufficiently pressed.
- *quantitative* devices, which actually measure the force and represent its values in terms of electrical signals, requiring a proper measuring system.

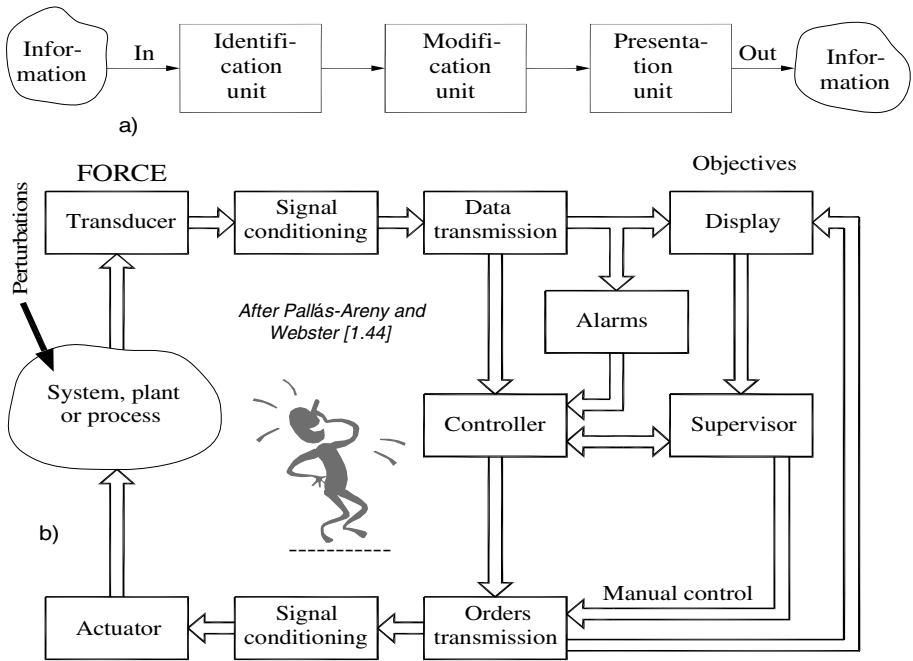


Fig. 1.10 Stages of data flow (a) and functional block diagram of a measurement and control system joining sensing and actuating (b)



Fig. 1.11 Engineering of Measurement Systems course (a), Peter Stein and DMS at IMEKO TC-3 Conference on Force, Torque and Mass, Madrid, 1996 (b)

Force transducers are most frequently used as part of a measurement or control system. Figure 1.10 shows the data flow in such a system [1.44]. In addition to the acquisition of information carried out by a sensor or a transducer, a measurement requires the processing of that information and the presentation of the result in order to make it perceptible to human senses.

The various electrical methods of sensing force can be categorized in arbitrary order of their practical utility as follows [1.33]:

- i) weighing the unknown force against the gravitational force of a standard mass [$G = m \cdot g$];
- ii) determining the *acceleration* of a known mass to which the force is applied [$F = m \cdot a$];
- iii) converting the concentrated force to a distributed fluid *pressure* and measuring that pressure [$p = F / A$];
- iv) balancing the force against an *electromagnetically* or *electrostatically* developed force {See some specific differences in Chapter 15!};
- v) measuring the *strain* produced in an elastic body by the unknown force. A dozen of elastic elements will be detailed in the Second Part of this volume.

A unified approach to the engineering of measurement systems has been presented by Peter Stein (Phoenix, AZ) in his book [1.45] as well as in worldwide courses (Fig. 1.11a) and conferences (Fig. 1.11b).

Table 1.2 looks at the five nonelectrical signal domains and defines a range of phenomena that will translate from one of these nonelectrical domains into electrical output [1.46]. There are a lot of transduction mechanisms: all can form independent sensors or act as information carriers from other transducers.

Whenever pressure is measured, it requires the measurement of force too. One could say that force is measured when dealing with solids, while pressure – when dealing with fluids (liquids or gases). Therefore, the author has decided to add FORCE to pressure in this Culsaw's table, extended on a couple of pages.

Table 1.2 A synoptical image of a wide range of techniques available for measurement

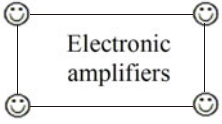
Input variable	Output variables			
	Current	Voltage	Resistance	Light
Current			Thyristor	Light bulb
Voltage			☹	Gas discharge
Resistance	Ohm's law	Ohm's law	☹	☹
Light	Photoelectric effect	Photovoltaic effect	Photo conductivity	Fluorescence
Temperature	☹	Thermocouple	Resistance thermometer	Pyrometers
Magnetic field	Faraday's / induction law	Hall effect	Magneto-resistance	Birefringence in domains
FORCE / Pressure	☹	Piezo-electricity	Piezo-resistance	Piezoelectric breakdown
Strain	☹	Piezo-electricity	Piezo-resistance	☹
Chemical	Ionic concentrator	Electro-chemical cells	Chemi-sorption	Chemi-luminescence

Table 1.2 (*continued*)

Output variables				
Temperature	Magnetic field	FORCE / Pressure	Strain	Chemical
Joule heating	Ampere's law	Via e-m forces	Magnetostatic forces	Electrolysis
Resistive / Joule heating	Via current Amp's law	Via e-m force	Electrostatic force	Ionization potentials
☹	☹	☹	☹	☹
Absorption bolometry	☹	Radiation pressure	Radiation pressure	Photo etching photosynthesis
☹	☹	Thermal stresses	Thermal expansion	Thermal decomposition
Dynamic hysteresis	☹	Magnetic forces	Magnetostriction	☹
Dynamic stressing	Magnetostriction	Fluidic amplifiers	Diaphragm motion	Phase changes
Dynamic straining	Magnetostriction	Direct displacement	Lever	☹
Heat of reaction	☹	Volume change in reaction	Volume / heat of reaction	All chemical reactions

Adapted after Brian Culsaw, *Smart Structures and Materials*,
Artech House, Inc., Norwood, MA, © 1996

The signal domains do clearly overlap, but their classification is useful and illustrates the diversity of sensing technologies. The function of this synoptical image is to graphically emphasize the large variety of transduction techniques while at the same time allowing some common features to be relieved. Force is a derived quantity in the SI system but a fundamental physical measurand on which many other quantities as torque, pressure and acceleration are based. The need for an electronic/electrical output signal is obvious since this is the field in which the necessary signal-processing capabilities are available.

REFERENCES

1. Fletcher, R.: Force transduction materials for human-technology interfaces. *IBM Systems Journal* 35(3&4), 630–638 (1996)
2. Tuning into the virtues of virtual labs. research eu – results supplement, No. 16, p. 36. Image © Shutterstock 2009, European Research Area (July/August 2009)
3. Israelachvili, J.N.: Intermolecular and surface forces, 2nd edn. Academic Press, London (1995)
4. Braginsky, V.B., Manukin, A.B., Douglass, D.H.: Measurement of Weak Forces in Physics Experiments {Translation from Russian of *Izmerenie malykh sil v fizicheskikh eksperimentakh*}. The University of Chicago Press, London (1977)
5. Horowitz, P., Hill, W.: *The Art of Electronics*. Cambridge University Press, Cambridge (1989)
6. Patterson, M.: Force, Pressure, and Torque (January 2007), <http://academic.udayton.edu/MarkPatterson/ECT459/force>
7. Yaniv, S.: Why measure force? (March 2005), <http://www.mel.nist.gov/div822/why.htm>
8. Silver, F.H.: *Mechanosensing and Mechanochemical Transduction in Extracellular Matrix. Biological, Chemical, Engineering, and Physiological Aspects*. Springer, Heidelberg (2006)
9. Ștefănescu, D.M.: Strain gauged elastic elements for force and related quantities measurement. In: CD Proc. IMEKO Int'l Conf. Cultivating Metrological Knowledge, Merida, Mexico, November 27-30, Paper 22 (2007)
10. Letter symbols to be used in electrical technology, 6th edn. Ref. number CEI/IEC 27-1 (1992)
11. Koch, S.J., Thayer, G.E., Corwin, A.D., de Boer, M.P.: Micromachined piconewton force sensor for biophysics investigations. *Applied Physics Letters* 89, Paper 173901. American Institute of Physics, New York (2006)
12. Paetow, J.: Weighing cell and force transducer – there is a difference. In: Private discussions at Hottinger Baldwin Messtechnik, Darmstadt, Germany (November 1987)
13. Grave, H.F.: *Elektrische Messung nichtelektrischer Größen*. Akademische Verlagsgesellschaft Geest & Portig KG, Leipzig, DDR (1965)

14. Duffait, R., Nogarede, B.: Mesure des faibles couples dans les microsystems. In: Actes des conferences Metrologie 1997, Besançon, France, October 20-23, pp. 171–177 (1997)
15. Hunt, A. (Coord.): Guide to the Measurement of Force. The Institute of Measurement and Control, London (Published 1998); ISBN 0-904457-28-1
16. Ilincioiu, D., Păsărin, C., Petrișor, D.: Force indicator. In: Proc. 14th Symposium Danubia-Adria on Experimental Methods in Solid Mechanics, Poreč, Croatia, October 2-4 (1997)
17. Milea, T., Bit, C.: Force measurement method by means of elasto-optical contact. Private communication, Transylvania University, Brașov, Romania, May 20 (1993)
18. Wyrembeck, E.P.: Inductively modeling parallel, normal, and frictional forces. *The Physics Teacher* 43, 107–110 (2005)
19. Ngai, V., Medley, J.B., Jones, L.: Friction of hydrogel (long-wear silicone and soft disposable) contact lenses. The inaugural Ontario Biomechanics Conference, Session 1.4, Barrie, Canada, February 27-29 (2004)
20. Sajewicz, E., Kulesza, Z.: A new tribometer for friction and wear studies of dental materials and hard tooth tissues. *Tribology International* 40(5), 885–895 (2007)
21. Krim, J.: QCM tribology studies of thin absorbed films. *nanotoday* (ISSN 17480132), 2(5), pp. 38–43. Elsevier Ltd., Amsterdam (2007)
22. Makarov, A.R., Renski, A.B., Borkunski, G.H., Etingof, M.I.: Tensometry in Machine Building. Izdat Mashinostroenie, Moskva (1975) (in Russian)
23. Evans, M.S., Stoughton, R.S., Kazerooni, H.: Hydrostatic force sensor. In: Proc. 5th Int'l Symp. on Robotics & Manufacturing, Maui, Hawaii (August 1994)
24. de Volder, M., Ceysens, F., Reynaerts, D., Puers, R.: A PDMS lipseal for hydraulic and pneumatic microactuator. *J. Micromech. Microeng.* 17, 1232–1237 (2007)
25. Hydraulic load cells. *International Equipment News*, No. 9, p. 21 (September 2002)
26. Hadăr, A., Szabo, A., Gheorghiu, H.: Cylinder with diffract piston for measuring masses and weights. November 13-15, Salon INNOVA Eureka, Brussels, Belgium (2008)
27. Buchner, C.: Determination of micro-forces from 1 μ N up to 10 N realized with a full automatically dead load machine developed by the BEV. In: Proc. XIX IMEKO World Congress on Fundamental and Applied Metrology, Lisbon, Portugal, September 6-11, pp. 397–401 (2009)
28. Tita, I., Bârsănescu, P., Schultes, G.: HydroWIM – Hydraulic sensor for Weigh in Motion application. Research report, Hochschule für Technik und Wirtschaft des Saarlandes, Saarbrücken, Deutschland (2005)
29. Ariel, G.B., Penny, M.A.: The computerized resistive exercise dynamometer (December 2002),
http://www.sportsci.com/topics/ces/red_nasa/red1991.html
30. Regtien, P.P.L.: Instrumentation Electronics: Basic Electronic Theory and Techniques, p. 2. Prentice Hall, New York (1992)
31. Ștefănescu, D.M.: Methods for increasing the sensitivity of strain gauge force transducers. PhD Dissertation, p. 4, “Politehnica” University of Bucharest (1999)

32. Pedersen, H.C.: Measurement techniques and data acquisition. Lecture notes for the 6th semester course, Aalborg, Denmark (January 2006)
33. Fraden, J.: Handbook of Modern Sensors – Physics, Design and Applications, 3rd edn. Springer, Heidelberg (2004)
34. Norton, H.N.: Handbook of Transducers for Electronic Measuring Systems. Prentice Hall, Inc., Englewood Cliffs (1969)
35. The inside story: Pressure sensors or pressure transducers? Leaflet from Data Instruments – Transducer Products Group, Lexington, MA (no year)
36. Fleming Dias, J.: Transducers. In: Coombs, C.F. (ed.) Electronic Instrument Handbook, ch. 5, 3rd edn. McGraw-Hill, New York (1999)
37. Bethe, K.: Optimization of compact force-sensor/load-cell family. Sensors and Actuators A: Physical 42(1-3), 362–367 (1994)
38. Nishimoto, Y., Taguchi, T., Masumoto, K., Ogita, K., Nakamura, M., Taguchi, S., Uesugi, T., Takada, N., Suita, S.: Real-time monitoring for detecting rejection using strain gauge force transducers in porcine small bowel transplantation. Transplantation Proceedings 36, 343–344 (2004)
39. Force sensing – instruments, sensors and equipment for measuring static or dynamic force or torque, August 27 (2009),
http://sensors-transducers.globalspec.com/.../force_sensing
40. Busch-Vishniac, I.J.: Electromechanical Sensors and Actuators. Springer, Heidelberg (1999)
41. Usher, M.J., Keating, D.A.: Sensors and Transducers – Characteristics, Applications, Instrumentation, Interfacing, 2nd edn. MacMillan, Houndmills (1996)
42. Middelhoek, S., Audet, S.A.: Silicon Sensors. Academic Press Ltd (Harcourt Brace Jovanovich Publishers), London (1989)
43. Imerito, T.: MEMS – Imagination for Microelectronics. Science and Technology Communications, Pittsburgh Technology Council, PA (March 2006)
44. Pallás-Areny, R., Webster, J.G.: Sensors and Signal Conditioning. John Wiley & Sons, Inc., New York (1991)
45. Stein, P.K.: The Unified Approach to the Engineering of Measurement Systems for Test and Evaluation, Part I – Basic Concepts. Fifth Printing with Revisions. Stein Engineering Services, Inc., Phoenix, AZ (1995)
46. Culsaw, B.: Smart Structures and Materials. Artech House, Boston (1996)

Chapter 2

ELECTRICAL METHODS OF FORCE MEASUREMENT

The nonelectric force measuring methods are history already. Anyway, the mechanic, pneumatic or hydraulic devices do not have the sensitivity of the electronic ones, as no physical phenomenon directly transforms force into electric signal [2.1]. Force is a mechanical measurand, and its applying modifies the electric, magnetic, acoustic and/or optical properties of specific materials. The key component within the measurement system is the transducer (Fig. 2.1), which can use various measurement principles or methods. The most convenient description of the transducer field is offered by the physics-oriented approach [2.2]. There are generally accepted six signal domains containing the main physical parameters: mechanical (acoustic included), thermal, electrical, magnetic, radiant (optical), and chemical.

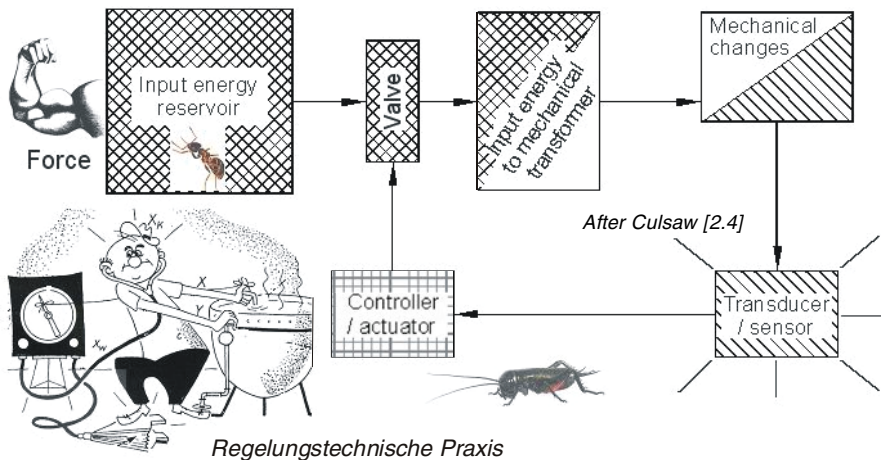


Fig. 2.1 Energetical transformations in the automatic process of force measurement combining hard work and soft control like in the fable “The cricket and the ant”

Technical systems can directly produce different energy forms, e.g. mechanical and thermal. Biological systems (e.g. muscles) can also produce mechanical energy due to their movement. Appropriate measurement technique is necessary, often connected with automatic control of the process.

2.1. ENERGETICAL ASPECTS IN FORCE TRANSDUCTION

A suggestive way of describing the different transducer possibilities is by applying a 3D energy space diagram [2.3], like in Figure 2.2a, in which:

- X-axis represents the input energy domain. It contains the required auxiliary energy only, if a modulating transducer is involved. In the case of a self-generating transducer it represents the energy and information bound to it.
- Y-axis represents the output energy domain in which the outcoming information content is available.
- Z-axis represents the modulating energy domain in which the incoming information is available, if an auxiliary energy source is required.

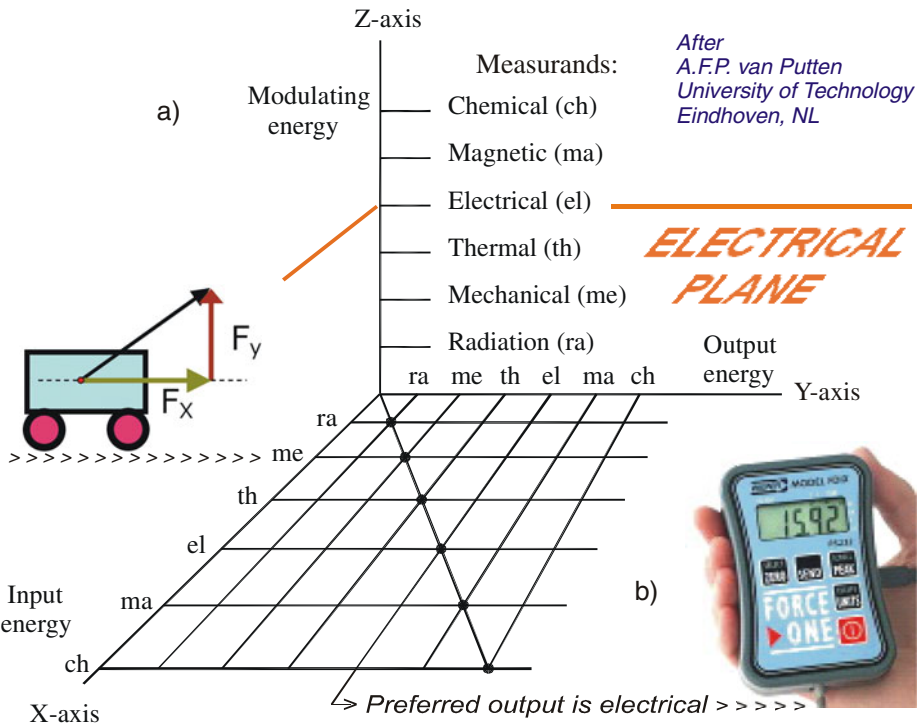


Fig. 2.2 a) A 3D representation of the energetical transduction process (Transducers' cube). b) Example of mechanical force input "transduced" into a digital signal output.

In the X-Y plane (so-called input-output plane), all 36 possible self-generating transducers can be found. In the transducers placed on the main diagonal, i.e. modifiers (shown by dots), no energy conversion is involved, but an energy shape conversion is executed only.

If somebody represents the entire transducer cube, as it was imagined by Middelhoek, in each elemental box within this cube a complete transduction system could be defined [2.4]. A wide range of physical and/or chemical phenomena can be used to fulfill the transduction process represented by that box. In practice, only devices offering an electric output are called transducers, because the most measurement systems use electric signal. In other words, the output signal must lie in the electrical plane, but the input signal applied to the modulating channel can exist anywhere within the 36 options inside that plane. An example of modulating transducer is the magnetoresistor, which has the Miller index of transduction [el, el, ma], i.e. the conventional abbreviations for input, output and modulating energies. The digital Force One Indicator is an example of electric output transducer (Fig. 2.2b).

Following the definitions given by Rosenberg & Karnopp (1983) and Middelhoek & Hoogerwerf (1986), the most complete definition in this area is given by Irene Busch-Vishniac (1989) [2.5]: *A transducer is a device which transforms energy from one type to another, even if both energy types are in the same domain (e.g. a wheel changing rotation into translation movement); the latter situation is represented with close loops (Fig. 2.3). Often this process is bidirectional.*

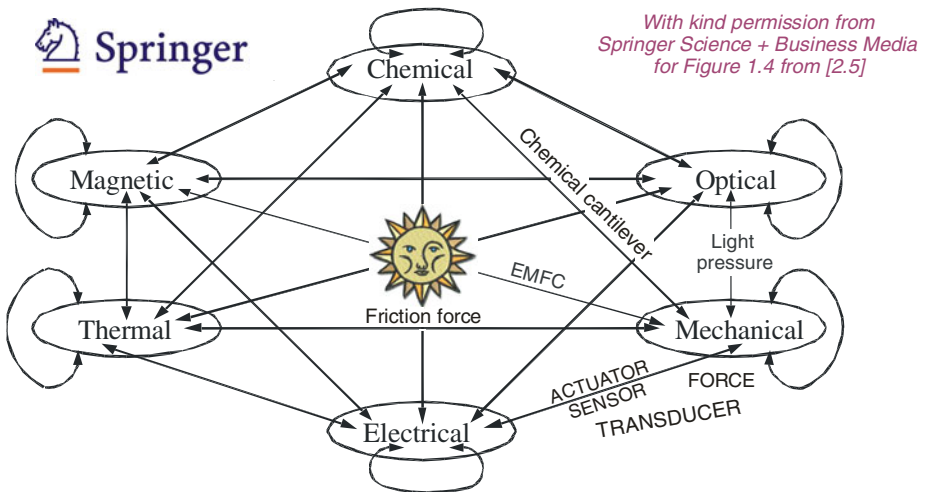


Fig. 2.3 A suggestive positioning of the six energy domains in order to represent their complex interactions and transformations between basic energies

Specific examples of energetical transformation are given in [2.6] and their names are written on the connection arrows in the above-mentioned figure:

- Friction force is presented in subchapter 1.3 while some thermal processes are described in the following subchapter.
- Electromagnetic force compensation (EMFC) principle is presented in C.7.4 and C.8.1...C.8.3.
- Embedded piezoresistive cantilevers can react volumetrically when exposed to various analyte molecules; the mechano-chemical reactions might be absorption, diffusion or adsorption [2.7], as detailed in C.23.3.
- James Clerk Maxwell has stated that the pressure of strong sunlight on a square mile is about 14.5 N [2.8].
- Our focus is electro-mechanical and it is “localized” in the lower right corner of Figure 2.3. In this reversible process, a bidirectional force transducer can be seen as a sensor from the mechanical input to the electrical output or as an actuator (referring to the opposite direction).

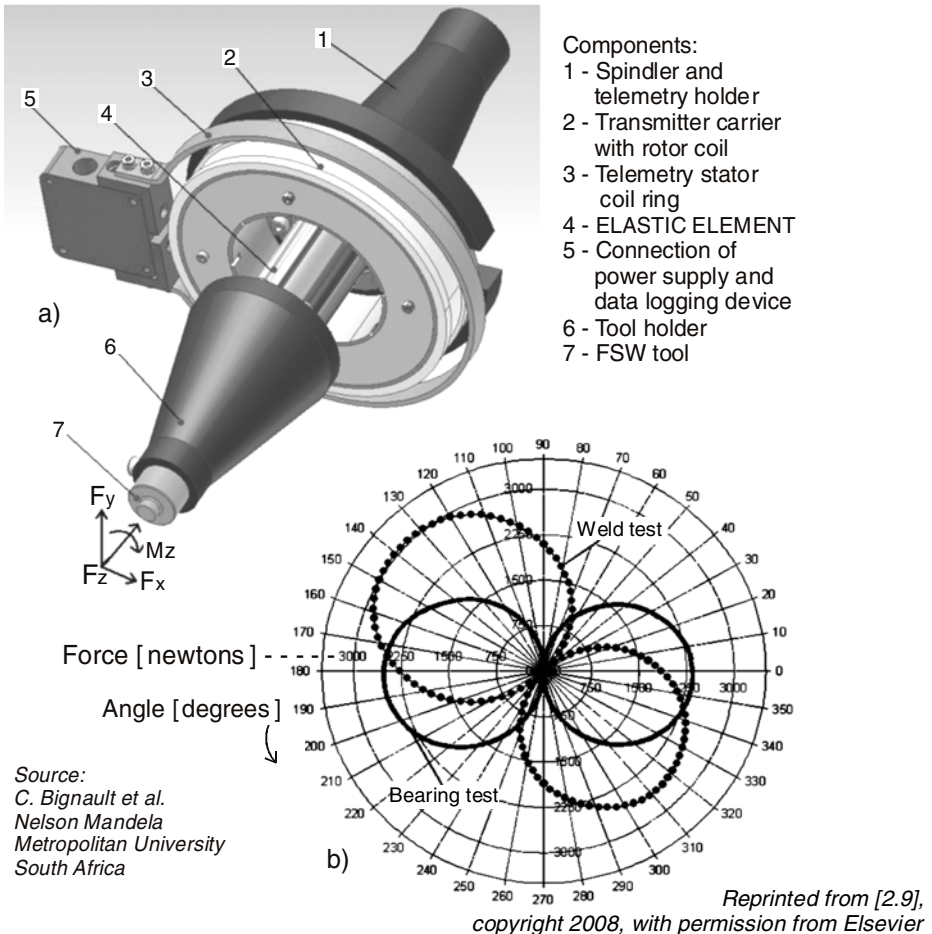
The most useful effects in the mechanical energy domain are summarized in Table 2.1, including their Miller indices and short explanations. In real measurements, these effects are more complex and closely interconnected, e.g. the triboelectric rubbing of materials produces thermal effects too, and they are very useful within the applications presented below.

Table 2.1 Some effects in mechanical force domain and their short description

Effect	Notation	Macroscopic description	Chapter
Piezoresistance	[el, el, <i>me</i>]	Change in semiconductors <i>conductivity</i> due to a mechanical force	C.3.5.
Piezoelectric	[<i>me</i> , el, 00]	Generation of a <i>surface charge</i> due to a mechanical force	C.6
Triboelectric	[<i>me</i> , el, 00]	<i>Positive or negative charges</i> generation due to the surface rubbing of materials	—
Acoustoelectric	[<i>me</i> , el, 00]	Generation of an <i>electric current</i> by a traveling acoustic wave (SAW)	C.13.5
Thermoelastic	[th, el, <i>me</i>]	<i>Voltage</i> generation in two regions of a metal due to a mechanical strain and a temperature difference in those regions	—
Magnetoelastic	[<i>me</i> , ma, 00]	Change in <i>magnetization</i> by a mechanical force	C.9
Piezooptic	[ra, ra, <i>me</i>]	Change in <i>refractive index</i> due to a mechanical force	Fig. 1.5b
Photoelastic	[ra, ra, <i>me</i>]	Generation of <i>double refraction</i> by a mechanical force	Fig. 32.2

2.2. EXAMPLES OF FORCE MEASUREMENT IN THERMAL PROCESSES

Friction stir welding (FSW) is an autogenous solid-state technique that uses a nonconsumable tool to generate frictional heat (Fig. 2.4) [2.9].



VERTICAL FORCE $F_z = 60 \text{ kN}$ compressive strain HBM XK51 3/350	HORIZONTAL FORCE $F_x/y = 8 \text{ kN}$ shear strain HBM XK11 3/350	APPLIED TORQUE $M_z = 400 \text{ N-m}$ bending strain HBM DK11 3/350
---	--	---

Fig. 2.4 Four-component force and torque transducer for friction stir welding (a) and “force footprints” for weld and bearing tests (b). The polar diagram Force versus Angle has radial data expressed in newtons and angular data in degrees.

There is a complex interaction between the rotating tool and the alloy, making difficult the contribution determination of various process parameters (tool geometry, temperature, rake angle, speed and feed) to the desired weld properties. A system functions with four degrees-of-freedom (DoF) namely F_x , F_y , F_z and M_z is presented in Figure 2.4a. The transducer design is based on a strain gauged hollow steel shaft acting as elastic element.

The concept of “force footprint” describes the resultant horizontal force variation during a single revolution of the instrumented FSW tool. Such a presentation like in Figure 2.4b is useful if supposing the area of the polar plot as a measure of the energy input into the weld, while the angle subtended by the direction of travel and the force maxima and minima is likely to reflect details of the weld flow mechanisms. The force transducer is designed to provide output data for on-line video rendering of force footprint polar plots.

A telemetric system, achieved by capacitive coupling of FDM (Frequency Division Multiplexed) modulated signals, provides a high-speed unidirectional data link between the rotating and stationary components.

The molecular dynamics is a valuable tool to simulate the nanoscale cutting of a Cu single crystal using a conical diamond (Fig. 2.5a). The authors of the paper [2.10] introduce the nanoscale contact pressure (NCP) factor, defined as the ratio between the action/cutting force and the tool-workpiece contact projection area. This model for estimating the nanoscale cutting force requires only the average cutting depth (proportional to the thrust force) and the “melting” area in the cutting direction to be measured. The diagrams for thrust and cutting forces versus the cutting travel distance are shown in Figure 2.5.b.

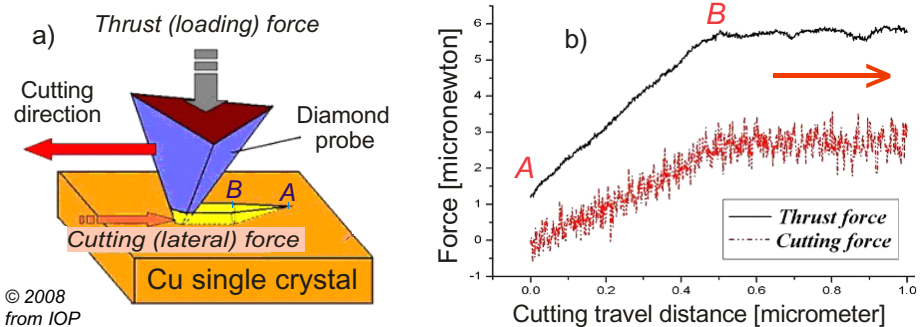


Fig. 2.5 Two-directional loading for nanoscale cutting of a Cu single crystal using a conical diamond (a) and the appropriate curves of thrust and cutting forces (b)

Energy dissipation due to friction in telescopic carbon nanotubes (CNTs) is modeled by molecular dynamics over a wide temperature range [2.11].

The friction force between the inner and outer CNTs is strongly related to thermal effects and shows a minimum as temperature increases. At ultra-low temperatures, thermal lubrication, i.e. the reduction in the friction force because of thermal activation, plays a dominant role because energy barriers for the relative translational movement of the concentric nanotubes are so small that the thermally activated jumps effectively reduce the friction force.

2.3. TYPICAL REQUIREMENTS FOR FORCE TRANSDUCERS

Force has a “variable” position among the mechanical quantities. It takes the first place for Middelhoek & Audet [2.2] and Bau, de Rooij & Kloeck [2.12], being followed by torque, power, stress and other energy-oriented variables. Force is on the third place for Fraden [2.13] and on the fourth position for van Putten [2.3], Usher [2.14] and Sze [2.15].

Irrespective of the position assigned in various classifications, the measurement of force is important in a wide range of applications, starting from the atomic level and extending to the interplanetary one, due to the space vehicles launched from the Earth.

Any force measuring system is inherently amenable to the environment interaction [2.16] expressed by mechanical, chemical, thermal and radiation factors (Fig. 2.6). According to P.K. Stein [2.17] there are 32 combinations (syndromes) of responses to environment, out of which 16 are critical.

The disturbance factors can be eliminated by specific action for each case. Here are two “minor” examples: firstly, the conditions to neglect load variation produced by creep [2.18]:

- the transducer is stabilized by several loading–unloading cycles (in order to reduce its inherent influences over zero and sensitivity [2.19]);
- time depending loading configuration is maintained constant;
- reading time on each stage is the same.

Secondly, measures have to be taken to reduce induced mechanical strain by a DC electric field in thin organic materials included into force transducers [2.20].

The selection of an appropriate transducer usually involves some basic considerations [2.21]:

- measurand (i.e. FORCE), range (expressed in newtons or its multiples and submultiples), overload, accuracy, frequency response;
- transduction principle, deeply connected with measurement method;
- measurement system capability: signal conditioning, data processing (filtering, errors compensation), transmission and display;
- available space, ambiental and functional/working conditions;
- economic aspects: performance-cost ratio, possibilities of reusing or redesign, periodic verification of technical characteristics.

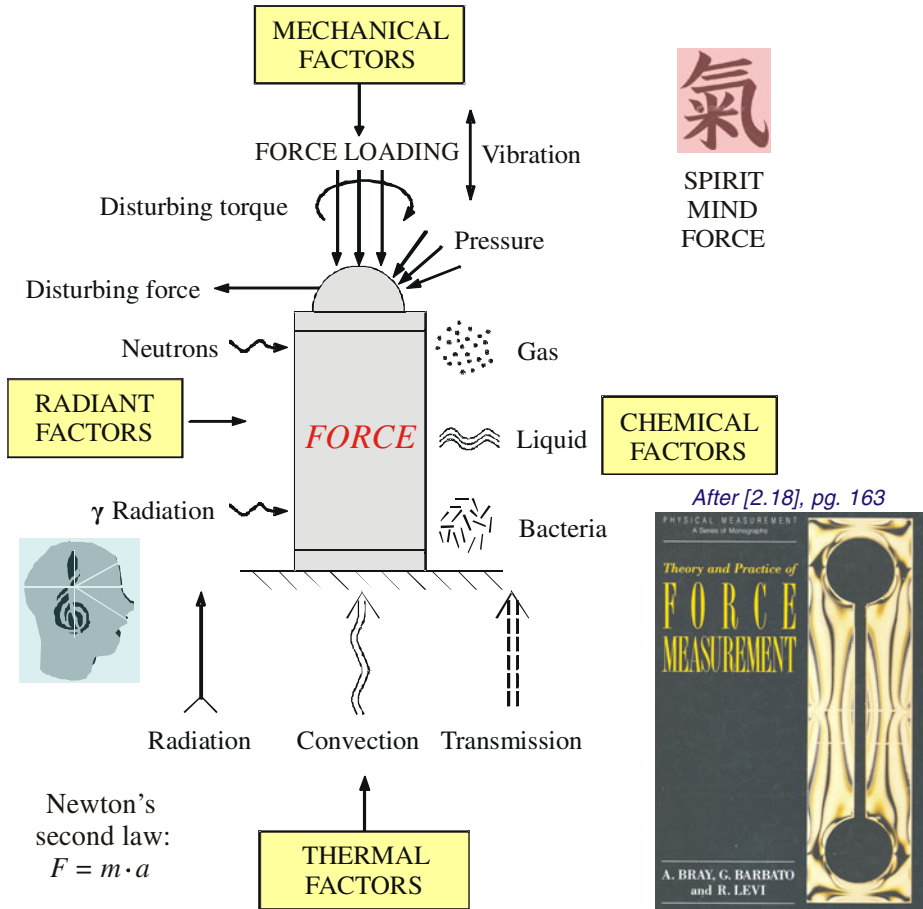


Fig. 2.6 Parasitic factors in mechanical force measurements. Note that radiation can be thermal or ionizing as well. If mechanical, chemical, thermal and radiant factors can be the influence factors, it results that the electrical and magnetic phenomena are the useful ones for mechanical force measurements.

2.4. FORCE TRANSDUCERS (FTs) CLASSIFICATIONS

2.4.1. First attempts of force transducers systematization

As V. Gordon Childe said, “*The aim of science is surely to amass and systematize knowledge.*” Electronic engineers prefer to classify transducers according to some variable parameters (resistance, inductance, capacitance), and then to add transducers generating voltage, charge or current, and other sensing devices not included in the preceding groups [2.22].

A *variable-impedance transducer* contains an elastic component and a potentiometric, inductive or capacitive component [2.23]. In Figure 2.7 the concentrated force and/or distributed pressure act on a flexible diaphragm. The displacement of this elastic element under load is transferred to the moving part of the transduction element and provides the change in resistance or reactance. Bridge-type circuits are quite commonly used to obtain a voltage output which is proportional to the applied load.

The *biparameter* method of force measuring {resistive + inductive}, proposed in [2.24], includes three steps:

- i) a coil assembly and a quantum tunneling composite, wherein the coil is adapted to carry an electric current, and wherein the quantum tunneling composite is electrically insulated from the coil and disposed in a magnetic path created by the coil when an alternating current is present in the coil;
- ii) positioning the coil assembly with the quantum tunneling composite in a load path of a force and under strain from the force, the electrical resistance R of the quantum tunneling composite changes with the force variations;
- iii) determining the force using at least the measured inductance L in the coil.

A classical and minimal classification of transduction principles has been made by Seipel in 1983, adding to the parametric transducers {resistive (SG - strain gauge and piezoresistive), inductive (LVDT) and capacitive} two “new” types: piezoelectric transducer and electromagnetic balance [2.25]. The Mettler-Lexicon “adds” magnetoelastic and vibrating wire principles for weighing applications [2.26].

The following measurement techniques are competitively compared in [2.27], considering the technical specifications for some commercial products:

- Strain gauge – metallic: Siemens Teleperm M 56454,
– diffused silicon: Honeywell 411 Series,
- Variable inductance: Hartmann & Braun 15750,
- Differential capacitance: Rosemount 1151 DP and Fischer & Porter 50 DPF,
- Resonant / vibrating wire: Foxboro 823 DP,
- Force balance: Schlumberger Thermis C.

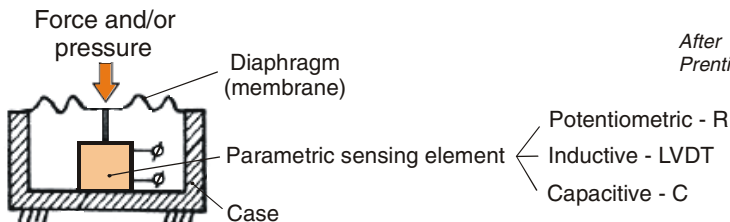


Fig. 2.7 Global representation of force and/or pressure sensing based on a parameter variation: R (resistive), L (inductive) or C (capacitive)

Besides mechanical (springs and levers) and optical devices (photoelastic and Fabry-Perot interferometer) for force measurement, seven types of force transducers suitable for industrial robots are presented in the Romanian handbook [2.28]: resistive (SGs and piezoresistive), inductive (including eddy current detectors), capacitive, piezoelectric, electromagnetic (among them magnetoresistors), magnetoelastic and vibrating wire devices.

An extensive table, intended to systematically present the possibilities of electrical measurement of forces and other mechanical quantities, is given in [2.29], also including some thermal, acoustic or optical effects (geometrical and physical). Apart from the above mentioned measuring principles, there exist others that would be difficult to classify in these categories, like those used in solid-state electronic devices (here dealt with in subchapter 16.1).

2.4.2. German FT classifications

Professor Klaus Horn, T.U. Braunschweig, has been active for a long time in the systematization of the physical principles and the basic geometrical shapes that occur in the electrical measurement of the force and pressure [2.30 – 2.32]. A measurement specialist will realize an overwhelming quantity and variety of industrial and customized products, due to their operational principles, shapes of elastic elements, and rated loads [2.33]. It is also remarkable the attempt toward a “standardized” representation of four different force transducers (Fig. 2.8):

- a) Independent from whether load F is applied punctually or as a surface-distributed force, a load-input element is used as force adapter. The height H must be designed according to the Saint Venant’s principle: $H > 5 D$. This way, a system of forces statically equivalent to that actually applied has the same effect at a sufficiently large distance from the loading point.
- b) A capacitive force transducer (FT) contains a movable center electrode CE, which is a circular plate straight and parallel guided by the diaphragms DG between two differential electrodes E_1 and E_2 .
- c) Practical realization of a piezoelectric FT makes use of two thin quartz discs with $H < 0.3$ mm, arranged with opposite polarization and preloaded with force F_p by tightening screws. The central electrode is placed between two outer electrodes: one is formed by the rigid force adapter and other by the base element. The output voltage U_m is a measure of the applied force.
- d) An energy reduction process is achieved by built-in energy transformers. A force-pressure transformer is used to convert a very large longitudinal force F_L into a pressure p , which is generated in a thin layer (0.3 mm) of a hydraulic fluid of low compressibility in a small reservoir together with compensation body CB, inserted into a borehole CB_+ . DG is a flexible ring used as guided diaphragm, DT is the transformer diaphragm and DM is the measuring diaphragm, i.e. a profiled membrane with four strain gauges.

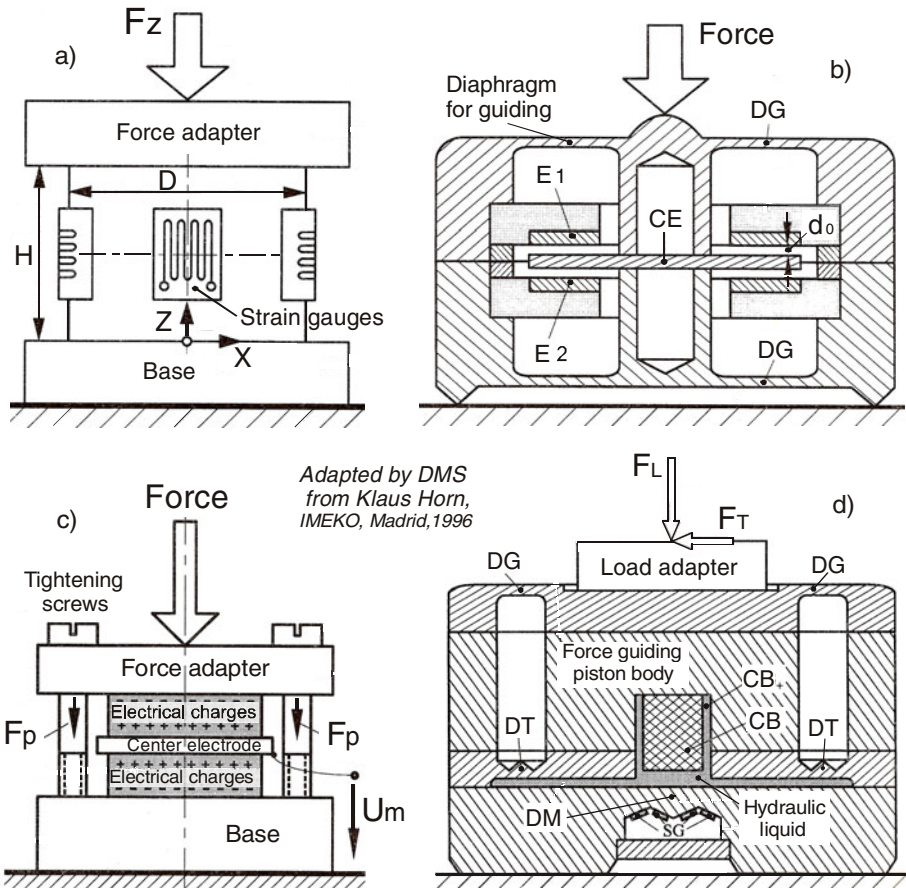
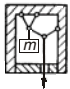
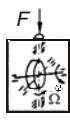
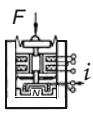
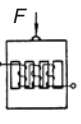
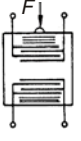
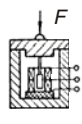
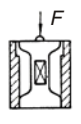


Fig. 2.8 The coexistence of mechanical and electrical aspects in the representation of force transducers: a) Resistive force transducer (FT) with four strain gauges bonded on the columnar elastic element and connected in Wheatstone bridge. b) Differential capacitive FT with circular plates. c) Piezoelectric FT. d) hybrid hydraulic-electric FT, finally based on a strain gauge profiled membrane.

“Extreme” solutions of force transducers proposed by K. Horn are the inductive or magnetoelastic ones for large loads and optical interferometer or tunnel scanning microscope techniques for very small forces.

Seven types of force transducers are presented in Table 2.2 [2.34]. In fact, the RLC one represents three types: potentiometer, inductive coil and variable capacitor. There are seven suggestive miniatures (small-scale reproductions) and the associated formulas indicating the force dependence of their principal parameter, left to right:

Table 2.2 Survey of measurement principles for force transducers – Theiß (1983)

Working principle	Vibrating wire	Gyro-dynamic	Force balance	Magneto-elastic	Acoustic (SAW)	RLC displacement	Metallic strain gauge
Symbolic layout							
Physical formula	$f \sim \sqrt{\frac{F}{m}}$	$\Omega \sim \frac{F}{E}$	$i \sim F$	$\mu \sim F$	$f \sim f_0(1 - \epsilon)$	$s \sim \frac{F}{k}$	$\frac{\Delta R}{R} \sim \epsilon \sim F$
Load range	< 1kg	< 10kg	< 1kg	0,1->1000t	< 10kg	1g->100t	1kg->1000t
Deflection [mm]	< 0,2	< 0,1	0	< 0,5	< 0,2	< 1	< 0,5
Linearity error	< 0,02%	< 0,02%	< 0,01%	> 1%	> 0,1%	> 0,5%	< 0,02 - 1%

- f – resonance frequency for vibrating-wire force transducer,
- Ω – angular velocity for gyroscopic force transducer,
- i – current in the feedback loop for electromagnetic force compensation,
- μ – magnetic permeability for magnetoelastic force transducer,
- f – acoustic frequency for surface acoustic waves force transducer,
- S – displacement sensitivity for the linear potentiometer, LVDT and plane plates capacitor, respectively,
- ϵ – strain inside the elastic element of force transducer.

Load range is indicated in mass units, having in view that the precise mass determination is made by measuring its force effect in the gravitational field of the Earth [2.35].

2.4.3. Dutch FT classifications

The Dutch school contribution to the general picture of force measurements is reflected in a lot of valuable handbooks and PhD dissertations.

Dr. H.A.C. Tilmans, Universiteit Twente, The Netherlands, has shown that, while the electromagnetic (reluctance type) transducer is too vague concerning the parts description (a yoke, a resonating beam and a driving coil with an excitation winding of n turns), a separate category should be constituted by the electrodynamic transducer in which a vibrating beam, placed in a magnetic field, is passed by AC and the resulting Lorentz force provides the driving force [2.36]. Due to the beam motion, the flux linkage of the current loop changes, thereby inducing a voltage that determines the detection signal. More generally, a so-called “continuum transducer” has a permanent coupling with the elastic media and important interactions between the electric, magnetic, mechanical and thermal energy domains have to be considered.

Table 2.3 Classification of measurement principles for force transducers (Blom, 1989)

FORCE TRANSDUCER	Normal range [N]	Resolution [ppm]	Thermostability [ppm]
DIRECT CONVERSION			
Vibrating wire	5 ... 100	100	10
Piezoelectric	$10^3 \dots 10^7$	10000	200
Resonant quartz beam	1 ... 10	20	10
COMPOSITE CONVERSION			
Strain gauge	1 ... 10^7	100	15
Displacement: LVDT	$10^{-2} \dots 10^4$	1000	500
Capacitive	10 ... 100	2000	200
Hydraulic	500 ... 2×10^5	10000	1000
Gyroscopic	50 ... 250	10	1
Magnetoelastic	$2 \times 10^3 \dots 10^7$	500	30
FORCE COMPENSATION			
Balance	maxim 10^4	1	20
Electromagnetic compensation	$10^{-3} \dots 10^2$	1	10

Dr. Fr. Blom, Twente University of Enschede, gives a clear classification of transduction considering the fundamental conversion process, as described in the Table 2.3 [2.37]:

- Direct conversion in which the stress in the elastic body directly generates the electrical signal.
- Composite conversion – the stress in the elastic body is transformed into an electrical signal by means of a displacement measurement that can be performed in a different signal domain, for instance magnetically.
- Force compensation – the measuring device generates a counterforce, which equals the measurand; it is a zero displacement measurement, based on its continuous control in a feedback loop.

In this classification are not included other types of resistive transducers besides strain gauges while force balance is a measurement technique applied to different types of transducers, using various measurement principles (as presented in Chapter 15). The principles under development in 1989 – such as force transducers with piezoresistive devices, magnetic ribbons or surface acoustic wave (SAW) resonators – were not listed in this Dutch table.

2.4.4. English FT classifications

In his summary table of transducer characteristics for measurement of force, weight and torque, Mansfield has included only the following types in 1973: resistive, magnetoelastic and piezoelectric (charge amplifier, quartz oscillator and special piezo-transistor) [2.38].

A quarter century later, Morrison, focused on computerized measurement particularities of mechanical quantities, has limited his selection to piezo-electric, piezoresistive and capacitive transducers [2.39].

As a consequence of technological advance and industry requirements for regulations, the UK National Physical Laboratory edited in 1998 “*Guide to the Measurement of Force*” [2.40]. In the Table 2.4 are presented nine “electric” force transducers types. While the resistive transducers are splitted in three categories (without pretensioned and/or wrapped wires), the LVDT, capacitive, tuning-fork and vibrating wire are grouped in the same central row!

A more detailed classification of measurement principles has been given by NPL in its “*Guide to the Measurement of Pressure and Vacuum*” [2.41]; there are indirect and direct methods, among the latter being pressure balances and transducers based on mechanical deformation of their elastic elements.

Table 2.4 Classification of measurement principles for force transducers (NPL, 1998)

FORCE TRANSDUCER TYPE	Typical range of rated capacities	Typical total uncertainty
Hydraulic	500 N to 5 MN	$\pm 0.25\%$ to $\pm 5\%$
Pneumatic	10 N to 500 kN	$\pm 0.1\%$ to $\pm 2\%$
Strain gauge load cells:		
Foil gauges	5 N to 50 MN	$\pm 0.02\%$ to $\pm 1\%$
Semiconductor gauges	1 N to 10 kN	$\pm 0.2\%$ to $\pm 1\%$
Thin film gauges	0.1 N to 100 N	$\pm 0.02\%$ to 1%
LVDT, capacitive, tuning-fork, vibrating wire	10 mN to 1 MN	$\pm 0.02\%$ to $\pm 2\%$
Piezoelectric crystal	1.5 mN to 120 MN	$\pm 0.3\%$ to $\pm 1\%$
Electrostatic or electromagnetic force balance	0.25 N to 20 N	1 part in 10^6
Magnetoelastic	2 kN to 50 MN	$\pm 0.5\%$ to $\pm 2\%$
Gyroscopic	50 N to 250 N	$\pm 0.001\%$

Other comments related to the English metrological classification are:

- Hydraulic and pneumatic devices are nonelectrical force transducers; in this Handbook they were presented in Chapter 1.4.
- Electromagnetic and electrostatic force balances have some specific differences, properly presented in Chapters 15.2 and 15.3, respectively.
- More details on the uncertainty of calibration results in force measurements are given in the Publication Reference EAL-G22, European Accreditation Laboratory, Edition 1, August 1996.

2.5. NONCONVENTIONAL TYPES OF FORCE TRANSDUCERS

The sixth category designated by van Putten (see Figure 2.2) is the radiant energy (i.e. electromagnetic, acoustic or optical), which can be measured by means of microwave or infrared radiometers. The radiometric technique is also used for weighing in nuclear physics where the mass-energy equivalence relation has an important implication [2.42]. A special device, the Crookes radiometer, wherein a rotor with dark and light vanes spins when exposed to light in a partial vacuum, but their reason for rotation has been the cause of much scientific debate [2.43].

Encyclopedia Britannica considers the *electromagnetic transducers* as a large group [2.44], the major categories of which are differential transformers (LVDT), inductance transducers, induction transducers, Hall-effect magnetic transducers, and saturable reactors. Béla Lipták, Foxboro also includes inductive, reluctance and LVDT transducers within the magnetic category [2.45]. We propose two important delimitations in the area of electromagnetic force transducers:

- the inductive ones as a distinct chapter of parametric force transducers (C.4),
- the induction transducers (with moving coils) as a separate chapter of electrodynamic force transducers (C.8).

In their turn, the *acoustic* and *optical methods* need a more detailed treatment in connection with the force measurement.

2.5.1. Electrodynamic force transducers

More specific among the electromagnetic methods, the introduction of “feedback control represents the basis of free magnetic suspension which enables the weighing of an object in a closed container with an external balance and the measuring of forces on a body in controlled *motion*” [2.46].

On the other hand, in large range weighing systems an applied mass generates a force under the influence of gravity, but the conversion from force to current is not achievable [2.47]. This leads to a compensation principle where the force due to the mass is compensated by a counterforce so that the difference between the two forces is zero. The current used to achieve the equilibrium in this *dynamic* process is proportional to the force.

An extended presentation of the electrodynamic force transducers is made in Chapter 8.

2.5.2. Galvanomagnetic force transducers (based on Hall effect)

A group of 24 Hall-effect magnetic sensors defines all the components of magnetic gradients needed to calculate the three-dimensional magnetization force acting on nonmagnetic materials [2.48].

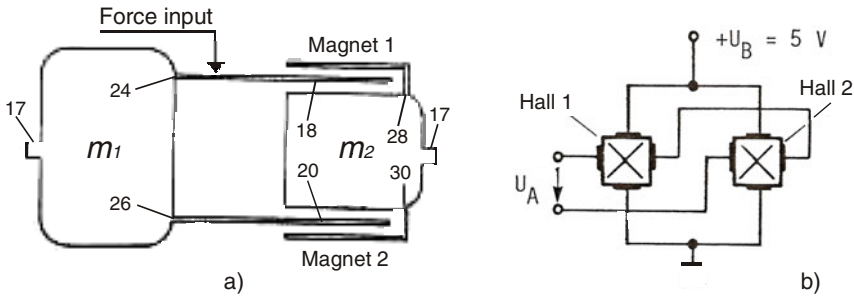


Fig. 2.9 Force transducer based on galvanometric Hall-effect (a) and the symbolization of Hall devices and their differential connection (b)

A micromachined force transducer using a three-axis Hall probe is able to measure forces as small as 1 pN in both air and water [2.49]. Their results show that these force transducers can be useful for magnetic force calibration and also for on-chip measurement of biophysical forces.

Lucas Automotive GmbH utilizes Hall devices for the detection of an actuation force of a brake pedal [2.50] while Key Safety Systems, Inc. uses them to measure the force inside the seat belt [2.51].

A dynamometric cell having an elastically deformable force transducer for receiving a weight force and a Hall sensor arrangement for detecting the deformation of the force transducer and its conversion into an electric weight signal is disclosed by Bizerba GmbH in [2.52]. The force transducer is designed as a hollow bar with two attenuation zones spaced in the longitudinal direction.

A device for measuring displacement and force comprises two masses of material linked together by a parallel beam linkage which permits displacement of one mass relative to the other in a single direction (Fig. 2.9a). The force or displacement to be measured is applied to one of the masses in the allowable direction and is sensed by a sensor. In a preferred embodiment [2.53], this is a Hall-effect sensor, attached to one of the masses (m_1) and positioned between two magnets attached to the other mass (m_2). Movement of one mass relative to the other changes the magnetic field around and is sensed by the Hall sensing device. A more sensitive solution is the differential one [2.54], using two Hall devices (e.g. Siemens KSY-10) connected like in Figure 2.9b.

An extended presentation of the force transducers based on the Hall effect is made in Chapter 10.

2.5.3. Acoustic force transducers (SAWs)

Sensing devices based on longitudinal-mode thin-film bulk acoustic-wave resonators (FBAR), monolithically integrated with silicon high-frequency technologies, have been developed for inertial force detection [2.55].

European Craft Pro2Control project, leading German, French, Italian and Spanish companies, universities and industries are defining and implementing a zero-defect forming control system [2.56]. Commonly integrated transducers (force and acoustic) do not allow detecting all types of faults in this kind of applications, so they have considered a multisensor approach, associating artificial vision to the previous transducers.

NovuSonic [2.57] disclosed an acoustic transducer which comprises a microfabricated, sound generating, or receiving, diaphragm, a conductive leaf cantilever actuator, and a counter electrode. In the acoustic transducer, the electrostatic attraction force between the counter electrode and the leaf cantilever due to an imposed electrical potential is utilized to generate a deflection of the diaphragm attached to said cantilever. In operation, the cantilever collapses on to the counter electrode, causing a significant increase in actuator driving force due to the reduction, and partial elimination, of the air gap in the transducer.

Rosemount Aerospace Inc. [2.58] disclosed a SAW sensing element operatively associated with a clevis insert for detecting mechanical strain imparted to this insert when a force acts on it through the pin.

A comprehensive survey on SAW devices and their best representation (Fig. 2.10) is given in [2.59] helping a designer to find the parameters required to achieve a specified accuracy or uncertainty of measurement. Two examples of coefficients for physical effects on SAW substrate materials are: 10 ppm/kN for force loading and 2 ppm/kPa for applied pressure.

By bending, stretching, and compressing the SAW substrate, transducers for torque, force, displacement, vibration or acceleration were made, e.g. the “intelligent tire” developed to monitor the tire pressure as well as the friction force between the tire and the road surface.

An extended presentation of SAW devices is made in subchapter 13.5.

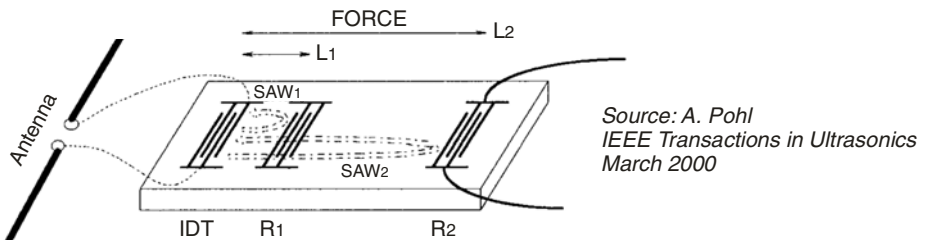


Fig. 2.10 The principle of wireless SAW sensing device and its force transducer representation. IDT means interdigitated transducer, R₁ is the first reflector and R₂ is the second one. The applied force F increases the length L_1 and L_2 and, consequently, modifies the propagation characteristics of the surface acoustic waves.

2.5.4. *Optical devices for force measurements*

There is a huge “spectrum” of optical methods used in force measurements too. The optic fiber devices [2.60] are in full development at present; these type of strain gauges, invented in 1978, need however expensive instrumentation, as the Mach-Zehnder interferometer. Here are two applications using advanced opto-electronics:

- A *vision-based force measurement technique* is proposed at the University of Toronto (Canada) for determining the microgripper deflections during the microassembly process [2.61]. A video microscopic system is used to measure the deflections in the gripper’s jaws, connected to a robotic work-station through thin elastic compliant beams. Finite element analysis (FEA) simulations are used to obtain information of possible beam deflections and their corresponding microforces.
- A high-sensitivity, high-resolution *interferometric micro-opto-electro-mechanical system* (MOEMS) for measuring acceleration, force, and pressure of fluids during flow is described in the patent [2.62]. The MOEMS structure may be integrated with a planar waveguide and a photodetector.

In this Handbook we have not a special chapter devoted to optical devices for force measurements, maybe an independent and multidisciplinary book will be necessary.

We analyze the following specific applications in the area of force transducers:

- C.14.4 – Optical gyroscopes (fiber optic or laser);
- C.15.4 – Optical devices based on force feedback;
- C.16.4 – Force transducers involving optical techniques.

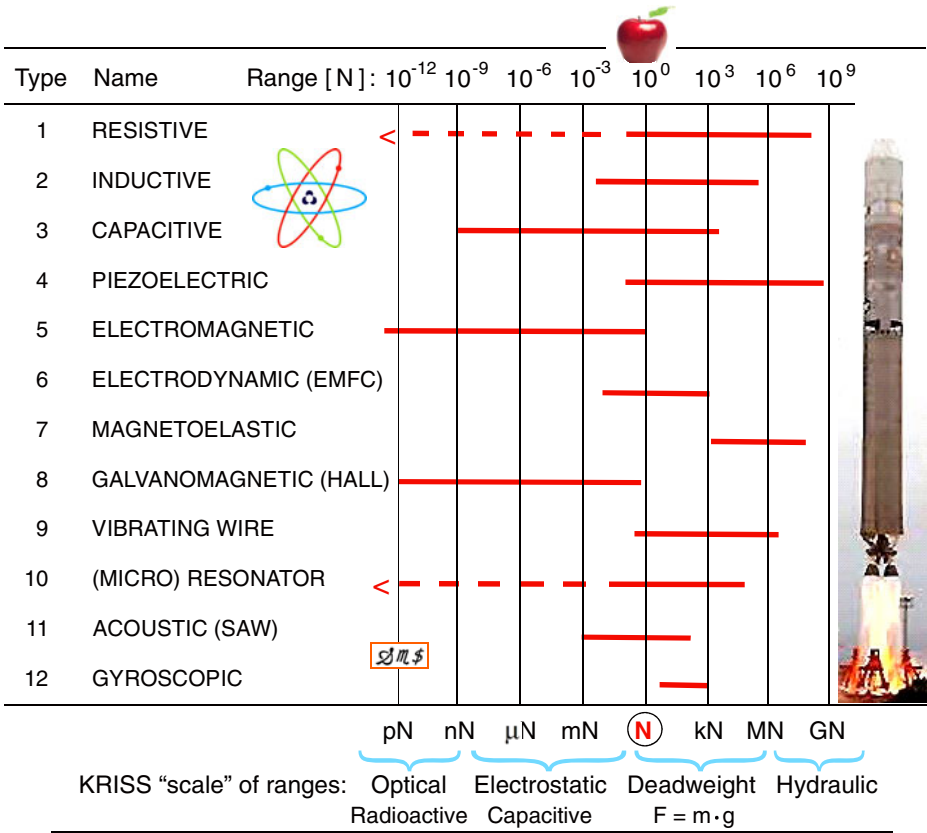
2.6. AN ENLARGED CLASSIFICATION OF FORCE TRANSDUCERS

In this complex, inter- and multi-disciplinary area of force transducers the consensus concerning their classification is difficult to forge but not impossible. Following the systematic approach developed in his doctoral thesis [2.63], the final variant of the classification proposed by the author is given in Table 2.5.

Accordingly, the twelve categories chosen offer a better delimitation of the force transducers (FTs) types, that are thoroughly described in a dozen of chapters (C.3...C.14), plus a chapter devoted to force balances (C.15) and another to mixed methods (C.16).

In the previous tables (T.2.2...T.2.4), various FT types were systematized under different forms, which complete each other. In this way, for the selected force transducers are shown: typical range of rated capacity, resolution, thermostability and linearity error, deflection of elastic element under load, and typical total uncertainty.

Table 2.5 Classification of measurement principles for force transducers (DMS, 2009)



The range of forces depicted by the Korean Research Institute of Standards and Science has in view four different categories, from nanoforce measuring equipment to standard testing machines for metrological calibration.

We emphasize firstly the *range*, through a graphical representation more suggestive than that strictly based on numerical figures. One can see that the totality of these twelve categories of force transducers is „centered” upon the value of 1 N (just the force measurement SI unit!). However, the scales are more extended toward submultiples of the newton than its multiples, which is in full concordance with recent advances in the field of nanotechnologies, atomic force microscopy and magnetic flux quantum based techniques.

For illustrating the lower limit of force measurements (weighing included), the following references are significant:

- atto-newton force detection (10^{-18} N) using ultrathin silicon cantilevers investigated by *atomic force microscopy* [2.64];

- sub-piconewton weighing ($< 10^{-12}$ N) based on magnetic flux quantum phenomenon [2.65];
- single atom weighing by means of *carbon nanotubes* [2.66]. A carbon nanotube is an extremely thin but stiff resonator. If a suspended CNT is “vibrated” at its natural frequency, this frequency will fall proportional to the number of atoms or molecules attached to it.

The opposite “extreme” is determined by the necessity for measurement of very large forces, up to several tens meganewton, in ship building, civil engineering, metallurgical industry (rolling mills) and, more spectacular, the thrust measurement for the Space Shuttle solid rocket booster [2.67]. Two reusable SRBs provide the main thrust to lift the shuttle off the launch pad and up to an altitude of about 46 km. While on the pad, the two SRBs carry the entire weight of the external tank and orbiter and transmit the weight load through their structure to the mobile launch platform. Each booster has a liftoff thrust of approximately 12.5 MN at sea level, increasing shortly after liftoff to about 13.8 MN. So, the scaling extends from the atomic to the geophysical range, but not reaching yet the value of 1 GN (giga = 10^9).

Maximum values for force are indicated in the Table 2.4 for piezoelectric force transducers (120 MN), followed by magnetoelastic and resistive (strain gauges) ones. For example, 48 plate-rings combined in parallel and in series into one compact, strain gauged elastic structure, with lower profile and smaller weight as compared with a classical load cell for 20 MN [2.68].

We consider as most logical and intuitive our option for the 12 types of force transducers and the succession of their study. It is to be mentioned that this FT classification is compatible with most older global (Tables 2.2, 2.3 and 2.4) or partial classifications:

- *Vibrating FTs*, containing vibrating wires, tuning-fork resonators and SAW devices (ultrasonic transmitters), grouped in Table 12.2 [2.40].
- *Digital FTs* (with frequency output), containing vibrating wires, tuning-fork resonators and gyroscopic transducers [2.69].
- *Interdigital transducers* (like combfingers) can be resonant, acoustic (SAW), as well as capacitive force transducers, and they are applicable for the measurement of a wide range of mechanical quantities [2.70].

An adequate terminology is generally a delicate matter. Long before the publication of the International Vocabulary of Metrology (VIM), Aurel Millea tried to differentiate the concepts of measuring “principles” and “methods” [2.71]. Presently, the unanimously accepted definitions are the following [2.72]:

- **Principle:** physical phenomenon or effect serving as a basis of a measurement;
- **Method:** generic description of a logical organization of operations used in a measurement.

In our case, it is possible to classify force transducers as follows:

- 4...8 FT types, based on piezoelectric and magnetic effects, may best be introduced in the category of *principles*;
- 9...12 FT types better suit the class of *methods*, since the vibrating and digital force transducers involve more complex measurement procedures;
- 1...3 FT types may be equally seen as belonging to both categories, they using distinct physical principles while implying also complex measuring methods e.g. the differential one.

Excepting the gyroscopes, all types of force transducers are found together in the “frequency scale” presented in Figure 13.2 [2.73]:

- parametrical – R, L and C as constitutive parts of the impedance,
- piezoelectric – mainly in dynamic regime and for actuators,
- electromagnetic (electrodinamic, magnetoelastic and galvanomagnetic),
- resonators (vibrating wire and tuning fork) and acoustical ones.

It is difficult to maintain equally deep and comprehensive treatment of all these principles but not impossible. In Figure 2.11 the Newton's “cake” is presented, in which the dozen of “slices” symbolizes the 12 types of force transducers. Note that the thinnest slice is half as stick as the biggest one, and, although the author has not beforehand planned any lengths of the respective chapters, their weight reflects the relative practical importance of every FT type.

On the first place there are the “traditional” resistive FTs, and they have the most extended range while gyroscopes have the narrowest force range. On the next places are the vibrating, resonator and acoustic FTs, followed by the piezoelectric, capacitive and electromagnetic ones. The magnetoelastic, galvanomagnetic (Hall effect), gyroscopic, inductive and electrodynamic types complete a consistent and coherent classification of force transducers.

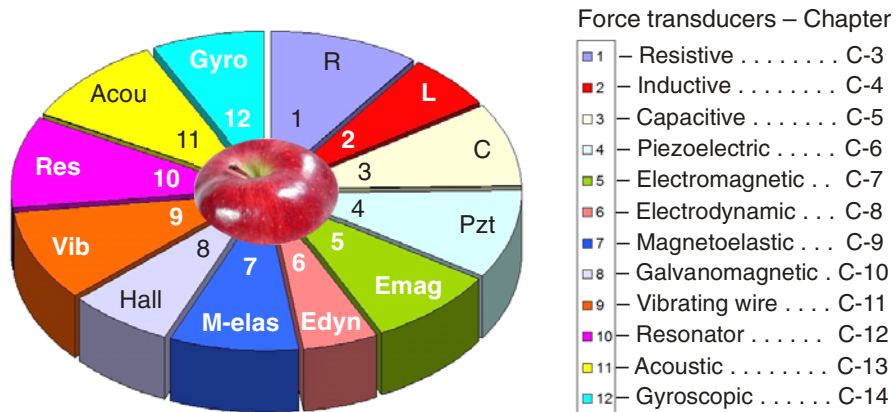


Fig. 2.11 The Newton’s “cake” representing the weight of 12 types of force transducers

Force has an important position among the mechanical quantities, most of them being connected by physical formulas and able to be measured with the same kinds of elastic elements and measurement methods, often by resistive strain gauges [2.74], as presented in the next chapter.

REFERENCES

1. Kersten, J.: *Innovative Load Cell Technology. Application Note ISWM*, Revere Transducers Europe, Breda, The Netherlands (1995)
2. Middelhoek, S., Audet, S.A.: *Silicon Sensors*. Academic Press Ltd (Harcourt Brace Jovanovich Publishers), London (1989)
3. van Putten, A.F.P.: *Electronic Measurement Systems*. Prentice Hall, New York (1988)
4. Culsaw, B.: *Smart Structures and Materials*. Artech House, Boston (1996)
5. Busch-Vishniac, I.J.: *Electromechanical Sensors and Actuators*. Springer, Heidelberg (1999)
6. Isihara, H., Arai, F., Fukuda, T.: *Micro mechatronics and micro actuators*. IEEE/ASME Transactions on Mechatronics 1(1), 68–79 (1996)
7. Porter, T.L., Delinger, W.: *Electronics for LabView based piezoresistive micro-cantilever sensor system*. Sensors & Transducers Magazine 68(6), 568–574 (2006)
8. Carson, R.: *Blavatsky's foreknowledge of the wave / particle duality of light (1996-2004)*, <http://www.seekerbooks.com>
9. Blignault, C., Hattingh, D.G., Kruger, G.H., van Niekerk, T.I., James, M.N.: *Friction stir weld process evaluation by multi-axial transducer*. Measurement 41, 32–43 (2008); ScienceDirect
10. Lin, Z.-C., Huang, J.-C.: *A study of the estimation method of the cutting force for a conical tool under nanoscale depth of cut by molecular dynamics*. Nanotechnology 19, Paper 115 701 (2008)
11. Chen, Y., Yang, J., Wang, X., Ni, Z., Li, D.: *Temperature dependence of frictional force in carbon nanotube oscillators*. Nanotechnology 20, Paper 035704 (2009)
12. Bau, H.H., de Rooij, N.F., Kloeck, B. (eds.): *Mechanical Sensors*. VCH, Weinheim (1994)
13. Fraden, J.: *Handbook of Modern Sensors – Physics, Design and Applications*, 3rd edn. Springer, Heidelberg (2004)
14. Usher, M.J., Keating, D.A.: *Sensors and Transducers – Characteristics, Applications, Instrumentation, Interfacing*, 2nd edn. MacMillan, Houndmills (1996)
15. Sze, S.M.: *Semiconductor Sensors*. John Wiley & Sons, Inc., New York (1994)
16. Vervuren, W.: *Loadcells and their environment*. In: Kemény, T., Havrilla, K. (eds.) *Force Measurement and Weighing in the 90s*. IMEKO TC Event Series, vol. 29, pp. 189–195. MTE SZ Házinyomda, Budapest, 1104-91
17. Stein, P.K.: *The Unified Approach to the Engineering of Measurement Systems for Test and Evaluation; Part I – Basic Concepts*. Fifth Printing with Revisions, Stein Engineering Services, Inc., Phoenix, AZ (1995)

18. Bray, A., Barbato, G., Levi, R.: *Theory and Practice of Force Measurement*. Academic Press, London (1990)
19. Peters, M.: Force measurement, present and future. In: *Proc. IMEKO XIIIth World Congress, Turin, Italy, September 5-9, vol. III*, pp. 2295–2296 (1994)
20. Zegnini, B., Boudou, L., Martinez-Vega, J.: An optical technique to measure the induced mechanical strain by a DC electric field in thin organic insulating film. In: *Proc. 15th IMEKO TC-4 Symp. Novelties in Electrical Measurements and Instrumentation, Jassy, Romania, September 19-21, vol. II*, pp. 387–390 (2007) ISBN 978-973-667-260-6
21. Norton, H.N.: *Sensor Selection Guide*, 1st edn. Elsevier Sequia S.A., Lausanne, Switzerland (1983)
22. Pallás-Areny, R., Webster, J.G.: *Sensors and Signal Conditioning*. John Wiley & Sons, Inc., New York (1991)
23. Khazan, A.D.: *Transducers and Their Elements*. Prentice Hall Inc., A Pearson Education Company, Upper Saddle River, NJ (1994)
24. Baudendistel, T.A.: Force sensor, strain sensor and methods for measuring same. US Patent 2006 0137464, June 29 (2006)
25. Seippel, R.G.: *Transducers, Sensors & Detectors*. Prentice Hall, Reston Publishing Company, Reston (1983)
26. Biétry, L., Kochsiek, M.: *Mettler Wägelexikon. Praktischer Leitfaden der wägetechnischen Begriffe*. Mettler Instrumente AG, Greifensee, Switzerland, ME-720113-84
27. 823 DP series d/p Cell Transmitter – Competitive comparisons. Foxboro Company, Foxboro, MA, TI 37-75
28. Dolga, V.: *Sensors and Transducers for Industrial Robots*. Editura Eurobit, Timișoara (1999) (in Romanian); ISBN 973-99-227-9-1
29. Pantelimon, B., Iliescu, C.: *Mesures électriques et transducteurs, Tome 2*. Editura Matrix, București, Romania (2006)
30. Horn, K.: Elektrische Messung von Kräften und Drücken. VDI-Berichte Nr. 54, pp. 11-19 (1961)
31. Horn, K.: Physikalische Prinzipien für elektromechanische Wägezellen – Aufnehmerprinzipien für die Umformung der mechanischen Meßgröße 'KRAFT' in elektrisch nutzbare Meßgrößen. wd – wägen & dosieren, Heft 1, S.5–S.16, Deutschland (1976)
32. Horn, K.: Wägeprinzipien. In: Kochsiek, M. (ed.) *Handbuch des Wägens*, 2. Auflage. Friedrich Vieweg & Sohn, Braunschweig – Wiesbaden (1989)
33. Horn, K.: Design of sensors with very high stiffness. In: *Proc. 15th Int'l Conf. on Accuracy Assurance in Force, Torque and Mass Measurements, Madrid, Spain, October 7-11*, pp. 285–294 (1996)
34. Theiß, D.: Die Wägezelle: Von Wägegut zum Meßsignal. Auszug aus: 'Industrielle Wägetechnik' von A. Schuster, Eigenverlag Schenck, S21–S36, Darmstadt (1983)
35. Paetow, J.: Weighing cell and force transducer – there is a difference. Private discussions at Hottinger Baldwin Messtechnik GmbH in Darmstadt, West Germany (November 1987)

36. Tilmans, H.A.C.: Micro-mechanical sensors using encapsulated built-in resonant strain gauges. PhD dissertation, Twente University of Enschede (1993)
37. Blom, F.R.: Resonant silicon beam force sensor. PhD dissertation, Twente University of Enschede, The Netherlands (1989)
38. Mansfield, P.H.: Electrical Transducers for Industrial Measurement. Butterworth, London (1973)
39. Morrison, T.P.: The Art of Computerized Measurement. Oxford University Press, Oxford (1997)
40. Hunt, A. (Coord.): Guide to the Measurement of Force. The Institute of Measurement and Control, London, UK (Published 1998); ISBN 0-904457-28-1
41. Cuscó, L. (Coord.): Guide to the Measurement of Pressure and Vacuum. The Institute of Measurement and Control, London, UK (Published 1998)
42. Škundrić, S., Kovačević, D.: Elektromehaničke vage (Merenje mase mernim pretvaračima sile na bazi tenzometarskih traka). Štampa BMG, Beograd, Serbia (1995)
43. October 15 (2009),
<http://www.en.wikipedia.org/wiki/Radiometer>
44. Britannica Online Encyclopedia, October 15 (2009),
<http://www.britannica.com/EBchecked/topic/602499/transducer>
45. Lipták, B.G. (ed.): Instrument Engineers' Handbook: Process Measurement and Analysis, 4th edn., pp. 758–759. CRC Press – ISA, Boca Raton, FL (2003)
46. Gast, T.: The impact of feedback on the determination of masses and forces in controlled atmospheres. *Termochimica Acta* 236, 277–290 (1994)
47. Reber, D.: Electrodynamic force compensation devices in mass comparators. In: Proc. 13th Int'l Conf. Force and Mass Measurement, Helsinki, Finland, May 11-14, pp. 205–210 (1993)
48. Maki, S., Ataka, M.: Magnetization force sensor. *Rev. Sci. Instrum.* 76, Paper 066106 (2005)
49. Koch, S.J., Thayer, G.E., Corwin, A.D., de Boer, M.P.: Micromachined piconewton force sensor for biophysics investigations. *Applied Physics Letters* 89, Paper 173901 (2006)
50. Ohlig, B., Giering, W.: Device for the detection of an actuation force of a brake pedal and brake system. European Patent EP1608940-2005
51. Grzic, R.: Seat belt force sensor. European Patent EP1350681-2003
52. Selig K.P., Wurster K.: Force transducers. US Patent 2006 0053898, March 16 (2006)
53. Carignan, F.J.: Displacement / force transducers utilizing Hall effect sensors. Data supplied from the worldwidesep@cenet database WO9318380-1993
54. Zabler, E., Heintz, F.: Neue, alternative Lösungen für Drehzahlsensoren im Kraftfahrzeug auf magnetoresistiver Basis. Artikel 9.8, *Sensoren Technologie und Anwendung*, Bad Nauheim, Deutschland (1984)
55. Campanella, H., Plaza, J.A., Montserrat, J., Uranga, A., Esteve, J.: High-frequency sensor technologies for inertial force detection based on thin-film bulk acoustic wave resonators (FBAR). *Microelectronic Engineering* 86(4), 1254–1257 (2009)

56. Fillatreau, P., Bernard, F.X., Aztiria, A., Sáenz de Argandoña, E., García, C., Arana, N., Izaguirre, A.: Sheet metal forming global control system based on artificial vision system and force–acoustic sensors. *Robotics and Computer-Integrated Manufacturing* 24(6), 780–787 (2008)
57. Pedersen, M.: Electrostatic acoustic transducer based on rolling contact micro actuator. Data supplied from the worldwideesp@cenet database WO2007078433-2007
58. Isebrand, S., Powel, J.: Force sensing clevis insert. European Patent EP2042429, April 1 (2009)
59. Pohl, A.: A review of wireless SAW sensors. *IEEE Transactions on Ultrasonics, Ferroelectrics, and Frequency Control* 47(2), 317–332 (2000) (Invited paper)
60. Washabaugh, P.D., Peters, K.J.: Sensitive structures that retain stiffness by incorporating finite length measurement paths. In: *Proc. SPIE N-Amer. Conf. Smart Structures and Materials*, Orlando, FL, February 13-18 (1994)
61. Anis, Y.H., Mills, J.K., Cleghorn, W.L.: Zero-crossing edge detection for visual force measurement in assembly of MEMS devices. In: *Proc. SPIE 6109 on MOEMS-MEMS 2006 Micro & Nanofabrication, Session 5, Paper 19*, San Jose, CA, January 21 (2006)
62. Li, C.C.: Interferometric MOEMS sensor. US Patent 7518731, April 14 (2009)
63. Ștefănescu, D.M.: Methods for increasing the sensitivity of strain gauge force transducers. PhD dissertation (160 pages, 26 tables, 86 figures, 336 references), Universitatea “Politehnica” București, Romania, September 10 (1999) (in Romanian)
64. Stowe, T.D., Yasumura, K., Kenny, T.W., Botkin, D., Wago, K., Rugar, D.: Attonewton force detection using ultrathin silicon cantilevers. *Appl. Phys. Lett.* 71, 288–290 (1997)
65. Choi, J.-H., Choi, M.-S., Kim, M.-S., Park, Y.-K.: Magnetic flux quantum as a sub-pico-newton weight. In: *Proc. Asia-Pacific Symp. Mass, Force and Torque, APMF 2005, Jeju Island, Korea, August 30 - September 3*, pp. 99–104 (2005)
66. Hakonen, P.: Nanotubes weigh the atom. *research*eu results supplement No. 17*, p. 43 (September 2009),
<http://cordis.europa.eu/ictresults/index.cfm?section=news&tpl=article&ID=90708>
67. http://en.wikipedia.org/wiki/Space_Shuttle_Solid_Rocket_Booster (October 19, 2009)
68. Zhang, S., Chen, W.: Development of the integrated multiple plate-ring type load cell with large capacity. In: Shi, C., Zhang, Y. (eds.) *Acta APMF 1996 – Present Situation and Progress of Measurement on Mass and Force*, Beijing, China, August 20-22, pp. 151–153 (1996)
69. Zecchin, P. (Chair.): *Digital Load Cells – A Comparative Review of Performance and Application*. The Institute of Measurement and Control, London, UK, Document WP0803 (2003)
70. Varadan, V.K.: Tutorial Course on Smart Sensors and Materials. In: *Proc. 11th Conf. Asia-Pacific Nondestructive Testing, Jeju Island, South Korea, November 4 (2003)*

71. Millea, A.: Electrical Measurements. Principles and Methods. Editura Tehnică, București, Romania (1980) (in Romanian)
72. International Vocabulary of Metrology (VIM 3) – Basic and General Concepts and Associated Terms, ISO (ISO/IEC) Guide 99-12:2007, Geneva, Switzerland (2008)
73. Mamishev, A.V., Sundara-Rajan, K., Yang, F., Du, Y., Zahn, M.: Interdigital sensors and transducers. Proc. IEEE 92(5), 808–845 (2004)
74. Ștefănescu, D.M.: Strain gauged elastic elements for force and related quantities measurement. In: CD Proc. IMEKO Int'l Conf. Cultivating Metrological Knowledge, Merida, Mexico, November 27-30, Paper 22 (2007)

Chapter 3

RESISTIVE FORCE TRANSDUCERS

The most common method to measure force relies on resistive sensing. The advantages of resistive sensors are their reliability, simple construction, adjustable resolution, and maintenance-free technology. Electrical resistance is also the easiest electrical property to measure precisely over a wide range at moderate cost. These important features have often made resistive sensors the preferred choice in sensor designs [3.1].

A series of textbooks [3.2] – [3.6] and review articles [3.7], [3.8] on instrumentation present resistive sensors used in force transducers; the most popular are strain gauges (SGs) and force sensing resistors (FSRs).

Strain gauges (Fig. 3.1a and b) are devices which utilize piezoresistive properties (i.e., change in resistance due to strain) of an elastic material: metal, alloy, semiconductor or cermet. This change in resistance takes place both due to change in the resistive element dimensions as well as change in the material resistivity. The resistance change can be measured by inserting the strain-sensitive resistor in one of the arms of a Wheatstone's bridge.

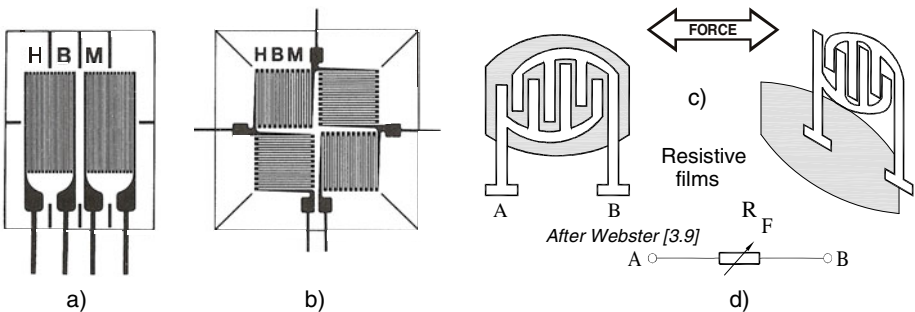


Fig. 3.1 Classic strain gauges: double (a) and quadruple (b); modern force sensing resistors (c) and a symbol of the resistor value depending on the applied force (d)

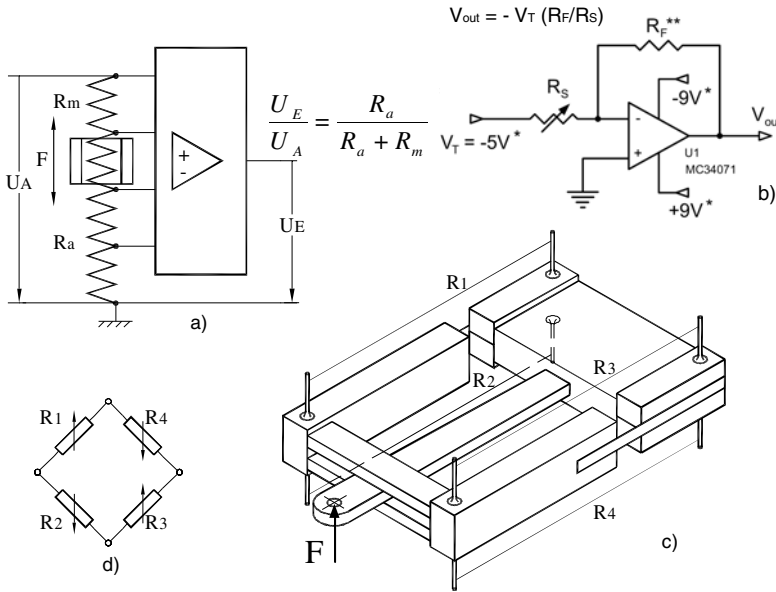


Fig. 3.2 Potentiometer (a), FSR and Op Amp (b), pretensioned wires (c) and Wheatstone bridge connection for strain gauged force transducers (d)

Force sensing resistors (Fig. 3.1c, d) utilize the property of certain polymer thick-film devices to exhibit decreasing resistance with the increase of an applied force [3.9]. A FSR is made up of two parts: a resistive material applied to a film and a set of digitating contacts applied to another film. The resistive material completes the electrical circuit between the two sets of conductors on the second film. When a force is applied to this sensor, a better connection is made between the contacts; hence, the conductivity is increased. Over a wide range of forces, it turns out that conductivity is a linear function of force.

3.1. RESISTIVE FORCE TRANSDUCERS TYPES

Tensometric force transducers make use of the following resistive measuring means [3.10]: potentiometer, resistive network, pretensioned wire configuration and strain gauges (classic or semiconductor) in Wheatstone bridge connection. All these elements are based on the electrical resistance R whose variation can be produced by modifying any of the three parameters from the equation:

$$R = \rho \cdot l / A \tag{3.1}$$

where ρ is resistivity, l – conductor length, and A – cross section area.

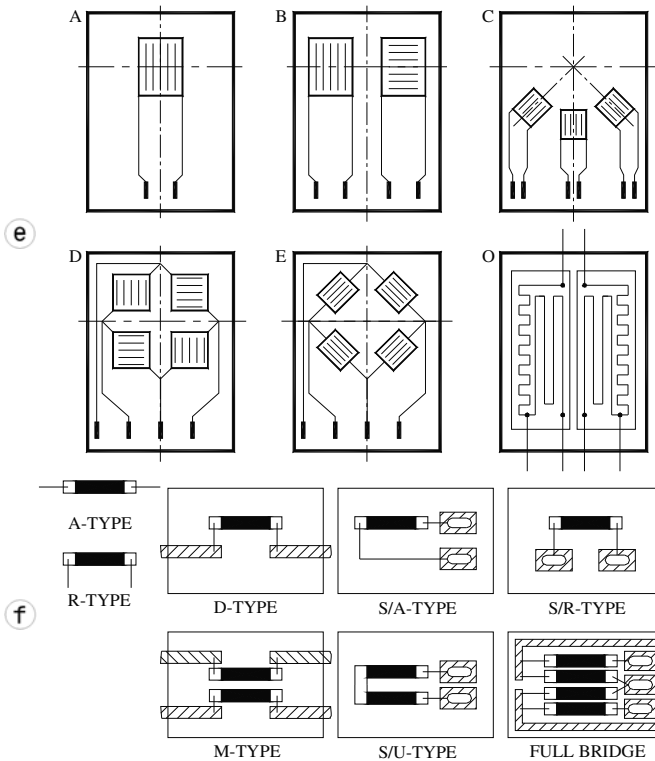


Fig. 3.2 (continuation) Classic (e) and semiconductor (f) strain gauges

Figure 3.2 shows the most important resistance-type transducers and their associated electronic circuits:

- a) *Potentiometer (rheostat)*, where the force/torque determines a linear/angular movement of a contact. It is a resistive divider of $500 \Omega \dots 5 \text{ k}\Omega$, equivalent to a Wheatstone half-bridge. The moving contact (slide wire variable resistor) is suitable for various mechanical quantities measurement [3.11].
- b) *Resistive network* – a solution introduced by Albert Haug [3.12] under the name of *Flexmetall*; its latest version is *Flexiforce* [3.13]: a flexible network based on semiconductor inks, in which each intersection is a force sensor; by electronic scanning (20 kHz/channel) and measuring of resistance variation (a direct method as in the case of the tensometric bridge) load distribution on complex structures (sport equipment, ergonomic chairs for surgeries, control chambers or special vehicles) can be determined.
- c) *Pretensioned resistive wires*, stretched but not soldered on structure – a different, ingenious electroresistive effect used by Perry [3.14], by Romanian I.P.A. in Bucharest or foreign companies [3.15].

- d) In a classic or semiconductor strain gauge transducer, the measurand (force) is converted into a resistance change, due to strain, usually in two or four arms of a *Wheatstone bridge*. A complete bridge together with signal conditioning circuitry can be *integrated on a silicon chip*. The upward arrows in the schematic diagram indicate increasing resistances while the downward arrows indicate decreasing resistances.
- e) *Classic strain gauges* – based on the specific deformation/elongation of a “comb”-shaped conductor under mechanical load. The multitude of strain gauge models can be noticed: A – uniaxial; B – biaxial; C – tridirectional rosette; as well as complete Wheatstone bridge (quadruple): D – for bending or E – for shearing [3.16]. Model O is a special BLH strain gauge for high temperatures (500 °C), corrosion or underwater environment [3.17].
- f) *Semiconductor strain gauges* – illustrated by five simple models (a quarter of a bridge), two double models (half-bridges) and a complete bridge [3.18]. Considering the great progress in the field of thin coatings (10 μm) [3.19] or thick coatings (100 μm) [3.20] and in the field of silicon technology [3.21], the applicability of strain gauges has considerably widened. They can detect relative variations of length and, implicitly, of resistance under 1 ppm. The advanced technologies apply simultaneously to elastic and electronic microstructures as well as PC components (Silicon Valley).

3.2. POTENTIOMETERS

A classic analog potentiometer is shown in Figure 3.3a, illustrating the force – displacement duality. For accurate tensometric measurements, a digital potentiometer is recommended. For example, WinPot (Fig. 3.3b), used for analog circuitry calibration, has the following features [3.22]:

- resistance values: 10, 50 and 100 kΩ,
- ultra-low power consumption in stand-by: 1 μA (with output buffer inactive),
- single, dual or quad channels,
- four programmable presets with power-on recall,
- 256 linear taps, SPI interface.

Commercial digital potentiometers have a limited resistance range; to overcome the discrete nominal resistance values was developed an interface circuit for resistive sensors in bridge configuration utilizing digital potentiometers in order to implement an automatic calibration procedure [3.23]. Such an approach facilitates the use of digital signal processing with high flexibility and increased resolution compared to a simple potentiometer circuit.

A number of various potentiometric goniometers have been developed for gait (Fig. 3.3c), being usually associated with multicomponent strain gauge force transducers (SGFTs).

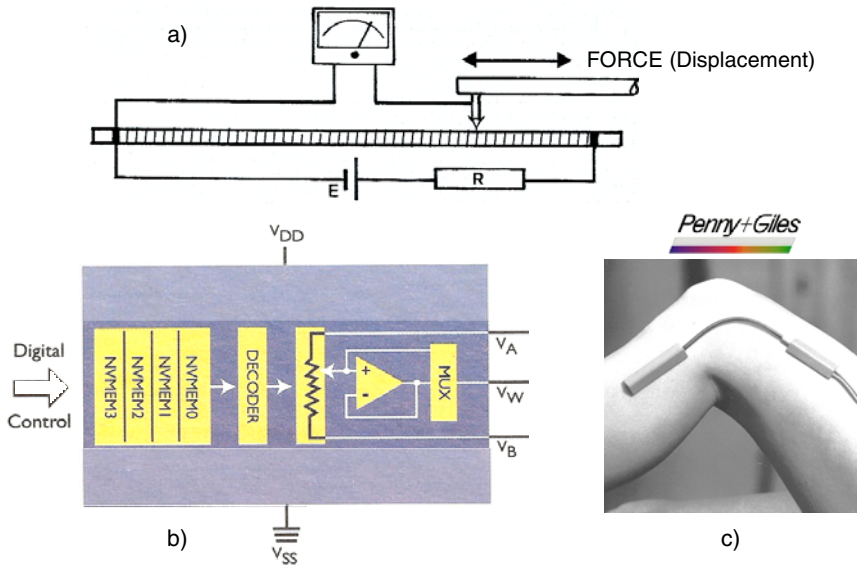


Fig. 3.3 Analogic (a) and digital potentiometer (b). A Penny & Giles strain gauged electrogoniometer applied to the knee (c).

3.3. PRETENSIONED WIRES

As an example, the first Romanian load cell has been realized with unbonded wires in 1966, at the Enterprise for Automation Elements (IPA) in Bucharest, Romania [3.24]. The constructive solution is depicted in Figure 3.4. The four resistance windings are pretensioned under equal tension for zero applied force. When force is applied to the mobile part, strain increases in R_1 and R_3 , and decreases in R_2 and R_4 .

There were manufactured load cells of 0.35; 0.5; 1 and 2 kN (accuracy class 0.5) and 5; 10; 20; 50 kN (accuracy class 1), successfully used at that time in the field of electronic weighing.

Some multifunctional transducers based on tensioned wires are summarized in Table 3.1.

Table 3.1 Tensioned wires devices for measuring force, mass and displacement [3.25]

Transducer type	Force [N]	Mass [kg]	Displacement [mm]
SG 3	12	1.2	± 0.035
SG 4	0.95	0.095	± 0.35
SG 47 M	0.035	0.0035	1

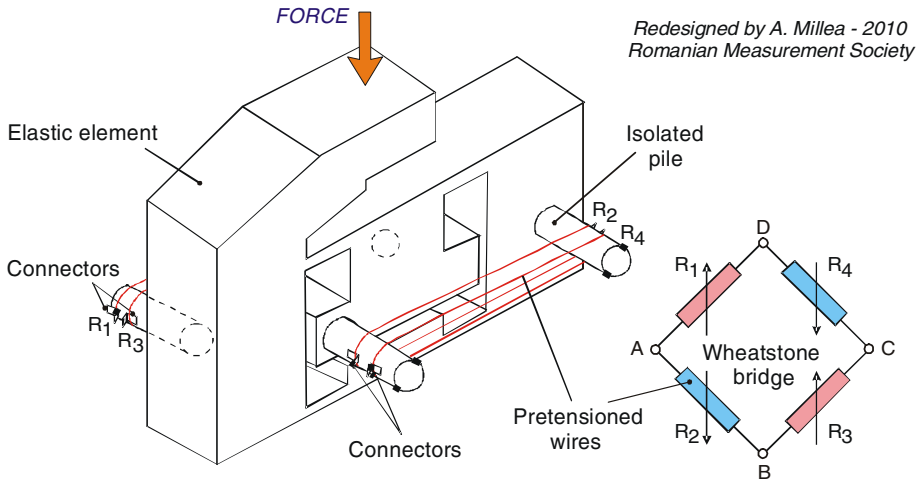


Fig. 3.4 A four-arm unbonded strain gauged force transducer

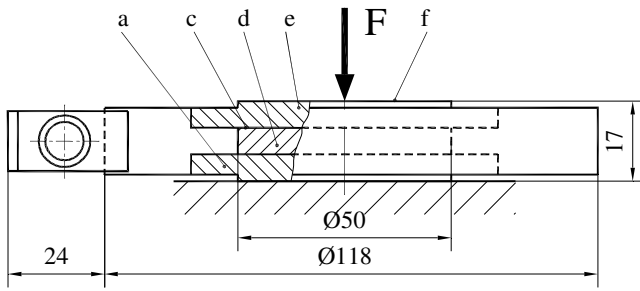
A strain wire has been interwired to provide four active arm Wheatstone bridge on a pressure diaphragm [3.26]. Other models of force transducers with pretensioned wires were presented in [3.6] and [3.27].

3.4. STRAIN GAUGES

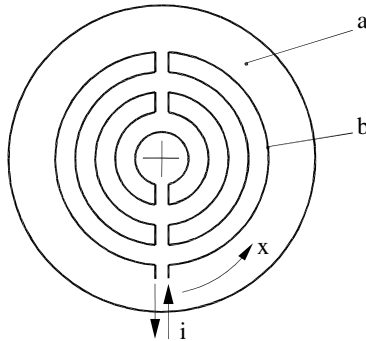
Bonded strain gauges are so-called because they are attached to the elastic element surface. They may be metal foils, thin or thick films, silicon and solid-state devices. A series of author's applications are presented in [3.28] – [3.33].

Force transducers of small height have been developed incorporating a grid of zernin or manganin arranged transverse to the lines of force [3.34]. A flat conductive filament made of resistive alloy is firmly attached, in the form of two semi-spiral cross-deformed metal strips, by sputtering or photo-lithographic etching technique, to the surface of a carrying body and exposed to a stress field (Fig. 3.5). Force F represents the integral of the stress σ acting on the area covered by the manganin grid ($R = 3.8 \text{ k}\Omega$). The resistance materials used for the filament must possess sufficient sensitivity to transverse stress to allow the processing of the measurement data by standard tensometrical equipment. The full scale output for 500 kN is about 1.5 mV/V for manganin (quarter-bridge), and nonlinearity, hysteresis and creep after 30 minutes did not exceed 0.5 %.

The alloy manganin is a suitable material for the active zone of another piezoresistive sensor, depicted in [3.35]. It has a small temperature coefficient and an adequate pressure coefficient. Aluminum oxide has been used to create two insulating coatings, so the global sensor can be deposited on steel shafts.



Source: Oppermann
IMEKO – Prague, 1985



Force sensor assembly:
 a - carrying assembly
 b - measuring grid
 c - intermediate layer
 d - transmission plate
 e - input plate
 f - force input surface

Fig. 3.5 Force transducer with two semi-spiral flat resistive filaments

Physical vapour deposition and photolithographic processes were used for plating and sensor structuring of the manganin layer. The sensor total thickness lying within the manufacturing tolerances is about 10 µm.

The basic functioning principle of liquid metal strain gauge (LMSG) is the measurement of strain-induced electrical-resistance-change of the liquid metal capillary that is contained within the soft polymer encasement [3.36]. In biological measurements, especially blood flow or tissue swelling, a variant called mercury-in-rubber strain gauge is used. This SG kind consists of a small amount of liquid mercury enclosed in a small rubber tube, which is applied around, e.g. a toe or leg. Swelling of the body part results in stretching of the tube, making it both longer and thinner, which increases its electrical resistance. Mercury-in-rubber strain gauges are also used in plethysmography for determining changes in the volume of various parts of the body from changes in their girth [3.37].

The Indium-Gallium SG consists of a fine-bore rubber tube filled with a mixture of Indium and Gallium, which is sealed at both ends with platinum electrodes. A continuous electrical signal records changes in electrical output caused by expansion of the gauge. For Erectionmeter, this strain gauge is positioned two-thirds of the way down the shaft of the penis toward the base.

Calibration is accomplished using the same procedure as described for the mechanical strain gauge.

A novel fluidic strain sensor is proposed using a mixture of glycerin with aqueous sodium chloride encapsulated within an elastomer for piezoresistive large strain measurement up to about 40 % [3.38]. Electrochemical impedance spectroscopy (EIS) is applied for strain response measurement and equivalent circuit analysis is conducted to explain the strain-affected ion transportation behavior of the sensor. The use of ionic liquids for green chemistry and of electrical conductive media in large strain sensor technology is environmentally friendly and suited for industrial fabrication.

3.5. PIEZORESISTIVE SENSORS

Traditional strain gauges have a spatial distribution of several millimeters, so the force transducer can not be arbitrarily small. It has a relatively low stiffness as well as some mass; the resulting lower natural frequency has to be considered when performing dynamic measurements [3.39]. Sometimes semiconductor (also called piezoresistive) strain gauges are recommended instead of metal foil SGs; they are characterized by a much higher gauge factor, i.e. higher output signal as a function of a given sensed strain (Smith, 1954). This means that they can be much stiffer, compared to transducers based on foil gauges, resulting in a higher natural frequency for dynamic measurements.

Gauge factor k , also called *strain coefficient of resistance*, is defined as

$$k = \frac{\Delta R / R}{\Delta l / l} = 1 + 2 \nu + \frac{\Delta \rho / \rho}{\Delta l / l} \quad (3.2)$$

where ν is the Poisson's ratio, while the relative variation $\Delta l / l$ is just the strain ϵ . Other parameters are defined as those related to the formula (3.1).

The advantages of semiconductor SGs in transducers applications are [3.17]:

- wide resistance ranges, gauges having resistance from 10 Ω to 10 k Ω ,
- high sensitivity – a gauge factor k of 50...70 times that of a metal foil SG ($k = 2$ for constantan), and this value may be positive or negative depending upon whether p- or n-type silicon has been used to manufacture the gauge,
- single crystal silicon has zero hysteresis,
- high fatigue life, greater than 10^8 fully reversed cycles at $\pm 1000 \mu\text{m/m}$,
- small size minimizes power dissipation and self-heating effects, thus enabling miniature transducers to be achieved.

Piezoresistivity derives its name from the word *piezin*, meaning “to press” in Greek. It is an effect exhibited by various materials that are changing their resistivity due to an applied pressure. The effect was first discovered by

Lord Kelvin in 1856, who noted that the resistance of copper and iron wires increased when in tension. The first application of the piezoresistive effect did not appear until the 1930s, when Dr. Edward Simmons (Caltech) has invented the strain gauges. Rather than using metal wires, these SGs are generally made from a thin metal foil mounted on a backing film, which can be glued onto a surface. The use of glue can limit both the accuracy of measurement, due to incomplete transmission of strain to the gauge, as well as the maximum temperature at which the device may be used. These limitations can be overcome in a thin film strain gauge, which consists of a thin piezoresistive material deposited directly on an insulating surface of the strainable device [3.40]. At the beginning of the 1970s Honeywell (US), Druck Ltd (UK) and Philips Research Center in Hamburg, Germany launched the piezoresistive sensors in pressure measurement and now they are commonly used to measure force, acceleration, vibration and other mechanical quantities too. Piezoresistive sensors are normally assumed to refer to semiconductor devices [3.41].

3.5.1. Silicon devices

Van Putten, in his chapter on mechanical energy in silicon microtransducers [3.42], explains all *piezo* significances (Fig. 3.6):

- Piezoresistor*: In response to strain, a diffused resistor in silicon changes its resistance value.
- Lateral photo-effect* could be connected with other strain measurements.
- Piezojunction*: When a silicon pn-junction is stressed, the current-to-voltage characteristics change.
- Piezo-transistor*: A transistor shows the same strain sensitivity as a piezo-junction, but, in addition, it presents a current gain factor which is also strain-sensitive. The solid-state devices are presented in the subchapter 16.1.

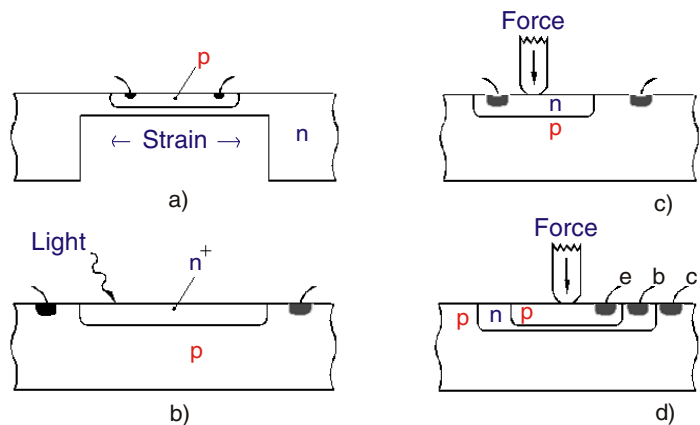


Fig. 3.6

Si devices:

- piezoresistor
- photo-effect
- piezojunction
- piezotransistor

The performance of semiconductor SGs based on p-type silicon microcrystals with different impurity doping, mounted on elastic elements made of invar were studied in the temperature range (4.2...300) K [3.43]. The development of high-sensitive transducers operable in liquid helium temperature range is possible on the basis of giant nonclassic piezoresistance in p-silicon using silicon SGs with boron doping near metal-insulator transition from the insulating side.

A set of semiconductor force and pressure transducers developed on the basis of hetero-epitaxial layers of silicon-on-sapphire is described in [3.44]. Physico-technological optimization of the SOS sensing elements makes it possible to create force transducers for measurements in cryogenic (down to 1 K), normal- and high-temperature (up to 350 °C) media.

Key phases of force transducers development in the Institute of Physical Measurements from Russia since 1961 till now are shown in [3.45]. The performance data of intelligent force transducers and the underlying resistive-strain sensors for space-rocket applications are presented. The problem of minimizing the destabilizing factors distorting the informative signal of thin-film tensoresistive pressure sensors (TRPS) is described in [3.46], particularly the effects of temperature and vibro-acceleration.

A silicon load cell based on a new operating principle is presented in [3.47]. The force is measured by compressing a meander-like strain gauge. A second SG, not loaded, is used to compensate temperature, as well as bending and stretching stresses within the chip. The Wheatstone bridge output is a linear function of the total force, and independent of the force distribution on the square silicon chip. Silicon does not suffer from creep and hysteresis. Measurements up to 1000 kg show a short-term repeatability of 0.1 %.

A new analog technology to adjust resistance values using Rejistor (*Resistive+Adjustor*) is presented in [3.48]; its performance compares favorably to its digital counterpart, the digital potentiometer. Microbridge's Rejistor is a passive, VLSI and MEMS compatible, adjustable microresistor. It is based on standard CMOS technology, a polysilicon resistance and its associated heating resistor being on a suspended microstructure created by bulk micromachining.

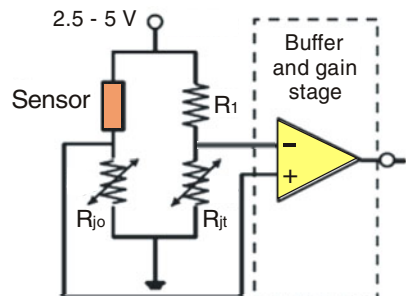


Fig. 3.7 Rejistor inserted in a classical Wheatstone bridge circuit

The most obvious application of Rejutors to sensor conditioning is to use them in the arms of the Wheatstone bridge, both as reference and ratio resistors (Fig. 3.7). The resistance of the Rejutor can be varied after packaging, so that adjustment by the user in field conditions is not only feasible but desirable for a lot of applications.

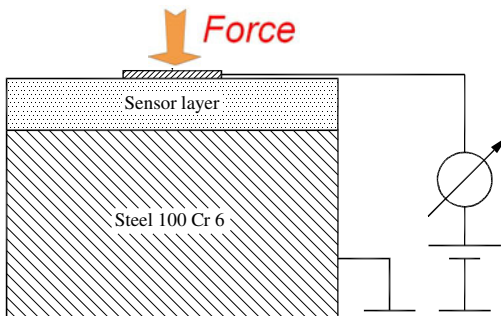
3.5.2. Carbon film coatings and carbon nanotubes (CNTs)

The piezoresistivity of graphitic carbon films was a research topic four decades ago [3.49]. Nowadays, the diamond-like carbon (DLC) coatings have been optimized for sensing the variation of the applied mechanical forces up to 500 N [3.50]. Because of the extreme hardness and high elasticity, (15...30) GPa and (140...270) GPa, respectively, the coating can be applied directly to mechanical parts, obtaining a cheap but effective force and/or pressure transducer (Fig. 3.8). The fabrication was done by sputtering and plasma CVD (chemical vapor deposition) techniques.

Requirements for further development of force sensitivity multifunctional coatings are the following:

- high mechanical, long term and corrosion stability,
- low friction and wear resistant,
- low price and flexible application,
- on-line and continuous control.

A report on successful integration of amorphous carbon (a-C) as a piezoresistive strain gauge into a silicon microcantilever force sensor has been presented at the 13th International Conference on *Solid-State Sensors, Actuators and Microsystems*, Seoul, Korea, 5-9 June 2005 [3.51]. Linear characteristics of the SG resistance versus the applied force (0 to $\pm 600 \mu\text{N}$) were obtained, revealing piezoresistive gauge factors of a-C within 36...46. This value is between those of the coefficients k for metals (0.5...6) and silicon (65...180).



Reprinted with permission from [3.50],
copyright 2002 IEEE



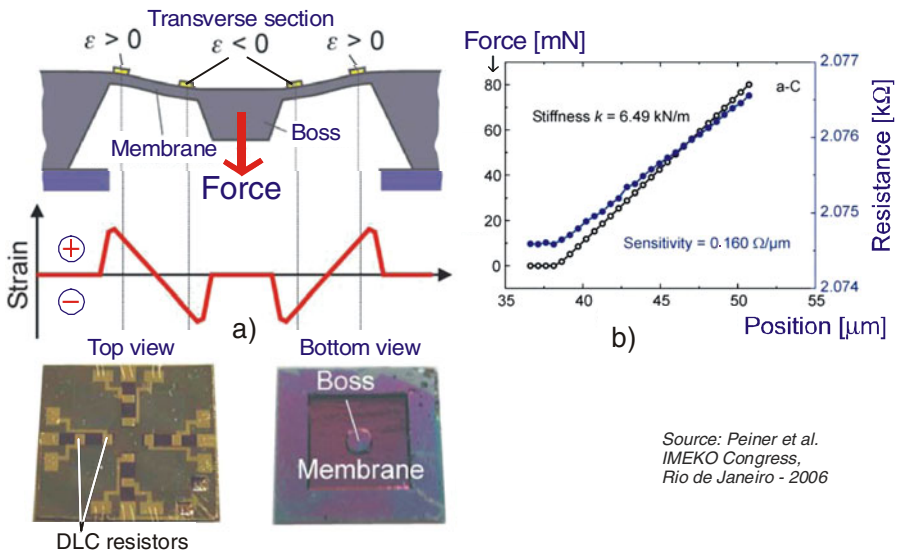
Fig. 3.8 DLC (diamond-like coating) resistivity is measured applying a defined current through the load generating system

For piezoresistive applications it is also attractive the polycrystalline diamond (poly-C), which is successfully used for cochlear implant probes due to its biocompatibility and chemical inertness [3.52]. Hydrogenated (a-C:H) and hydrogen-free (a-C) amorphous DLC strain gauges have been successfully integrated on micromachined silicon boss-membrane force sensors. They reveal gauge factors k in the range of 20...30 (a-C) and 50...90 (a-C:H).

Sensor prototypes with integrated DLC resistors were realized using a bulk silicon micromachining process based on standard photolithography, thermal oxidation and wet etching.

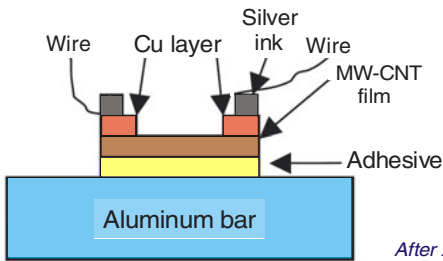
An applied force F causes the boss to be deflected out of its initial position (Fig. 3.9a). Transverse tensile ($\epsilon > 0$) and compressive ($\epsilon < 0$) strain, respectively, are generated at the top surface of the membrane, which is S-shape deformed, and transferred to the diamonds-like coating strain gauges located close to the frame and the boss. The square membrane and the boss have areas of $(4 \times 4) \text{ mm}^2$ and $(2 \times 2) \text{ mm}^2$ respectively, and thicknesses of $(30...70) \text{ }\mu\text{m}$ and 0.4 mm , respectively. The DLC resistors have an area of $(0.6 \times 0.8) \text{ }\mu\text{m}^2$ and a thickness of 0.5 to $1.0 \text{ }\mu\text{m}$.

Figure 3.9b exhibits typical load – deflection – resistance characteristics measured with a-C resistors on a boss membrane ($h = 49 \text{ }\mu\text{m}$) under tensile strain. A force sensitivity of $1.2 \text{ \%}/\text{N}$ is observed and corresponds to a gauge factor k of 18.



Source: Peiner et al.
IMEKO Congress,
Rio de Janeiro - 2006

Fig. 3.9 S-shape deformed square diaphragm (a) and its load – deflection – resistance characteristics measured with a-C strain gauges (b)



After X. Li et al., *Nanotechnology* - 2008

Fig. 3.10 A new type of strain gauge based on carbon nanotube film

The possibility of using multi-walled carbon nanotube (MWCNT) films as strain sensors is analyzed in [3.53]. Such films were taken from Nano-Lab Inc. (Newton, MA, USA), prepared by a solution / filtration method, and bonded directly onto specimens by a nonconductive adhesive (Fig. 3.10). Optimal aspect ratio (length versus width greater than 7) is considered.

For comparison, conventional foil strain gauges were also bonded to the structure on the opposite side. To ensure good electrical contact between carbon nanotube film and the wires, a thin layer of copper was thermally deposited on both ends of the film as electrodes, and the wires were connected to the electrodes by silver ink.

The sample resistances were typically between 30 and 300 Ω . The calculated gauge factor was between 2 and 3.76, close to the gauge factor of foil strain gauges. Wheatstone bridges were used to convert the resistance changes of the MWCNTs to voltage output.

The specimens were subjected to uniaxial tensile load-unload cycle to investigate their static sensing properties. Results indicated that this new sensor is better than the conventional foil strain gauge for high frequencies, and useful for structural health monitoring and vibration control applications.

Based on the molecular structure mechanics method, the dynamic properties of super carbon nanotubes were compared by the researchers of Engineering Mechanics Dept., Tsinghua University of Beijing [3.54] with those of the single-wall carbon nanotube (SWCNT). These super CNTs have ultra-low density, ultra-high sensitivity to mass (10^{-24} g) and to strain (887 Hz/nm/m, i.e. about 1 kHz per nanostrain!) as well as a lower fundamental frequency, being recommended for a new generation of sensors for strain and mass.

Because the elastomers are not suitable for creating force transducers, an attempt to increase the force sensitivity of polymer thick-film resistors was successfully made by blending carbon and silver-filled commercial pastes with elastomers [3.55]. A high solid content may increase the polymer's rigidity but enhances its stability too.

3.6. FORCE SENSING RESISTORS (FSRs)

A resistive tactile sensor can be fabricated by using materials whose electrical resistances are functions of strain, e.g. conductive rubber obtained by using carbon powder as an impregnating material [3.56]. Operating principles of elastomeric sensors are based either on varying the contact area when the elastomer is squeezed between two conductive plates or in changing the thickness when the external force varies (Fig. 3.11a). The contact area at the interface between the pusher and the elastomer changes, resulting in a reduction of electrical resistance (Fig. 3.11b).

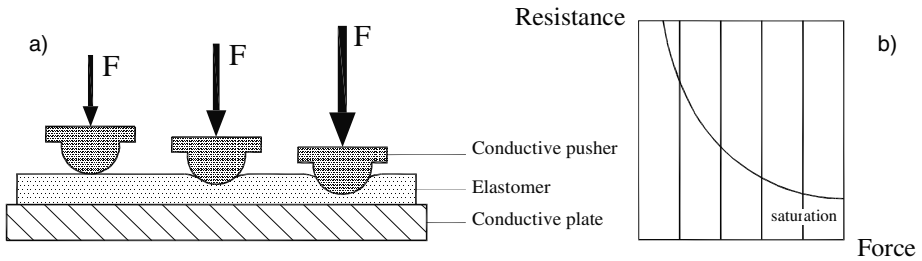


Fig. 3.11 Three stages of pushing on a resistive tactile sensor (a) and its characteristic Resistance versus Force (b). Without applied load, the value of the force sensing resistor (FSR) is over 100 k Ω , while after loading its resistance falls to 1 k Ω .

An unconventional design sandwiched a wire strain gauge between two layers of elastomer (Fig. 3.12a), so that force normal to the sensor surface produced Poisson strain that, being horizontal, had a maximum effect on the strain gauge [3.57]. Discrete FSRTM (Interlink Inc) sensors are constructed by the opposition of two polymer membranes; one membrane has interdigitating electrodes printed on its inner surface whereas the adjacent surface of the other membrane has been treated chemically to render it electrically conductive (Fig. 3.12b). Contact of the two adjacent surfaces allows a current to flow between electrodes through the conductive surface.

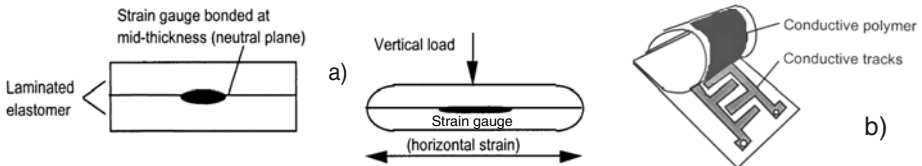


Fig. 3.12 Wire strain gauge sandwiched between two layers of elastomer (a) and a single force sensing resistor with conductive polymer (b)

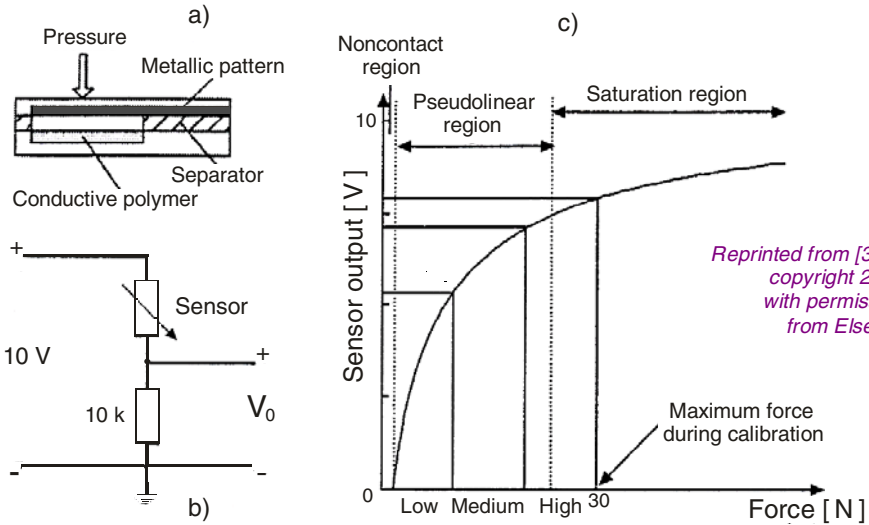
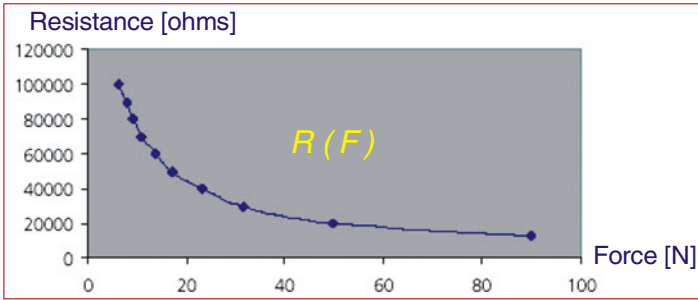


Fig. 3.13 Structure of the conductive polymer pressure sensor (a), resistance voltage divider (b) and voltage-force characteristic (c)

A multilevel input system is described in [3.58]: a metal layer with two interdigitated electrodes is separated from a conductive polymer layer by a cavity of 0.5 mm height (Fig. 3.13a). A simple circuit for resistance-voltage conversion converts the sensor resistance into a voltage output that changes with the applied force (Fig. 3.13b). The typical resistance values are 100 k Ω for a light touch and 1 k Ω for a heavy push. A typical voltage-force curve can be divided into three regions: noncontact, pseudolinear and saturation (Fig. 3.13c).

The therapeutic robotic companion Huggable [3.59] features four modalities of somatic information (pain, temperature, touch, and kinesthetic information) and need a large combination of resistive sensors over the entire surface. The form of a Teddy Bear was chosen since it has a wide appeal among all age groups across different cultures. For touch are used both electric field and QTC (quantum tunneling composite) force transducers. 100 k Ω NTC thermistors are utilized for temperature and a voltage divider with a 1 M Ω potentiometer for kinesthetic information (moderate touch).

Quantum tunneling composites are materials which normally act as insulators, but when deformed they become highly conductive due to quantum tunneling effects. Figure 3.14. shows a plot of resistance as a function of force for the Peratech QTC switch substrate used in the Huggable toy. In the current implementation, a force range from less than 100 gf to greater than 5 kgf can be sensed, just within the usual range of forces from human contact.



Source:
 W.D. Stiehl et al.
 MIT Media Lab.
 Cambridge, MA.
 Copyright 2005
 IEEE

Fig. 3.14 Plot of Resistance vs Force for the Quantum Tunneling Composites switch

A new generation of flexible, thin-film contact resistive force and pressure sensors printed on polyester substrates, made by Tekscan, Inc., is available in both *single load cell* and *grid-based configurations* [3.60]. A simple excitation circuit, like that presented in Figure 3.2b, should be used with the FlexiForce sensor to provide a constant drive voltage. This circuit helps ensure an output voltage proportional to the applied force. Reference resistance R_F is 1 k Ω to 100 k Ω . Sensor resistance R_s at no load is > 5 M Ω . Maximum recommended current: 2.5 mA.

Due to their 100 μm thickness, minimal disturbance to the true force and pressure patterns occurs (Fig. 3.15a and b) and therefore they are proving themselves useful in manufacturing (smart membrane switches, infusion pumps, pedals, etc) as well as research in bioengineering [3.61] and medical sciences, e.g. new electrolarynx “Evada” using a force sensing resistor to simultaneously control the voice intensity and frequency during conversation [3.62].

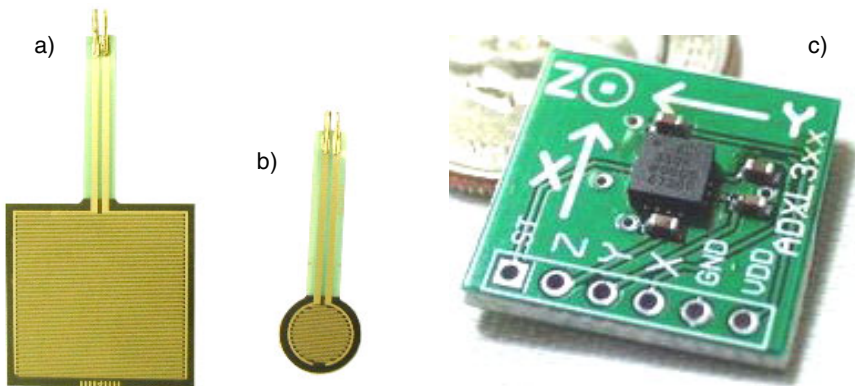


Fig. 3.15 Square (a) and circular (b) force sensing resistors, and a silicon triaxial force sensor on a flip chip microassembly, reprinted with permission from Elsevier (c)

Tekscan's *FlexiForce* sensors [3.63] are used in a variety of applications, performing a multitude of functions such as:

- detect and measure a relative change in force or applied load,
- detect and measure the rate of change in force,
- identify force thresholds and trigger appropriate action,
- detect contact and/or touch.

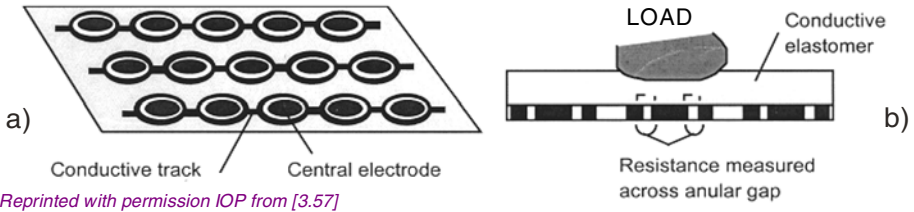
The miniaturization of microelectromechanical systems can be achieved by flip chip assembly directly onto a flexible circuit substrate [3.64], enabling scaling down of MEMS sensorized devices for biomedical applications (Fig. 3.15c). The heat bondable anisotropic conductive film 5552R (3M) allowed mechanical robust and low resistance electrical bondings together with a short process cycle time.

3.7. FORCE SENSING RESISTIVE NETWORKS

Tekscan's matrix-based pressure measurement systems, fabricated by means of the same technology used for the single-element force sensors, are thin, flexible, and trimmable [3.60]. They consist of silver electrodes printed as a matrix of intersecting rows and columns. An additional layer of semiconductive ink provides an electrical resistance at each intersection on the matrix. Sandwiching these two layers together creates an array sensor. The conductance of these sensors generally can be tailored to vary from zero (without external forces) to hundreds of microsiemens for the maximum applied force.

With multiplexing hardware based on a microprocessor circuit, the resistance output is read and displayed graphically on a PC. Changing the formulation of the ink produces different sensitivity ranges; varying the spacing between rows and columns yields finer resolution. Flexible, unobtrusive, and available in a multitude of force and pressure ranges, these sensors provide accurate feedback with a high degree of spatial resolution (0.0229 mm^2). Sampling rates can also vary; systems that sample upward of 470 000 elements have been built, ideal for improving sport equipment or developing medical research.

Paper [3.65] describes a system that measures forces over the entire hand using thin-film sensors and associated electronics to obtain force readings from up to 60 thin-film sensors at rates of up to 400 samples/s per sensor. The sensor readings, together with a video stream containing information about hand posture, are logged into a portable computer using a multiplexer, analogue-to-digital converter and appropriate software. Applications include measuring forces for driving a vehicle, hitting a golf ball, evaluating the hand strength following disease, trauma or surgery, and enabling quantitative ergonomic investigations.



Reprinted with permission IOP from [3.57]

Fig. 3.16 Resistive sensors array for plantar pressure measurement (a) and resistance measurement scheme by pushing the conductive elastomeric “floor” (b)

An array of resistive sensors for plantar pressure measurement [3.57] was created by placing a conductive elastomeric sheet on a flat matrix of regularly arranged metallic electrodes (Fig. 3.16a). Each sensor consisted of two copper electrodes, a central one and an outer ring, between which a voltage was applied. Compression of the rubber decreased the resistance across the annular gap and the corresponding increase in current was measured (Fig. 3.16b).

Yabuki *et al.* [3.66] have compared the ratio of the normal and tangential forces with the measured friction coefficient of a vibratory finisher (Fig. 3.17a) under dry and water-wet conditions. The integrated contact force transducer is based on one normal and three tangential sensors (Fig. 3.17b and c) made by Tekscan Inc. (Flexiforce sensor model A101-1).

Reprinted with permission from Elsevier
 Source: Yabuki *et al.*
Wear – 2002

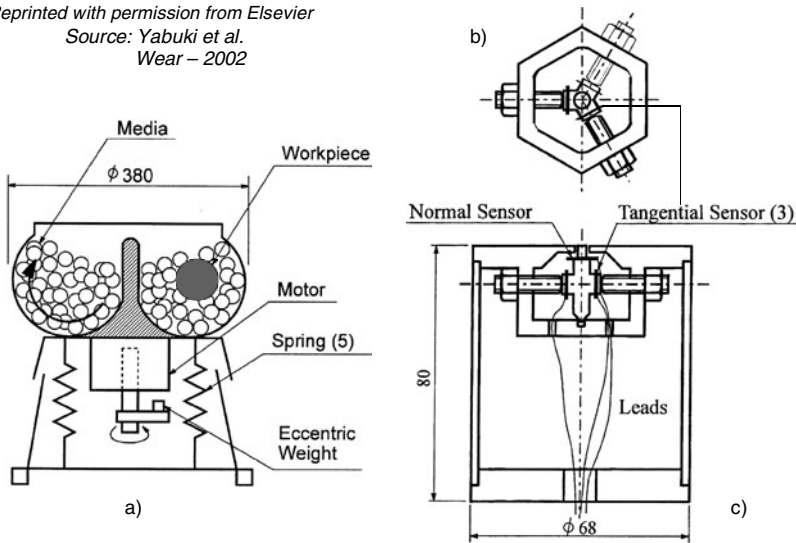


Fig. 3.17 Schematic diagram of a bowl-type vibratory finisher (a) and the new surface force transducer (cylindrical workpiece) in plan view (b) and cross-sectional view (c)

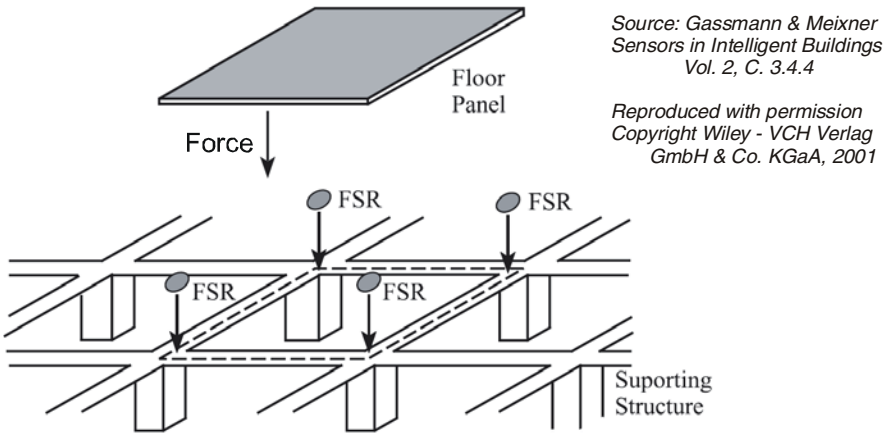


Fig. 3.18 Force sensing resistors supporting an “intelligent floor”

Four force sensing resistors (Fig. 3.18), manufactured by Interlink Electronics (Camarillo, CA), are placed between the floor panels’ corners and their supporting structures [3.67]. Each sensor has a circular active sensing area of 12.7 mm in diameter and is connected as a variable resistor in a simple force-to-voltage conversion configuration. The analog voltage level is then sent to a computer and digitized as an 8-bit integer. Real-time data acquisition is accomplished with a PC board that can support 64 analog inputs simultaneously at a sampling rate of up to 500 kHz (National Instruments, ATMIO-64E-3).

On-line data processing is performed with the LabVIEW software that features a graphical-based programming environment. Readings from the four sensors corresponding to the same floor panel are summed and compared with an empirically determined threshold. If the total force reading exceeds the threshold, an icon representing the floor panel will change its color from green to black on the computer screen. When sensor readings are stable, the system can correctly track a person walking across the active floor area.

Another example is given in [3.68], consisting in a grid of 256 sensors distributed by 64 tiles (8×8 array) each having 60 cm by 60 cm. Force sensing resistors having 6.4 mm radius are used as force and/or pressure transducers beneath the “intelligent floor.”

Smart textiles using fabric-based sensors to monitor gesture, posture or respiration have been exploited in many applications [3.69]. Most of fabric-based sensors were manufactured by either coating piezoresistive materials on a fabric or directly knitting electroconductive fibers into fabrics. In these complex resistive networks the relationship of resistance versus strain cannot be described as a linear function and is modeled as a second order equation.

Performances of the designed yarn-based sensors were experimentally evaluated by measuring their resistance changes under variable loading. Fiber meshed resistive strain transducers were clamped between the cross bars of a tensile tester Instron 5500 [3.70].

InControl Solutions Company has achieved a smart force joystick designed for portable and low-power applications with simple input acquisition, stable response, and a small form factor [3.71]. Conventional joysticks move a game character at a constant rate, no matter how hard the user presses, but adding proportional control would vary this rate based on touch: apply more pressure to the joystick, and the character would move faster! In this respect, the Multipath force transducer combines screen print technology with a unique, patented design that places a resistor on one sheet and a silver shunt (or pattern of shunts) on the opposing sheet. The resistor is a rectangular area of carbon ink printed over two silver ink traces. When the transducer sandwich is lightly pressed, the silver begins to contact the high points on the carbon resistor surface. As more pressure is applied, the number of contact points increases, causing the resistance to decrease and following a force-resistance relationship established for an individual configuration of force transducer. Worth to mention is the Multipath ability to create various sensing element arrays based on adaptive algorithms: from proportional switches to fast directional controls.

A vertical thick-film resistor for a fine-pitch-array sensor with a large number of sensing points (6400) for measuring the relief (footprint) of a pressure of up to 6 bar on an area of $(0.4 \times 0.4) \text{ m}^2$ has been presented in [3.72]. The resistor dimensions are $(0.6 \times 0.6 \times 0.12) \text{ mm}^3$. These resistors made by stainless steel screen (DuPont 8059) are vertically oriented inside an assembly with high density and large number of sensing elements, each “point” being accessible with a computer-controlled measuring system.

REFERENCES

1. Du, W.Y., Yelich, S.W.: Resistive and capacitive based sensing technologies. *Sensors & Transducers Journal* 90, 100–116 (2008)
2. Dally, J.W., Riley, W.F., McConnell, K.G.: *Instrumentation for Engineering Measurements*. John Wiley & Sons, Inc., New York (1993)
3. Doebelin, E.O.: *Measurement Systems: Application and Design*. McGraw-Hill Book Company, New York (1966)
4. Neubert, H.K.P.: *Instrument Transducers – An Introduction to Their Performance and Design*. Clarendon Press, Oxford (1975)
5. Norton, H.N.: *Handbook of Transducers for Electronic Measuring Systems*. Prentice Hall, Inc., Englewood Cliffs (1969)
6. Stere, R.: *Electronic Apparatus for Measurement and Control*. Editura Didactică și Pedagogică, București (1968) (in Romanian)

7. Ștefănescu, D.M.: Resistive transducers utilized in machine-building. In: Proc. 4th Conf. Vibration in Machine Design, Timișoara, vol. 4, pp. 297–304 (1982) (in Romanian)
8. Ștefănescu, D.M.: Resistive force transducers for testing in aeronautical industry. *Rev. Transp. și Telecom XIII(2)*, 26–31 (1986) (in Romanian)
9. Webster, J.G. (Editor-in-Chief): *The Measurement, Instrumentation and Sensors Handbook*. CRC Press – Springer – IEEE Press, Boca Raton, FL (1999)
10. Sheingold, D.H. (ed.): *Transducer Interfacing Handbook. A Guide to Analog Signal Conditioning*. Analog Devices, Norwood, MA (1980)
11. Unimeasure/80 – A multipurpose transducer (US Patent 3842385). Unimeasure, Inc., Grants Pass, OR (1986)
12. Haug, A.: Übersicht über die Dehnung verschiedener Körperformen bei Belastung. Reprint Hottinger Baldwin Messtechnik GmbH, Darmstadt, 2–68
13. FlexiForce. Sensing solutions for the 21st century. Tekscan Inc., South Boston, MA, Technical Data Sheet Model A 101-98
14. Perry, C.C., Starr, J.E., Weidner, J.R.: Modern strain transducers: their design and construction. In: Hannah, R.L., Reed, S.E. (eds.) *Strain Gage Users' Handbook*, SEM Edition (1992); ISBN 0-912053-36-4
15. Kraftaufnehmer Produkt Information. Hellige-Fabrik wissenschaftlicher Apparate, Freiburg im Breisgau, Bundesrepublik Deutschland (1977)
16. Solid state transducer technology short form catalog. Kulite Semiconductor Products, Inc., Ridgefield, N.J., Bulletin SF-1C-88
17. Window, A.L., Holister, G.S.: *Strain Gage Technology*. Elsevier Applied Science, London, New York (reprinted 1989)
18. Load cells, weighing equipment & systems. Kubota Corporation, Osaka, Japan, Catalog 1102-99
19. Henning, W.: Mikroelektronik-Sensoren. Vortrages anlässlich des 3. Kolloquiums der Österreichischen Tribologischen Gesellschaft, pp. 3-15. Siemens, München (1981)
20. Sarro, P.M., van Herwaarden, A.W.: Silicon cantilever beams fabricated by electrochemically controlled etching for sensor applications. *J. Electrochem. Society* 133, 1724–1729 (1986)
21. Middelhoek, S., Audet, S.A.: Silicon sensors: full of promises and pitfalls. *J. Phys. E: Sci. Instrum.* 20, 1080–1086 (1987)
22. Low power 'Set and Lock' digital pots. Winbond Electronics Corporation America. In: *Europe Electronics Express*, Info Card 1421, San Jose, CA (May 2003)
23. Leinonen, M., Juuti, J., Jantunen, H.: Interface circuit for resistive sensors utilizing digital potentiometers. *Sensors and Actuators A: Physical* 138(1), 97–104 (2007)
24. Popescu, A., Mocanu, D.R., Ștefănescu, D.M.: Historical aspects of using resistive strain gages for producing load cells in Romania. In: *History of strain gages, brittle coatings and loadcells – Retrospection in 19 countries at 50-year Jubilee*, preprints IMEKO, Houston, Texas, October 19, pp. 209–213 (1988)
25. Elektrische Geräte für Messung von Kraft, Masse und Länge (Position). Swema, Stockholm, Sweden, Katalog T.169.78.10.1
26. Bonfig, K.W., Bartz, W.J., Wolf, J.: *Sensoren und Meßaufnehmer. Neue Verfahren und Produkte für die Praxis*. Expert Verlag, Grafenau, Deutschland (1988)

27. Northrop, R.B.: Introduction to Instrumentation and Measurements. CRC Press, Boca Raton (1997)
28. Ștefănescu, D.M.: Strain gauge transducers for measurements in Electrotechnics and Energetics. *Revue Roumaine de Sciences Techniques – série Électrotechnique et Énergétique*, Tome 32(4), 413-418 (1987)
29. Mocanu, D.R., Bârsănescu, P.D., Ștefănescu, D.M.: How to select the strain gauge to minimize the measurement error due to the integration tendency. In: Proc. 9th Int'l Conf. Experimental Mechanics, Copenhagen, Denmark, vol. 1, pp. 326–332 (1990)
30. Ștefănescu, D.M., Ștefănescu, V.: Strain gauge force transducers. In: Abstracts European Conference Junior - Euromat, Lausanne, Switzerland, pp. 442–443 (1992)
31. Ștefănescu, D.M., Mănescu, T., Ion, I.: Strain gauges emplacement possibilities for force/torque transducers in Robotics. In: Proceedings IMEKO XV World Congress Measurement to Improve the Quality of Life in the 21st Century, Osaka, Japan, June 13-18, vol. 10, pp. 117–124 (1999)
32. Ștefănescu, D.M., Marinescu, A.: Strain gauged elastic elements for measuring large forces in Mechatronics. In: Proceedings 3rd IFAC Symposium on Mechatronic Systems, Sydney, Australia, September 6-8, pp. 439–444 (2004)
33. Ștefănescu, D.M.: Strain gauged elastic elements for force and related quantities measurement. In: CD Proc. IMEKO Int'l Conf. on Cultivating Metrological Knowledge, Merida, Mexico, November 27-30, Paper 22 (2007)
34. Oppermann, K.: Force sensor with metal measuring grid transverse to the lines of force. In: Proc. Xth IMEKO World Congress, Prague, Czech, Paper 358 (1985)
35. Löffler, E., Siewert, C., Ascher, C.: Manganin thin film sensor for force sensing. *Surface and Coatings Technology* 174-175, 1287–1292 (2003)
36. Ravary, B., Pourcelot, P., Bortolussi, C., Konieczka, S., Crevier-Denoix, N.: Strain and force transducers used in human and veterinary tendon and ligament biomechanical studies. *Clinical Biomechanics* 19, 433–447 (2004)
37. Youdin, M., Reich, T.: Mercury-in-rubber (Whitney) strain gauge. *Annals of Biomedical Engineering* 4(3), 220–231 (1976) by SpringerLink Netherlands, 24 March (2007)
38. Cheung, Y.-N., Zhu, Y., Cheng, C.-H., Chao, C., Leung, W.F.: A novel fluidic strain sensor for large strain measurement. *Sensors and Actuators A: Physical* 147(2), 401–408 (2008)
39. Hjelmgren, J.: Dynamic measurement of force – A literature survey. Swedish National Testing and Research Institute, Boras, SP Report 27 (2002)
40. Chopra, K.L., Kaur, I.: Thin Film Device Applications. Plenum, New York (1983)
41. Cuscó, L. (Coord.): Guide to the Measurement of Pressure and Vacuum. The Institute of Measurement and Control, London (published 1998); ISBN 0-904457-29-X
42. van Putten, A.F.P.: Electronic Measurement Systems. Prentice Hall, New York (1988)
43. Druzhinin, A.A., Maryamova, I.I., Kuttrakov, A.P., Pavlovsky, I.V.: On the possibility to create high-sensitive piezoresistive mechanical sensors for cryogenic temperatures. *Sensors and Systems Journal* (7) (July 2005) (in Russian)
44. Stuchebnikov, V.M.: SOS strain gauge sensors for force and pressure transducers (December 2004), http://www.midaus.com/docs/publ_2.pdf

45. Shamrakov, A.L., Timofeev, V.A.: Force transducers for space-rocket technologies. *Sensors and Systems Journal* (9) (September 2005) (in Russian)
46. Mokrov, E.A., Vasiliev, V.A., Belozubov, E.M.: Application of systemology elements for minimizing the effect of destabilizing factors on thin-film tensoresistive sensors. *Sensors and Systems Journal* (3) (March 2005) (in Russian)
47. Zwijze, R.A.F., Wiegerink, R.J., Krijnen, G.J.M., Lammerink, T.S.J., Elwenspoek, M.: Low-cost piezoresistive silicon load cell independent of force distribution. *J. Micromech. Microeng.* 10, 200–203 (2000)
48. Cheeke, D.: Sensor signal conditioning. *Sensors & Transducers* 82(8), 1381–1388 (2007)
49. Devenyi, A., Gheorghiu, A., Belu, A., Korony, K.: Electrical transport and structure of vacuum deposited carbon films. In: *Proc. Physics & Chemistry of Semiconductors Conference, Budapest, Hungary*, pp. 11–17 (November 1970)
50. Biehl, S., Lüthje, H., Bandorf, R.: Novel force sensor based on hard Diamond-like-Carbon films. In: *Abstracts 16th European Conf. on Solid-State Transducers, Prague, Czech Republic, September 15-18, vol. 2*, pp. 427–428 (2002)
51. Peiner, E., Tibrewala, A., Bandorf, R., Biehl, S., Lüthje, H., Doering, L.: Micro force sensor with piezoresistive amorphous carbon strain gauge. *Sensors and Actuators A: Physical* 130-131, 75–82 (2006)
52. Peiner, E., Tibrewala, A., Lüthje, H., Bandorf, R., Biehl, S., Doering, L.: Piezoresistive diamond-like carbon micro strain gauges. In: *CD Proc. XVIII IMEKO World Congress on Metrology for a Sustainable Development, Rio de Janeiro, Brazil, September 17-22, Paper 426* (2006)
53. Li, X., Levy, C., Elaadil, L.: Multiwalled carbon nanotube film for strain sensing. *Nanotechnology* 19(4) (2008)
54. Li, Y., Qiu, X.M., Yang, F., Wang, X.-S., Yin, Y.: Ultra-high sensitivity of super carbon-nanotube-based mass and strain sensors. *Nanotechnology* 19, Paper 165502 (2008)
55. Papakostas, T.V., White, N.M.: The effect of blending polymer thick-film resistors with elastomers on the force sensitivity of the films. In: *Abstracts of Eurosensors XIV, Copenhagen, Denmark, August 27-30, pp. 293–294* (2000); ISBN 87-89935-51-9
56. Fraden, J.: *AIP Handbook of Modern Sensors – Physics, Design and Applications*. American Institute of Physics, New York (1993)
57. Urry, S.: Plantar pressure-measurement sensors (review article). *Measurement Science and Technology* 10, R16–R32 (1999)
58. Tang, H.: Multilevel input system. *Int. J. Human-Computer Studies* 54, 495–507 (2001)
59. Stiehl, W.D., Lieberman, J., Breazeal, C., Basel, L., Lalla, L., Wolf, M.: Design of a therapeutic robotic companion for relational, affective touch. In: *Proc. IEEE Int'l Workshop on Robots and Human Interactive Communication*, pp. 408–415. MIT Media Lab, Cambridge, MA (2005)
60. Lowe, M., King, A., Lovett, E., Papakostas, T.: Flexible force sensors – In touch with modern technology. *Sensors online* (June 2004), <http://www.sensorsmag.com>

61. Bachus, K.N., DeMarco, A.L., Judd, K.T., Horwitz, D.S., Brodke, D.S.: Measuring contact area, force, and pressure for bioengineering applications: Using Fuji Film and TekScan systems. *Medical Engineering & Physics* 28, 483–488 (2006)
62. Choi, H.-S., Park, Y.J., Lee, S.M., Kim, K.-M.: Functional characteristics of a new electrolarynx 'Evada' having a force sensing resistor sensor. *Journal of Voice* 15(4), 592–599 (2001)
63. FlexiForce®, the leader in standard & custom OEM force sensing solutions. Tekscan, Inc., South Boston, MA, PDF on Internet (created on November 17, 2006)
64. Sieber, A., Valdastrì, P., Houston, K., Menciassi, A., Dario, P.: Flip chip micro-assembly of a silicon triaxial force sensor on flexible substrates. *Sensors and Actuators A: Physical* 142(1), 421–428 (2008)
65. Nikonovas, A., Harrison, A.J., Hault, S., Sammut, D.: The application of force-sensing resistor sensors for measuring forces developed by the human hand. *Proc. Inst. Mech. Eng. [H]* 218(2), 121–126 (2004)
66. Yabuki, A., Baghbanan, M.R., Spelt, J.K.: Contact forces and mechanisms in a vibratory finisher. *Wear* 252, 635–643 (2002)
67. Gassmann, O., Meixner, H. (eds.): *Sensors in Intelligent Buildings*, vol. 2. C. 3.4.4. Wiley-VCH Verlag, Weinheim (2001)
68. Nunes, A., Piedade, M., Neves, R.: Cost effective immersive room with pressure sensing floor. In: *CD Proc. IMEKO Int'l Conf. Cultivating Metrological Knowledge*, Merida, Mexico, November 27–30, Paper 71 (2007)
69. Huang, C.-T., Shen, C.-L., Tang, C.-F., Chang, S.-H.: A wearable yarn-based piezoresistive sensor. *Sensors and Actuators A: Physical* 141(2), 396–403 (2008)
70. Wijesiriwardana, R., Dias, T., Mukhopadhyay, S.: Resistive fibre-meshed transducer. In: *Proc. 7th IEEE Int'l Symp. on Wearable Computers, ISWC 2003* (February 2006)
71. Haverty, C., Fildes, G.: Enhancing computer game joysticks with smart force transducers. *Sensors Magazine* (September 1998)
72. Belavic, D., Hrovat, M., Pavlin, M.: Vertical thick-film resistors as load sensors. *Journal of the European Ceramic Society* 21, 1989–1992 (2001)

Chapter 4

INDUCTIVE FORCE TRANSDUCERS

There is a great variety of induction coil sensors. The designs for coils with air or ferromagnetic cores are compared, their frequency properties are analyzed and various methods for output signal processing are presented in [4.1]. It is our aim to estimate their usefulness in force measurement.

Several research teams have developed prototype microprobes with nanometer repeatability. The systems from PTB [D] and TUE [NL] use piezoresistive sensors placed on a membrane or on microlevers while that from NPL [UK] uses capacitive sensors. Swiss Top Nano 21 research project [4.2], with the Ecole Polytechnique Federale de Lausanne, industrial partner Mecartex and METAS, developed a 3D touch probe for coordinate measuring machines using probing forces below 0.5 mN; x , y and z translational motion components are measured by three inductive transducers.

Figure 4.1 presents the measurement principle with variable inductance. The variable (passive) parameter could be one of these: differential transformer (LVDT), reluctance, mutual inductance and impedance (by eddy current) [4.3].

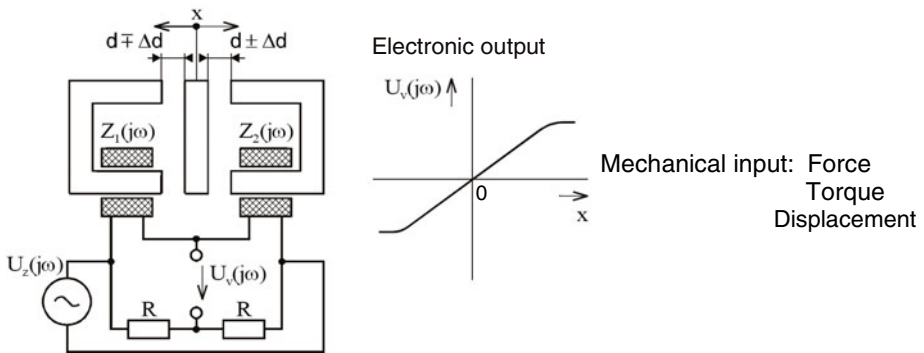


Fig. 4.1 The principle of differential transducer with variable inductance

4.1. LVDT (Linear Variable Differential Transformer)

In most sensors force is not directly converted into an electric signal; instead, their working principle relies upon combining a position sensor and a force-to-displacement converter. The latter may be a simple coil spring, whose compression displacement x can be defined through the spring coefficient k and compressing force F as

$$x = k \cdot F \quad (4.1)$$

The horizontal transducer shown in Figure 4.2a is composed of a spring and a LVDT displacement sensor [4.4]. Figure 4.2b shows the optimal vertical assembly of LVDT force transducer and bending spring in order to prevent lateral movements.

Within the linear range of the spring, the LVDT sensor produces a voltage which is proportional to the applied force. With LVDT sensors, resolutions of $1 \mu\text{m}$ or less are possible [4.5], this principle being especially appropriate for force transducers with very small capacities (0.1 N).

Hooke's law states that an elastic body subjected to a force load within its elastic limit will deflect in direct proportion to that force. The combination of an elastic element with an LVDT produces a force transducer, generally known as an LVDT load cell [4.6]. AC and DC variants are available.

The bidirectional nature of the displacement characteristic of an LVDT perfectly complements the bidirectional deflection of an elastic element. Thus, an LVDT load cell produces an output voltage that is proportional to the axial force load and that also undergoes a phase or polarity reversal when it changes from tension to compression. This assumes that the LVDT is adjusted to zero or null output when the elastic body is unloaded. Optimum operating characteristics are developed when the linear range of the LVDT corresponds to the deflection of the elastic element.

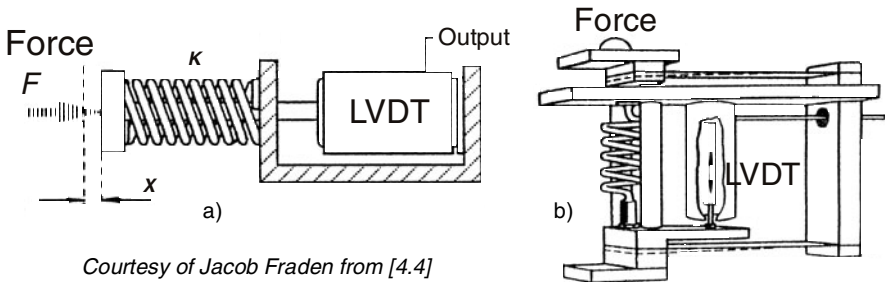


Fig. 4.2 Two spring systems (a – Fraden, b – Wieringa) used to convert force into displacement, which is measured by a LVDT.

Typical examples of LVDTs combined with elastic elements [4.6] are illustrated in Figure 4.3. The bending beam (Fig. 4.3a) can be loaded in tension or compression. The extension spring (Fig. 4.3b) must be loaded either way, but is usually used for tensile loads. Proving rings (Fig. 4.3c) and configurations of multiple beams (Fig. 4.3d) are elastic elements most often used in commercial LVDT force transducers.

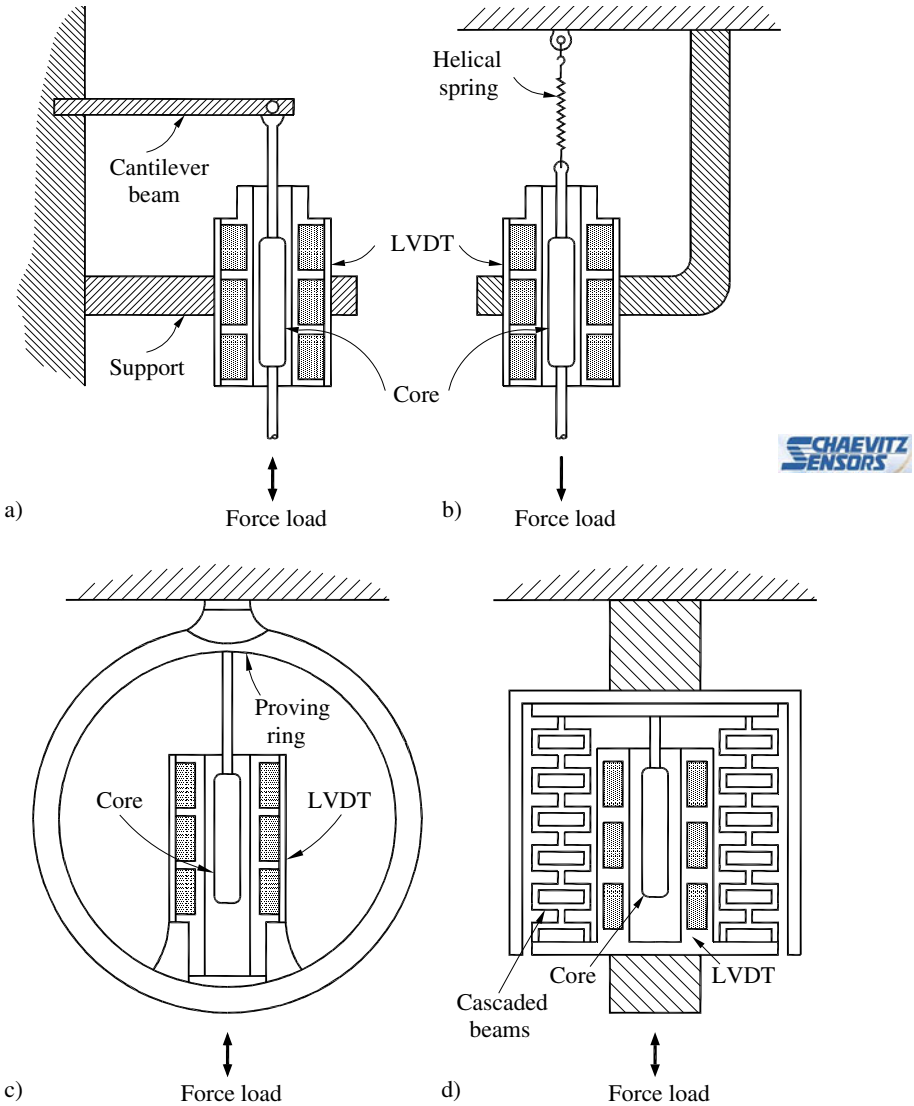


Fig. 4.3 Different combinations of elastic elements and LVDTs for force transducers

LVDTs are inductive devices that act as position sensors and may be attached to other deflecting components such as diaphragms. They comprise a cylinder of ferromagnetic material which is moved inside a tube with three separate windings: a central coil is excited with an alternating voltage and there are two sensing coils, one on either side. As the magnetic plunger moves within the tube, the magnetic field coupling is changed; with suitable electronics a linear relationship between cylinder position and output can be obtained.

This method may be used to select displacements of movable magnetic cores from less than a millimeter to several hundreds of millimeters. For pressure transducers [4.7] the plunger is attached to the center of a diaphragm or at the end of a bellows, they operating between 0.01 Pa and 10 MPa. Macro Sensors [4.8] designed a pressure-balanced, oil-filled and double bellows-sealed LVDT assembly to enhance the reliability of multiple redundant LVDT-based extensometers monitoring the structural integrity for offshore platforms.

LVDT (linear variable differential transformer) electrical connections are depicted in Figure 4.4. They can work as inductive half-bridges, inductances being represented by black rectangles (RMP Rheinmetall Meß- und Prüftechnik – Fig. 4.4a) or by half-spirals (RDP Group – Fig. 4.4b).

If LVDT contains one primary and two secondary coils (Fig. 4.4c), connected like in Figure 4.4d, the differential effect is obtained between the two secondaries. When the core is moved, an AC-signal is produced that can be used to determine amplitude and direction of the core movement [4.9]. The resulting transducer can be made stiff and with low mass, that makes it suitable for dynamic measurements.

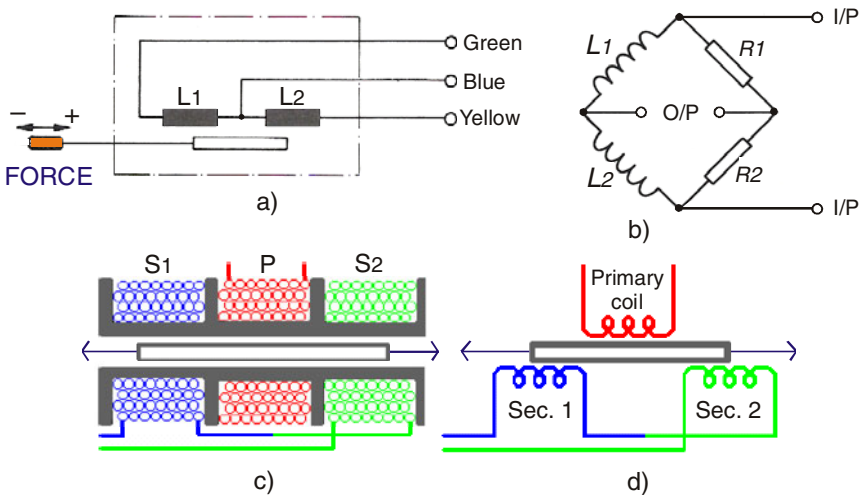


Fig. 4.4 Different electrical connections symbolization for LVDT force transducers

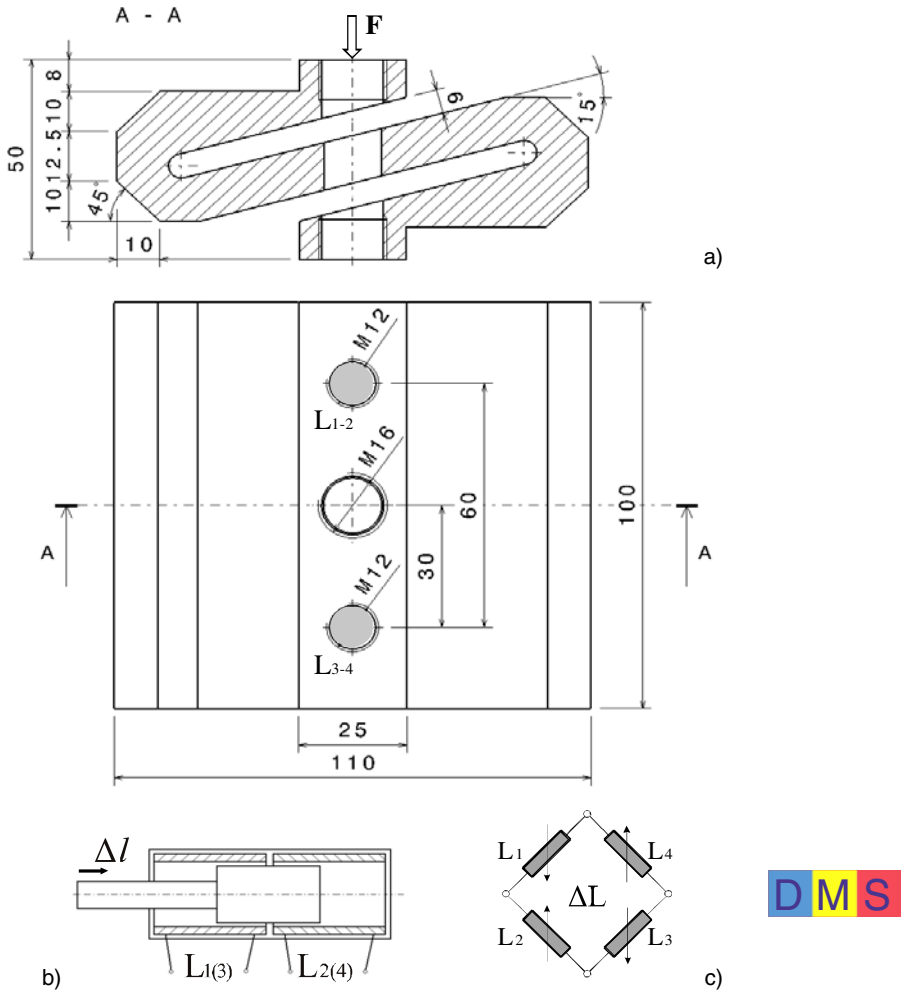


Fig. 4.5 S-shaped spatial elastic element for inductive force transducer (a), LVDT displacement sensor (b), full-bridge connection for two LVDT devices (c)

A robust transducer, designed as a “spatial S” with two oblique slots and two positions for associated inductive transducers, mounted on a cutter device with alternating motion equipping the farming combine (Fig. 4.5), is described in [4.10]. Inductive displacement transducers, combined with strain gauges bonded on a cage-shaped elastic element force transducer, are shown in [4.11]. LVDTs and piezoelectric force sensors integrated with a magnetorheological damper, in order to facilitate its closed-loop structural vibration control, are presented in [4.12].

4.2. VARIABLE RELUCTANCE TRANSDUCERS

A variable reluctance pressure transducer [4.13] uses a magnetically conductive diaphragm to modulate the magnetic reluctance of a differential transformer just like in proximity detectors. Figure 4.6 illustrates the basic idea behind the magnetic flux modulation. The core and coil assembly produces a magnetic flux whose field lines travel through the core, the air gap and the diaphragm. The permeability of the core magnetic material is at least 1000 times higher than that of the air gap, and, subsequently, its magnetic reluctance is lower than the reluctance of air. Since the magnetic reluctance of the air gap is much higher than the reluctance of the core, it is the gap which determines the inductance of the core-coil assembly. When the diaphragm deflects, the air gap increases or decreases depending on the direction of deflection, thus causing the modulation of the inductance.

Figure 4.7 shows a proving ring sensing element employed in a relative force transducer, axially loaded in tension and/or compression [4.14]. When a compression force is measured, the elastic ring is deformed and, by the construction of the assembly, the distance between one of the coils and the corresponding armature-leg decreases while the distance between the other coil and its adjacent armature-leg increases. This process is bidirectional, the proximity variations in dual coil transducer being opposite for tension forces.

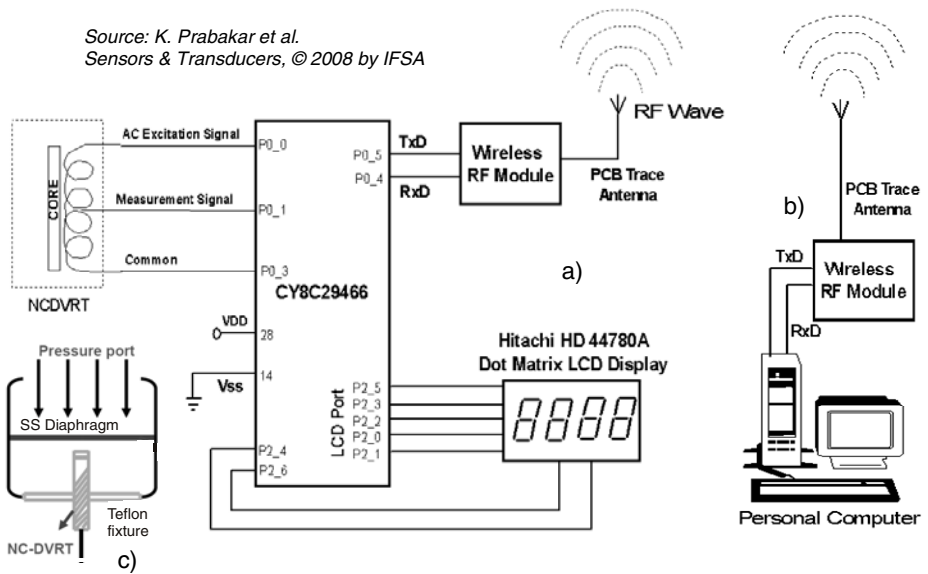


Fig. 4.6 Wireless measuring system using noncontact differential variable reluctance transducer: a) emitter with μ C and 2.4 GHz RF module, b) receiver, c) pressure sensor

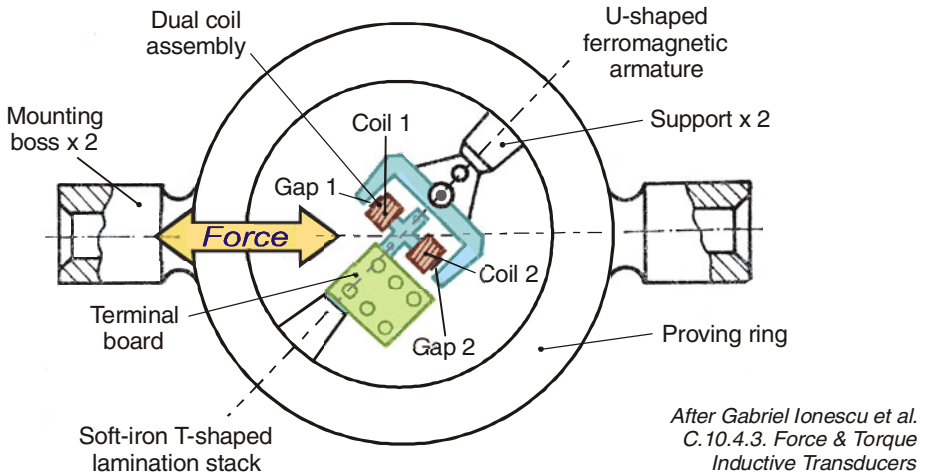


Fig. 4.7 Relative force transducer with a proving ring as a dual sensing elastic element and a differential variable reluctance transducer (DVRT)

For both coils, the soft-iron T-shaped lamination stack constitutes the common core. The output AC signal is obtained at the diagonal of a four-arm bridge, whose arms are the two coils and two matched resistors. The bridge is nulled without applied force, the relative measuring device having equal gaps between the armature and both coils. When a force is applied, the coil inductances vary in opposite directions generating an unbalance signal proportional to the force magnitude. Phase sensitive detection allows to sense the direction of the input force.

The same design, but using four coils electrically connected as four active arms of an AC bridge, can be adapted for a relative torque transducer [4.15].

4.3. MUTUAL INDUCTANCE VARIATION FORCE TRANSDUCERS

The mutual inductance variation measurement systems (Fig. 4.8) cover a wide range, from 0.5 N to 200 kN, as presented in Table 4.1. These force transducers consist of small displacement sensors working on the “electrical comparator” principle, which measure the deformations of elastic bodies under load [4.16].

Table 4.1 Measurement range with mutual inductances for various elastic elements

	Measurement range	Elastic element type
Small	0.5 N ... 20 N	Diaphragm/membrane
Medium	10 N ... 20 kN	Diaphragm or full cylinder
Large	5 kN ... 200 kN	Tube

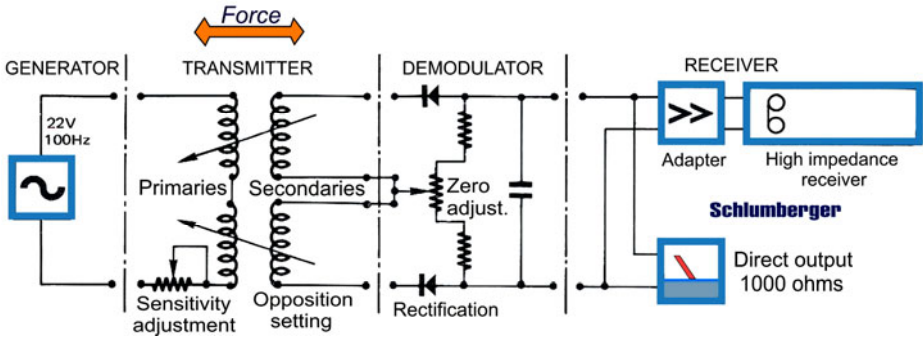


Fig. 4.8 Mutual inductance variation system (with zero and sensitivity adjustments) for measurement of tensile, compressive or alternating forces

The main characteristics of the mutual inductance variation devices are:

- conditioners working either with 50 Hz mains supply (ground equipment) or with 27 V_{DC} supply (airborne),
- sensitivity on direct output: $\pm 210 \mu\text{A}$ (traction and compression recorders) with a load of 1 k Ω ,
- linearity (terminal deviation): 1 %,
- repeatability: $< \pm 0.05 \%$,
- hysteresis: between $\pm 0.25 \%$ and $\pm 0.5 \%$.

The invention entitled “*Mutual inductance force sensor (MIFS)*” offers a new design in input sensor technology [US Patent 7047826 / 23 May 2006]. This novel and robust, multi axis, force input sensor is based on the principle of mutual inductance [4.17]. Here, the movement between two parallel flat coil sets, printed on opposing surfaces, is detected. The surfaces or boards are held in proximity by some elastomeric structural component/housing. This enables a sensor that functions in a variety of ways, including as a flat “pad” type controller/pointer with response actions similar to that of a joystick. The sensor is immune to unwanted temperature induce effects, external magnetic fields and can operate in wet and dry environments. Other advantages are:

- inexpensive, simple and easy to produce (“print and fold”), cheap to replace,
- variety of configurations for measuring multiple axes of force and torque,
- linear response over a wide range of input forces,
- thin, low profile – can be used on flex surfaces,
- durable and rugged.

Applications include automotive detectors, medical research sensors and rehabilitation equipment, computer games, and other systems to detect input forces along one or several axes.

4.4. INDUCTIVE EDDY CURRENT TRANSDUCER

The monitoring bridge construction can be performed by optimized eddy-current transducers to recognize damages earlier and to reduce rehabilitation expenses. The aim is to measure the coil impedance of an eddy-current sensor positioned close to a prestressing cable and to conclude the change of stress in steel of reinforced concrete elements [4.18]. The principle of the experimental set-up is depicted in Figure 4.9. While a coil is wound up on a ferrite core and put on a steel sample, the steel is loaded with tensile stress, being certain that the ferrite U-core rests without air gap, close to the steel bar (a square profile reduces this air gap). Since the magnetic circuit is closed over the iron, impedance variations can be measured during mechanical stressing.

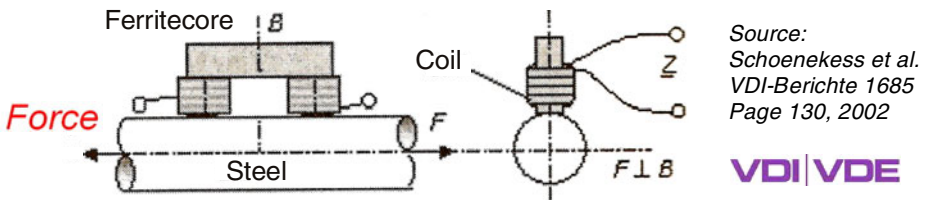


Fig. 4.9 Force and stress measurement with coil and ferrite core coupled on a steel bar

An impedance analyzer HP 4284A and a load cell with measuring range of 25 kN are utilized for several consecutive measurement cycles under an input terminal voltage of 480 mV, at a frequency of 1 kHz. The curves measured on soft steel show a climbing tendency of inductance and reluctance by increasing tensile stress, the relative change of reluctance being smaller than that of the inductance. So, the inductive effect in the impedance assembly is a measure of the applied tensile force (with a mean correlation coefficient better than 0.996).

4.5. BIPARAMETRIC INDUCTIVE FORCE TRANSDUCERS

4.5.1. Biparametric LR

Magnetoinductive magnetometers are relatively new, with the first patent issued in 1989 [4.19]. Such a sensor is simply a single winding coil on a ferromagnetic core that changes permeability within the Earth's field. The sense coil is the inductance element in a LR relaxation oscillator. The frequency of the oscillator is proportional to the field being measured (Fig. 4.10a).

The oscillator frequency can be monitored by a microprocessor's capture/compare port to determine field values. These magnetometers are simple in design, low cost, and low power. They are available from Precision Navigation, Inc. and used in compass applications.

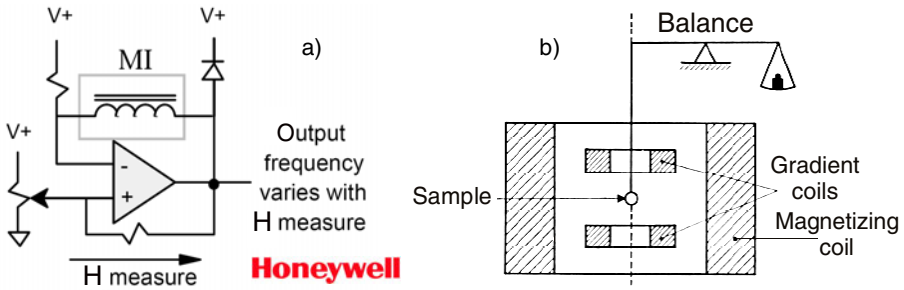


Fig. 4.10 Magnetoinductive (a) and force based (b) magnetometers

Remember that the first and simplest of the force based magnetometers was developed by Faraday and is called magnetic balance (Fig. 4.10b). Here a set of magnetizing coils are used to magnetize a sample while a second set of coils generates a field gradient which results in a force on the sample which is measured by a balance or force transducer [4.20].

In magnetic force microscopy (MFM) a small magnetic dipole is flown over the surface of a magnet (10...100 nm off the surface). The force on the dipole is then used to measure local variations in the material magnetization.

4.5.2. Biparametric LC

As the mechanical or hydraulic dynagraphs which are still utilized are provided with old recording devices operating with a high inertia, they do not allow an accurate reproduction of the load variations during the oil pumping cycle. There is a permanent interest in developing modernized dynamometers. In this respect an electronic dynagraph equipped with biparameter frequency transducers and a new measurement system able to eliminate the influence of the assembling tubes have been made within the Automatics and Electronics chairs from the Romanian Oil and Gas Institute [4.21].

The operation principle of this digital display dynamometer results from Figure 4.11a, where V represents the force transducer output after establishing the relation between the applied force and the frequency f of a sinusoidal signal. The transducer is a frequency discriminator: when f complies with the applied force, the output voltage is naught. The frequency discriminator characteristic is linear, so the output voltage V (which can be considered a deviation signal) is proportional to the frequency deviation; this voltage is applied to the input of a chopper provided DC amplifier. Hence, it appears that the dynamometer operates according to the automatic compensation principle of the discriminator frequency which makes up the transducer electronic circuit. Thus the transducer itself contains only passive elements (L and C), leading to a better stabilization than in case of an embedded electronic oscillator.

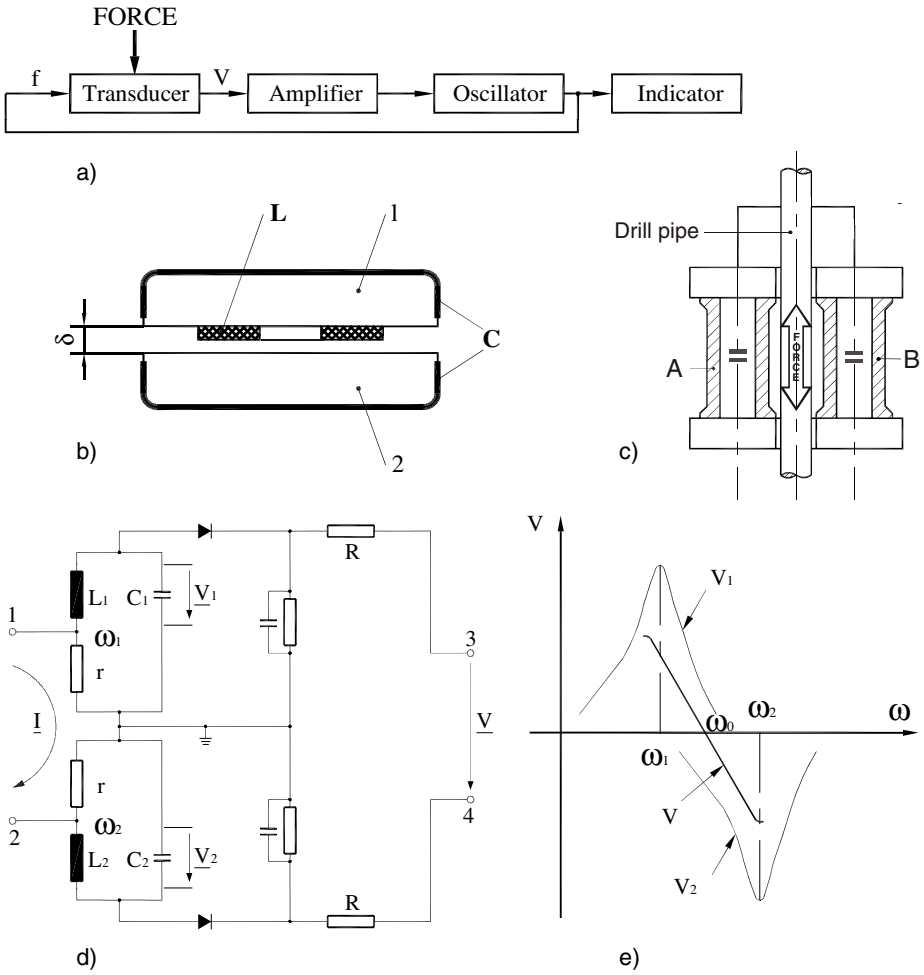


Fig. 4.11 Biparametric force transducer oscillation scheme (a), based on LC sensing devices (b), sized within two elastic elements A and B (c); frequency discriminator (d) with passive elements (L and C) and linear force – frequency characteristic (e)

Figure 4.11b shows the biparametric force transducer measurement principle. The two electrodes 1 and 2 are ferrite-made tips, outer-plated. These two metallized plates represent the electrodes of the capacitor C. On the inner side of one of the tips a one-layer plane coil L is printed. Both the coil inductance L and the capacitor capacitance C vary depending on the distance δ between the electrodes. The coil and the capacitor can be connected as an LC oscillator circuit.

By compressing the elastic bodies A and B (Fig. 4.11c) during pumping, the two electrodes of the internal LC sensitive device become closer, that leads to the frequency variation of the discriminator which is proportional to the applied force. The symmetrical location of the two elastic bodies ensures random bending compensation, so the dynamometer effectively measures the axial stress of the smooth drill pipe.

Due to the fact that in each elastic body there is such a circuit, a discriminator can be made up using the two LC circuits (Fig. 4.11d). The achievement of the linear zone of the combined characteristics for this biparametric force transducer is shown in Figure 4.11e.

The LC biparametric force transducer has superior performances such as:

- linear working characteristic (force – frequency),
- high sensitivity (up to 1 kHz/ μm),
- lack of inertia (measurement possibilities in dynamic conditions),
- utilization of digital technique for measurement, display and recording.

A micromechanical pressure transducer is disclosed in Figure 4.12, in which a capacitive transducer structure is integrated with an inductor coil to form a LC tank circuit [4.22], the resonance frequency of which may be remotely detected by imposing an electromagnetic field on the transducer.

The capacitive transducer structure comprises a conductive movable diaphragm, a fixed counter electrode, and a predetermined air gap between said diaphragm and electrode.

The diaphragm deflects in response to an applied pressure, leading to a change of capacitance in the structure and hence a shift of resonance frequency of the LC tank circuit.

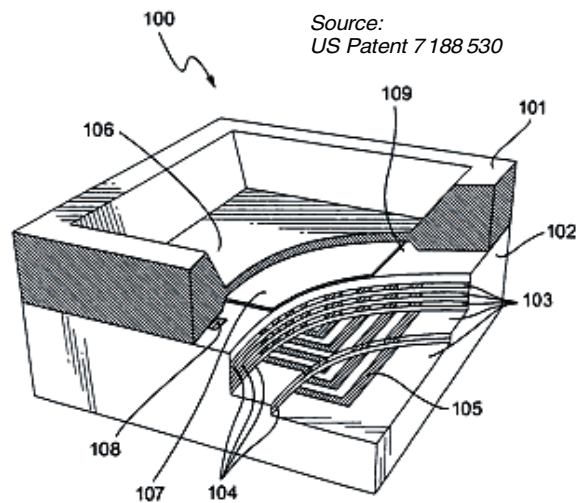


Fig. 4. 12 Micro-mechanical inductive-capacitive transducer for relative or absolute pressure sensing

The resonance frequency of the LC circuit can be remotely detected by measuring and determining the corresponding peak in the force transducer electromagnetic impedance.

REFERENCES

1. Tumanski, S.: Induction coil sensors – a review. *Measurement and Science Technology* 18, R31–R46 (2007)
2. Kueng, A., Meli, F., Thalmann, R.: Ultraprecision micro-CMM using a low force 3D touch probe. *Meas. Sci. Technol.* 18, 319–327 (2007)
3. Platil, A.: Mechatronics sensors. PPT-02-position-b-bw on Internet (Created on November 10, 2004)
4. Fraden, J.: *AIP Handbook of Modern Sensors – Physics, Design and Applications*. American Institute of Physics, New York (1993)
5. Wieringa, H.: Electrical force measuring transducers. In: *Proc. Symposium Force, Pressure, Displacement and Flow Sensors*, Twente University of Technology, Enschede, The Netherlands, May 13-14, pp. 179–197 (1982)
6. Herceg, E.E.: *Handbook of Measurement and Control (An authoritative treatise on the theory and application of the LVDT)*. Schaevitz Engng., Pennsauken, NJ (March 1989)
7. Cuscó, L.(Coord.): *Guide to the Measurement of Pressure and Vacuum*. The Institute of Measurement and Control, London, UK (published 1998); ISBN 0-904457-29-X
8. High pressure and chemically resistant LVDTs enhance performance of extensometers used to monitor structural integrity of off-shore platforms. *Product News: Macro Sensors*, Pennsauken, NJ. *Sensors & Transducers e-Digest*, 101(2) (February 2009); ISSN 1726-5479
9. Hjelmgren, J.: Dynamic measurement of force – a literature survey. Swedish National Testing and Research Institute, SP Report 27 (2002); ISBN 91-7848-918-0
10. Ștefănescu, D.M., Ion, I.: Force and torque measurement at the farm equipment for thick plants cutting. In: *Proceedings XIIth IMEKO Conference on Mass and Force Measurement for Improving the Efficiency*, Szeged, Hungary, September 4-7, pp. 49–52 (1990)
11. Bădescu, G., Ștefănescu, D.M.: Installation for determining the elastic constants of rocks. *Studii și cercetări de mecanică aplicată*, Tom 40(3), 451–466 (1981) (in Romanian)
12. Lam, K.H., Chen, Z.H., Ni, Y.Q., Chan, H.L.W.: A magnetorheological damper capable of force and displacement sensing. *Sensors and Actuators A: Physical* 158(1), 51–59 (2010)
13. Prabakar, K., Usharani, R., Jayapandian, J.: Wireless pressure sensor using non-contact differential variable reluctance transducer. *Sensors and Transducers* 99(12), 102–108 (2008)
14. Norton, H.N.: *Handbook of Transducers for Electronic Measuring Systems*. Prentice Hall, Inc., Englewood Cliffs (1969)

15. Ionescu, G., Dobrescu, R., Droașcă, B., Guțu, A., Hohan, I.: Transducers for Industrial Automatization, vol. I, ch. 10.4.3, Force and Torque Inductive Transducers, Editura Tehnică, București (1988) (in Romanian)
16. Fast response force transducers for measurement of tensile, compressive or alternating forces. Schlumberger Instruments et Systems, Velizy – Villacoublay, France, Catalog CD0272E/1/10/71
17. Peshkin, M.: Mutual inductance force sensor. Technology Transfer Program NU 20084, Northwestern University, Chicago, IL (April 2007)
18. Schoenekess, H.C., Ricken, W., Liu, J.-G., Becker, W.-J.: Eddy-current sensors and their applications to force and stress measurement in steel reinforced concrete. VDI-Berichte Nr. 1685, pp. 129-134 (2002)
19. Caruso, M.J., Bratland, T., Smith, C.H., Schneider, R.: A new perspective on magnetic field sensing. Bulletin 5/98
20. http://www.physics.uwa.edu.au/_data/page/41376/Fields_and_Magnets_notes.pdf (May 9, 2006)
21. Racoveanu, N., Dumitrescu, I., Tertîșco, M.: Dynamometer with digital read-out for deep pumping wells. Automatica și Electronica 9(5), 212–217 (1965) (in Romanian)
22. Pedersen, M., Ozgur, M., Huff, M.A.: Micro-mechanical capacitive-inductive sensor for detection of relative or absolute pressure. US Patent 7188530 (March 13, 2007)

Chapter 5

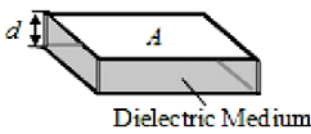
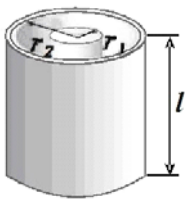
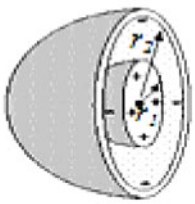
CAPACITIVE FORCE TRANSDUCERS

Resistive and capacitive transducers are the most spread in force measurements. Following some estimations, more than 30 % of modern transducers are direct or indirect applications of the RC sensing principles [5.1]. Capacitive transducers are the most precise of all electrical ones and are known for their extremely high sensitivity and resolution, large bandwidth, robustness, stability, and drift-free measurement capability. They can be used in severe environments (high temperature, magnetic fields, and radiation) as well as in various non-contact or nonintrusive applications.

5.1. CAPACITIVE FORCE TRANSDUCERS CLASSIFICATION

At the heart of any capacitive-sensing system is a capacitor (formerly named condenser). Capacitors are available in three configurations: flat (parallel), cylindrical (coaxial), and spherical (concentric), as shown in Table 5.1.

Table 5.1 Fundamental types of capacitive force transducers (CFTs)

Type	Flat Parallel	Cylindrical Coaxial	Spherical Concentric
Layout	 <p>Dielectric Medium</p>		
Formula	$C = \frac{\epsilon_r \cdot \epsilon_0 \cdot A}{d}$	$C = \frac{2\pi \epsilon_r \cdot \epsilon_0 \cdot l}{\ln(r_2 / r_1)}$	$C = \frac{4\pi \epsilon_r \cdot \epsilon_0 \cdot r_1 \cdot r_2}{r_2 - r_1}$

ϵ_r is the relative permittivity of the medium between the electrodes while ϵ_0 is the vacuum permittivity; the rest are geometric factors. Varying any of these parameters will change the capacitance, which then can be accurately measured and thus defines the operating principle of capacitive transducers.

All capacitive transducers fall into one of these three design classifications, with the flat and cylindrical being the most commonly used forms and presented in separate subchapters.

Spherical capacitive transducers are not as popular as the parallel or cylindrical configurations. This is largely due to the spherical design's complexity and higher manufacturing cost. However, the spherical geometry does provide several unique features, that neither flat-plate nor coaxial capacitors have, such as higher capacitance within a limited or compact space, a shape that is more readily adaptable to measure irregular surfaces, spherical equipotentials, and wider bandwidth.

A spherical capacitor provides the ideal shape for generating a nonlinear electric field gradient between its central electrode and its inner surface. This unique feature was utilized by scientists at NASA (National Aeronautics & Space Administration) to create the geophysical fluid flow cell. This cell uses spherical capacitors to simulate gravitational field conditions for studying the behavior of fluids. By applying an electric field across a spherical capacitor filled with a dielectric liquid, a body force analogous to gravity is generated around the fluid. The force acts as a buoyant having the magnitude proportional to the local temperature of the fluid and in a radial direction perpendicular to the spherical surface.

5.2. CAPACITIVE FORCE TRANSDUCERS (CFTs) WITH PLATES

The most usual types of capacitive force transducers with plates are presented in Table 5.2, together with their layouts, formulas and graphs of capacity versus linear or angular displacement [5.2]. Here S is the plate's area.

5.2.1. CFT with variable thickness of the dielectric pad

The contact force sensor for artificial hands with a digital interface for a controller [5.3] consists simply of two parallel plates separated by an elastic material that also acts as a dielectric (Fig. 5.1a). This prosthetic force sensor up to 100 N has a small size (an area less than 100 mm²) and is thin in depth for mounting on fingers and palm.

Applying a force across the plates increases the capacitance. The material between the two plates should deform sufficiently under low loads, in an ideal elastic (without hysteresis) and repeatable manner. Disc springs (or Belleville washers) are ideal devices for high loads in small spaces.

Table 5.2 Main types of capacitive force transducers (CFTs) with plates

Type	Layout	Formula	Graph
Variable air gap		$\frac{\Delta C}{\Delta d} = -\frac{C}{d} \left(1 - \frac{\Delta d}{d}\right)$	
Variable differential air gap		$\frac{\Delta C}{\Delta d} = -\frac{C}{d} \left[1 + 2 \left(\frac{\Delta d}{d}\right)^2\right]$	
Variable thickness of dielectric pad		$C = \frac{\epsilon_1 S}{d_0 - d_1(x) \left(1 - \frac{\epsilon_1}{\epsilon_2}\right)}$	
Angular variable overlapping		$C = \epsilon \frac{S(\alpha)}{d}$	

Linking the change in force applied across the plates to a change in either S , d or ϵ_r , through a suitable dielectric (e.g. elastomer) creates a transducer (Fig. 5.1a) whose capacitance varies as the inverse function of force. A convenient method to convert this capacitive change into a signal is to use a relaxation oscillator, like in Figure 5.1b, reprinted with permission of IOP from [5.3].

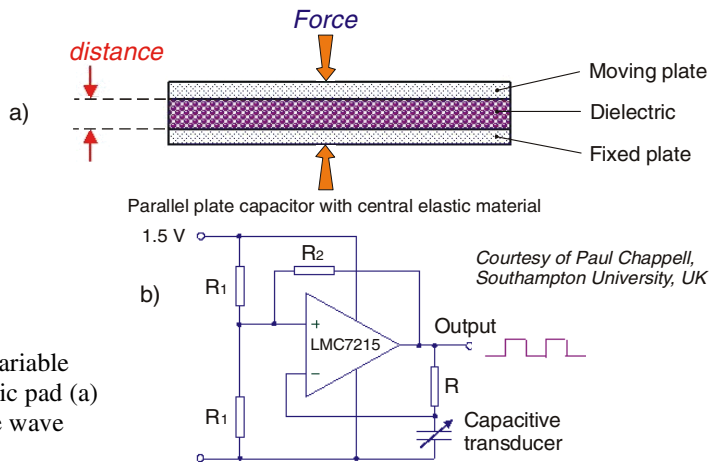


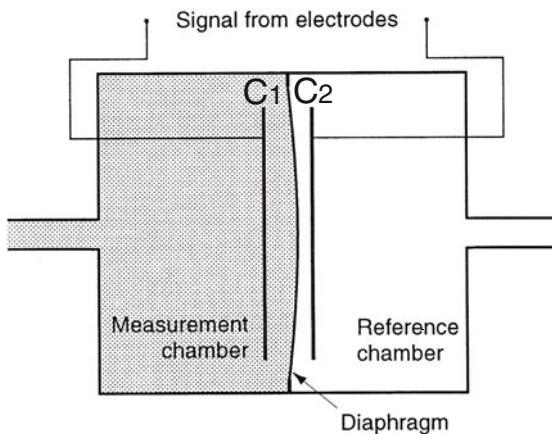
Fig. 5.1 CFT with variable thickness of dielectric pad (a) and associate square wave oscillator (b)

Capacitive transducer designs based on variation of the dielectric constant are often found in force or pressure, humidity, chemical-substance, and biocell sensing applications. For example, the transducer developed by ONERA French Aerospace Lab. detects a change in relative permittivity of the dielectric ϵ_r between two electrodes when a force or pressure is exerted on the plates; it is a very thin transducer (80 μm) and can measure micropressures. Advantages of such pellicular transducers are their compactness, resistance to vibration, and high bandwidth (50...200) kHz but they are temperature sensitive.

5.2.2. CFT with variable distance between plates

Capacitive techniques are used in conjunction with a diaphragm which may form one plate of a capacitor, with the pressure containing cover the other plate [5.4]. The symmetrical design shown in Figure 5.2 provides a more linear relationship between pressure and electrical output and easily measures differential pressures. To measure absolute pressures the reference chamber is evacuated. The metallized diaphragm and the two electrodes form two capacitors which are incorporated into an AC bridge circuit. When a pressure is applied to one side of the diaphragm, the diaphragm deflects, changing the values of the capacitances C_1 and C_2 .

For small or differential pressures or accelerations the electrostatic force compensation principle is useful, the deformable parallel-plate capacitor acting both as sensing element and as deflection-restoring electrostatic system [5.5]. The main technological problem is the design of a sufficiently high-compliance capacitive transducer, based on a thin CuBe membrane (25 μm) with well-defined tension and fixed between two outer rigid electrodes [5.6].



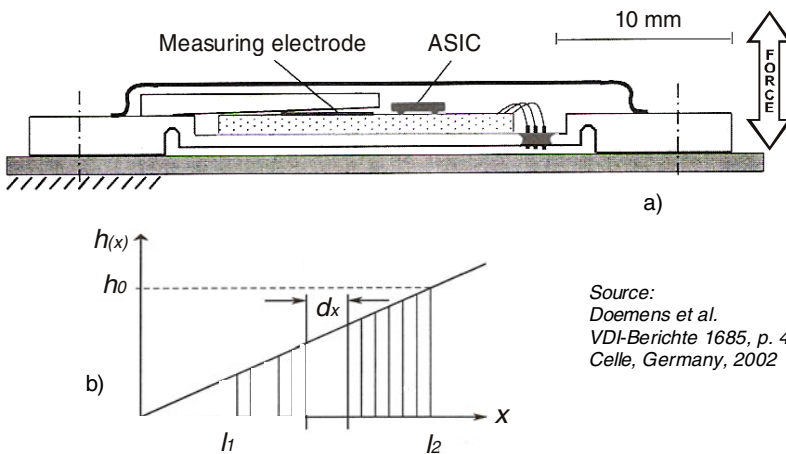
Courtesy of The Institute of
Measurement and Control,
London, Copyright 1998

Fig. 5.2 Capacitance manometer (diaphragm gauge)

5.2.3. CFT with plates arranged under a certain angle

The measurement of force and torque is primarily based on the acquisition of the mechanical strain occurring as deflection or elongation of the stressed unit or as torsion of a shaft. In the range of nominal load these deformations usually are in the range of a few microns. For a precise transformation of this extremely small mechanical measurand in an electrical signal the application of capacitive techniques is advisable using the variation of the distance between the capacitor electrodes [5.7]. The principle of measurement is based on the mechanical acquisition of the distortion between two points in a specified distance and the transformation into a corresponding modification of the gap between the electrodes and the angle, respectively. The design of the capacitor itself can be performed in different ways. Within a former development the capacitor was consisting of two planar combs providing a high output capacitance due to number of parallel electrode pairs. The torsional displacement resulted in a variation of the air gap and thus in a change of the capacitance. Due to technological and functional reasons the transducer principle has been simplified by the application of two electrodes which are arranged under a certain angle (Fig. 5.3a).

Depending on the applied load the angle between the two electrodes is changing and causes an alteration of the transducer's capacitance. The value of the capacitance can be calculated by the integral of the incremental capacitances of the corresponding distances between the electrodes (Fig. 5.3b). By theory, the calculated capacitance is reciprocally proportional to the applied force or torque, respectively.



Source:
Doemens et al.
VDI-Berichte 1685, p. 412
Celle, Germany, 2002



Fig. 5.3 Capacitive force transducer with a certain angle between its plates (a) and the capacitance dependence on the “angular plate” dimensions: l – length and h – height (b)

5.3. MULTIPLE PLATES CAPACITIVE FORCE TRANSDUCERS

A new type of dynamometer, composed of three separate sensitive elements, and designed to work in hostile atmosphere has been developed [5.8]. The device can simultaneous monitor the weight variations of three composite-material specimens, exposed to hygro-thermal cycling within a temperature range from 250 to 330 K and a humidity range from 0 to 95 %. The particular application concerns a high dimensional stability structure designed by Alenia Spazio (as a support of an onboard ultra-violet spectrograph of the artificial satellite SOHO) within a joint international program of research on the Sun.

In principle, the device is based on the elastic deflection of a cantilever beam. The free end of the beam, whose deflection is proportional to the suspended weight, determines the difference between two electrical capacitances formed by the beam itself with two fixed electrodes faced to it. If the two capacitances (upper and lower) are the comparison arms of a transformer bridge, the unbalance signal of the bridge, conveniently converted into a DC signal, can be considered as the output of a weight-to-voltage transducer.

The multiple dynamometer (Fig. 5.4a) consists of three cantilever beams symmetrically arranged at 120° and sandwiched between two glass plates. This arrangement allows to measure at the same time several samples, also if irregularly shaped. The dynamometer can be held stable with only one fixed point.

The three elastic elements (item 1) are surrounded by an electrostatic shield (item 2) and they are connected by means of thin grooved strips to the common annular body. In this central area the mobile part is clamped between the two glasses by means of spacers made in zerodur, 100 μm and 300 μm thick. By choosing the proper spacers thickness it is possible to have the three elastic beams exactly halfway between the upper and lower glass plates, when the specimens under test are hung to the mobile ends of the dynamometer. The metal used for the beams and shield was cut and worked from the same sheet of a Ni-Cu alloy (Monel), that was chosen because of its nearly temperature-independent elastic modulus in the considered temperature range. The two glass plates (item 3) that clamp the cantilever beams and its rim, are made in zerodur (the same material used for the spacers), a glass-ceramic typically used for precision optical components. On the areas facing upward and downward the free ends of the beams, the fixed electrodes of the capacitive transducers are made by thin-film technique.

In order to ensure the best measurements repeatability and accuracy, the dynamometer is kept in a compact copper mounting frame that gives thermal uniformity and good electrical shielding to the device (Fig. 5.4b).

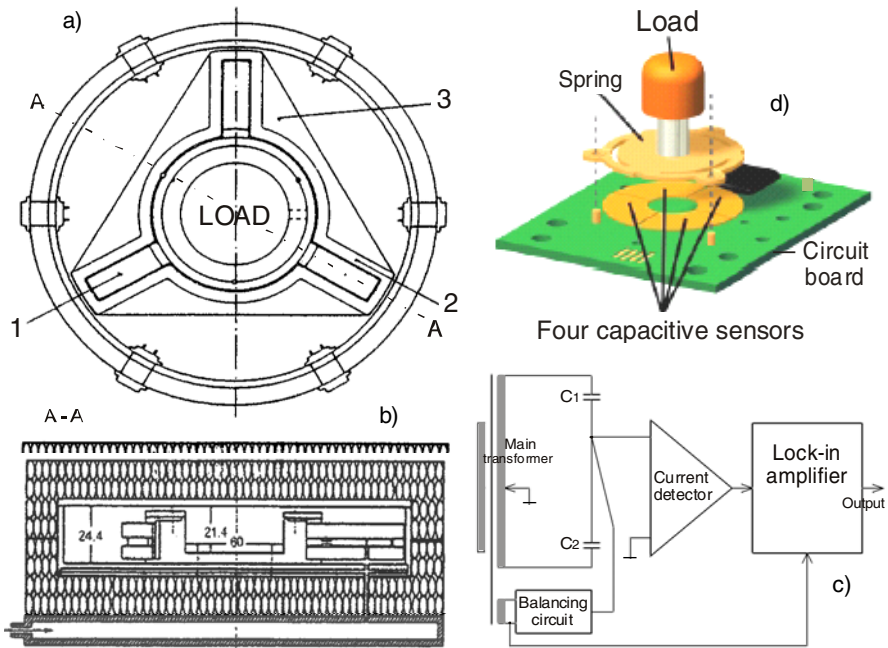


Fig. 5.4 Multiple dynamometer (three cantilever beams), presented at IMEKO, Turin, 1994: a) top view, b) cross section. c) Measurement scheme with transformer bridge and lock-in amplifier. d) CFT “joystick” with four circular sectors of parallel plates.

The monel beam and the faced electrodes on the two triangular plates of each dynamometer form a differential couple of plane-parallel capacitors whose capacitance difference varies as a function of deflection. The differential configuration has several advantages:

- nearly insensitive to dimensional variations of the elastic cantilever beams,
- a doubled sensitivity,
- partial linearization of the nonlinear dependence of the characteristic displacement vs. capacitance.

Each of the three differential capacitive transducers constitutes the comparison arms of a transformer bridge, the triangular symmetry being related to the electronic signal processing. For small changes of the specimens mass each dynamometer beam changes its position as a linear function of mass variations. The consequent capacitance variation forces the AC transformer bridge, which forms the measuring system, to deviate from its original balance condition. The current signal, which is rising from capacitances variation and is proportional to it, is converted into a voltage signal by a transconductance pre-amplifier and is measured by means of a synchronous detector (Fig. 5.4c).

Other example when capacitance between two metal plates is changed with the distance between them is presented in [5.9]. Force can be measured if the metal plates are connected to an elastic element. This idea is applied in some miniaturized force transducers as the one in Figure 5.4d, having four pairs of “circular sector” plates.

5.4. INTERDIGITATED AND MATRIX OF CAPACITIVE SENSORS

5.4.1. CFT with interdigitated electrodes

A surface micromachine chip is stiffly mounted to a rod under load (or a torsionally deformed shaft) the same way as resistive strain gauges are applied. The transducer consists of freestanding interdigitated electrodes which form a variable capacitor changing its capacitance in accordance to an applied force or torque [5.10]. The connected side of the combs is anchored to the substrate (Fig. 5.5a) and thus a shear-deformation of the substrate caused the fingers to change their relative position to the substrate (Fig. 5.5b). So the capacitance between two combs changes according to the shear deformation of the test body. Regarding a little piece of an element, like that in Figure 5.5c, a relation between the main strain direction σ_1 , σ_2 and the strain in a rotated coordinate system σ_φ , τ_φ can be found:

$$\sigma_\varphi = \frac{\sigma_1 + \sigma_2}{2} + \frac{\sigma_1 - \sigma_2}{2} \cdot \cos(2\varphi) \tag{5.1}$$

$$\tau_\varphi = \frac{\sigma_1 - \sigma_2}{2} \cdot \sin(2\varphi) \tag{5.2}$$

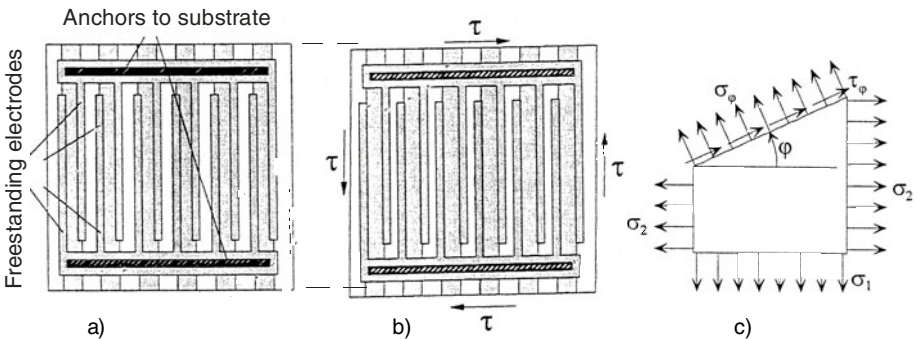


Fig. 5.5 Capacitive change of freestanding interdigitated combfingers (a) due to shear deformation (b) and shear and strain relationship (c)

From the last equation it can be seen that shear stress reaches its maximum for $\varphi = 45^\circ$. If additionally $\sigma_2 = -\sigma_1$, there is only shear stress, no strain, within this plane.

Usually the sensitivity for piezoresistive strain gauges is described by a k -factor which gives the proportionality between strain and relative change of resistance. In a similar way a K_C -factor for a change of capacitance is defined:

$$K_C = \frac{\Delta C / C}{\varepsilon} = \dots = \frac{l \cdot (1 + \nu)}{d} \quad (5.3)$$

where l and h are the geometric parameters of a combfinger, d is the distance between two combfingers and ν is the Poisson's coefficient.

These formulas are valid for a single axis strain state and the sensing structure being mounted in a way that its combfingers are in a 45° -angle towards the main strain direction (maximum shear stress).

A variable capacitance type transducer is designed to measure the penetration force during intracytoplasmic sperm injection of egg cells for artificial fertilization as well as for other biomedical applications in the force range $(1 \dots 500) \mu\text{N}$ [5.11].

The MEMS based transducer measures triaxial forces using a system of flexible beams subjected to bending and torsion, combined with ten interdigitated (combfinger) capacitors (Fig. 5.6). The force versus displacement characteristic of the transducer can be fully described by a 6×6 positive definite stiffness matrix.

A quantitative model of the transducer behavior was derived and simulated using MATLAB. It has been demonstrated analytically that using nonsymmetric electrode placement, one can minimize the cross talk between the x and y displacement modes. The process is relatively simple and allows for easy modification of the force range.

Source: Enikov & Nelson
University of Minnesota

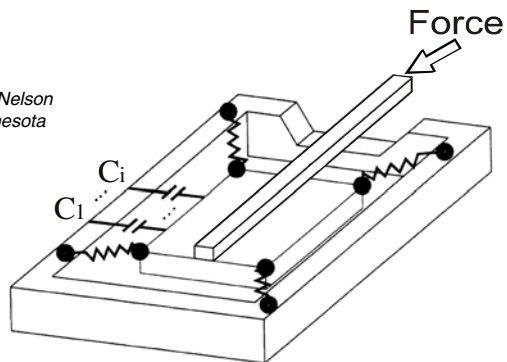


Fig. 5.6 Ten interdigitated capacitors for measuring triaxial forces in artificial fertilization

The strain sensing properties of interdigitated and sandwich thick film capacitors, using titanium dioxide as the dielectric and tunnelling as the dominant conduction mechanism, were investigated in [5.12]. The gauge factor, which demonstrates the devices sensitivity, was found by dividing the fractional change in capacitance by the applied strain. A gauge factor of 5 and 30 was recorded for interdigitated and sandwich capacitors, respectively.

5.4.2. CFT using a matrix of capacitive sensing elements

Monocrystalline silicon does not suffer from hysteresis and creep and therefore it is an ideal material for use in a load cell. To minimize the influence of non-homogeneous load distributions, it appears to be necessary to use an array of sensing elements evenly distributed over the transducer chip. An earlier design with 16 sensing elements resulted in an accuracy of 0.2 % of full scale [5.13].

The actual chip (Fig. 5.7: a – general view, b – cross section, c – bottom view) contains 10000 load bearing poles and capacitor poles [5.14]. It appears that the error is less than 0.03 % if at least 25 groups of capacitors are measured individually (each consisting of 400 capacitors connected in parallel).

The top-wafer contains poles which bear the load. The bottom-wafer contains an electrode pattern forming an array of capacitors with the top wafer as a common electrode. On application of a load the poles will be compressed and the distance between the metallic electrodes and the top-wafer will decrease thereby increasing the capacitance.

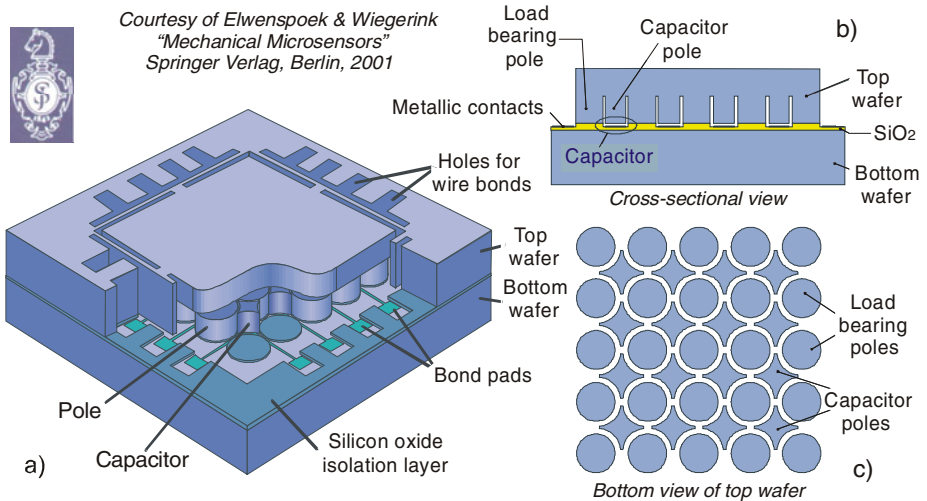


Fig. 5.7 Array of small capacitors distributed over the entire chip (a), cross-section of the distributed capacitive load cell (b) and bottom view of its top wafer (c)

5.5. CYLINDRICAL CAPACITIVE FORCE TRANSDUCERS

The coaxial configuration is the second most popular design in capacitive transducers. A simple displacement transducer can be easily built using a cylindrical capacitor if the inner conductor can be moved in and out of the outer conductor. The capacitance of such a transducer is in a linear relationship with the displacement l . Besides the resistive or inductive ones, the differential capacitive transducers are used for a large range of applications [5.15]. There are specialized companies such as Eilersen (Denmark) which produce high performance capacitive force transducers.

The cylindrical capacitor is easier to be achieved and has a lateral sensitivity twice less than the one with plane plates [5.16]. The sensitivity S of the round electrodes is about two times higher than the sensitivity of the flat electrodes, and the change in the sensitivity $\Delta S/S$ as a result of small capsule displacement in high-speed precision weighing of pharmaceutical capsules is one order of magnitude higher for the round electrodes [5.17].

The capacitance formula for a tubular capacitor is shown in Figure 5.8a, in which ϵ_r represents the relative permittivity (2.3 for the ANG 10 liquid), D – the internal diameter of the external tube (98 mm), d – the external diameter of the internal tube (96 mm), l – the overlapping length of the two mountings.

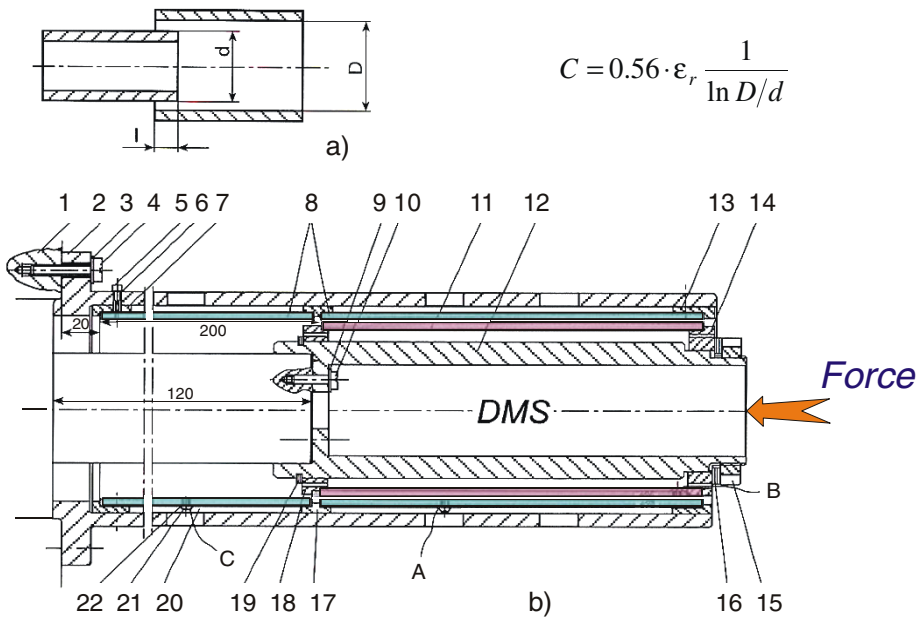


Fig. 5.8 Schematic representation of a tubular capacitive transducer (a) and differential capacitive transducer for measuring the fluid compressibility (b)

The capacitive transducer is based on the variation of one of the quantities in the above formula, the length in this case, that is the overlapping surface. Turicin underlines the tendency of diminishing the distance between the tubular mountings to increase the sensitivity and linearity, the limitation being given by the breakthrough voltage.

The differential variant sensibly reduces the errors and improves the linearity. The differential capacitor is connected in the bridge to a carrier frequency amplifier operating in unbalance state, a signal proportional to the motion being obtained at the output, which is the piston stroke from the fluid compression chamber having the already-known initial volume. One of the half-bridge is located under pressure at the entrance and the other outside (eventually also in a oil bath but not under pressure). Unlike the differential capacitive transducer HITEC, used for measuring the specific deformations of the Boeing aviation structures [5.18], at which the excitation tubular mountings are located inside and the sensitive ring outside, in our application, because some functional and available space reasons, the final choice is the version with an inside gliding cylinder. We have to use an accurate technological processing (unitary boring H7/h6) and a tidy electrical installation with screened wires, insulated passages through the recipient wall and floating exits, to reduce parasitic capacitances as possible. The maximum sensitivity is obtained when the bridge is symmetrical to both diagonals (for supply and measurement).

The constructive solution, depicted in Figure 5.8b, includes the following items: 1 – basic pad, 2 – box, 3 and 9 – washers, 4, 5, 10, 21 – screws, 6 – insulating element, 7 – insulating guide I, 8 – external electrode, 11 – internal electrode, 12 – gliding element, 13 – insulating guide II, 14 – insulating body I, 15 – special nut, 16 – spacer, 17 – insulating guide III, 18 – insulating body II, 19 – safety ring, 20 – electrical connection wire, 22 – connection washer for electronic bonding.

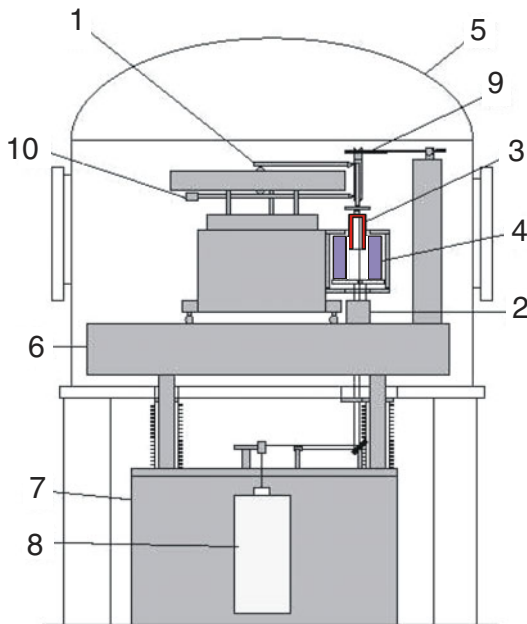
The 1 mm resolution for a usable motion of the 200 mm piston provides 0.5 % accuracy, sufficient to determine the fluid compressibility coefficient.

The American NIST (National Institute of Standards and Technology) has a primary standard of small force (micronewton level) traceable to the International System of Units (SI) [5.19]. They have constructed a series of increasingly refined systems to achieve force using an arrangement of coaxial cylindrical capacitors.

The balance (Fig. 5.9) has been assembled on a custom optical table in a specially designed free standing vacuum chamber (approximately 1 meter in diameter). Functionally, the EFB consists of an electrostatic force generator that acts along a vertical axis (z-direction) aligned to the local gravity to within a few milliradians. Forces are generated when voltages are applied to the pair of nested, coaxial hollow cylinders (items 3 and 4). The outer high voltage cylinder is fixed while the inner electrically grounded cylinder is free

to translate along the z-axis, varying the degree of overlap. The capacitance of this geometry is in principle a linear function of the overlap of the two cylinders. For a perfectly coaxial arrangement, the in-plane capacitance gradient possesses radial symmetry so that the resulting electrical force is directed solely along the z-axis. To define this axis of symmetry, the inner cylinder is suspended from a counterbalanced parallelogram linkage (item 1) that employs a series of crossed-flexure pivots.

The NIST electrostatic force balance generates electrical forces, F_e , in response to loads along the balance axis. Weighings and force comparisons are accomplished by controlling the voltage on the main electrodes to maintain the null position of the balance. They use a proportional integral-derivative (PID) servocontroller implemented on a dedicated processor in a separate chassis, with high-level operator control through an ordinary PC. For typical balance operation, a mechanical imbalance is imposed on the counterweight side which is countered by an electrostatic force applied by the controller to maintain null as measured by the interferometer (item 2). Therefore, the measurement standard of microforce would be traceable to the primary standards of length and voltage instead of the mechanical artifact for the SI mass unit.



Source: Pratt & Kramar
NIST - 2006

Components:

- 1 - Parallelogram balance
- 2 - Differential plane mirror interferometer
- 3 - Main inner electrode
- 4 - Main outer electrode
- 5 - Vacuum chamber
- 6 - Optical table
- 7 - Granite foundation block
- 8 - Heterodyne laser light source
- 9 - Mass lift
- 10 - Counterweight

Fig. 5.9 The American primary microforce standard based on the principle of electrostatic force balance (EFB – NIST)

5.6. APPLICATIONS BASED ON ELECTROSTATIC FORCES

5.6.1. Electrostatic force balances

For most current semiconductor sensors the actuating force is generated electrostatically [5.20]. An implementation of the force feedback circuit is shown in Figure 5.10. The movable microstructure forms one plate MP of two variable capacitors C_1 and C_2 , while two fixed plates FP-1 and FP-2 form the other two plates of these capacitors. Plates FP are controlled with drive signals V_D , and the signal induced on plate MP is buffered by a high-impedance circuit. When MP is in its neutral position, we have $C_1 = C_2$ and no signal is generated. As MP moves in response to the parameter of interest (i.e. force F), the charge induced on it is non-zero and a signal is created being proportional to the differential charge in the C_1 - C_2 capacitor pair. This signal is filtered and amplified to generate the signal V_0 which is fed back to MP through an isolation buffer stage, to relocate the central plate to its neutral position in this “differential” capacitor.

The Mass and Force Group, Division of Physical Metrology within KRISS, Republic of Korea uses a nano force calibrator (NFC), which consists of a microbalance that measure the force and a piezoelectric actuator that displaces the cantilever whose displacement is measured using its internal capacitive feedback transducer [5.21].

A disc-pendulum with electrostatic stiffness reduction allows a quasi-static force to be measured in a range $< 10^{-5}$ N with 10^{-12} N force resolution. The functional diagram, presented in Figure 5.11, is based on a conductive disc-pendulum arranged between two external parallel plates with which the conductive disc-pendulum forms two parallel-plate capacitors [5.22].

Application of electric voltages on the capacitors allows the stiffness of the pendulum to be adjusted. The horizontal forces to be measured cause a deflection of the disc-pendulum which is compensated with the aid of a servo-system composed of interferometric deflection measurement and electrostatic counterforce generation. This principle offers an especially large range for stiffness adjustment only by varying the electric voltage on the capacitor plates.

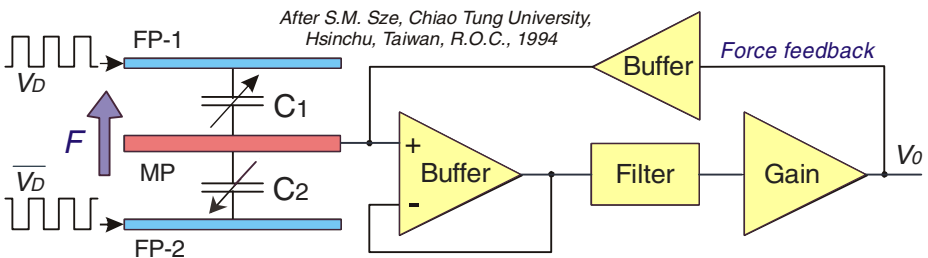
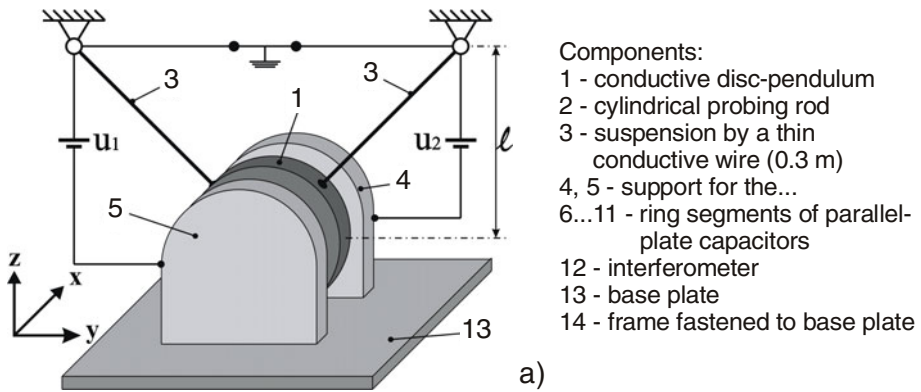
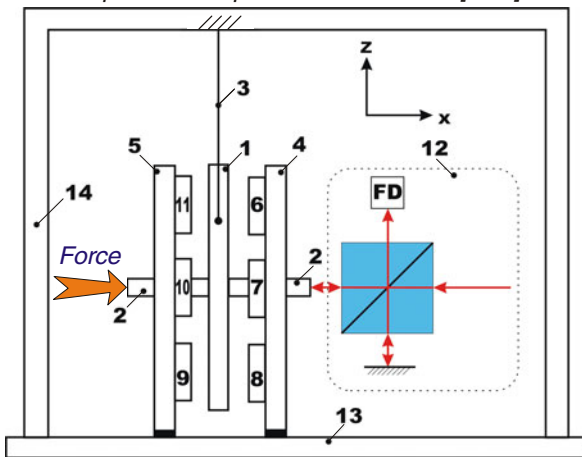


Fig. 5.10 Electrostatic force feedback application in a differential solid-state transducer



Reprinted with permission IOP from [5.22]



Courtesy of
Vladimir Nesterov
PTB

Fig. 5.11 Functional diagram for very small quasi-static force measurement (a) and schematic side view of the PTB experimental set-up with parallel-plate capacitors (b)

The principal disturbance variable of the new nanoforce measuring device is the seismic noise. To reduce this influence, two identical disc-pendulums were used: a measuring pendulum and a reference one [5.23]. The latter serves to measure and eliminate the seismic variations and the thermal drift. The complete set-up stands on a pneumatically damped optical table with active inclination stabilization. A large pendulum having the mass $m = 200$ kg, which can be deflected with the aid of a nano-positioning device, acts as an adjusting element of the control device. Without inclination stabilization, the variation of the table position in pendulum direction amounts to 1×10^{-6} rad/h, while with inclination stabilization, this value is reduced to 1×10^{-8} rad/h, and it is sufficient for the measurement of nanoforces.

A first force measurement to determine the resolution has been performed with a stiffness reduction to 0.003 N/m. With a measuring duration of 100 s, force resolution was < 0.1 nN. Therefore, a first proof of the efficiency of this measuring principle has been furnished. There are increasing expectations of an attainable force resolution of 1 pN combining the force calculated from the optical power of a laser with the reflection factor of the disc-pendulum based on electrostatic force compensation [5.24].

In the Center for Measurement Standards from Hsinchu, Taiwan two force-generation mechanisms, namely the electrostatic force by the capacitive actuation unit and the optical force from the radiation pressure, were designed and calibrated by means of the gravitational force [5.25].

5.6.2. Other applications of electrostatic forces for the measurement of mechanical quantities

Microtubules are polymers of tubulin subunits arranged on a hexagonal lattice. Each tubulin dimer is modeled as an electrical dipole coupled to its neighbors by electrostatic forces. Mechanical forces that act on the microtubule affect the distances between the dimers and alter the electrostatic potential. So, the microtubules can be used as mechanical force sensors; they can detect the force directions and magnitudes in various biomedical applications [5.26].

A high-resolution load-displacement transducer for nanoindentation was developed based on a capacitive-plate configuration [5.27]. The transducer applies a force via electrostatic actuation and senses displacement via monitoring the change in capacitance. The external applied load on the transducer is measured as the difference between the electrostatic force and the spring force induced by the displacement. The transducer has a *rms* load resolution of 3 nN when it is tested in a reduced vibration environment, and 10 to 20 nN when is directly attached to a multimode AFM (atomic force microscopy) for performing *in situ* nanoindentation and adhesion (pull-off) force measurements. The high resolution of the transducer enables the observations of clear loading-unloading curves in the sub-10-nm nano-indentation and “jump-on” phenomena in pull-off force measurements, being superior to other commercially available transducers.

A transducer designed to be used with an electrostatic film motor that features mechanical flexibility, but can also be used as an independent transducer, is presented in [5.28]. It employs three-phase electrodes both in sliding and stationary parts and estimates displacement and bending from the change of the capacitance between the electrodes. The paper describes an equivalent capacitance-network model. Based on this model, sensing principles for both displacement and bending are experimentally verified using a prototype, proving little interference between them.

A vertical array of Faraday pail sensors was developed to partially separate bipolar charged polydisperse powder and measure the charge-to-mass ratio of powders deposited in each Faraday pail using an electrometer to evaluate the electrostatic field [5.29].

At the Department of Electrical and Computer Engineering, University of Manitoba, Canada, an electric field transducer was made which uses a micromachined microspring supported membrane as the sensing element [5.30]. The sensing mechanism involves electrostatic force to deflect the membrane, and an optical position transducer to measure its movement. Measurement resolution was 5 kV/m for a DC field and 140 V/m for a 49 Hz AC field. It is shown that a bias voltage applied to the membrane can be used to increase measurement sensitivity. With a 17 kV/m DC bias field, a 0.3 V/m AC field at 97 Hz was detectable.

The force generated by a spark discharge in a pin-to-plate system has been investigated in [5.31]. It is difficult to measure the force directly over a short sparking period. Axial vibration was observed for the pin electrode supported flexibly by a cantilever to the axial direction at the spark discharge that occurred periodically. The force was implicitly calculated in the case that the calculated vibration agreed with the measured. The result indicated that the force was very small, almost 0 N, during the spark period. The vibration was generated not by the force at the spark discharge but by alternative of the Coulomb force at the period of no discharge and reaction force due to the ionic wind at the Corona discharge.

5.7. ELECTRONIC CIRCUITS FOR CAPACITIVE TRANSDUCERS

Capacitive transducers are traditionally divided into two basic classifications: *passive* or *active*, based on whether or not there are any electronic components within the transducer [5.1]:

- *Passive transducers* do not have any internal electronics, thus minimizing guard size. They have some significant advantages: greater flexibility in probe configuration, more stable and cost less than active systems. Their disadvantages include lower bandwidth and lower drive frequency, which makes them unsuitable for some applications.
- *Active transducers* have electronics, usually a small circuit board, packaged inside them. Active transducers operate at much higher frequencies and bandwidths, and are particularly well suited to applications which may involve stray electrical noise on the target. Their disadvantages include higher costs and less configuration flexibility.

There exists a wide range of modern signal conditioning and measuring circuits for capacitive transducers [5.2]:

- *charge pumps* – for solid state devices (e.g. made by CMOS technology);
- *transformer bridges* (like in Figure 5.4c) – expensive and noncompatible with IC technologies;
- *oscillators*: a square wave RC generator was shown in Figure 5.1b, while a sinusoidal LC oscillator was depicted in Figure 4.11. An RF capacitive force transducer operates based on the modification of the distance between two electrodes; its capacitor is connected in parallel with a coil, forming together an oscillating circuit [5.32].
- *converters*: capacitance-to-frequency or capacitance-to-voltage (the capacitor presence in the feedback loop eliminates the frequency dependence). Analog Devices, Inc. has introduced a series of the high-precision, fully integrated converters that address the complex and difficult task of direct capacitance-to-digital conversion [5.33].

A new method for measuring displacement on the nanometer scale in a surface-force apparatus (SFA) (Fig. 5.12) is based on a capacitor included in an *oscillator*, followed by a high sensitivity *frequency-to-voltage converter* [5.34]. This method of capacitance measurement is low cost and does not require the use of a carrier frequency or a lock-in amplifier, without loss in resolution and dynamic performance.

When it is used in conjunction with the interferometer technique, this transducer can perform nanorheological determinations or measurements of contact forces between two surfaces, usually a sphere and a plane.

Loadstar Sensors Inc. of Mountain View, CA has launched a new line of products based on its patent protected capacitive sensing technology [5.35]. These new “direct meters” offer a large (0...5) V measurable output without the need for external signal conditioning equipment in a compact, rugged, stainless steel package. As the producer states: Just supply 5 V_{DC} power to the transducer and measure the DC output using a common digital multimeter! The small size and threaded mounting holes provided on the top and bottom of the transducers, make possible to mount them conveniently and fit them into tight spaces. In addition, their low power consumption (only 0.01 mW) makes them suitable for use with batteries. By comparison, the cost, size and complexity of conventional strain based resistive load cells make the latter more difficult to incorporate into various industrial applications.

A novel MEMS-based capacitive transducer for combined force and elasticity modulus measurements is presented in [5.36]. The proposed device can measure both the contact force and the stiffness of the object under contact. The sensing concept utilizes multiple silicon nitride membranes with varying stiffnesses; their relative deflection can be measured to calculate the stiffness or the elasticity modulus of the targeted object. These new MEMS capacitive transducers, having a (1 × 1) mm² square active sensing area, can discriminate

elasticity variation of polymer specimens with a resolution of 0.1 MPa over a range of (0.7...1.2) MPa. Their force sensing resolution is as small as 0.2 mN over a force range up to 0.5 N.

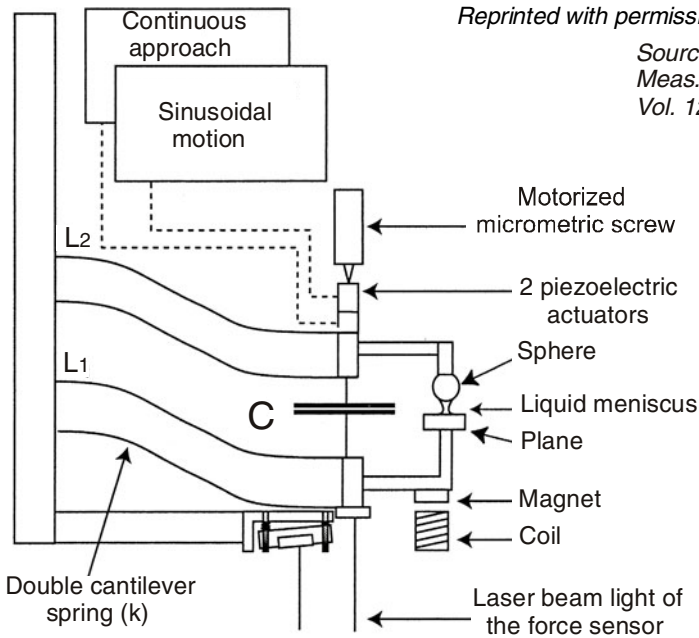


Fig. 5.12 The force spring bending deflection is measured with an interferometric transducer while the separation between the surfaces is capacitively sensed.

In conclusion: Advantages of capacitive transducers are their simple structures, high sensitivity and resolution, reduced temperature dependence, long-term stability, and durability. Some capacitive devices can achieve sub-nanometer position resolution (< 0.01 nm), having a bandwidth up to 100 kHz. Capacitive transducers can provide contact or noncontact measurement of various physical or chemical quantities representing force and related quantities: distance, proximity, acceleration, flow, pressure, separation, connected with various biocells, chemical substances and mechatronic devices.

REFERENCES

1. Du, W.Y., Yelich, S.W.: Resistive and capacitive based sensing technologies. *Sensors & Transducers Journal* 90, 100–116 (2008)
2. Platil, A.: *Mechatronics sensors: Measurement of position. position-c-bw.ppt*, November 11 (2004)

3. Chappell, P.H., Elliott, J.A.: Contact force sensor for artificial hands with a digital interface for a controller. *Measurement and Science Technology* 14, 1275–1279 (2003)
4. Cuscó, L. (Coord.): *Guide to the Measurement of Pressure and Vacuum*. The Institute of Measurement and Control, London, UK (Published 1998)
5. Bethe, K.: Dynamometrical sensors: (Many) problems (some) solutions. *Sensors and Actuators A: Physical* 26(1-3), 285–293 (1991)
6. Schucht, C.: Capacitive pressure transducer with electrostatic compensation of displacement. *VDI/VDE – Fachtagung Sensoren, VDI-Berichte No. 677*, p. 119, Bad Nauheim, F.R.G (1986)
7. Doemens, G., Spriegel, D., Wünsche, H.: Microsystem for capacitive force and torque measurement. *VDI-Berichte Nr. 1685*, pp. 411–415 (2002)
8. Cabiati, F., Nerino, R., Clari, F., Giaretto, V., Miraldi, E., Ruscica, G.: Multiple dynamometer for hostile atmosphere based on differential capacitive transducers. In: *Proc. XIIIth IMEKO World Congress, Turin, Italy, September 5-9, vol. III*, pp. 1899–1903 (1994)
9. Hjelmgren, J.: *Dynamic measurement of force – a literature survey*. Swedish National Testing and Research Institute, Boras, Sweden, SP Report 27 (2002); ISBN 91-7848-918-0
10. Meckes, A., Aigner, R., Dorfinger, G., Wachutka, G.: Capacitive silicon micro-sensor for force and torque measurement. In: *Int'l Conf. Transducers XI and Eurosensors XV, Munich, Germany, June 10-14, Paper 2A3.05* (2001)
11. Enikov, E.T., Nelson, B.J.: MEMS based single cell penetration force sensor. In: *SPIE Conf. Microrobotics and Microassembly, Boston, MA, vol. 3834*, pp. 40–46 (September 1999)
12. Arshak, A., Arshak, K., Morris, D., Korostynska, O., Jafer, E.: Investigation of TiO₂ thick film capacitors for use as strain gauge sensors. *Sensors and Actuators A: Physical* 122(2), 242–249 (2005)
13. Wiegerink, R., Mateman, R., Zwijsze, R., Krijnen, G., Lammerink, T., Elwenspoek, M.: Quasi monolithic silicon load cell for loads up to 1000 kg with distributed capacitive sensing. In: *Proc. 13th European Conf. on Solid-State Transducers, The Hague, The Netherlands, September 12-15*, pp. 545–546 (1999)
14. Elwenspoek, M., Wiegerink, R.: *Mechanical Microsensors*. Springer, Heidelberg (2001)
15. Pavlenko, V.A., et al.: Capacitive transducers in test equipment. In: *Proc. 3rd Conf. on Testing Equipment for Experimental Investigations of Mechanical Properties of Materials and Structures, Moscow, Soviet Union, October 9-14, vol. 1*, pp. 543–552 (1989)
16. Ștefănescu, D.M., Mănescu, T.: Differential capacitive transducer for measuring fluid compressibility. *Instrumentația VII(6)*, 24 (1998) (in Romanian)
17. Burmen, M., Pernus, F., Likar, B.: High-speed precision weighing of pharmaceutical capsules. *Meas. Sci. Technol.* 20, Paper 115203 (2009)

18. Procter, E., Strong, J.T.: Capacitance strain gauges. In: Window, A.L., Holister, G.S. (eds.) *Strain Gage Technology*. Elsevier Applied Science, London (reprinted 1989)
19. Pratt, J.R., Kramar, J.A.: SI realization of small forces using an electrostatic force balance. In: *CD Proc. XVIII IMEKO World Congress on Metrology for a Sustainable Development*, Rio de Janeiro, Brazil, September 17-22, Paper 109 (2006)
20. Sze, S.M.: *Semiconductor Sensors*. John Wiley & Sons, Inc., Chichester (1994)
21. Kim, M.-S., Choi, I.-M., Park, Y.-K., Choi, J.-H., Kim, J.-H.: Characterizing Atomic Force Microscope cantilevers using a precision balance. In: *Proc. Asia-Pacific Symp. Mass, Force and Torque (APMF 2005)*, Jeju Island, Korea, pp. 89–94 (2005)
22. Nesterov, V.: Facility and methods for the measurement of micro and nano forces in the range below 10^{-5} N with a resolution of 10^{-12} N (development concept). *Meas. Sci. Technol.* 18, 360–366 (2007)
23. Test of a new electrostatic nanoforce measuring principle. PTB, Micro- and Nanoforce Metrology, Internet, May 12 (2008)
24. Brand, U.: Measuring nano- and piconewtons. *PTB News – Metrology, Technology, Services, Cooperation*, p. 1, Bulletin 08.3
25. Chen, S.-J., Pan, S.-S.: Nanonewton force generation and detection based on a sensitive torsion pendulum. *IEEE Transactions on Instrumentation and Measurement* 58(4), 897–901 (2009)
26. Karafyllidis, I.G., Lagoudas, D.C.: Microtubules as mechanical force sensors. *BioSystems* 88(1-2), 137–146 (2007)
27. Yu, N., Bonin, W.A., Polycarpou, A.A.: High-resolution capacitive load-displacement transducer and its application in nanoindentation and adhesion force measurements. *Review of Scientific Instruments* 76 (April 2005)
28. Nishijima, T., Yamamoto, A., Higuchi, T.: A flexible sensor measuring displacement and bending. *Meas. Sci. Technol.* 20, Paper 045205 (2009)
29. Zhao, H., Castle, G.S.P., Inculeț, I.I.: The measurement of bipolar charge in polydisperse powders using a vertical array of Faraday pail sensors. *Journal of Electrostatics* 55, 261–278 (2002)
30. Roncin, A., Shafai, C., Swatek, D.R.: Electric field sensor using electrostatic force deflection of a micro-spring supported membrane. *Sensors and Actuators A: Physical* 123-124(C), 179–184 (2005)
31. Kawamoto, H., Umezu, S.: Force at spark discharge in pin-to-plate system. *Journal of Electrostatics* 65(2), 75–81 (2007)
32. Ionescu, G., Dobrescu, R., Droașcă, B., Guțu, A., Hohan, I.: *Transducers for Industrial Automatization*, Vol. I, Editura Tehnică, București (1988) (in Romanian)
33. Martenson, S.: Capacitance-to-digital converter simplifies instrumentation and sensor design. *Sensors & Transducers e-Digest* 59(9) (September 2005)
34. Restagno, F., Crassous, J., Charlaix, E., Monchanin, M.: A new capacitive sensor for displacement measurement in a surface-force apparatus. *Meas. Sci. Technol.* 12, 16–22 (2001)

35. Harish, D.: CS-series of integrated load sensors based on innovative capacitive sensing technology. *Sensors & Transducers e-Digest: Product News* 69(7) (July 2006)
36. Peng, P., Sezen, A.S., Rajamani, R., Erdman, A.G.: Novel MEMS stiffness sensor for force and elasticity measurements. *Sensors and Actuators A: Physical* 158(1), 10–17 (2010)

Chapter 6

PIEZOELECTRIC FORCE TRANSDUCERS (PZFTs)

The first demonstration of the direct piezoelectric effect was in 1880 by the brothers Pierre and Jacques Curie as a phenomenon where electric dipole (developing potential difference) is generated in anisotropic natural crystals subjected to mechanical stress. Woldemar Voigt's *Lehrbuch der Kristallphysik* (*Textbook on Crystal Physics*), published in 1910, describes the 20 natural crystal classes which are capable of piezoelectricity, and rigorously defines the piezoelectric constants using tensorial analysis.

The most often cited difference is that quartz is the better choice for measuring dynamic forces while strain gauges are more suitable for static forces [6.1]. Piezoelectric quartz frequency response is up to ten times higher than that of the equivalent piezoresistive transducer but a large number of applications fall into this overlapping frequency range where both types of transducers are viable candidates for measuring force. (Some authors consider "Piezoelectric" and "Piezoresistive" like cousins not brothers!) The measurement process complexity, regardless of the utilized principle [6.2], is shown in Figure 6.1.

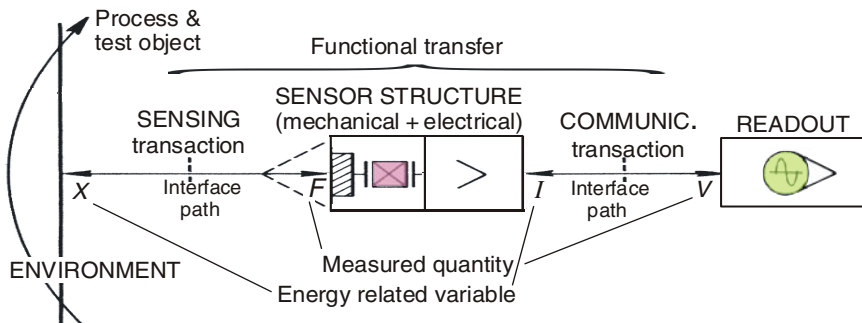


Fig. 6.1 General view of a measuring system for various mechanical quantities. Here the measurand is force F and the transducer symbol means "piezoelectric".

Passive sensor elements (R, L, C) that are designed to deflect under load result in several drawbacks:

- Sensing element structures are subject to fatigue failure.
- Frequency response is limited by sensing element stiffness. Quartz sensor is typically ten times stiffer than SG sensor of equivalent capacity.
- Temperature changes affect mechanical and electrical properties of elastic elements, bonding agents and resistive sensors, causing output signal changes unrelated to applied force.
- Sensitivity drifts with time due to aging of sensing element materials and bonding agents. Periodic recalibrations are usually required.

The most impressive advantage of piezoelectric force transducers is their “rangeability”, extended from milli- to mega-newtons. They have instantaneous “zoom-in” capability (up to 10^5) and provide higher accuracy and finer resolution measurements of small force changes in the presence of a much larger background force. Finally, piezoelectric transducers sizes are smaller but they cost more than SG sensors of equivalent capacity.

6.1. PIEZOELECTRIC MATERIALS

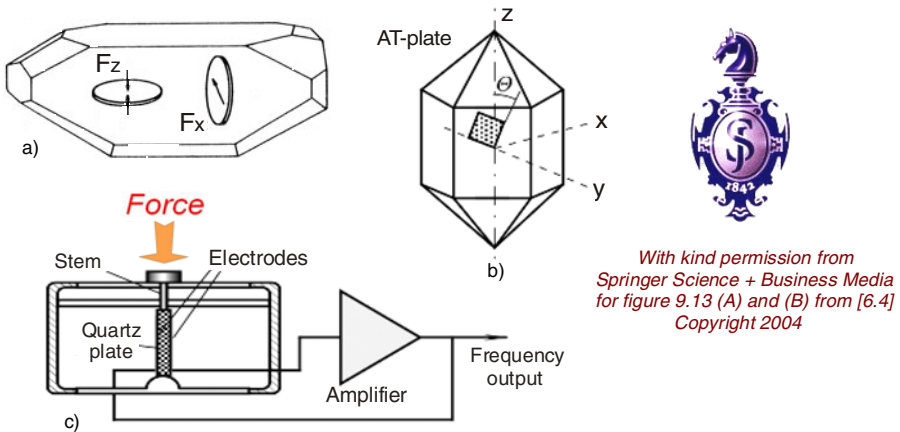
6.1.1. Quartz crystals

Quartz is the main material employed, although certain ceramics also exhibit the piezoelectric effect. If a disc cut out of this material is deformed, a voltage is generated between the end planes [6.3]. Crystalline quartz is naturally piezoelectric and produces an electric charge output in direct response to an applied force. The separation of the components is ensured by the fact that each crystal is sensitive only to a certain component. Because of this it is important to precisely position the sensitive axis with respect to the assembly and the transducer with respect to the vector of the forces to be measured.

Figure 6.2a shows how the discs have to be cut out for different force directions. In Figure 6.2b is an AT-cut of a quartz crystal reported to the triaxial system [6.4]. The quartz crystal has three co-planar electrical axes x , three neutral (or mechanical) axes y in the same plan as the first but at 90° angle, and an optical axis z perpendicular to all others.

Fig. 6.2c presents the transducer structure, with its surface electrodes for utilizing the piezoelectric effect, which are connected in a positive feedback of an oscillator. Details on quartz crystals as resonators are given in Chapter 12.2.

GaPO_4 (gallium orthophosphate) has twice the sensitivity of conventional quartz (SiO_2) and high thermal stability of many piezoelectric properties [6.5]. Its intrinsically large electrical resistance enables the production of transducers with excellent sensing behavior in extremely high temperature and pressure. [European FP5 program, Gapogrowth project with Austrian partner Piezocryst].



With kind permission from
Springer Science + Business Media
for figure 9.13 (A) and (B) from [6.4]
Copyright 2004

Fig. 6.2 Piezoelectric crystals (a), with different orientation to the axes system (b) and assembled force transducer with frequency output (c)

6.1.2. Sensors with organic polymers

The large piezoelectric effect of polyvinylidene fluoride has been demonstrated by Kawai in 1969. A piezoelectric tactile transducer (Fig. 6.3a) has three films laminated together [6.4]. The upper and the bottom films are PVDF while the center film is for the acoustic coupling between the other two. The softness of the central film determines the sensor sensitivity and its operating range. The bottom piezoelectric film is driven by an AC voltage from an oscillator. This excitation signal results in mechanical contractions of the film which are coupled to the compression film and, in turn, to the upper piezoelectric film, which acts as a receiver. Because piezoelectricity is a reversible phenomenon, the upper film produces alternating voltage upon being subjected to mechanical vibrations from the compression film. These oscillations are amplified and fed into a synchronous demodulator which is sensitive to both the amplitude and the phase of the received signal. When compressing force F is applied to the upper film, mechanical coupling between the three-layer assembly changes affecting the amplitude and the phase of the received signal. These changes are recognized by the demodulator and appear at its output as a variable voltage.

A new PVDF-based force transducer (Fig. 6.3b) uses a cable consisting of an internal semiconductive electrode (1), a PVDF layer (2) and an external electrode made of a copper wire layer (3) and a conductive lacquer coating (4). The tested transducer samples were polarized by a voltage of 30 kV using the Corona technique (an electrical discharge brought on by the ionization of a fluid surrounding a conductor, which occurs when the strength of the electric field exceeds a certain value) and stabilized for five months [6.6]. Its geometrical parameters are: $a = 1.62$ mm, $b = 2.18$ mm, $l_{el} = 90$ mm and $l_c = 180$ mm.

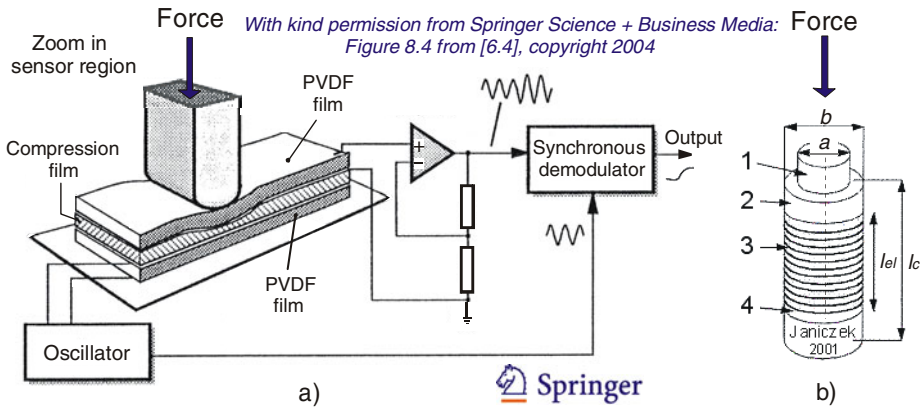


Fig. 6.3 PVDF force transducers based on thin films (a) or on copper wire windings (b)

Electromechanical film (EMFi) is a thin, cellular, biaxially oriented polypropylene film that can be used as an electret-type active material [6.7]. Electret is the electrostatic equivalent of a permanent magnet (as it has been attested by Heaviside in 1885). Having a special voided internal structure and high resistivity it is capable of storing large permanent charge. The surface charge is injected during manufacturing by a Corona method using high electric field. High sensitivity, light weight and relatively low cost EMFi is capable of measuring force and pressure changes. This material shows a strong quasi-piezoelectric response when compressed. The charge signal ΔQ at the electrodes is proportional to the dynamic force ΔF exerted to the film surface. The signal voltage across the sensor film is given by the relationship

$$\Delta V = \frac{\Delta Q}{C_s} = \frac{d_e \cdot \Delta F}{C_s} \quad (6.1)$$

where d_e is the piezoelectric constant, which is the equivalent of the sensitivity factor (2.3 pC/N for X-cut quartz plate) and C_s is the sensor film capacitance.

Easy to cut to almost any shape and size, EMFi can be integrated as a functional part in different mechanical structures. Flexible and thin sensors are useful especially in physiological applications where sensor arrays are often used in contact with skin or clothing. The Institute of Measurement and Information Technology from Tampere, Finland has constructed a special chair equipped with EMFi sensors in order to measure pulse, breathing and other activities of a person sitting on the chair for studying human behavior in different computer using situations.

An one-directional position-sensitive force transducer based on polypropylene electret film is described in [6.8]. While the voltage amplifier had relatively low input impedance, the dynamic response of the transducer in the dilatation phase (recovering of micropores) was four times more intensive than during compression. The preliminary test was done with eight subjects using the prototype of the pressure sensitive lock (PSL).

A novel force and force rate sensory system to advance applications in micromanipulation using an *in situ* polyvinylidene difluoride piezoelectric sensor is presented in [6.9]. Highly sensitive 1D and 2D sensors detect real-time microforce and force rate information during the manipulation process, with a resolution in the range of sub-micronewtons. A tele-micromanipulation platform, which performs tele-microassembly of the MEMS structures and tele-cell-manipulation with tactile force feedback via Internet was built successfully.

An efficient technique based on piezoelectric transducers is proposed for identifying the impact force acting on carbon fibers reinforced polymer (CFRP) laminated plates [6.10]. Chebyshev polynomial is employed to approximate the impact force history. His coefficients are directly used as unknown parameters. The relation between these unknown parameters and the strain responses at the specified positions is formulated through the finite element method and the mode superposition method. By comparing the numerically estimated strains and the experimental ones, an optimization model is set up to solve this inverse problem by employing the quadratic programming method.

6.1.3. Solid state devices

The paper [6.11] explains the action of piezoelectricity in the MIS (metal-insulator-semiconductor) diodes, formed on n-GaN with SiO₂, for capacitive strain sensing. These diodes, when subjected to static load, were found to exhibit a steady-state change in capacitance.

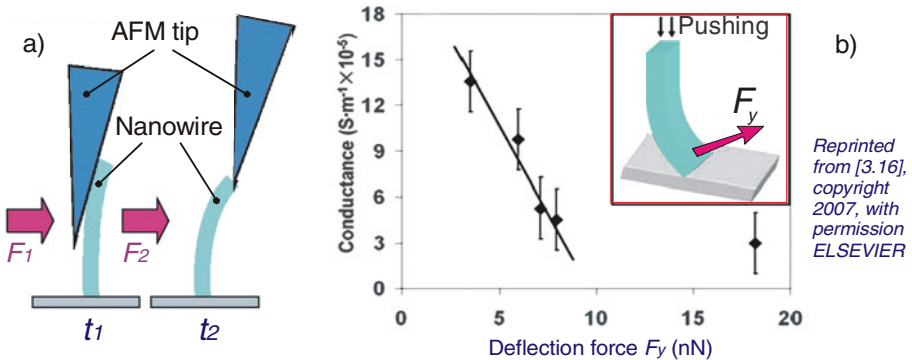


Fig. 6.4 ZnO nanowire (a) and piezoelectric FET (b) for nanoscale force measuring

Figure 6.4a shows an experimental setup for generating an electric signal through the deformation of a semiconducting piezoelectric nanowire (NW).

The piezoelectric FET (field-effect transistor) is a new type of transistor, turned on/off by applying a mechanical force [6.12]. By connecting a ZnO nanowire across two electrodes that can apply a bending force, the piezoelectric field created across the bent NW serves as the gate for controlling the electric current flowing through it. By bending, the width of the conducting channel in the nanowire becomes smaller, while the depletion region becomes larger. The increase in bending contributes to the dramatic drop in the conductance of the ZnO NW. Based on this principle, a nanoscale force or pressure transducer can be demonstrated [6.13], with an almost linear relationship between the bending force and the conductance (Fig. 6.4b). The mechanical force applied to the nanowire can be determined from its bent shape in the nanonewton range.

6.2. UNIDIRECTIONAL PIEZOELECTRIC FORCE TRANSDUCERS

In piezo force transducers the sensing element is the same as the transduction element which produces the electrical output signal from an acting force. It is mounted directly in line with the force path and the entire force is measured (Fig. 6.5a). High accuracy is obtainable and virtually independent of the point of the force application. When force transducer cannot be installed directly into the force path, an indirect (or shunt) force transducer can be used (Fig. 6.5b).

It is possible to use an assembly of stacked piezoelectric plates and stressed with the same force in series. Electrically the plates can be wired parallel – so a lower output impedance results, or in series – in order to get a larger voltage output. For example (Fig. 6.6a), a 2-kN force properly applied to a cubic-centimetersized quartz crystal produces over 12.5 kV [6.14]. A charge-collection electrode is sandwiched between two quartz-crystal elements. The transducer can be preloaded so that the dynamic forces applied act in comparison to a static level, compared to which alternating increases and decreases appear, so that fluctuating tension-compression loads can be evaluated [6.15].

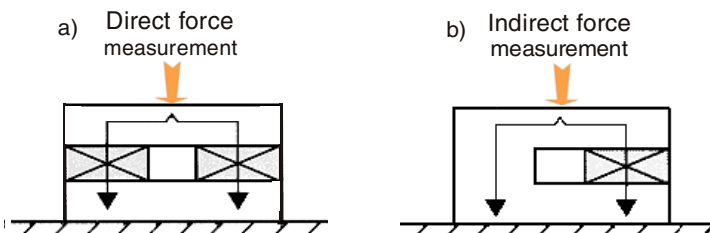


Fig. 6.5 Force transducer installation: direct (a) and indirect method (b)

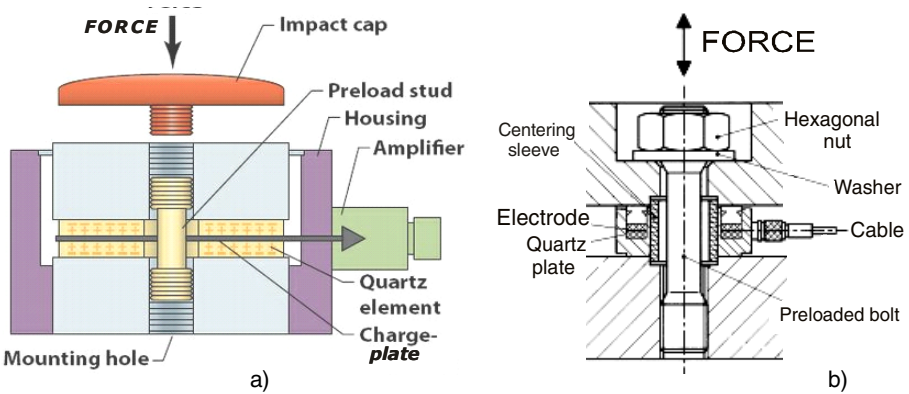


Fig. 6.6 Two models of piezoelectric force transducers: a) Repass, b) NPL

Any force applied to the sensing element produces a separation of charges within the atomic structure of the material, generating an electrostatic output voltage which can be routed directly to a charge amplifier or converted to a low-impedance signal for an internal MOSFET amplifier. Internal leakage paths are formed by impurities within the crystal while external paths are created by the electronics used to measure the voltage generated. The discharge time constant (DTC) typically follows an exponential curve similar to an RC time constant and determines the transducer's lowest frequency response. The piezoelectric transducer capacitance is low (10...100 pF), so isolation resistances over $10^{10} \Omega$ are necessary to have DTC over 1 second.

These devices are often known as *piezoelectric crystals* or *quartz force transducers* [6.16]. They are different from most other sensing techniques because they are active sensing elements (also called self-generating sensors). No power supply is needed and the deformation to generate a signal is very small – an advantage of high frequency response of the measuring system without introducing geometric changes to the force measuring path. When packaged as a load washer, as in Figure 6.6b, and compressed under a force of 10 kN a typical piezoelectric transducer deflects only 0.001 mm. The high frequency response (up to 100 kHz) enabled by this stiffness and the other inherent qualities of the piezoelectric effect makes the quartz crystal sensors very suitable for dynamic force measurements such as oscillation, impact, or high-speed compression or tension. Measurements can be made over a period of minutes or even hours and piezoelectric transducers are said to take “quasi-static” measurements.

A piezoelectric force sensing apparatus for monitoring the bond force in an ultrasonic welding machine is presented in [6.17]. The force transducer is a piezoelectric one (Fig. 6.7a) but could also be a magnetostrictive transducer.

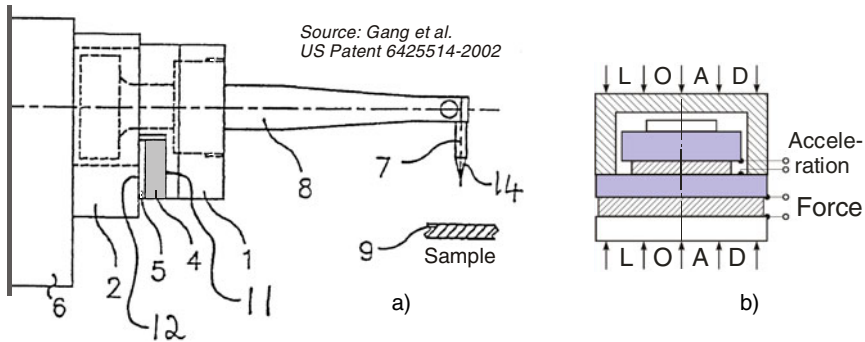


Fig. 6.7 Applications with piezoelectric force transducers: a) ultrasonic welding machine, b) impedance head for mobility measurements

An “impedance head” (e.g. type 8001 Bruel & Kjaer), joining in the same mounting the force and acceleration piezoelectric transducers (Fig. 6.7b), has some advantages:

- smaller sizes as compared with the two separate coaxial transducers, easily fulfilling the condition of measuring force and acceleration in the same point and without phase errors,
- a more reduced total mass,
- easier to install it on the structure,
- versatility in various applications.

An installation for mobility and mechanical impedance measurements at the “Politehnica” University of Bucharest, Romania is described in [6.18].

Transducers convert one form of energy to another; the piezoelectric transducers are typically used in a double role [6.19]:

- *Piezo sensors* convert mechanical energy into electrical energy, and they are referred to as “generators”.
- *Piezo actuators* convert electrical energy (voltage and charge) to mechanical energy (force and motion), and they are referred to as “motors.”

A hybrid-type microgripper with an integrated force transducer has been achieved within the project Brain Korea 21 [6.20]:

- microfingertips fabricated using micromachining technology to integrate a very sensitive *force sensor* for measuring the gripping force with a sensitivity of 667 N/V,
- piezoelectric gripper finger *actuators* that are capable of large gripping forces and moving strokes.

During the testing experiments it was found that the frictional forces between the working plane and the microobject could be utilized to facilitate the release of microobjects from the microgripper.

There is a huge variety of applications with piezoelectric force transducers, for example they can be used as ballistocardiographs [6.21] as well as in underwater weighing system utilizing “force cube” transducers [Akers and Buskirk, *Journal of Applied Physiology*, **26**, pp. 649-652, 1969]. Gautschi [6.22] covers the entire field of piezoelectric transducers for mechanical measurands (force, strain, pressure, acceleration, acoustic emission).

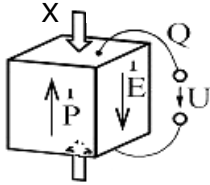
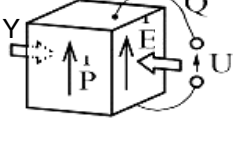
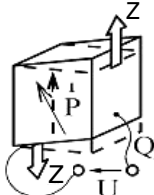
The paper [6.23] presents the analytical modeling of a piezoelectric multilayer cantilever used as a micro-electro-mechanical-system (MEMS) chemical sensor. It is an array of piezoelectric cantilevers with voltage output in the millivolt range that replaces the conventional laser-based position-sensitive detection (PSD) systems. The sensing principle is based upon changes in the deflection induced by environmental factors in the medium where a micro-cantilever is immersed. Bending of the cantilever induces the potential difference on opposite sides of the piezoelectric layer providing an information signal about the detected chemicals. Finite element method (FEM) simulations using CoventorWare (a MEMS design and simulation program) were performed to obtain optimum design for the chemical sensor parameters.

Two sets of piezoelectric force transducers for measuring in-plane magnetic force generated by two radial magnetic bearings are presented in [6.24], offering valuable information for operation monitoring, unbalance evaluation, cutting force control and *in situ* system parameter identification.

6.3. TRIDIRECTIONAL PIEZOELECTRIC FORCE TRANSDUCERS

The principle of operation of a piezoelectric transducer is that a physical quantity, transformed into a force, acts on two opposing faces of the sensing element. Depending on the design, different “modes” to load the piezoelectric element can be used: longitudinal, transverse and shear (Table 6.1).

Table 6.1 Piezoelectricity types depending on mechanical loading (after [6.25])

Type	Longitudinal	Transverse	Shear stress
Layout			
Stress direction	Electrical axis	Mechanical axis	Shape distortion
Characteristic	Charge depends on crystal dimensions	Charge depends on crystal shape	Less influenced by thermal dilatation

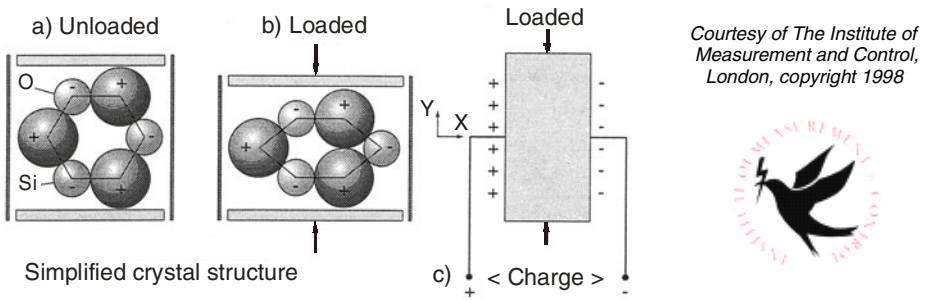


Fig. 6.8 Transverse piezoelectric effect [6.26]

An example of transverse piezoelectricity is presented in Figure 6.8. A load in the Y direction results in a charge across the X direction.

Multicomponent piezoelectric force transducers (Fig. 6.9) measure the forces in three orthogonal axes [6.27]. Force F is transmitted to each of 3 discs with the same magnitude and direction. Each piezoelectric crystal ring (shown “exploded”) has been cut along a specific axis and the orientation of the sensitive axis coincides with the axis of the force component to be measured. Each then produces a charge proportional to the force component specific to that disc. The charge is collected via the electrodes inserted into the stack.

A new transducer for measuring normal and shear stresses in physical modeling is presented in [6.28]. Its sensing element is a stack of piezoelectric plates which measures directly three components of the applied force.

Force and pressure measurements were performed in a high Reynolds number facility, at the Cryogenic Ludwig-Tube in Germany [6.29]. The balance based on multicomponent piezoelectric force transducers was applied totally in the cryogenic environment. The highest possible Reynolds number in most nearly incompressible flow ($Re = 5.8 \times 10^6$) was achieved at the temperature of $T = -150$ °C, the highest pressure possible, $p_0 = 10$ bar, and the lowest attainable Mach number of $Ma = 0.28$. The results show that, in spite of the pulse operating mode of the wind tunnel, the steady and unsteady processes can be measured very well by means of a piezoelectric balance.

High sensitivity, miniature series 209C quartz piezoelectric force transducers from the Force/Torque Division of PCB Piezotronics, Inc. measure dynamic compression and tensile forces in a wide variety of biomedical tissue product testing applications [6.30]. Transducers feature ICP[®] voltage output, and have an extremely high sensitivity of 500 mV/N at a force range of 10 N in compression and 4.5 N in tension. ICP (integrated circuit piezoelectric) force transducers contain built-in microelectronics to convert the high impedance charge to a low impedance voltage, which eliminates the noise associated with charge amplifiers and the required high impedance cables.

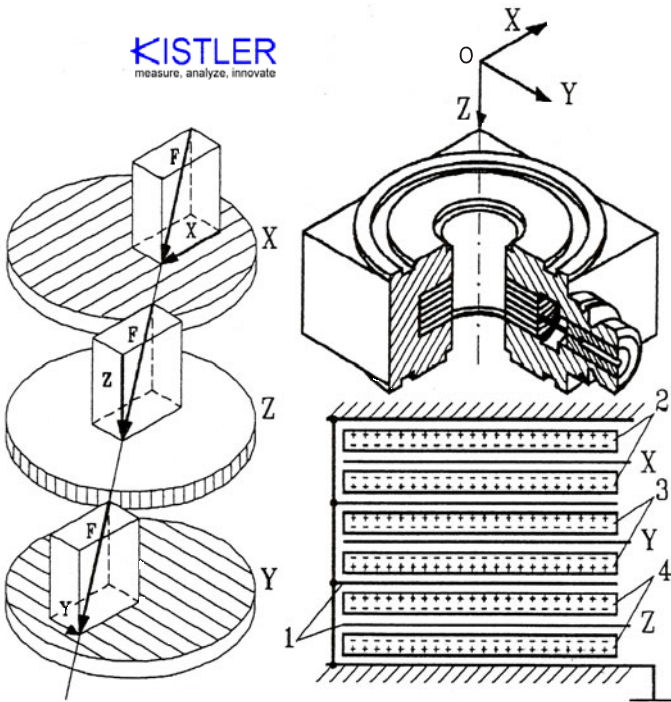


Fig. 6.9 Component separation within a triaxial force transducer: 1 – electrodes, pair of crystals for X (2), Y (3) and, respectively, Z (4) components

Another biomedical application: a hip stem instrumented with four piezoelectric transducers (PZTs) was successfully implanted in a composite femur and tested under shear and axial eccentric loads [6.31].

Instrumented manual contact force measuring can be direct one-dimensional (1D) or indirect three-dimensional (3D). Direct measurement is defined as taking place at the interface of force delivery and force sensing. A new hand/palm-held computerized measuring system enables recording and presenting of 3D manual contact forces at the patient-practitioner interface [6.32]. These 3D direct force measures have the potential to give a more complete and differentiated characterization of patient and practitioner forces than 1D forces.

Manual techniques play a prominent role in chiropractic, massage therapy and osteopathy. The more completed 3D manual contact force description also can help practitioner and students to improve both manual force perception and delivery skills by providing higher standardization and real-time objective feedback about performance.

The 3D force measuring chain consists of the following components:

- a 3D piezoelectric force sensor, preloaded with 5 kN (VarioCOMP multi-component force sensor 9601A31, Kistler Instrumente AG Winterthur, CH);
- a charge amplifier (Kistler multichannel charge amplifier 5034A3);
- an analog-to-digital converter (ADC-card PCL-1800, Advantech, Taiwan);
- a PC with data acquisition and real-time data presentation software (LabVIEW 5.1, National Instruments).

6.4. PIEZOELECTRIC BIMORPH AS FORCE TRANSDUCER

Piezoelectric bimorphs (Fig. 6.10c) consist of two flat strips of piezoelectric elements joined one to each other, provided with electrodes in such a manner that when an electric field is applied, one strip elongates while the other contracts. They are sensitive to bending and/or torsion loads [6.33].

A bimorph consisting of two rectangular piezoelectric strips that are connected back-to-back on a thin metallic center electrode, forming a millinewton range force sensor with dynamic excitation, is presented in [6.34]. This planar, parallel and symmetrical bimorph is modeled by finite element analysis with a static, analytical expression for generated charge, voltage, displacement and force that correspond to the deflection of a freely oscillating piezoelectric bimorph. A circuit that is used to actuate the bimorph is described, as well as the measured results from the actuator and the sensor side of the bimorph in both free oscillation and blocked cases.

In order to maximize the electrical admittance [6.35] two electrodes of the bimorph are formed on an annular piezoelectric disc (Fig. 6.10a). Two discs are clamped together to form a piezoelectric bimorph (Fig. 6.10b) which is sensitive to variable compression loads [6.36].

An experimental set-up to investigate the hysteretic behavior of a piezoelectric bimorph (285-784 M641, Sensor Technology[®]) is shown in [6.37]. To monitor the PZT displacement a strain gauge based system has been adopted, with a differential amplifier (INA111, Burr-Brown[®]) as a conditioning circuit (Fig. 6.11a).

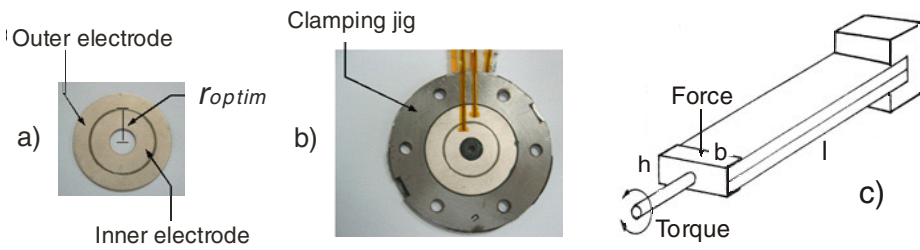


Fig. 6.10 Piezoelectric bimorphs made of rings (a), discs (b) or strips (c)

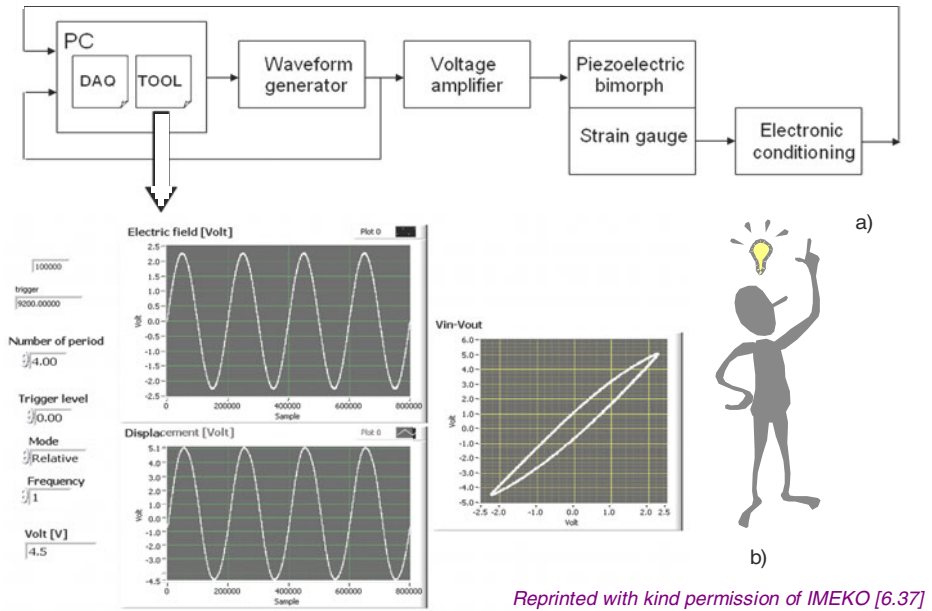


Fig. 6.11 a) A schematic representation of the set-up for the piezoelectric bimorph characterization. b) The virtual instrument front panel for signal acquisition and data processing. X-Y graph represents the hysteresis characteristics of the piezo bimorph.

A high voltage source, driven by an arbitrary waveform generator, stimulates the PZT actuator, whose deflection is captured by SG signals from the readout electronics and forcing waveforms are acquired by a PCI 3036E DAQ card.

Figure 6.11b is a typical view of front panel of the virtual instrument (DAQ card PCI-6111E), developed in LabVIEW™ environment, during the signal acquisition phase in order to obtain information about piezo deflection and state diagram. During the calibration phase, the piezoelectric actuator is driven at a very low frequency (0.1 Hz) and the actual deformation is estimated by processing images recorded with CCD (charged coupled device) camera.

A pair of bimorph cantilevers, glued opposite along an insulating layer, can achieve force or moment generation as they are electrically connected in parallel or in series, respectively [6.38]. Another twin device “faced” structure, achieved by placing the piezoelectric actuator and sensor opposite each other, ensures high sensitivity to longitudinal and transversal waves. The actuator stimulates the unknown surfaces, and the transmitted acoustic wave is picked up by the sensor to extract the material properties [6.39]. The functional scheme of the smart tactile transducer (Fig. 6.12) includes sensors and actuators, driving and signal conditioning circuits as well as a data processing subsystem.

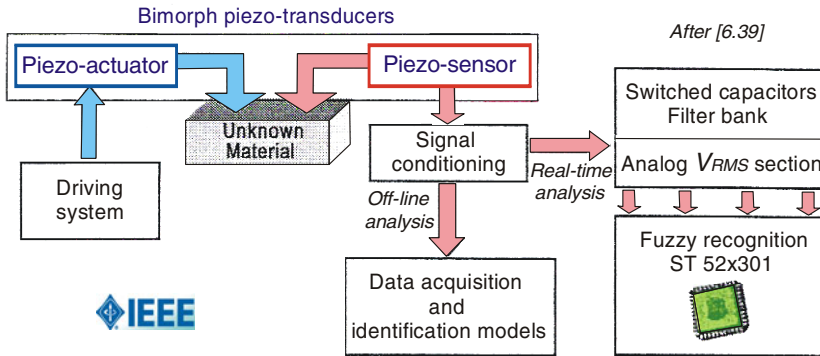


Fig. 6.12 Tactile recognition of surfaces based on bimorph piezo-actuators and -sensors

Two different strategies are possible:

- “*off-line*” approach, based on both time- and frequency-domain signal processing implemented using MATLAB and LabVIEW, allows identifying suitable numerical models to classify various surfaces.
- “*real-time*” strategy is based on the analysis of the spectral power densities of the signals acquired in various frequency ranges. A band-pass filter bank and an analog circuit for the computation of the root mean square value V_{RMS} of each filter output are used. This information is processed by a classification algorithm based on fuzzy logic and implemented using a low-cost dedicated microcontroller.

All the hardware and software can be integrated into a small portable device.

A.M. Stewart, Research School of Physical Sciences and Engineering, The Australian National University Canberra, used a bimorph to measure a cantilever deflection as an effect of colloidal forces between transparent surfaces in liquids and gases [6.40].

A research team of Caltech, working for NASA's Jet Propulsion Laboratory, proposed the development of bimorph actuators and force transducers based on carbon nanotubes (CNTs) [6.41]. Such devices could make it possible to generate, sense, and control displacements and forces on a molecular scale, and could readily be integrated with conventional electronic circuits. They would exploit the dependence of nanotube length on charge injection that has been observed in mats of disordered carbon single-wall nanotubes [R.H. Baughman *et al.*, “Carbon Nanotube Actuators”, *Science* **284**, 1340 (1999)]: CNTs become elongated or shortened when biased at negative or positive voltage, respectively. This result suggests that one could produce opposing changes in length in pairs of side-by-side, oppositely-biased nano-tubes, resulting in a lateral deflection of the unsecured tube ends. These devices would make possible novel MEMS, and even microscopic robots.

6.5. ELECTRONIC CIRCUITS FOR PIEZO FORCE TRANSDUCERS

There is a wide variety of electronic circuitry associated with piezoelectric force transducers, oscillators (See Figures 6.2c and 6.3a), generators (Fig. 6.11a) and charge amplifiers being the most widely used.

A comparison between different plastic films for tactile sensing is made in [6.42]. A passive capacitive sensing film behaves like a modulator type sensor (Fig. 6.13a), and thus needs electronic excitation that probes the capacitance. While a capacitive film sensor can be used for detection of a static force, like the weight of an object, piezoelectric and electret sensors measure only dynamic forces; they behave like a capacitive generator type sensor giving an output signal without any external electric excitation (Fig. 6.13b).

In case of a charge amplifier, the high-pass frequency of the system depends on the feedback capacitor C_f and resistor R_f of the amplifier:

$$f_{HP} = \frac{1}{2\pi R_f \cdot C_f} \tag{6.2}$$

The amplifier acts as a charge integrator above the cut-off frequency f_{HP} and as a current amplifier below that frequency.

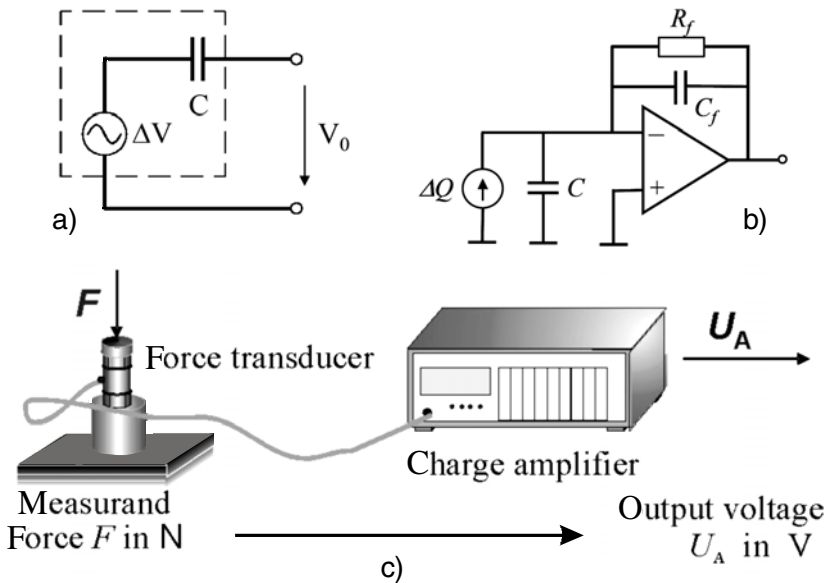


Fig. 6.13 Passive capacitive (a) and active piezoelectric sensing (b) for static and dynamic forces. c) Charge amplifier, typical for piezoelectric force transducers.

Figure 6.13c shows a schematic drawing of a measuring chain with a piezoelectric force transducer (PZFT) and a charge amplifier to measure the induced charge. The paper [6.43] presents a new method for calibrating PZFTs using static forces. Load cycles with pilgrim-steps and a special evaluation of the measuring results permit the determination of transducer coefficients that are independent of the charge amplifier linear drift. So, the piezoelectric coefficients are independent of the measurement time and the time of load change of the force standard machine in use.

Since the charge inevitably leaks out due to finite resistance and capacitance, the piezoelectric transducer is not suited for static measurements. The measuring system is characterized by a so-called discharge time that describes the time-rate of charge leakage [6.44].

The induced charge as a function of mechanical stress is not easy to be measured. Generally, the high-impedance charge signal is converted via a charge amplifier to a "low-impedance" voltage signal that can be measured (and displayed) using standard instruments. A charge integrator, associated with a piezoelectric cantilever, improves the low-frequency measurements, making them suitable for chemical and biological detection [6.45].

A complete piezoelectric force measurement chain made by H.B.M. is PACeline CFW [6.46]. This piezoelectric force washer with innovative design is available with nominal (rated) forces of 50 kN and 140 kN. Since the sensitivity of 4.3 pC/N is independent of measuring range, all common assembly and testing applications can be covered.

A new scheme of oscillation generation for mass-sensitive sensors is developed in [6.47]. The application of Schmitt triggers enables to diminish the oscillator frequency jitter. This results in a short-term instability decrease that reduces detection limits and improves the analysis precision.

Active oscillators for piezoelectric resonators which allow performing microweighing in liquid media are considered in [6.48]. The paper offers a modified oscillator circuit that enables a piezosensor to operate in a wide range of sorbent masses (up to 50 μg).

Piezoresponse force microscopy (PFM) has emerged as a preeminent tool for nanoscale imaging, spectroscopy, and manipulation of ferroelectric materials [6.49]. The basic idea of PFM is to affect locally the piezoelectric sample surface by the electric field and to analyze the resulting displacements [6.50]. This technique is based on the converse piezoelectric effect, which is a linear coupling between the electrical and mechanical properties of a material. Since all ferroelectrics exhibit piezoelectricity, an electric field applied to a ferro-electric sample results in its dimensional changes. An AFM (atomic force microscope) tip is used as a top electrode moved over the sample surface in order to detect the polarization orientation. The electric field generated in the

sample causes the domains with the polarization parallel to the field to extend and the domains with opposite polarization to contract. The amplitude of the response measures the local electromechanical activity of the surface while its phase informs on the polarization direction.

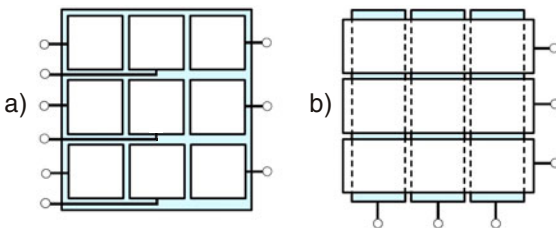
6.6. COMPLEX APPLICATIONS WITH PIEZOELECTRIC DEVICES

Film sensors, able to locate the acting point of a force or a moving object, can be realized in many ways [6.42]: resistive, capacitive, piezoelectric. The area can be divided into smaller areas and addressed individually (Fig. 6.14a). Several acting points can be monitored in the same time but for these “matrix” type solutions the readout electronics complexity increases quickly when high resolution is needed. A single element of the matrix can be also addressed by multiplexed amplifier and common row and column electrodes (Fig. 6.14b). An economic problem is the multiplexing rate for a great number of acting points.

Piezoelectric microbalances are used as very sensitive chemical and biological sensors. For the mass based sensing applications utilizing a Quartz Crystal Microbalance, a piezoelectric crystal, made of AT-cut quartz wafer at an angle of $35^{\circ}15'$ and sandwiched between a pair of electrodes, is generally used.

Piezoelectric crystal immunosensors work on the principle of measuring a small change in resonant frequency of an oscillating piezoelectric crystal due to change in mass on the sensor surface [6.51]. Because of their low cost and high Q -factors, these miniaturized sensors show fast response time, high sensitivity, and are suitable for mass production using standard fabrication techniques. Arrays of such sensors could be fabricated to cover ranges of a particular sensing property and have the potential for seamless integration with CMOS-based electronics.

Fig. 6.15a shows the piezoelectric crystal construction and its vibration in thickness shear mode. A QCM sensor typically consists of a thin AT-cut quartz disc with circular electrodes on both sides of the quartz. Due to the piezoelectric properties of the quartz material a voltage between these electrodes leads to a shear deformation of the quartz crystal.



Source:
Lekkala et al.
IMEKO World Congress
Dubrovnik, Croatia, 2003

Fig. 6.14 Individual (a) vs multiplex measurement (b) for forces acting points location

Fig. 6.15b depicts a multi-channel QCM system comprising of seven interdigital piezoelectric quartz crystals (AT-cut with gold electrodes, 10 MHz each) encapsulated in a detector cell coupled with frequency oscillating and monitoring devices.

Antigen detection is made with piezoelectric crystal bound with receptor molecules (Fig. 6.15c).

The relationship between the resonant frequency f_r of an oscillating piezoelectric crystal and the mass deposited on the crystal surface is

$$f_r = \frac{\rho_q \cdot N \cdot A}{m} \quad (6.3)$$

where ρ_q is the density of the quartz (2.65 g/cm^3), N is the frequency constant, A is the area (cm^2) of the electrodes of quartz plate, and m is the mass (g) of the oscillating quartz.

The QCMs measure the resonant frequency f_r of a quartz crystal, which is a linear function of the mass of material deposited on the crystal surface (as described by Sauerbrey, Metrologia Berlin, in 1959). There are many different kinds of detection mechanism based on changes in one or more of the physical characteristics of a thin film or layer in contact with the device surface.

A novel biosensing interfacial design strategy has been produced by assembling nano-Au particles on amine-terminated plasma-polymerized films [6.52]. A quartz-crystal microbalance (QCM) is used as a model transducer in order to evaluate the chemical process and could be combined with odor sensors fabricated by depositing nanocrystalline Indium Tin Oxide thin films on AT-cut quartz crystals [6.53]. The change in frequency characteristics and surface resistance as a function of time was measured for odors from different groups of foods and drinks.

Due to their small dimensions and high stiffness piezoelectric transducers are predestined for dynamic force measurements [6.54]. Besides microsensing applications, the piezoelectric measurement technology for high nominal loads, in conjunction with mechatronic systems and low-drift charge amplifiers, seems to offer unused potentials.

REFERENCES

1. How to select a force sensor. Kistler Instrument Corporation, Amherst, NY, Catalogue KI 6.001e – 99
2. Seippel, R.G.: Transducers, Sensors & Detectors. Prentice Hall (Reston Publishing Company), Reston, VI (1983)

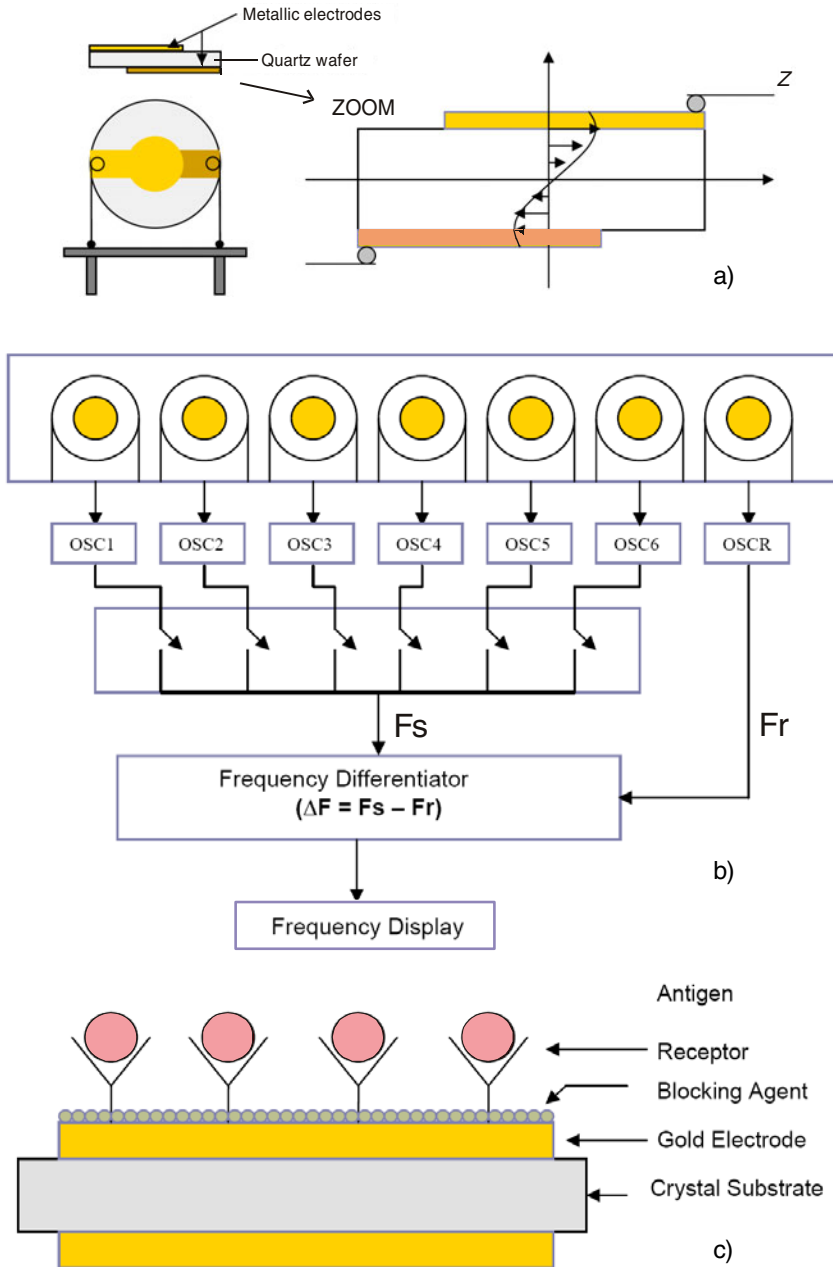


Fig. 6.15 Piezoelectric crystal immunosensors: a) Thickness shear mode vibration and b) multichannel system with frequency display. c) Schematic diagram of piezoelectric crystal bound with receptor molecules for antigen detection. (Courtesy of IFSA ©2006)

3. Wieringa, H.: Electrical force measuring transducers. In: Proc. Symposium Force, Pressure, Displacement and Flow Sensors, May 13-14, pp. 179–197. Twente University of Technology, Enschede (1982)
4. Fraden, J.: Handbook of Modern Sensors – Physics, Design and Applications, 3rd edn. Springer, Heidelberg (2004)
5. Novel piezoelectric crystals for sensor applications. Cordis focus – RTD Results Supplement, No. 68, p. 44, offer ID 3491 (December 2007); ISSN 1025-4013
6. Janiczek, T.: Analysis of PVDF transducer signals stimulated by mechanical tension. Journal of Electrostatics 51-52, 167–172 (2001)
7. Paajanen, M., Lekkala, J., Kirjavainen, K.: Electro-Mechanical Film (EMFi) – A new multipurpose electret material. Sensors and Actuators 84, 95–102 (2000)
8. Evreinov, G., Raisamo, R.: One-directional position-sensitive force transducer based on EMFi. Sensors and Actuators A: Physical 123-124(C), 204–209 (2005)
9. Shen, Y., Xi, N., Lai, K.W.C., Li, W.J.: A novel PVDF microforce/force rate sensor for practical applications in micromanipulation. Sensor Review (Emerald Group Publishing Limited) 24(3), 274–283 (2004)
10. Hu, N., Fukunaga, H., Matsumoto, S., Yan, B., Peng, X.H.: An efficient approach for identifying impact force using embedded piezoelectric sensors. Int'l Journal of Impact Engineering 34(7), 1258–1271 (2007)
11. Strittmatter, R.P., Beach, R.A., Picus, G.S., McGill, T.C.: Piezoelectrically enhanced capacitive strain sensors using GaN metal-insulator-semiconductor diodes. Journal of Applied Physics 94(9), 5958–5963 (2003)
12. Wang, X., Zhou, J., Song, J., Liu, J., Xu, N., Wang, Z.L.: Piezoelectric field effect transistor and nanoforce sensor based on a single ZnO nanowire. Nano Letters 6(12), 2768–2772 (2006)
13. Wang, Z.L.: The new field of nanopiezotronics. materialstoday 10(5), 20–28 (2007)
14. Repass, R.: Sensor sense: piezoelectric force sensors. Internet, February 7 (2009)
15. Ionescu, G., Dobrescu, R., Droaşcă, B., Guţu, A., Hohan, I.: Transducers for Industrial Automatization, Vol. I. Editura Tehnică, Bucureşti (1988) (in Romanian)
16. What is the general principle of a force transducer?, http://www.npl.co.uk/instmc_weighing_panel/weigforc.html; Crown Copyright 2003. (reproduced by permission of the Controller of HMSO)
17. Ou, G., Widdowson, G.P., Shing, K., Kwan, K.: Force sensing apparatus. US Patent 6425514, July 30 (2002)
18. Ştefănescu, D.M.: Equipment for mobility and mechanical impedance measurement. Studii şi cercetări de mecanică aplicată, Tom 41(4), 501–513 (1982) (in Romanian)
19. Introduction to piezo transducers. Piezo Systems, Inc., Cambridge, July 21 (2006)
20. Park, J., Moon, W.: A hybrid-type micro-gripper with an integrated force sensor. Microsystem Technologies 9(8), 511–519 (2004)
21. Rogallo, V.L., Jenkins, R.S., Deboo, G.J.: A piezoelectric transducer for measuring cardiac and gross motor activity of small organisms. NASA Tech. Note D-4590/68
22. Gautschi, G.H.: Piezoelectric Sensorics. Springer, Berlin (2005)
23. Zhou, W., Khaliq, A., Tang, Y., Ji, H., Selmic, R.: Simulation and design of piezoelectric microcantilever chemical sensor. Sensors and Actuators A: Physical 125(1), 69–75 (2005)

24. Kim, S.-J., Lee, C.-W.: On-line identification of current and position stiffness by LMS algorithm in active magnetic bearing system equipped with force transducers. *Mechanical Systems and Signal Processing* 13(5), 681–690 (1999)
25. Platil, A.: *Mechatronics Sensors*. PPT-05-force-b on Internet, January 3 (2005)
26. Cuscó, L. (Coord.): *Guide to the Measurement of Pressure and Vacuum*. The Institute of Measurement and Control, London, UK (published 1998)
27. Hunt, A. (Coord.): *Guide to the Measurement of Force*. The Institute of Measurement and Control, London, UK (published 1998)
28. Rosochowski, A.: Technical feasibility of a three-axis force transducer for measuring pressure and friction on the model die surface – prototype development. *Journal of Material Processing Technology* 115, 192–204 (2001)
29. Schewe, G., Steinhoff, C.: Force measurements on a circular cylinder in a cryogenic Ludwig-Tube using piezoelectric transducers. *Experiments in Fluids* 42(3), 489–494 (2007)
30. Munschauer, P.: High sensitivity force sensors for dynamic biomedical tissue product testing. On-line Magazine 'Sensors & Transducers' (S&T e-Digest) 64(2) (February 2006)
31. Cristofolini, L., Marchetti, A., Cappello, A., Viceconti, M.: A novel transducer for the measurement of cement-prosthesis interface forces in cemented orthopaedic devices. *Medical Engineering & Physics* 22, 493–501 (2000)
32. van Zoest, G.G.J.M., van den Berg, H.T.C.M., Holtkamp, F.C.: Three-dimensionality of contact forces during clinical manual examination and treatment: A new measuring system. *Clinical Biomechanics* 17, 719–722 (2002)
33. Stere, R.: *Electronic Apparatus for Measurement and Control*. Editura Didactică și Pedagogică, București (1968) (in Romanian)
34. Kursu, O., Kruusing, A., Pudas, M., Rahkonen, T.: Piezoelectric bimorph charge mode force sensor. *Sensors and Actuators A: Physical* 153(1), 42–49 (2009)
35. Lim, C., Choi, S.B.: Vibration control of an HDD disk-spindle system using piezoelectric bimorph shunt damping. *Smart Materials and Structures* 16, 901–908 (2007)
36. http://www.ssslabs.com/ehtml/images/3/Piezo_Bimorph.jpg, June 13 (2009)
37. Andò, B., Giannone, P., Graziani, S., Pitrone, N.: Measurement system for the characterization of piezoelectric bimorphs. In: CD Proc. 19th IMEKO TC-3 Int'l Conf. Force, Mass & Torque Measurements: Theory and Application in Laboratories and Industries, Paper 14, Cairo, Egypt, February 19-23 (2005)
38. Hou, X.: A bimorph moment / force actuator for dynamic testing. *Sensors and Transducers Journal* 108(9), 128–138 (2009); ISSN 1726-5479
39. Baglio, S., Muscato, G., Savalli, N.: Tactile measuring systems for the recognition of unknown surfaces. *IEEE Transactions on Instrumentation and Measurement* 51(3), 522–528 (2002)
40. Stewart, A.M.: The use of piezoelectric bimorphs to measure forces in colloidal systems. *Meas. Sci. Technol.* 6, 114–123 (1995)
41. Hunt, B., Noca, F., Hoenk, M.: Carbon nanotube bimorph actuators and force sensors. NASA Tech Briefs NPO-21153, Pasadena, CA, October 3 (2005)

42. Lekkala, J., Tuppurainen, J., Paajanen, M.: Material and operational properties of large-area membrane type sensors for smart environments. In: CD Proc. XVIIth IMEKO World Congress Metrology in the 3rd Millenium, Cavtat-Dubrovnik, Croatia, June 22-27, pp. 2045–2048 (2003)
43. Mack, O.: A new calibration method with static loads for piezoelectric force transducers. In: Proc. XVIII IMEKO World Congress on Metrology for a Sustainable Development, Rio de Janeiro, Brazil, September 17-22, Paper 22 (2006)
44. Hjelmgren, J.: Dynamic measurement of force – a literature survey. Swedish National Testing and Research Institute, Boras, Sweden, SP Report 27 (2002)
45. Isarakorn, D., Linder, M., Briand, D., de Rooij, N.F.: Evaluation of static measurement in piezoelectric cantilever sensors using a charge integration technique for chemical and biological detection. *Meas. Sci. Technol.* 21, Paper 075801 (June 2010)
46. PACeline CMC – Piezoelectric force measurement chain (June 2009), <http://www.hbm.com/en/menu/products/transducers-sensors/force-transducers/piezo/single...>
47. Korenman, Y.I., Kiselyov, A.A., Kadantsev, A.V.: Quartz generator effect on accuracy characteristics of mass-sensitive sensors. *Sensors and Systems Journal* (1) (January 2005) (in Russian)
48. Kalach, A.V., Ryzhkov, V.V., Sitnikov, A.I.: Active oscillators for piezoelectric microweighing in liquid media. *Idem* (2) (February 2005)
49. The Piezo Force Module for electromechanical measurements. Asylum Research – Atomic Force Microscopes, Santa Barbara, CA, PDF Data Sheet 27, April 9 (2009)
50. Alexe, M., Gruverman, A. (eds.): *Nanoscale Characterisation of Ferroelectric Materials. Scanning Probe Microscopy Approach.* Springer, Berlin (2004)
51. Raman Suri, C.: Quartz crystal based microgravimetric immunobiosensors. *Sensors & Transducers* 66(4), 543–552 (2006); ISSN 1726-5479
52. Wang, H., Wang, C., et al.: A novel biosensing interfacial design produced by assembling nano-Au particles on amine-terminated plasma-polymerized films. *Analytical and Bioanalytical Chemistry* 377(4), 632–638 (2003)
53. Patel, N., Huebner, J., Saredy, J., Stadelmaier, B.: Odor sensing with indium tin oxide thin films on quartz crystal microbalance. *Sensors & Transducers Journal* 91(4), 116–126 (2008)
54. Mack, O.: Investigations of piezoelectric force measuring devices for use in legal weighing metrology. In: CD Proc. 19th IMEKO TC-3 Int’l Conf. Force, Mass & Torque Measurements: Theory and Application in Laboratories and Industries, Cairo, Egypt, February 19-23, Paper 28 (2005)

Chapter 7

ELECTROMAGNETIC FORCE TRANSDUCERS

7.1. CLASSIFICATION

Sensing magnetic fields has evolved from ancient navigation purposes to the increasing need for improved sensitivity, smaller form factor, compatibility with modern electronic systems within airport security and structural stability [7.1].

Frost + Sullivan analyze the following magnetic field measuring methods:

- silicon-based magnetic sensors: anisotropic/giant/colossal magnetoresistance,
- different types of search coils (induction methods),
- fluxgate (force-based or induction-based) magnetometers,
- Hall / galvanomagnetic sensors,
- SQUIDs (superconducting quantum interference devices).

Figure 7.1 compares these magnetic sensors sensitivities and indicates the chapters in this Handbook where they are presented in detail.

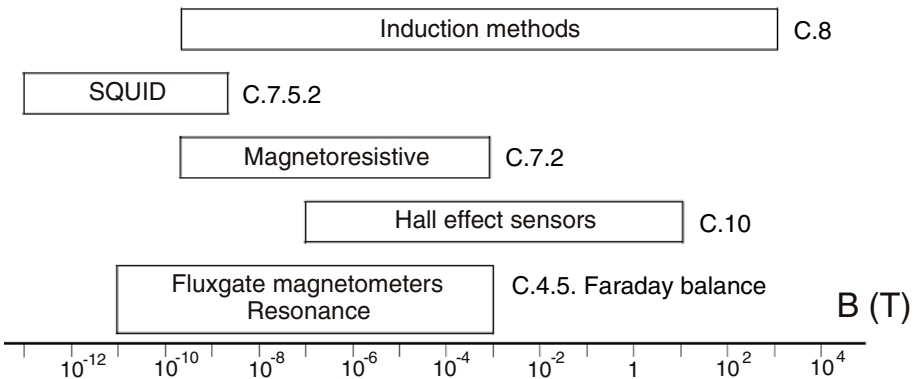
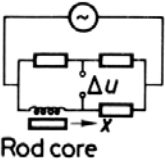
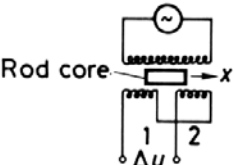
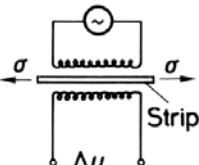
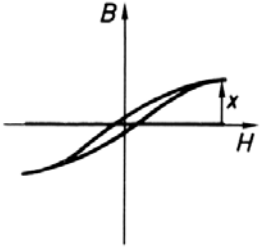
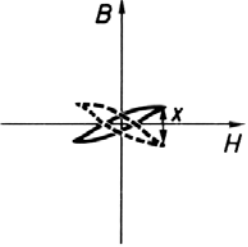
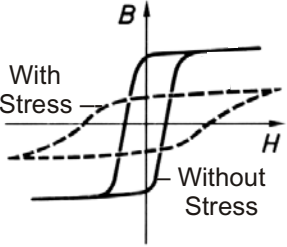


Fig. 7.1 Relative sensitivity for various magnetic field measurement techniques (redrawing from [7.1]). B is the magnetic induction, expressed in T (tesla).

Table 7.1 A review of magnetic sensor principles for various measurands – first part

Displacement x		Force F
Alternating current		
Inductance change ↓ Differential voltage	Change of flux distribution ↓ Differential voltage	Elastic strain ↓ Permeability change
 <p>Rod core</p>	 <p>Rod core</p>	 <p>Strip</p>
(A) 	(B) 	(C) 
Permeability, saturation	Permeability, saturation	Magnetostriction elasticity limit

Note the rows significance: 1. Process variable (displacement, force, magnetic field, rotational speed and current); 2. AC or DC option; 3. Fundamental and functional principles; 4. Schematic layout; 5. Magnetic characteristic and determinant property.

Table 7.1 A review of magnetic sensor principles for various measurands – second part

D.C. magnetic field H_0	Speed n	Current I
Direct current		
D.C. field magnetic biasing ↓ Occurrence of harmonics	Galvanomagnetic effect ↓ Hall voltage	
<p>(D)</p>	<p>(F)</p>	<p>(G)</p>
Initial and maximum permeability	Coercive field strength demagnetization curve	Permeability, magnetic resistance of the return path

Table 7.1 is a selective review of magnetic sensor principles for various measured quantities, made by SIEMENS AG [7.2]. Magnetic sensors are understood as those based on the principles and effects of the electromagnetic field and in some form or another contain magnetic material as the principal functional element. The following measurement principles are adaptable for

force transducers: changes in inductance (sketch A) or in flux distribution in a coil system (sketch B), elastomagnetic or magnetostrictive (sketch C), DC field magnetic biasing (sketch D) and galvanomagnetic ones (sketches F and G).

Parametric measuring systems utilize inductive changes; they are presented in Chapter 4. Here a coil is used either as an active element in a bridge circuit or as a frequency-determining element in an oscillator circuit. The bridge diagonal voltage or the oscillator frequency is an indication of the inductance. The magnetic circuit may be laid out in different ways, two distinctive types of configuration being *inductor* and *transformer* [7.3]:

- A magnetic workpiece approaches a coil system and increases the inductance (proximity switch type).
- A soft magnetic core moves in and out of a coil thus increasing or decreasing its inductance (LVDT: a pair of coils “penetrated” by a plunger).

Other types of electromagnetic force transducers are presented in this chapter and in the next three chapters as follows:

- C.8 – *Electrodynamic* force transducers based on moving coils;
- C.9 – *Magnetoelastic / magnetostrictive* force transducers;
- C.10 – *Galvanomagnetic* force transducers based on the Hall effect.

Figure 7.2, adapted by professor Aurel Millea [7.4], presents some typical measurement errors: offset, sensitivity, linearity and hysteresis. In order to choose the best measurement variant from the Table 7.1, it is recommended for B (magnetic induction) versus H (magnetic field intensity) diagrams to be linear, intersecting or approaching the origin point, being bidirectional (both in tension – first quadrant and compression – the “opposite” one) and having low hysteresis. In this respect, the optimum order for electromagnetic measurement principles connected with force transducers is G (Hall sensors) – D (DC field magnetic biasing, see Figure 7.11) – A or B (variable inductance, e.g. linear variable differential transformer) – C (magnetoelastic / magnetostrictive).

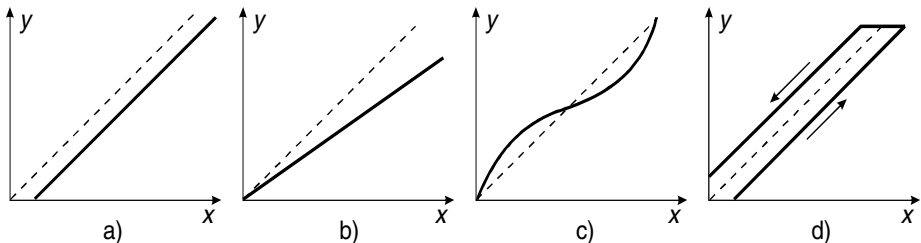
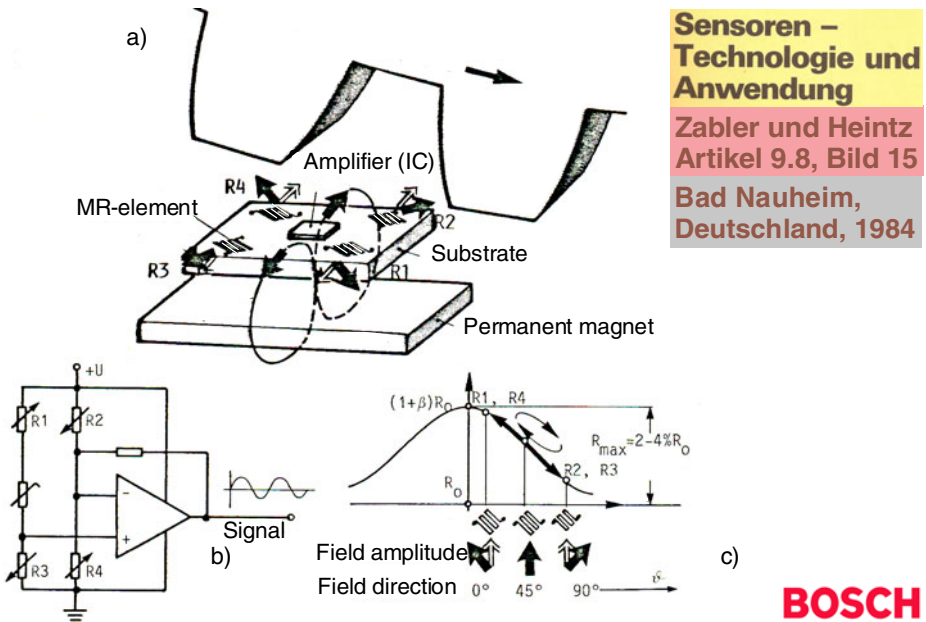


Fig. 7.2 Measurement errors: a) offset (additive), b) sensitivity (multiplicative), c) linearity, d) hysteresis (dotted line – ideal case, continuous line – real case)

7.2. MAGNETORESISTIVE FORCE TRANSDUCERS

The principle of anisotropic magnetoresistive (AMR) transducers is based on the fact that metals (e.g. bismuth), when cooled to low temperature, show a change of resistivity when subjected to an applied magnetic field [7.5].

The basic cause for the magnetoresistivity is the Lorentz force, which causes the electrons to move in curved paths between collisions [7.6]. For small values of the magnetic field, *the change in resistance R is proportional to the square of the magnetic field strength H*. A so-called “barber pole” structure consists of a series of strips with high electrical conductivity that force the current flow into an angle of 45° with respect to the easy axis (energetically favorable direction of the spontaneous magnetization in a ferromagnetic material) [7.7]. Each strip is arranged in a meander pattern and forms an arm of a Wheatstone bridge. The degree of bridge imbalance is then used to indicate the magnetic field strength, or more precisely, the variation in magnetic field in the plane of the permalloy strips normal to the direction of current. Two additional fixed resistors, formed on a silicon substrate, may be laser trimmed to balance the bridge under zero-magnetic field conditions.



**Sensoren –
Technologie und
Anwendung**
Zabler und Heintz
Artikel 9.8, Bild 15
Bad Nauheim,
Deutschland, 1984

BOSCH

Fig. 7.3 Magnetoresistive sensor for measuring rotational speed and power: a) Magnetoresistors positioning, b) Wheatstone bridge connection and measurement scheme, c) Output signal diagram

An industrial application (Fig. 7.3) is the magnetoresistive transducer for measuring rotational speed (and resulting power) [7.8]. A force transducer of 1 N (Fig. 7.4), patented by professor Klaus Horn from T.U. Braunschweig, was designed and tested being connected with springs of high rigidity [7.9]. With an appropriate arrangement of the field plates into a functionally designed transducer, a linear behavior and a high resolution of 2 nm is obtainable.

The 2007 Nobel Prize for Physics went jointly to Albert Fert of Université Paris-Sud, France, and Peter Grünberg of Forschungszentrum Jülich, Germany, for independently discovering the giant magnetoresistance (GMR) effect in 1988. The phenomenon of GMR is where weak magnetic changes in magnetic resistance give rise to big differences in electrical resistance; it is also worthily to support higher area density for hard discs.

Magnetoresistors are the simplest of Lorentz force devices, using semiconductors such as InSb and InAs [7.10]. The magnetoresistive effect depends on the electron mobility in the semiconductive material.

To date the best utilization of GMR materials for magnetic field sensors has been in Wheatstone bridge configurations (Fig. 7.5), although simple GMR resistors and GMR half-bridges can also be fabricated [7.11]. A sensitive bridge can be fabricated from four photolithographically patterned GMR resistors, two of which are active elements. These resistors can be as narrow as 2 μm allowing a serpentine 10 kW resistor to be patterned in an area as small as $(100 \times 100) \mu\text{m}^2$. The very narrow width also makes the resistors sensitive only to the component of magnetic field along their long dimension.

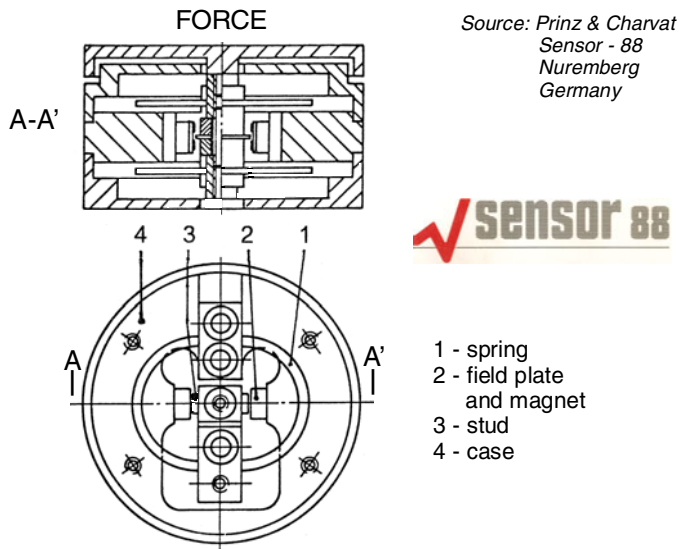


Fig. 7.4 Prototype of magnetoresistive force transducer (1 N)

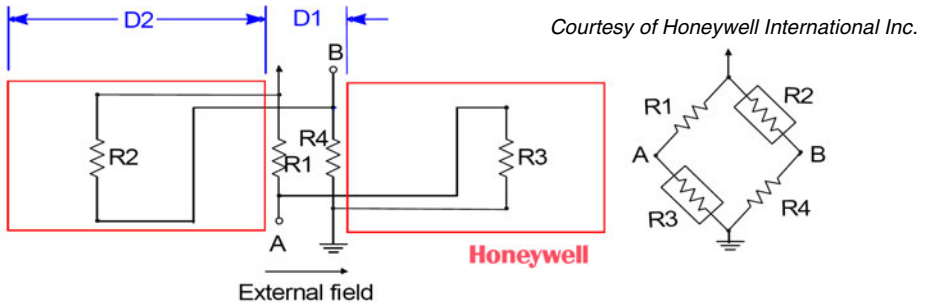


Fig. 7.5 GMR resistors in a Wheatstone bridge force transducer: R_1 and R_4 are active while R_2 and R_3 are for reference. D_1 is the length of the gap between the flux concentrators, D_2 is the length of one flux concentrator.

Small magnetic shields are plated over two of the four equal resistors in a Wheatstone bridge, protecting these resistors R_2 and R_3 from the applied field and allowing them to act as reference resistors. Since they are fabricated from the same material, they have the same temperature coefficient as the active resistors. The two remaining GMR resistors (R_1 and R_4) are both exposed to the external field. The bridge output is therefore twice the output from a bridge with only one active resistor. The bridge output for a 10 % change in these resistors is approximately 5 % of the voltage applied to the bridge.

Additional permalloy structures are plated onto the substrate to act as flux concentrators. The active resistors are placed in the gap between two flux concentrators as is shown in Figure 7.5. These resistors experience a field which is larger than the applied field by approximately the ratio of the gap between the flux concentrators, D_1 , to the length of one of the flux concentrators, D_2 .

The sensitivity of a GMR bridge transducer can be adjusted in design by changing the lengths of the flux concentrators and the gap between them. In this way, a GMR material which saturates at approximately 300 Oe can be used to build different sensors which saturate at 15, 50, and 100 Oe. External coils and feedback can be used to produce magnetoresistive transducers with higher sensitivity, in the 100 mA/m range.

The offerings from Honeywell [7.12], Philips Semiconductors [7.13] (e.g. the KMZ51 package) and Zetex Semiconductors [7.14] concerning the magnetic field sensors appear to be about the same in capability.

Hottinger Company proposes a robust, magnetic speed measuring system with high resolution [7.15], possible to use in complex applications together with torque, rotational speed, angle and power transducers.

The voyage of NASA's robot SPIRIT over the red planet's surface has been precisely controlled with 78 magnetoresistive sensors manufactured by Sensitec GmbH.

7.3. FORCE MEASUREMENTS IN MAGNETIC FIELD

A variety of forces have to be considered in magnetic separation of artificially synthesized liquids which are strongly magnetized: traction force, gravity, friction in the carrier medium and interparticle scattering. Force measurement in magnetic field is a difficult task, still depending on the modeling and computation procedures [7.16].

In using electromagnetic force to press uniformly a ferromagnetic soft mold written with microlens array cavity into a UV-curable resin on a glass substrate, a polymeric 300×300 microlens array with a diameter of $150 \mu\text{m}$ and a pitch of $200 \mu\text{m}$ has been successfully fabricated within the Department of Power Mechanical Engineering, National Tsing Hua University of Taiwan, R.O.C. [7.17].

Scanning electron microscopy (SEM) and optical observations confirm that these polymer microlens arrays, produced by electromagnetic force-assisted imprinting facility with UV exposure capacity, are without defects or distortion and have good pattern fidelity over a large area.

Figure 7.6 shows the electromagnetic force-assisted UV-imprint system consisting of a UV-transparent top plate (glass plate), an imprinted substrate, a UV lamp and an electromagnet with a power supply. A UV-curable resin Ormocomp (Micro Resist Technology GmbH), with the refractive index 1.52 at the 633 nm wavelength, is used. The current of the electromagnet is controlled by the power supply, through which the imprinted force is controlled. The wavelength of the UV lamp is between 365 and 410 nm while the intensity at 365 nm is $100 \text{ mJ}\cdot\text{cm}^{-2}$.

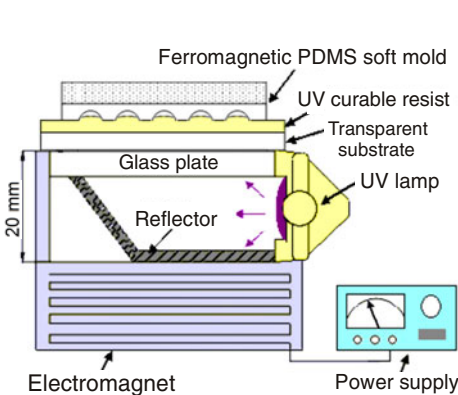


Fig. 7.6 Schematic functional diagram of electromagnetic force-assisted imprinting equipment

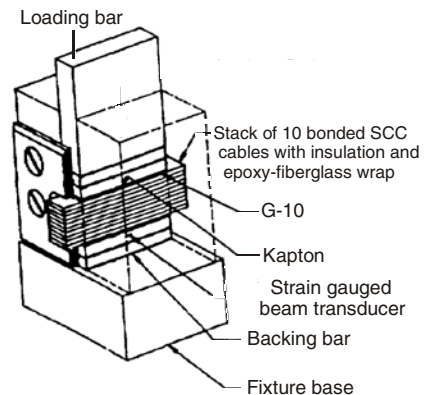


Fig. 7.7 Strain gauged cantilever for measuring internal forces in superconducting accelerator magnet

7.3.1. Resistive force transducers in magnetic field

The UniMeasure/80F force transducer [7.18] is a solid-state device which generates a linear output of resistance versus force. In fact, it is a semiconductor chip whose resistance varies as it is moved with the shaft in a controlled permanent-magnet field. The resistance output can be read directly on a conventional ohmmeter or digital multimeter and converted to force. The force can also be read directly in engineering units on a special digital panel meter. The principal specifications are:

- pull force is standard, but push or push-pull options are also available,
- linear load range: max. 3 kgf,
- nominal sensitivity: 0.11 ohms/gram,
- combined linearity and hysteresis error is equal to the deviation from the best straight line as a percentage of force reading.

A mechanism to vary magnetically the resistance of a linear fluid damper for exercise machines is illustrated in [7.19].

The measurement of internal forces in superconducting accelerator magnets (compressive stresses in coils and end restraint forces on the coils) by using bending mode deflections for sensing the applied loads with strain gauged cantilever at Brookhaven National Laboratory (US) is depicted in [7.20]. The beams are mounted in the SSC magnet collar packs. The strain gauge is bonded relatively far from the edge of the bar and thus is uniformly strained when subjected to bending from the pressure of the coil on the opposite face of the beam. The ends of the SSC dipole magnets are also subjected to a large axial Lorentz force (about 850 kN at 6.6 Tesla).

Calibrations are performed on a pair of strain gauged beams at ambient temperature, in the fixture shown in Figure 7.7. A known total load is applied with a press or other type of loading machine to a stack of 10 layers of cable type superconductor.

Figure 7.8 presents two variants of elastic elements for measuring the axial loads transmitted to the foundation by high voltage electromagnetic circuit breakers when acting [7.21]: a) longitudinal and transverse strain gauges have to be bonded on the classical tube; b) SGs with $\pm 45^\circ$ directions to be prepared for the tube with lateral holes.

A research team from T.U. Kaunas and Ekranas Company (Lithuania) succeeded in the shrinking force measurement of cathode ray tube's shrink fit rim band [7.22]. They have compared the following measurement methods:

- Magnetization method – applicable only for strongly magnetized materials;
- Barkhausen's noise method – effective only when controlling the shrinking force of shrink fit rim band top layers;
- CRT imitator-measurer is a meter simulating the tube base perimeter, designed only for a certain type of cathode ray tube.

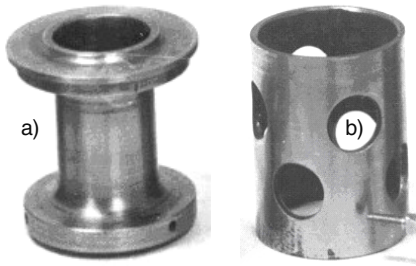


Fig. 7.8 Load cell elastic elements for high voltage circuit breakers [DMS]

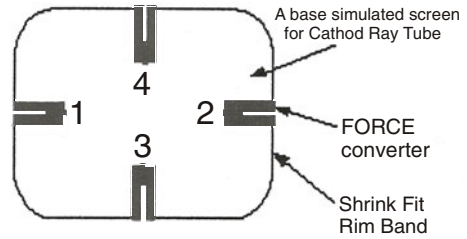


Fig. 7.9 Shrinking force measurement of cathode ray tube's shrink fit rim band

Four strain gauged load cells type HLC – H.B.M. having low overall height and maximum range of 17.6 kN were mounted like in Figure 7.9. The main characteristics of the cathode ray tube imitator-measurer are:

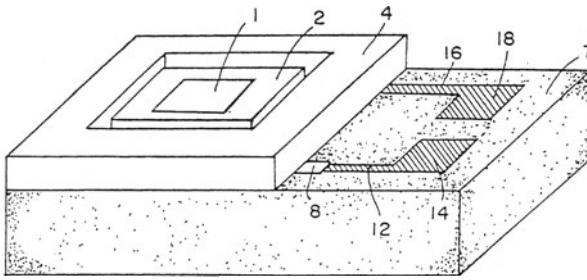
- number of measuring channels: 4,
- maximum value of measured force: 16 kN,
- max. measurement error: ± 50 N,
- resolution: 1N.

A micromachined piezoresistive cantilever magnetometer, with a self-calibration function on-chip integrated is presented in [7.23]. When the cantilever is subjected to a magnetic field to be measured, the magnetic force will exert upon the magnetized nickel thin-film pattern that is located at the cantilever end. The magnetic force bends the micromechanical cantilever, which is further read out by an integrated piezoresistor.

For realizing the self-calibration function, an aluminum spiral is integrated around the cantilever to provide an artificial magnetic field, when an electric current flows through the spiral coil. The artificial magnetic field can be used to drive the cantilever bending and causes a self-calibration output signal. With this on-chip self-calibration scheme, the detection of magnetic field can be immune to the long-term drift in remanence of the magnetized nickel pattern, thereby, improving the sensing stability. The formed sensor (by bulk micro-machining technologies) is used for magnetic-field measurement, resulting a piezoresistive sensitivity of $1.06 \times 10^{-4} / \text{mT}$ and sensing resolution of $4.6 \mu\text{T}$.

7.3.2. Capacitive force transducers in magnetic field

A research team of the Honolulu University in Hawaii has patented a magnetic and electric force sensing method using a static force responsive transducer made of a micromachined, solid state magnetic sensor consisting of a central silicon platform surrounded and supported by a thin silicon membrane [7.24]. This assembly geometry determines linearity, sensitivity and measuring range.



Source:
Holm-Kennedy + Umemoto
US Patent 5036286-1990

Fig. 7.10 Capacitive force sensing by solid state magnetic sensor

The Earth's magnetic field or a magnetic field of other origin acts as an attractive or repulsive force towards the magnetic material placed onto the silicon platform (Fig. 7.10). The magnetic force mechanically displaces the silicon platform and diaphragm membrane which is translated to an electrical signal where a change in capacitance is measured by variable overlapping.

7.3.3. Pressure transducers based on magnetic higher-order harmonic fields

A wireless, passive pressure transducer (without supply), based on the change in magnetic higher-order harmonic fields is described in [7.25]. This complex device is made of an airtight pressure chamber with two opposite membranes: a flexible membrane attached to a permanent magnetic strip (biasing element) and a rigid membrane attached to a magnetically soft ferromagnetic strip (sensing element). The flexible membrane of the chamber deflects with changing pressure, thus varying the separation distance between the sensing and biasing elements. This distance change alters the biasing field experienced by the sensing element, varying the pattern of its magnetic higher-order harmonic fields and allowing remote pressure monitoring through a magnetic coil. When exposed to an AC magnetic field, a magnetically soft ferromagnetic material generates a series of higher-order harmonic fields due to the nonlinearity behavior in magnetic induction.

Figure 7.11 illustrates the experimental setup. As depicted by the authors, the sensor was placed at the bottom of a pressure chamber. A pressure gauge was attached to the pressure chamber to record the actual pressure, and a bicycle pump was used to pressurize the chamber. The sensor was inside the pressure chamber and placed on the detection coil and the excitation coil. The excitation coil consisted of two sets of superimposed Helmholtz coils with a diameter of 25 cm. The sensor tracked the pressure variation by measuring the change in the magnetic 2nd order harmonic field. Finally, the sensor signal, recorded by the spectrum analyzer, was sent to the PC for processing through a GPIB interface with customized software in Visual Basic.

Reprinted with permission from [7.24],
copyright 2008

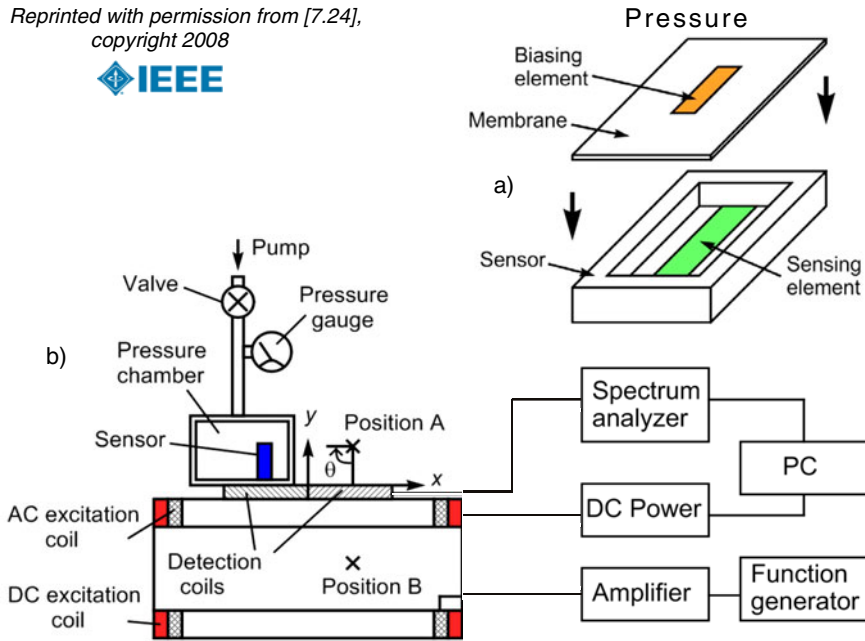


Fig. 7.11 Pressure transducer (a) based on the change in magnetic higher-order harmonic fields; experimental setup and measurement scheme (b)

Diaphragm-based pressure transducers have various applications including force, acceleration, fluid flow, and displacement measurements. Unlike pressure detectors that convey information through high frequency electromagnetic fields (MHz range), such as those based on an LC tank circuit or an RF transponder, the described transducer is interrogated with low frequency magnetic field (a few hundred Hz). This allows the output signal to pass through an electrically dense media (human body or water) without significant energy loss, extending thus the detection range.

7.4. ELECTROMAGNETIC WEIGHING BY FORCE COMPENSATION

EMFC is the classical abbreviation for electromagnetic force compensation: In the servocontrolled weighing systems the applied force is electromagnetically compensated [7.26]. The loading point displacement, caused by the force variation, is electrically measured and the resulting signal is fed back to the electromagnet (an *electric* coil associated with a permanent *magnet*). The current needed for compensation, digitally processed and displayed in engineering units, is a measure of the applied load (Fig. 7.12).

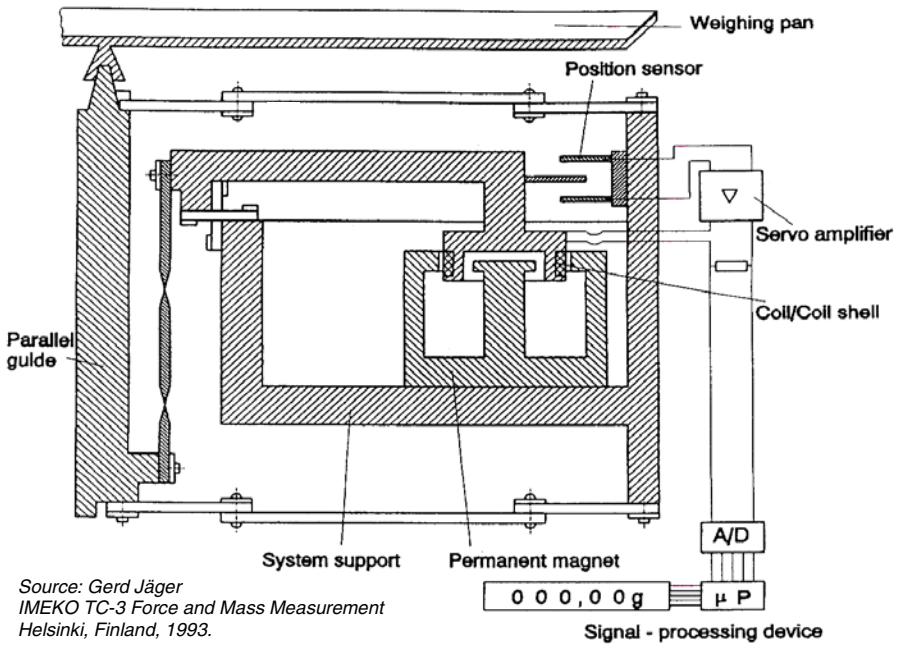


Fig. 7.12 Weighing cell based on electromagnetic force compensation (EMFC) [7.27]

This force feedback weighing machine is a complete measuring system, which combines sensing with actuating [7.28]: the applied force is directly proportional to the current through the actuator coil, and calibration is possible by finding the current required to balance a known mass m (or force $m \cdot g$).

Some companies, for example Mettler-Toledo, use the term Electro-Magnetic Force Restoration (instead of ... Compensation) [7.29]. Over the last years, the increasing performance of SGFT (strain gauged force transducers) has allowed them to compete with the EMFR load cells on their low end of the application cost versus characteristics spectrum (Fig. 7.13).

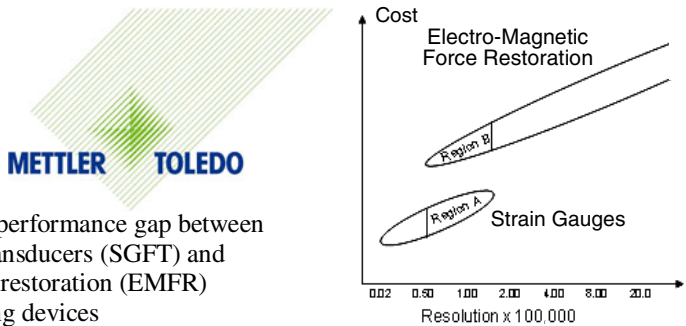


Fig. 7.13 Closing the performance gap between strain gauged force transducers (SGFT) and electromagnetic force restoration (EMFR) load cells and weighing devices

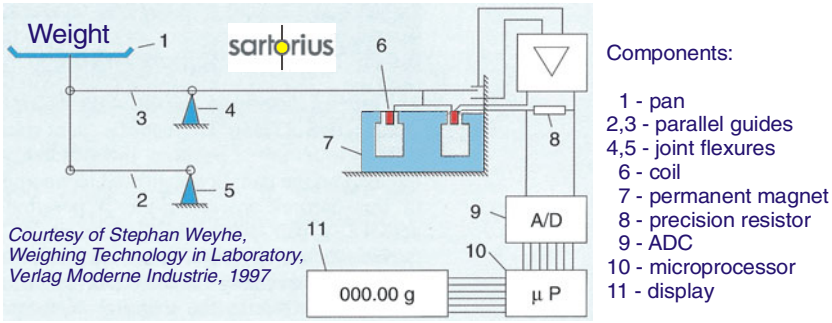


Fig. 7.14 Working principle of electromagnetic force compensation weighing cells

The weighing cells made by Sartorius [7.30] function according to the EMFC principle (Fig. 7.14) and feature a patented, completely monolithic design. The function of the parallel guides (2, 3) is to intercept the additional torque generated when a sample is off-centered on the weighing pan (1). All moving parts of the system rest on rugged joint flexures (4, 5), an excellent compromise between elasticity and rigidity. The force applied by the mass of a sample being weighed is compensated by the magnetic force of a coil (6) through which current flows. This coil is located in the gap of a permanent magnet (7), replacing the second pan with weights or the switching weights on the conventional balance. A precision resistor (8), integrated into the control loop, “transduces” the current into a voltage, proportional to the load on the pan. This signal is transmitted to the analog-to-digital converter (9), then filtered and digitally compensated by the microprocessor (10) and shown on a display (11). This rugged technology delivers the highest weight resolution along with the greatest accuracy and shortest response times.

7.5. ELECTROMAGNETIC DEVICES FOR SMALL FORCES

7.5.1. Electromagnetic probes for micro- and nano-force measurements

National institutes of metrology are developing nanoforce standards by using electrostatic force balances and transfer standards based on the EMFC principle. The active measurement method by null balance is more accurate and sensitive than the passive one utilizing piezoresistive cantilevers (Fig. 7.15).

KRISS has developed an electromagnetic probe to generate and to measure the micro- and nano-forces [7.31]. A thin cantilever mounted with a NiCr conducting wire (about 1 μm diameter) has been fabricated by MEMS process (Fig. 7.16a). This high sensitivity cantilever can be driven by Lorentz force generated by applying current into the wire under uniform magnetic flux.

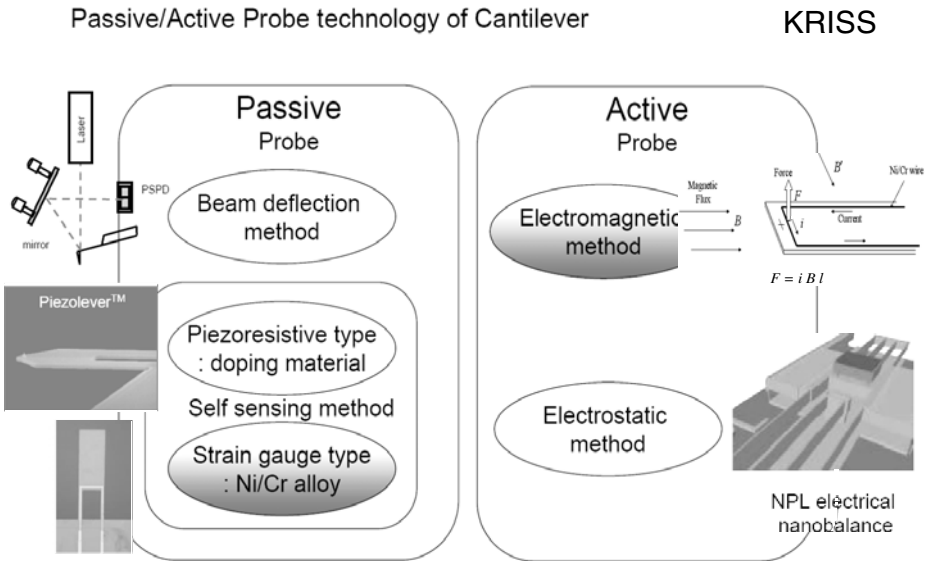


Fig. 7.15 Measuring micro/nano forces by cantilever probes in different technologies: passive (piezoresistive) and active (electromagnetic or electrostatic)

This simple electromagnetic circuit was analyzed by finite element analysis (FEA) and constructed to obtain high magnetic flux density. It has a spring constant around 0.01 N/m, ensuring high force sensitivity.

Source: In-Mook Choi et al.
 IMEKO TC-3 Conference on Force,
 Mass and Torque Measurements,
 Cairo, Egypt, 2005.

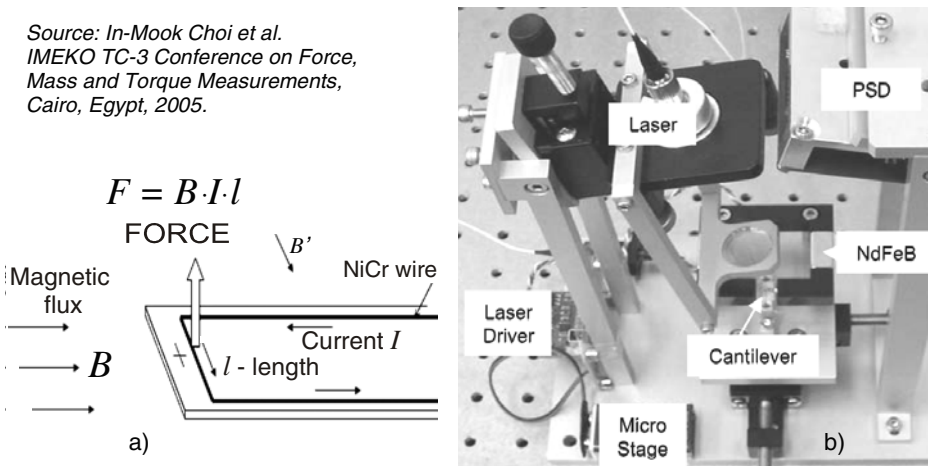


Fig. 7.16 High sensitivity cantilever driven by Lorentz force under uniform magnetic flux (a) and optical devices for detecting the electromagnetic probe deformation (b)

The system has permanent magnets for uniform magnetic flux generation and optical devices for detecting the cantilever deformations (Fig. 7.16b). A laser beam deflection system, including a laser diode and a PSD, detects the deformation of the electromagnetic active probe. In order to precisely measure micro/nano forces, the cantilever null position is controlled with the Lorentz force opposing to a vertical input force. This probe can be used as a transfer standard for microforce evaluation or in various researches, such as binding-force measurement between molecules, force lithography, and nanoindentation.

A planar integrated microdynamometer system with gear coupling and electronically controlled electromagnetic brake to provide variable mechanical loading is described in [7.32].

7.5.2. *Magnetic flux quantum as a sub-pico-newton weight*

As KRISS documentation states: Small force metrology, which is generally accepted as metrology for force below micronewton level, is attracting strong interest in pace with developing nano-science, but on the other hand staying almost uncultivated in a sense that there is too wide range from micronewton to zeptonewton (10^{-21} N) inside a simplified terminology of “small.”

A few-micron-sized superconducting ring or superconducting quantum interference device (SQUID) circuit is mounted on an ultrasoft micro-cantilever [7.33]. In a calibrated magnetic field gradient, dB/dz , a force is created on the superconducting ring. Through a designed procedure of magnetic field and temperature, which is different for a superconducting ring and SQUID, one can control the number of quanta and change the realized force by step. A quantum-weight generating cantilever device comprising a 20 micron-sized ring-shaped niobium film, deposited on the paddle of an ultrasoft single-crystalline silicon cantilever, is depicted in [7.34].

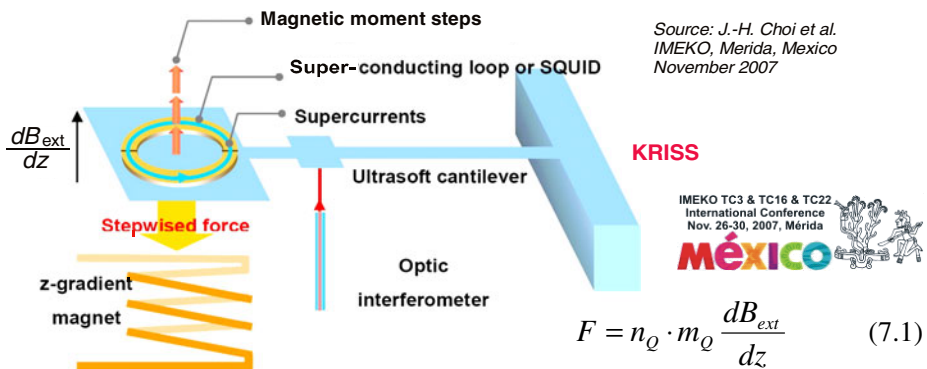


Fig. 7.17 Schematic of quantum-weight generating cantilever device

High-quality niobium film was patterned by optical lithography and deposited using an ultra-high-vacuum sputter system within the micro-fabrication process of cantilevers, which adopts double-side reactive-ion-etching.

A superconducting loop is mounted on an ultrasoft microcantilever with an external magnetic field gradient applied in a perpendicular direction. In superconducting state, magnetic flux through the loop is quantized, and the resultant magnetic moment has a component with constant steps. The step size is determined by fundamental constants such as electron charge and the length of the loop.

The force created on the superconducting loop is given by the relation (7.1), presented in Figure 7.17, where dB/dz is the magnetic field gradient, m_Q is a magnetic moment step by adding one flux quantum and n_Q is an integer. The field gradient, dB/dz , can be determined *in situ* from the resonance frequency shift of the cantilever.

Considering a niobium ring of inner and outer radii $5\ \mu\text{m}$ and $10\ \mu\text{m}$, respectively, and thickness of $50\ \text{nm}$, a force step is numerically estimated as $1.84 \times 10^{-13}\ \text{N}$ with dB_{ext}/dz of $10\ \text{T/m}$. This “smallest” measurable force (approx. $0.2\ \text{pN}$) causes a static displacement of about $2\ \text{nm}$ for a cantilever with an elastic constant $k_c = 10^{-4}\ \text{N/m}$, detectable by optical interferometry, a bare optical fiber end and a force device constituting a Fabry-Perot cavity.

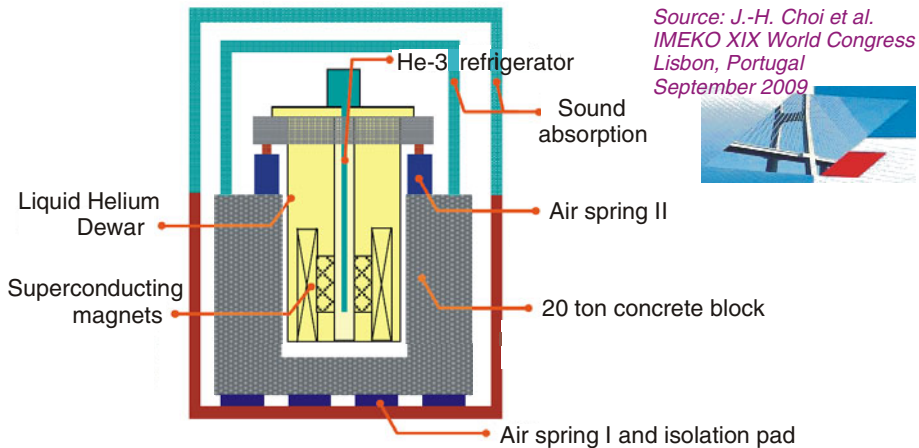


Fig. 7.18 Schematic of flux-quantum-based force facility at the Korean Research Institute of Standards and Science [7.35]. Superconducting magnets for generating uniform and gradient magnetic field are immersed in liquid helium and surrounds the piconewton standard force realization stage in an inner vacuum chamber installed at the bottom of He-3 refrigerator.

In order to produce and measure the discrete magnetic force on a superconducting ring in terms of the number of flux-quantum, a modern instrumentation has been developed to provide all the necessary conditions such as low temperature (4 K to 280 mK), high field-gradient (12 T/m), vibration isolation (-95 dB at 30 Hz), and high vacuum (Fig. 7.18).

Klaus von Klitzing was awarded the 1985 Nobel Prize for Physics for his work on Quantum Hall effect.

7.5.3. Casimir forces and levitation pressures measurement

Casimir force is a macro quantum effect strongly depending on the shape of the boundaries that confines the electromagnetic fields. Demonstrating this dependence requires geometries with interactions that deviate significantly from the pair-wise summation of two-body potentials.

The paper [7.36] presents Casimir force measurements between a gold-coated sphere and a silicon plate with an array of nanoscale, high-aspect-ratio rectangular trenches. A micromachined torsional oscillator acts as a force transducer, allowing measuring the interactions between the surfaces at high sensitivity. Channels with widths ranging from 200 to 500 nm and depth of 1 μm are fabricated on a silicon substrate. Such measurements open up new possibilities to manipulate the Casimir force by tailoring the shape of the interacting surfaces.

Due to the extremely small distances (under 1 μm) at which the Casimir force reaches measureable levels, an experimental verification succeeded only in 1996 [7.37]. Casimir force in the micrometer scale is negligible but at distances of 10 nm it means a pressure of 10 tons per square meter! Reducing distances further increases the forces dramatically. In fact, sticking, and the resulting high friction, is one of the most challenging topics in nano technology and tribology. Specialized software is capable to compute Casimir forces in really arbitrary geometries for nanoscaled machines (MEMS and NEMS). It features state-of-the-art mesh technology as well as a high degree of parametrizability in Finite Element Analysis.

A methodology involving a micromachined parallel-plate geometry to measure the Casimir force and its dependence on the boundary conditions of the electromagnetic field is presented in [7.38]. This is a new setup of micro-electromechanical means for parallelism control aiming to measure the Casimir force at sub-micron separation distances.

Hull and Komori [7.39] present a levitational system comprising a stationary, bulk high-temperature superconductor (HTS) and a levitated component (rotor) that consists of a cylindrical permanent magnet surrounded by an annular HTS. The rotor is cooled in a liquid nitrogen bath below the critical temperature of the HTS while surrounded by a ferromagnetic cage. When the

ferromagnetic cage is removed, the flux from the permanent magnet is essentially excluded from the interior of the high-temperature superconductor. When brought into proximity with the HTS stator, the cage-cooled rotor experiences a levitational force. This force is measured with a strain-gauge force transducer located outside of the liquid nitrogen bath.

As it can be seen in Figure 7.19, there exists a complex interdependence between the electromagnetic quantities and the other physical quantities. In this “planetary” system, the quantity “energy” is in a central position, that best characterizes the various transformation processes within the force transducers.

REFERENCES

1. Magnetic Sensors – Emerging Technology. Frost & Sullivan research service, May 3 (2009), <http://www.researchandmarkets.com/reports/c49941>
2. Boll, R., Borek, L.: Magnetic sensors of new materials. SIEMENS Forschungs- und Entwicklungsberichte 10(2), 83–90 (1981)
3. Regtien, P.P.L.: Instrumentation Electronics: Basic Electronic Theory and Techniques. Prentice Hall, New York (1992)
4. Millea, A.: Book of Metrologist. General Metrology. Editura Tehnică, București (1985) (in Romanian)
5. Webster, J.G. (Editor-in-Chief): The Measurement, Instrumentation and Sensors Handbook. CRC Press – Springer – IEEE Press, Boca Raton, FL (1999)
6. Fraden, J.: AIP Handbook of Modern Sensors – Physics, Design and Applications. American Institute of Physics, New York (1993)
7. Hauser, H., Stangl, G., Fallmann, W., Chabicovsky, R., Riedling, K.: Magnetoresistive sensors. In: Proc. Workshop on Preparation, Properties, and Applications of Thin Ferromagnetic Films, Vienna, Austria, June 15-16, pp. 15–27 (2000)
8. Zabler, E., Heintz, F.: Neue, alternative Lösungen für Drehzahlsensoren im Kraftfahrzeug auf magnetoresistiver Basis. Sensoren Technologie und Anwendung, Artikel 9.8, Bad Nauheim, Deutschland (1984)
9. Prinz, R., Charvat, R.: Sensor mit magnetoresistivem System zur Messung extrem kleiner Wegdifferenzen. In: Proc. Sensor 1988, Int’l Exhibition with Congress and Special Show for Research, Development and Application, Messezentrum Nürnberg, Deutschland, May 3-5, pp. 319–334 (1988)
10. Wecker, J.: Magnetoresistive Schichtsysteme und ihre Anwendungen. Fachveranstaltungsunterlagen “Magnetwerkstoffe für technische Anwendungen”, Haus der Technik, Aachen, Deutschland (2003)
11. Caruso, M.J., Bratland, T., Smith, C.H., Schneider, R.: A new perspective on magnetic field sensing. Honeywell International Inc., Morristown, NJ (May 1998)
12. Holman, P.A.: Magnetoresistance (MR) transducers and how to use them as sensors, 1st edn. Honeywell International Inc., Morristown, NJ (July 2004)
13. Magnetoresistive sensors for magnetic field measurement. PDF SC17 General Magnetism, Philips Semiconductors, Eindhoven, The Netherlands, September 6 (2000)

14. Hübschmann, S., Schneider, M.: Magneto-resistive sensors – Principles of operation and applications. Zetex Semiconductors plc, Oldham, UK, Application Note 20-96
15. Schicker, R.: Master of the rings – a robust, magnetic speed measuring system with high resolution. *Hotline Hottinger* (2), 14–16 (2003)
16. Henjes, K.: The traction force in magnetic separators. *Meas. Sci. Technol.* 5, 1105–1108 (1994)
17. Wen, T.-T., Hocheng, H.: Innovative rapid replication of microlens arrays using electromagnetic force-assisted UV imprinting. *J. Micromech. Microeng.* 19, Paper 025012 (2009)
18. UniMeasure / 80F force transducer. UniMeasure, Inc., Grants Pass/Corvallis, OR
19. Levins, B., Gravagne, I.: A magnetically controllable valve to vary the resistance of hydraulic dampers for exercise machines. In: *Proceedings IEEE/ASME International Conference on Advanced Intelligent Mechatronics*, Monterey, CA, July 24–28, pp. 492–497 (2005)
20. Goodzeit, C.L., Anerella, M.D., Ganetis, G.L.: Measurement of internal forces in superconducting accelerator magnets with strain gauge transducers. In: *Proc. Applied Superconductivity Conference*, San Francisco, CA, August 21–25 (1988)
21. Ștefănescu, D.M.: Load cells for measuring axial loads transmitted to foundation by high voltage circuit breakers when acting. *Buletinul Institutului Politehnic București – seria Mecanică*, Tom XLIII (3), 77–84 (1981) (in Romanian)
22. Augutis, V., Gailius, D., Milinskas, A.: Measurement of the shrinking force of cathode ray tube's shrink fit rim band. In: *CD Proc. XVII IMEKO World Congress on Metrology in the 3rd Millennium*, Dubrovnik, Croatia, TC-15, pp. 1926–1929 (2003)
23. Liu, J., Li, X.: A piezoresistive microcantilever magnetic-field sensor with on-chip self-calibration function integrated. *Microelectronics Journal* 38(2), 210–215 (2007)
24. Holm-Kennedy, J.W., Umamoto, D.K.: Magnetic and electric force sensing method and apparatus. US Patent 5036286 – 1990
25. Pereles, B.M., Shao, R., Tan, E.L., Ong, K.G.: A remote query pressure sensor based on magnetic higher-order harmonic fields. *IEEE Sensors Journal* 8(11), 1824–1829 (2008)
26. Wieringa, H.: Electrical force measuring transducers. In: *Proc. Symp. Force, Pressure, Displacement and Flow Sensors*, May 13–14, pp. 179–197. Twente University of Technology, Enschede (1982)
27. Jäger, G.: High-speed weighing engineering. In: *Proceedings 13th IMEKO TC-3 Conference on Force and Mass Measurement*, Helsinki, Finland, May 11–14, pp. 230–236 (1993)
28. Usher, M.J., Keating, D.A.: *Sensors and Transducers – Characteristics, Applications, Instrumentation, Interfacing*, 2nd edn. MacMillan, Houndmills (1996)
29. Sawh, C.: Closing the performance gap between strain gage and electro-magnetic force restoration load cells. In: *Proc. 6th APMF*, Shanghai, China, November 3–6, pp. 183–188 (2003)
30. Weyhe, S.: *Weighing Technology in the Laboratory: Technology and Applications*. Sartorius + Verlag Moderne Industrie, Landsberg/Lech (1997)

基本單位與導出單位關係圖 Derivation of Base Units

DMS

氣

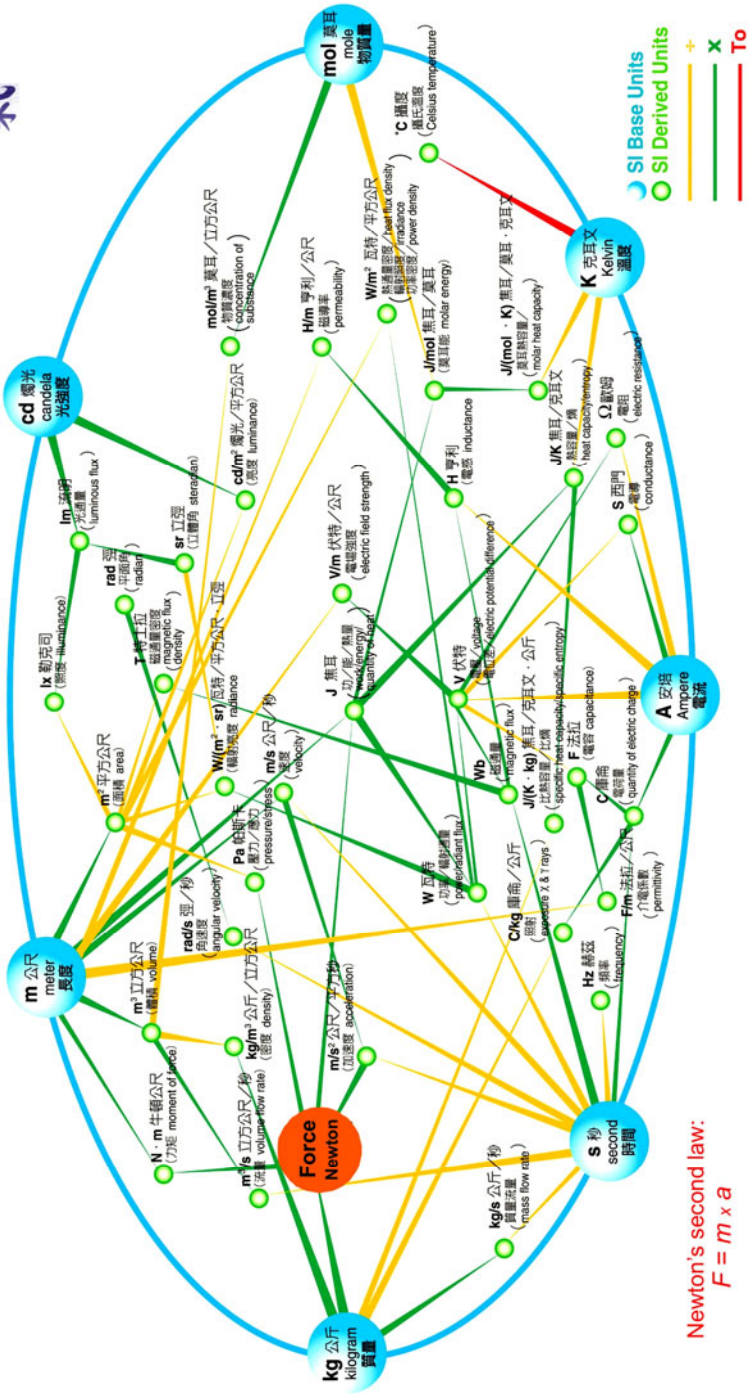


Fig. 7. 19. A planetary system of representation of the SI base and derived measurement units

31. Choi, I.-M., Kim, J.-H., Lee, H.-J., Kim, M.-S., Park, Y.K., Woo, S.Y., Kang, D.-I.: Development of electromagnetic probe for micro force measurement. In: CD Proc. 19th IMEKO TC-3 Int'l Conf. Force, Mass & Torque Measurements: Theory and Application in Laboratories and Industries, Cairo, Egypt, Paper 46 (2005)
32. Christenson, T.R., Klein, J., Guckel, H.: An electromagnetic microdynamometer. In: Proc. IEEE MEMS, Amsterdam, Netherlands, January 20-February 2, pp. 386–391 (1995)
33. Choi, J.-H., Choi, M.-S., Kim, M.-S., Park, Y.-K.: Magnetic flux quantum as a sub-pico-newton weight. In: Proc. Asia-Pacific Symp. Mass, Force and Torque (APMF 2005), Jeju Island, Korea, August 30-September 3, pp. 99–104 (2005)
34. Choi, J.-H., Lee, K.-C., Kim, Y.-W., Kim, M.-S.: Characterization of quantum-weight generating cantilever device. In: CD Proceedings IMEKO Int'l Conf. Cultivating Metrological Knowledge, Session 1.1, Merida, Mexico, November 27-30 (2007)
35. Choi, J.-H., Kim, M.-S., Park, Y.-K., Kim, Y.W., Kang, D.-I.: KRISS approach to pico-newton standard force realization. In: Proc. XIX IMEKO World Congress on Fundamental and Applied Metrology, Lisbon, Portugal, pp. 406–409 (2009)
36. Bao, Y., Ho, B.C.: Casimir force measurements between a sphere and a surface with high-aspect ratio, nanoscale channel arrays. American Physical Society, Ref. (March 1, 2007)
37. Casimir force simulation and nanomachines, May 6 (2009), http://www.functional-materials.at/rd/rd_spa_casimir_en.html
38. Nawazuddin, M.B.S., Lammerink, T.S.J., Wiegerink, R.J., Elwenspoek, M.C.: Measurement setup for detecting the Casimir force between parallel plates separated at a sub-micron distance. *J. Micromech. Microeng.* 20, Paper 064005 (June 2010)
39. Hull, J.R., Komori, M.: High levitation pressures with cage-cooled superconductors. *Supercond. Sci. Technol.* 15(5), 763–768 (2002)

Chapter 8

ELECTRODYNAMIC FORCE TRANSDUCERS

Table 8.1 Electromagnetic versus Electrodynamic – specific differences and possibilities of interchangeability

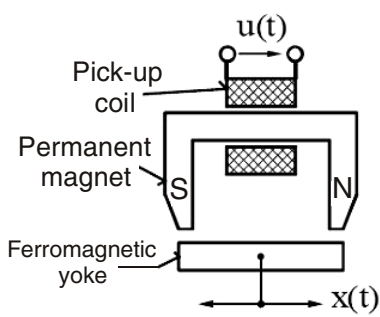
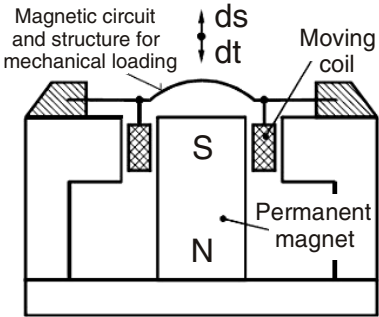
ELECTROMAGNETIC	ELECTRODYNAMIC
Moving magnet or magnetic circuit part	Moving coil
	
FARADAY'S LAW (1831)	INDUCTION LAW
$u = - N \cdot d\Phi/dt$ <p>where $\Phi = B \cdot A$</p> <p>u – electromotive force</p> <p>B – magnetic induction</p> <p>Φ – magnetic flux</p> <p>N – number of turns</p> <p>A – turns cross section area</p> <p>t – time</p>	$u = B \cdot l \cdot v$ <p>where $v = ds/dt$</p> <p>u – electromotive force</p> <p>B – magnetic induction</p> <p>l – conductor length</p> <p>v – speed of moving coil</p> <p>s – space of movement</p> <p>t – time</p>

Table 8.1, including two redrawn figures after Antonin Platil [8.1], shows the main characteristics of electromagnetic and electrodynamic devices, as well as their fundamental difference: voltages are induced by transformation or by moving. Certain authors use interchangeably the two words; they have the same “root.” These terms, like their defined phenomena, are strongly connected. Here are four different examples:

- Electromagnetic propulsion and its inverse, electrodynamic braking, in space sailing applications [8.2];
- Schneider Electric Ind SA designed an electromagnetic compensation for a circuit breaker with high electrodynamic force [8.3];
- The electromagnetic force analysis for an electrodynamic suspension [8.4] requires extended interdisciplinarity: magnetic levitation, eddy current, lift to drag (force) ratio, finite element method and so on;
- US Patent subclass 335/195 is entitled: Magnetic or electrodynamic force!

These two terms symbiosis is illustrated in Figure 8.1, representing an electrodynamic field generator with crossed electric and magnetic force vectors.

The official name of the StarDrive “Electronic Dynamo”, discovered by Mark Tomion, is Electrodynamic Field Generator [8.5]. The EDF generator uses banks of permanent magnets and rotating field coils to produce a very-high DC rotor voltage, and plane-parallel ring electrode arrays to electrostatically expand and control that voltage as applied to the outer hull, so that huge quantities of external field electrons may be accelerated to energy levels which are usually achieved only with a particle accelerator!

As the author states, this electrodynamic field generator is a marvelous synthesis of proven and familiar modern technologies to achieve a remarkable machine. The synergistic union of electrical dynamo and vacuum tube technologies yields a device which may result in surprising new vistas for humankind after building “The Time Machine.”

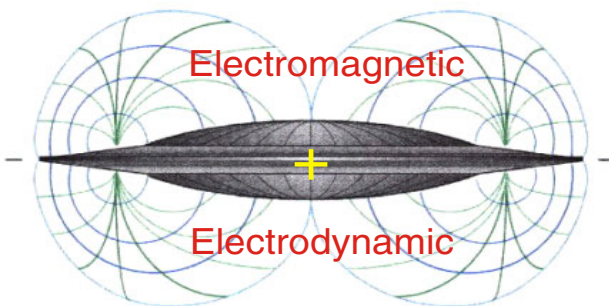


Fig. 8.1 Electrodynamic field generator configuration showing the crossed electric and magnetic force vectors

8.1. ELECTRODYNAMIC FORCE COMPENSATION PRINCIPLE

A current flows in a magnetic field generates a force [8.6]. The resultant force F is proportional to the magnetic field B , the current I and the path length l in the magnetic field. Since for weighing applications the magnetic field is perpendicular to the direction of the current flow, the force is perpendicular to both the magnetic field and the current flow (Fig. 8.2a). If B and l are constant, the proportionality between force and current can be easily measured.

$$F = B \cdot I \cdot l \quad (8.1)$$

In weighing systems an applied mass generates a force under the influence of gravity. The conversion from a force to a current is not achievable. This leads to a compensation principle where the force due to the mass is compensated by a counter force so that the difference between the two forces is zero. The current used to achieve the equilibrium is proportional to the force.

This equilibrium is not static so that the current has to be controlled by a regulator, which uses the coil position as input. If the coil is not at the zero position, the current is changed in the direction indicated by the sign of the positional deviation so that the coil is moved back to zero (Fig. 8.2b). This is a *dynamic* system and the principle is often called *electrodynamic force compensation*. The advantages of such a system are:

- there is no friction,
- the system is active, that means it is controllable,
- no coil displacement at the time of measurement, so the system measures always at the same set point.

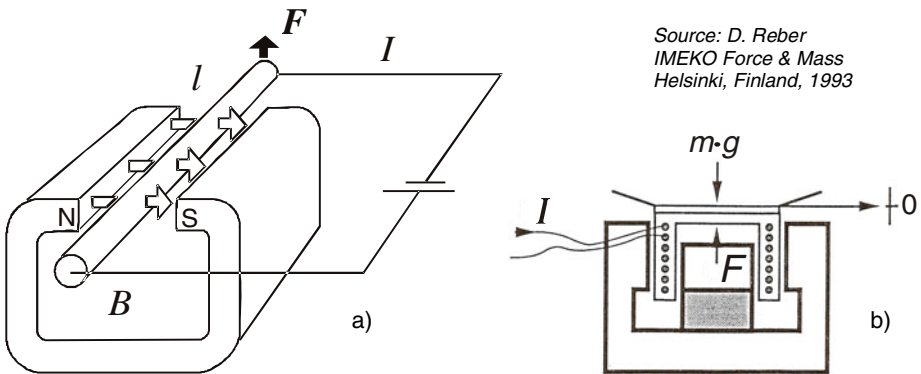


Fig. 8.2 A current I flowing through a conductor l in a magnetic field with induction B generates a force F (a). Electrodynamic force compensation for weighing balances (b).

8.2. LOAD CELLS WITH ELECTRODYNAMIC FEEDBACK

Closed-loop, electrodynamic force cells are used for weighing light objects in the range of 0.1 mg to 100 g [8.7]. Figure 8.3a shows how an upward force F_i is generated electromagnetically to equal the external, downward force F_e . Equilibrium position can be sensed electro-optically or with a high-resolution LVDT. The electromagnetic force is generated by a coil and permanent magnet assembly, similar to that used in loudspeakers, but without spring. The LVDT output is conditioned by a phase-sensitive rectifier and low-pass filter, then by a proportional plus derivative compensator (COMP) and integrator (INT); its output, V_c is processed by a transconductance amplifier (VCCS), and its output, i_c is the input of the force coil. The block diagram is depicted in Figure 8.3b.

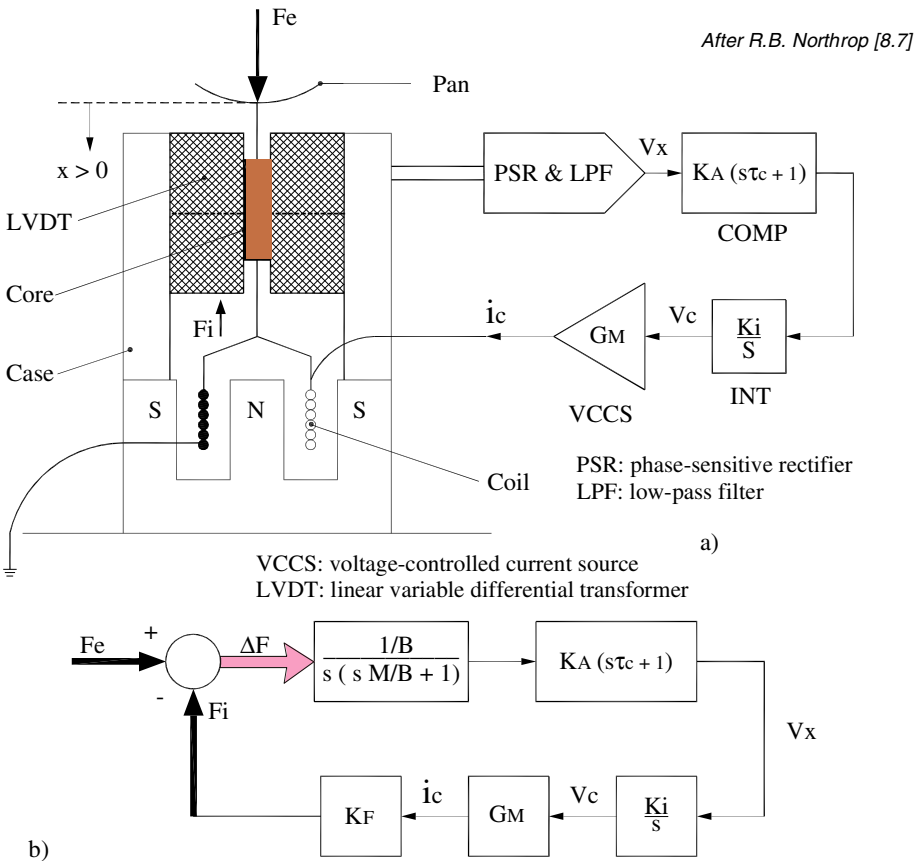


Fig. 8.3 Section through an electrodynamic feedback load cell (a) and equivalent block diagram of the electrodynamic measurement system (b)

Computer aided modeling and parametrical design of electrodynamic force transducers are presented in [8.8]. The design, construction and calibration of an electrodynamic shaker or vibrator for lightweight structures at high frequencies (several kHz) are described [8.9]. This electrodynamic force generator uses a conventional wire-wound coil onto which is assembled a force gauge. The force transducer is made by using a miniature piece of piezoelectric material, being useful for frequency response function measurements.

An electrodynamic force transducer used as an actuator in the active vibration control of various electromechanical systems is presented in [8.10].

8.3. ELECTRODYNAMIC FORCE COMPENSATION BALANCES

8.3.1. Hydrodynamic gravimetric balance

A 30-ton weighing system [8.11] had to achieve a resolution of 3 million increments with the guarantee that the expanded measurement uncertainty would not exceed 0.01 %. The final decision fell in favor of a dual-balance weighing system (Fig. 8.4) that combines two different principles of force measurement, respectively:

- three independent strain gauge force transducers (SGFTs), arranged to support the weighing tank and, below these,
- a “classic” beam scale with electronic readout for an electromagnetic force compensation (EMFC) weighing system. Conforming to the usual duality of terms, this main component of the Hydrodynamic Test Field is denominated “lever balance with electrodynamic force compensation.”

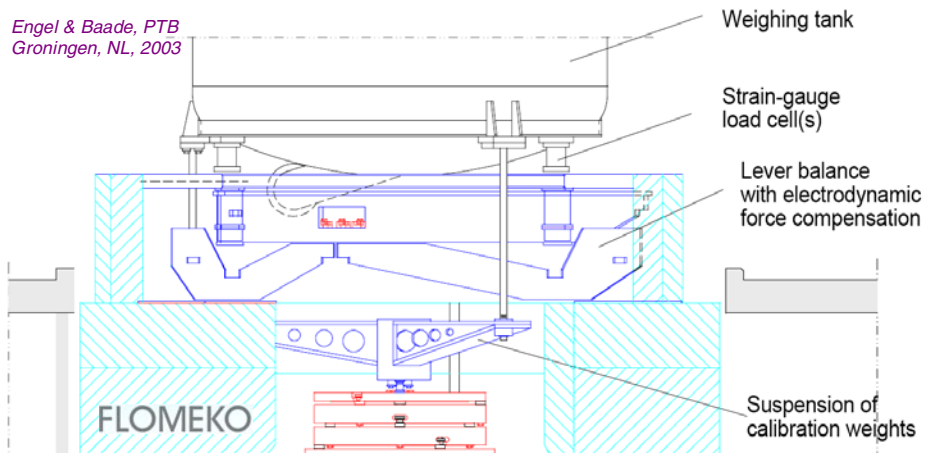


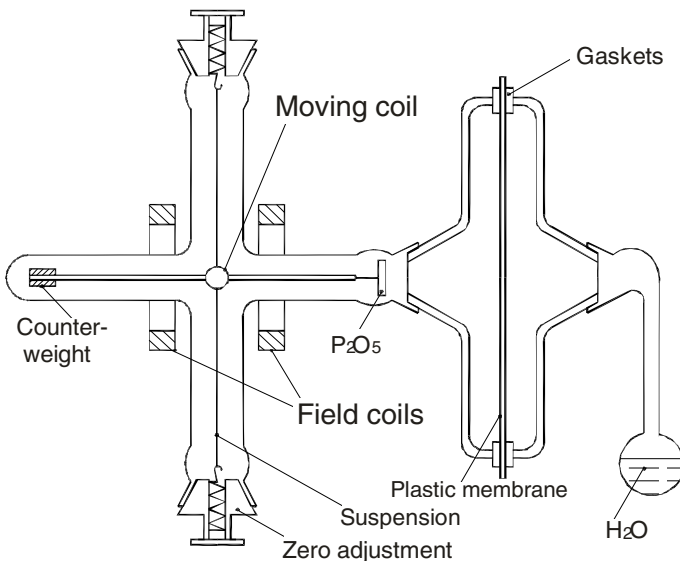
Fig. 8.4 Dual-balance (strain gauged load cells and electrodynamic force compensation lever) as gravimetric reference system at Physikalisch-Technische Bundesanstalt

8.3.2. *Electrodynamic vacuum microbalance*

In the age of microsystems and nanodevices technology, traceability of smallest forces in the μN and nN range is demanded by industry [8.12]. The precise electrodynamic compensating balance permits weight forces to approx. 12 N to be measured with a resolution of $10\ \mu\text{N}$. The precision piezoelectric device allows displacement by up to $100\ \mu\text{m}$, with a resolution of $1\ \text{nm}$ and a repeatability of the position of $\pm 5\ \text{nm}$.

The introduction of feedback control [8.13], applicable to all basic mechanical balances, resulted in improved performance with reduced demands of mechanical design. Compensation by electromagnetic or electrostatic forces is by far more elegant and easily lends itself to automation with the aid of feedback control. It also facilitates the simultaneous observation of different measurands, such as mass, force and torque components.

The closed loop of an electromagnetic balance contains a comparator (e.g. a balance beam), a deflection sensor, a controller and an electromagnetic actuator. The input is a weight or a force; the output may be a current. The sensor can be based on diverse physical effects, such as electrostatic or electro-magnetic induction, and various optical methods, like interferometry or polarization. {Observe the perfect agreement with Figure 7.15, illustrating the active and passive probe procedures within KRISS!}



Source:
Th. Gast
T.U. Berlin

Fig. 8.5 Permeation measurement with the electrodynamic vacuum microbalance using inductive sensors and amplitude modulation of the carrier frequency (Reprinted from [8.13], copyright 1994, with permission from Elsevier)

If the electromagnetic actuator is replaced by an electrodynamic one, with a moving coil in the air gap of a magnet, the well-known electrodynamic balance results, as it is built by many corporations today.

For the vacuum microbalance (Fig. 8.5) an electrodynamic torque motor was used, consisting of a pair of Helmholtz coils rigidly mounted outside the vacuum chamber, and a moving coil attached to the balance beam inside the chamber. The moving coil was suspended in taut bands of platinum-nickel alloy. They served as electrical connections and could be twisted from the outside by ground-in metallic stoppers in order to tare the balance.

With a constant current exciting the field coils and an arbitrarily variable and measurable current flowing through the moving coil, this system represents a dynamometric electrobalance, if the direction of the balance beam is optically detected and kept horizontal by adjusting the current, having an operator as controller!

The combination of field coils and moving coils represents a variable transformer. In order to be self-compensated, the system needs alternating excitation too, two kinds of currents (AC and DC) flowing simultaneously through the Helmholtz coils. An electronic circuit like in Figure 8.3b is recommended to ensure the automatic compensation of the microbalance.

8.3.3. Electrodynamic devices for small particles experiments

Historically, electrodynamics began when Gauss and Weber generalized Coulomb law for the case of moving charges postulating that interaction force between two charges depends on their velocities difference, i.e. on their relative movement [8.14].

A team of Physics Department, Texas A&M University employed a Paul-Straubel ring-type electrodynamic trap to study the movement of the single microparticles [8.15] while the researchers from Chemical Engineering Dept, University of Bremen presented a method to determine the drag force for a spherical particle in a double ring electrodynamic trap [8.16].

The thermophoretic force on single microspheres has been measured over a wide range of Knudsen numbers and particle thermal conductivities for solid and liquid spheres in air [8.17]. The measurements were accomplished by electro-dynamically levitating the particle between heated and cooled plates mounted in a vacuum chamber.

A time-domain analysis of an active medium based on a coupled quantum mechanical and electromagnetic model to accurately simulate the dynamics of silicon-based photonic devices is presented in [8.18]. This approach has been used to electro-dynamically model the light amplification and amplified spontaneous emission in 1D silicon nanocrystals, as well as the novel photonic crystal-based silicon microcavity.

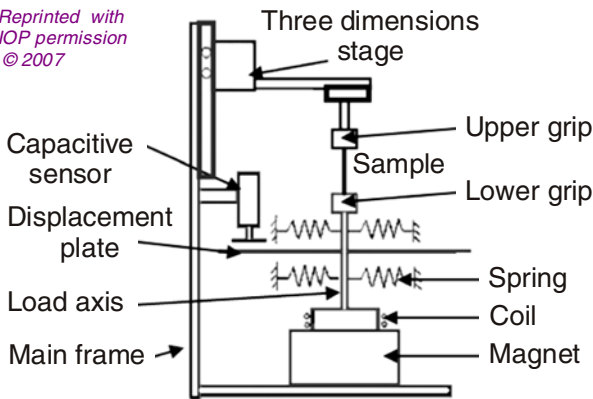
8.4. MICROMECHANICAL TESTERS WITH MOVING COILS

An electrodynamic transducer includes a frame and contains at least one electric coil which is placed in a static magnetic field and which can move about a rest position in a vertical free space [8.19]. The coil(s) is/are wound around and fixed to a mandrel and a return member is used to return the coil-bearing mandrel to the rest position in the absence of an external bias, the straight cylinder defining an inner volume and an outer volume. The magnetic field is produced by outer and inner magnetic structures, each comprising at least one fixed permanent magnet in the form of a ring.

An invention of an electrodynamic force measuring apparatus [8.20] comprises a force coil arranged in a stationary magnetic field and movable out of a null position by the action of the force which is to be measured; this force coil is supplied with a current through the agency of an amplifier as a function of its deviation out of the null position as detected by a feeler, and this current producing, under the action of the stationary magnetic field, a restoring force which forces back the force coil into the null position.

A moving-coil tester, named as MicroUTM (Universal Testing Machine), has been developed for testing various samples in tension, compression and bending experiments [8.21]. The main component is a moving coil suspended in a uniform magnetic field through a set of springs (Fig. 8.6). This coil has a double function: it is driven as an actuator and, at the same time, it senses the applied force. When a current passes through the coil, the electromagnetic force is proportional to the current magnitude in the region of the uniform magnetic field, subtracting the spring force induced by the displacement. So, the load is sensed by this current while the displacement is measured using a non-contact capacitive sensor.

Reprinted with
IOP permission
© 2007



Source:
Yong Huan et al.
Chinese Academy of
Sciences, Beijing

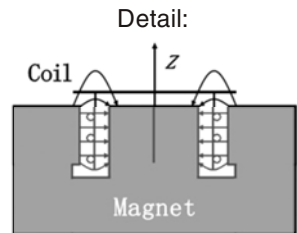
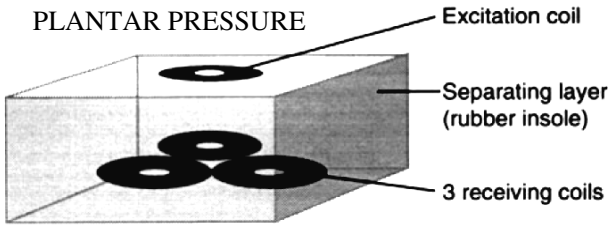


Fig. 8.6 Moving-coil micromechanical tester for tension-compression experiments



*Source: Stephen Urry
Meas. Sci. Technol.
R16 - R32, 1999*

Fig. 8.7 A 3D force and displacement transducer based on moving coils as alternative to FSRs (force sensing resistors). Reprinted with permission IOP Publishing from [8.22].

A four-coil triaxial transducer for plantar pressure measurements is presented in [8.22] being first time described in [8.23]. This technique uses one coil for excitation and other three for sensing (Fig. 8.7). The three receiving coils are symmetrically arranged about the center of the excitation coil and separated from it vertically by a silicone rubber insole. Application of a force produces the excitation coil movement and induces emfs in the sensing coils to be processed for estimating their displacement in three orthogonal directions.

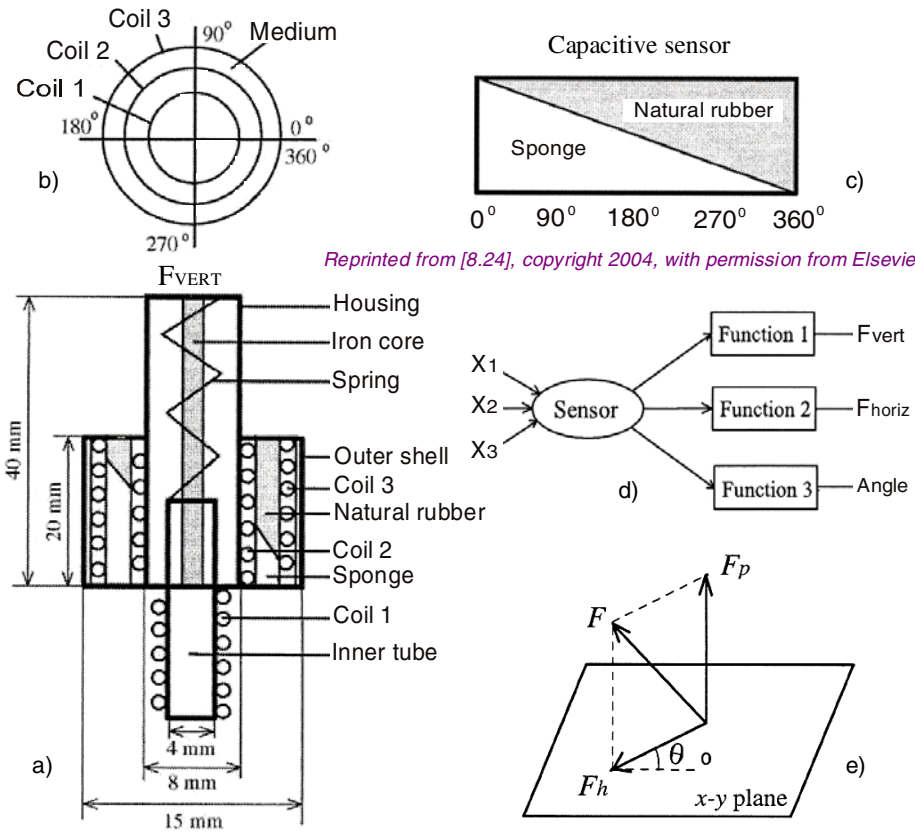
8.5. MULTIFUNCTIONAL TRANSDUCERS WITH MOVING COILS

A multifunctional transducer can be defined as a complex device having more than one sensing function [8.24]. In Figure 8.8 is depicted such a transducer having the following measurement functions:

- vertical (perpendicular) force – measured by inductive sensing,
- horizontal force magnitude – measured by induced sensing,
- horizontal force direction – measured by capacitive sensing.

Fig. 8.8a is a schematic cross section presenting three coaxial cylindrical acrylic structures: an inner tube with bottom, housing and outer shell. Then, an iron core in the middle of the transducer, with the same length as the housing, the top end of which is fixed on the housing. The inner tube can move up and down along the iron core. A fine copper wire is wound to make a coil from the bottom of the inner tube and a spring is mounted to connect the housing with the inner tube. Between the housing and the outer shell, there are two coaxial coils (2 and 3) and a tube-shaped dielectric medium which completely fills the space between the two coils. This medium is made of two elastic, dielectric materials: natural rubber and sponge, having the relative permittivities 4 and 2.5, respectively.

Fig. 8.8b shows the bottom view of the transducer assembly. In the second mode of operation, a force is applied only to the midpoint of the outer shell. A source of sinusoidal voltage is applied across coil 2, while a digital multimeter measures the amplitude of the electromotive force across coil 3.



Reprinted from [8.24], copyright 2004, with permission from Elsevier

Fig. 8.8 Multifunctional force transducer: a) sectional view with inductive plunger and coaxial induction coils; b) bottom view of three concentric coils; c) unfolded dielectric surface for capacitive sensing; d) block diagram for three measured variables; e) final results for vertical force F_{vert} , horizontal force F_{horiz} and the associated in-plane angle θ

Fig. 8.8c shows the unfolded dielectric medium. The same coils 2 and 3 work as two tube-shaped electrodes and the capacitance C between them is measured by an LCR meter, which, like the previously mentioned digital multi-meter, is used as an additional control means. Because the compositions of the two elastic materials which make up the dielectric medium between the two coils are different, the ratio of natural rubber to sponge is different at various angles (two opposite triangular surfaces). When a force is applied in different directions in turn, different capacitive changes occur.

Fig. 8.8d represents the block diagram of the multifunctional force transducer. A synthesized vision of the three-dimensional force measurement system, combining three different sensing principles, is presented in Table 8.2.

Table 8.2 Multifunctional and multicomponent force transducer using three different measurement principles

Func- tion	Measured variables	Components in Figure 8.8	Type of sensing	Chapter in this Handbook
1	Force F_{vert}	Coil 1 + iron core	Inductive	4
2	Force F_{horiz}	Coil 2 as exciter Coil 3 as detector	Induced	8.4
3	Angle θ	Coil 2 + 3 as tubular electrodes	Capacitive	5

This ingenious assembly permits the measurement of three different quantities with a single transducer. It resolves only two components of the force F : one in the perpendicular direction (z-axis), F_p and other in the horizontal direction, F_H . The angle θ is measured in polar coordinates within the horizontal plane x-y (Fig. 8.8e).

REFERENCES

1. Platil, A.: Mechatronics sensors: Direct measurement of velocity. PDF (January 2005)
2. http://www.bestsyndication.com/072407_solar-power-sailing-in-outer-space-extend-long-distance-travel.htm, July 24 (2007)
3. Rival, M., Blancfene, M., Grelier, C.: Circuit breaker with high electrodynamic force and breaking capacity. Abstract of JP 2000106075, data supplied from the esp@cenet database, May 9 (2009)
4. Iwatani, Y., Torii, S.: Analysis of electromagnetic force of electrodynamic suspension with quasi-three dimensional analysis. *International Journal of Applied Electromagnetics and Mechanics* 25(1-4), 61–67 (2007)
5. Tomion, M.: StarDrive Engineering. US Patent 6404089, June 11 (2002)
6. Reber, D.: Electrodynamic force compensation devices in mass comparators. In: Proc. 13th Int'l Conf. Force and Mass Measurement, Helsinki, Finland, May 11-14, pp. 205–210 (1993)
7. Northrop, R.B.: Introduction to Instrumentation and Measurements. CRC Press, Boca Raton (1997)
8. Pedraza, B.: Computer aided modeling and design of electrodynamic force transducers. *Electronics and Electrical Engineering, computer science in UK Collections*. City University of London (1983)
9. Grice, R.M., Pinnington, R.J.: An electrodynamic shaker with an integral force gauge for high-frequency measurements on lightweight structures. In: Proceedings of the Institution of Mechanical Engineers, Part C, vol. 214(10), pp. 1285–1297 (2000)

10. Lozina, Z., Vučina, D., Sedlar, D.: Active vibration control of electro-mechanical system with step excitation and electromagnetic actuator. In: *Procs. Int'l Symp. Coupled Methods in Numerical Dynamics*, Split, Croatia, September 16-19, pp. 345–350 (2009)
11. Engel, R., Baade, H.-J.: New-design dual-balance gravimetric reference system with PTB's new 'Hydrodynamic Test Field'. In: *Proc. 11th Int'l Conf. Flow Measurement – FLOMEKO*, Groningen, The Netherlands, May 12-14 (2003)
12. New force measuring device from 10 mN to 10 N. *Physikalisch-Technische Bundesanstalt, Annual Report* (2002), <http://ptb.de/en/publikationen/jahresberichte/jb2002/nachrdjahres/s16e.html>
13. Gast, T.: The impact of feedback on the determination of masses and forces in controlled atmospheres. *Termochimica Acta* 236, 277–290 (1994)
14. Klyushin, J.G.: On electrodynamic forces. Reprint of the Academy of Civil Aviation, St. Petersburg, Russia, May 12 (2009)
15. Kolomenskii, A.A., Jerebtsov, S.N., Stoker, J.A., Scully, M.O., Schüssler, H.A.: Storage and light scattering of microparticles in a ring-type electrodynamic trap. *Journal of Applied Physics* 102(9), Paper 094902 (2007)
16. Göbel, G., Wriedt, T., Bauckhage, K.: Periodic drag force and particle size measurement in a double ring electrodynamic trap. *Rev. Sci. Instrum.* 68(8), Paper 3046 (1997)
17. Li, W., Davis, E.J.: Measurement of the thermophoretic force by electrodynamic levitation: Microspheres in air. *Journal of Aerosol Science* 26(7), 1063–1083 (1995)
18. Shi, S., Redding, B., Creazzo, T., Marchena, E., Prather, D.W.: Quantum electrodynamic modeling of silicon-based active devices. *Advances in Optical Technologies*, Article ID 615393 (2008)
19. Richoux, B., Lemarquand, G., Lemarquand, V.: Electrodynamic transducer and use thereof in loudspeakers and geophones. US Patent Application No. 2009 0028375, January 29 (2009)
20. Fischer, P.: Electrodynamic force measuring apparatus. US Patent 4020687, May 3 (1977)
21. Huan, Y., Zhang, T., Yang, Y.: A moving-coil designed micro-mechanics tester with application on MEMS. *Meas. Sci. Technol.* 18(11), 3612–3616 (2007)
22. Urry, S.: Plantar pressure-measurement sensors (review article). *Measurement Science and Technology* 10, R16–R32 (1999)
23. Warren-Forward, M.J., Goodall, R.M., Pratt, D.J.: Three dimensional displacement and force transducer. *IEEE Proceedings A* 139, 21–29 (1992)
24. Chi, Z., Shida, K.: A new multifunctional tactile sensor for three-dimensional force measurement. *Sensors and Actuators A: Physical* 111, 172–179 (2004)

Note for reference 18: *Copyright © 2008 Shouyuan Shi et al.* This is an open access article distributed under the Creative Commons Attribution License, which permits unrestricted use, distribution, and reproduction in any medium, provided the original work is properly cited.

Chapter 9

MAGNETOELASTIC FORCE TRANSDUCERS

Magnetic and mechanical behaviors are coupled. It means that the magnetic behavior cannot be accurately determined unless the mechanical fields are taken into account, and, in the same time, the deformation state is depending on the magnetic configuration.

Romanian researcher Nicoleta Lupu has presented a complete vision on the magnetoelastic and (reciprocal) elastomagnetic effects at the European School on Magnetism [9.1]. In Table 9.1 are noted with capitals the useful magnetoelastic effects for force (Villari) or torque (Matteucci) transducers, respectively. The main statements are:

- *Magnetostriction* (with a valuable overview written by Ekreem *et al.* in [9.2]) is only a part of the magnetoelastic phenomenon.

Table 9.1 Magnetoelastic and elastomagnetic effects for transducer applications

Magnetoelastic / direct effects	Elastomagnetic / inverse effects
Joule magnetostriction (1842) <i>Change of the sample dimensions in the direction of the applied magnetic field</i>	VILLARY EFFECT <i>Change in magnetic susceptibility due to applied mechanical stress</i>
Magnetoanisotropy effect <i>Magnetoelastic contribution to the magnetocrystalline anisotropy</i>	ΔE effect <i>Magnetically induced changes in the elasticity module</i>
Wiedemann effect <i>Twisting induced by helical magnetic field anisotropy</i>	MATTEUCCI EFFECT <i>Helical anisotropy and electromotive force induced by a torque</i>
Magnetovolume effect <i>Volume change due to magnetization (mostly near the Curie temperature)</i>	Nagaoka-Honda effect <i>Change in the magnetic state due to a change in the volume</i>

- The use of contactless *magnetoanisotropic* devices for measuring sheet rolling effort in rolling mills is described in [9.3]; their results, as compared with those of strain gauged transducers and magnetoelastic dynamometers, indicate an error of 12 %.
- The ΔE effect is an apparent loss of linearity in the elastic behavior of demagnetized specimens [9.4]. This is due to the superimposition of the magnetostriction strain to the elastic one during the strain measurement. Linear behavior is recovered when the mechanical stress is high enough to saturate magnetostriction.
- Force measurement applications based on the *magnetovolume* (Nagaoka-Honda) effect are not found in technical literature.

9.1. THE MAGNETOSTRICTIVE PRINCIPLE

The magnetostriction of ferromagnetic materials manifests itself in shape and volume changes during magnetization and, is the reason for elastomechanical stressing of a magnetic body leading to reversible changes of the magnetization curves (See Table 7.1, Sketch C!). In other words: The loading applied on the magnetoelastic element of a force transducer modifies the properties of its magnetic circuit.

Figure 9.1 depicts a cold-rolled sheet package where two perpendicular windings (primary for excitation and secondary for detection) are located [9.5]. Permeability of the material between holes (μ_x) does not vary because of the holes shielding effect, but it is variable on the force direction (μ_y). Permeability decreases along the applied direction of the compression force, magnetic flux increases in the transverse plane and therefore increases the induced voltage in secondary winding. A reverse phenomenon occurs when applying tensile force.

The output voltage of the magnetoelastic force transducer is given by

$$e(t) = - \frac{d\phi_r}{dt} = - \frac{d}{dt}(M \cdot i) \quad (9.1)$$

where ϕ_r is the total flux in the measuring winding, M – mutual inductance between the windings, and i – the instant value of the current (with frequency ω) in excitation winding. Two loading regimes are possible:

- (*quasi*)static force and sinusoidal excitation current with constant amplitude I , resulting the output signal given by the relationship

$$e(t) = -M \frac{di}{dt} = -M \cdot I \cdot \omega \cdot \cos \omega t \quad (9.2)$$

where the variation of magnetic coupling under the applied load modulates the output signal. This regime may be also used in case of variable forces, on the condition that the frequency of the excitation current is much higher than the maximum frequency of the applied force.

- *variable force* and DC excitation $i(t) = I$, resulting the output voltage given by the relationship

$$e(t) = -I \frac{dM}{dt} \tag{9.3}$$

where the output voltage is proportional to the variation speed of the mutual inductance M :

$$M = L_{12} = K_m \sqrt{L_1 \cdot L_2} \tag{9.4}$$

where K_m is the coupling factor while L_1 and L_2 are the self-inductances of the two coils.

When magnetoelastic force transducers are concerned, in addition to a high coupling factor (as close as possible to unity), a linear dependency between mechanical stress and magnetization curve is desired, if possible. Usually, a differential arrangement of the windings (differential transformer) enables that $M = 0$ when the applied force is zero.

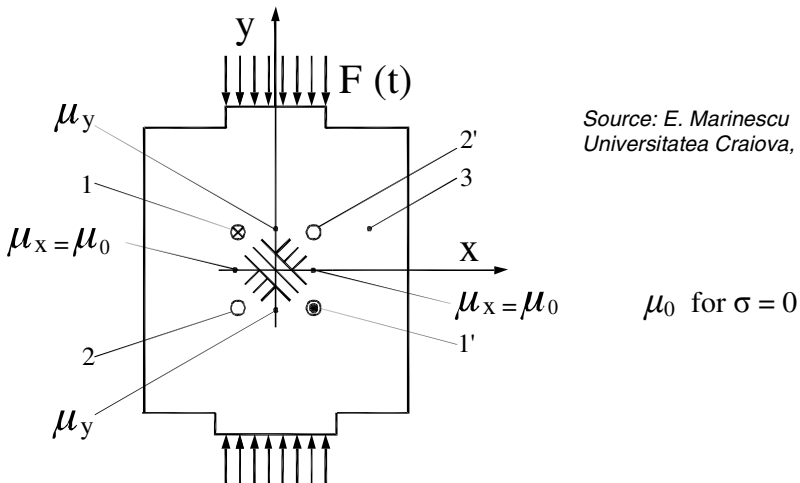
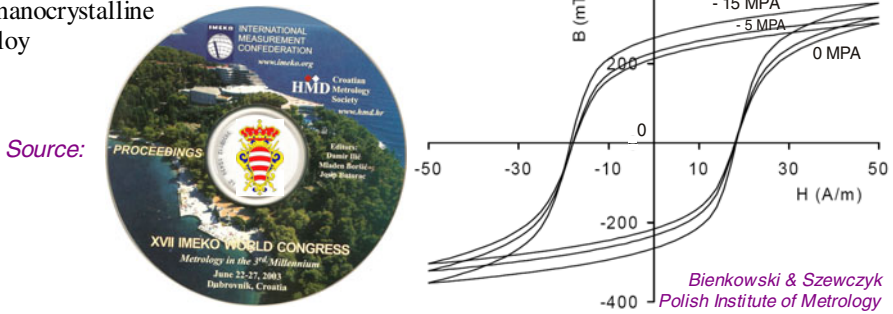


Fig. 9.1 Magnetoelastic force transducer – Pressductor type

Fig. 9.2 Positive magnetostriction hysteresis loops for a nanocrystalline alloy



The SIEMENS document [9.6] states that the slope of the magnetization curve (i.e. permeability) is inversely proportional to the applied tensile stress and corresponds to the negative magnetostriction while the compressive stressing describes the case of positive magnetostriction. The influence of the compressive stress σ on the quasistatic hysteresis loop of the core made of $\text{Fe}_{73.5}\text{Nb}_3\text{Cu}_1\text{Si}_{13.5}\text{B}_9$ in quenched state [9.7] is shown in Figure 9.2.

9.2. CLASSIFICATION OF MAGNETOELASTIC FTs

In magnetoelastic / magnetostrictive transducers a change of length or strain caused by external forces has the effect of changing the magnetic permeability or distorting the hysteresis loop [9.8].

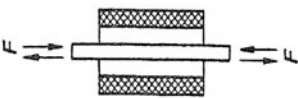
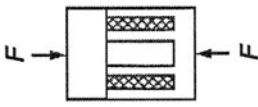
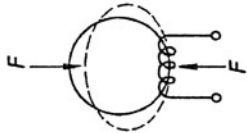
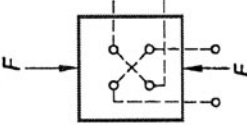
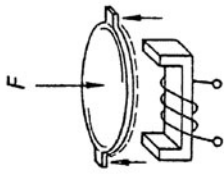
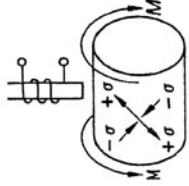
The basic elastomagnetic transducers could be:

- Unidimensional systems having predefined magnetic flux paths where the inductance or permeability is changed by mechanical loading;
- Two or three dimensional systems having flux configurations which change their hysteresis loop due to loading and for which the vectorial change of the magnetic properties has to be evaluated [9.6].

Table 9.2 proposes an extended survey on magnetoelastic structures for measuring force, torque, pressure and other related quantities. It combines typical elastic elements with adapted magnetic circuits in order to process a multitude of variables. Here are depicted seven of the twelve elastic elements which are presented in the second part of this Handbook.

Daga *et al.* [9.9] presents the magneto-electro-elastic transducers characteristics under transient mechanical loading using the finite element method. There are different locations for sensors along the top surface of a mild steel beam, subjected to clamped-free and simply supported boundary conditions. A transient sensing response of PZT-5 and (Terfenol-D)-epoxy mixed components is also studied by ANSYS 8.1 in order to validate their behavior with the computer code.

Table 9.2. Magnetoelastic force and torque transducers: elastic elements and magnetic circuits

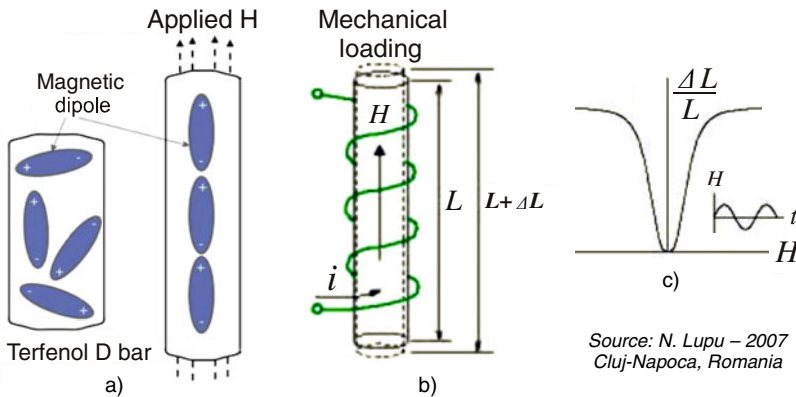
Flux configuration	1-dimensional		2-dimensional		3-dimensional	
Elastic element	A: Rod	B: Frame or Tube	C: Ring	D: Block	E: Membrane	F: Shaft
Magnetic circuit layout						
Mechanical loading	Tension	Compression	Bending	Compression	Bending	Torsion
Process variable	Force Displacement	Force	Force	Force Vibration	Force Pressure	Torque

9.3. AXIAL MAGNETOELASTIC FORCE TRANSDUCERS

9.3.1. Magnetostrictive strips and bars

Magnetostriction is the deformation that spontaneously occurs in ferromagnetic materials when an external magnetic field is applied. This coupling effect can be used to build magnetostrictive actuators and transducers. The reciprocal effect, the change of the magnetic susceptibility of a material when subjected to a mechanical stress, is called the Villari effect.

The simplest example is a soft magnetic strip subjected to an axial tensile load while a Terfenol-D bar (Fig. 9.3) can be bidirectionally loaded.



Source: N. Lupu – 2007
Cluj-Napoca, Romania

Fig. 9.3 A Terfenol bar aligning its dipoles in magnetic field (a) and under mechanical loading (b); time variable dependence: relative inductance vs magnetic field intensity (c)

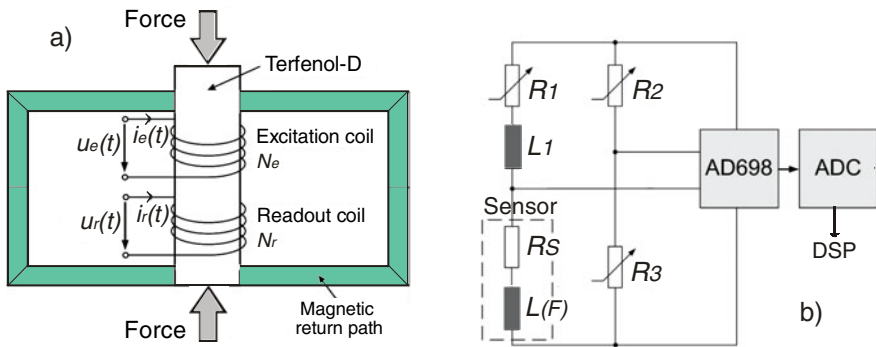
The researchers from the Institute for Measurement Technology, Johannes Kepler University Linz, Austria [9.10] had an idea to increase the magnetoelastic force transducers sensitivity using Terfenol-D, a rare earth element alloy of terbium, dysprosium and iron, having one of the largest known magnetostrictive constants.

The force transducer prototype (Fig. 9.4a) comprises two coils (excitation and read-out). The main part of the set-up is the Terfenol-D rod with a diameter of $d = 13$ mm and a length of $l = 28$ mm. A magnetic return path of ferrite material is implemented to close the magnetic circuit, with reduced eddy current losses. Since Terfenol-D is a rather brittle material, it can easily be destroyed by tensile stress, so only compressive forces were applied.

Then they minimized the complexity of the sensor arrangement by using a single coil to determine the magnetic reluctance R_m of the closed magnetic circuit comprising the sensor. R_m is also depending on the permeability of the sensor material and can be determined by measuring the force dependent inductance $L(F)$ of the sensing coil (Fig. 9.4b). This coil is part of a quarter

AC-bridge with an appropriate impedance (L_1, R_1) and two variable resistances (R_2, R_3), in order to balance the bridge which is driven by a small excitation signal with a frequency of 20 kHz. The bridge signal is demodulated by the linear variable differential transformer (LVDT) chip AD698 (Analog Devices). Following a demodulation and an analog-to-digital conversion step, the signal is further processed in a digital signal processing unit (Blackfin DSP, AD).

In Figure 9.4c the relative changes of the magnetic resistance R_m are plotted vs the probe loading and the excitation current frequency, respectively. The mechanical load was applied by a tensile testing machine (TIRA Test 2703) in quasi-static 100 N compressive force steps in the range of $0.1 \leq F_c \leq 2$ kN.



Source: Oppermann & Zagar, IMEKO, Lisbon, Portugal, September 2009

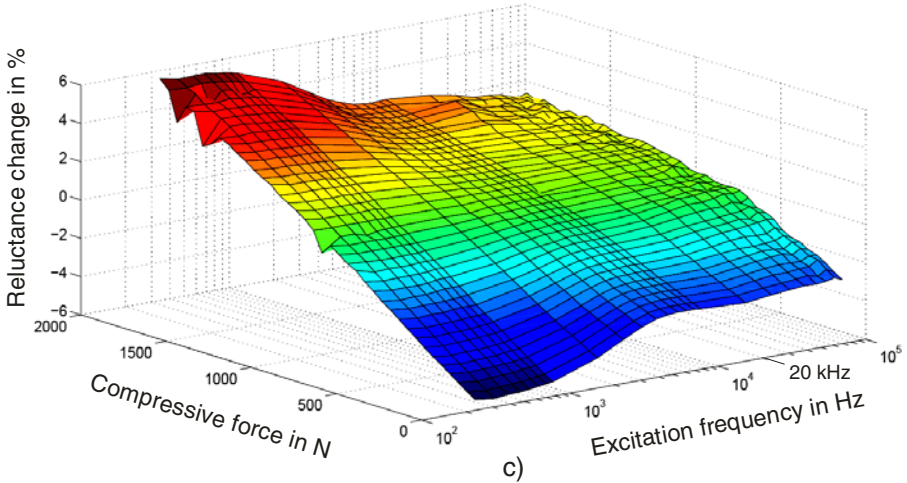


Fig. 9.4 Magnetoelastic force transducer based on a Terfenol-D rod (a), block diagram of the electronic circuits (b) and 3D dependencies of the magnetic reluctance relative change on the mechanical load (up to 2 kN) and the excitation frequency (c)

The diagram 9.4c shows the sensitivity decreasing with higher driving frequencies. The best trade-off between excitation frequency (determining the dynamic behavior) and the measurement sensitivity was found, attesting the performances of this new, robust and cheap magnetoelastic force transducer.

9.3.2. Magnetostrictive amorphous wires

Although the magnetoelastic effects occur in all ferromagnetic alloys, they are particularly prominent in the amorphous magnets. The internal structure of MAW (magnetostrictive amorphous wires) consists of an inner core where easy axis (referred to the energetically favorable direction of spontaneous magnetization in a ferromagnetic material) is parallel to the wire axis and an outer shell in which the easy directions are basically radial [9.11].

Transducer, built around a MAW having composition $\text{Fe}_{77.5}\text{Si}_{7.5}\text{B}_{15}$, and 125 μm in the as-quenched state is supplied by Unitika Ltd. Japan. The wire (1) is axially mounted inside the exciting coil (2) which creates the magnetic field (Fig. 9.5a). Two covers (4 and 5) laterally close the iron case (3). Cover (4) is copper made and has the possibility of circular moving together with the shaft of the sensor. Cover (5) is made by insulated material and is fixed on the case. The spring (6) permits the creation of an axial tensile stress into the wire.

A supplementary force F can be applied to the shaft (7), thus enabling the using as a force transducer.

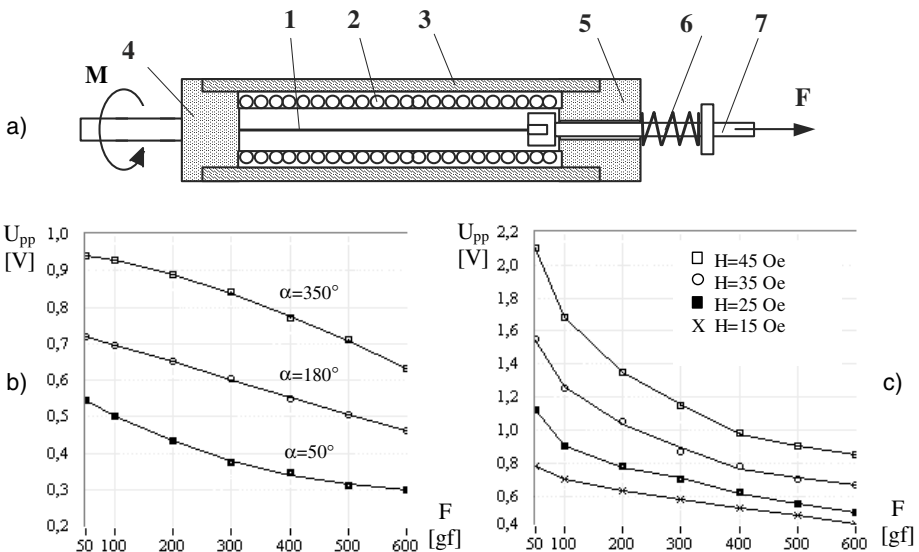


Fig. 9.5 Magnetostrictive amorphous wire transducer (a): output signal dependence on the axial force when varies the shaft angle (b) or the magnetic field intensity (c)

The exciting coil (2) has the intensity and the frequency of the current adjusted by a programmable AC source. This current causes an alternating magnetic field axially oriented and, in conjunction with the helical anisotropy induced in the wire due to the rotation of the sensor shaft, determines the apparition of Matteucci voltage pulses (See Table 9.1) at the ends of the wire (pieces 4 and 7) constituting the output signal.

One can study the dependence of the peak-to-peak value of the Matteucci pulses (U_{pp}) with respect to various forces F , as well as for angles in the range of 0 to 360 degrees, under the influence of several external factors such as: intensity, shape and frequency of the excitation field, wire diameter and length.

The transducer characteristics were automatically traced using two-channels digital oscilloscope, PC interfaced by means of a digital acquisition board. The measuring system was conceived as a virtual instrument in LabVIEW package. Figure 9.5b shows the output variation with respect to the axial tensile stress applied to the wire. The best linearity is obtained when the shaft is half turned (180°). The field intensity influence on the voltage-force curves is shown in Figure 9.5c. Raising the field intensity affects the linearity. If H is too small, the system becomes unstable. The optimum was found in the range 15 to 25 Oe.

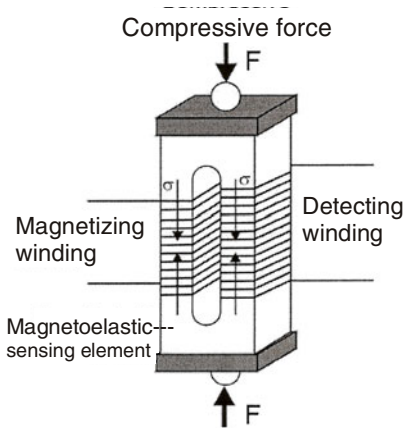
Another contribution of the Romanian “school of magnetism” is an experimental set-up with an amorphous wire of $\text{Fe}_{77.5} \text{Si}_{7.5} \text{B}_{15}$, 125 μm diameter, vertically positioned and acting as a magnetostrictive delay line (MDL) [9.12]. Tensile stress was applied along the length of 400 mm by putting weights at the free end of it. The dependence of the peak-to-peak amplitude on the applied force could be fitted by a linear curve, the sensitivity being 10 mV/N.

9.4. FRAME-SHAPED MAGNETOELASTIC FORCE TRANSDUCERS

In case of sensing elements made of bulk magnetic materials, such as ferrites, the frame-shaped core method can be used. The model presented in Figure 9.6 provides the closed magnetic circuit and enables compressive force to be applied in the range up to 60 MPa. On the frame-shaped core both magnetizing and detecting winding were made. These windings enable measurement of the magnetic hysteresis loop $B(H)$ changes under the influence of the compressive stresses σ [9.13].

Other variants are mostly of pot-core like design and are in principle iron-closed chokes, the inductance changes (ΔL) of which are used as an indication of the applied force.

Magnetic permeability variation $\Delta\mu$ is the main factor of the magnetoelastic sensitivity [9.14] and it is strongly connected with strain ε variation during magnetoelastic functioning:



Reprinted with permission from Elsevier, copyright 2004

Source: Biełkowski & Szewczyk
Sensors and Actuators A: Physical,
Vol. 113, No. 3, 2004.



Fig. 9.6 Method of applying the compressive stress to the frame-shaped magnetoelastic sensing element made of ferrite

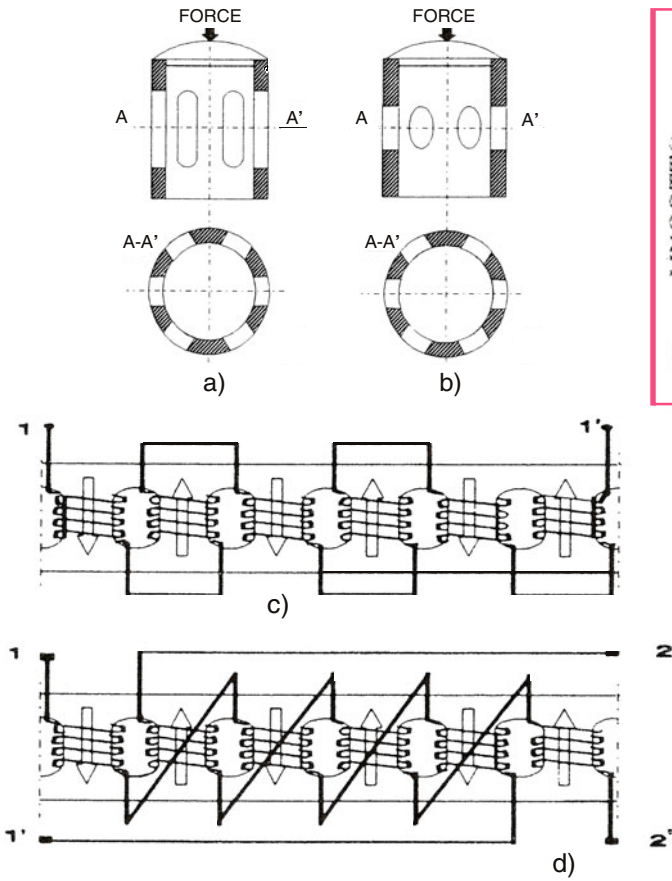
$$S_m = \frac{\Delta L / L}{\Delta l / l} = \frac{\Delta \mu / \mu}{\Delta l / l} = \frac{\Delta \mu / \mu}{\epsilon} \quad (9.5)$$

Comparing with the resistive strain gauges sensitivity [factor k from the formula (3.2)], the magnetoelastic relative sensitivity S_m is much higher (15 to 1000 times), but, unfortunately, the hysteresis is substantially greater than that of the piezoresistive devices (0.5 ... 3 %).

9.5. TUBULAR MAGNETOELASTIC FORCE TRANSDUCERS

Magnetoelastic force transducers are not as popular as strain gauged load cells, because of their greater hysteresis and uncertainty. They possess many advantages such as a high and powerful output signal which facilitates the use of simple and cheap primary electronics, high admissible mechanical overload and good temperature features. Due to their sturdy construction, high signal level and small internal resistance, the magnetoelastic load cells can be used in rough and electrically disturbed environments such as in rolling mills [9.15].

Two materials are in common use for the transducer cores: electro-technical steel and permalloy. They are manufactured on a large scale as thin laminated sheets to avoid losses. On the other hand, equal force distribution throughout all stressed parts of the transducer is easier to achieve in massive core construction. Thus the problem of satisfy two contrary requirements arises. This problem is solved either by sticking the sheets together or by designing complicated constructions of transducers (Fig. 9.7).



With kind permission of IMEKO Paper of J. Zakrzewski

Fig. 9.7 Windings of the columnar (a) or hole-shaped (b) tubular elements, connected either as a choke-type (c) or as a transformer-type (d) magnetoelastic force transducer

Magnetoelastic force transducers are constructed in such a manner that their elements stressed by the measured force are fully penetrated by magnetic flux. The penetration of flux is limited by eddy currents according to [9.16]:

$$d_p = \sqrt{\frac{\rho}{\pi \mu \cdot f_f}} \tag{9.6}$$

where d_p is the depth of penetration, ρ – resistivity, μ – permeability of the magnetic core material and f_f – the field frequency. The penetration depth d_p for a field frequency of 500 Hz extends to approximately 1.8 mm.

Equal force distribution between all active parts of the transducer is achieved by tubular elastomagnetic elements, made by Canthal type FeNiAl alloys and having rectangular slots (Fig. 9.7a) or circular holes (Fig. 9.7b). The number and the size of such “windows” determine the force transducer range, usually between 100 N and 5 kN.

The basic idea of tubular transducer operation depends on the change of magnetic properties of the core due to mechanical stress:

- In *column-shaped transducers* the flux density direction coincides with the stress direction, especially in the most stressed parts which are the columns.
- In *hole-shaped transducers* the vector of the flux density changes its value along the flux path and its direction does not coincide with that of mechanical stress, hence the relatively lower sensitivity of the second model of magneto-elastic force transducer.

These columnar and hole-shaped tubular transducers may be used for two configurations which require pull-through windings:

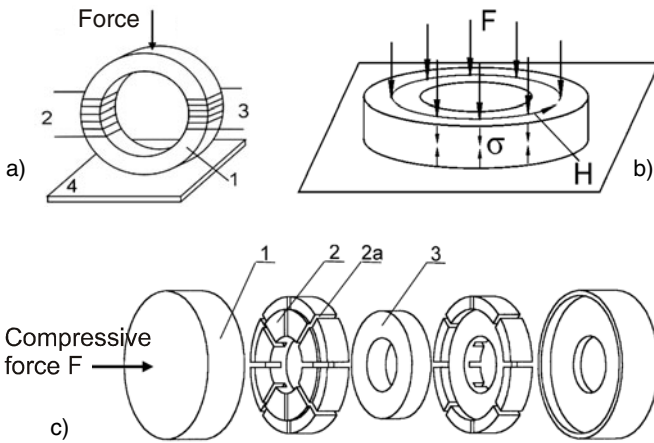
- *choke-type transducer* (Fig. 9.7c) where the coil impedance depends on the stress in the core material; either the current or the voltage of the coil may be treated as the transducer output quantity.
- *transformer-type transducer* (Fig. 9.7d) where the cross-inductance change caused by the measured force determines a change in the output voltage of the secondary coil. This secondary voltage creates the output signal of the magnetoelastic force transducer.

9.6. CIRCULAR MAGNETOELASTIC FORCE TRANSDUCERS

Both compressive and tensile stresses occur when a circular ring is deformed to an ellipse (Fig. 9.8a), so the magnetoelastic sensitivity of the vertical ring is significantly reduced and it is not recommended for force transducers based on magnetic properties.

In the horizontal core method (Fig. 9.8b), the compressive force F is applied to the ring-shaped sensing element perpendicularly to the magnetizing field H , so a uniform, compressive stress σ can be reached on the all length of the magnetic circuit of the sensing element. So, the ring-shaped cores, which are commercially available, can be used as magnetoelastic force and/or stress transducers.

A special device for applying stresses to the ring core [9.17] is presented in Figure 9.8c. Base backings (1) allow a ring core (3) to be subject of the compressive force F . Due to the special, non-magnetic cylindrical backing (2), the distribution of stresses in the core is uniform. Measuring and magnetizing windings are placed in grooves (2a) at the cylindrical backings (2).



Sources:
 Bieńkowski & Szewczyk
 IMEKO Congress – 2003,
 Dubrovnik, Croatia

and

Journal of Optoelectronics
 and Advanced Materials,
 Vol. 5, No. 3, 2003.

Fig. 9.8 a) Idea of applying the compressive force in the direction of the diameter of the ring-shaped sensing element: 1 – sensing core, 2 – magnetizing winding, 3 – sensing winding, 4 – base plane. b) Horizontal ring-shaped core principle applied for magnetoelastic force transducers. c) Device for applying the compressive stress on a ring-shaped sensing element (Polish patent P-345758).

Another contribution of the Polish “school of magnetism”, the device for application of uniform torque to ring-shaped sensing elements [9.18] is presented in Figure 9.9a, together with the torque influence on the hysteresis loop of an alloy subjected to thermal annealing in the temperature 550 °C for one hour (Fig. 9.9b).

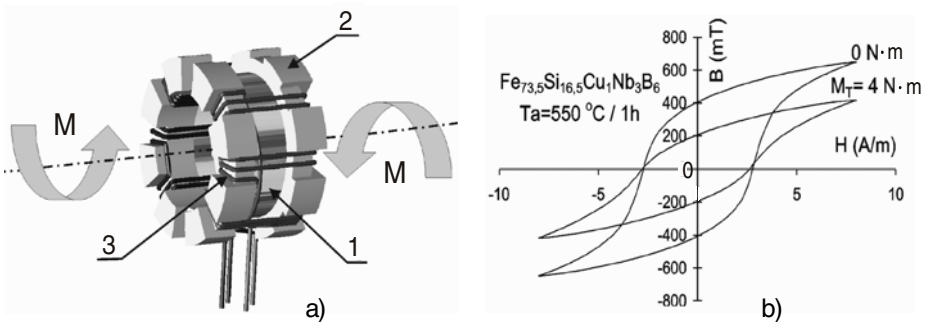


Fig. 9.9 a) Magnetoelastic ring-shaped torque transducer components: 1 – ring-shaped core, 2 – magnetizing and measuring windings, 3 – non-magnetic backing with grooves. b) $B(H)$ characteristics for negative magnetostriction.

One can remark there are two kinds of magnetostriction [9.19]:

- positive – when the slope of hysteresis diagram increases with applied stress (e.g. permalloy),
- negative – when the slope of hysteresis diagram decreases with applied stress (e.g. nickel).

In the same time, the magnetostriction sign depends upon the loading, being negative for tension (Fig. 9.9b) or positive for compression (Fig. 9.2), and confirming the bidirectional significance of the word “striction.”

9.7. BLOCK-SHAPED MAGNETOELASTIC FORCE TRANSDUCERS

Transducer systems falling into this category are known as “pressductors”. The effect exploited in this case is that when stressed, a magnetically isotropic material is modified to a different degree longitudinal and transverse to the load axis, i.e. it becomes magnetically anisotropic.

Where materials having positive magnetostriction are subjected to compressive stressing, the permeability is reduced in the load direction and increased at right angles to it. This can be seen as a modification of the originally symmetrical flux line pattern (Fig. 9.10a). This modification can be picked up by primary (C_1) and secondary (C_2) coils, mutually offset by 90° [9.20].

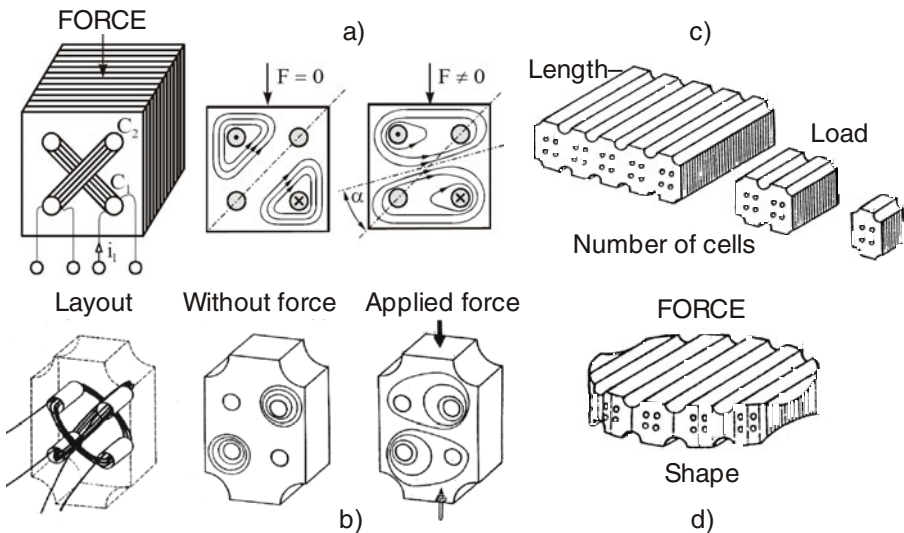


Fig. 9.10 Magnetoelastic principle illustrated by Platil with sheets (a) and by Wieringa with massive core construction (b). Combined methods for adjusting the capacity of the magnetoelastic force transducers by length and number of cells (c) and by shape (d).

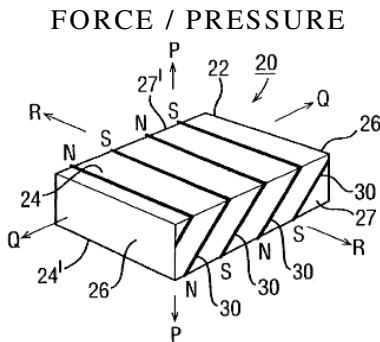
Another representation and its associated description have been given by Wieringa in [9.21]: In a block made from ferromagnetic steel four holes are made at the corners of a square (Fig. 9.10b). Diagonally two coils are positioned through these holes. One of the coils is supplied with an alternating current. No voltage will be induced in the second coil, since the two coils are perpendicular to each other; therefore no magnetic lines pass through the second coil.

If the steel block is loaded, the coils are no longer perpendicular to each other due to the deformation and, moreover, the magnetic properties in the two perpendicular directions change. Now some magnetic lines will pass through the second coil inducing a voltage in it. The magnetic flux through the second coil is proportional to the applied force.

This principle has been introduced by ASEA Company in Sweden. By using long steel blocks (so-called “serial combination”) and/or several blocks “in parallel” (Fig. 9.10c), the nominal capacity of the magnetoelastic force transducer can be adjusted or enlarged.

The advantage of this transducer is that it is simple, robust and it has a small height. The force over the square or circular surface is integrated, so it is not important how the force is distributed on the sensing device (Fig. 9.10d).

Other magnetoelastic solution for force or torque transducers is described in the patent abstract [9.22]: A force transducer element (20) comprises a body (22) of magnetizable material having at least one magnetized region (30) at an angle, say 45°, to the force-sensing direction (P-P). The element may be a block having opposite force receiving surfaces (24, 24'). Preferably, there are pluralities of parallel magnetized regions of alternating opposite polarity of magnetization to form closed loops. Another embodiment (Fig. 9.11) contains plural transducer elements angled to one another to resolve force directions. The principle is extended to a circular transducer element, i.e. membrane type. The invention may be implemented in a flexible magnetic tape too.



*Lutz Axel May
Fast Technology AG, Ottobrunn
Euro Patent 1274974 - 2003*

Fig. 9.11 Magnetoelastic block with oblique slices to resolve loading directions

9.8. MAGNETOELASTIC SHAFTS FOR TORQUE TRANSDUCERS

The “pressductor” effect can be applied for measuring torque at shafts, namely “torductors” [9.23]. The changes in magnetic properties of the shaft surface are measured by means of staggered yokes which are arranged close to the surface. The magnetic loading is complicated in this case since the permeability must be considered as a tensorial quantity.

According to the producer, the Torductor[®]-S design gives a non-contact and rugged torque transducer without moving parts. Since the sensor is part of the load-carrying shaft, the measured torque is the true transmitted torque. This enables the Torductor to combine high accuracy with high overload capacity and fast response at all times. A high output signal ensures immunity against electrical or magnetic interference from the surroundings. The Torductor is designed to work in harsh environments where other transducers have poor reliability. The typical environment found within an engine power train in terms of vibrations, temperature, lubricants or magnetic components is not a problem for this transducer. The Torductor[®]-S is the ideal choice for measurement under demanding and hostile conditions.

The stress in a (magnetoelastic) shaft is proportional to the applied torque, i.e.

$$\tau = \frac{M_t \cdot r}{I_p} \quad (9.7)$$

where τ is the maximum shear stress at the shaft surface, M_t is the torsion moment, r is the shaft radius and I_p is the polar moment of inertia. It follows that torque must change the permeability of the shaft if it is made of a magnetic material such as steel.

The torque transducer shown in Figure 9.12 consists of five coils wound onto a common five-armed core [9.24]. The central coil can be thought of as the primary winding of a transformer and the four circumferentially positioned coils act as transformer secondaries. Magnetic coupling between the primary and the secondaries is provided by the steel shaft, which is positioned close to the transducer. The primary coil is excited by an alternating current, and produces an oscillating magnetic field within the shaft. The four secondary coils are connected together in a Wheatstone-bridge arrangement and are positioned so that they lie over the lines of principal stress, which follow a helical path at 45° for a cylinder in torsion.

When the shaft is not under torsion, equal currents are induced in the four secondaries and out-of-balance voltage of the bridge is zero. Applying torque to the shaft, the permeabilities in the tension and compression

directions will change by equal but opposite amounts and the amplitude of the resulting bridge output voltage is proportional to the applied torque.

*Reprinted with permission of
Institute of Physics – London
from [9.24]*

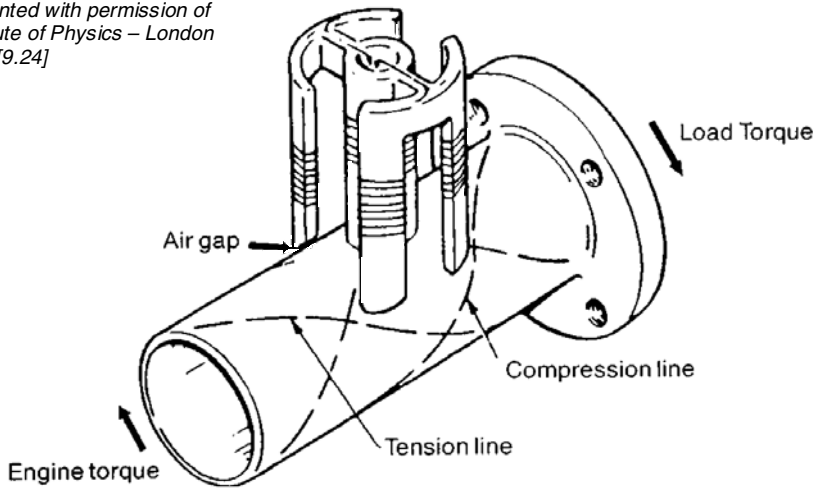


Fig. 9.12 Magnetoelastic / magnetostrictive force transducer

The main problems with this type of torque transducer are:

- inhomogeneity of the shaft material (permeability can vary by up to 50 % around the circumference of the shaft),
- sensitivity to changes in the sensor-shaft gap,
- excessive stress and aging, which cause permanent changes,
- variations in the transducer output due to changes in the shaft-rotation speed. For a constant torque the output signal can “ripple”, at a frequency equivalent to the rotation rate, being difficult to measure the instantaneous torque.

Here are some applications with magnetoelastic measuring shafts [9.25]:

- electronic weighing equipment for foundry travelling cranes,
- electric load limiter for cranes in civil engineering and harbours,
- equipment for tension control in laminated tapes.

9.9. MAGNETOELASTIC FTs ELECTRONIC CIRCUITRY

Besides the different solutions of force transducers presented in Table 9.2, there are other primary sensing possibilities based on the magnetostrictive principle:

- magnetoelastic strain gauge (Fig. 9.13a), based on the relative variation of the coil inductance due to the applied force [9.14];

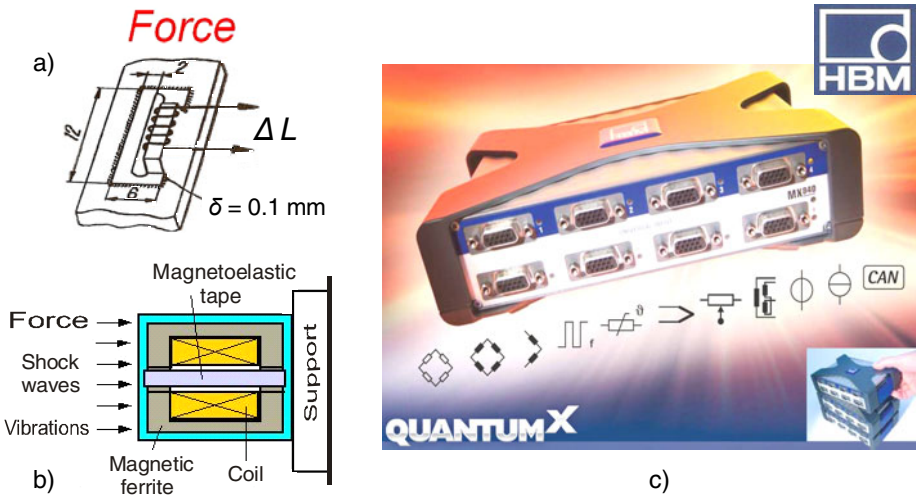


Fig. 9.13 Old magnetoelastic strain gauge (a) and modern magnetoelastic tape (b) for force transducers. QuantumX – universal conditioner and tensometric amplifier (c).

- magnetoelastic tape (Fig. 9.13b) where quasistatic force, wave or vibration loading change the material permeability. Strains less than 10^{-10} are detected with small magnetoelastic sensors developed by Chen Yang – ISM [9.26].

QuantumX is a multifunctional conditioner and amplifier for numerous transducers having different measuring principles (Fig. 9.13c). A single MX840 module has eight universal connectors that suit all common transducer technologies, whatever the combination [9.27].

Alongside the elastic material and the magnetic circuit shape, the electronic circuitry is also a decisive factor for magnetoelastic force transducers. Transformer, oscillator and multivibrator are usual solutions in this respect, and analog or binary output signals are obtained, either frequency (up to 20 kHz).

There are many variants of implementing the magnetoelastic transducers:

- depending on the position of the coils and their connection to the measuring scheme, it can be differentially inductive or transforming;
- according to the way the force is applied, it can have one or more active sections to channelize the magnetic field [9.28].

Additionally to the circuits shown in the previous subchapters, Koga and Sasada [9.29], Institute of Electrical Engineers of Japan, utilize the mutual induction of planar coils. Ong *et al.* [9.30] use the change in magnetostatic coupling between elements to modulate the coercive force and $B(H)$ loop switching characteristics of the force transducer, or the mass-sensitive change in the magnetoelastic resonant frequency of an amorphous ferromagnetic ribbon.

At the Marine Technological College, Hyogo, Japan [9.31], a prototype digital force transducer was fabricated to convert a compression load into an oscillation frequency in an Esaki diode relaxation oscillator circuit, using the magnetomechanical (Villari) effect of ferrites.

REFERENCES

1. Lupu, N.: Magnetostriction versus magnetoelastic effects. European School on Magnetism, Cluj-Napoca, Romania, September 9-18 (2007)
2. Ekreem, N.B., Olabi, A.G., Prescott, T., Rafferty, A., Hashmi, M.S.J.: An overview of magnetostriction, its use and methods to measure these properties. *Journal of Materials Processing Technology* 191(1-3), 96–101 (2007)
3. Zheleznov, Y.D., Grigoryan, G.G., Zhuravskii, A.G., Kondratov, A.I., Chernyi, V.A.: Application of magnetoanisotropic transducers for measuring force in rolling. Translated from Russian "Izmeritel'naya Tekhnika" (8), 27 (August 1974)
4. Daniel, L., Hubert, O., Billardon, R.: Homogenization of magneto-elastic behavior: from the grain to the macro scale. *Computational and Applied Mathematics* 23(2-3) (May- December 2004)
5. Marinescu, E.: Measurement of time-varying forces by magnetoelastic transducers. In: Proc. 2nd Romanian Symposium of Tensometry, Cluj-Napoca, pp. 193–199, vol. I, June 11-14 (1980)
6. Boll, R., Borek, L.: Magnetic sensors of new materials. *Siemens Forschungs- und Entwicklungsberichte* 10(2), 83–90 (1981)
7. Bieńkowski, A., Szweczyk, R.: Possibilities of utilising newly developed nanocrystalline materials as stress and force sensors. In: CD Proc. XVIIth IMEKO World Congress Metrology in the 3rd Millenium, Cavtat-Dubrovnik, Croatia, pp. 397–400, June 22-27 (2003)
8. Hauptmann, P.: *Sensors: Principles and Applications*. Carl Hanser Verlag, Munich (1991)
9. Daga, A., Ganesan, N., Shankar, K.: Behavior of magneto-electro-elastic sensors under transient mechanical loading. *Sensors and Actuators A: Physical* 150(1), 46–55 (2009)
10. Oppermann, K., Zagar, B.G.: A novel magneto-elastic force sensor design based on Terfenol-D. In: Proceedings SENSOR + TEST Conference 2009, Nuremberg, Germany, May 26-28, vol. 2, pp. 77–82 (2009)
11. Foşalău, C., Postolache, O., Creţu, M.: A novel transducer for force and angle measurements based on magnetostrictive amorphous wires. In: Proc. 44th International Scientific Colloquium IWK 1999, Ilmenau, Germany, September 20-23, pp. 257–261 (1999)
12. Chiriac, H., Hristoforou, E., Neagu, M., Borza, F.: Force measurements using Fe-rich amorphous wire as magnetostrictive delay line. *Sensors and Actuators A: Physical* 91, 223–225 (2001)
13. Bieńkowski, A., Szweczyk, R.: The possibility of utilizing the high permeability magnetic materials in construction of magnetoelastic stress and force sensors. *Sensors and Actuators A: Physical* 113(3), 270–276 (2004)

14. Stere, R.: *Electronic Apparatus for Measurement and Control*. Editura Didactică și Pedagogică, București (1968) (in Romanian)
15. Hunt, A. (Coord.): *Guide to the Measurement of Force*. Institute of Measurement and Control, London (published 1998)
16. Zakrzewski, J.: New magnetoelastic force transducer. In: Proc. XIIIth IMEKO World Congress, Turin, Italy, September 5-9, vol. I, pp. 241–245 (1994)
17. Szewczyk, R., Bieńkowski, A., Salach, J., Fazakas, E., Varga, L.K.: The influence of microstructure on compressive stress characteristics of the Finemet-type nanocrystalline sensors. *Journal of Optoelectronics and Advanced Materials* 5(3), 705–708 (2003)
18. Salach, J., Bieńkowski, A., Szewczyk, R.: Magnetoelastic, ring-shaped torque sensors with the uniform stress distribution. *Journal of Automation, Mobile Robotics & Intelligent Systems* 1(1), 66–68 (2007)
19. Ionescu, G., Dobrescu, R., Droașcă, B., Guțu, A., Hohan, I.: *Transducers for Industrial Automatization*, vol. I. Editura Tehnică, București (1988) (in Romanian)
20. Platil, A.: *Mechatronics Sensors*. PPT-05-force-b on Internet, January 3 (2005)
21. Wieringa, H.: Electrical force measuring transducers. In: Proc. Symposium Force, Pressure, Displacement and Flow Sensors, May 13-14, pp. 179-197. Twente University of Technology, Enschede, The Netherlands (1982)
22. May, L.A.: Magnetic-based force/torque sensor. European Patent EP 1274974 (2003)
23. Torductor[®]. Torque measurement with Pressductor[®] Technology. ABB Automation Products AB, Västerås, Sweden, PDF created on October 16 (2007)
24. Turner, J.D., Austin, L.: Sensors for automotive telematics (review article). *Measurement Science and Technology* 11, R58–R79 (2000)
25. Equipment for measuring torque moment, speed and power – type IM-TnP. Research Institute and Factory “Electroputere” Craiova, Romania (1986)
26. GMR, eddy current, capacitive and magnetoelastic sensors for mechanical quantities. ChenYang Technologies GmbH & Co. KG, Finsing, Germany (May 19, 2009), <http://www.chenyang-ism.com/Sensors.htm>
27. Boersch, J.: QuantumX – the new, multi-functional amplifier system. In: Hotline Hotline Hottinger – News from the world of test and measurement (2), Darmstadt, Germany, 4-5 (2007)
28. Trendafilov, G.I.: Magnetoelastic force-measuring transducer. *Facta Universitatis (Niš, Serbia), Series Electronics - Energetics* 9(2), 263–273 (1996)
29. Koga, F., Sasada, I.: Magnetostrictive effect type force (strain) sensor using mutual induction of planar coils. *IEEE Transactions on Fundamentals and Materials* 127(6), 355–360 (2007)
30. Ong, K.G., Paulose, M., Jain, M.K., Gong, D., Varghese, O.K., Mungle, C., Grimes, C.A.: Magnetism-based remote query glucose sensors. *Sensors* (Published by Molecular Diversity Preservation International) (1), 138–147 (2001)
31. Takahashi, Y.: Digital force transducer utilizing magnetomechanical effect. *Energy Technology Data Exchange Web by World Wide Science*, March 19 (2009)

Chapter 10

GALVANOMAGNETIC FORCE TRANSDUCERS

The general class of phenomena called galvanomagnetic (or reciprocal magnetogalvanic) includes the *Hall effect* and the *magnetoresistance* one [10.1]. The Hall effect is the generation of a transverse electromotive force in a sample carrying an electric current and exposed to a perpendicular magnetic field. Depending on the geometry, this force may cause the appearance of a current deflection in the sample or a transverse voltage across the sample, called Hall voltage. At the same time, the resistance increases under the magnetic field influence, and this is called magnetoresistance effect (See details in C.7.2).

One way to fabricate the Hall sensor [10.2] is to use a silicon p-substrate with ion-implanted n-wells (Fig. 10.1a). Electrical contacts provide connections to the power supply (or control) terminals (E) and from the differential outputs (V_H). A Hall element is a simple square well with four electrodes attached to the ends of its diagonals (Fig. 10.1b). A helpful way of looking at the Hall sensor is to picture it as a resistive bridge (Fig. 10.1c). This representation makes its practical applications more conventional because the Wheatstone bridge circuits are the most popular networks with well established design methods.

Courtesy of Jacob Fraden from [10.2]

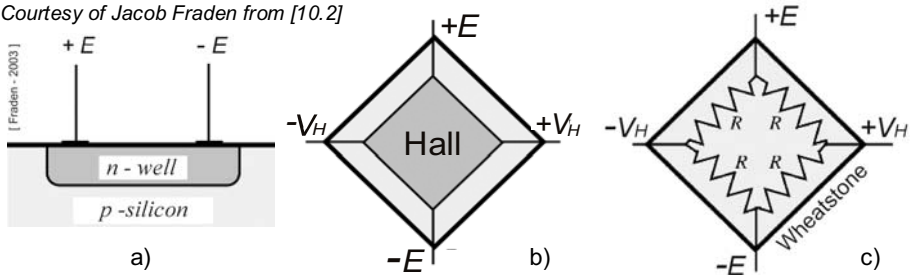


Fig. 10.1 Silicon Hall-effect sensor with n-well (a), Hall sensor symbol (b) and its equivalent resistive bridge circuit, used for magnetoresistors too (c)

Generally, every piece of electrically conductive material, fitted with four electrical contacts, could be used as a Hall device. However, to be reasonably efficient and convenient for practical applications, a Hall device is made in the form of a plate. The contacts are positioned at the boundary of the plate, far away from each other. Two contacts are for the current source (E). The other two contacts, used for sensing the Hall voltage (V_H), are placed to attain approximately equal potentials at a zero magnetic field; then the potential difference at the sense contacts equals to Hall voltage. To simplify the design and fabrication of a Hall plate, a highly symmetrical shape and a uniform material and thickness of the plate are usual chosen. So, a four-way symmetric Hall-effect transducer can be viewed as a Wheatstone bridge.

10.1. HALL EFFECT AND ITS APPLICATIONS

Edwin Herbert Hall was an American physicist who discovered in 1879 the “Hall-effect”, i.e. development of a transverse electric field in a solid material (metal or semiconductor) when it carries an electric current and is placed in a magnetic field that is perpendicular to the current. This effect is stronger in semiconductive materials than in metallic ones.

If a magnetic field B is applied orthogonal to a current I then there will be a Lorentz force acting on the moving charges orthogonal to both the field and current direction (Fig. 10.2). This Lorentz force can be described by an electric field (Hall voltage V_H), which is given by:

$$V_H = \frac{R_H \cdot I \cdot B}{d} \quad (10.1)$$

where d is the thickness of the conductor and R_H is the Hall coefficient, which is inversely proportional to the number of charge carriers.

The Hall-effect is a consequence of the Lorentz force in semiconductor materials [10.3]. When a voltage is applied from one end of a slab of semiconductor material to the other end, charge carriers start to flow with velocity v . If at the same time a magnetic field is applied perpendicular to the slab, the current carriers are deflected to the side by the Lorentz force. Charge builds up along the side until the resulting electrical field produces a force on the charged particle q sufficient to counteract the Lorentz force. Since the quantities F_L , v , and B are vector quantities, they have both magnitude and direction. The Lorentz force F_L is proportional to the cross product between the vectors representing velocity and magnetic field, being perpendicular to both of them and, for a positively charge carrier, has the direction of advance of a right-handed screw rotated from the direction of v towards the direction of B .

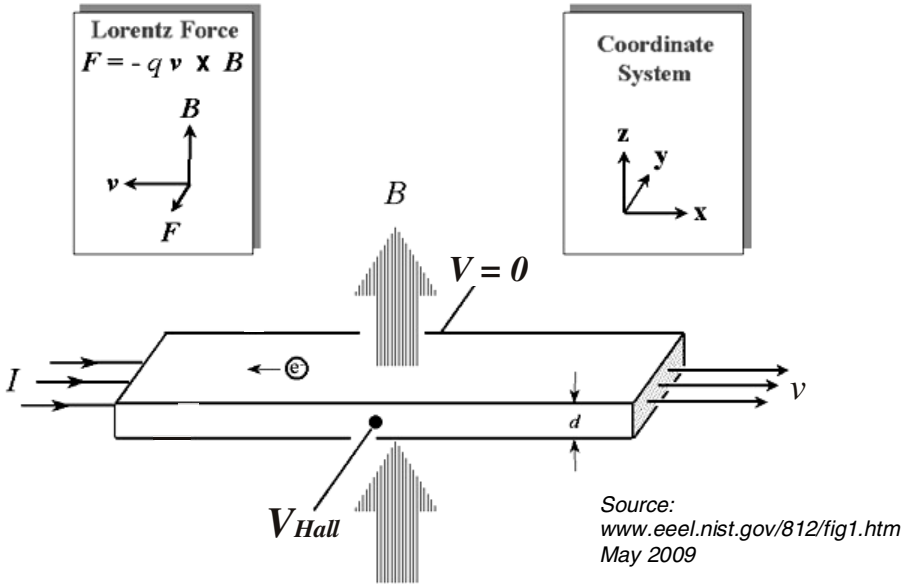


Fig. 10.2 Schematic of the Hall-effect in a long, thin bar of semiconductor having the current I along the x -axis [10.4]. The direction of the magnetic field B is along the z -axis and the sample has a finite thickness d . The resulting Hall voltage (which is negative for n-type semiconductors and positive for p-type ones) is along the y -axis.

The Hall magnetic devices have complex applications for measuring mechanical quantities (e.g. force transducers), magnetic fields or electric current, power and energy [10.5]. These multifunctional devices are also suitable as multiplicative circuits for analogic computation [10.6].

Galvanomagnetic effects, in particular the Hall-effect, have already found many applications in various transducers after the discovery of the III-V semiconductors with very high electron mobility. Two possible applications for mechanical measurands are mentioned in [10.7]: speed and current transducers. (See Table 7.1, Sketch F and G, respectively!)

The current sensors represent a further development of DC transformer with Hall elements originally intended for heavy currents (Fig. 10.3). Today they are used in electronic circuits, for example in switched-mode power supplies for closed-loop control and protective tasks. These electromagnetic transducers comprise a Hall element arranged in the gap of a slotted highly permeable nickel-iron toroidal core or a laminated core, being dimensioned for various current wave forms. The Hall-effect method is good for measurement of high fields up to $12 \text{ MA}\cdot\text{m}^{-1}$ but has a limited sensitivity of about $8 \text{ A}\cdot\text{m}^{-1}$.

Source:
NK Technologies
San Jose, CA
2009

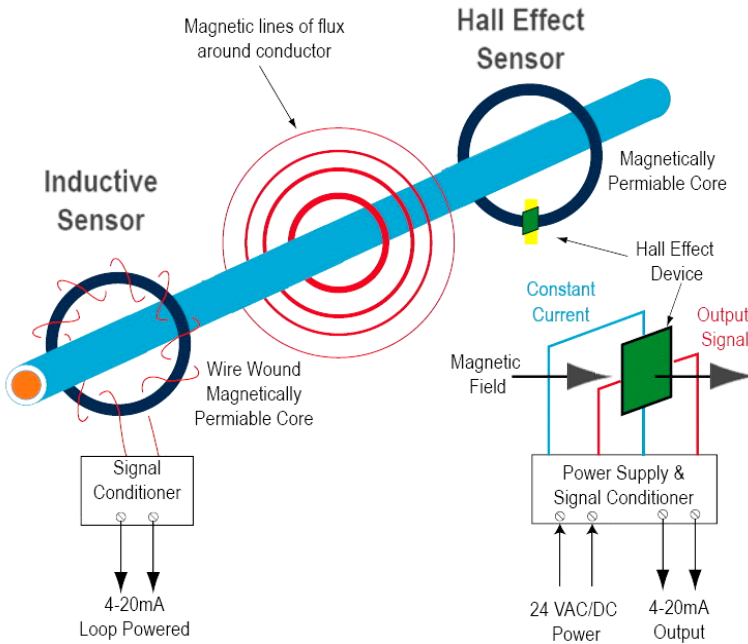


Fig. 10.3 Hall-effect sensor – current sensing for automation applications

Galvanomagnetic Hall-effect transducer can be viewed as an alternative to the inductive one [10.8], consisting of three basic components: the core, the Hall-effect device and signal conditioning circuitry. When the energized Hall sensor is exposed to a magnetic field from the core, it produces a potential difference (voltage) that can be measured and amplified into process level signals such as (4...20) mA or a contact closure.

These sensors are typically direct current energized, deliver a high DC output which varies linearly with magnetic flux density over a specified range, and have, nowadays, excellent zero and span temperature stability. They are also light (0.35 g), small and cheap.

Many Hall-effect sensors are fabricated from silicon slabs and fall into two general categories – the basic sensors and the integrated ones. Other sensitive materials used for the element fabrication include InSb, InAs, Ge and GaAs. In the silicon element, an interface electronic circuit can be incorporated into the same wafer. This integration is especially important since the Hall-effect voltage is quite small.

Careful choice of semiconductor materials and circuit design give Hall-effect sensors (often called Gaussmeters) with a highly linear dependence of voltage on magnetic field: *the greater the magnetic field, the greater the voltage.*

10.2. FORCE TRANSDUCERS BASED ON THE HALL EFFECT

10.2.1. Hall effect in geotechnical engineering

Experience of the University of Surrey shows that linear-output Hall-effect sensors can be easily and cheaply utilized for *ad hoc* development of the geotechnical laboratory instrumentation [10.9]. These devices are used as sensing elements in transducers to measure:

- axial and radial displacement,
- the resulting normal and shear stresses respectively,
- as well as the overall forces.

Linear-output Hall-effect sensors are usually used to measure displacements; they are located inside some magnetic field where the flux density along some path varies linearly with the position relative to the sensor. If such holding parts are machined to adequate shapes from spring materials with good elastic properties, then forces or other mechanical quantities may be similarly measured. The deflection produced by the applied force to the elastic structure changes the magnetic field geometry and, as a logical consequence, the resulting Hall voltage.

The principle chosen for the force transducer (Fig. 10.4a) was the measurement of bending displacements of two stiff blocks connected by a number of slender beams (Fig. 10.4b). Linear-output Hall-effect sensors were bonded to small steel studs, which were subsequently bonded to one block. Pairs of magnets were connected to the opposite block in a similar way. The material integral construction technique and hardening treatment were used.

A configuration of two sensors and four magnets which has been useful in the measurement of forces is shown in Figure 10.4c. In this configuration, each sensor is displaced in relation to a pair of magnets in such a way it passes over first one magnetic pole and then the opposite one. The resultant output vs. displacement relationship for each individual sensor is linear near to the middle of separation, S , between the magnets. The sensitivity can be increased (up to about 15 mV/ μm) by decreasing the separation between the pair of magnets to zero, and the gap, G , between the sensor and the pair of magnets to the minimum feasible (about 0.1 mm). It is possible to redesign them using linear-output Hall-effect sensors as a low-cost in-house option, with the further advantage of possibly achieving much higher full scale output than in the case of conventional strain-gauged instruments.

Benefits result from the measurement of the whole configuration output (Fig. 10.4d) as the difference between the individual outputs of the pair of Hall sensors. The large zero offset voltage characteristic of each sensor (about 4 V) is then removed and sensitivity is doubled with an appropriate arrangement of the magnets.

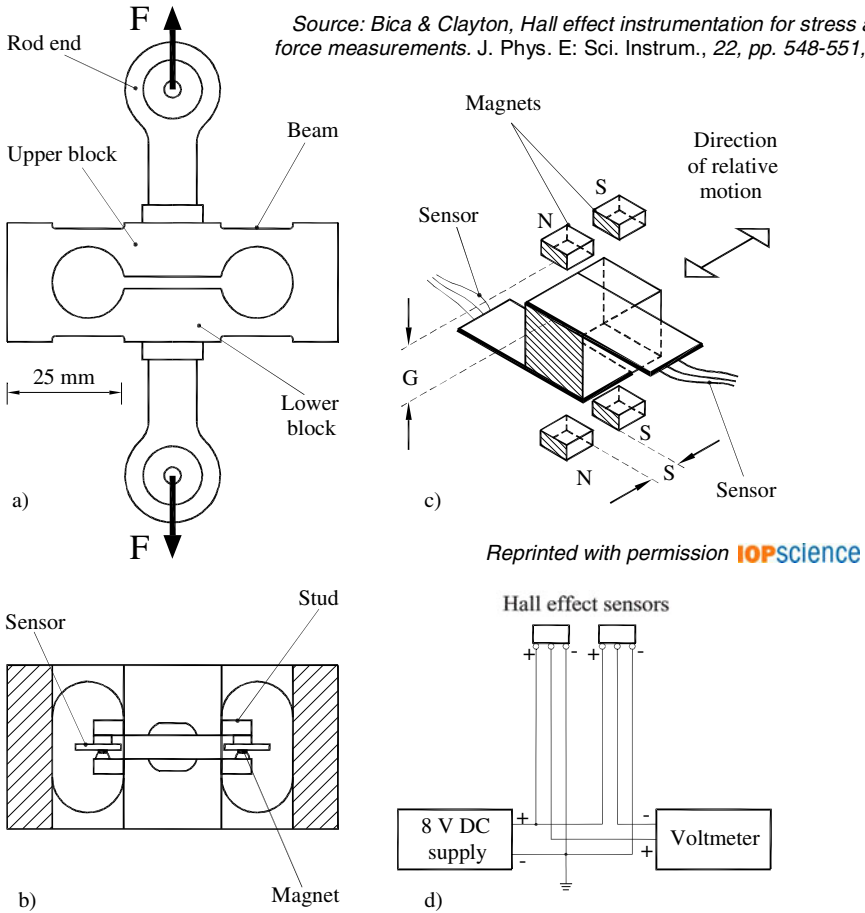


Fig. 10.4 Hall-effect force transducer: lateral view (a) and middle cross section (b). A pair of Hall sensors (c) and their electrical connection (d).

10.2.2. Medical applications with Hall sensors

An apparatus for measuring abduction strength of a patient's thumb is presented in [10.10]. A force transducer is mounted to the thumb engaging means for detecting the transmitted force. The transducer utilized in this embodiment is based on a Hall-effect device which produces an output representative of the detected force.

An isotonic transducer based on the Hall effect is depicted in [10.11]. An isotonic saline solution with the same osmotic pressure as the blood is considered the optimal medium to estimate the tension within two or more muscles under biomechanical tests.

10.3. HALL DEVICES FOR OTHER MECHANICAL QUANTITIES

10.3.1. Displacement and position measurements using Hall sensors

Biomechanical studies often aim at determining the contributions of a tendon or ligament in posture, gesture and locomotion in terms of load or strain, which are strongly connected by the Hooke's law of elasticity, but also by using the same measurement equipment. The Hall-effect strain transducer is a steel tube covered with teflon and coupled to a Hall generator [10.12]. A magnetic core or a metal wire charged magnetically slides freely within the tube. One end of the tube is bonded to a fixation pin and the distal end of the magnet is similarly armed. The fixation pins serve to attach the transducer to the tendon or ligament. The transducer signal, i.e. the Hall generator output voltage, is proportional to the magnetic field strength and the magnetic core displacement.

A device adapted for replaceable implantation in soft body tissue for the measurement of the mechanical behavior of the soft tissues of the body is presented in [10.13]. The device consists of a Hall-effect strain transducer that detects the linear motion of a magnetic core. The barb force transducer has pressure sensors located within the body of the probe that detect the squeezing of the tissue fibers against the sides of the transducer. The combination of the Hall-effect strain transducer and the barb force transducer allows the operator to simultaneously measure the strain and force on a specific soft tissue.

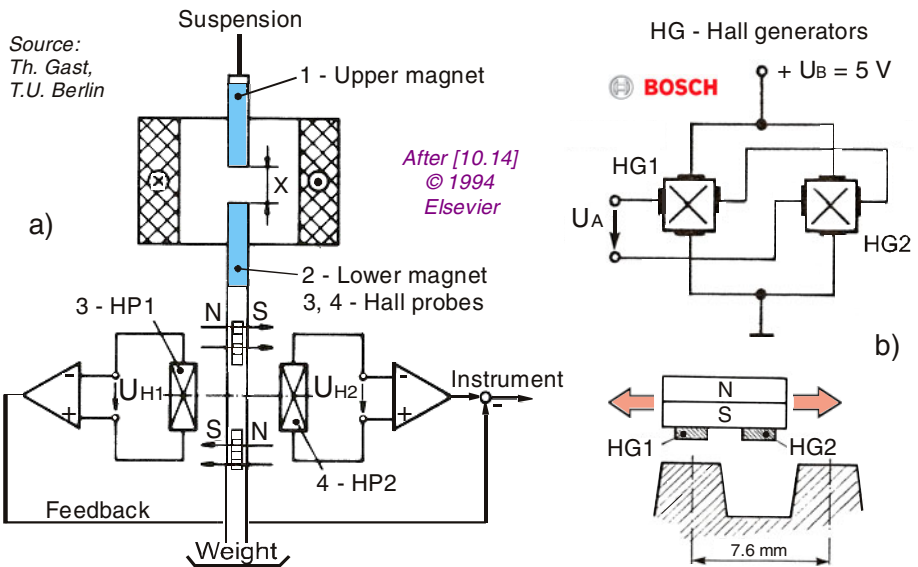


Fig. 10.5 Hall devices' symbolization and circuitry for vertical (a) and horizontal (b) positioning with galvanomagnetic transducers

Figure 10.5a presents a suspension balance with Hall sensors [10.14]. The magnetostatic principle is taken into account when reactions under high pressures are to be investigated. Two small bar magnets are attached to the shaft (2), which connects the suspended bar magnet (1) to the balance pan. They generate a magnetic field of cylindrical symmetry with a horizontal plane of zero radial field strength. This plane travels along the Hall sensors (3 and 4), arranged opposite to one another near the container wall. The sum of the Hall voltages is proportional to the vertical deviation x of the lower magnet from a chosen position, which can be adjusted by shifting the Hall sensors parallel to the axis of the suspended magnet. With the aid of a PD-controller, this magnet is maintained in stable magnetostatic equilibrium. A superimposed control loop keeps the mean value of the control current at zero. Hall generators and circuitry for determining the horizontal position on a cog rack are shown in Figure 10.5b.

10.3.2. Weighing based on Hall devices

The patent of Newton, not Isaac Newton, but Robert from Connecticut [10.15], presents a lightweight and portable “book scale” (Fig. 10.6a) comprising two weighing assemblies (Fig. 10.6b) connected by a flexible joint (22) so that the two assemblies may be folded against each other to form a compact case. Weight measurement is made by a Hall-effect sensor (Fig. 10.6c) in each assembly which measures the variation in magnetic flux density caused by the movement of magnets (44, 46) mounted on the platform. Output from the Hall-effect sensors is summed and the total weight is displayed on a digital read-out.

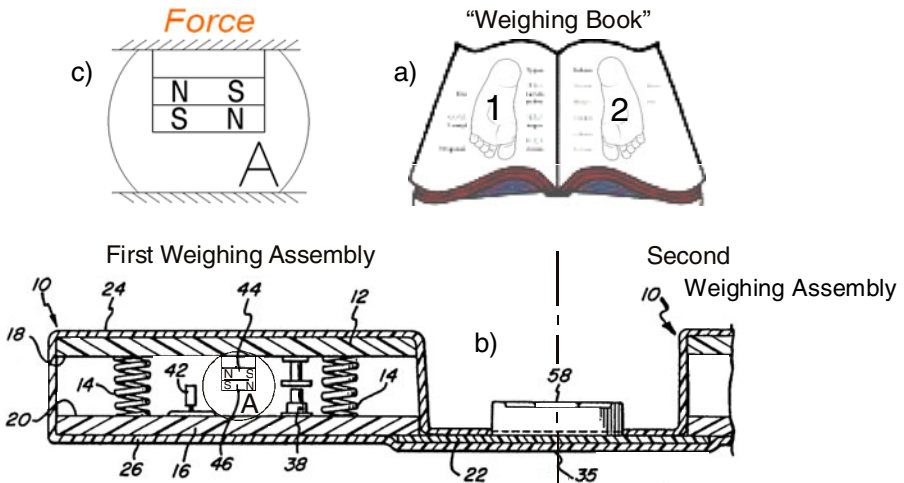


Fig. 10.6 An “open book” for weighing (a) based on Hall devices mounted under the platform (b). Detail with galvanomagnetic sensing devices (c).

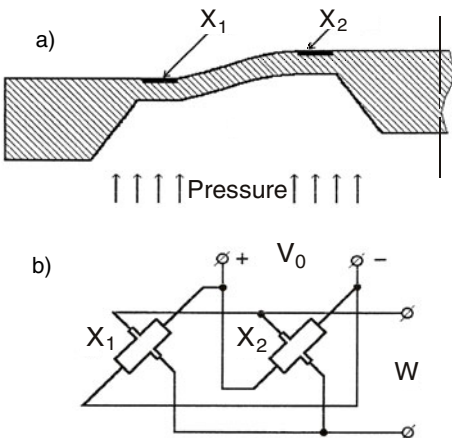
10.3.3. Pressure and flow measurements by means of Hall sensors

The most efficient and cost-effective solution to incorporate electronic functionality into mechanical gauges, by directly sensing the deflection of the needle pointer is to use a novel magnetic sensing technology based on the Hall-effect [10.16].

A Hall-effect sensor is an intelliGAUGE transducer that varies its output voltage in response to changes in the magnetic field. This has been achieved with no physical contact between the gauge pointer and sensor, preventing any interference with the mechanism. This maintains the inherent high accuracy of the gauge and leads to maximum reliability and robustness, bridging the gap between the traditional analogue mechanical pressure gauge and solid state electronic devices.

The sensitive element of other modern silicon pressure transducers, the operational principle of which is based on the transverse electromotive force effect [10.17], is often used alongside with the Wheatstone piezoresistive bridge. The sensitive element known as the four-terminal gauge or the transverse voltage strain gauge (TVSG) has a form of a single piezoresistive element with two current and two potential terminals. It can be viewed as the mechanical analog of a Hall-effect device.

As opposite to the piezoresistors in the Wheatstone bridge, the linear size directions of the TVSG do not usually coincide with the principal axis of the conductivity tensor.



Source: Zhadko et al.
Institute of Semiconductor Physics
Kyiv, Ukraine – 2001

Reprinted from [10.17],
copyright 2001,
with permission from

ELSEVIER
SCIENCE

Fig. 10.7 Piezoresistive transducers integrated in the planar side of the silicone square-shaped diaphragm with a center boss (the E-type diaphragm) near the two sides of the diaphragm thin part (valley) (a). They are included into two parallel connected four-terminal piezoresistive transducers with quasi-Hall topology, i.e. transverse voltage strain gauges – TVSG (b).

The load application, uniformly distributed over the diaphragm, produces a stress in the TVSG position with opposite signs (Fig. 10.7a): one of the gauges is axially compressed (X_1) while another is axially stretched (X_2), or *vice versa*. The directed deforming stress induces conductivity anisotropy in a normally isotropic silicon crystal. So in the longitudinal electrical field the charge carriers (holes) drift along the field and deflect in the direction with the high mobility. As the result, the holes are forced to one side of the transverse voltage strain gauges. Their accumulation on one side will create an electrical transverse field, which counteracts the deflection. This opposing electrical field resulting from the redistribution of holes in the plate under the influence of the conductivity anisotropy generates the transverse electromotive force, which can be picked up by the voltage taps placed at the opposite edges of the device.

From the circuit in Figure 10.7b, one can see that the output voltage of the pressure transducer W is a difference of the transverse voltages generated by the two transverse voltage strain gauges.

TVSG has a number of important advantages in comparison with the Wheatstone piezoresistive bridge as follows:

- smaller zero pressure offset,
- less scatter of temperature sensitivity variation from gauge to gauge,
- simpler additional circuitry for the nominal output signal unification and for sensitivity temperature compensation.

Flowmeters, for fluids in which – as for the Hall-effect – the deflection of mobile charge carriers in a magnetic field is utilized, also belong to the current sensor group. In this case a strong, temperature-stable permanent magnet of large dimensions is required, whereby AlNiCo magnets find the most application.

10.3.4. Shock measurements using Hall devices

When a probe, which is in free fall condition, meets on its trajectory an obstacle, for example a cantilever beam, an energetic transfer will be made between this two parts of the system [10.18]. Practically, the potential energy stored, during the time of the displacement (Fig. 10.8a), will be transferred to the beam according to a parabolic formula:

$$m \cdot g (h + y) = 0.5 k_H \cdot y^2 \quad (10.2)$$

where m is the probe's mass [kg], g – the gravitational acceleration [m/s²], h – the throwing height [m], y – the displacement of the beam [m] and k_H – the elastic constant [N/m].

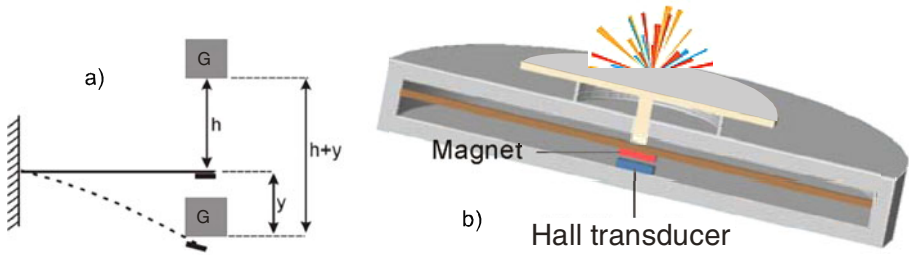


Fig. 10.8 A probe falling on a cantilever beam (a) and a shock transducer based on a Hall-effect sensor (b)

In Figure 10.8b is presented a shock detector based on a double cantilever beam. Starting from the top, the device consists of the following components: detecting plate, spring, elastic beam, permanent magnet and Hall-effect transducer (the classical tandem), and detector's case.

The most important part of the mobile assembly is the excitation coil, in a planar configuration, having the role to generate the magnetic field required for the correct functioning of the sensing element. The fix assembly has to be made from the same non-conducting and non-magnetic material, but also able to absorb the parasite external vibration.

The main part of the detector is the analog Hall-effect transducer, made by impurifying, if the transducer's support is made from a semiconductor material, or in thin film technology, if the transducer will be attached after the building process. Signal processing circuits are integrated on the same chip or film with the transducer. The transducer is emplaced in such manner that interaction with the magnetic field generates a measurable, repetitive and easy to process Hall voltage.

10.3.5. Penetration velocity and rotational speed measured with Hall sensors

Due to the evident influence of the penetration velocity on the measurement of cone index, diverse motor-operated penetrometers have been designed to keep the velocity with a constant into various soils [10.19]. Unlike other methods employing various principles to measure the penetration force, this method used a Hall-current-sensor to dynamically measure the operating current of a permanent magnet DC-motor.

The Hall-effect tachometric transducer [10.20] has a wide range of measuring frequencies, sensing the changes in the internal magnetic field of the gear speed sensor (Fig. 10.9a). Easy installation, oil and water proof qualities have granted this type of transducer wide applications in various industries such as automobiles, ships, electricity and petrochemicals.

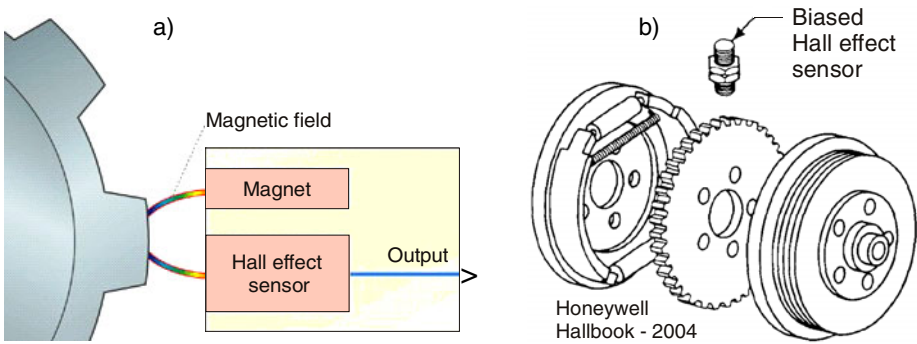


Fig. 10.9 Hall-effect tachometric transducer (a) and anti-lock braking system (ABS) based on a biased Hall-effect sensor (b)

10.4. GALVANOMAGNETIC FTs IN COMPLEX MEASUREMENT CHAINS

10.4.1. Combined measurands in galvanomagnetic force transducers

Figure 10.9b shows a possible solution for controlling the braking force of a wheel so that it does not lock-up [10.21]. A biased Hall-effect sensor is used in this respect. The sensor is positioned to sense an internal tooth gear. The gear could be the disc brake hub. The reaction time of the braking system will determine the frequency of the signal as a function of wheel revolution, avoiding its blockage.

The high-resolution, magnetic speed measuring system HBM is based on the non-contact sampling of a magnetized rotor by means of magnetostrictive sensors [10.22]. It uses giant magnetostrictors (GMRs), comprising two half-bridges which are turned 90° in opposite directions to allow absolute determination of angle (Fig. 10.10).

Torque flanges are utilized with integrated magnetic speed measuring system. Some demands made on the speed measuring system are:

- Mechanical and application-specific features of measurement flanges must not be impaired by the speed measuring system.
- A high resolution system that simultaneously allows a lot of relative movements between the rotor and the stator is needed.
- Possible contamination due to the open optical system design must be eliminated.
- Geometrically simultaneous recording of torque and speed (and then calculating the power) requires a large internal diameter and the transfer of torque flange breaking moments.

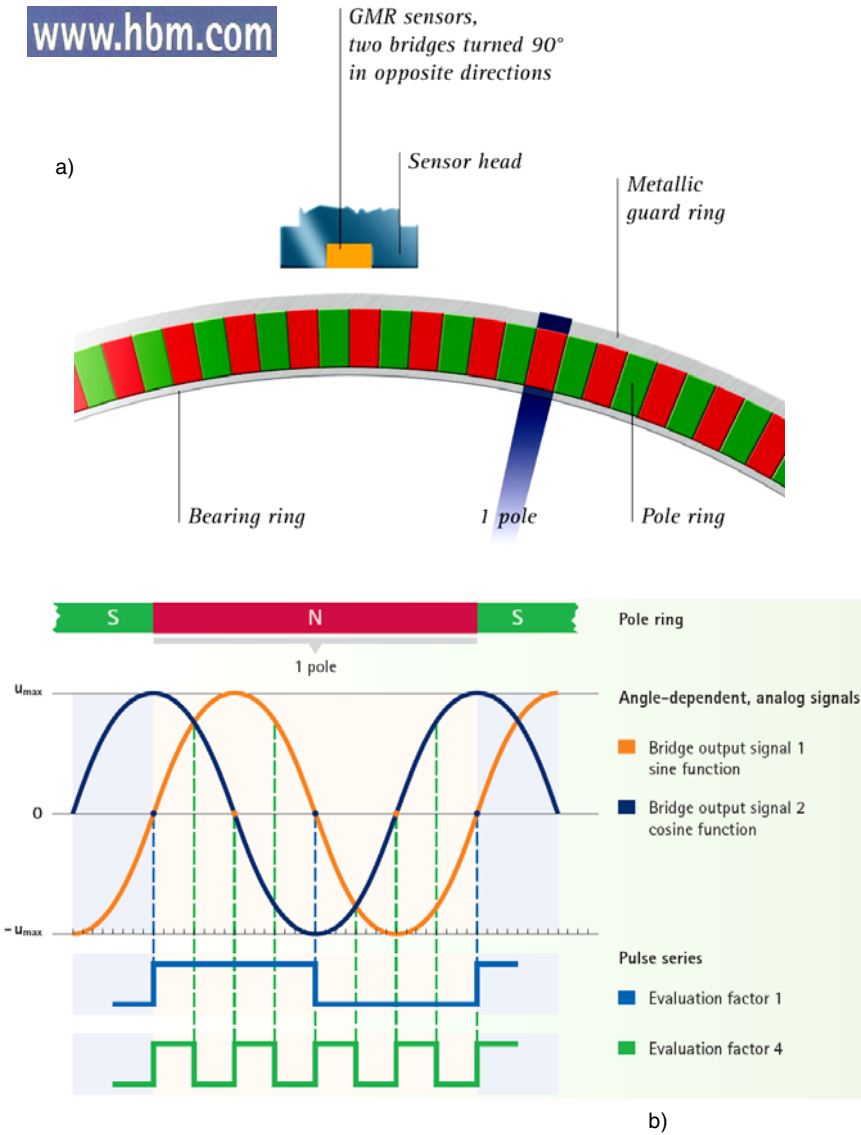


Fig. 10.10 High-resolution speed measuring system using giant magnetoresistors (a) and an example of pulse multiplication (b)

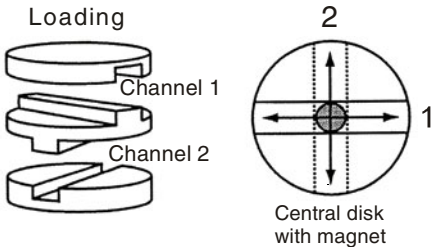
A hybrid position and force controller card has been designed for a linear hydraulic actuator [10.23]. Position and force variables of each actuator are sensed by a LVDT and a Hall-effect force transducer, respectively, and the associated card performs signal conditioning process on the sensed signals.

The development of an advanced sensor for atomic force-guided scanning Hall probe microscopy whereby both a high mobility heterostructure Hall-effect magnetic sensor and an n-Al_{0.4}Ga_{0.6}As piezoresistive displacement sensor have been integrated in a single III–V semiconductor cantilever is reported in [10.24]. This allows simple operation in high-vacuum/variable-temperature environments and enables very high magnetic and topographic resolution to be achieved simultaneously.

10.4.2. Triaxial galvanomagnetic force transducers

Measurement of the horizontal components of discrete forces under the foot was first attempted by using a “Hall-effect magnetoresistive sensor.” Note that both galvanomagnetic effects are connected in the same expression by Stephen Urry! Moreover, the orthogonal shear stresses and the normal (compressive) stress could be simultaneously measured. As described by the author [10.25], the transducer design comprises two outer discs of aluminum with a central disc of acetal to minimize friction. The three discs were bounded together with separating layers of natural rubber sheet that offered a good compromise between rebound resilience (the recovery speed) and a low set under compression (the recovery degree). The middle disc contained a centrally placed magnet whereas each outer disc contained a magnetoresistor. Relative motion of the three discs was constrained by ridges and grooves so that the outer two discs slid orthogonally with respect to the inner disc. The normal component of force was detected by means of a strain-gauged diaphragm attached to the shear section. So, this is a triaxial force transducer combining three measurement principles (Hall sensors, magnetoresistors, strain gauges).

A new shape of Hall device is the circular one [10.1], having geometrical factor $G_H = 1$. The novel “3D Wheel Hall Sensor” exploits the signal attributes of an “ideal” Hall voltage, Hall current and/or geometric magnetoresistive effect. It senses all the three dimensions of the field, namely the flux-density of B_z which is proportional to the DC component, whereas B_x and B_y components are proportional to the first harmonic of the output signal.



*Reprinted with permission from
Institute of Physics - London*

*Source: St. Urry
Plantar pressure measurement
Meas. Sci. Technol. - 1999*

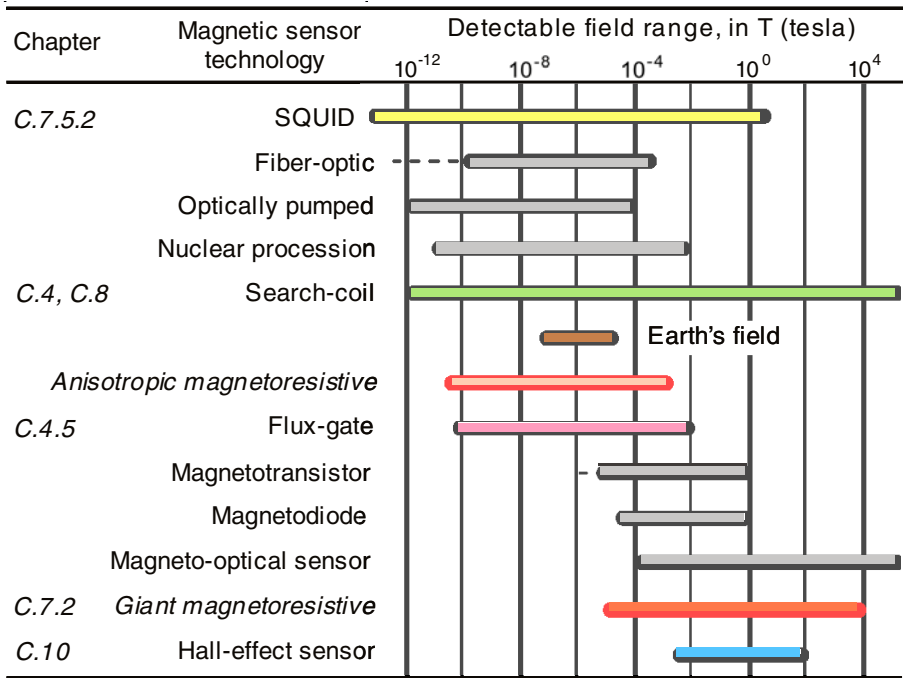


Fig. 10.11 Bidirectional shear force transducer using galvanomagnetic sensors

10.5. OTHER ELECTROMAGNETIC PRINCIPLES IN FORCE MEASUREMENT

Galvanomagnetic force transducers include the Hall-effect based- and the magnetoresistive types (anisotropic – AMR and giant – GMR). Their positions among other electromagnetic transducers are shown in the Table 10.1.

Table 10.1 Magnetic sensor technology “field distribution” (adapted from [10.3])



C - Chapters in this Handbook where they are presented

Magnetoresistive force transducers were detailed in C.7.2. They are based on magnetically controllable resistors, discovered by Lord Kelvin in 1856. The determining factor for the specific resistance is the angle formed by the internal direction of magnetization and the direction of current flow. Usually, the highly conductive material is applied below an angle of 45°. Four magnetic field sensitive resistors are interconnected to form a Wheatstone bridge [10.26].

Comparing the galvanomagnetic methods: the magnetoresistors detect a larger magnetic field than the Hall-effect sensors but the latter satisfy a wider range of applications related to the measurement of mechanical forces. And, these Hall devices, invented in 1879, have the best linearity among all electromagnetic force transducers.

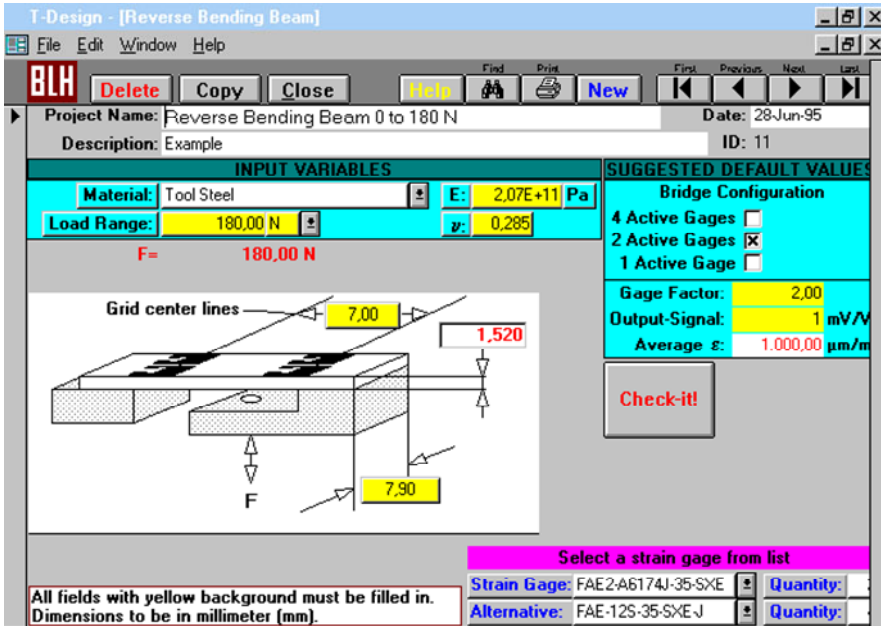
Hall-effect sensors, as well as magnetoresistors, may be associated with many types of elastic elements:

- cantilever beam: Figures 10.4 and 10.8,
- stretched / compressed bar: Figure 10.5,
- square membrane / diaphragm: Figures 10.6 and 10.7,
- disc: Figure 10.11,

similarly to the resistive strain gauges, connected into Wheatstone bridges as well (Fig. 10.12).

REFERENCES

1. Petousis, V.N., Dimitropoulos, P.D.: Galvanomagnetic effects “Sensors based on Hall Effect” (lecture note). *Journal of Engineering Science and Technology Review* 2(1), 1–7 (2009)
2. Fraden, J.: *AIP Handbook of Modern Sensors – Physics, Design and Applications*. American Institute of Physics, New York (1993)
3. Caruso, M.J., Bratland, T., Smith, C.H., Schneider, R.: A new perspective on magnetic field sensing. Courtesy of Honeywell International, Inc. 5/98 and copyright (2010)
4. The Hall Effect and the Lorentz Force. NIST Electronic & Electrical Engineering Laboratory, May 23 (2009), <http://www.eeel.nist.gov/812/fig1.htm>
5. Popovic, R.S.: Hall effect devices. In: Jones, B.E., Spillman, W.B. (eds.) *Series in Sensors*, 2nd edn., Institute of Physics, Bristol, PA (2004)
6. Grave, H.F.: *Elektrische Messung nichtelektrischer Grössen*. Akademische Verlagsgesellschaft Geest & Portig KG, Leipzig, DDR (1965)
7. Boll, R., Borek, L.: Magnetic sensors of new materials. *SIEMENS Forschungs- und Entwicklungsberichte* 10(2), 83–90 (1981)
8. Katasak, J.: High performance current sensing for automation applications – Hall effect sensor. [Images/current-sensor.gif](http://www.nktechnologies.com/images/current-sensor.gif), NK Technologies, San Jose, CA (2010)
9. Bica, A.V.D., Clayton, C.R.I.: Hall effect instrumentation for stress and force measurements. *J. Phys. E: Sci. Instrum.* 22, 548–551 (1989)
10. Boatright, J.R., Peindl, R.D.: Apparatus and method for measuring abduction strength of a patient’s thumb. US Patent: 5471996-95, <http://www.freepatentsonline.com>
11. Grade isotonic transducer or Hall effect isotonic transducer (May 2006) http://adstruments.com/products/datasheets/Panlab_Organ_30Series_Low
12. Ravary, B., Pourcelot, P., Bortolussi, C., Konieczka, S., Crevier-Denoix, N.: Strain and forces transducers used in human and veterinary tendon and ligament biomechanical studies. *Clinical Biomechanics* 19, 433–447 (2004)
13. Arms, S.W.: Implantable displacement sensor means. US Patent 4813435-89
14. Gast, T.: The impact of feedback on the determination of masses and forces in controlled atmospheres. *Termochimica Acta* 236, 277–290 (1994)
15. Newton, R.F., Sundermeyer, F.D.: Folding scale. US Patent 4765421-88
16. IntelliGAUGE – Contact-free sensor technology for WIKA. PDF created on April 23 (2009), <http://www.sagentia.com>



Classical design of strain gauged elastic element

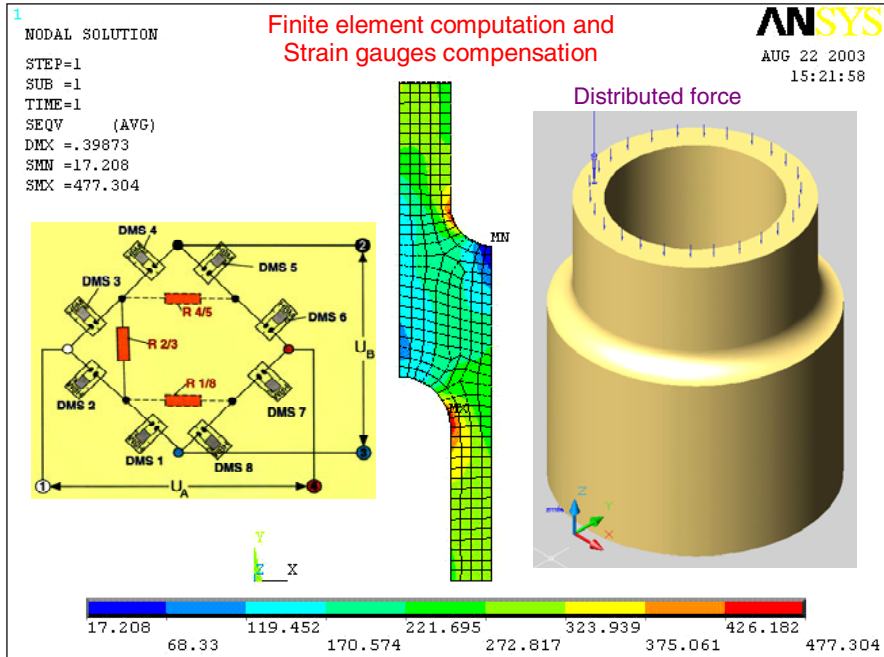


Fig. 10.12 Classical and Finite Element design of strain gauged elastic elements

17. Zhadko, I.P., Babichev, G.G., Kozlovskiy, S.I., Romanov, V.A., Sharan, N.N., Zinchenko, E.A.: Silicon pressure transducer with differential sensitive element based on transverse electromotive force effect. *Sensors and Actuators A: Physical* 90, 89–95 (2001)
18. Târnovan, I.G., Tebrean, B., Crişan, T.E.: Shock transducer with Hall sensing element. In: *Proc. 15th IMEKO TC-4 Symp. Novelties in Electrical Measurements and Instrumentation*, Jassy, Romania, September 19–21, vol. 2, pp. 581–586 (2007)
19. Sun, Y., Lin, J., Ma, D., Zeng, Q., Lammers, P.S.: Measurement of penetration force using a Hall-current-sensor. *Soil and Tillage Research* 92(1–2), 264–268 (2007)
20. Hall effect tachometric transducer / Speed sensor / Gear sensor. China Internet Information Center, May 23 (2009)
21. Hall Effect Sensing and Application. PDF Hallbook Honeywell (January 28, 2004)
22. Schicker, R.: Master of the rings – a robust, magnetic speed measuring system with high resolution. *Hotline Hottinger* (2), 14–16 (2003)
23. Sadjadian, H., Taghirad, H.D.: High precision parallel shoulder manipulator. Tehran, Iran, May 23 (2009),
<http://saba.kntu.ac.ir/eecd/aras/projects/HPPSM.htm>
24. Brook, A.J., Bending, S.J., Pinto, J., Oral, A., Ritchie, D., Beere, H., Henini, M., Springthorpe, A.: Integrated piezoresistive sensors for atomic force-guided scanning Hall probe microscopy. *Applied Physics Letters* 82(20), 3538–3540 (2003)
25. Urry, S.: Plantar pressure-measurement sensors (review article). *Measurement Science and Technology* 10, R16–R32 (1999)
26. Magnetoresistive sensors – the measurement principle. PDF-Datenblatt, February 22, pp. 32–38. RheinTacho Messtechnik GmbH, Freiburg, Germany (2002)

Chapter 11

VIBRATING-WIRE FORCE TRANSDUCERS

The resonators (wires – as described in this chapter, rods, beams or tubes) are mechanical modifiers in which an elastic element is excited into vibration at its natural frequency, the value of which depends on the desired input quantity, e.g. force [11.1]. The output is thus at a frequency depending on the measurand.

11.1. VIBRATING WIRE AS FORCE MEASUREMENT PRINCIPLE

Reports of the use of vibrating-wire transducers (VWT) have appeared in 1928, in a paper by Davidenkoff, while the initial experiences in the UK were gained at the Building Research Station [11.2]. As related by a founder's nephew [11.3], the Wirth-Gallo company first started building vibrating-wire transducers in USA decades ago, but today there are modern incarnation, compact and inexpensive aluminum units having smart geometry (Fig. 11.1).

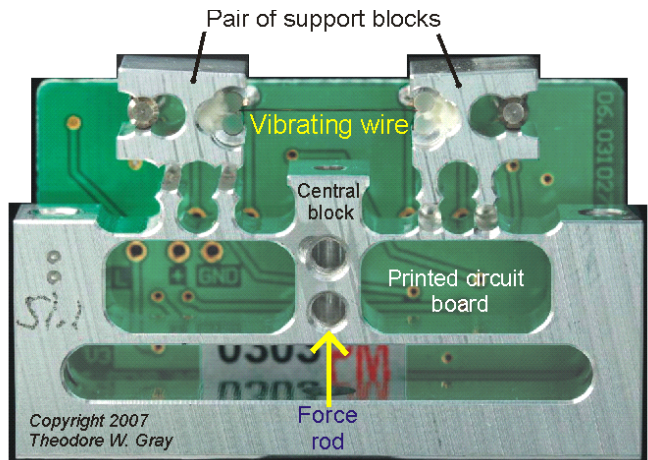


Fig. 11.1
Vibrating-wire
force transducer
(VWFT) as adapted
by DMS from TWG

The idea is quite simple: A wire is stretched between two points and vibrates while an alternating current runs through it. The natural magnets around the wire have been removed from this photo so you can see the wire stretched across the center near the top of the unit. It is held on either side by a pair of sapphire cylinders squeezed together by conical steel pins pressed into the opposite sides of the two blocks on top.

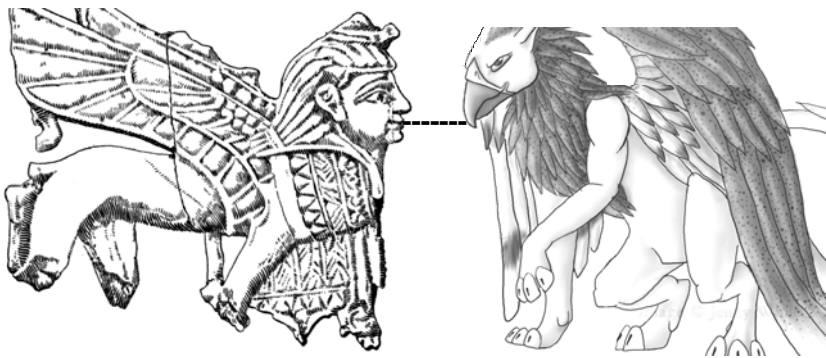
In use, the force to be measured is applied to a rod inserted through the hole in the thick bottom section and fastened with set screws to the block in the center of the machined aluminum unit. As you can see from the geometry of the device, if you push up on the center block it will deflect upwards, causing the two sets of horizontal supports to angle outwards (going from rectangular to parallelogram shape), which in turn will cause the two blocks holding the wire to be pulled farther apart. The actual movement is microscopic: The mechanism is designed to transfer force to the wire, not actually move any significant amount. (In fact the whole complex geometry is designed to minimize the negative effects, like metal creep and fatigue.)

Why not just use piezoelectric crystals or strain gauged force transducers? Because it is difficult to keep them accurate under severe operating conditions. Imagine wanting to be able to weigh the garbage collected from each individual house on a collection route, by putting transducers on all four wheels of the garbage truck. This is not only being done in a number of European countries, but soon will be a legal requirement that all garbage collection service be priced by their weight! Transducers on the wheels of a garbage truck have what can only be described as a hard life. One minute they are being run over pot holes at high speed, slamming a truck weighing many tons down hard on the transducer. The next minute they are being asked to accurately weigh a few kilograms of garbage, by measuring the increases in weight of the multiton truck when a new bin is tipped into it. The basic requirement for profitability is the ability to accurately weigh truckloads [11.4]. The better systems are highly sensitive to ever incremental weight changes and compensate for environmental factors (e.g. ambient temperature).

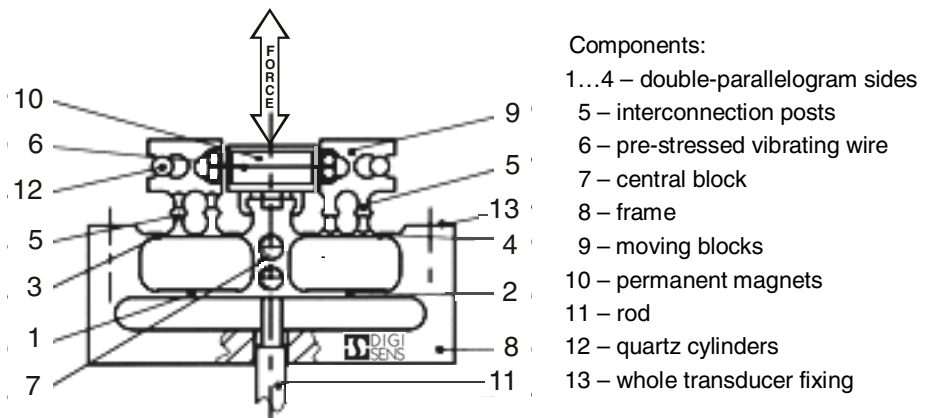
A good image is worth a thousand words; the exact functioning of a VWFT can be explained in Figure 11.2 [11.5]: Between the two supporting blocks (9) is a prestressed wire (6). The two permanent magnets (10) produce a magnetic field perpendicular to the wire (6). If a current is applied, the wire deflects due to the electromagnetic force. With the help of exciter electronics the wire can be put into vibration. The frequency of the vibration is determined by the stress applied to the wire by the two fixing blocks (9). The two quartz cylinders (12) pressed into the fixing blocks guarantee a constant retaining force on the wire. A force applied to the rod (11) acts on the central block (7) and deforms the double-parallelogram device composed of positions 1, 2, 3 and 4.

The stress on the wire varies due to the interconnection posts (5) and the two moving blocks (9). We could imagine two fantastic creatures, looking like zoomorphic elastic elements! A Korean Chinese Foo Dog? An ancient Sphinx or a Greek lion-woman? The most spectacular “tandem” is composed by an Egyptian winged sphinx and an American Gryphon – the mythical beast of folklore, a combination of Gyrfalcon and Snow Leopard!

The excitation electronics, directly fixed to the transducer, supplies the wire with the required energy for vibration, amplifies the frequency signal and changes it from a sinusoidal into a square-wave (TTL) signal. Such a signal can be transmitted interference-free and most microprocessors can directly accept it for further processing. The high output signal, comparing with strain gauged force transducers, is amongst other things responsible for the exceptional precision and stability.



Fantastic moving blocks: Sphinx versus Gryphon



- Components:
- 1...4 – double-parallelogram sides
 - 5 – interconnection posts
 - 6 – pre-stressed vibrating wire
 - 7 – central block
 - 8 – frame
 - 9 – moving blocks
 - 10 – permanent magnets
 - 11 – rod
 - 12 – quartz cylinders
 - 13 – whole transducer fixing

Fig. 11.2 Vibrating-wire force transducer components and “mythological” sensing

11.2. VWFTs’ STRUCTURES AND CHARACTERISTICS

A vibrating-wire force transducer (VWFT) is a complex structure strongly connecting a mechanical assembly based on a piano wire, an electromagnetic excitation and a digital measurement system (Fig. 11.3).

When a length of piano wire is held in tension and plucked, it will vibrate at its natural frequency f_0 . A small relative movement of the end fixings causes a change in the measured frequency of vibration. The wire can be used as strain gauge or in other types of transducer that respond to small deformations, such as load cells [11.6].

The fundamental frequency f_0 of the vibrating wire, expressed in hertz, is given by the equation for simple harmonic motion in the mechanics of oscillation:

$$f_0 = \frac{1}{2l} \sqrt{\frac{\sigma}{\rho}} \tag{11.1}$$

where l is the vibrating wire length, σ – its stress (tension) and ρ – the wire density.

Just like in force transducers based on elastic elements with bonded strain gauges, the mechanical stress σ under the applied load on the vibrating wire is converted into specific strain ϵ , following the Hooke’s law of elasticity:

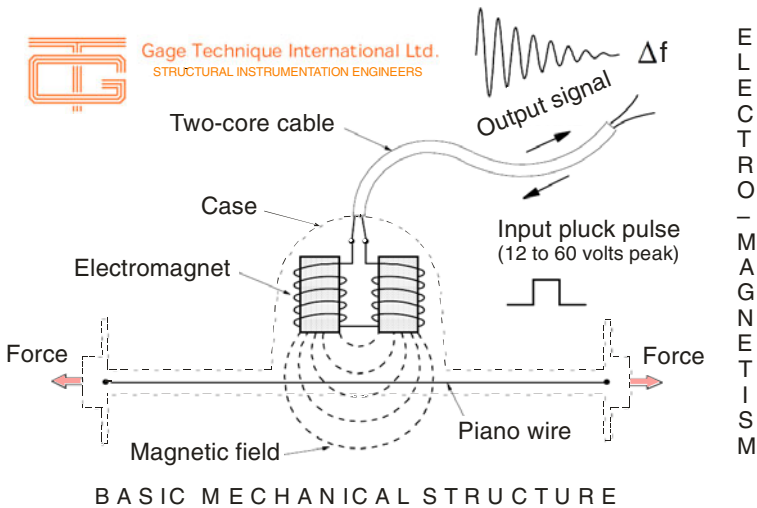


Fig. 11.3 A vibrating-wire force transducer: a piano wire electromagnetically plucked (The digital readout is not represented in this picture)

$$\sigma = E \cdot \varepsilon \quad (11.2)$$

where E is the elasticity modulus of the vibrating-wire material.

Combining the first two relations and having in view that E and ρ are constant parameters of the material, the vibrating-wire strain ε can be written as a parabolic dependence:

$$\varepsilon = k_f \cdot f^2 \quad (11.3)$$

where k_f is the gauge factor of the force transducer, usually expressed in units of microstrain per frequency squared. Each vibrating-wire transducer has its own constant, which is affected only by a change of the wire length.

This description of the operation of the “plucked” VWFT is didactically more suggestive and easier to understand. However, in practice the transducer of this type is inserted in the feedback loop of an electronic oscillator, in order to generate continuous oscillations on the vibrating-wire resonance frequency. The existence of a variation in electric current does not affect the gauge constant and therefore does not impair the measurement accuracy.

Readout units usually measure the frequency f or its inverse T , which is the period of the vibrating-wire element in the transducer. A measurement in engineering units, such as kN or microstrain (strain multiplied by 10^{-6}), is calculated by comparing two types of readings: an initial one is taken soon after the transducer is installed and other subsequent readings can then be referred back to the original datum. A positive change indicates a compressive strain.

The sensitivity of the vibrating-wire transducer, S_{vw} is defined as the ratio between the relative variation of frequency and the relative variation of wire length, which is the specific deformation ε [11.7]. The final form of this relation, as a result of a finite difference computation, taking into account that Δl is much smaller than l_0 and after replacing ε according to (11.2) is:

$$S_{vw} = \frac{\Delta f / f_0}{\Delta l / l_0} = \dots = 0.5 \frac{E}{\sigma_0} \quad (11.4)$$

One may notice that vibrating-wire sensitivity S_{vw} increases directly proportional with the elasticity module, E and inversely proportional with the initial stress, σ_0 which cannot be reduced below a certain limit, in order to ensure its proper functioning.

Practical work has demonstrated that the sensitivity of the force measurement by means of vibrating wires differentially installed on an elastic element, e.g. a ribbed membrane, is higher than using other parametric

transducers (R, L or C). This sensitivity reaches the value of 300 in case of this VWFTs as compared to the 250 in case of the differential capacitor (formerly called condenser) and with the 200 in case of the semiconductor strain gauged transducers (Table 11.1).

A series of tests were carried out in the Material Strength and Transducers laboratories of the “Politehnica” University of Bucharest within three closely linked domains: learning – research – production [11.8].

Various materials for manufacturing the wire were tested (enameled copper, wolfram or steel), as well as various methods for fixing and pre-straining of the vibrating wire. Finally the option was the diametrical installation of the VW inside of a ring-shaped elastic element. This ring has an external diameter $D = 120$ mm, while the internal one is $d = 100$ mm and its width $a = 5$ mm. Applying the force $F = 1$ kN on a steel piano chord, pre-fastened with screws at the two endings, a frequency variation from 3 to 4 kHz which can also be auditive sensed.

Such tests can also be performed at various levels of education: student scientific circles, diploma papers, Master and PhD dissertations. A superior stage in this respect is the structural optimization of the VWT elastic elements. For example one can install two perpendicular vibrating wires on the opposite faces of a ribbed membrane sized ($\varnothing 120$ mm \times 24) mm². Using the finite element method the influences of various size modifications can be studied: the reduction of the circular rib thickness from $b_3 = 6.5$ mm to $b_1 = 1.3$ mm leads to the increase of the VWT sensitivity by 24.7 % as an effect of increasing variation of the length δ .

Numerous contributions concerning the methods of increasing the strain gauged force transducer sensitivity (including the ones with vibrating wire) can be found in the author’s PhD work [11.9].

Table 11.1 Performance comparison for some measuring principles of force transducers

Performance	Principle	Vibrating wire	Variable inductance	Differential condenser	Strain gauges	
					Metallic	Semicond.
Range ratio		0.6	0.8	0.6	1	
Sensitivity factor		300	100	250	2	200
Accuracy [% of full scale]		0.2	0.35	0.25	0.5	0.35
Linearity error [%]		0.02	0.5	0.5	0.02	1
Thermal effect [% / 50 °C]		1	1.2	1.2	0.5	10
Stability [% / year]		0.01	0.5	0.05	0.5	0.05
Maximum frequency [kHz]		0.1	0.5	0.1	1	
Price ratio		1	0.4	0.9	0.3	0.2

11.3. ELECTRONIC CIRCUITS FOR VWTs

The vibrating-wire instruments are called “auto-resonating” that is the gauge wire is maintained in vibration, producing a continuous output signal as long as the power is applied; details are given in the Norwegian Geotechnical Institute's reference [11.10]. These resonators are well suited for dynamic measurements and have an advantage over conventional analog transducers because the output is a time-dependent signal, which can be measured, directly in digital systems by pulse counting.

11.3.1. Vibrating-wire excitation methods

The simplest form of excitation is to pluck the stretched wire by hand, and the simplest form of measurement is to determine the pitch or tone of the sound generated by the vibrating wire. For this reason vibrating-wire strain gauges are sometimes referred to as acoustic transducers (category presented in Chapter 13). The earliest recorded account of using a plucked stretched string to measure deformation was made in Italy by Pietro Cardani (1888), based on the modulus of elasticity measurement. He plucked the wire manually with small tweezers and determined the string frequency both by ear and with a stroboscope, reporting an accuracy of approximately 0.003 mm. Jump now to the lovely electric guitar, having mahogany body and neck, a resonator cone with a Highlander piezo-transducer and a lipstick tube single coil by the neck!

The most common methods of exciting vibrating-wires are depicted in Figure 11.4. In the first example, a coil with a permanent magnetic core is placed close to the gauge-wire (Fig. 11.4a). When a current pulse is applied to the coil, the wire made by ferromagnetic steel is plucked electromechanically and it will oscillate until it stops due to dampening. This is the noncontinuous “pluck-and-read” mode of operation in geotechnical and structural instruments.

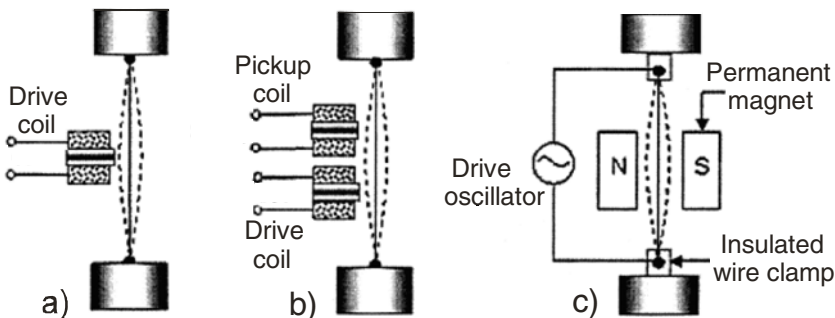


Fig. 11.4 Vibrating-wire excitation schemes: a) single coil, b) tandem of coils, c) feedback loop of an electronic oscillator generating continuous oscillations

To keep the gauge-wire oscillating, it is necessary to have an electronic drive circuit to maintain the oscillation and to provide the output signal. The vibrating-wire transducer consists of a taut ferromagnetic wire that is excited into transverse vibrations by a drive coil and these vibrations are detected utilizing an added pick-up coil, as in Figure 11.4b. Both coils have permanent magnetic cores and once the wire has been excited to its resonance frequency for an applied stress, it is maintained at this frequency by connecting the two coils by a feedback loop through an amplifier to form a self-oscillating system. Each resonant frequency is a measure of the tension in the wire and hence, applied force at that instant [11.11].

Another convenient way to induce a mechanical vibration in the gauge-wire is to place it in a permanent magnetic field and drive it with alternating current to set up transverse vibrations, which are picked up by a detector coil magnetically coupled to the wire and this signal is fed to a driving oscillator forming a close loop (Fig. 11.4c). The disadvantage of the concept: it is generally more difficult to design electrically insulated fixation points for the vibrating wire.

In the NGI measuring system, presented in Figure 11.5, the vibrating-wire transducer and coils are configured as a simple oscillator circuit. When a voltage is applied to the oscillator terminals, the gauge-wire will automatically start to vibrate and it will continue to vibrate at its resonant frequency as long as voltage is applied to the terminals. The connection between the exciter circuit and the vibrating-wire transducer is via a two-conductor long-cable, typical for geotechnical applications. The maximum cable length used to date between the VWT and the excitation and control circuits is approximately 12 km.

Note that the world's first truly electronic watch, Bulova Accutron, put on the market in 1960, had an electrically excited tuning fork controlled by a similar transistorized circuit.

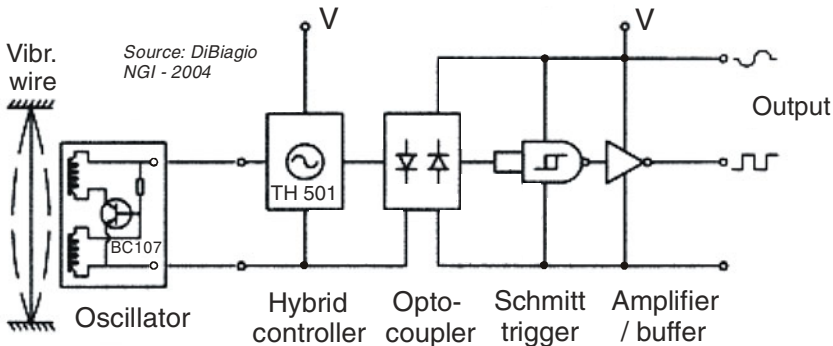


Fig. 11.5 Typical vibrating-wire system at the Norwegian Geotechnical Institute

11.3.2. Measuring circuits for vibrating-wire transducers

The most representative electronic schemes associated with the VWTs evolution stages are the following [11.8]:

- low frequency generator, that is an audio-frequency amplifier incorporating a vibrating-wire resonator (Fig. 11.6a);
- Wheatstone bridge resistively balanced where electromechanical oscillations on the wire resonance frequency are produced;
- VW as part of an oscillatory circuit LC (the Foxboro solution) resulting an unified signal proportional to the frequency squared and appropriately processed in a scheme presenting the automatic adjustment loop [11.12];
- a combination of a vibrating wire with a piezoelectric transducer which, being a reversible one, behaves as an active element (actuator), exciting the VW according to its basic frequency. The force – frequency characteristic is nonlinear but its evaluation does not raise any problem, the frequency of the output signal of the oscillatory circuit being easily processed using a programmable microprocessor;
- the intelligent force VWT in the numerical weighing system, SFT2 (K-Tron) model, presented in Figure 11.6b: the digital filtration stops the interference noises in the installation; there are also thermal compensation circuits and the incorporated microprocessors provide the maximum resolution, without the need for *in situ* recalibration.

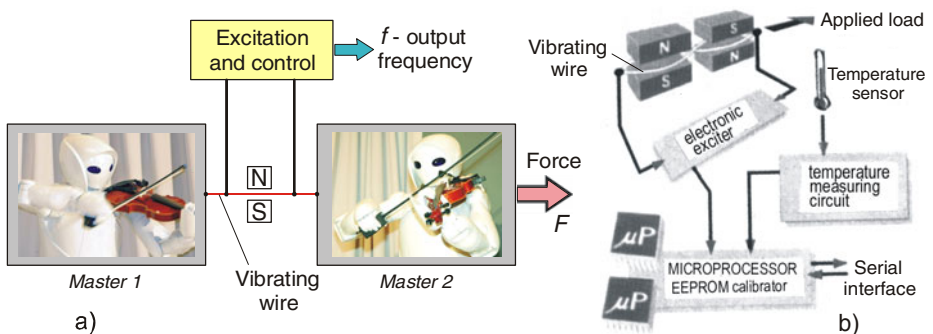


Fig. 11.6 Classical (a) and modern (b) vibrating-wire systems together with Toyota Partner Robots playing violins (drawing styles correlated with technical evolution)

11.3.3. Digital weighing based on vibrating-wire transducers

The Smart Force Transducer III (SFT III) incorporates the latest digital weighing technology into their weigh-feeding and metering equipment [11.13]. With a mechanical package specifically designed and optimized for duty in process applications involving single-point weighing, the SFT III is the standard in the company's SWB300 and SWB600 smart weigh belt

feeders, K4G multi-ingredient loss-in-weight feeding system, and SFM350 smart flow meter. Other K-Tron gravimetric equipment employs multi-point weighing and retains the company's current SFT II transducer.

The SFT III's single vibrating wire and unique parallelogram design resists torsional loading making it suitable for unconstrained single-point weighing. Its monolithic structure produces a stiff and responsive measurement system with very low deflection and no barometrically sensitive components.

The SFT III is the latest incarnation in more than 30-year evolution of digital transducers beginning with K-Tron pioneering the introduction of the digital mass transducer employing vibrating dual-wire weighing technology. The SFT III marks the sixth generation of digital weighing technology using a single vibrating wire that is characterized by significant advancements over vibrating dual-wire technology in all aspects of performance including high-resolution and stability, data communications and networking, vibration immunity, as well as mechanical simplicity, reliability and robustness.

A double parallelogram structure is presented by Brabender [11.14]. It is a deflectionless single *vibrating-wire load cell* with microprocessor, EEPROM for linearity optimizer, internal resolution of 1 ppm, software filter for vibration attenuation and serial weight transmission.

A compensated *vibrating-wire force transducer* with its indicating device have a typically combined nonlinearity, hysteresis and repeatability error of 0.025 % fsd in the temperature band of $-10\text{ }^{\circ}\text{C}$ to $+40\text{ }^{\circ}\text{C}$ [11.15].

11.3.4. Virtual musical instruments investigated by means of VWFTs

In order to design "virtual" musical instruments, measurements of the mechano-acoustic impulse responses have been made using a Maximum Length Sequence signal, generated by PC, sampled by the A/D board, and cross-correlated with the original one, to obtain the impulse response directly in the time domain, thanks to the Alrutz fast deconvolution algorithm [11.16].

For direct measurements (Fig. 11.7), this signal, properly amplified, was sent to a *Dunnwald-like copper wire force transducer*: the force exerted over the bridge is proportional to the current passing through the wire, as it is located in a strong, permanent magnetic field. The acoustic pressure radiated from the violin's body is then sampled by a microphone located in the anechoic chamber of the Cremona's Violin Making School, and the impulse response is obtained by cross-correlation of the acoustic signal with the excitation signal. Then this "anechoic" input force signal can be used as a starting point for producing music samples played on "virtual" violins.

Another solution consists in measuring the force applied from the vibrating chords to the bridge, during a musical performance.

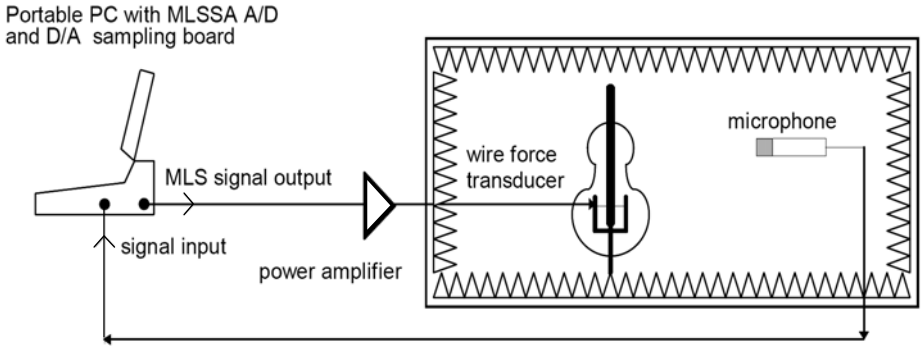


Fig. 11.7 Testing “virtual” music performance using the “anechoic” input force signal

However this is not an easy task: miniaturized load cells have to be inserted between the chords and the bridge, and their mass and stiffness are anyway too large to avoid any change in the dynamic response of the instrument. For this reason, it was chosen an indirect technique, in which the input force signal is reconstructed by inverse filtering of response signals.

Although there are differences between activation through the bow or (electro)magnet, like in the reaction way into the measurement scheme, the force which acts on the strings (producing their stretching or bending) determines the responding frequency.

11.4. DIFFERENT TYPES OF VIBRATING-WIRE TRANSDUCERS

Vibrating-wire force transducers (VWFT) belong to the category of frequency-output transducers and have all their advantages: high accuracy and repeatability, possibility for remote measuring and digitalization of results. As anyone who has tuned a guitar knows, the resonant frequency of a stretched wire depends on how tightly it is tensioned. So, the frequency is a measure of the force stretching the wire, and therein lies a vibrating-wire transducer.

The operating principle consists in the modification of the self-resonance frequency (f_0) as a result of the mechanical stress variation inside the wire, according to other form of the Equation (11.1):

$$f_0 = \frac{1}{2l} \sqrt{\frac{F}{\rho \cdot A}} \tag{11.5}$$

where l is the gauge length, A – the wire section, ρ – the material density and F – the force by which the wire is extended.

The fundamental resonance frequency, f_0 may be modified in two ways:

- by modifying the strain inside the wire at a *constant length*, a version in which the tensile stress ($\sigma = F/A$) should be directly measured;
- by modifying the wire length under *fixed stress*, a situation in which extensions can be measured as relative variations of length ($\epsilon = \Delta l/l$).

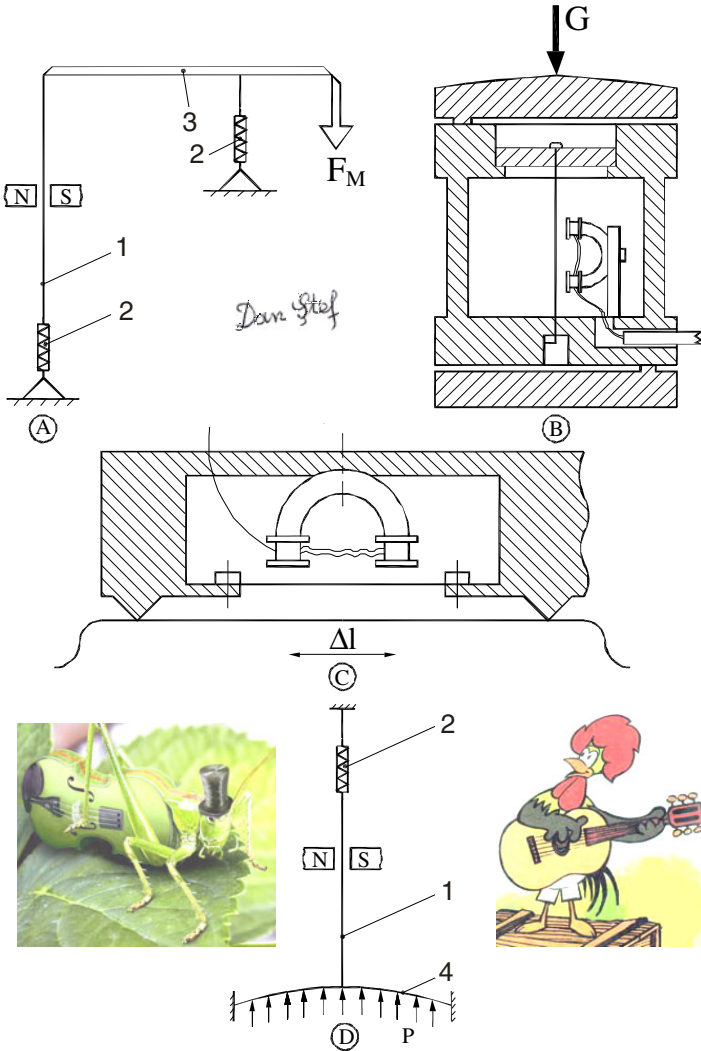


Fig. 11.8 Some mechanical quantities measurement using vibrating wires: a) force (Erdem), b) mass (Rohrbach), c) displacement (Maihak), d) pressure (Milohin). Parts significance: 1 – vibrating wire, 2 – spring, 3 – lever, 4 – diaphragm.

Because it is difficult to maintain the wire under constant strain in the case of the VWTs, one should measure the mechanical stress variations and, implicitly, the variations of the wire frequency. These could be produced by various quantities, such as: force (Fig. 11.8a), associated with weighing by levers [11.17], mass (Fig. 11.8b), displacement or vibration (Fig. 11.8c), pressure (Fig. 11.8d) and others which could be turned into extensions: thermal dilatations, density, viscosity, strain deformations, torsion couples, level variations, etc.

To ensure the stability in operation and a maximum sensitivity, the transducer should maintain its wire in resonance by means of a feedback signal. In this respect there are two constructive versions, concerning the excitation system (the electronic circuits are not represented in Figure 11.8):

- the wire location (usually on the vertical direction) in a constant magnetic field produced by a *permanent magnet* (Fig. 11.8a and d);
- the wire incorporation in a controlled oscillator, being excited by an *electromagnet* (Fig. 11.8b and c).

Other possibility: the vibrating wire introduced into the Wheatstone bridge, located on the response loop of an electronic amplifier, leads to an electro-mechanical (or mechatronic) oscillator.

In the large constructive variation of VWTs, especially for customized industrial measurements [11.18], the remarkable contribution of reputed measurement schools is worth mentioning:

- British: R.S. Jerret, R.V. Jones;
- German: H.F. Grave, Albert Haug;
- Russian: N. Davidenkoff, A.M. Turicin.

A vibrating-wire force transducer, used as tensometer for monitoring concrete structures, is depicted in Figure 11.9, conforming to the Sketch 11.8C.

Another VWFT design provides a highly stable and sensitive means of monitoring water levels [11.19]. The main component of the precision water level monitoring system 4675LV is a cylindrical weight suspended from the vibrating-wire force transducer. The cylinder hangs partially in the water whose level is to be monitored. As the water level changes, the changing buoyancy force on the cylinder acts directly on the vibrating-wire transducer altering its tension and hence its resonant frequency.

The main advantage of the 4675LV system lies in its high sensitivity and stability, which allows water level changes of as little as 0.1 mm to be measured accurately. The force transducer is immune to zero drift and has a very low response to temperature changes. As with all vibrating-wire transducers, because the output is a frequency, it is not affected by changes of cable resistance and hence long signal cables are not a problem. The frequency is measured by either a portable readout box or a datalogger.

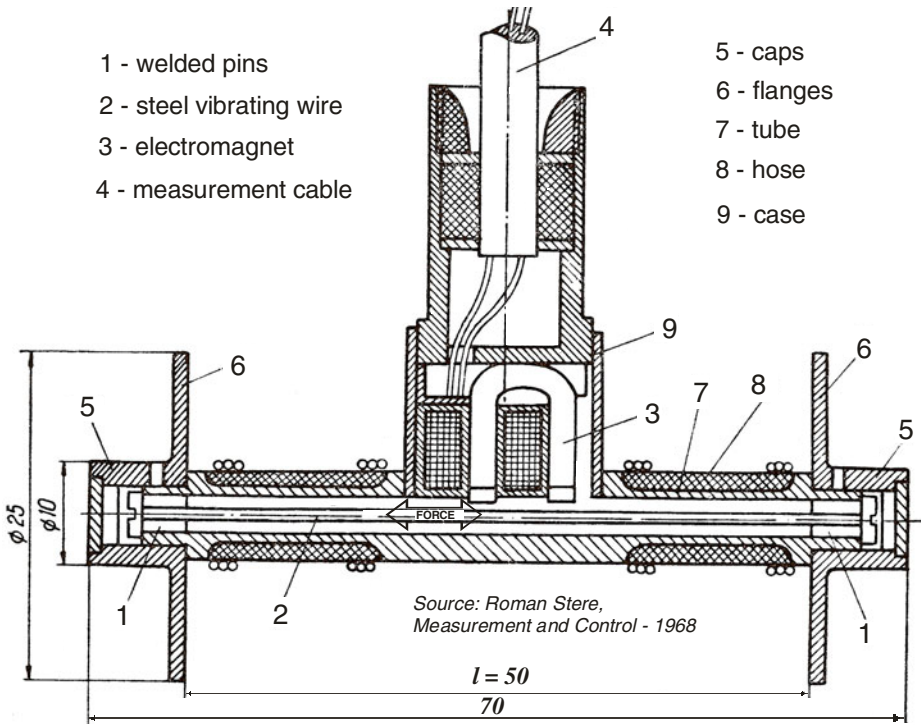


Fig. 11.9 Sectional drawing of a vibrating-wire tensometer (measurement base of 50 mm) for monitoring concrete stress within constructions of great importance

Relationship between the vibration frequency and the applied load is in the form of a parabola (Equation 11.3), which may be linearized electronically (using a microprocessor) or by mechanical arrangements, e.g. two vibrating mechanical systems, one of them producing contraction and the other extension as compared to the initial (preloaded) state.

The differential method is based on the vibrating dual-wire technique (Fig. 11.10a), doubling the measurement sensitivity as compared with a single VW [11.20]. There are two pretensioned wires inside a rigid frame, each wire being excited by two “opposite” magnets (N-S). Applying a load (force, mass, pressure or other related quantity) on the central yoke, one vibrating-wire is supplementary tensioned, increasing its vibration frequency f_1 , while the second one is “detensioned”, reducing its vibration frequency f_2 . This two oscillating frequencies are mixed together, as shown in Figure 11.10b, and, finally, their digitally indicated difference is proportional to the mechanical loading.

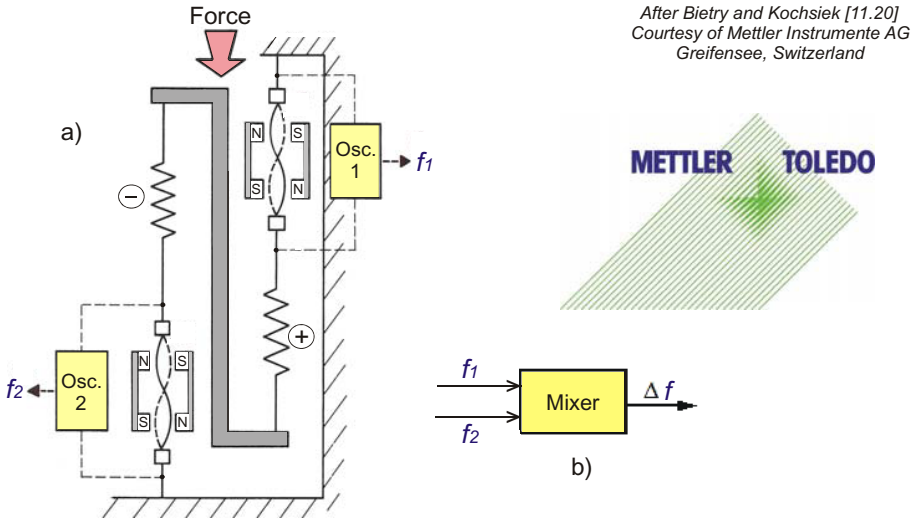


Fig. 11.10 The differential solution for vibrating-wire force transducer (a) and the mixing of the two oscillating frequencies (b) in order to indicate various applied loads

11.5. VWTs' APPLICATIONS FOR OTHER PHYSICAL QUANTITIES

The thermophysical properties of fluids are required for the design of many industrial processes. Experience has demonstrated that these features can be provided for mechanical properties by the application of vibrating objects with a variety of geometries. In such instruments the complex resonance of a vibrating object immersed in a fluid is measured and then related to the required thermophysical properties using working equations founded on the principles of physics [11.21].

11.5.1. Viscometers and densimeters

The viscosity of DIDP (diisodecyl phthalate), a fluid which could be used as a viscometer calibrant at viscosities of the order of 100 mPa·s, has been measured with a variety of methods including vibrating-wire viscometers. This instrument consists of a metallic wire, usually made from tungsten (a steel-gray metal with the chemical symbol W and atomic number 74) or stainless steel, which is tensioned, either by a mass, suspended from its lower end, or by being clamped between two rigid supports. A current is then passed through the tensioned wire which, in a permanent magnetic field perpendicular to its length, forces it to move. A continuous alternating current can be used (forced vibrations) or a direct current may be applied to displace the wire from its rest position, and the decay of amplitude measured after release (transient).

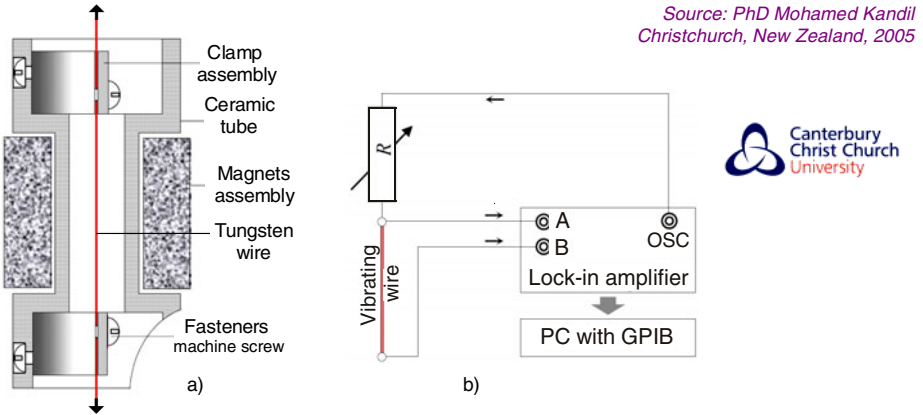


Fig. 11.11 Vibrating-wire viscometer (a) and its associated electronics (b) used for precision determinations in laboratory applications

Measurements of the current induced in the wire by its motion in the magnetic field provide the resonance in the forced oscillation mode or the logarithmic decrement and frequency in the transient decay mode.

From either measurement method, it is possible to determine the viscosity and when a mass is suspended from one end it is also possible to obtain density of the fluid using an appropriate model. A vibrating-wire densimeter uses the buoyancy force exerted by the sample fluid on an immersed buoy to alter the tension of a wire from which it is suspended [11.22]. The data obtained have a precision of $\pm 0.05\%$ and an estimated accuracy of $\pm 0.1\%$.

Kandil [11.23] has achieved a vibrating-wire viscometer, with an electrically insulating tensioning mechanism, to measure the viscosity of fluids over a wide range of temperature and pressure. Two vibrating wires were constructed of nominal length 40 mm, having nominal diameters of 0.05 and 0.15 mm; increasing the wire diameter increases the upper operating viscosity range of the viscometer. A schematic cross section, illustrated in Figure 11.11a, is conforming to the sketch B from Figure 11.8. The signal of the induced voltage was measured with a lock-in amplifier (PerkinElmer™ model 7265) connected to a computer equipped with a general purpose interface board (GPIB) controlled by Agilent Vee™ data acquisition software (Fig. 11.11b).

The properties of a vibrating wire in vacuum and in superfluid $^3\text{He-B}$ at temperatures well below transition temperature, where the properties are analogous with that of quantum vacuum, are presented in [11.24]. It is shown that the wire, as a simple mechanical resonator, can be used to measure such fundamental physical quantity as the energy gap in a spectrum of quasiparticle excitations of the superfluid $^3\text{He-B}$.

11.5.2. "Piezometers" (for underground water pressure)

Two basic designs are used in the construction of vibrating-element pressure transducers [11.25]. A pressure-sensitive element (diaphragm or bellows) develops a force against a tensioned wire or quartz crystal whose natural mechanical frequency of vibration depends on the stress due to the force. As a result, the frequency is a function of pressure. Electromagnetic and piezoelectric effects are utilized to pick up signals proportional to the deflection of the elements and to exert the driving forces on the vibrating member.

The instrument used to measure the pressure of the underground water in the clay (usually referred to as the pore-water pressure) is called piezometer, the name being derived from two Greek words *piezein* (to press) and *metron* (a measure) [11.26]. The "string" in a vibrating-wire piezometer is a steel wire stretched between a fixed block and a metal diaphragm, like in sketch D from Figure 11.8. Pore-water pressure pushes against the other side of the diaphragm which bends as pressure increases (Fig. 11.12a). As the diaphragm bends so the tension on the wire decreases which in turn causes the note it produces when plucked to change. In fact it produces a lower note (with a lower frequency).

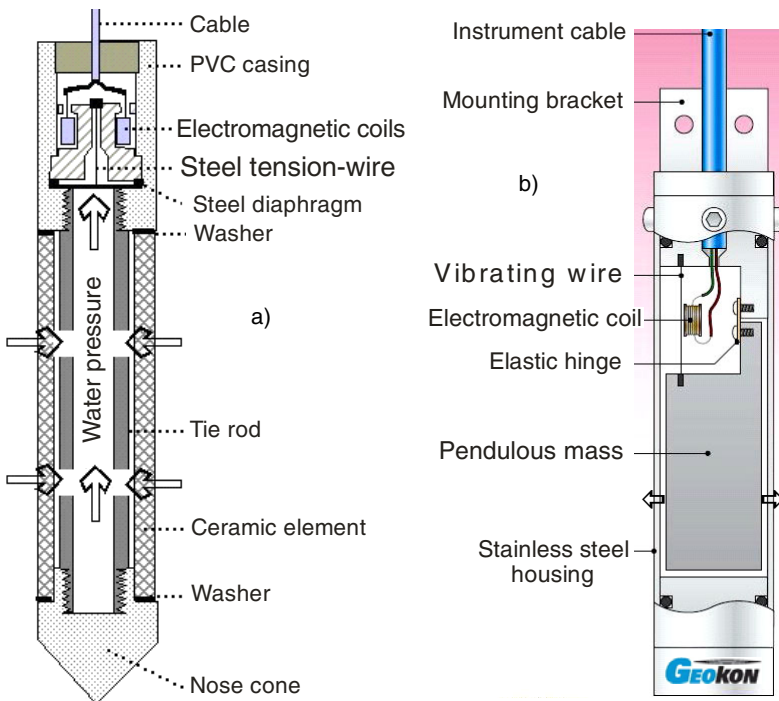


Fig. 11.12 Piezometer for underground water pressure (a) and tiltmeter with pendulous mass (b) based on vibrating-wire measurement principle

Because the piezometer is many meters underground, the operator can not pluck the wire himself. Instead electromagnetic coils are fitted on each side of the tension-wire and these are connected to the surface by ordinary copper wires. An electrical pulse sent down to the coils from the surface “plucks” the tension-wire and the two coils then sense the subsequent vibration and convert it to an electrical alternating-current output whose frequency is related to the tension in the wire and hence to the pore-water pressure.

11.5.3. Tiltmeters / inclinometers and slope indicators

Gage Technique International manufacture, supply, and install geotechnical and structural transducers, based on vibrating-wire strain gauges, for monitoring strain, tilt, displacement, and pressure [11.27]. The entire product range of Slope Indicators includes electrolevels, inclinometers, piezometers, pressure cells, extensometers, crackmeters, settlement systems, and many other.

The model 6350 Tiltmeter (Fig. 11.12b) is designed for attachment to structures, on either vertical or horizontal bracket, and for the subsequent measurement of any tilting that may occur [11.28]. When at rest, in vertical configuration, a pendulous mass inside the transducer, under the force of gravity, attempts to swing beneath the elastic hinge on which is supported but is restrained by the vibrating wire. As the tilt increases or decreases the mass attempts to rotate beneath the hinge point and the tension in the vibrating wire changes, altering its vibrational frequency.

Vibrating-wire tiltmeters combine a high range with high sensitivity, and very high calibration accuracy. They have excellent long-term stability and their temperature dependence is close to zero. The transducer output is a frequency, which can be transmitted over long cables, and renders the transducer less susceptible to the effect of moisture intrusion.

Biaxial measurements of angles can be achieved by mounting the tiltmeter in pairs, each member oriented at 90° to the other.

11.6. VWTs’ PROGRESS AND THEIR EXTENDED UTILIZATION

The evolution of vibrating-wire technology is driven by specific applications and economic needs. The most important categories of utilization and their advantages are the following:

a) Industrial, commercial and private weighing

Since its introduction in current use, the vibrating-wire weighing technology has established a certified reputation in the process marketplace for its high accuracy, long term stability, and operational reliability. The range of applications is extended from domestic (popular kitchen balances and bath

scales) to dynamic weighing in rough industrial environment and transportation of various objects including garbage.

b) Structural testing in Civil Engineering

The vibrating-wire method is strongly recommended for real-time and remote testing *in situ* being very convenient for measuring static or quasi-static phenomena on huge structures [11.29]. Its innate qualities, such as cheapness, long-service stability and tolerance to electrical troubles, make it particularly suitable for experiments in long tunnels [11.30]. Monitoring programs for constructions of great importance (road bridges, dams, and nuclear containments) can be watched in order to detect any departure from the design limits, improving the safety of all engineering structures.

c) Determination of thermophysical properties for fluids

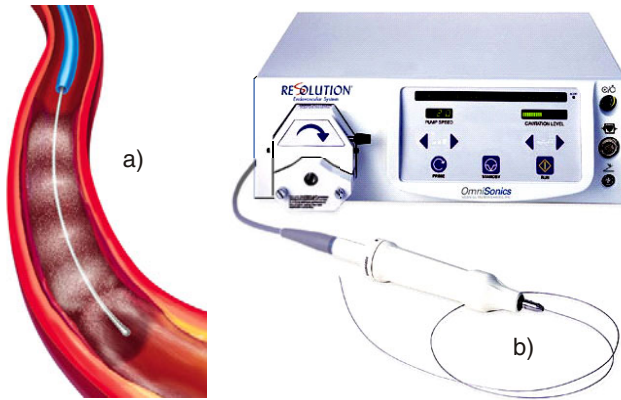
By the end of the 1960s only few techniques had emerged having both a rigorous mathematical description of the experimental method and technical innovation to render precise measurements in fluids for gas or liquid phases, up to high pressure and in wide temperature range [11.31]. The vibrating-wire technique has made “the journey from accuracy to fitness for purpose” to succeed in high-resolution determinations of fluid thermophysical properties like density, viscosity, conductivity, intermolecular pair potentials, etc.

d) Medical procedures

Some basic probe vibrating assemblies have been extended through various medical purposes. The vibrating motion, produced by a needle, wire or electrode, has a key role in endoscopic procedures [11.32] or as a lifesaver for millions of people suffering vascular occlusive diseases [11.33]. OmniSonics Medical Technologies of Wilmington, MA, has directly applied sound energy to clots using a narrow wire that is guided to the trouble spot (Fig. 11.13). High-frequency sound waves radiate outward from the wire, breaking the clot into particles smaller than red blood cells and the body naturally flushes them away. The wire stays cool throughout the procedure, preventing damage to the surrounding tissue, a significant improvement over earlier healthcare technology.

e) Biological investigations

Here are two applications: a platinum wire acting as a microvibrating electrode to measure the local mechatronic property of biological gel [11.34] and a vibrating probe, an insulated, sharpened metal wire with a small platinum-black tip (10...30 μm), which can detect ionic currents in the μA per cm^2 range for cellular samples in physiological saline [11.35].



Source:
Popular Mechanics,
August 2009

Fig. 11.13 Blood clots busted with a vibrating wire (a) and the associated apparatus developed by OmniSonic Medical Technologies (b)

The probe is vibrated at about 300 Hz by a piezoelectric bender. In the presence of a bioelectric current, the probe detects a voltage difference between the extremes of its movement. This basic, low-cost measurement system is readily adaptable to most laboratories interested in measuring physiological electric currents associated with wounds, developing embryos and other biological systems.

f) Advanced scientific research

The scientists of the Kavli Institute for Nanoscience at T.U. Delft have conceived a suspended vibrating carbon nanotube (CNT), comparable to an ultra-small violin string in an inventive “orchestration” [11.36]. When they applied an alternating electric field (using an antenna), the suspended nanotube begins to vibrate at a certain frequency. Moreover, the nanotechnologists were able to vary the number of electrons on the CNT, causing very slight changes in its vibration behavior each time an electron is added. They have succeeded in charting the influence of the presence of just a single electron in a measurement environment cooled to almost absolute zero.

NOTE: All the above-mentioned devices could be treated as vibrators or resonators as well, but we consider the vibrating-wire technique as a distinct and large-spread method for measuring the force and other physical quantities.

The vibrating-wire force transducers (together with their associated electronics) are solid and stable, complex mechanical devices involved in numerous applications regarding the electronic measurement of various physical

parameters. Although their measurement range is more reduced (due to the prestressing) and they cannot be easily miniaturized, the VWFTs present the advantages of an increased sensitivity and high resolution using frequency output.

This innovative vibrating-wire concept, connected with large-scale integrated MEMS and modern digital technology, has proved significant advances over the analog resistive (strain gauges), inductive (LVDT) and capacitive sensors in widespread use within force transducers.

In the context of the wide diversity of force measuring principles, illustrated in Figure 11.14, selecting of a certain type of force transducer is sometimes a complex problem, which is more extensively analyzed in Chapters 2, 16 and 34.

REFERENCES

1. Usher, M.J., Keating, D.A.: *Sensors and Transducers – Characteristics, Applications, Instrumentation, Interfacing*, 2nd edn. MacMillan, Houndmills (1996)
2. Hornby, I.W.: The vibrating wire strain gauge. In: Window, A.L., Holister, G.S. (eds.) *Strain Gage Technology*. Elsevier Applied Science, London (reprinted 1989)
3. Wirth, J.: Vibrating wire sensor. An example of the element Copper. Internet text updated, September 5 (2007)
4. Duffy, D.P.: What you should know about weighing systems. *MSW Management (Online)*. The Journal for Municipal Solid Waste Professionals, 1–11 (November–December 2003)
5. Digi Sens Technology: Vibrating-Wire, <http://www.digisens.com/typo3temp/2c573a3114.gif> (last updated: June 14, 2006)
6. Lock, S.: The theory of vibrating wire transducers. PDF created by Gage Technique International Ltd., Trowbridge, November 18 (1999)
7. Stere, R.: *Electronic Apparatus for Measurement and Control*. Editura Didactică și Pedagogică, București (1968) (in Romanian)
8. Ștefănescu, D.M.: Vibrating-wire transducers. *Automatizări și instrumentație (Sisteme – măsurări – elemente de execuție – acționări – comunicații – calculatoare de proces)*. Anul X (serie nouă) (4), 19–21 (2001) (in Romanian)
9. Ștefănescu, D.M.: *Methods for increasing the sensitivity of strain gauge force transducers*. PhD dissertation (160 pages, 26 tables, 86 figures and 336 references), Universitatea “Politehnica” București, Romania, September 10 (1999) (in Romanian)
10. DiBiagio, E.: A case study of vibrating-wire sensors that have vibrated continuously for 27 years. PDF created on August 3 (2004)
11. Hunt, A. (Coord.): *Guide to the Measurement of Force*. The Institute of Measurement and Control, London (1998)
12. Hulsing, R.H.: Vibrating beam force transducer with automatic drive control. US Patent 5417120 (May 23, 1995)

13. K-Tron smart force transducer weighing technology for gravimetric feeding, batching and metering. Thomas Publishing Company (2009), http://www.ktron.com/images/imagelib//graphics/PIC_S
14. Intelligent Digital Load Cell IDL-F. PDF created on April 5 (2004), http://www.brabender-technologie.com/mainpage/feeding/english/idl-f_e.htm
15. Zecchin, P. (Chair.): Digital Load Cells – A Comparative Review of Performance and Application. The Institute of Measurement and Control, London WP0803-2003
16. Farina, A., Langhoff, A., Tronchin, L.: Realization of “virtual” musical instruments: measurements of the impulse response of violins using MLS technique. PDF created on October 7 (2000), <http://pcfarina.eng.unipr.it/Public/Papers/068-Ciarm95...>
17. Erdem, U.: Force and weight measurements. *Journal of Physics E: Scientific Instruments* 15, 857–872 (1982)
18. Holst, P.A.: Resonant wire technology applied to process control instrument design. Acta IMEKO VIII (Moscow, Soviet Union), Session 11, A-21 (1980)
19. Vibrating wire weir monitor. Geokon – Geotechnical Instrumentation, Lebanon, NH, June 22 (2009)
20. Biétry, L., Kochsiek, M.: Mettler Wägelexikon. Praktischer Leitfaden der wägetechnischen Begriffe. Mettler Instrumente AG, Greifensee, Ch, ME-720113-84
21. Wakeham, W.A., Fitt, A.D., Ronaldson, K.A., Goodwin, A.R.H.: A review of vibrating objects for the measurement of density and viscosity in oilfields including devices fabricated by the method of MEMS. *High Temperatures – High Pressures* 37, 137–151 (2008)
22. Pádua, A.A.H., Fareleira, J.M.N.A., Calado, J.C.G., Wakeham, W.A.: A vibrating-wire densimeter for liquids at high pressures: The density of 2,2,4-trimethylpentane from 298.15 to 348.15 K and up to 100 MPa. *International Journal of Thermophysics* 15(2), 229–243 (1994); (SpringerLink Netherlands: April 22, 2005)
23. Kandil, M.: The development of a vibrating wire viscometer and a microwave cavity resonator. PhD Dissertation, University of Canterbury, Christchurch, New Zealand, PDF created on January 30 (2006)
24. Človečko, M., Hanušin, T., Král, M., Skyba, P.: Vibrating wire: A probe for the energy gap measurement in superfluid $^3\text{He-B}$. *Acta Physica Slovaca* 54(6), 525–533 (2004)
25. Khazan, A.D.: *Transducers and Their Elements*. Prentice Hall Inc., A Pearson Education Company, Upper Saddle River, NJ (1994)
26. Vibrating wire piezometers. In: *The Management of Coastal Erosion – Report 2* (June 23, 2009), <http://www.canterbury.gov.uk/images/coastal/Diag103.jpg>
27. About Gage Technique, Allington, Maidstone, Kent, UK, June 23 (2009), <http://www.gage-technique.demon.co.uk/images/piezoes.jpg>
28. Vibrating wire tiltmeter. Geokon – Geotechnical Instrumentation, Lebanon, NH (June 22, 2009)
29. Jávör, T.: General recommendation for the vibrating-wire measuring method and its equipment. *Materials and Structures* 10(4), 255–257 (1977); (SpringerLink Date: September 21, 2006)

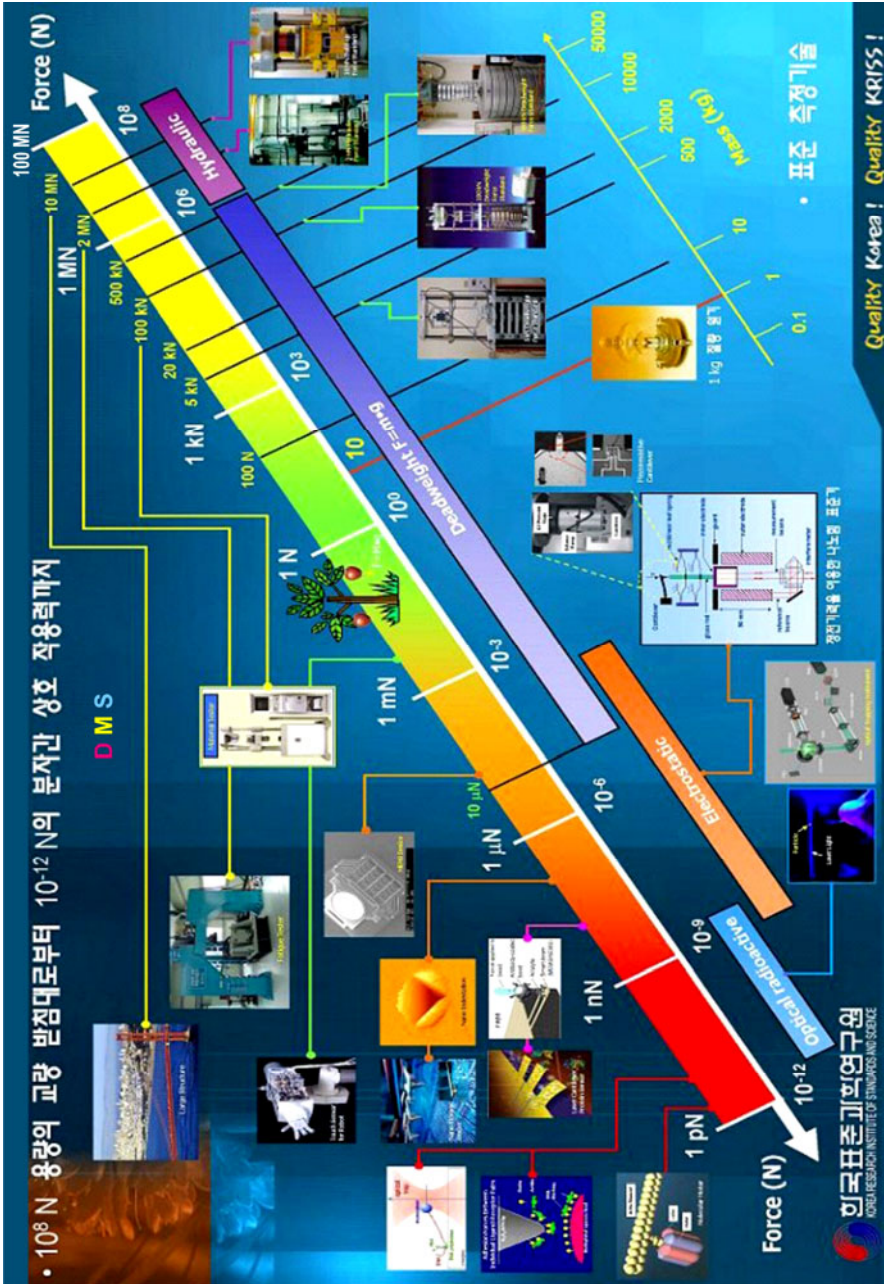


Fig. 11.14. Principles, ranges and applications in the field of Force Measurement (courtesy of KRISS)

30. Thomas, H.S.H.: The measurement of strain in tunnel linings using the vibrating-wire technique. *Strain (An International Journal for Experimental Mechanics)* 2(3), 16–23 (2008)
31. Wakeham, W.A., Assael, M.A., Atkinson, J.K., Bilek, J., Fareleira, J.M.N.A., Fitt, A.D., Goodwin, A.R.H., Oliveira, C.M.B.P.: Thermophysical property measurements: the journey from accuracy to fitness for purpose. *International Journal of Thermophysics* 28(2), 372–416 (2007)
32. Parasher, V.K., Miller, N.J.: Probe vibrating assembly for endoscopic procedures. US Patent 7048684, May 23 (2006)
33. Sound busts blood clots. Published in the March 2003 issue and online (August 2009),
<http://www.popularmechanics.com/technology/industry.html>
34. Furukawa, T., Hashimoto, S., Mochizuki, S., Otani, H., Imamura, H., Iwasaka, T.: Measurement of local mechatronic property of biological gel with micro-vibrating electrode. *Journal of Biomechanics* 39 (Suppl. 1), S654 (2006)
35. Reid, B., Nuccitelli, R., Zhao, M.: Non-invasive measurement of bioelectric currents with a vibrating probe. *Nature Protocols* 2(3), 661–669 (2007)
36. Steele, G.A., Hüttel, A.K., Witkamp, B., Poot, M., Meerwaldt, H.B., Kouwenhoven, L.P., van der Zant, H.S.J.: 'Nano violin string' made of vibrating carbon nanotube (w/Video). Published online in *Science Express Reports*, July 23 (2009)

Chapter 12

RESONATOR FORCE TRANSDUCERS

The resonator sensors (wires, beams, membranes, cylinders or tubes) are mechanical modifiers in which an elastic element is excited into vibration at its natural frequency, the value of which depends on the desired input quantity [12.1]. The output is thus at a frequency proportional to the measurand of interest, e.g. force or pressure. Like in properly excited parametric transducers, the stress applied to an elastic body generates a proportional signal. Resonant sensors are based on the fact that the resonance frequency (or relative phase of oscillation) of a vibrating micromechanical structure is a highly sensitive device for parameters that alter the resonator stiffness or geometry [12.2].

The general scheme of a resonant microsensor is shown in Figure 12.1a. The resonator element is inserted into the feedback loop of an electronic oscillator [12.3]. Stress effects occur due to the applied force, which increase the resonator stiffness, thus changing its resonance frequency. The oscillator output is fed to a frequency counter recording the load-dependent signal.

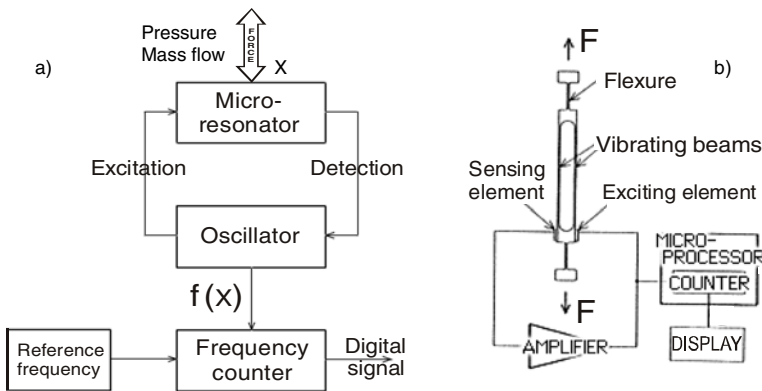


Fig. 12.1 Resonator force transducer: a) block diagram and b) tuning fork scheme

Table 12.1 Actuating and sensing variants for microresonators (after [12.3])

Chapters	DMS	Excitation / Actuating	Detection / Sensing
	C.3	Electro-thermal	Piezo-resistive
	C.5	Electrostatic	Capacitive
	C.6	Piezo-electric	
	C.7	Electro-magnetic	
	Diverse	Optical	

For excitation and detection of the micromechanical resonators the following techniques are most frequently applied and presented in Table 12.1. In principle two approaches can be used:

- a single element for both excitation and detection, corresponding to an electrical one-port network;
- separate elements for excitation and detection, modeled as an electrical two-port resonator.

The vibrating wires were presented in the previous chapter. Other vibrating elements, which are strips or plates, are made from a material with good elastic properties such as quartz, piezoceramic material, Elinvar (Nickel steel with 13 % Chromium) or beryllium copper. Usually, they are formed into a shape similar to a double tuning fork, generally referred as DETF (double-ended tuning fork) devices. Each element of the fork is forced into oscillation, which is maintained at a specific frequency in a closed loop feedback system (Fig. 12.1b). Two piezoceramic elements, close to the lower ends of the vibrating beams, are connected to the output and input terminal of an amplifier respectively, acting to sustain the vibration, one for exciting and the other for sensing. Change of frequency is a function of the applied force. A transducer of this type may have a maximum measuring range of about 30 kg, with a general performance specification complying with 6000 divisions to OIML R60 [12.4].

12.1. RESONATOR PRINCIPLE IN FORCE MEASUREMENT

Mechanical resonators have excellent stability and potentially low hysteresis [12.5]. Adding the frequency output feature, a considerable practical interest is achieved. Digital transducers have many advantages over conventional analog transducers in that their output can be measured accurately with inexpensive frequency counters, they have reliability, low error rates, reduced susceptibility to degradation of transmitted signals by electrical interference, and low dependence on change in electrical characteristics with time.

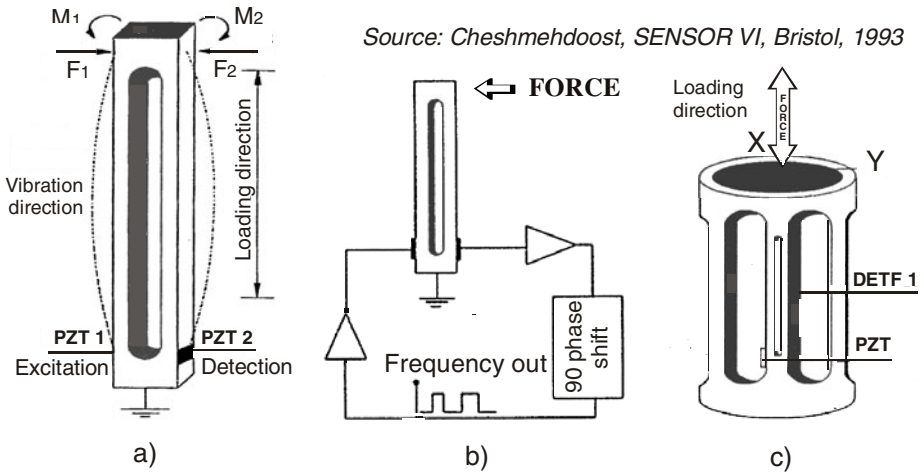


Fig. 12.2 Double-ended tuning fork (DETF) excitation and detection (a) and its closed-loop resonant circuit (b). Tubular resonator with four equi-spaced DETFs (c).

The double-ended tuning fork basic structure consists of twin beams which are coupled at their roots (Fig. 12.2a). When one of the tines in this symmetrical structure is excited at its fundamental frequency, the opposite tine resonates sinphasically. Due to symmetrical vibration of the DETF, the vibration of counterforces F_1 , F_2 and bending moments M_1 , M_2 cancel at the roots, so that at each end of the resonator beyond the roots. This unique property of the DETFs allows them to be clamped beyond their vibrational roots without significant loss of vibrational energy or reduction in their mechanical quality factor Q .

The fundamental frequency of a beam is a function of its parental material property, and dimensions. This frequency increases with increasing applied axial force, and the equation governing the vibration of a beam under tension T is given by:

$$T \cdot \frac{d^2Y}{dX^2} - E \cdot I \cdot \frac{d^4Y}{dX^4} = \rho \cdot A \cdot \frac{d^2Y}{dt^2} \tag{12.1}$$

where: I – second moment of area: $(b \cdot h^3) / 12$

E – Young’s modulus of the material

ρ – the material density

A – cross-sectional area of the beam ($b \cdot h$)

b and h are breadth and height of the beam, respectively

t – time

Assuming a simple harmonic motion and applying the boundary conditions, the natural frequency f_{01} , when axial force $T = 0$, is given by the expression below:

$$f_{01} = \frac{a^2}{2\pi \cdot l^2} \sqrt{\frac{E \cdot I}{\rho \cdot A}} \quad (12.2)$$

where: a – value determined by mode number of vibration $n_v \approx (1 + 2n) \pi/2$,
and

l – beam length.

However, when $T \neq 0$, the natural frequency of the beam under axial force f_{T1} becomes:

$$f_{T1} = f_{01} \cdot \sqrt{1 + \frac{1}{a^3} \cdot th \frac{a}{2} \cdot \left(a \cdot th \frac{a}{2} - 2 \right) \cdot \frac{l^2 \cdot T}{2E \cdot I}} \quad (12.3)$$

These equations define the motion of a DETF under stress and they may be used to design a DETF to operate at a particular frequency; it is also possible to determine the total frequency shift of a DETF under full-scale load. However, in practice other important parameters should be considered in order to realize a DETF-based force transducer.

An electronic closed-loop circuit tracks the resonant frequency (output of each DETF) and incorporates a digitally generated 90° phase-shift to bring input and output in phase. This arrangement (Fig. 12.2b) keeps each device in continuous oscillation, and as the structure is loaded each closed-loop circuit tracks the resonant frequency and maintains respective oscillation.

12.2. MATERIALS FOR RESONATORS AND THEIR Q-FACTORS

Since early 1980's, Shinko Denshi Co. Ltd. has developed metallic resonant tuning fork balance and since early 1990's, Avery Berkel and Weigh-Tronix (now Avery Weigh-Tronix) have achieved quartz resonant tuning fork weighing scales while Druck Ltd has developed silicon resonant pressure transducers.

NOTE: In this chapter, and in others as well, the term "quartz resonator" refers to a sensor type in which the property of a quartz crystal to electro-mechanically oscillate on certain resonance frequencies is exploited, and not simply the classical piezoelectric effect (as treated in Chapter 6), consisting in generating an emf proportional to the applied mechanical load.

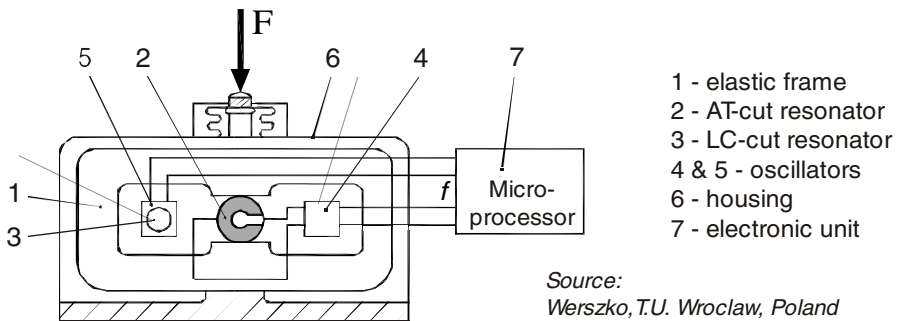
12.2.1. Quartz resonators for force transducers

The exceptionally high elasticity accompanied by practically negligible hysteresis and the high chemical resistivity make single-crystal quartz a most suitable material for microresonators with long-term stability. Besides electrical charging effect and resulting output voltage [12.6], the intrinsic piezoelectric effect can easily be used to excite stable mechanical resonance vibrations with a high Q value. The quartz resonator mechanical deformation causes a change in resonance frequency which can be related to the applied pressure or force.

A force transducer, developed in T.U. Wroclaw, Poland [12.7] and shown in Figure 12.3, consists on an elastic frame (1), a C- or U-shaped AT-cut resonator (2) for force measurement, an LC-cut resonator (3) for temperature measurement, two oscillators (4 and 5), a housing (6) and a microprocessor-based electronic unit (7). Under the force F action the resonant frequency f of the resonator, connected with oscillator 4, is changed, producing the output signal of the transducer.

The resonance frequency changes of the thickness-shear vibration of symmetrical incomplete circular AT-cut quartz crystal resonators (QXRs) are used for sensing elements in digital force transducers [12.8]. The incomplete circular shape can be applied to a larger load than the circular disc because the flat regions of the incomplete shape provide a distributed load application without the problems of stress concentration of a point force inherent to a circular disc. This shape increases the force sensitivity when compared with the complete disc near azimuth angle 0° .

The quality factor Q is a dimensionless parameter that describes how underdamped a resonator is, or equivalently, characterizes a resonator's bandwidth relative to its center frequency. Requirements relative to the Q factor are in general conflicting, depending on the application considered, e.g. if a system is submitted to a wide band excitation it should have a low Q value, while an oscillator is more stable when the Q value of its resonator is higher.



Source:
Werszko, T.U. Wroclaw, Poland

Fig. 12.3 Force transducer with quartz resonator (Courtesy of IMEKO, Budapest)

The Q value is a “sharpness” measure for resonance or frequency selectivity of a vibratory system with a single mechanical or electrical degree of freedom [12.9]. A Q -control device has been implemented and used to decrease the quality factor of the quartz tuning fork in Atomic Force Microscopy [12.10].

A quartz tuning fork resonator with smaller dimensions results in the reduced spring constant with important performance improvements in scanning probe microscopes and force sensing instruments [12.11]. A spring constant of 480 N/m and a mechanical quality factor Q of 27500 are nearly optimal values needed for frequency modulated AFM. Its noise-floor factor of $6.5 \text{ fN/Hz}^{1/2}$ – a measure of the minimum contact force attainable by the system – provides better force sensitivity than previously reported larger quartz tuning forks.

An experimental characterization of the dynamics of oscillating quartz tuning forks, increasingly used in scanning probe microscopy as force sensors, is made in [12.12]. The tuning forks can be described as a system of coupled oscillators. The coupling between the quartz tuning fork prongs has a strong influence on the dynamics and the measured motion is in remarkable agreement with a simple model of coupled harmonic oscillators (in-phase and anti-phase eigenmodes). The precise determination of the elastic coupling between the prongs allows the obtaining of a quantitative relation between the resonance frequency shift and the force gradient acting at the tuning fork free end.

Quartz microbalances based on quartz crystals coated with organic materials present high selectivity and absorptivity for the investigated compounds in chemical gas sensing [12.13]. The output signal of the QMB transducers, connected to Colpitts or TTL customized oscillators, is the shift of the resonance frequency, which is proportional to the absorbed analyte mass. The proportionality constant includes the square of the initial resonance frequency of the coated quartz crystal and the reverse of its area.

Two AT-cut quartz-crystal resonators, with 6.2 MHz nominal frequency, were coated with 600 nm layers of silicon dioxide on one side [12.14]. One of these resonators was exposed to the cosmic environment by actuating an electromagnetic shutter, while the other, situated in the close neighbourhood, was not. The difference between the two frequencies was converted into an analog signal and, through the telemetry system, recorded on the Earth. This “Nanobalance” experiment was performed during the Soviet – Romanian joint space flight on the space laboratory “Saliut-6” (14-21 May 1981).

12.2.2. Silicon resonators for force transducers

The classical example (Fig. 12.4b) is a silicon beam force transducer with piezoelectrically driven resonant strain gauge and an electronic oscillator which uses the resonator as the frequency defining element [12.15]. The most complex are MEMS and NEMS resonators which bear great potential for applications as RF sensors in life sciences or information technology [12.16].

A semiconductor fabrication process has been applied to prepare resonant AlN (aluminum nitride) and SiC (silicon carbide) beams (Fig. 12.4a), to be operated at frequencies between 0.1 and 2.1 MHz. The metallized beams were actuated by the Lorentz force in a permanent magnetic field of about 0.5 T produced by four NdFeB-magnets. A RF current sets the beam in oscillation. The induced voltage was measured using *time domain* (by digital oscilloscope) or *frequency domain* techniques, obtaining the resonant frequency dependence on tensile axial strain.

A systematic study of the RF response of double clamped beams of different materials and various geometries has been made under various operating conditions, including pressure-dependent viscosity and vacuum. The geometric dimensions varied from 10 to 500 μm in length l , from 1 to 8 μm in width w and from 100 to 250 nm in thickness t . The induced response of the resonators is smaller than the exciting signal by 5 to 7 orders of magnitude.

The resonant response of the beam structures can also be studied in the frequency domain, employing a balanced or bridge measurement technique. The major challenge consists of precisely adjusting the amplitude and phase of the reference (cable and resistor), to suppress the strong drive signal sufficiently at the input port of the differential amplifier (Fig. 12.4c). High resonant frequencies and quality factors are beneficial for high sensitivity.

An atomic force microscope is used as a nanometer-scale resolution tool for characterization of the electromechanical behavior of a polysilicon resonant cantilever-based mass sensor, actuated electrostatically by applying DC and AC voltages from a driver electrode placed closely parallel to the cantilever [12.17].

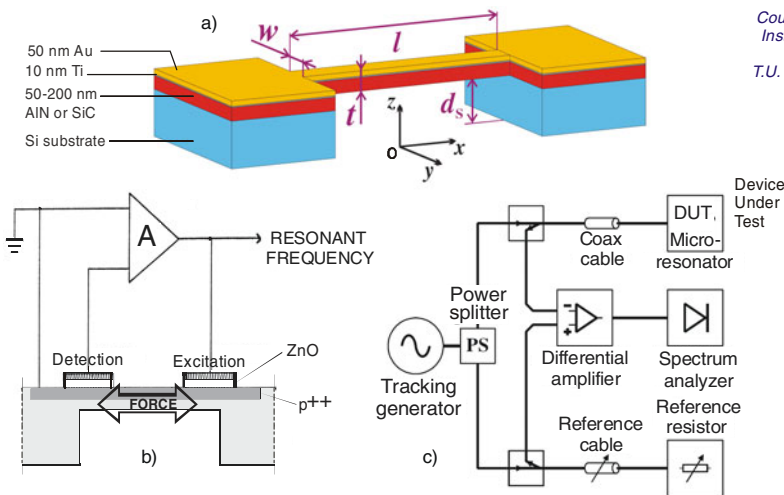


Fig. 12.4 Silicon resonator (a) in classical oscillator (b) or in RF strain transducer (c)

The dependence of the static cantilever deflection on DC voltage and of the oscillation amplitude on the AC voltage frequency are measured and the results are fitted by a simple nonlinear electromechanical model.

Doubly-clamped beam nanoresonators based on nanoelectromechanical systems (NEMS) with operating frequencies up to the microwave L-band have been achieved, through the development of improved materials and novel detection techniques [12.18]. An in-plane nanoresonator based on electrostatic actuation and silicon nanowire piezoresistive detection is presented in [12.19].

Another possibility is the SiC free-free beam nanomechanical resonators offering significant improvement in quality factor Q as compared to a doubly-clamped beam design operating at similar frequencies. Eddy current damping inherent to the widely-used magnetomotive transduction scheme (balanced-bridge detection) is experimentally measured using a top-down nanofabricated SiC nanowire device.

Two advances have been crucial to breaking the 1-GHz barrier in NEMS [12.20]: the use of 3C silicon carbide epilayers, and the development of balanced, high frequency displacement transducers. This achievement represents a significant advance in the quest for extremely high frequency nanoelectromechanical systems.

Apart from 3C-SiC epilayers on silicon, polished 6H-SiC bulk material based NEMS are also made possible using a tilted electron cyclotron resonance (ECR) etching technique. A suspended nanoscale, doubly clamped beam resonator has been made as an initial demonstration of this new fabrication method. Fundamental flexural mode mechanical resonance is detected at 171.2 MHz, with a quality factor Q of about 3000.

Magnetomotive transduction has been used extensively in the above achievements, where eddy current damping is usually negligible. However, it was realized that such damping phenomena may turn out to be crucial for doubly clamped beam nanotube mechanical resonators. This concept has been experimentally demonstrated. Silicon carbide material is used to create a dummy nanotube, and in turn being used to investigate the role of eddy current damping phenomena in the context of studying nanotube mechanical motion.

A novel nanotube-based device, carrying a single domain nanomagnet paddle and forming a torsional mechanical resonator, appears capable of force sensing in zepto-newton/Hz^{1/2} range at room temperature. By cooling down GHz nanomechanical resonators to low temperatures, the devices approach their quantum regime of operation.

Graphene-based resonators [12.21] that can be optically or electrically actuated have been fabricated by researchers from Cornell University and Pomona College [Bunch *et al.*, *Science* (2007) **315**, 490]. They have developed a mechanical technique to exfoliate single or multilayered sheets of graphene over preprepared trenches on SiO₂ substrates. The suspended graphene sheets

can be described as micron-scale cantilevers clamped to the surface by van der Waals forces. These cantilevers are set into vibrating motion through the application of a time-varying radio frequency voltage or by focusing a diode laser onto the surface. The resulting megahertz-range mechanical vibrations can be detected by optical interferometry. These mechanical properties make graphene suitable for force and mass sensing applications. By using a single layer of graphene atoms as a cantilever, the ultimate limit of two-dimensional nanoelectromechanical systems, such a sensor could detect ultra-small masses.

12.3. VARIOUS SHAPES OF RESONATORS

The measurand typically alters the stiffness or shape of the resonator, hence causing a change in its resonant frequency. The resonating elements can be cylinders (or tubes), membranes, tuning forks, strings, rods, or micromachined pieces of quartz [12.22]. Some simple shapes are presented in Figure 12.5:

- Piezoelectric disc resonator [12.23] or silicon ring resonator [12.24] as diametrical force transducer.
- Single-ended, U-shaped, torsional-mode tuning fork, used for temperature sensing [12.25]; the change in resonant frequency of the temperature sensitive quartz resonator can conveniently be utilized to compensate for thermal effects in the DETF force / pressure transducer mechanisms [12.26].
- Resonating beams for force measurement are often in the form of two U-shaped tuning forks connected tine-to-tine and resulting the typical DETF.

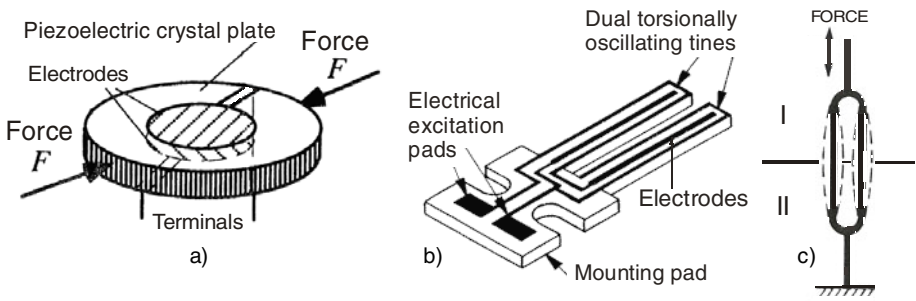


Fig. 12.5 Different shapes of plates and beams used for resonating force transducers: a) disc, b) dual tines (like musical diapason) and c) double-ended tuning fork (DETF)

12.3.1. Resonating beams for force transducers

A beam (3D) in a flexural vibration will change its resonant frequency, as stress is applied to it (Fig. 12.6a), in the same way as the resonant frequency of a vibrating wire or string (1D) is a function of applied mechanical tension [12.27].

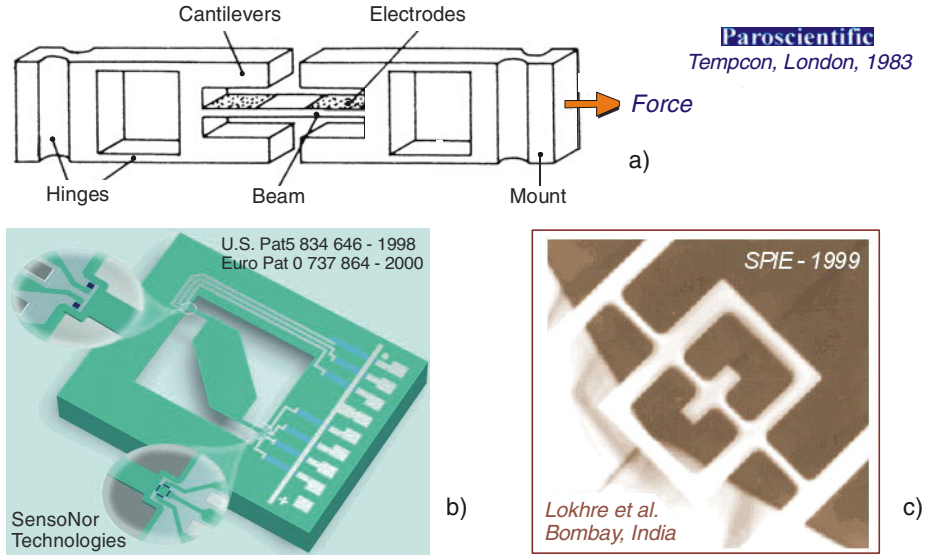


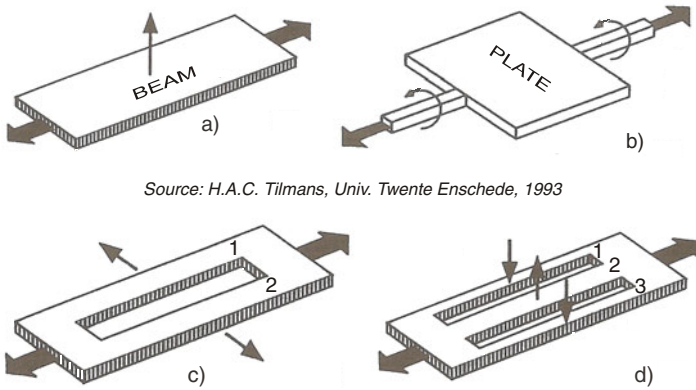
Fig. 12.6 Three specific resonating beams for force transducers: a) vibrating quartz Paroscientific transducer, b) accelerometer with inertial mass between two cantilevers, c) torsional and flexural MEMS resonator

As they are made from a piezoelectric material, they can be used as circuit elements simply by attaching appropriate connections and maintained in oscillation electronically.

The *two-beam* accelerometer pictured in Figure 12.6b has been developed by Sensonor for automotive applications [12.28]. The SA30 crash transducer, based on a thermally excited, acceleration-sensitive resonant structure, features self-test and self-calibration functions.

The Solid State Electronics Department of Tata Institute of Fundamental Research in Bombay, India [12.29] has designed, fabricated and tested a balanced doubly suspended versatile, torsion and flexural, MEMS resonator structure (Fig. 12.6c). FEM analysis has been used to compute the most likely six vibrational modes and their frequencies of free vibration, including flexure, torsion and mixed modes. The resonator arms are symmetrically deposited with magnetic films so as to give desired bending/twisting moments to the structure.

Figure 12.7 shows four examples of resonant strain gauges as clamped-clamped beams with a rectangular cross section or a combination of parallel band splines in a double or triple configuration [12.30]. Beams (sketches a, c and d) or plates (sketch b) are widely described in standard mechanical textbooks and their “adaptation” for micromechanical transducers is achieved by Bao within the series of “*Handbooks of Sensors and Actuators*” [12.31].

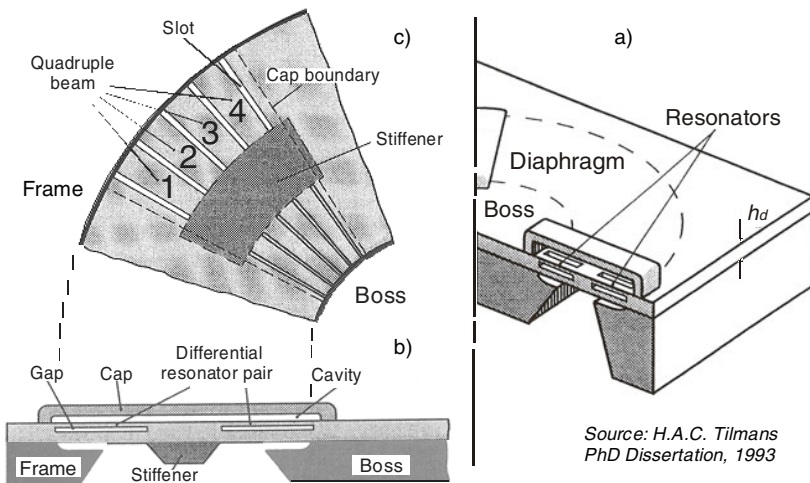


Source: H.A.C. Tilmans, Univ. Twente Enschede, 1993

Fig. 12.7 Examples of resonator configurations: a) simple flexural beam, b) torsional resonator plate, c) double-ended tuning fork, d) triple beam. The “wide” arrows indicate the applied axial force while the “narrow” arrows suggest the vibration modes.

12.3.2. Resonating diaphragms / membranes for force / pressure transducers

Figure 12.8a shows a 3D drawing of a differential pressure transducer. This structure can also be applied as a force transducer if the load is concentrated to the boss. In order to improve the equality of axial load transfer to the horizontal beams of the resonators, the region in between the resonators is stiffened.



Source: H.A.C. Tilmans PhD Dissertation, 1993

Fig. 12.8 a) 3D sketch of the right part of a differential pressure transducer with circular bossed diaphragm and embedded DETFs as differential resonators. b) Cross sectional view of the left part diaphragm. c) Top view of a sealed resonator pair, indicating the radial construction of the quadruple beams (adapted from the Dutch school [12.30]).

Other resonant structures associated with diaphragms are self-supporting such as single or multiple beams to give high natural frequencies without pre-tensioning [12.32].

Vibration modes and parameters of a square silicon membrane and of an oval membrane (micromachined quartz), both having apertures which delimitate microresonators [12.3], are presented in Table 29.1.

Metallic glasses (cut in the form of small strips of amorphous iron alloys) are also used as resonating elements for tensile force transducers.

12.3.3. Resonating tubes for force transducers

The load bearing capability of a DETF is determined by its material's yield strength and cross-sectional area. In designing the high capacity load cell a simple approach of integrating the DETFs and their support was chosen, they being fabricated from one piece of material in order to reduce the potential hysteresis due to the materials mismatch [12.5]. Four equi-spaced DETFs were fabricated in the walls of a hollow stainless steel cylinder at 90° relative to each other as depicted in Figure 12.2c.

The cylinder's four identical DETFs have tines with (1×4) mm² cross-sectional area and length of 20 mm. The load cell is designed for operation either in tension or compression. The load capability of this type of load cell may be easily varied by changing the dimensions of the supports. Finite element analysis has been used to establish an optimum static loading model for the device. The 20 kN load cell is quite insensitive to off-axial loading which may occur in real applications; this immunity is achieved by averaging the frequency outputs of all four double-ended tuning forks around the cylinder.

The tubular DEFT based load cell was tested under open-loop condition using a spectrum analyzer to obtain the frequency response under zero load conditions. The natural frequencies of all four DETFs were found to be around 6 kHz (less than 5 % variation between them); they have a Q greater than 1500.

The open-loop characterization of the DETFs showed that *the lower the drive voltage the higher the Q* . The high level of drive voltage causes loss of energy from the system by means of sound and/or heat.

12.4. SINGLE BEAM (MICRO)RESONATORS

Table 25.2 gives a summary of resonant force microsensors which have been developed by the Institut für Mikrotechnik der Technischen Universität Braunschweig in Germany [12.3]. Vibration modes and associated parameters are presented for single-, double- and triple-beam resonators.

Other examples illustrating these categories of (micro)resonators are detailed in separate subchapters.

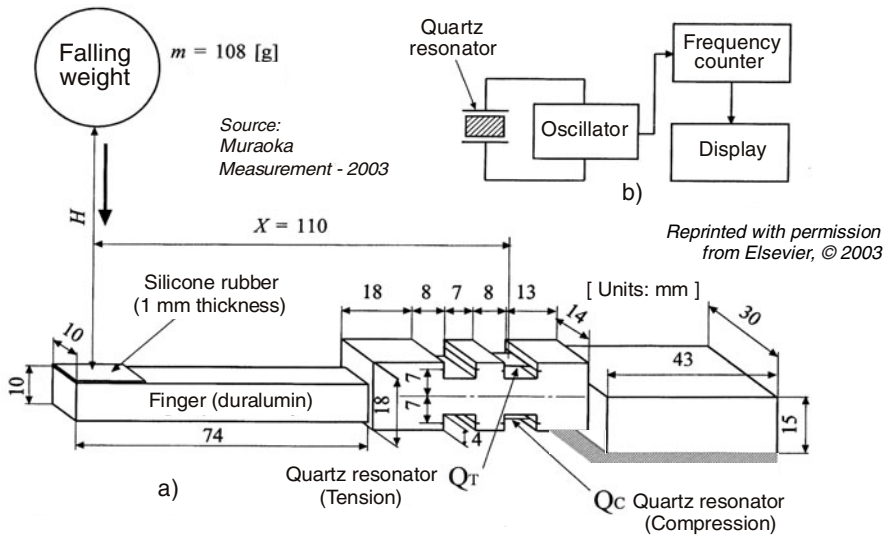


Fig. 12.9 AT-cut quartz profile built-in a finger tested by an impulsive force (a) and block diagram of the monitor system, including the quartz resonator symbol (b)

A force transducer based on a quartz resonator is inherently insensitive to noise, since the output is frequency shifted by the external force. The robot finger is regarded as a “profiled” cantilever [12.33] to improve its sensitivity in tension and, respectively, in compression for associated quartz resonators (Fig. 12.9a). The fundamental frequency is $10 \pm 0.5 \text{ MHz}$, the vibration mode is a thickness shear one, and the fast response is monitored by a digital display (Fig. 12.9b).

Four different resonance-based vector touch sensor designs are analyzed in [12.34]. A VTS probe would detect the magnitude and direction of contact force ranging from 10 to 100 mN between the probe tip and a specimen. The VTS resonating system is composed of a rigid rectangular metal bar with a ruby sphere attached to one end (Fig. 12.10a). Several pairs of piezoelectric elements (PZTs) are bonded on each side of the metallic bar. Functionally, PZTs will work to expand and contract when energized by an AC signal. Hence, several strategically placed PZTs are used as actuators to the probe and additional PZTs detect the strains as they propagate through the rectangular body.

Piezoelectric ceramics, when bonded to a rigid body and subject to applied electric fields, may be used to impose surface stress. Fig. 12.10b shows a resonator in which a thin PZT plate with electrodes on each of its two faces is bonded to the structure using electrically conductive epoxy. A PZT bonded to an oscillating structure will produce a voltage that is proportional to the strain in the probe and, therefore, the amplitude of oscillation of the structure.

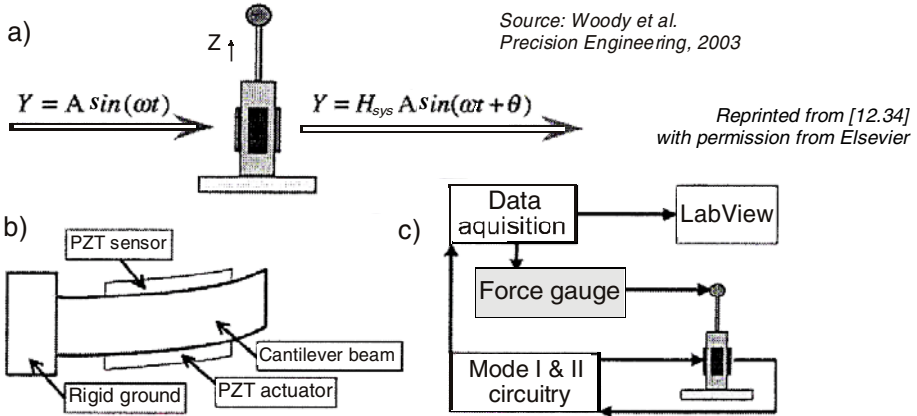


Fig. 12.10 Resonating probe input and output signals (a) and system response due to PZT excitation (b). Experimental setup for VTS (vector touch sensor) probe (c).

In the majority of applications contact forces will occur on the probe tip's outer hemisphere. A force gauge and probe mount are designed to contact the probe through a load cell while simultaneously measuring sensor output in both mode I (lock into a desired frequency and monitor phase response) or mode II operation (lock into a certain phase and then monitor frequency), an open and closed loop scheme, respectively (Fig. 12.10c). The mechanical apparatus to characterize VTS probes consists of the following major components:

- a force gauge to contact the probe head with a range and resolution comparable to current triggering and scanning CMM probes;
- motion control stages capable of moving the force gauge relative to the contact probe head to provide a complete scan over the outer hemisphere;
- a rigid clamp mechanism so that the probe body and force gauge must be rigidly fixed prior to measurement;
- automated data collection and storage using LabVIEW™ software.

An AFM cantilever for which the second flexural mode frequency can be tailored to reduce its stiffness relative to the first one is presented in [12.35]. This design allows to control the ratio of the first two resonant modes f_2/f_1 over the range 1.6 to 4.5, improving the dynamic tip-surface contact measurements.

12.5. DOUBLE BEAM (MICRO)RESONATORS

12.5.1. Classical double-ended tuning forks (DETFs)

VIBRA is the first electronic weighing scale based on tuning-fork vibrating principles, successfully developed by Shinko Denski Tokyo. When a tensile or compressive load is applied to a monoblock vibrator constructed in the form of two tuning-forks whose tips are jointed to each other, the vibrating frequency

will increase or decrease with high fidelity and accuracy according to the applied load (Fig. 12.11a). This frequency is counted and displayed digitally.

The new vibrational force transducer (DETF type) and its applications are presented in [12.36]. The tuning-fork force sensor developed by Shinko Denshi is used as a controlling device for the mirror surface of Subaru, the world's largest optical telescope on Hawaii Island, and it has shown successful results such as the discovery of a distant galaxy 128 billion of light years away from the Earth [12.37]. There are 261 actuators of precision tuning-fork sensors that continuously control the main mirror, which has a diameter of 8.3 m, 20 cm thick and weighs 20 t for ultra precise mirror control.

The paper [12.38] proposes a force transducer based on a DETF directly machined in a circular metallic plate after designing by means of finite element simulations. It is a specific, small height, tubular elastic element bonded on a thin circular plate, "transforming" the applied compressive force into a tensile force in the DETF beams (Fig. 12.11b). An original electronic device, using analog and logic functions, realizes the frequency shift measurement.

The tuning fork force transducer model TL-6000 made by Shinko Denshi Co. Ltd. for 50 N capacity is suitable as reference because of its long-term sensitivity stability and small hysteresis (Fig. 12.12). Its repeatability and reproducibility are satisfactory for calibrating other force transducers [12.39]. Other advantages – as expressed by the producer – are the following:

- i) *Simple construction.* The tuning-fork sensor is of such simple construction that it is trouble-free.

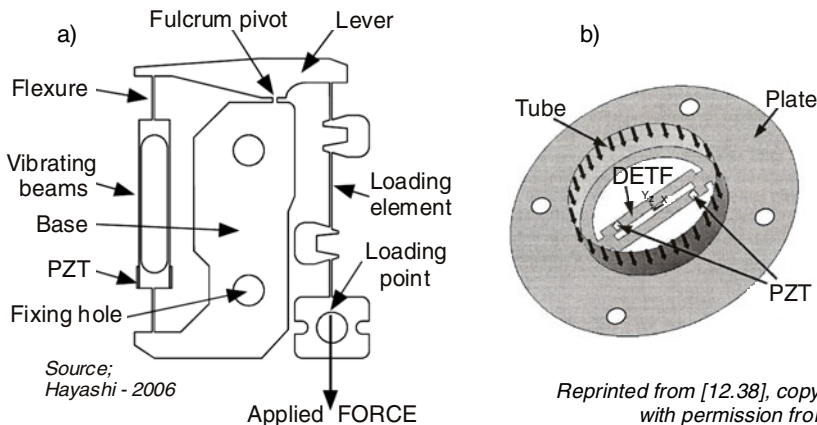


Fig. 12.11 a) Double-ended tuning fork sensor unit, ready for mounting in various applications. b) Special geometric structure, like a "hollow hat", transforming the vertical compressive force into a horizontal tensile force within DETF.

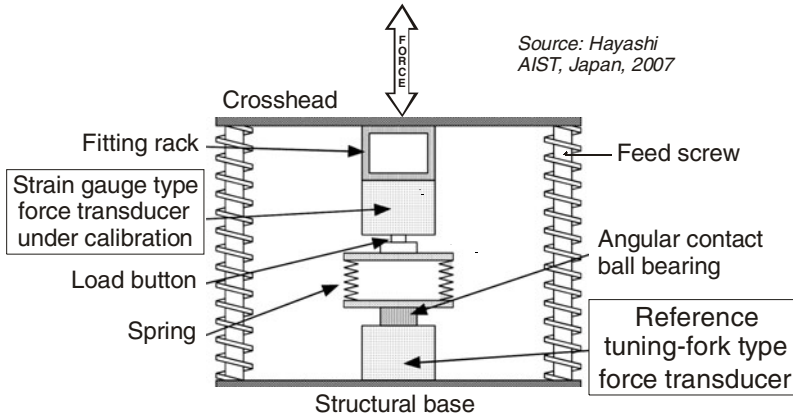


Fig. 12.12 Force comparator with reference to DETF type of force transducer

- ii) *Elimination of A-D conversion.* Since the detected value is in digital quantum, as expressed by a frequency level, there is no need for A-D converter. This leads to simplicity in electronic circuits and high accuracies.
- iii) *Wide measurable range.* It is possible to relate to a high degree of accuracy at large load with large sensors as well as at small load with smaller sensors.
- iv) *Minimum power consumption.* The power consumed by the sensor is in order of microwatts, adequate for battery operation, telemetering and explosion-proof application.
- v) *High accuracy.* The obtained accuracy in VIBRA is at least an order higher than that in the strain gauged load cells.
- vi) *No warm-up time.* Measurement may be carried out instantaneously without warm-up as the sensor and measuring circuit are operable upon energizing.

12.5.2. Modern solutions for DETF resonators

The key sensing element in primary pressure standards (dead weight testers) is a vibrating quartz crystal whose resonant frequency changes with pressure-induced stress [12.26]. Figure 12.13a shows a DETF resonator design consisting of two identical beams flexing 180 degrees out of phase to cancel the opposing forces and moments, thus transmitting very little energy to the mounting pads. Even though the quartz crystal has a high Q and a long-lasting resonance, a small amount of energy must be supplied to achieve and maintain oscillation of the DETF. Surface electrodes piezoelectrically drive and detect the resonant frequency through an external oscillator circuit. The electrode pattern is produced as an integral part of the photolithographic and chemical milling methods used in DETF manufacturing. The resonant frequency of the tines is a function of the dimensions, composition, and applied load.

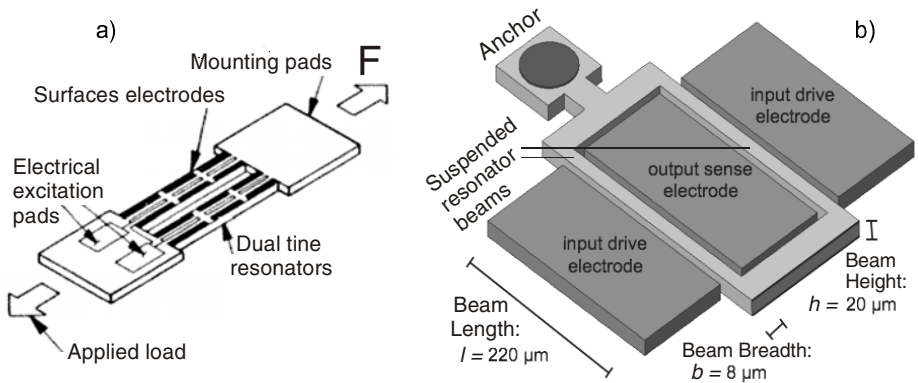


Fig. 12.13 New models of DETF sensing devices: a) vibrating quartz crystal for dead weight tester, b) high Q , single-anchored silicon MEMS resonator

Transducer resolution of parts per billion of full scale output allows observation of piston-cylinder nonuniformity and taper equivalent to changes in diameter of one molecular layer.

New micromechanical resonators, like those illustrated in Figure 12.13b, were fabricated using the “epi-seal” process in single crystal silicon and encapsulated with epitaxially deposited polysilicon [12.40]. Each beam of the tuning fork measures $(220 \times 20 \times 8) \mu\text{m}^3$ and the resulting transducer has a resonant frequency of approx. 1.3 MHz and quality factor $Q = 10^4$, at room temperature. The sensitive quartz resonators are actuated and sensed electrostatically.

An ANSYS microsystem analysis example, namely “*Application High Q Resonator Beam*” is presented in [12.41]. The objective of the paper was to demonstrate that it is possible to fabricate vibrating beam micromechanical resonators with high Q factors by placing support beams at the node points for the fundamental flexural mode. The support beams are subjected to torsion when the resonator beam flexes. This arrangement creates a beam that is essentially unrestrained (free-free) in the flexure mode.

This work demonstrates ANSYS Multiphysics’s capabilities in the following areas:

- Parametric modeling of MEMS geometry
- Static Analysis
- Contact Analysis
- Modal Analysis
- Prestressed Modal Analysis
- Electrostatic Pull-In Calculations
- Prestressed Harmonic Analysis

A parametric solid model and FEA mesh were created using ANSYS Multiphysics Release 6.1. The resonator beam, supporting beams, dimples, and anchors were modeled using the 8-noded SOLID45 element. The mesh contained 15252 elements and 20229 nodes.

This ANSYS Multiphysics evaluation focused on the 50 MHz beam geometry. The lowest natural frequency dominated by flexure of the resonator beam is mode number 15, and its calculated value is 51.6 MHz.

12.6. METALLIC TRIPLE BEAM RESONATORS (MTBRs)

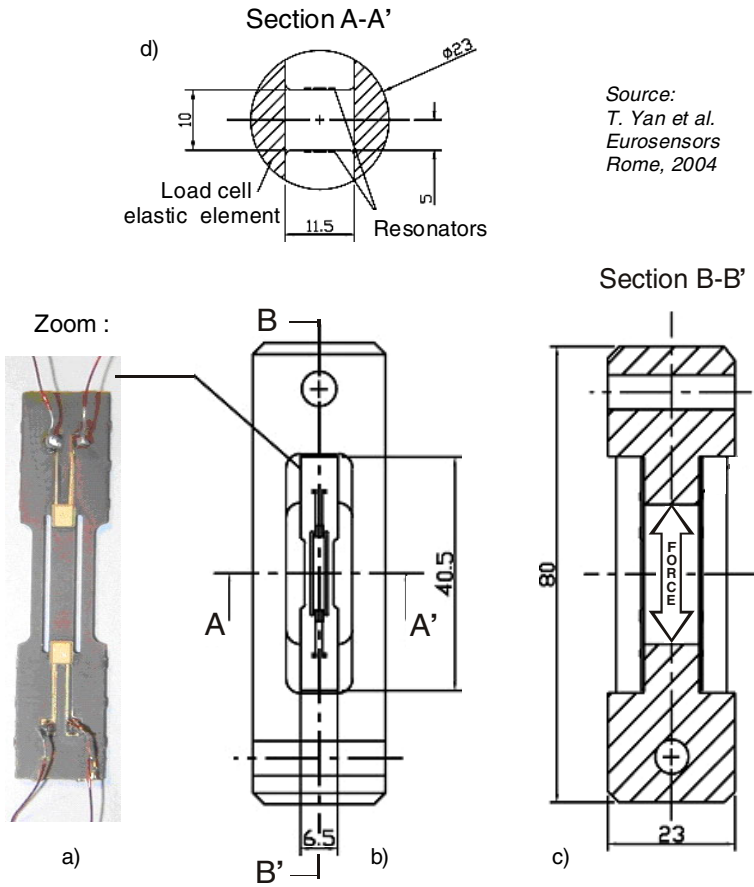
A thin-film multilayer structure of piezoelectrically driven silicon triple-beam resonators is presented in [12.42]. A joint Brunel – Southampton Universities' research team has developed digital strain gauges based on a metallic triple-beam resonator (MTBR) structure with thick-film piezoelectric sensor elements. The resonator, an oscillating structure vibrating at resonance, is designed such that its resonant frequency is a function of the mechanical measurand. The resonator substrate was fabricated by a double-sided photochemical etching technique and the thick-film piezoelectric elements were deposited by a standard screen-printing process. The new metallic digital strain gauges can be used on stiff structures, have high overload capacities, low power consumption, frequency output for digital processing, and offer prospects for wireless-batteryless operation. The device can be easily mass-produced at low cost for use in a wide range of measuring systems, e.g. load cells, weighing machines, torque transducers and pressure sensors.

12.6.1. Force transducers with MTBRs

The paper [12.43] reports on the design, construction and characteristics of a novel force transducer with resonators having stiffness and potential overload capability some 10 times that of a resistive strain gauge load cell. The experimental cell loaded up to 600 kg gives a direct output frequency change of 870 Hz (safety factor of 5).

The MTBR substrate (Fig. 12.14a) is photochemically etched from 430S17 stainless steel. The screen printing process was successfully used to deposit piezoelectric materials for fabrication of triple-beam tuning-fork resonators having a load capacity of 100 N, with a safety factor of over 2.

Figure 12.14b shows the load cell design, made from a 17-4 PH stainless steel rod with slots milled at two sides, and the central slot section of the rod machined throughout (Fig. 12.14c). In order to achieve mechanical balance of the load cell, two resonators are mounted into the slots with one on each side (Fig. 12.14d) using epoxy-phenolic adhesive. Pinholes have been drilled at 90° to each other at the ends of the rod for applying the load.



Source:
 T. Yan et al.
 Eurosensors
 Rome, 2004

Fig. 12.14 a) Metallic triple-beam resonator (MTBR) mounted inside a load cell, which is presented in front view (b), as well as in longitudinal (c) and cross section (d)

The load cell was calibrated on an industrial calibration machine at Applied Weighing International Ltd. The load distributed to each resonator is calculated to be 3.75 kg (37 N), corresponding to 180 microstrain ($\mu\text{m}/\text{m}$) in the resonator beams and the load cell (instead of 2000 $\mu\text{m}/\text{m}$ for strain gauges). Here is the summary of the main load cell characteristics:

- Rated load 600 kg
- Load sensitivity 1.45 Hz/kg
- Nonlinearity 0.7 %
- Hysteresis 1.2 %
- Repeatability 0.1 %
- Stability (at 300 kg for 30 min) 0.05 % (percentages reported to full scale)

The resonant frequency of the resonator operating in air, measured in an open loop with a vector signal analyzer HP 89410A, is 6547 Hz, and the value of the Q -factor is 3100.

12.6.2. Torque transducers with metallic triple-beam resonators

A new torque transducer of the above-mentioned British school, with high overload capability and direct frequency output [12.44], employs the MTBR sensing devices with thick-film printed lead zirconate titanate (PZT) drive and pickup elements (Fig. 12.15).

The transducer has a sensitivity of 40 Hz/N·m in a torque range of up to 20 N·m, resulting in a strain level of 400 $\mu\text{m}/\text{m}$ on the measurement shaft surface and giving a large frequency-change output of 800 Hz.

The strain level required by the new torque transducer can be much lower ($\sim 100 \mu\text{m}/\text{m}$) than the level usually required by conventional metallic resistance-strain-gauge-based torque transducers, thus increasing the transducer overload capability by a large factor. Nevertheless, under such a low strain level, this tuning-fork torque transducer can still output an adequately large frequency change of 200 Hz for measurement. Having a large overload capability is very important in many torque measurement applications where rapid and large overloads can occur.

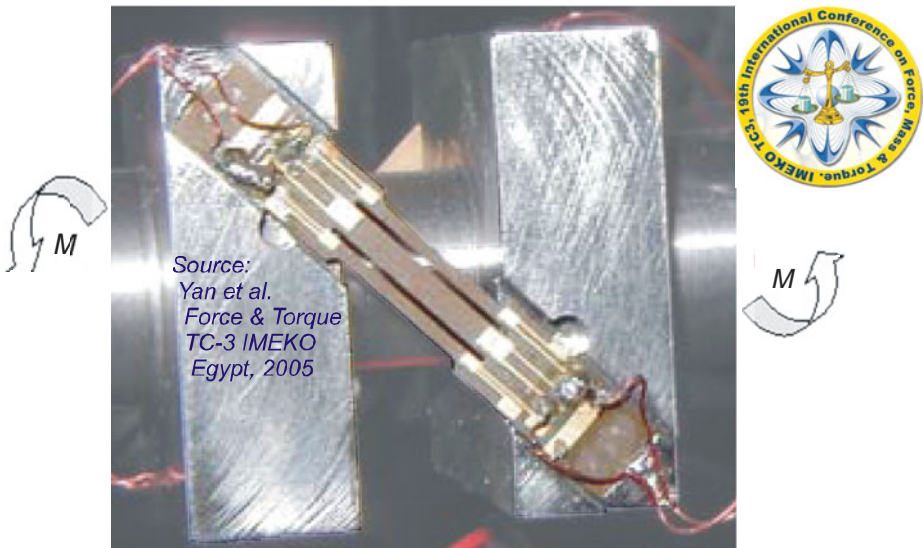
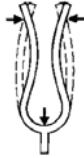


Fig. 12.15 Torque transducer with metallic triple-beam resonator achieved by a joint Brunel – Southampton Universities’ research team in the United Kingdom

Table 12.2 Vibrating elements for force, torque and other mechanical measurands

Chapter DMS	Denomination Typical sensing	Category	Associated quantities and phenomena
C.11	Vibrating wire	Electromagnetics	Thermophysical: viscosity, density
C.12	Microresonators DETF (tuning fork)	Electromagnetics	Vibrations
C.13	Surface acoustic wave Comb-shaped inter- digitated electrodes	Acoustics	Ultrasounds Acoustic emission Acousto-optics



As a conclusion, the resonator type force transducers are considered “vibrating elements” [12.45] together with vibrating wire transducers (previous Chapter) and surface-wave resonators (next Chapter). Table 12.2 suggests the “passage” from one dimension (wires) to tridimensional structures (spatial surfaces) for these vibrating force transducers and presents some specific differences and connections between various mechanical quantities.

REFERENCES

1. Usher, M.J., Keating, D.A.: *Sensors and Transducers – Characteristics, Applications, Instrumentation, Interfacing*, 2nd edn. MacMillan, Houndmills (1996)
2. Buser, R.A.: Resonant sensors. In: Bau, H.H., de Rooij, N.F., Kloeck, B. (eds.) *Mechanical Sensors*, vol. 7, pp. 205–284. VCH Weinheim, Germany (1994)
3. Büttgenbach, S., Fabula, T., Schmidt, B., Wagner, H.-J.: Resonant force and pressure microsensors. 7. Intern. Fachmesse mit Kongress für Sensoren, Meßaufnehmern und Systeme – Sensor 95, 27–32 (1995)
4. Zecchin, P. (Chair.): *Digital Load Cells – A Comparative Review of Performance and Application*. The Institute of Measurement and Control, London, Document WP0803 (2003)
5. Cheshmehdoost, A., Jones, B.E.: A new cylindrical structure load cell with integral resonators. In: *Proc. SENSORS VI: Technology, Systems and Applications*, pp. 429–434. IOP Publishing, Bristol (1993)
6. Fraden, J.: *Handbook of Modern Sensors – Physics, Design and Applications*, 3rd edn. Springer, New York (2004)
7. Werszko, M.: Force transducers with quartz resonator. In: Kemény, T., Havrilla, K. (eds.) *Force Measurement and Weighing in the 90s*, IMEKO TC Event Series, vol. 29, pp. 295–299. MTESZ Házinyomda, Budapest, 1104-91
8. Wang, Z., Zhu, H., Dong, Y., Wang, J., Feng, G.: Force-frequency coefficient of symmetrical incomplete circular quartz crystal resonator. *IEEE*, Los Alamitos (2001)

9. Blom, F.R.: Resonant silicon beam force sensor. PhD dissertation. Twente University of Enschede, The Netherlands (1989)
10. Tung, V.T., Chizhik, S.A.: Quartz tuning fork Atomic Force Microscopy using a quality-factor control. In: Source: Physics, Chemistry and applications of nanostructures reviews and short notes, pp. 535–538. World Scientific Publishing Co., Singapore (2009)
11. Barbic, M., Eliason, L., Ranshaw, J.: Femto-Newton force sensitivity quartz tuning fork sensor. *Sensors and Actuators A: Physical* 136(2), 564–566 (2007)
12. Castellanos-Gomez, A., Agraüt, N., Rubio-Bollinger, G.: Dynamics of quartz tuning fork force sensors used in scanning probe microscopy. *Nanotechnology* 20, Paper 215502 (2009)
13. Oprea, A., Henkel, K., Oehmgen, R., Appel, G., Schmeißer, D., Lauer, H., Hausmann, P.: Increased sensor sensitivities obtained by polymer-coated quartz microbalances. *Materials Science and Engineering C* 8-9, 509–512 (1999)
14. Mecea, V.M.: Loaded vibrating quartz sensors (Review paper). *Sensors and Actuators A: Physical* 40(1), 1–27 (1994)
15. Elwenspoek, M., Wiegerink, R.: *Mechanical Microsensors*. Springer, Heidelberg (2001)
16. Brückner, K., Cimalla, V., Niebelschütz, F., Stephan, R., Tonisch, K., Ambacher, O., Hein, M.A.: Strain- and pressure-dependent RF response of microelectromechanical resonators for sensing applications. *J. Micromech. Microeng.* 17(10), 2016–2023 (2007)
17. Abadal, G., Davis, Z.I., Borrísé, X., Boissen, A., Barniol, N., Pérez-Murano, F., Serra, F.: Atomic force microscope characterization of a resonating nanocantilever. *Ultramicroscopy* 97, 127–133 (2003)
18. Huang, X.M.H., Feng, X.L., Zorman, C.A., Mehregany, M., Roukes, M.L.: VHF, UHF, and microwave frequency nanomechanical resonators. *New Journal of Physics* 7(247) (2005)
19. Mile, E., Jourdan, G., Bargatin, I., Labarthe, S., Marcoux, C., Andreucci, P., Hentz, S., Kharrat, C., Colinet, E., Duraffourg, L.: In-plane nanoelectromechanical resonators based on silicon nanowire piezoresistive detection. *Nanotechnology*, 21(16), Paper 165504 (2010)
20. Huang, X.M.: Ultrahigh and microwave frequency nanomechanical systems, April 12 (2003), <http://resolver.caltech.edu/CaltechETD>
21. Busuttill, K.: Putting graphene in the balance. *materialstoday* 10(3), 15 (2007)
22. DiBiagio, E.: A case study of vibrating-wire sensors that have vibrated continuously for 27 years. Norwegian Geotechnical Institute, PDF (created on August 3, 2004)
23. A piezoelectric disk resonator as a diametrical force sensor. *Ekspierimentalne tehnike u fizici*, Universitas Studiorum Zagrabiensis, Croatia, June 30 (2009), http://www.phy.hr/~nnovosel/etuf/nastavni_materijali.php
24. Walter, B., Faucher, M., Algre, E., Legrand, B., Boisgard, R., Aime, J.-P., Buchaillot, L.: Design and operation of a silicon ring resonator for force sensing applications above 1 MHz. *J. Micromech. Microeng.* 19, Paper 115009 (2009)

25. Survey of quartz bulk resonator sensor technologies. IEEE Ultrasonics, Ferroelectrics and Frequency Control Society (June 2009), http://www.ieee-uffc.org/frequency_control/teaching...
26. Wearn Jr., R.B., Paros, J.M.: Measurements of dead weight tester performance using high resolution quartz crystal pressure transducers, Redmond, WA, June 27 (2009), <http://www.paroscientific.com>
27. Kirman, R.G.: A vibrating quartz force sensor. Transducer Temponcon Conference Papers, London, June 14-16, pp. 99-121 (1983)
28. Force Sensor. US Patent 5834646 (1998), European Patent EP 0737864 B1 (2000)
29. Lohkre, S.G., Virwani, K., Gajanan, B., Pai, S.P., Apte, P.R.: Study of vibrational modes of MEMS-resonators. In: Proceedings SPIE, vol. 3903, pp. 32-41 (1999)
30. Tilmans, H.A.C.: Micro-mechanical sensors using encapsulated built-in resonant strain gauges. PhD dissertation, Twente University of Enschede, Holland (1993)
31. Bao, M.-H.: Micro Mechanical Transducers: Pressure Sensors, Accelerometers and Gyroscopes. In: Regtien, P.P.L. (ed.) Handbook of Sensors and Actuators, 2nd edn. Elsevier, Amsterdam (2004)
32. Cuscó L. (Coord.): Guide to the Measurement of Pressure and Vacuum. The Institute of Measurement and Control, London, UK (Published 1998)
33. Muraoka, S.: Application of a quartz resonator to a force sensor built in a robot finger for use in grasp or recognition environment. Measurement 34, 229-244 (2003)
34. Woody, S.C., Smith, S.T.: Resonance-based vector touch sensors. Precision engineering 27(3), 221-233 (2003)
35. Felts, J.R., King, W.P.: Mechanical design for tailoring the resonance harmonics of an atomic force microscope cantilever during tip-surface contact. J. Micromech. Microeng. 19, Paper 115008 (2009)
36. Kobayashi, M.: New technology for measuring force and mass. In: Proc. 2nd Int'l Symp. Measurement of Force and Mass between Japan and China, May 23-24, pp. 79-84. Tsukuba Science City, Japan (1994)
37. Okazaki, M.: Development of the world's first precision tuning-fork force sensor. Companies from Ibaraki Prefecture, Japan, p. 44, PDF created on October 14 (2008)
38. Barthod, C., Teisseyre, Y., Géhin, C.I., Gautier, G.: Resonant force sensor using a PLL electronic. Sensors and Actuators A: Physical 104, 143-150 (2003)
39. Hayashi, T., Katase, Y., Ueda, K., Hoshino, T., Suzawa, H., Kobayashi, M.: Performance of force comparator with reference to tuning-fork type force transducer. In: IMEKO Int'l Conf. Cultivating Metrological Knowledge, Merida, Mexico, November 27-30, Paper 58 (2007)
40. Hopcroft, M.: High-stability silicon MEMS resonators. DARPA HERMIT Research Program (July 2009), <http://www.micromachine.stanford.edu/.../resonators.html>
41. Wang, K., Wong, A.C., Nguyen, C.T.C.: VHF free-free beam high-Q micro-mechanical resonators. Journal of Microelectromechanical Systems 9(3) (September 2000)

42. Fabula, T., Wagner, H.-J., Schmidt, B., Büttgenbach, S.: Triple-beam resonant silicon force sensor based on piezoelectric thin films. *Sensors and Actuators A: Physical* 41-42, 375–380 (1994)
43. Yan, T., Jones, B.E., Astrup, J., Rakowski, R.T., Tudor, M.J., Beeby, S.P., White, N.M.: Stiff load cell with high overload capability and direct frequency output. In: *Proc. 18th Conf. Solid-State Sensors (Eurosensors 2004)*, Rome, Italy, September 12-15 (2004)
44. Yan, T., Jones, B.E., Rakowski, R.T., Tudor, M.J., Beeby, S.P., White, N.M.: Stiff torque transducer with high overload capability and direct frequency output. In: *CD Proc. 19th IMEKO TC-3 Int'l Conf. Force, Mass & Torque Measurements: Theory and Application in Laboratories and Industries*, Paper 47, Cairo, Egypt, February 19-23 (2005)
45. Hunt, A. (Coord.): *Guide to the Measurement of Force*. The Institute of Measurement and Control, London (Published 1998); ISBN 0-904457-28-1

Chapter 13

ACOUSTIC FORCE TRANSDUCERS

An acoustic force transducer is a device in which an acoustic signal (sonic, ultrasonic, etc) is used as an intermediate quantity between its input (in this case, force) and output. There is a great variety of acoustic methods for the measurement of force and other related quantities, the primary one being the surface acoustic wave (SAW) method; others will be discussed together with industrial and medical applications. Alex Mamishev, University of Washington at Seattle, associates the acoustic sensing with the electromagnetic one [13.1].

For example, the piezoelectric interdigital transducers (IDTs), the most commonly used periodic electrode structures, are key components of the SAW devices (Fig. 13.1a).

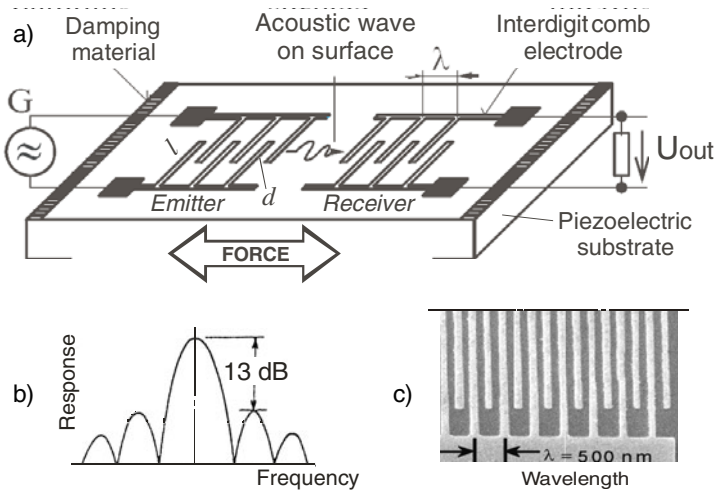


Fig. 13.1 SAW (surface acoustic wave) force transducer configuration (a): its frequency response curve (b) and a half-pattern of an IDT (interdigitated transducer) (c)

They contain a basic delay line configuration made by depositing two thin-metal IDTs as two interlocking comb-shaped on a polished piezoelectric plate (White and Voltmer, 1965).

The most important SAW property is associated with the confinement of acoustic energy near the surface of a solid. The attenuation (typically 1.5 dB for 10^4 wavelengths) is much smaller than that for em waves of the same frequency. For the simplest version, when the comb finger lengths are equal and the finger spacing is uniform, the frequency response is a $\sin x/x$ curve (Fig. 13.1b), with the primary side lobes 13 dB below the main peak.

SAWs have extremely low velocity, about 10^5 times that of electromagnetic waves, therefore resulting very small wavelengths and dramatic size reductions under the motto “*From microwaves to ultrasounds (and return)!*”

Fig. 13.1c depicts such a miniaturized IDT pattern. By contacting carbon nanotubes with metal leads, zero-dimensional systems with large charging energies can be defined. If a surface acoustic wave is applied, results in a quantized current transport [13.2]. Both mechanical and electrical SAW potential change the properties of the nanostructures. Additional gates and/or local doping allow the creation of a pn-junction and there the SAW mediated single charge transport leads to the emission of single photons.

13.1. INTERDIGITAL TRANSDUCERS (IDTs)

The paper [13.1] attempts to bring together and compare the inductive, capacitive, dielectric, piezoacoustic, chemical, biological, and microelectro-mechanical interdigitated (in the fashion of a zipper) sensors and transducers (e.g. SAWs).

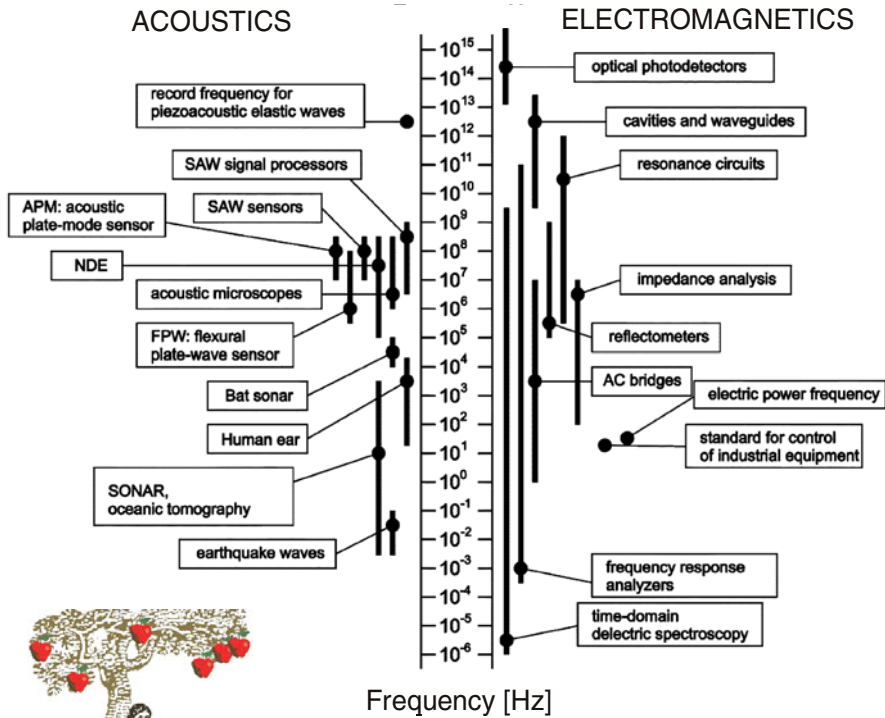
Figure 13.2 shows a “frequency scale”, gathering together most of the previously presented measurement principles for force transducers:

- parametrical – R , L and C constitutive parts of the impedance,
- piezoelectric – mainly in dynamic regime and actuators,
- electromagnetic (electrodynamical, magnetoelastic and galvanomagnetic),
- resonators (vibrating wire and tuning fork) and acoustical ones.

The term “interdigital” applied to acoustic and em transducers signifies a special technique of implementation rather than a distinct measuring principle.

The most common reason for making an interdigital electrode structure is to increase the effective length, and, therefore, the capacitance C between the electrodes. The major advantage of using electrostatic forces as opposed to magnetic forces is that a very high energy density can be achieved when the distance between the adjacent electrodes becomes small.

The longitudinal electrostatic force along the X axis (Fig. 13.3) in a comb drive is generated due to fringing fields at the ends of IDT electrodes [13.3]:



...frequency of apple falling?...

Source: Mamishev et al.
University of Washington,
Seattle, USA

Reprinted with permission IEEE, copyright 2004

Fig. 13.2 Frequency spectrum for acoustic and electromagnetic interdigital transducers

$$F = \frac{1}{2} V^2 \cdot \frac{dC}{dx} = \frac{V^2 \cdot \epsilon_0 \cdot n_e \cdot b}{w} \tag{13.1}$$

where F is the force developed by the finger interaction when applying voltage V , ϵ_0 is the vacuum permittivity, n_e – number of electrode fingers, b – electrode height, and w – gap between the electrodes.

This force is independent of the finger length and becomes especially significant at sub- and micrometer scales.

A specific invention [13.4] relates to an electroacoustic transducer, particularly an ultrasonic one, comprising a plurality of electrostatic microcells of the cMUT (capacitive micromachined ultrasonic transducer) type.

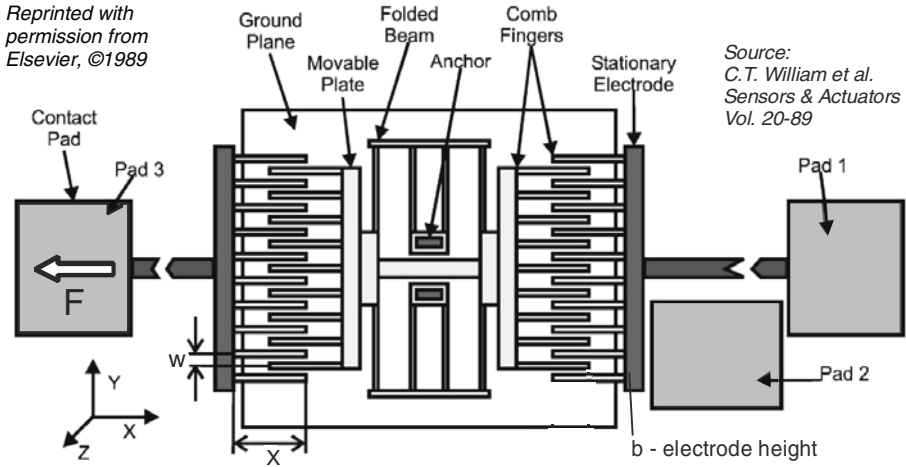


Fig. 13.3 Layout of a linear resonant plate force transducer based on axially loaded IDT electrodes. The original symbols (b and w) differ from the usual ones (h and d).

The electrostatic microcells are arranged in homogeneous groups with the same geometrical characteristics but their geometry is different in other groups. In the micromachined directional microphone [13.5] the capacitive couplings between the diaphragm and the backplates remain to play the role of voltage-to-force transducers through which feedback control voltages could be applied to possibly damp out the resonance peak of the rocking mode.

The IDT transducers are multifunctional, combining several measuring principles (capacitive, resonant or acoustic) and being applicable for the measurement of a wide range of mechanical quantities [13.6]. IDTs are primarily used to convert microwaves to surface acoustic waves, while the term “interdigital” has not the sense of “measuring force between human fingers”!

Besides SAWs, which belong to IDTs and to acoustic transducers as well, other acoustic measurement methods suitable for force transducers will also be presented: acoustic emission and wave guide, ultrasonic and acoustic radiation.

13.2. ACOUSTIC EMISSION AND WAVEGUIDES

13.2.1. Acoustic emission applications

In order to optimize the durability of the head/disc interface, it is necessary to minimize the contact force. Acoustic emission (AE) signals were utilized to investigate the contact force between the head and the disc of a computer hard drive [13.7]. The AE transducer was directly calibrated using the “ball drop method” and indirectly by system identification, utilizing a high bandwidth laser Doppler vibrometer (LDV).

The transfer function of the system is determined from the known input force and the measured AE output signal. So, any unknown input force can be obtained from this transfer function and the measured output signal “produced” by acoustic emission. Contact forces in the range of (5...25) mN were found for nano sliders and (2...10) mN for pico sliders.

A research team from AIST, Tsukuba, Japan uses a multi-functional composite of SMA (shape memory alloy) as both sensor and actuator for constructing intelligent materials with sensing and suppressing functions [13.8]. The acoustic emission signals induced by phase transformation were used to measure the amount of strain associated with different deformed locations.

As a result of acoustic emission, the noisy measurement data of the machine tool vibrations compromise the calibration accuracy of empirical cutting force models. A reliable calibration of a ball-end milling force model from noisy cutting force data is presented in [13.9].

13.2.2. Acoustic waveguides applications

Figure 13.4a shows the construction principle of a parallel-plate acoustic waveguide multifunctional transducer [13.10].

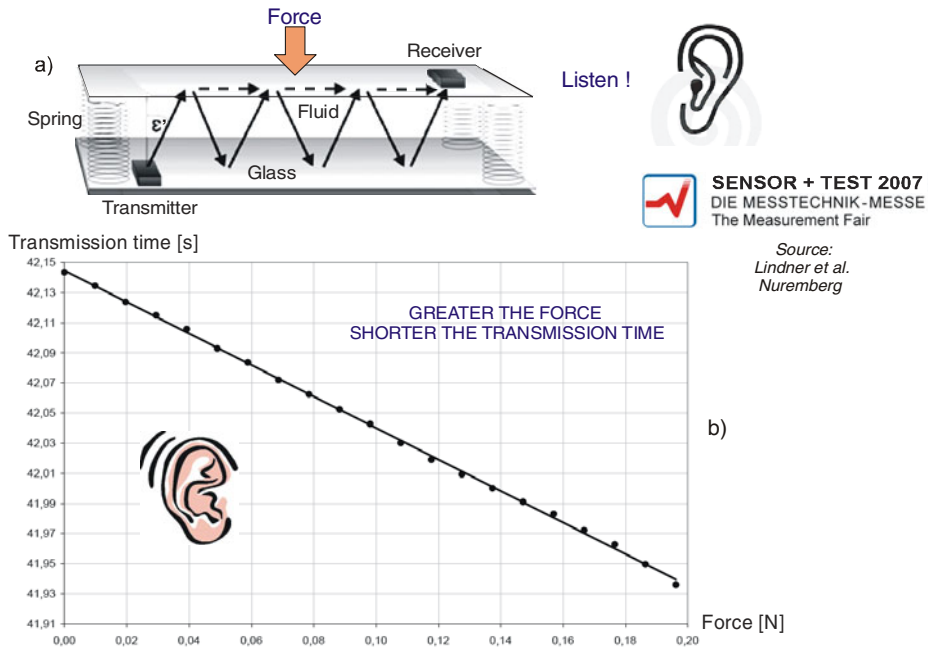


Fig. 13.4 Parallel plate acoustic waveguide force transducer with digital output (a) and associated force vs. slight variation of transmission time diagram (b)

SENSOR + TEST 2007
DIE MESSTECHNIK-MESSE
The Measurement Fair

Source:
Lindner et al.
Nuremberg

The traveling time of the transmission wave depends on the two glass plates arrangement (particularly on their distance) and on the radiation angle ε' . Since the time constants of the piezoceramic interdigital transducers are rather small and the transmission wave is radiated off from the substrates as a sharp beam, the different receiver signals from a single exciting burst and transmitted through fluid or glass are well separated in time. Thus, distance can be determined by measuring zero-crossings of the receiver signal near the maximum of its envelope.

For example, a force acting on the plates produces a deformation of the springs causing a corresponding time shift of the receiver signal. *Greater the force applied, shorter the distance between the plates, and, implicitly, shorter the measured transmission time*, displaying a near linear diagram (Fig. 13.4b)!

A first proof of this concept was achieved with elastic spacers made from rubber and gravitational force acting on the upper plate. It turned out that sub-newton forces down to 0.01 N could easily be detected with this set-up; the sensitivity was in the order of 1 s/N. Since a force of 1 N caused a deformation of about 2 mm with such spacers, the dynamic range of such an acoustic device may cover the range between 0.01 N to 10 N.

13.3. ULTRASOUND FORCE TRANSDUCERS

13.3.1. Industrial applications of ultrasound force transducers

An instrument for measuring clamping force of bolt connections, made by Hagiwara Electric [13.11], operates on the principle of ultrasonic wave transmission (Fig. 13.5). Tightening a bolt or turning a nut on induces a tensile stress in the bolt, causing an elongation. An ultrasonic wave, introduced at the bolt head by a probe, travels through the bolt and reaches the other end of the bolt where the wave is reflected back toward the head end.

The speeds of wave transmission decrease with increasing stresses and the elongation of the bolt lengthens the echo time intervals between introduction of the incident wave and reception of the returning wave. The instrument uses the combined effect of these two characteristics of ultrasonic wave transmission. The amount of initial tension σ (the stress induced by the tightening operation) is given by:

$$\sigma = K_U \cdot (T_p - T_o) \quad (13.2)$$

where K_U is a constant whose value is determined by the dimensions of the bolt to be tested.

Prior to the testing operation, the value K_U is determined and stored in the memory of the unit by entry of dimensional data for a given bolt.

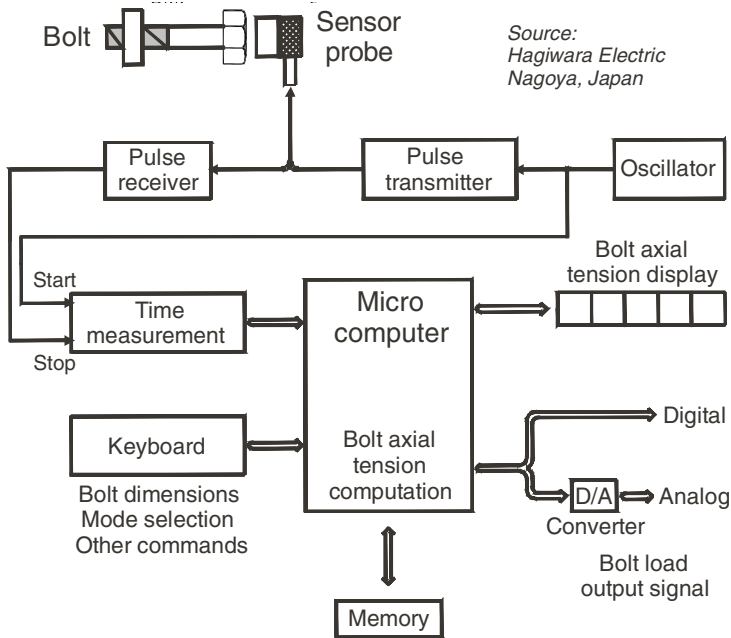


Fig. 13.5 Ultrasonic bolt clamping force meter

Before the bolt is tightened, the sensor probe is applied to the head end of the bolt to measure the time T_o and, after it has been tightened, the probe is again applied in the same way as before to measure the time T_p . The built-in microcomputer is programmed to give the σ value according to Eq. (13.2) and the digital display shows the result of computation, giving a direct reading of the bolt-load.

The advantage of this instrument is that it can measure the clamping force without loosening bolt connections or using measured or calculated values of the torque needed when tightening. The bolt connection remains “unchanged” during this measurement.

A method and apparatus for acoustically removing a frozen bolt from a metal structure having a bolt hole formed therein is presented in [13.12]: An acoustic transducer is removably mounted to the head of the bolt (...) and excites the bolt at that frequency specific resonance and predetermined amplitude, thereby loosening the bolt from the bolt hole.

Usually the contact force is measured by inserting a strain gauged elastic element into the tested structure, which may cause a difference in contact conditions. The ultrasonic technique facilitates the measuring of metal-metal contact interfacial pressure without any change in the contact region [13.13].

The relation between the intensity (acoustic pressure) of reflected wave P_r and incident wave P_i is given by the reflection ratio of acoustic pressure:

$$R_a = \frac{P_r}{P_i} = \frac{Z_B - Z_A}{Z_B + Z_A} \tag{13.3}$$

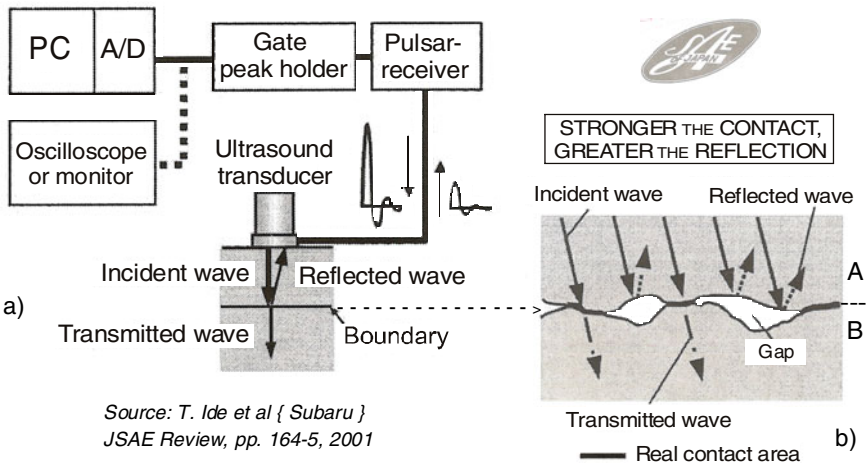
where Z_A and Z_B are the acoustic impedances of elastic bodies A and B, expressed by the product of the sound velocity c and the material density ρ .

There are two “extreme” situations:

- all the incident wave is transmitted, when the two bodies are made of steel ($Z_A = Z_B$) and $R_a = 0$;
- almost all the incident wave is reflected, if the material B is air, Z_B is negligibly small when compared with Z_A and R_a becomes nearly 1.

In the actual case (Fig. 13.6b), there are many microscopic gaps between the two bodies because of surface roughness and the two materials contact only in the real contact area. If the two materials have the same acoustic impedance, all the incident waves will go through the boundary, while only a part of waves will be reflected. Thus the macroscopic reflection ratio R_a is proportional to the ratio of the real contact area to the apparent one. Through an appropriate calibration, the contact force can be estimated by the reflection ratio under the rule: *Stronger the contact force, greater the reflection of acoustic waves!*

Fig. 13.6a depicts the measurement system schematic. The main part of the transducer is a piezoelement, embedded in a thin cylindrical metal case (diameter 6 mm) and attached on the material.



Source: T. Ide et al { Subaru }
 JSAE Review, pp. 164-5, 2001

Fig. 13.6 Contact force measurement by ultrasonic waves (a), contact region zoom (b)

When this piezoelement receives a high voltage pulse from the pulsar-receiver, it expands momentarily by a slight amount, giving an impact to the material surface. An ultrasonic plane wave with a frequency of 5 MHz is generated and propagates into the material; when it reaches the boundary, part of it is reflected as an echo, giving an impact to the piezoelement and a voltage pulse is generated in the transducer, which is sent back to the pulsar-receiver.

The pulsar-receiver consists of a high-speed pulse generator and a high gain amplifier with a dynamic range of over 100 MHz. The generated pulse has a rising time of 5 ns (90 %), width of 18 ns and a peak voltage of 88 V. The pulsation frequency is 1 kHz. The return voltage pulse from the transducer is amplified by the pulsar-receiver and sent to the peak holder, which outputs the peak value of the reflected pulse. Echo is generated many times but a gate is applied to catch only the first echo. The peak holder output, which is renewed at each pulse reception, is stored in a PC through an A/D converter.

Other application is a high power ultrasonic hammer, consisting of a front and a rear mass and two piezoelectric drivers on either side of a center mass, which mainly determines the resonance [13.14]. This special force transducer, ensuring possibilities to manipulate its mechanical coupling and electrical connections, is suitable for driving great mass loads such as the pipes contents.

13.3.2. Ultrasound force transducers for food and pharmacology

One of the most important quality indicators for fruits is their firmness, highly correlated with their elastic modulus. According to the traditional destructive method, a cylindrical rod of the penetrometer is pushed into the apple while measuring the penetrating force. A new measuring system [13.15] uses a pair of ultrasonic transducers to transmit and receive the ultrasonic wave; they have a diameter of 40 mm and a central frequency of 100 kHz. To match the acoustic impedances, transducers with curved wear plates for direct contact to the apple surface and vacuum grease are used. High power and low frequency ultrasonic pulser-receiver Pundit 6 (CNS Farnell Inc., US) generates the ultrasonic waves. The through-transmission mode is selected, the first transducer acting as transmitter, the second as receiver, both being connected to a digital storage oscilloscope (WaveRunner, LeCroy Co, US).

Apple firmness is measured using a compression test apparatus. A multiple linear regression model describes the relationships between firmness and ultrasonic parameters (wave velocity, attenuation and peak frequency). The correlation coefficients between elastic modulus and ultrasonic wave velocity or attenuation coefficient are 0.976 and 0.930, respectively. The elastic modulus decreases while the attenuation coefficient increases with storage time of apples. Using this nondestructive test (NDT) for apples makes possible to assess their maturity and to estimate their shelf life.

Digital sonomicrometry is very useful to evaluate different anaesthetics [13.16]. Two miniature piezoelectric crystals were implanted externally on the stomach fundus of an anaesthetized guinea pig (to measure “real-time” gastrointestinal contractility) or on the oesophagus of a Sprague–Dawley rat (to measure esophageal relaxation). *In vivo* measurement of the transmission time for ultrasonic pulses between the implanted crystals provided a continuous recording of inter-crystal distance and hence the muscle length variation.

13.3.3. Medical applications of ultrasound force transducers

Although electrocardiomyography (EMG), magnetic resonance, optical tomography and birefringence have all been used to image skeletal muscle during contraction, these techniques lack either spatial or temporal resolution to fully characterize dynamics inside the muscle. A real-time HF ultrasound acquisition system was used to describe coordination of individual muscle fibers during an isometric contraction [13.17]. Effects of contraction size and muscle fatigue on axial strain and strain rate were examined in isolated leg muscles. A single-element 10 MHz ceramic ultrasound transducer (Panametrics® V311, $f\# = 1.5$, focal length = 38 mm, spherically focused) was used to image the rat EDL (extensor digitorum longus). One end of the isolated muscle was fixed to a metal rod and the other (with intact tendon) to a force transducer lever, which measured the strength of each muscle contraction (Fig. 13.7a).

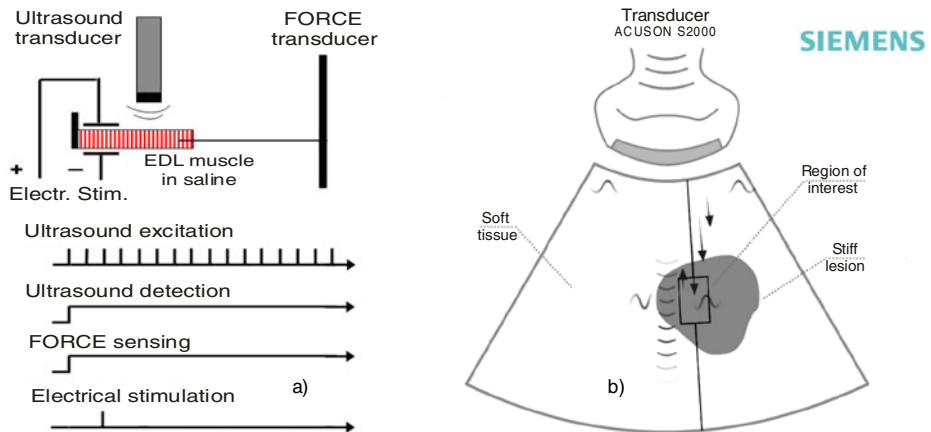


Fig. 13.7 a) Ultrasound imaging apparatus for muscle contraction and timing diagrams. b) Virtual touch tissue quantification utilizes an acoustic push pulse (like a half-circle) to generate shear waves (horizontal S-shaped) through a user-placed region of interest. When detection pulses (the arrows) interact with a passing shear wave, they reveal the wave’s location at a specific time, allowing calculation of the shear wave speed. This numerical value is related to the stiffness of the tissue within the region of interest.

Strain was estimated with a phase-sensitive speckle-tracking algorithm, capable of detecting displacements less than 100 nm. The spatial distribution of axial strain was not uniform and ranged from 0.5 to 5 % during twitch stimulation. Also, strain and strain rate paralleled contraction size and degree of muscle fatigue. Ultrasound has also been used to measure changes in length and degree of pennation of muscle fibers as a measure of force at low frame rate (< 100 Hz). This potentially noninvasive technique may be appropriate to assess severity of movement disorders, such as cerebral palsy, and track coordination during therapy and rehabilitation after muscle injury.

An ultrasonographic probe has been developed for earlier detection by noninvasive diagnosis of periodontal disease activity [13.18]. In order to evaluate its clinical effectiveness, a comparison study of this ultrasonographic probe to both a standard manual and a controlled-force probe was conducted.

A one-way analysis of variance was performed to compare the results for the three sets of probing depth measurements, followed by repeated measures analysis to assess the reproducibility of the different probing techniques. Future studies will complete the development of more effective automated feature recognition algorithms that convert the ultrasonographic echoes into pocket depth readings as Gingival Index scores.

13.4. ACOUSTIC RADIATION FORCE TRANSDUCERS

13.4.1. Acoustic radiation force transducers in medicine

Acoustic Radiation Force Impulse (ARFI) imaging is a method for characterizing local variations in tissue mechanical properties using a single ultrasonic transducer array to both apply temporally short localized radiation forces within tissue and to track the resulting displacements through time [13.19]. Nightingale *et al.*, Dept. of Biomedical Engineering, Duke University, Durham, NC show how images of tissue displacement immediately after force cessation, maximum tissue displacement, the time it takes for the tissue to reach its maximum displacement, and the recovery velocity of the tissue are generated from the ARFI datasets [13.20]. In soft tissues the following equation can be used to determine the radiation force magnitude:

$$F = \frac{W_{abs}}{c} = \frac{2\alpha \cdot I_t}{c} \quad (13.4)$$

where: F [$\text{kg}/(\text{s}\cdot\text{cm})^2$] is acoustic radiation force, W_{abs} [$\text{w}/(100 \text{ cm})^3$] – power absorbed by the medium at a given spatial location, c [m/s] – sound speed of the medium, α [m^{-1}] – absorption coefficient of the medium and I_t [w/cm^2] – *in situ* temporal average intensity at a given spatial location.

For tissues with relatively low attenuation (0.3...0.5) dB/cm/MHz, or, when relatively low frequencies (1...3 MHz) and low f -numbers (1...2) are utilized for radiation force excitation, the majority of the energy is absorbed within the focal region of the acoustic beam ($\sim 10 \text{ mm}^3$), which approaches a spatial impulse-like excitation volume.

f -number is defined as the ratio of the focal length of a lens to the effective diameter of its aperture.

For tissues with higher attenuations (0.7...1.5 dB/cm/MHz), or when higher frequencies (7...10 MHz) or higher f -number (3...5) focal configurations are utilized, the excitation energy is typically distributed throughout the geometric shadow of the active transmit aperture, and the excitation volume is larger, having a more complex spatial distribution ($\sim 200 \text{ mm}^3$).

Acoustic Radiation Force Impulse imaging is implemented on a modified diagnostic ultrasound scanner, using the same transducer for both the excitation and monitoring the tissue response both spatially and temporally. ARFI images are generated of the tissue displacement magnitude within the region of excitation at a given time after radiation force application. They demonstrate an improved contrast over conventional ultrasound displays.

For example, SIEMENS ACUSON™ ultrasound systems feature a comprehensive range of tissue strain analytic applications that enable qualitative visual or quantitative value measurements of the mechanical stiffness or elastic properties of tissue (Fig. 13.7b). This new dimension of diagnostic information is not available using conventional sonographic imaging (with classical echographs), and represents the most important development in ultrasound technology since the advent of Doppler imaging [13.21].

ARFI imaging, based on brief, high-intensity, focused ultrasound pulses to generate radiation force in tissues, has many clinical applications to detect abnormalities inside the breast [13.22], liver, prostate and colorectal imaging [13.23]. Ultrasound transducers are also used to measure the wave velocity in arterial walls [13.24]. A sinusoidally modulated force with a high frequency is noninvasively generated on the arterial wall by the radiation force and the resulting vibration in the artery is measured by ultrasound Doppler transceiver.

13.4.2. Acoustic radiation force transducers in metrology

The radiation force balance is a gravimetric balance, which means that the ultrasonic beam orientation is vertical (Fig. 13.8). The interaction between the beam and the target is mainly due to the reflection phenomenon. It is a stainless steel cone-shaped target connected to an analytical balance by means of an appropriate structure. The ultrasonic beam is directed downwards on the reflecting target (45° half angle and 2.5 cm of radius) and the radiation force exerted by the ultrasonic beam is measured by the balance in mass units and

converted to force units using the appropriate acceleration value due to gravity. INMETRO Brazil setup uses a microbalance model CP224-S (Sartorius), with 0.1 mg of readability and 220 g maximum load capacity [13.25].

For perfect reflecting targets, the ultrasonic output power P is given by:

$$P = \frac{c \cdot F}{2 \cos^2 \theta} \quad (13.5)$$

where c is the sound velocity in water (1491 m/s at 23 °C), F – radiation force and θ – angle between an incident wave and the normal to the reflecting surface.

The ultrasonic power is determined from the difference between the force measured with and without ultrasonic radiation.

The UK National Physical Laboratory developed a range of high quality Secondary Standard Radiation Force Balances (RFBs) for use by manufacturers of ultrasound equipment and by measurement laboratories [13.26]. Medical diagnostic and physiotherapy ultrasound equipment operates in the frequency range (1...10) MHz and power (calibration) range from 20 mW to 10 W, with type A (random) measurement uncertainties: the greater of 1 mW or 1 %.

For example, direct radiation force (DRF) and acoustic streaming provide the main influences on the behavior of particles in aqueous suspension in an ultrasound standing wave (USW). DRF, which drives suspended particles towards and concentrates them in acoustic pressure node planes, has been applied to rapidly transfer cells in small scale analytical separators. Capture of biotinylated particles and spores on a coated acoustic reflector in a quarter wavelength USW resonator was DRF-enhanced by 70- and 100-fold, respectively compared to the situation in the absence of ultrasound.

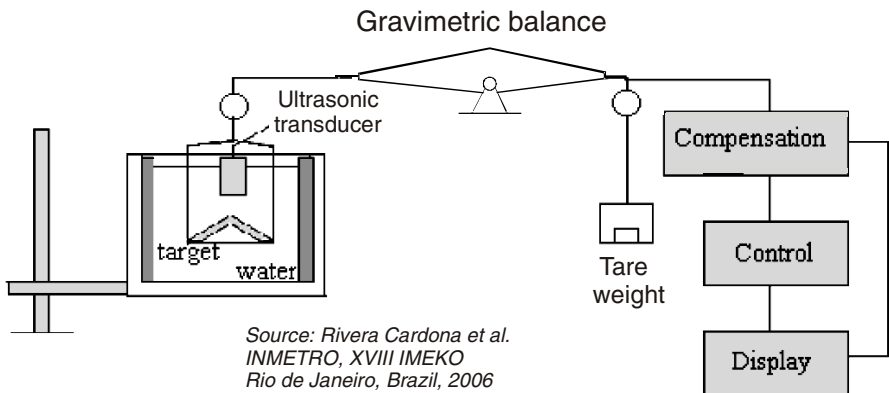


Fig. 13.8 Ultrasonic power measurement in liquids (Standard IEC 61.161)

In order to undertake irradiation of polymer blocks or films by ultrasound, Hallez *et al.* [13.27] deal with the measurements of ultrasonic power and its distribution within the cell by several methods. The electric power measured at the transducer input is compared to the ultrasonic power input to the cell evaluated by calorimetry and radiation force measurement for different generator settings. Valuable results were obtained using new transducer types (based on focused composites, i.e. HIFU: high intensity focused ultrasound) observing that measurement of radiation pressure for power evaluation is more adapted to low powers (< 15 W) and that calorimetry is a valid technique for global energy measurements. The ultrasonic intensity distribution is qualitatively depicted by sono-chemi-luminescence of luminol. Finally, the quantity of energy absorbed by samples placed in the sound field is determined and the temperature distribution monitored as a function of wall distance. This energetic balance allows understanding the global behavior of all experimental set-ups made up of a generator, transducer, liquid and sample.

13.5. SURFACE ACOUSTIC WAVE (SAW) TRANSDUCERS

SAW devices (Fig. 13.9a) are based on a theory propounded by Lord Rayleigh in his work "*On waves propagated along the plane surface of an elastic solid*" [Proc. London Math. Soc., **7**, pp. 4–11, 1885]. Surface acoustic (or Rayleigh) waves are elastic displacements propagating nondispersively (i.e. with velocity independent of frequency), in the microwave range (megahertz to gigahertz) at the stress-free boundary of a solid, with the amplitude decaying exponentially in the bulk with increasing distance from the surface [13.28]. Commonly used materials for commercial SAW devices are LiNbO_3 , LiTaO_3 and ST-cut quartz (SiO_2) as single crystals, UV curable semiconductive polymers, PVDF and ZnO in the form of thin film deposited by sputtering.

A SAW transducer is a device which converts electrical signals into surface acoustic waves and *vice versa*. The simplest type of transducer consists of a piezoelectric film or substrate with an alternate phase array of electrodes (also called interdigital comb), as shown in Figure 13.1a. To generate a SAW in an interdigital transducer (IDT), an alternating voltage is applied between the adjacent sets of fingers, which are separated by a distance d equal to half SAW wavelength (λ) at the design frequency. Increasing the number of finger pairs increases the efficiency of the transducer to a certain extent, at the cost of an accompanying decrease in the bandwidth, so that an optimum number of electrode finger pairs is required to obtain a maximum efficiency-bandwidth product. This is determined by the phase velocity of the SAW, which depends on the properties of the piezoelectric material and its orientation and thickness (in the case of thin films).

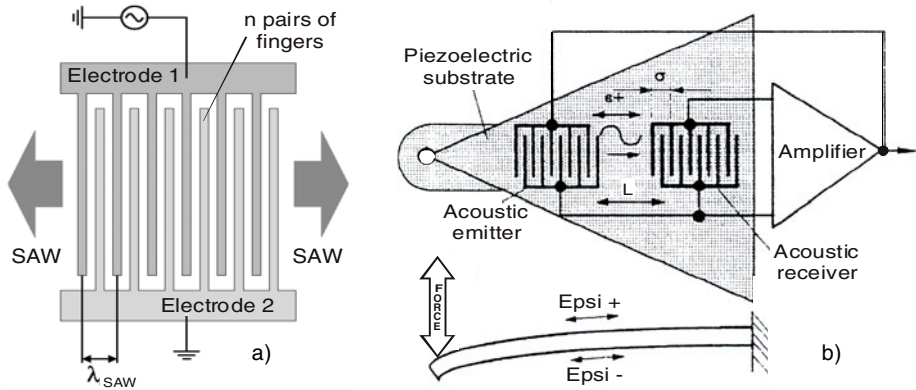


Fig. 13.9 Typical SAW device configuration (a) and resonator force transducer with a pair of IDTs on a bidirectionally bent cantilever (b)

The electrode dimensions, that is, the active length l of the fingers (the amount adjacent fingers overlap) and the periodic spacing d between them, determine the frequency response of the transducer.

SAW devices enable non-contacting strain measurement, being suitable for force, torque, pressure and other quantities measurement.

13.5.1. SAW force transducers

In the surface-wave resonator force transducer, an ultrasonic transmitter which is actuated by alternating voltage and consists of comb-shaped electrodes on a quartz substrate, emits surface acoustic waves directed according to the inverse piezoelectric effect [13.29]. A second system, arranged in the same way, converts these sound waves back into an alternating voltage, according to the piezoelectric effect. The amplifier is so arranged that the system vibrates on its natural frequency. The deformation of an elastic element, which depends on the applied force, changes the resonator frequency.

Figure 13.9b presents a resonator force transducer with SAW devices. One can obtain, using comb-like structured electrodes deposited on the piezoelectric substrate, mechanical vibrations which propagate as sound waves.

Applying simultaneously a pair of electrodes on either superior or inferior surface of a beam subjected to bending, one can measure the bending force, the frequency of the surface oscillations depending on the length of the beam. The signal generated by an acoustic transmitter is transmitted to an acoustic receiver (positioned at distance L from the transmitter) and then further transmitted to a stable-phased amplifier. Through a feedback reaction, a free oscillation is produced, whose resonance frequency depends on the surface strain, thus being proportional to the force that caused it.

13.5.2. SAW torque transducers

SAW torque transducer technology, like the piezoresistive and magnetoelastic ones, utilizes the principal tensile and compressive strains, which act at $\pm 45^\circ$ to the axis, on the surface of a shaft in torsion, for real-time torque measurement that can provide feedback for closed-loop control.

Typically, two SAW devices are used in one torque transducer and a differential measurement of resonant frequency (nominal value: 433 MHz) is performed in order to achieve temperature compensation and eliminate sensitivity to shaft bending [13.30].

Honeywell International Inc. (Morristown, NJ, US) designed a patented elastic structure in order to concentrate the mechanical strain into an etched diaphragm, thereby providing high strength, high sensitivity and ease of manufacturing thereof [13.31]. The annealed stainless steel casing, including the SAWs flat sensing device (Fig. 13.10a), has openings for the two connector pins that are hermetically sealed by glass fritting inside an oven [13.32].

The TorqSense classical solution, presented in Figure 13.10b, uses two SAW devices mounted directly on the shaft [13.33]. The two transducers are positioned at $\pm 45^\circ$ on the shaft, each forming part of an oscillator feedback loop, such that the output frequency is a function of the SAW geometry [13.34]. The two SAWs are connected in a half-bridge configuration, one being tensioned while the other is compressed. As a consequence of this differential measurement, the resulting frequencies are added or subtracted: their difference gives a torque measure while their sum can be used for temperature estimation. At a frequency of 500 MHz, a torsion moment of 1000 microstrains will alter the SAW frequency by 500 kHz.

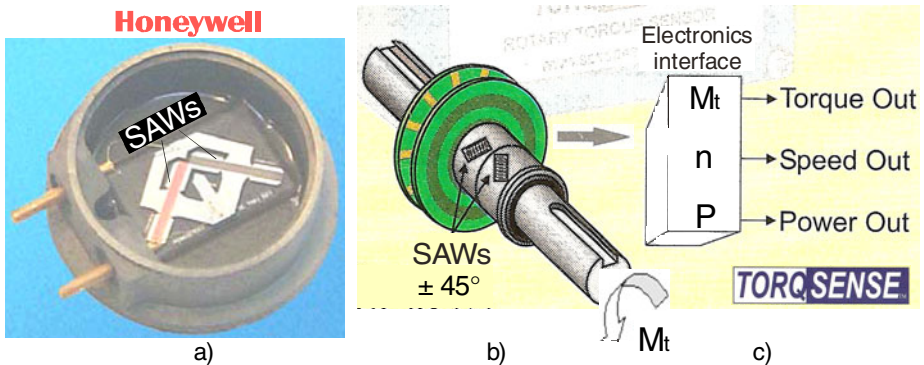


Fig. 13.10 Two variants of “double SAW” torque transducers: plane (a) and cylindrical (b) – courtesy of Honeywell Inc. and Sensor Technology Ltd. c) Electronic interface outputs for torque – M_t , rotational frequency – n and their product (power – P).

13.5.3. SAW pressure transducers

SAW devices are sensitive to mechanical and electrical properties occurring on their surface [13.35]. They are detecting mass loading and viscoelastic changes like stiffening and softening but also any property that interacts with the electrical field that is coupled to the propagating acoustic wave, namely electro-acoustic interactions. Cullen (1975) was the first reporting a SAW resonator use on a circular diaphragm [13.36]. SAWs are sensitive to stress or strain coupled into their substrate through the packaging too. Because of this, they make great platforms for pressure sensing applications (Fig. 13.11a).

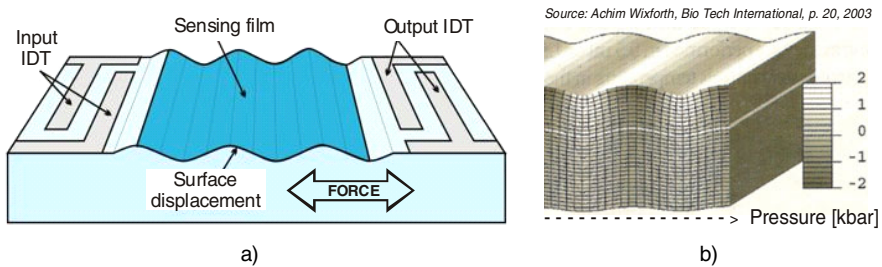


Fig. 13.11 Two-port SAW pressure platform under a nano-“earthquake” (a) and schematic picture of SAW propagation like marine waves (b)

Figure 13.11b shows a schematic representation of SAW propagation along a piezoelectric substrate, characterized by alternating regions of compressed and expanded material, as indicated in grayscale [13.37]. With wavelengths of only a few microns and amplitudes of nanometers, the applied forces and the electric fields are sufficient for a macroscopic effect.

A SAW-based element, implemented as a delay circuit on an AT-cut quartz crystal without sensitive coating, can be used as a pseudo-binary gas mixture composition analyzer due to its pressure sensitivity [13.38]. Therefore, a new express method for measuring physical parameters such as averaged molecular weight, density, and viscosity of binary gas mixtures (methane/air or propane/air) is actually available. A new type of sensing element for pressure gauges is the SAW-based dispersion strain gauging resonator with non-equidistant transducer, with tenfold improvement of its accuracy [13.39].

13.5.4. SAW fluidic transducers

A simplistic selectable SAW reflector array using fluidic channel control switches by interrogation signals [13.40] is presented in Figure 13.12a.

The next step towards microfluidic SAW application is to create “flatland” networks [13.37].

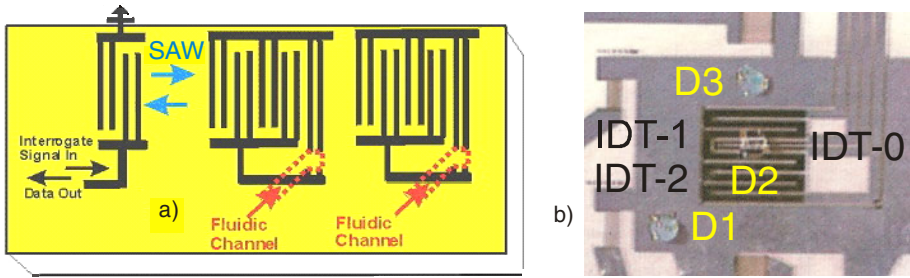


Fig. 13.12 a) A different 3D SAW device representation. b) A 2D SAW driven microfluidic processor with three droplets D1, D2, D3 (approx. 100 nl each) moved by nano-pumps, independently and by remote control, producing “nanochemical reactions” when are merged and mixed by the surface wave.

Crossing the border from the world of “macro” dimensions to that of the “micro” world, and also from 3D to 2D, produces an important effect namely that usually negligible physical phenomena become dominant, e.g. surface tension versus gravity.

Prototypic fluidic devices have already been constructed in which several droplets are moved using the SAW agitation phenomenon (Fig. 13.12b). The interdigital transducers IDT-1 and IDT-2 are driven 90° out of phase using a single generator IDT-0 with a $\lambda/4$ transmission line connecting them. Moreover, the simplicity of the fabrication process of such programmable bioprocessors makes them serious candidates for miniaturized laboratories on a chip.

13.6. SAW ELECTRONIC CIRCUITS

Piezoelectric SAW transducers utilize an oscillatory electric field to generate an acoustic wave that propagates on the substrate surface, then transforms back to an electric field for measurement.

A centrally placed interdigital transducer (IDT) converts the pulsed electrical input signal from the interrogator to a mechanical wave through the piezoelectric effect. These waves propagate from the resonator to the reflectors and back. This propagation continues to build energy until a resonance exists as a standing wave. The wavelength is roughly double the IDT spacing $\{\lambda = 2d\}$.

The resonant frequency is a function of strain in the interdigital transducer, in the direction of the single port resonator axis. Once the input signal stops, the IDT absorbs the acoustic energy and transmits the new frequency back to the receiver in the interrogation system. SAW transducer interrogation involves the measurement of frequency difference shifts between active and reference SAW devices to provide common mode rejection (CMR).

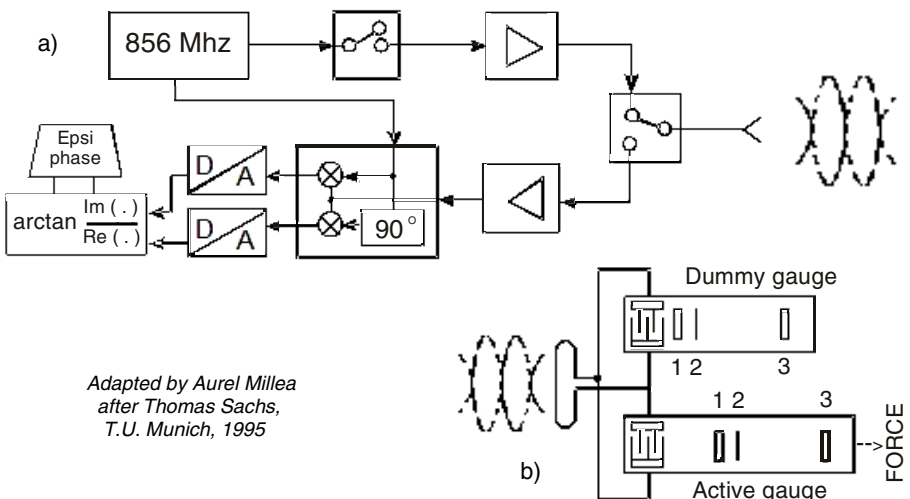
Coherent accumulation and averaging improves signal-to-noise ratio, while the measurement algorithm and monitoring of statistical variances promotes valid data. Such a measuring system uses patent protected methodology for sensing and reading / interrogation.

A new kind of strain transducer based on a SAW-device is presented in [13.41]. The measurement system (Fig. 13.13a) works in the MHz-range, so that it is possible to run by wireless transmission at about a distance of a few meters. The principle of “radar” signal processing is described as follows: some periods of a sine-wave are sent out every 10 μ s for a duration of approximately 100 ns.

The receiving device (Fig. 13.13b) is a delay line in which the signal is reflected three times. Because of the different types of reflectors, the first two reflections are partial and the third one is total. A few microseconds later the resulting signals are again transformed into electrical energy and received, amplified and phase detected with the oscillating signal which also generates the sending signal. A good representation of this reflecting process is given by Reindl [13.42].

The phase shift is a measure of the reflectors distance. If the transducer is compressed or stressed, a proportional phase shift can be observed. The most important advantage of this system is to measure forces and moments at rotating shafts or at locations not easily accessible.

Since many parameters contribute to frequency change of the SAW device, it is often difficult to determine the effect of a specific parameter on the change of frequency (Fig. 13.14a).



*Adapted by Aurel Millea
after Thomas Sachs,
T.U. Munich, 1995*

Fig. 13.13 a) Measurement scheme for surface acoustic wave transducers with wireless transmission. b) Half-bridge with two SAWs: reference and active due to applied force.

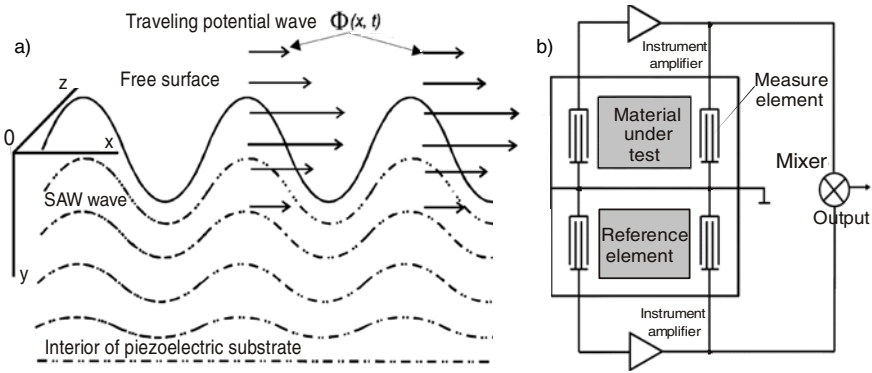


Fig. 13.14 a) Though the mechanism of the elastic wave propagation in a piezoelectric material is governed by mechanical motion and Maxwell's electromagnetic equations, the mechanical solution dominates as the propagation occurs at a velocity that is on the order of 10^5 less than that of light (C. Campbell, *SAW Devices*, Academic, N.Y., 1989). b) SAW configuration using a reference element in a bridge connection.

The most common way to solve this problem is to utilize the reference element [13.43], which is equal to the original SAW device except for the layer of coated material that is highly sensitive to the parameter of interest: force, torque, pressure, flow and other associated quantities. The diagram of such a device is shown in Figure 13.14b (reprinted with permission from Elsevier, copyright 1995); it looks like a bridge with four surface acoustic waves measurement elements!

The differential sensing scheme is implemented in hardware and external factors and signal drift due to temperature are avoided. The difference in frequency changes between these two elements reflects only the amount of change in the parameter of interest.

The researchers from the Shibaura Institute of Technology, Tokyo, Japan propose a two-dimensional strain transducer that simultaneously measures strains in two different directions using two delay lines that cross each other at right angles [13.44]. A single device was used to measure the strains in x and y directions. The elastic cantilever (Fig 13.15a) was vibrated by periodic force with 50 Hz. Measuring the amount of phase change between the input and output of a delay line caused by the mechanical strain, one can determine the magnitude of other related physical quantities, starting with the applied force.

An 128° Y-cut, X-propagating LiNbO_3 crystal was used, ensuring symmetric transmission characteristics about the x-axis. Installing two delay lines so that they were symmetric about the x-axis and intersecting each other at right angles ($X \pm 45^\circ$), a two-dimensional strain transducer has been achieved.

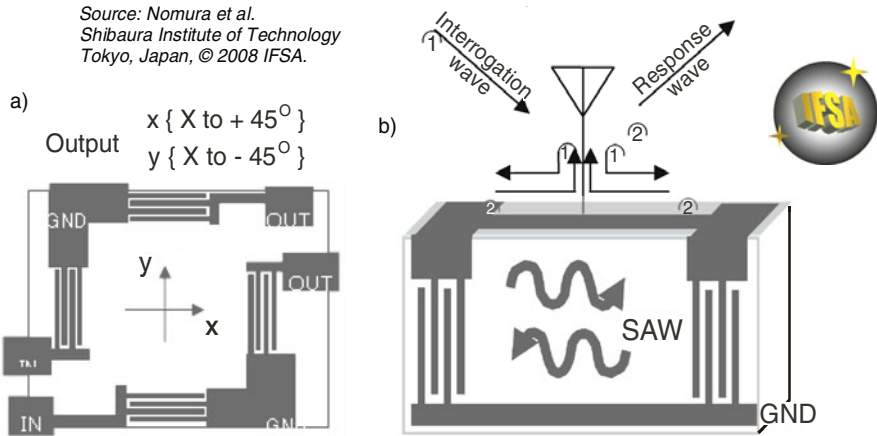


Fig. 13.15 Two-directional SAW strain (or force) transducer: a) “combined” output, b) wireless, passive remote sensing system (Courtesy of Sergey Yurish, © 2008 IFSA)

When this new SAW transducer is connected directly to an antenna, it is capable of passive remote sensing (Fig. 13.15b). Its response almost coincides with the results of conventional strain gauged transducers. Being slower than electromagnetic waves by approximately five orders of magnitude, SAWs can be made more compact, furthermore increasing of their frequency, as well as their precision and resolution.

SAW-based devices have also other advantages [13.1], [13.30]:

- They can be designed to provide complicated signal processing functions with a fairly simple and small structure (a single piezoelectric substrate with normally two IDTs).
- A broad range of response functions can be obtained through variation of electrode patterns, in a high measurement bandwidth (up to 1 kHz).
- Most SAW devices are manufactured using single-stage lithography, which is ideal for mass production of low-cost devices.
- They have the ability to withstand harsh environments (oil, electromagnetic interference, extreme temperatures) while are very sensitive detectors of ambiental changes (force, pressure, chemical contamination, etc.).
- SAWs prove outstanding reproducibility and accuracy, long-term stability.

The advent of wireless, batteryless sensing, using surface acoustic wave technology holds the promise of providing cost effective and elegant solutions to the challenges posed by high-speed rotating machine components [13.45]. Through the use of independent frequency bands, these transducers maintain their unique identification within the system architecture.

REFERENCES

1. Mamishev, A.V., Sundara-Rajan, K., Yang, F., Du, Y., Zahn, M.: Interdigital sensors and transducers. *Proceedings IEEE* 92(5), 808–845 (2004)
2. Ebbecke, J.: Deterministic single photon source in carbon nanotubes mediated by surface acoustic waves. PhD project, Heriot Watt University, UK, September 30 (2008)
3. William, C.T., Nguyen, T.H., Roger, T.H.: Laterally driven polysilicon resonant microstructures. *Sensors and Actuators A: Physical* 20, 25–32 (1989)
4. Caronti, A., Caliano, G., Savoia, A., Gatta, P., Pappalardo, M.: Microfabricated capacitive ultrasonic transducer for high frequency applications. *European Patent EP-1764162* (March 21, 2007)
5. Wu, N.E., Miles, R.N., Aydin, O.A.: A digital feedback damping scheme for a micromachined directional microphone. In: *Proc. 2004 American Control Conference*, Boston, MA, June 30 – July 2, pp. 3315–3320 (2004)
6. Varadan, V.K.: Tutorial Course on Smart Sensors and Materials. In: *Proc. 11th Conf. Asia-Pacific Nondestructive Testing*, Jeju Island, South Korea, November 4 (2003)
7. Knigge, B., Talke, F.E.: Contact force measurement using acoustic emission analysis and system identification methods. *Tribology International* 33, 639–646 (2000)
8. Oishi, R., Nagai, H.: Strain sensors of shape memory alloys using acoustic emissions. *Sensors and Actuators A: Physical* 122(1), 39–44 (2005)
9. Azeem, A., Feng, H.-Y., Orban, P.: Processing noisy cutting force data for reliable calibration of a ball-end milling force model. *Measurement* 38(2), 113–123 (2005)
10. Lindner, G., Faustmann, H., Koch, T., Krempel, S., Lind, F., Mick, H., Münch, M., Pflaum, K., Rothballer, S., Unterburger, M.: Digital precision measurement of force, pressure and other mechanical quantities with an acoustic waveguide sensor. In: *Proc. 13th Int'l. Conf. Sensor 2007*, Nuremberg, May 22–24, vol. I, pp. 91–96 (2007)
11. Ultrasonic bolt clamping force meter. Hagiwara Electric Co. Ltd., Nagoya, Japan (1983)
12. Ruffa, A.A.: Acoustic bolt removal. Report approved for public release. Department of the Navy, Washington DC, September 11 (1998)
13. Ide, T., Uchiyama, H., Yoneda, T., Tanaka, H.: Measurement of contact force between pulley sheave and metal pushing V-belt by means of ultrasonic waves. *JSAE Review* 22, 163–167 (2001)
14. Prokic, M., Tapson, J., Mortimer, B.J.P.: The ultrasonic hammer transducer. *IEEE*, Los Alamitos (2001), <http://www.mpi-ultrasonics.com/hammer-transducer.html>
15. Kim, K.-B., Kim, M.S., Park, J.-G., Lee, S.D., Kim, G.S., Jung, H.-M.: Determination of apple firmness by ultrasonic measurement. In: *CD Proc. XVIII IMEKO World Congress*, Rio de Janeiro, Brazil, September 2006, pp. 17–22, Paper 313 (2006)
16. Armstrong, S.R., McCullough, J.L., Beattie, D.T.: Measurement of 5-HT₄ receptor-mediated esophageal responses by digital sonomicrometry in the anesthetized rat. *Journal of Pharmacological and Toxicological Methods* 53(3), 198–205 (2006)

17. Witte, R.S., Dow, D.E., Olafsson, R., Shi, Y., O'Donnell, M.: High resolution ultrasound imaging of skeletal muscle dynamics and effects of fatigue. In: Proc. Joint 50th Anniversary Conf. IEEE Ultrasonics, Ferroelectrics, and Frequency Control, Montréal, Canada, August 24-27, pp. 764-767 (2004)
18. Lynch, J.E., Hinders, M.K., McCombs, G.B.: Clinical comparison of an ultrasonographic periodontal probe to manual and controlled-force probing. *Measurement* 39(5), 429-439 (2006)
19. Nightingale, K., Scott, M., Nightingale, R., Trahey, G.: Acoustic Radiation Force Impulse imaging: In vivo demonstration of clinical feasibility. *Ultrasound in Medicine & Biology* 28(2), 227-235 (2002)
20. Nightingale, K., Palmeri, M., Zhai, L., Frinkley, K., Wang, M., Dahl, J., Pinton, G., Hsu, S., Fahey, B., Dumont, D., Trahey, G.: Clinical applications of acoustic radiation force impulse imaging. In: Proc. 19th Int'l Congress on Acoustics, PACS: 43.80.Qf, Madrid, Spain, September 2-7 (2007)
21. Lazebnik, R.S.: Tissue strain analytics virtual touch tissue imaging and quantification - ACUSON S2000 ultrasound system. In: SIEMENS Medical Solutions - USA, Inc., Mountain View, CA, PDF created on November 5 (2008)
22. Melodelima, D., Bamber, J.C., Duck, F.A., Shipley, J.A., Xu, L.: Elastography for breast cancer diagnosis using radiation force: System development and performance evaluation. *Ultrasound in Medicine & Biology* 32(3), 387-396 (2006)
23. Palmeri, M.L., Nightingale, K.R.: On the thermal effects associated with radiation force imaging of soft tissue. *IEEE Transactions on Ultrasonics, Ferroelectrics, and Frequency Control* 51(5), 551-565 (2004)
24. Zhang, X., Greenleaf, J.F.: Measurement of wave velocity in arterial walls with ultrasound transducers. *Ultrasound Medical Biology* 32(11), 1655-1660 (2006)
25. Rivera Cardona, M.A., Alvarenga, A.V., da Costa-Felix, R.P.B.: Primary level ultrasonic output power measurement at laboratory of ultrasound of INMETRO. In: CD Proc. XVIII IMEKO World Congress on Metrology for a Sustainable Development, Rio de Janeiro, Brazil, September 17-22, Paper 124 (2006)
26. Kuznetsova, L.A., Coakley, W.T.: Applications of ultrasound streaming and radiation force in biosensors. *Journal of Biosensors & Bioelectronics* 22(8), 1567-1577 (2007)
27. Hallez, L., Touyeras, F., Hihn, J.Y., Klima, J.: Energetic balance in an ultrasonic reactor using focused or flat high frequency transducers. *Ultrasonics Sonochemistry* 14(6), 739-749 (2007)
28. Chopra, K.L., Kaur, I.: *Thin Film Device Applications*. Plenum, New York (1983)
29. Hunt, A. (Coord.): *Guide to the Measurement of Force*. The Institute of Measurement and Control, London, (Published 1998) ISBN 0-904457-28-1
30. Gierut, J., Lohr, R.: *Automotive powertrain & chassis torque sensor technology*. Honeywell International Inc. (2005)
31. Magee, S.J., Cook, J.D., Liu, J.Z.: Surface acoustic wave sensor methods and systems. US Patent 7165455 (January 23, 2007)
32. Fuhr, C.: SAW torque sensors for automotive applications help to improve fuel efficiency. Sensor Exhibiton in Hall 12, Booth No. 337 (Transense), Nuremberg, Germany, May 26-28 (2009)

33. Low-cost OEM rotary torque transducers. Special issue of IEN – Europe, PCNE 34, p. 32 (April 2004)
34. Turner, J.D., Austin, L.: Sensors for automotive telematics (review article). *Measurement Science and Technology* 11, R58–R79 (2000)
35. SAW Technology: Rayleigh surface acoustic wave delay line, July 13 (2009), http://www.sengenuity.com/tech_raleighSAW.html; 1997-2009 by Vectron International, Inc., A Dover Company
36. Drafts, B.: Acoustic wave technology sensors. *Sensors Magazine*, October 1 (2000), <http://www.sensorsmag.com/articles/.../main.shtml>
37. Wixforth, A.: Nanoquakes shake up biotechnology. *Bio Tech International*, pp. 20–22 (April/May 2003)
38. Soborover, E.I., Zyablov, V.L.: A SAW-based element without sensing layer as a gas and gas mixture sensor. (Russian) *Sensors and Systems Journal* (2) (February 2005)
39. Bogoslovsky, S.V.: SAW-based dispersion strain gaging resonator. *Sensors and Systems Journal* (Contents and abstracts translated from Russian) (7) (July 2007)
40. Campbell, C.K.: Understanding surface acoustic wave (SAW) devices for mobile and wireless applications and design techniques. Internet posting of “68 Questions and Answers for Year 2008” (2008)
41. Sachs, T.: Funkabfragbare OFW-Verzögerungsleitung zur Dehnungsmessung. In: 7. Internationale Fachmesse mit Kongress für Sensoren, Meßaufnehmern und Systeme – SENSOR 1995, Nürnberg, Deutschland, May 9-11, pp. 79–84 (1995)
42. Reindl, L., Mágori, V.: Funksensorik mit passiven Oberflächenwellen Komponenten (OFW). VDI – 515, Reihe 8: Meß-, Steuerungs- und Regeltechnik, pp. 62–79 (1995)
43. Benes, E., Burger, M.G.W., Schmid, M.: Sensors based on piezoelectric resonators. *Sensors and Actuators A: Physical* 48, 1–21 (1995)
44. Nomura, T., Kawasaki, K., Saitoh, A.: Wireless passive strain sensor based on surface acoustic wave devices. *Sensors & Transducers Journal* 90, 61–71 (2008)
45. Durdag, K.: Wireless surface acoustic wave sensors. *Sensors & Transducers Journal* 106(7), 1–5 (2009)

Chapter 14

GYROSCOPIC FORCE TRANSDUCERS

What is it gyroscope? One can find on Internet some very different definitions: a toy spinning while dangling on a string, a human, clownaround Orbitron or an extraterrestrial spacecraft... Planets and stars are also gyroscopes! In the known form of today (Fig. 14.1a) the gyroscope was invented in 1852 by Leon Foucault. A gyroscope is a physical device which demonstrates the principle of angular momentum conservation, based upon a spinning wheel on an axle. Once spinning, the device tends to resist changes to its orientation and to return in its initial position, like a boomerang!

14.1. THE GYROSCOPIC PRINCIPLE IN FORCE MEASUREMENT

To provide useful information, a gyro's spin axis must be related to some reference, usually the Earth's surface [14.1]. A force applied upward on the inner gimbal may be visualized as applied in an arc about axis Y-Y (Fig. 14.1b).

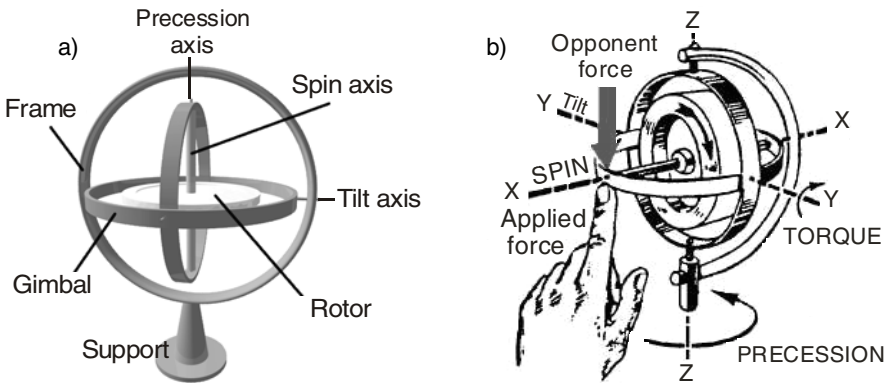


Fig. 14.1 Gyroscope composition (a) and its force / torque mechanism

This applied force is opposed by the resistance of gyroscopic inertia, preventing the gyro from rotating about axis Y-Y. With the rotor spinning clockwise, the precession will take place 90° clockwise from the point of applied force. The gyro precesses about axis Z-Z in the direction of the arrow.

A gyroscope exhibits a number of behaviors. Its motions can be analyzed according to three basic quantities:

- *spin* – angular velocity of the gyro rotor,
- *torque* – rotary motion applied to change the direction of the rotor axis,
- *precession* – resulting angular change of the spin axis when torque is applied.

Only those forces tending to tilt the gyro wheel will cause precession.

A classical example of actuating and sensing with tuning forks [14.2] is depicted in Figure 14.2a. The two tines of the tuning fork are excited in the X-direction by electrostatic, electromagnetic or piezoelectric force at the resonance frequency of the tines. If the sensor is then rotated around the Z-axis a movement of the tines in the Y-direction is induced. This movement is measured either capacitively, piezoresistively or piezoelectrically.

The gyroscope is a critical navigational instrument used for maintaining a fixed orientation with great accuracy, regardless of Earth rotation. If an airplane (Fig. 14.2b) is moving in X-direction, while its bounded frame (Earth) is rotating around Z-direction, the airplane will be affected by Coriolis force in Y-direction. The associated MEMS gyroscope consists of a sensing element as 2- μm -thick polysilicon structure having a dynamic range of 300 deg/s [14.3].

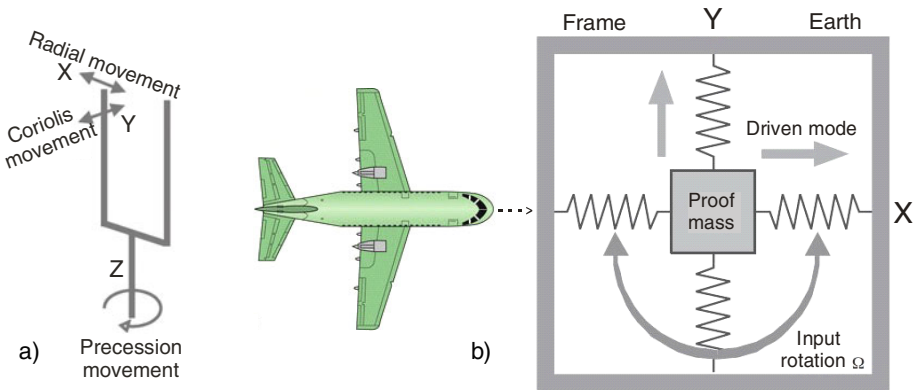


Fig. 14.2 a) Gyroscopic sensing principle: two tines are oscillating in the X-direction at their resonance frequency and, due to the Coriolis force, an oscillation in the Y-direction is induced when the sensor rotates around the Z-axis. b) The lumped model of actuating / driving and sensing for a gyroscopic proof mass.

Standard comb drive actuators are used to excite the structure to oscillate along one in-plane axis (X), which allows relatively large drive amplitudes. Any angular rate signal about the out-of-plane axis (Z) excites a secondary motion along the other in-plane axis (Y). Its proof mass is oscillated in certain direction, if any Coriolis forces (on the perpendicular direction) are sensed at the rotated frame.

Gyroscopic load cells exploit the force sensitive property of a gyroscope mounted in a (circular) gimbal or (square) frame system [14.4]. A commercially available device incorporates a dynamically balanced heavy rotor on a spindle, itself mounted in the inner frame of a two-gimbal system. The arrangement has three axes of rotational freedom mutually at right angles and origin on the gravity center of the rotor. The force to be measured by the gyroscopic transducer is applied through the lower swivel and a couple is produced on the inner frame causing the gimbals to precess. *The time taken for the outer gimbal to complete one revolution is a measure of the applied force.*

14.2. CONVENTIONAL GYROSCOPIC FORCE TRANSDUCERS

Together with vibrating wires and beams (e.g. tuning forks), gyroscopic force transducers are considered as true digital devices since they directly convert the applied load to a frequency output without analog-to-digital conversion [14.5].

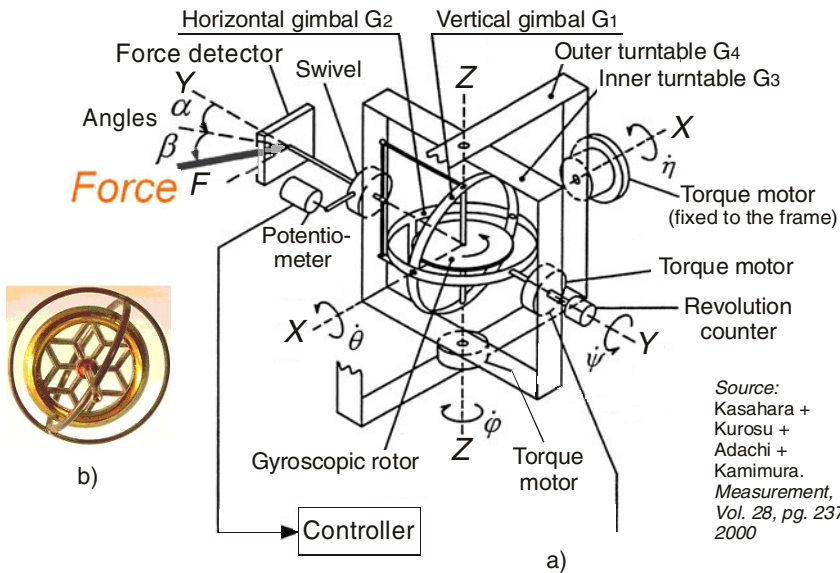


Fig. 14.3 Gyroscopic force measuring apparatus with horizontal outer gimbal and vertical inner gimbal (a). An optimized model of “whirligig” (b).

For a well-designed gyroscopic load cell it is generally claimed a temperature coefficient of 0.000 1 % fsd in the operating temperature range of -10 to $+40$ °C and a nonlinearity of 0.001 % fsd.

A gyroscopic measuring system for a vectorial force in three-dimensional space is described in [14.6]. In order to vectorially measure a force, two auxiliary turntables (driven by servomechanisms) are installed around the gyroscope, in which turntable outputs are required to follow some angles of incidence of a force vector (Fig. 14.3a). For accurate force measurement and disturbances suppression two types of compensation methods are proposed.

Two special features are used in comparison with other existing force measuring methods [14.7], namely:

- *Non-movement of the load.* The direction of a downward load to be measured is at a right angle to the one of the resulting movement in a horizontal plane. The gyroscope provides non-moving force balance measurement of wide range of loads, and the lever system is thus free from hysteresis and non-linearity. Its operation is unaffected by rotational friction which is detected and controlled by the use of torque motor.
- *Dynamically force-balanced.* The precession rate varies directly with the applied load, thus the gyroscope has an almost instantaneous response of precision rate to changes in applied couple, generating directly pulse signals. Since no springs and no balance weights are mounted in its structure, the response is the order of microseconds compared with its minimum measuring period of 0.5 s. It is unaffected by reaction forces from plant vibration because of the lack of hysteresis and of its high-speed of response.

Table 14.1 Performance comparison for two gyroscopes [14.8]

Characteristics	Producer →	Oyama N.C.T.	Stevens-Wöhwa
		Japan	Germany
Initial load [N]		36	20
Measuring range [N] with additional levers		150	200
Type of swivel (bearing)		Angular contact	Spherical thrust
Precession time [ms/rev]:			
– at zero load		1 100	2 700
– at full load		450	800
Allowable tilting angle [°]:			
– right and left		± 1.1	± 1.8
– back and forth		± 0.54	± 0.4
Non-linearity		1 / 30 000	1 / 10 000
Repeatability		1 / 30 000	1 / 10 000
Measuring time [s]		5 ... 6	5 ... 12

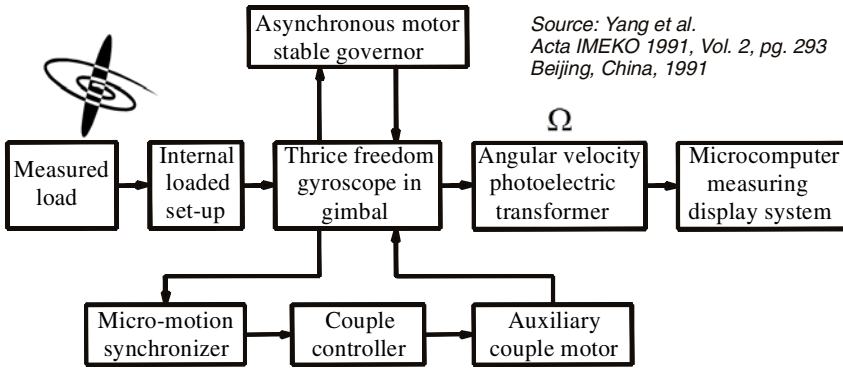


Fig. 14.4 Chinese 3 DoF gyroscope in gimbal together with internal loaded set-up, friction couple compensating system and revolution measuring microcomputer

Table 14.1 compares the Japanese gyroscope made by Oyama National College of Technology with German model achieved by Stevens-Wöhwa. The Chinese gyroscopic force transducer TLG-1 [14.9] has its block diagram depicted in Figure 14.4. It continually converts the maximum measured load (200 N) into unchanged couple on horizontal frame. Another variant is available for 500 kg platform with 5000 intervals.

14.3. TYPES OF MICRO-GYROSCOPIC FORCE TRANSDUCERS

There are a lot of micro-gyroscope types, not easy to arrange in classes; a basic device such as an IDT can be used as a resonator (Fig. 14.8b), a SAW sensor (Fig. 14.9) or a capacitive transducer, like in the application presented below.

The Charles Stark Draper Lab. designed an innovative electrostatic force compensated comb drive for a MEMS with a mechanism for providing an output signal representative of a physical quantity which the gyroscope is intended to detect [14.10]. This device is responsible for adjusting the output signal of the micro-electro-mechanical mechanism to compensate for errors in the output signal due to a change in the predetermined force.

14.3.1. Inertial gyroscopes

A MEMS transducer based inertial measurement unit (IMU) has been constructed in-house, intended to be used in a low-cost GNSS (global navigation satellite system) [14.11]. Calibration does not require a mechanical platform for the accelerometer but only a simple rotating table for the gyro. The proposed calibration methods utilize an ideal property, i.e. the ratio of the measured output of the accelerometer and gyro cluster, corresponding to the magnitude of applied force and rotational velocity, respectively.

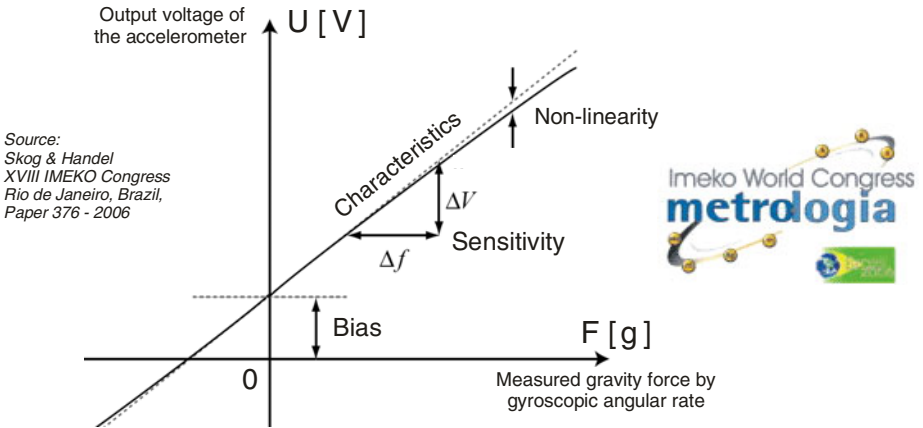


Fig. 14.5 The relationship between the accelerometer output voltage and the gyro angular rate is modeled as a linear function, describing the transducers scaling and bias.

The sensitivity quotient of the inertial gyroscope (Fig. 14.5), considering the accelerometer scale factor matrix K_a as a ratio between the output and input parameters (i.e. voltage and force relative variations), is given by

$$S_G = \frac{\Delta U}{\Delta F} \quad (14.1)$$

MEMS technology has made possible to cheaply fabricate a single chip accelerometer and gyroscopic transducer (Analog Devices). An inertial 6 DoF measurement unit has been constructed to measure accelerations and angular rates between $\pm 15 \text{ m/s}^2$ and $\pm 150 \text{ deg/s}$, respectively. The MEMS transducers output a voltage proportional to the physical quantities sensed by the transducers: acceleration and angular rate.

For vehicular and tactical-grade inertial navigation systems, high-performance MEMS gyroscopes are required with (1...100) deg/h stability. The fundamental operation of a new device is based on oscillating at its resonant frequency a Ni cantilever beam parallel to a Si substrate, defined as the horizontal direction, while sensing a modulated tunneling current normal to the substrate (the vertical direction), due to Coriolis force [14.12].

The horizontal movement of the end of the cantilever is sensed capacitively by using a triangular metal electrode on the substrate and a high-sensitivity RF tank circuit. A NASTRAN FEA program was utilized to model the vertical deflection of the cantilever over the tunneling tip produced by a distributed Coriolis force, obtaining a deflection sensitivity of 4.07 pm/deg/s.

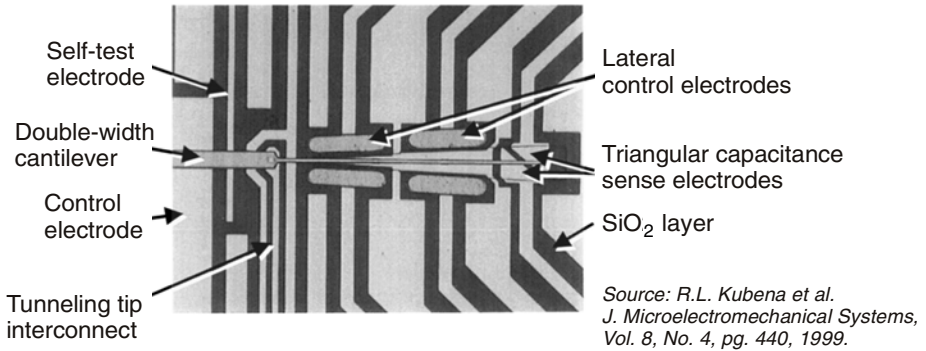


Fig. 14.6 Inertial rotation rate meter based on the “differential” sensing of a cantilever: horizontal – by triangular capacitance (principle in Fig. 5.3) and vertical – by tunneling

Kubena *et al.* have designed, fabricated and tested a highly miniaturized transducer that employs the high displacement sensitivity of quantum tunneling to obtain the desired resolution without the need for precise tuning the drive and sense resonant frequencies (Fig. 14.6). Their devices with 300- μm -long cantilevers have 27 $\text{deg/h/Hz}^{1/2}$ noise level, with promising possibilities of reducing to near the Brownian thermal noise level when a closed-loop servo, operating at the oscillation frequency, is implemented around the transducer. The use of a wide-bandwidth servo around the vertical loop opens the possibility of utilizing these transducers for both rotation and vibration sensing.

14.3.2. Piezoelectric gyroscopes

Piezoelectric gyroscopes are measuring the angular rotation of a system with respect to an inertial frame of reference by means of the Coriolis principle. A new dual-axis gyroscope made out of piezoelectric ceramic PZT [14.13] is capable to simultaneously measure the rotational velocity over two orthogonal axes with good enough sensitivity and distinction between the two components.

Usually the gyroscope operation principle incorporating a mechanical vibrator is to measure the variation of displacement induced by the Coriolis acceleration. The force rebalance loop is a kind of feedback control system that maintains the proof mass at a designed state with reciprocally balanced forces from mechanical and electrical sources (Fig. 14.7). The proof mass connected with the fixed outer frame through a beam spring sustains a driving oscillation in the X-axis and experiences an induced force in the Y-axis via the Coriolis acceleration when an angular velocity Ω is applied through the Z-axis. A systematic design approach of the force rebalance control is applied via a modified automatic gain control (AGC) method, which allows a simple linear approximation of the system’s dynamics [14.14].

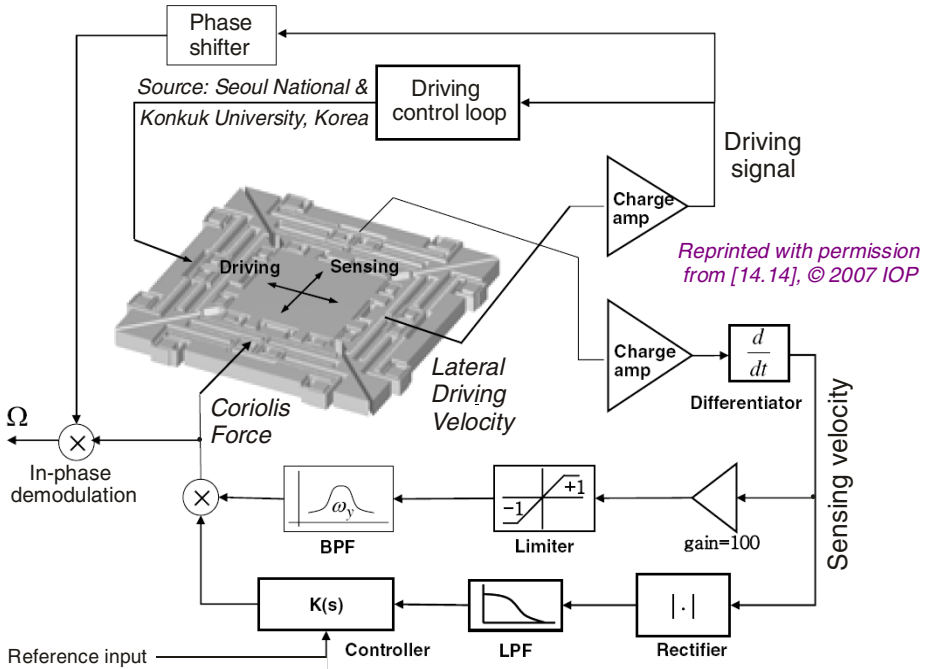


Fig. 14.7 MEMS vibratory gyroscope with automatic force rebalancing control

The lower loop is implemented for the force rebalance and the upper loop is for the lateral oscillation in the driving mode dynamics. Since the output of the charge amplifier is proportional to the displacement, an analog differentiator is applied to obtain the velocity signal handled in the loop. Precise reference signals are applied using an electrical force equivalent to the mechanical Coriolis force. Using the proposed modification of AGC and the rebalance strategy that maintains a biased oscillation, a number of performances appears, including bandwidth extension and widened operating range.

14.3.3. Resonator / vibrating gyroscopes

Almost all reported micromachined gyroscopes use vibrating mechanical elements to sense rotation [14.15]. They have no rotating parts that require bearings, so they can be easily miniaturized and batch-fabricated using micro-machining techniques. MEMS (micro-electro-mechanical system) gyroscopes have taken the idea of the Foucault pendulum, using a vibrating element. They are based on the transfer of energy between two vibration modes of different metallic structures caused by Coriolis acceleration. Much cheaper are different kinds of silicon micromachined vibrating structure gyroscopes (VSGs).

Several principles of vibratory gyroscopes have been produced, among them tuning forks and vibrating beams. A large manufacturer of MEMS gyroscopes is SDI (Systron Donner Inertial), producing, for example, guidance systems for ballistic missiles.

A tuning fork microgyroscope with 2 DoF sense modes, achieving a wide bandwidth without sacrificing mechanical and electronic sensitivity, is reported in [14.16]. This resonator microgyroscope, made by in-house silicon-on-glass micromachining process, is operated in a bandwidth of 1 kHz and ensures a raw mechanical sensitivity of $131 \mu\text{V}/\text{deg/s}$. The “scale factor” variation of the gyroscope is less than 0.38 % for large ambient pressure variations.

A single-crystal silicon-based tuning-fork gyroscope with electrostatic force-balanced driving and torsional Z-sensing is presented in [14.17].

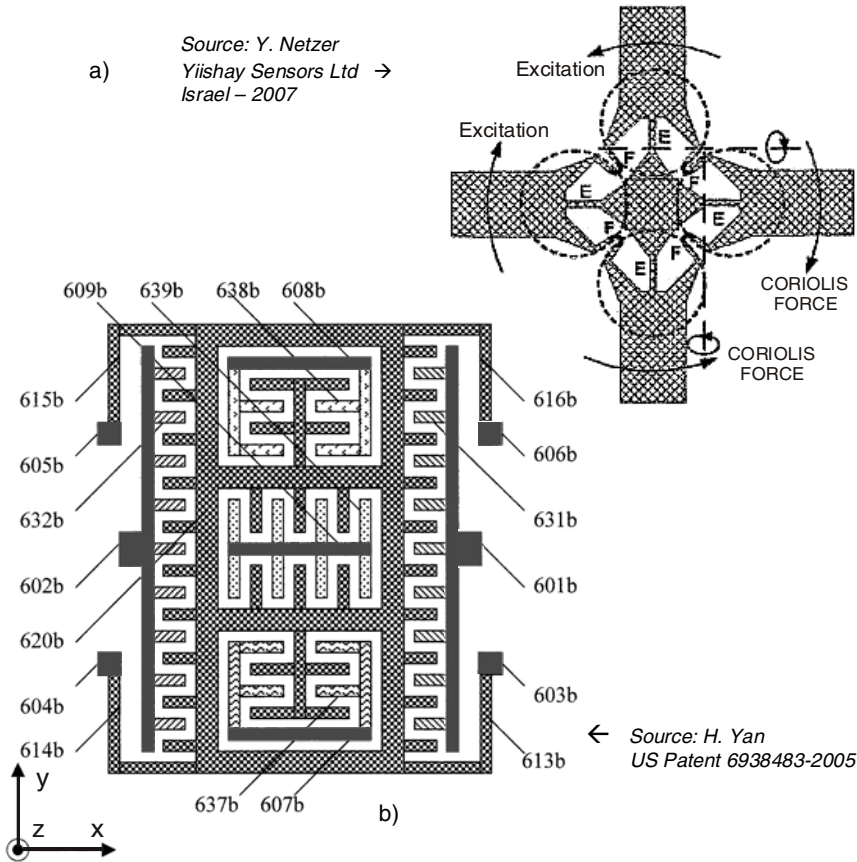


Fig. 14.8 Dual-axis gyroresonator (a) and IDT phase-locked vibratory gyroscope, with receiver section (index ‘b’) represented, emitter section (index ‘a’) being symmetric (b)

Invention [14.18] discloses an improved planar, dual-axis (X-Y), resonator gyroscope with mechanical coupling of adjacent vibrating members. The primary-mode flexible hinges include a tangential torsion element that largely decouples the out-of-plane resonant frequency from the wafer thickness (Fig. 14.8a). The use of separate plates for the force-balance and for the electric spring enables decoupling of the two functions. The invention also provides resonant frequency servo-loop for locking of the sense-mode resonant frequency to the drive-mode frequency, an online self-test, a split force balance loop for self-cancellation of the quadrature signal, decoupling of the force-balance and resonant frequency servo-loops and stabilization of the inertial rate-sensing sensitivity.

Another invention is related to a phase-locked mechanical resonator pair [14.19], which comprises at least two mechanical resonators wherein the resonance of the second mechanical resonator is phase-locked to the resonance of the first mechanical, and a micromachined vibration gyroscope that uses such phase-locked mechanical resonator pair as its resonating masses to generate differential Coriolis forces and to achieve inertial cancellation. This is a spectacular structure of Coriolis vibratory gyroscope (CVG) (Fig. 14.8b), combining series of horizontal and vertical interdigital transducers (IDTs).

14.3.4. Acoustic (and SAW) gyroscopes

The gyroscope has been used for navigational purposes since the 1920's, its accuracy improving as technology advanced. Nowadays optical gyroscopes are the most accurate on the market but, as Richard B. Johnson discovered, one does not need to use light [14.20]. One could use sound waves in air. Of course, the velocity of the sound is highly dependent upon temperature so such a device would be difficult to calibrate. The speed of sound at sea level on a standard day is about 340 meters per second. If we created a circular sound column 34 meters in length, a 10 kHz tone would undergo 1000 complete cycles during its passage through the circular pipe and the circulating sound would be affected by rotation for one tenth of a second round-trip time. Since the propagating sound is electrically generated, there is no need to use an interferometer to detect phase differences, just directly compare the output signal phase with the input signal phase. This is what Johnson's acoustic rate gyroscope did. This device, made in 1959 in a high school physics laboratory in Boston, was sensitive enough to detect, in première, the rotation of the Earth and became a Cold War top secret.

More advanced are devices with surface acoustic waves. Such a SAW gyroscope [14.21] uses the interference effect of two crossed SAWs, one is induced by the Coriolis force from the input rotation, and the other is from the SAW device with same operation frequency. A differential structure of two delay line oscillator is used to compensate the temperature effect.

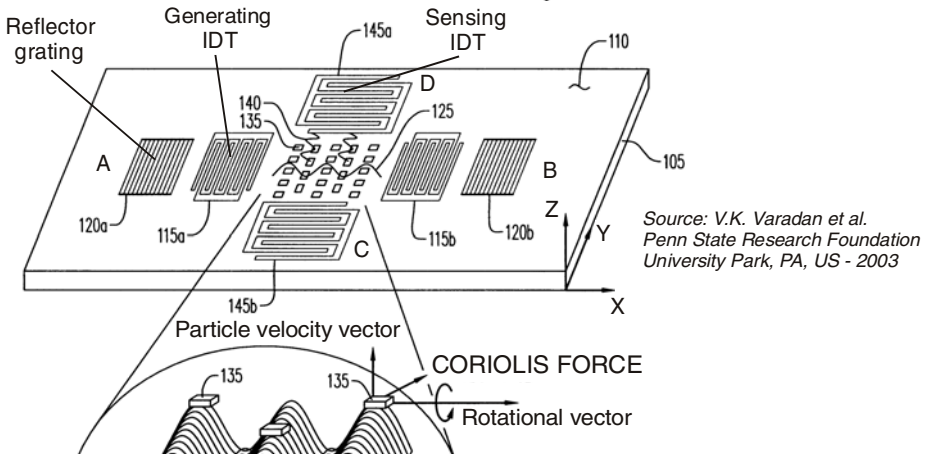


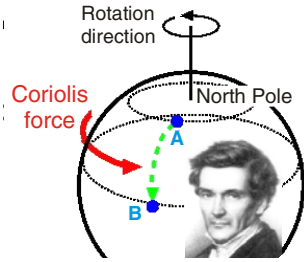
Fig. 14.9 Micro-electro-mechanical gyroscope with surface acoustic wave (SAW) devices and Coriolis force sensing

Based on the coupling of modes simulation, an 80 MHz two ports SAW resonator and dual-delay line were fabricated and characterized by the HP network analyzer. In the primary experimental results, a frequency change of 2.5 kHz was observed at rate of 500 deg/s from the SAW delay line, by interference effect between the secondary SAW induced by Coriolis force and the running SAW from the delay line.

An invention assigned to the Pennsylvania State Research Foundation (University Park, PA) is presented in [14.22] as follows: A gyroscope comprises a piezoelectric substrate having a polished surface (Fig. 14.9). Disposed on the surface are a resonator transducer (IDT – 115), a pair of reflectors (120), a structure such as a metallic dot, and a sensor transducer (IDT – 145). The resonator transducer creates a first surface acoustic wave on the surface. The pair of reflectors reflects the first SAW to form a standing wave within a region of the surface between the pair of reflectors. The structure is disposed on the surface within the region (A – B), wherein a Coriolis force acting upon the structure creates a second surface acoustic wave (namely C – D). The transducer senses the second SAW and provides an output indicative thereof.

14.3.5. Coriolis force transducers in medical applications

Cardiac apex rotation, quantified by sophisticated techniques (radiopaque markers and tagged magnetic resonance), has been shown to provide a sensitive index of left ventricle dynamics. The paper [14.23] describes the first experimental assessment of cardiac apex rotation using a gyroscopic transducer based on Coriolis force, epicardially glued on a sheep apex.



Due to the Earth's rotation, the force named after Gustav-Gaspard Coriolis (the French scientist who described it mathematically in 1835), is what causes objects in the Northern hemisphere to turn to the right and objects in the Southern hemisphere to turn to the left. The Coriolis acceleration arises in a referential rotating frame and is proportional to the rotation rate.

Fig. 14.10 Coriolis force explanation

The initial results suggest that the use of an implantable rotation transducer based on Coriolis force can be an efficient and effective tool to assess left ventricle torsional deformation both in normal and failing hearts.

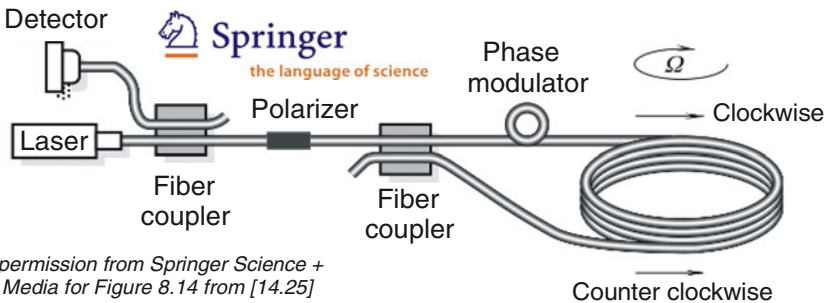
Another medical application (human gait analysis) depicts in-use calibration of body-mounted gyroscopes [14.24].

14.4. OPTICAL GYROSCOPES

14.4.1. Fiber optic gyroscopes (FOGs)

Rotation detection using light interference was discovered by Georges Sagnac in 1913. He showed that two waves acquired a phase difference by propagating in opposite directions around a loop interferometer, which was rotating about its axis. The effect was small, however, and measurement of slow rotations required a substantial interferometer.

An alternative and convenient method for increasing the sensitivity of passive Sagnac systems uses an optical fiber which may be wrapped many times around a small cylinder to increase the phase difference produced by rotation [Vali and Shorthill, 1976].



With kind permission from Springer Science + Business Media for Figure 8.14 from [14.25]

Fig. 14.11 Fiber-optic analog coil gyroscope sensing the rotation rate Ω

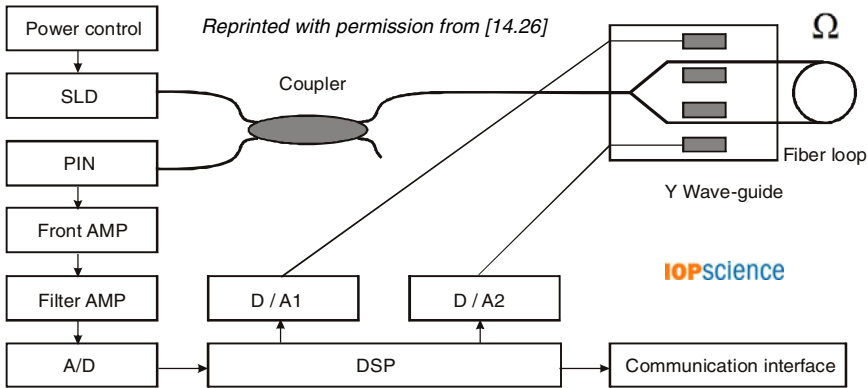


Fig. 14.12 MEMS / NEMS fiber optic gyroscope with closed-loop force feedback

The coil fiber gyroscope presented in Figure 14.11 contains a light source and a detector coupled to its optical fiber [14.25]. The light polarizer is positioned between the detector and the second coupler to ensure that both counterpropagating beams traverse the same path in the fiber-optic coil. The two beams mix and impinge onto the detector, which monitors the cosinusoidal intensity changes caused by rotationally induced phase changes between the beams. This type of optical gyroscope provides a relatively low-cost, small-size, rotation-sensitive sensor with dynamic range up to 10 000. Applications include yaw and pitch measurements, attitude stabilization, and gyrocompassing.

Closed-loop control schemes rely on feedback to control the position of the mass via a force feedback, or force rebalancing, at its rest position [14.26]. The force feedback required is proportional to the magnitude of the inertial load. Closed-loop force feedback systems have the potential for very high sensitivity and have been implemented in optic gyroscopic systems due to the minute forces. Based on closed-loop system, a new demodulator technology for fiber optic gyroscope (FOG) is presented.

Figure 14.12 shows the principle diagram of scanning phase shift FOG system. The light source of system used a super luminescent diode (SLD), light entrance the Y junction waveguide (LiNbO_3) through polarization maintain coupler (PM-BS). The each shoulders of Y waveguide were modulated by D/A1 and D/A2 converter controlling. One of them was used to phase shift keying (PSK); the other was used to phase expiation modulator (PEM). The opposite light create interference figure at PIN detector. Then the light signal was converted to voltage signal, which passed the front amplifier, noise filter, A/D (TI ADS5422), and putted into DSP (TI TMS320), which took charge creating the modulator wave and calculating the interference difference phase, as a measure of the angular velocity Ω .

14.4.2. *Laser gyroscopes*

A ring laser gyroscope (RLG) provides a dramatic improvement in optical gyroscope sensitivity; its beam is guided by mirrors inside the enclosure allowing the use of small loops, by internally converting the phase difference to a frequency difference digitally measured [Macek and Davis, 1963].

A research team from Princeton University has recently achieved for “John H. Glenn” Research Center, Cleveland, Ohio an experimental nuclear-spin gyroscope [14.27], based on an alkali-metal/noble-gas co-magnetometer, which automatically cancels the effects of magnetic fields and other external perturbations. The relationships among the electron polarization of the potassium atoms, the nuclear polarization of the helium atoms, the magnetic fields, and the mechanical rotation of the magnetometer are described by a system of coupled Bloch equations. A force-based magnetometer is depicted in Figure 4.10b. In comparison with fiberoptic gyroscopes, these gyroscopes would draw less power and would be smaller, lighter, more sensitive to rotation, and less costly.

14.4.3. *MOEMS (micro-opto-electro-mechanical system) gyroscope*

Compared with fiber-optic and ring laser gyroscopes, MOEMS gyroscopes, which appeared in 1980s, have the advantages of small size and light weight. They can be categorized into resonant (RMOG) and interferential micro-optic gyroscopes (IMOG). There is a kind of hybrid gyroscope as well that comprises a MEMS-like mechanical resonator to sense the inertial Coriolis force combined with an optical readout performed by an injection interferometer, as presented in [14.28].

Today optical gyroscopes are the most accurate sensing devices on the market but too expensive to be used for low-cost consumer applications. In contrast to conventional gyroscopes, optical gyroscopes have no rotating parts, which, generally, is an asset. An integrated approach to the design of a single-rotor optoelectronic gyrocoordinator is described in [14.29].

14.5. A TOPICAL REVIEW OF GYROSCOPES

A comprehensive paper on gyroscopes’ classification has been recently written by Chinese researchers in Shanghai [14.30]. They are grouped in macroscopic devices {classical gymbal (See C.14.2!) or ring laser} and micro-gyroscopes, combining the mechanical movement and sophisticated electronics, and mostly fabricated by silicon bulk-micromachining, as categorized in Table 14.2.

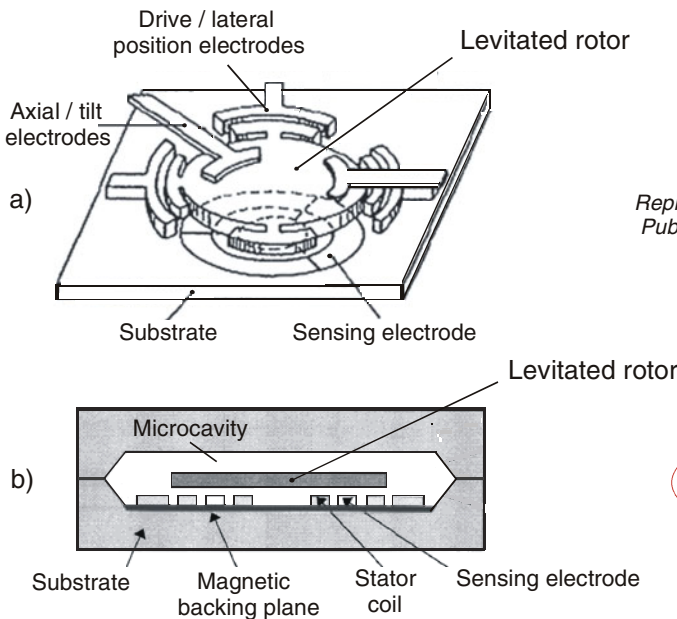
A levitated rotor gyroscope consists of a spinning rotor working on the principle of a classical gyroscope, and can be used as a dual-axis gyroscope but also as a tri-axis accelerometer.

Table 14.2 Different types of micro-gyroscopes

Micro-gyroscopic measurement principle	Section in this handbook
Coriolis Force	14.3
Levitated rotor	See below!
Optical (Sagnac and MOEMS)	14.4.1, 14.4.3
Nuclear magnetic resonance (NMR)	14.4.2, end of 14.5

There are two possibilities of levitation:

- Electrostatically suspended and sensed micromechanical rate gyroscope, demonstrated by SatCon Company early in 1990s [14.31], comprising a disc-shaped rotor with flange (the active conductive layer composed of structural polysilicon and separated from the other conductive layers by an insulating silicon nitride layer) and five sets of actuators for position control in both axial and radial directions (Fig. 14.13a).
- Electromagnetically levitated rotor based on the phenomenon that a conductive circular plate can be stably levitated above two groups of concentric coils (Fig. 14.13b); in 1995, Shearwood *et al.* realized such a structure by micromachining technology [14.32].



Reprinted with permission IOP Publishing Ltd. from [14.30]



Fig. 14.13 General view of an electrostatic levitation type of gyroscope (a) and schematic cross-section of an electromagnetic levitation micro-gyroscope (b)

Micro-gyroscopes based on nuclear magnetic resonance use the following phenomenon: if a static magnetic field H_0 is applied, the atoms tend to line up along the field lines and their magnetic moments will rotate about the direction of the intensity H_0 at a rate known as the Larmor precession frequency:

$$\omega_L = \gamma \cdot H_0 \quad (14.2)$$

where γ is a constant called the gyromagnetic ratio, depending on the type of material used.

In recent years, the combination of a cryogenic superconducting quantum interference device (SQUID) with the nuclear magnetic resonance in gyroscopes has overcome the difficulty of NMRGs picking-up of weak signals [14.33]. Such an inertial-grade atomic gyroscope achieves the highest performance in laboratory, being in connection with AFM (atomic force microscopy) technique.

The measurement of the rigid solids' rotation is of considerable interest in a number of areas. Rotation detectors are not only used in aircraft, missiles and other military fields, they have also been developed for new civil fields such as automobile navigation, antenna stabilization, crane control, unmanned vehicle control, wind and renewable energy platform stabilization.

REFERENCES

1. http://www.tpub.com/content/neets/14187/css/14187_137.htm
July 25 (2009)
2. Pörschmann, C.: 3-D audio in mobile communication devices: Methods for mobile head-tracking. *Journal of Virtual Reality and Broadcasting* 4(13) (October 2007)
3. Tawfik, H.H.: A glimpse at MEMS – An introduction to MEMS world, July 29 (2009), <http://knol.google.com/...tawfik/...glimpse...mems>
4. Hunt, A. (Coord.): *Guide to the Measurement of Force*. The Institute of Measurement and Control, London (Published 1998); ISBN 0-904457-28-1
5. Zecchin, P. (Chair.): *Digital Load Cells – A Comparative Review of Performance and Application*. The Institute of Measurement and Control, London (2003); Document WP0803
6. Kasahara, M., Kurosu, S., Adachi, M., Kamimura, K.: Analysis of a gyroscopic force measuring system in three-dimensional space. *Measurement* 28(4), 235–247 (2000)
7. Kurosu, S., Uchino, H., Kamimura, K.: Dynamical characteristics of gyroscopic force measuring apparatus. In: *Proc. 2nd Int'l Symp. Measurement of Force and Mass between Japan and China*, May 23-24, pp. 85–90. Tsukuba Science City, Japan (1994)

8. Kurosu, S., Adachi, M., Kamimura, K.: Performance of gyroscopic force measuring apparatus. In: Shi, C., Zhang, Y. (eds.) *Acta APMF 1996 – Present Situation and Progress of Measurement on Mass and Force*, Beijing, China, August 20-22, pp. 95–100 (1996)
9. Yang, J., Liu, S., Li, X., Zhi, J.: Studying and fabricating of model TLG-1 gyroscope force measurement transducer with high accuracy (GFMT). In: *Acta IMEKO XII, Measurement of Force, Mass, Pressure, Flow and Vibration*, Beijing, September 5-10, vol. 2, pp. 291–296 (1991); ISBN 7-80003-175-6/TB.18
10. Kourepenis, A.S., Weinberg, M.S., Elliott, R., Daley, S.: Force compensated comb drive. Patent Cooperation Treaty Application WO 2006099018, esp@cenet database (September 2006)
11. Skog, I., Händel, P.: Calibration of a MEMS inertial measurement unit. In: *CD Proc. XVIII IMEKO World Congress on Metrology for a Sustainable Development*, Rio de Janeiro, Brazil, September 17-22, Paper 376 (2006)
12. Kubena, R.L., Vickers-Kirby, D.J., Joyce, R.J., Stratton, F.P.: A new tunneling-based sensor for inertial rotation rate measurements. *Journal of Microelectromechanical Systems* (edited by IEEE) 8(4), 439–447 (1999)
13. Ryoo, H., Lee, Y., Roh, Y.: Design and fabrication of a dual-axial gyroscope with piezoelectric ceramics. *Sensors and Actuators A: Physical* 65(1), 54–60 (1998)
14. Sung, W.-T., Sung, S.K., Lee, J.G., Kang, T.S.: Design and performance test of a MEMS vibratory gyroscope with a novel AGC force rebalance control. *J. Micromech. Microeng.* 17(10), 1939–1948 (2007)
15. Bao, M.-H., Middelhoek, S.: *Pressure Sensors, Accelerometers & Gyroscopes*. In: *Handbook of Sensors and Actuators*, vol. 8. Elsevier Science, Amsterdam (2000)
16. Sahin, K., Sahin, E., Alper, S.E., Akin, T.: A wide-bandwidth and high-sensitivity robust microgyroscope. *Journal of Micromechanics and Microengineering* 19, Paper 074004 (2009)
17. Guo, Z.Y., Yang, Z.C., Zhao, Q.C., Lin, L.T., Ding, H.T., Liu, X.S., Cui, J., Xie, H., Yan, G.Z.: A lateral-axis micromachined tuning fork gyroscope with torsional Z-sensing and electrostatic force-balanced driving. *J. Micromech. Microeng.* 20, Paper 025007 (2010)
18. Netzer, Y.: Dual-axis resonator gyroscope. Patent Cooperation Treaty Application WO 2007105211, esp@cenet database, September 20 (2007)
19. Yan, H.: Phase-locked mechanical resonator pair and its application in micromachined vibration gyroscope. US Patent 6938483 (September 6, 2005)
20. Johnson, R.B.: The acoustic gyroscope, predecessor to the fiber-optic laser gyroscope (July 27, 2009), <http://www.abominablefirebug.com/AcousticGyro.html>
21. Oh, H., Lee, K., Wang, W., Yun, S., Yang, S.: Development of a novel surface acoustic wave MEMS-IDT gyroscope. In: Kullberg, R.C., Ramesham, R. (eds.) *Reliability, Packaging, Testing, and Characterization of MEMS/MOEMS and Nanodevices VIII*, Proc. SPIE, vol. 7206, February 9 (2009)
22. Varadan, V.K., Xavier, P.B., Suh, W.D., Kollakompil, J.A., Varadan, V.V.: Micro-electro-mechanical gyroscope. US Patent 6516665 (February 11, 2003)

23. Marcelli, E., Plicchi, G., Cercenelli, L., Bortolami, F.: First experimental evaluation of cardiac apex rotation with an epicardial Coriolis force sensor. *ASAIO Journal (American Society for Artificial Internal Organs)* 51(6), 696–701 (2005)
24. Scapellato, S., Cavallo, F., Martelloni, C., Sabatini, A.M.: In-use calibration of body-mounted gyroscopes for applications in gait analysis. *Sensors and Actuators A: Physical* 123-124, 418–422 (2005); French, P.J. (ed.): Special issue on the 18th Eurosensors conference on Solid-State Transducers
25. Fraden, J.: *Handbook of Modern Sensors – Physics, Design and Applications*, 3rd edn. Springer, Heidelberg (2004)
26. Zhang, B., Kahn, M.T.E.: Overview and improving fiber optic gyroscope based on MEMS/NEMS fabrication. *Journal of Physics: Conference Series* 34(1), 148–154 (2006)
27. Romalis, M., Kornack, T., Ghosh, R.: Nuclear-spin gyroscope based on an atomic co-magnetometer. Report for “John H. Glenn” Research Center, Cleveland, Ohio, January 1 (2008), <http://www.techbriefs.com/content/view/2565>
28. Norgia, M., Donati, S.: Hybrid optic-mechanical gyroscope with injection-interferometer readout. *Electronics Letters* 37, 756–758 (2001)
29. Raspopov, V., Ya., D.A.V.: The design of a single-rotor optoelectronic gyro-coordinator. (Russian) *Sensors and Systems Journal* (12) (December 2005)
30. Liu, K., Zhang, W., Chen, W., Li, K., Dai, F., Cui, F., Wu, X., Ma, G., Xiao, Q.: The development of micro-gyroscope technology (Topical review). *J. Micromech. Microeng.* 19, Paper 113001 (2009)
31. Torti, R., Gondhalekar, V., Tran, H., Selfors, B.: Electrostatically suspended and sensed micromechanical rate gyroscope. In: *Proc. SPIE*, vol. 2220, pp. 27–38 (1994)
32. Shearwood, C., Williams, C.B., Mellor, P.H., Yates, R.B., Gibbs, M.R.J., Mattingley, A.D.: Levitation of a micromachined rotor for application in a rotating gyroscope. *Electronics Letters* 32, 1845–1846 (1995)
33. Kornack, T.W., Ghosh, R.K., Romalis, M.V.: Nuclear spin gyroscope based on an atomic magnetometer. *Physical Review Letters* 5, Paper 230801 (2005)

Chapter 15

FORCE BALANCE TECHNIQUES

The three main methods used for the force measurement (Fig. 15.1) are:

- a) Mass balance, i.e. the unknown force is balanced against a known mass;
- b) Force balance, i.e. balancing force via a spring or magnet-coil arrangement;
- c) Deflection type transducers – measuring the deflection of an elastic element.

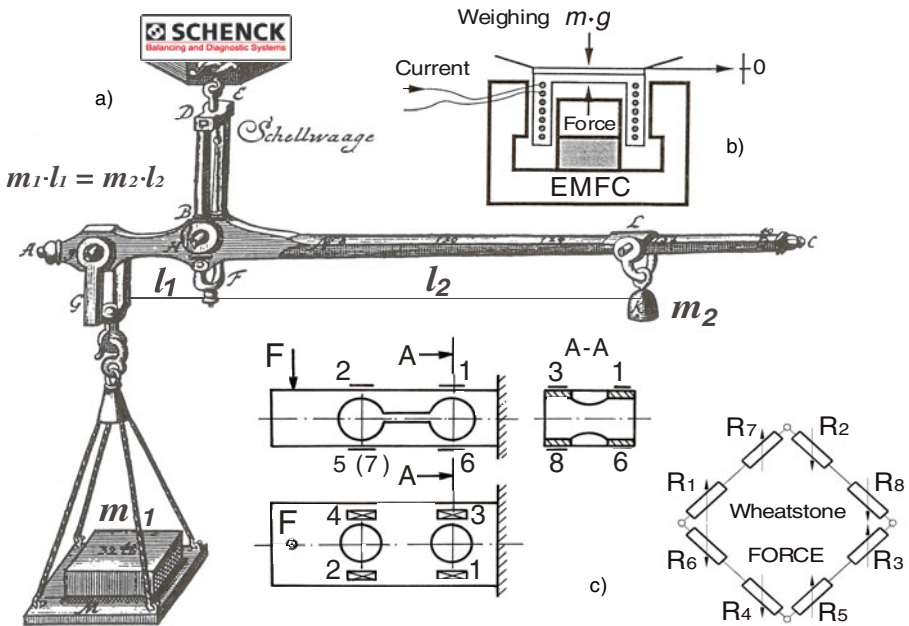


Fig. 15.1 a) Design drawing for a steelyard scale from the book “*Theatrum Staticum*” by Jacob Leupold [15.1]. b) Weighing by electromagnetic force compensation (EMFC) [15.2]. c) “Diagonal” combinations of strain gauges on a miniaturized elastic element for weighing and their Wheatstone bridge connection [15.3].

Force balance devices are often in the form of a beam balance operated as a feedback system, the tendency for displacement being detected and converted into a current fed to a magnet-coil, and producing a balancing force [15.4]. Feedback systems, sometimes referred to as inverse transducers, have considerable advantages in linearity and in calibration, since the overall response is governed by the passive feedback element.

15.1. FORCE BALANCE PRINCIPLE APPLIED TO TRANSDUCERS

There are differences between the transducers for measuring masses and forces not only by their definition [15.5]. Mass is a basic quantity of the SI System; force, on the contrary, is a derived quantity. The connection between the two is given by the acceleration ($F = m \cdot a$) but, in practice, only the forces effects can be sensed, using very different measurement principles (a dozen was widely described in Chapters 3 – 14).

Mass is a material property while force is a vector quantity. The mass standard for Metrology is achieved as an arbitrary artifact while force standards are derived from the mass ones. Both quantities cannot be measured directly, only by their effects which can be of manifold nature. The precise mass determination is made by measuring its force effect in the gravitational field of the Earth. The usable effects of force measurement techniques are mainly deformations and movements, as reactions in the sense of Newton's 3rd law. These can be as follows:

- weight forces and moments, acting directly or via levers and utilizing well-defined “balancing” procedures;
- field effects (e.g. electromagnetic or electrostatic);
- specially designed elastic elements, based on more complicated physical relationships (to be thoroughly presented in Chapters 21 – 33).

Pressure balance (Fig. 15.2a) is an alternative principle of force balance, usual for dead weight testers with hydraulic multiplication. The “balance” of pressures is illustrated by the following formula

$$p = \frac{F}{A_1} = \frac{F_w}{A_2} \quad (15.1)$$

where: F is the measured force, F_w is the force applied in the working system, A_1 and A_2 are the piston area for the measuring and working system.

The basic model of servo-type pressure-transducer (Fig. 15.2b) contains a pressure-sensitive element, whose deflection under pressure P provides an error signal that is fed into an amplifier.

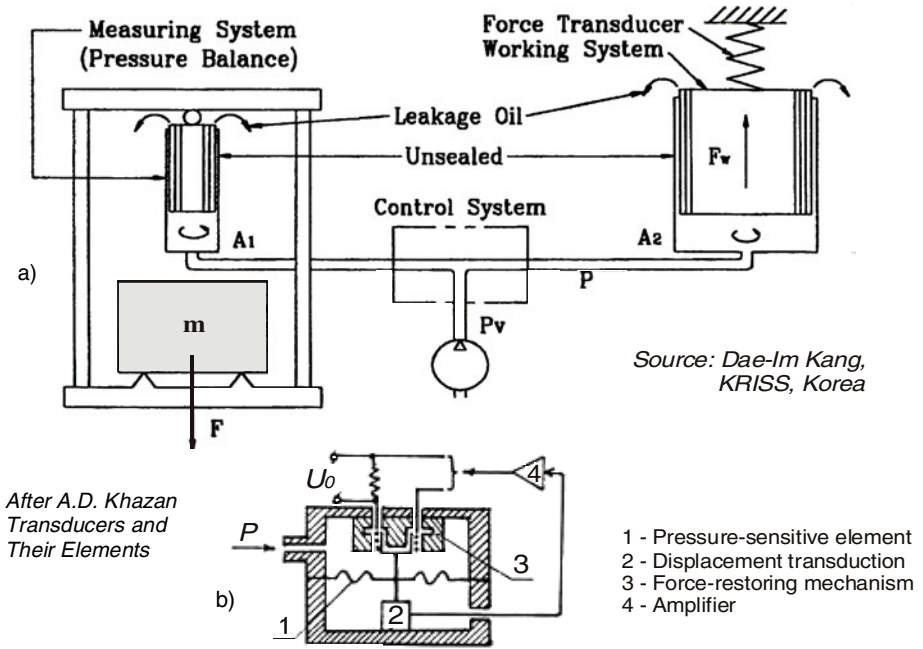


Fig. 15.2 a) Pressure balance (measuring system) + force transducer (working system) [15.6]. b) Servo-type pressure transducer based on a force-restoring mechanism [15.7].

The amplified signal excites a force-restoring mechanism that balances the force developed in the spring element due to the applied pressure. The current I_0 or voltage V_0 feeding the restoring system at the state of balance is a measure of the pressure.

Force-balancing is performed by a servomotor, the force coil of an electromagnetic system, or by a capacitive actuator while the displacement of the sensing element is detected by a transduction element (differential transformer, variable capacitor, photoelectric cell, etc.).

The dynamic analysis of a Foxboro force balance pressure transducer is described in [15.8]. Macro Sensors Company designed a pressure-balanced, oil-filled and double bellows-sealed LVDT assembly to enhance the reliability of multiple redundant LVDT-based extensometers mounted longitudinally around the circumference of the structural member to monitor overall integrity of offshore drilling platforms [15.9].

An accelerometer-based force balance system for shock tunnel testing is presented in [15.10]. As one can see, there is a close connection between force, torque, pressure, acceleration and other mechanical quantities. An integrated strain and force feedback system is described in [15.11].

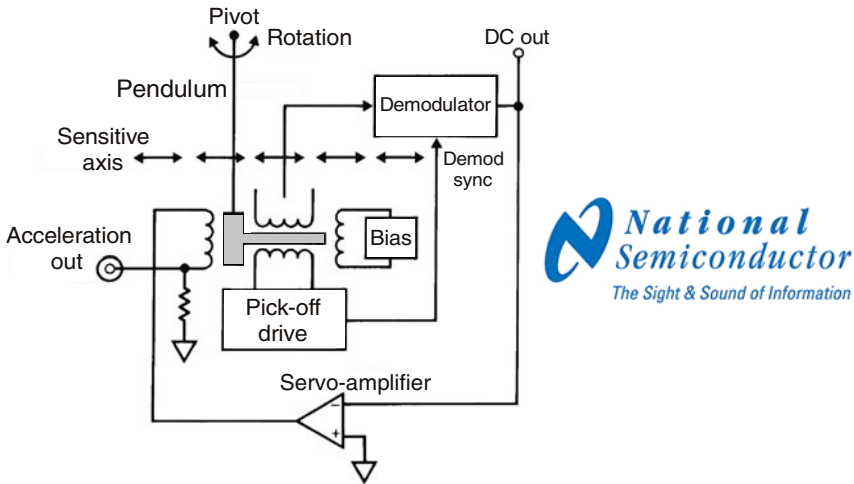


Fig. 15.3 Force-balanced accelerometer with linear variable differential transformer

The original advanced rheometric expansion system (ARES) had a force rebalanced transducer (FRT) installed in the system [15.12], which gives a good response for low torque application, but has a limited range (torque 0.02 kgf·m, force 2 kgf). The new ARES has a custom designed strain gauge transducer (Sensotec) that is more robust (torque 0.2 kgf·m, normal force 5 kgf) and gives better results. This is an “active” transducer using servo-controlled motor drive system back to its zero position after the capacitive sensing of displacement.

Strain gauged force transducers connected in Wheatstone bridges may be operated either in deviation mode or in self-balance mode.

The operating principles of the LVDT are applied in the force-balanced pendulous accelerometer [15.13]. These transducers feature wide dynamic range, high linearity and accuracy. Fig. 15.3 shows a conceptual form of this accelerometer. The device operates by means of an LVDT-type pick-off to determine the position of the pendulum. The DC output of the LVDT is fed to a servo-amplifier which drives the torque coil whose magnetic output completes a servo loop around the pendulum, forcing it to become immobile. Because the torque coil’s field can only attract the pendulum, a second bias coil provides a steady force for the torque coil to work against. When an input acceleration occurs along the sensitive axis, the servo applies the necessary current to the torque coil to keep the pendulum from moving. The amount of current required is directly proportional to the value of the input acceleration.

Force-balanced accelerometers are widely applied in aircraft inertial guidance systems, aerospace applications, seismic monitoring, shock and vibration studies, oil drilling platform stabilization and similar applications.

The force balance technique is also applied to other types of transducers, using various measurement principles:

- The radiation force balance is a gravimetric balance for determining the ultrasonic power in liquids (Fig. 13.8).
- A gyroscope is a dynamically force-balanced transducer. Figure 14.7 has depicted a MEMS gyroscope with automatic force rebalancing control.
- A floating rotameter, acting as force balance indicator, is depicted in [15.14].
- A model of force balance between the electrical forces and fluidic drag for ethanol-suspended SnO_2 nanobelts in a PDMS channel was developed in order to estimate the frequency-dependent dielectrophoresis (DEP) force and torque magnitudes from the angular motion induced by repulsive forces [15.15]. This experimental method can be also used for the electrokinetic characterization in the low frequency range (<100 kHz) electric fields of other elongated nanostructures, such as nanowires and nanotubes.
- A capillary force balance objective microscope (a feedback-loop in Atomic Force Microscopy) for studying sludge particles dispersion within the Environmental Management Science Program is presented in [15.16].

15.2. ELECTROMAGNETIC FORCE COMPENSATION (EMFC)

Historically, the first force based magnetometer has been called Faraday (or magnetic) balance (Fig. 15.4a). It has a set of magnetizing coils used to magnetize a sample while a second set of coils generates a field gradient which results in a force on the sample to be measured by a balance or force transducer.

The electromagnetic force balance uses a feedback circuit to compare the electrical output to the force input [15.17]. A typical EMFC system [15.18] has attached to the force input part an electrical coil which operates in the flux gap of a permanent magnet (Fig. 15.4b). An electric current passed through this coil generates a restoring force in opposition to the applied force.

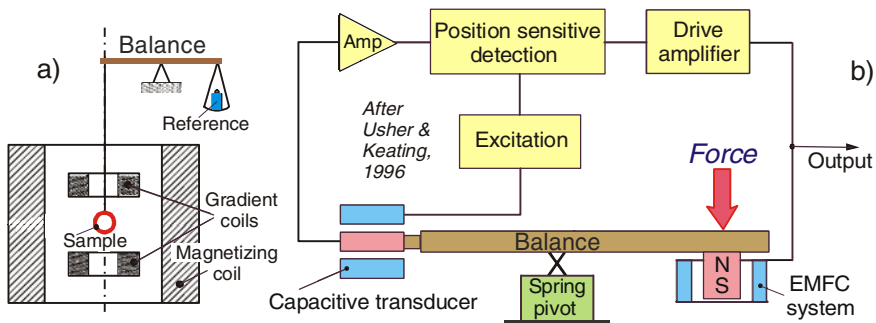


Fig. 15.4 Schematic of magnetic (a) and electromagnetic (b) force balances

A capacitive transducer is used to sense the displacement of the force input lever, its output being amplified and used to control the current in the coil until the restoring force exactly balances the applied force and restores the force input lever to its initial position. The coil current to achieve this balance is proportional to the applied force and is measured as a voltage sensed across a resistor in series with the coil. This balance has good dynamic performance, small deflection and low sensitivity to environmental conditions.

EMFC devices for weighing were detailed in Figures 7.12 and 7.14. They are reliable and well-established weighing instruments having mass ranges from two grams to several kilograms. They also represent a highly stable and linear force scale. An application for conveyor belts is presented in [15.19].

Here is another kind of application for force standard machines (FSM) having a range of a few newtons and a feed-back stabilized resolution of micro-newtons [15.20]. The set-up diagram of an electromagnetically compensated balance (ECB) is shown in Figure 15.5. Sartorius WZ 215-cw (210 g) or WZ 1203 (1200 g) are used as force transducer. The piezoactuator is a 100 μm PIFOC[®] with a capacitive transducer and a PI controller. A U1A strain gauged transducer and a precision DMP40 amplifier (HBM) serve for testing purposes. The rack, including the traverse, the stage and the basis, clamps the ECB, the force transducer under test and the force generator together. The spring constant of this rack is 1 MN/m, i.e. applying a load of 1 N produces a 1 μm bending.

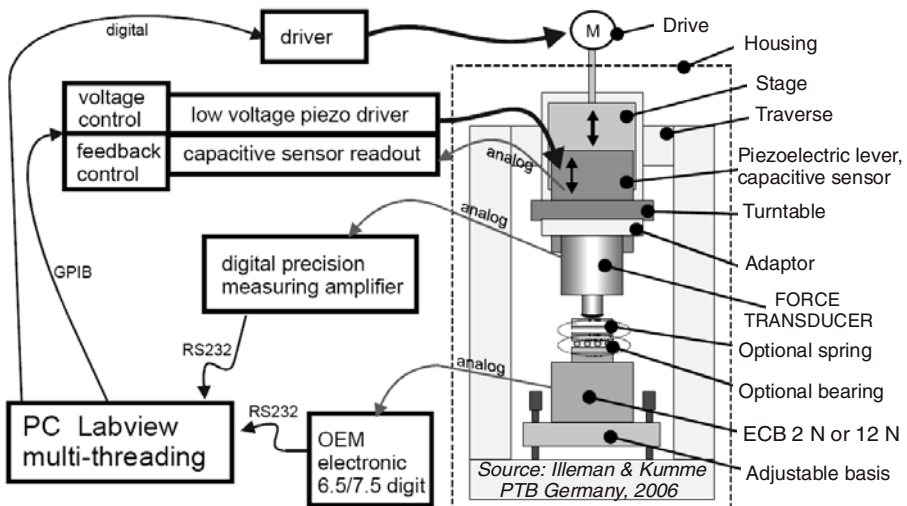


Fig. 15.5 The PTB electromagnetically compensated balance (ECB) – a suggestive representation of a variety of measurement principles (resistive – using strain gauges, capacitive, piezoelectric and electromagnetic) and computerized signal processing

The traceability to the force definition is realized by the subsequent calibration of this balance with newton-equivalent deadweights.

The universal force microscope for surface force measurements has replaced the mechanical spring of the original apparatus (Israelachvili, 1978) with a bimorph. The bimorph is operated as a force detector by producing an electric charge upon its plates, but this charge will decay away through the stray resistance.

With the electromagnetic force-feedback technique a force equal in magnitude but opposite in sign to the surface force is applied externally by a negative feedback system to return the bimorph voltage to zero with the object of minimizing its deflection [15.21]. Thus, using an amplifier with a very high input impedance to buffer the bimorph, the integrator time constant is much smaller than that of the bimorph and the errors are negligible.

15.3. ELECTROSTATIC FORCE COMPENSATION

Just like the electromagnetic (or electrodynamic) force compensation, the electrostatic force compensation uses “active” cantilever probes [15.22] for measuring micro- and nano-forces (See Figure 7.15).

The capacitive force-balance sensing technique [15.23] is illustrated in Figure 15.6. Through a large-valued resistor, R_{FB} , a DC voltage can be fed back. Two equal-valued but opposite-sign DC voltages $+V_0$ and $-V_0$ are added to the top and bottom plates driving signals, respectively, and a synchronous demodulator is inserted between the buffer and the amplifier A_0 .

Originally, the movable plate is at its balance position just in between two fixed plates. The distances on both sides are d_0 . In this case, the driving signal creates no signal at the input of the amplifier ($V_i = 0$) and no net force on the central plate.

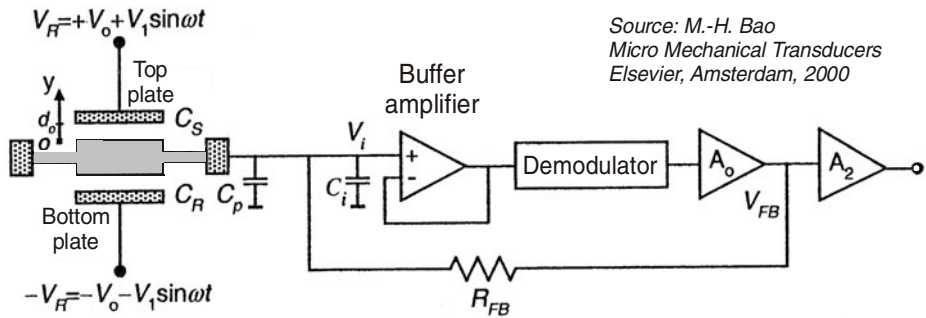


Fig. 15.6 Electrostatic force-balanced sensing technique (© 2000 Elsevier)

If the movable plate is then forced to move up by a distance y (i.e., in positive direction) by the action of a measurand (for example, an upward inertial force, $m \cdot a$, caused by a downward acceleration, a), an alternative signal V_i (with the amplitude V_1) appears at the input of the amplifier as:

$$V_i = \frac{y}{d_0} \cdot V_1 \cdot \sin \omega t \tag{15.2}$$

This signal is amplified and processed to feed back via R_{FB} a DC voltage, V_{FB} , to the input. If C_p and C_i are negligible, V_{FB} can be written as:

$$V_{FB} = +A_1 \cdot V_1 \cdot \frac{y}{d_0} \tag{15.3}$$

where A_1 is the open loop gain resulting from the buffer, the demodulator and the operational amplifier A_0 . Supposing that A_1 is positive and large, due to the positive DC voltage at the central plate, the electrostatic forces from the top plate and the bottom plate are no longer equal. The electrostatic force on the movable plate caused by the feedback is negative (i.e. in opposite direction to that of the inertial force, $m \cdot a$). Therefore, the displacement of the central plate is reduced by the electromechanical feedback. It can be proved that the displacement can be reduced significantly if A_1 is large enough so that the central plate remains at its original balanced position. Since the displacement of the central plate is very small, the measurand, a , is measured by the electrostatic force that balances the external force caused by the action of the measurand.

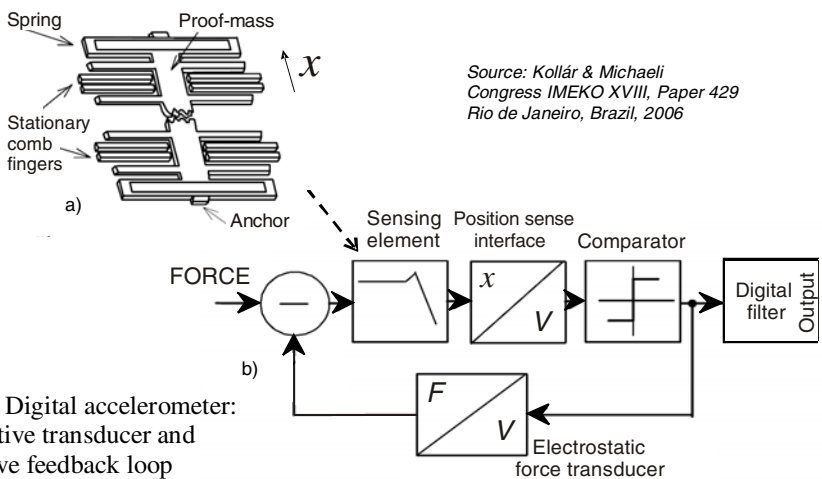


Fig. 15.7 Digital accelerometer:
a) capacitive transducer and
b) negative feedback loop

As the DC feedback voltage changes the electrostatic forces between the electrodes, the feedback is an electromechanical one. Thus, it is not a pure electrical measurement for capacitance but a close-loope electromechanical operation based on the capacitive sensing that gives results directly corresponding to the measurand. This measurement technique is referred to as capacitive force-balance method.

In a digital capacitive accelerometer [15.24], the proof mass is suspended above a substrate by compliant springs. Two nominally equal-sized sense capacitors are formed between the electrically conductive proof mass and stationary electrodes. When the substrate undergoes acceleration, the proof mass displaces from the nominal position, causing an imbalance in the capacitive half-bridge (Fig. 15.7a), measured by charge integration technique. Force balancing of the proof mass is attained by enclosing it in a negative feedback loop (Fig. 15.7b), which measures the deviations of the proof mass from its nominal position and applies a force to keep it centered. The digital accelerometer output is taken as the force needed to null or zero the position.

Another force-balanced MEMS transducer was developed to measure the forces between two surfaces with controllable distance [15.25]. Its mechanical structure is like a pendulous micromachined accelerometer, and it is designed as a closed-loop system with electrostatic force compensation.

The realization of micronewton forces in a manner traceable to the International System of Units using the NIST electrostatic force balance (EFB) (Fig. 15.8) is reported in [15.26].

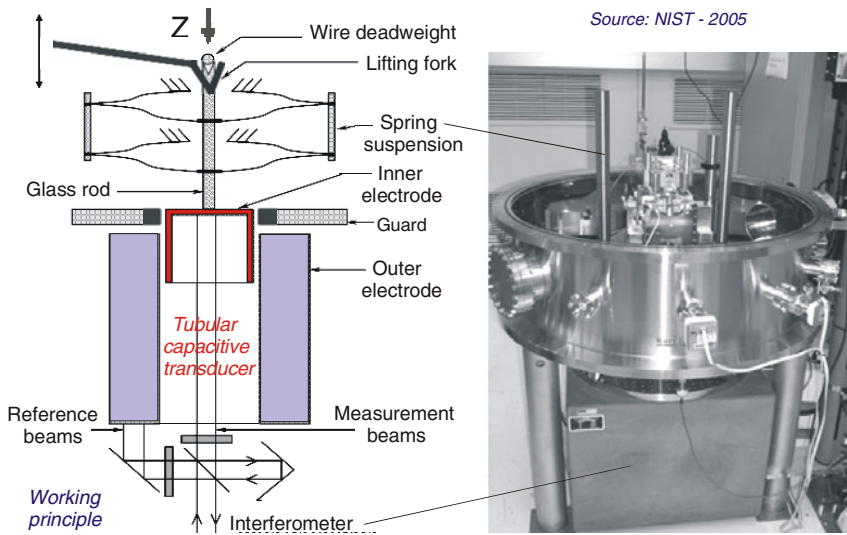


Fig. 15.8 SI realization of small forces using an electrostatic force balance

A comparison between the deadweight method and EFB is presented at a force level of approximately 200 μN , demonstrating a good agreement between these two independent measurements, at a level consistent with the uncertainties in 20 mg mass artifacts. The force sensitivity of an atomic force microscope can be directly calibrated using an *in situ* realization of a primary standard based on electrostatic forces ranging from 320 pN to 3.3 nN with an accuracy of a few percent [15.27].

15.4. OPTICAL DEVICES BASED ON FORCE FEEDBACK

A 5 mm diameter tri-axial force transducer has been developed for minimally invasive robotic surgery [15.28] within a research sponsored by the Belgian programme on Interuniversity Poles of Attraction. To define the required force range and resolution, a needle driver has been equipped with strain gauges and tested *in vivo*. The three components (F_x , F_y , F_z) should be measured with a range of ± 2.5 N. The required resolution is set to 0.01 N (0.2 % of the range) to assure a minimum of feeling during manipulation of soft tissues like liver.

The design tries to decouple the deformations caused by axial and radial forces, by using four identical parallelograms placed in an axisymmetric arrangement (Fig. 15.9a). An axial force causes the thin horizontal beams to bend, while the thick vertical beams deform negligibly. For a radial force, the opposite occurs: the vertical beams deform while the horizontal beams are mainly stressed longitudinally, a direction in which they have a high stiffness. The flexible structure is optimized using finite elements calculations, and the circular holes are starting points for the wire-EDM (electro-discharge machining) process used to machine the L-shaped slits.

The new transducer is based on a flexible titanium alloy (Ti6Al4V) of which the deformations are measured through reflective measurements with three optical fibers. Titanium material has a good corrosion resistance, superior biocompatibility, low Young's modulus and high strength (both maximizing transducer displacement), high fatigue resistance, and good shock resistance.

A design based on optical fibers that enable force reflection in the masters was chosen for reasons of safety as no leakage currents or interference signals can originate from it (Fig. 15.9b). It consists of two parts connected by a flexible connection. The upper part is connected to the tool while the lower part is connected to the instrument shaft. Three optical fibers, arranged at 120° intervals in the lower part, measure the relative displacement between upper and lower part through the intensity of the reflected signal. Axial forces cause identical displacements above all three fibers, while radial forces (in fact the related torques) result in different or opposite displacements.

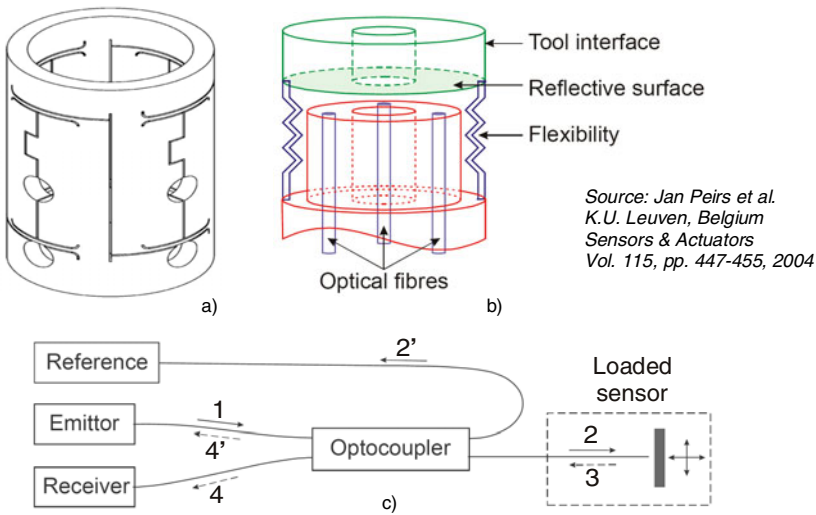


Fig. 15.9 Microoptical device with force feedback during minimally invasive robotic surgery: a) the optimized FEM design of the micromachined elastic structure; b) the basic layout of the optical device in which three optical fibers measure the deformation of the flexible structure through the intensity of the reflected light; c) two successive splittings (2-2' and 4-4') for the optical signal (Reprinted with Elsevier permission).

Figure 15.9c shows a possible configuration for each of the three sensing fibers in which the light is reflected back into the same fiber. An optocoupler has to be used to couple the emitter (LED) and receiver (photodiode) to the same measurement fiber. Maximum sensitivity is obtained when a 50/50-opto-coupler is used. This means that 50 % of the emitted signal (1) is coupled into the measurement fiber (2) while 50 % (2') goes to the reference photodiode. Similarly, the reflected signal (3) is split equally into the receiver (4) and emitter (4') fibers. So, after two successive splittings, maximally 25 % of the originally emitted light is sent back to the receiver (when this optical device reflects all incoming light).

Honeywell components were used for emitter (HFE4225) and receiver (HFD3228), and a 200 μm diameter sensor grade optical fiber with a numerical aperture of 0.37 (F-MBB, Newport). The emitter is fed with a 5 kHz sinusoidal signal with 0.85 V amplitude and 3.35 V offset, such that the LED remains in its linear domain. The receiver signal is filtered and amplified by two bandpass filters of 5 kHz in series.

These optical instruments are mounted on robot manipulators controlled by the surgeon through “joysticks” (masters). This way, the surgeon can perform the operation in a more ergonomic way and his hand movements can be scaled and filtered to remove trembling and to enhance accuracy.

Commercial robots for minimally invasive surgery are the ZEUS[®] system from Computer Motion and the Da Vinci[®] system from Intuitive Surgical.

After this review of a variety of *force balance* techniques, it is necessary to emphasize the different meanings of the term “*balance*”, e.g. weighing scale, wheel, tyre or gravimetric *balances*. From the point of view of the measuring methods, one of the most complex applications is represented by the multicomponent *tensometric balance* (Fig. 15.10) [15.29].

REFERENCES

1. Giesecke, P., Preusser, T.: Of scales and scale builders. Master craftsmanship presented by Carl SCHENCK AG, Darmstadt, Germany (1991)
2. Reber, D.: Electrodynamic force compensation devices in mass comparators. In: Proc. 13th Int'l Conf. Force and Mass Measurement, Helsinki, Finland, May 11-14, pp. 205–210 (1993)
3. Constantinescu, I.N., Ștefănescu, D.M., Sandu, M.A.: Mechanical Quantities Measurement by Tensometry. Editura Tehnică, București (1989) (in Romanian)
4. Usher, M.J., Keating, D.A.: Sensors and Transducers – Characteristics, Applications, Instrumentation, Interfacing, 2nd edn. MacMillan, Houndmills (1996)
5. Paetow, J.: Weighing cell and force transducer – there is a difference. Private discussions at Hottinger Baldwin Messtechnik GmbH in Darmstadt, West Germany (November 1987)
6. Kang, D.-I.: Design and application of force measuring system using build-up technique. PhD dissertation, KAIST, Daejeon, South Korea (1994)
7. Khazan, A.D.: Transducers and Their Elements. Prentice Hall Inc., a Pearson Education Company, Upper Saddle River, NJ (1994)
8. Soares, A.J., Kerlin, T.W., Miller, L.F.: Dynamic analysis of a Foxboro force balance pressure transducer. Trans. Am. Nucl. Soc. 43, November 19 (1982); Energy Technology Data Exchange Web, Washington, DC, USA, March 19 (2009)
9. High pressure and chemically resistant LVDTs enhance performance of extensometers used to monitor structural integrity of offshore platforms. Product News: Macro Sensors, Pennsauken, NJ. In: Sensors & Transducers e-Digest 101(2) (February 2009)
10. Sahoo, N., Mahapatra, D.R., Jagadeesh, G., Gopalakrishnan, S., Reddy, K.P.J.: Design and analysis of a flat accelerometer-based force balance system for shock tunnel testing. Measurement 40(1), 93–106 (2007); ISSN 0263-2241
11. Fleming, A.J., Leang, K.K.: Integrated strain and force feedback for high-performance control of piezoelectric actuators. Sensors and Actuators A: Physical 161(1-2), 256–265 (2010)
12. McKenna, G.B.: Advanced Rheometric Expansion System (ARES) (January 2007), <http://www.che.ttu.edu/McKennaGrp/ares.htm>

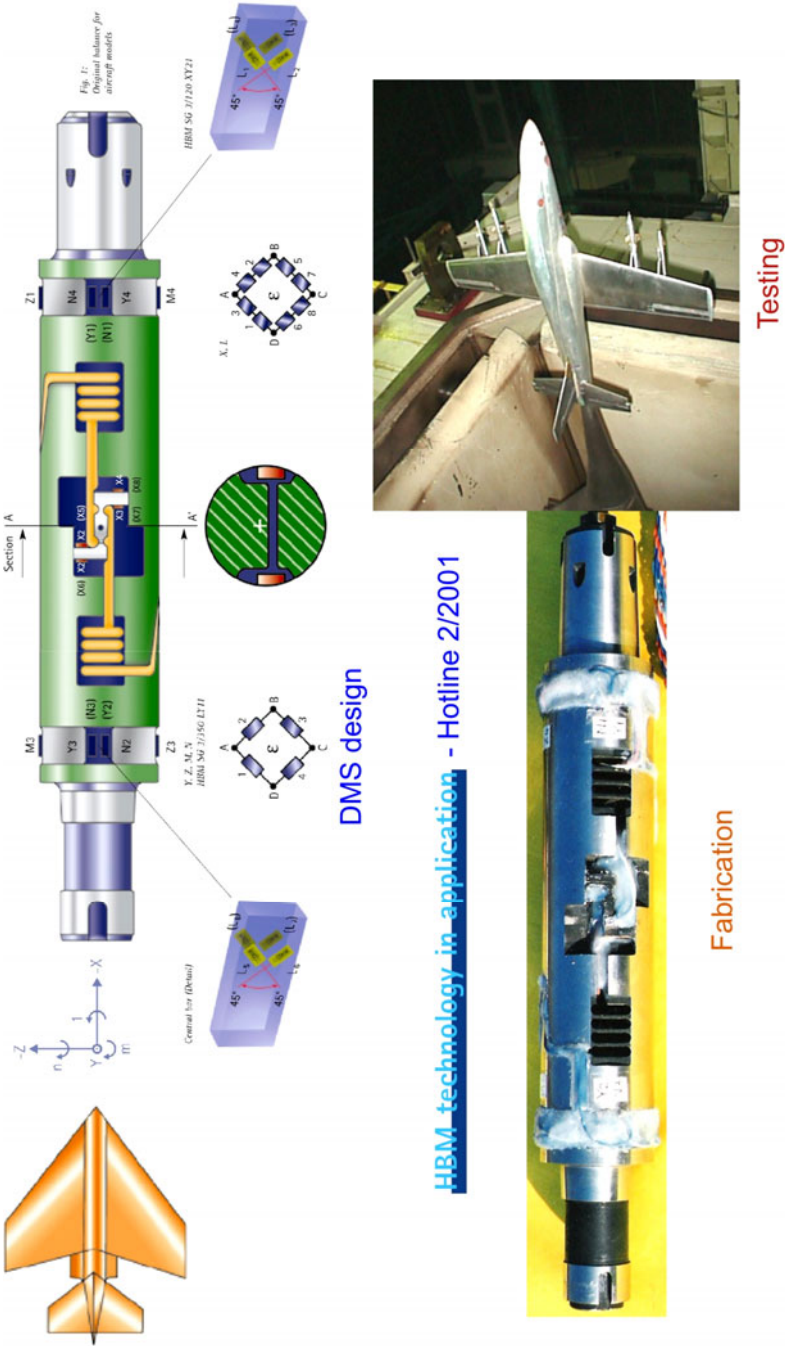


Fig. 15.10. Multicomponent strain gauge balance for wind tunnel

13. Signal conditioning for sophisticated transducers. Application Note AN 301–82 (2002) © 2002 National Semiconductor Corporation
14. Platil, A.: Mechatronics sensors: flow and level. PDF created on April 19 (2005)
15. Kumar, S., Hesketh, P.J.: Estimation of frequency-dependent electrokinetic forces on tin oxide nanobelts in low frequency electric fields. *Nanotechnology* 21, Paper 325501 (July 2010)
16. Hobbs, D.: A Capillary Force Balance objective microscope for studying sludge particles dispersion (January 2007),
<http://www.srs.gov/general/scitech/srtc/srtchtm/emsp>
17. Hunt, A. (Coord.): Guide to the Measurement of Force. The Institute of Measurement and Control, London (Published 1998); ISBN 0-904457-28-1
18. Usher, M.J., Keating, D.A.: Sensors and Transducers – Characteristics, Applications, Instrumentation, Interfacing, 2nd edn. MacMillan, Houndmills (1996)
19. Yamakawa, Y., Yamazaki, T., Tamura, J., Tanaka, O.: Dynamic behaviors of a checkweigher with electromagnetic force compensation. In: Proc. XIX IMEKO World Congress, Lisbon, Portugal, September 6-11, pp. 208–211 (2009)
20. Illemane, J., Kümme, R.: Research for a national force standard machine in the range from micro Newton to Newton relying on force compensation. In: Proc. XVIII IMEKO World Congress, Rio de Janeiro, Brazil, September 17-22, Paper 180 (2006)
21. Stewart, A.M.: The use of piezoelectric bimorphs to measure forces in colloidal systems. *Meas. Sci. Technol.* 6, 114–123 (1995)
22. Kim, M.-S., Choi, I.-M., Park, Y.-K., Kim, J.-H., Kang, D.-I.: SI traceable force balance at the micronewton to nanonewton level. In: Zhang, Y., et al. (eds.) Proc. 6th Asia-Pacific Symposium on Measurement of Mass, Force and Torque, APMF 2003, Shanghai, China, November 3-6, pp. 53–56 (2003)
23. Bao, M.-H.: Micro Mechanical Transducers – Pressure Sensors, Accelerometers and Gyroscopes. In: Middelhoeck, S. (ed.) *Handbook of Sensors and Actuators*. Elsevier, Amsterdam (2000)
24. Kollár, M., Michaeli, L.: Determination of the power spectral density in capacitive digital accelerometers using theory of limit cycles. In: Proc. XVIII IMEKO World Congress, Rio de Janeiro, Brazil, September 17-22, Paper 429 (2006)
25. Chen, H., Chen, D.: A new method to measure adhesion and surface forces using a closed-loop accelerometer. *Journal of Adhesion Science and Technology* 20(4), 307–318 (2006)
26. Pratt, J.R., Kramar, J.A.: SI realization of small forces using an electrostatic force balance. In: Proc XVIII IMEKO World Congress on Metrology for a Sustainable Development. Rio de Janeiro, Brazil, September 17-22, Paper 109 (2006)
27. Chung, K.-H., Shaw, G., Pratt, J.R.: Accurate picoscale forces for in situ calibration of AFM. In: Proc. XIX IMEKO World Congress on Fundamental and Applied Metrology, Lisbon, Portugal, September 6-11, pp. 402–405 (2009)
28. Peirs, J., Clijnen, J., Reynaerts, D., van Brussel, H., Herijgers, P., Corteville, B., Boone, S.: A micro optical force sensor for force feedback during minimally invasive robotic surgery. *Sensors and Actuators A: Physical* 115, 447–455 (2004)
29. Ștefănescu, D.M.: DMS in Windkanal — Rumänische Windkanalwaage mit Dehnungsmeßstreifen vom HBM. *Hotline HBM* (2), 12–13 (2001)

Chapter 16

MIXED METHODS IN FORCE MEASUREMENTS

This chapter comprises some applications which combine two or more force measurement principles, as well as force transducers based on sensors difficult to include in a certain category, like carbon nanotubes (CNTs).

With small dimensions and a combination of excellent mechanical and electrical properties, CNTs could find their way into nanoelectromechanical systems [16.1]. They have a Young's modulus of 1 TPa, i.e. five times larger than the best steel and also five times larger than high-quality carbon fibers, being considered to be the "ultimate" devices in this field. Their electronics applications spectrum includes field effect transistors and FET arrays, CMOS-integrated chemical- and bio-sensors, interconnected circuits for VLSI chips (vias). Two examples of mechanical quantities measurement are presented in Figure 16.1, with proper explanations given in Chapter 16.3.

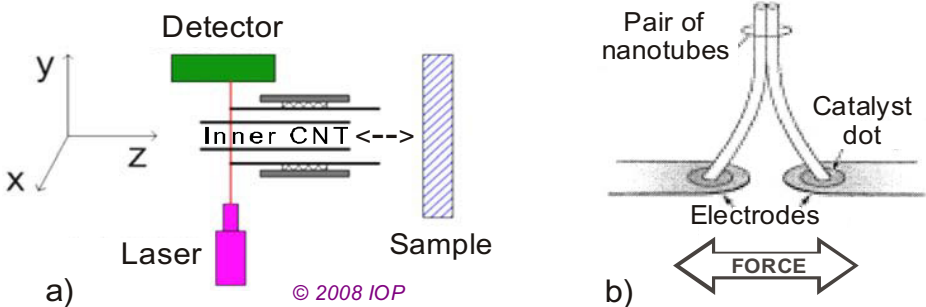


Fig. 16.1 a) A practical device for surface profiling, based on the nano-oscillator concept in the GHz range, where an inner tube from a finite length double wall CNT oscillates inside an open ended outer nanotube acting as a shutter for the laser beam path to the detector. b) Two CNTs grown out from catalytic metal dots on electrodes and attached to each other by van der Waals forces to form a bimorph sensor / actuator.

16.1. FORCE TRANSDUCERS USING ADVANCED ELECTRONICS

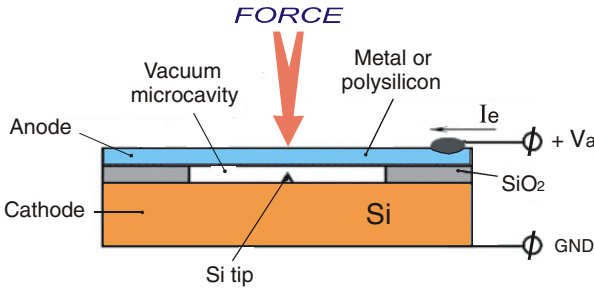
Solid-state piezoresistive potentiometers have replaced the classical ones (with wiper sliding on resistive wires or films), utilized in the field of mechanical quantities measurement [16.2]. Furthermore, their steady evolution has gone to silver-complexes as reversible electron transfer agents between the organic polymer film and the underlying solid-state conductor, resulting in highly reproducible starting EMF (electromotive force) values and improved initial signal stability [16.3]. Polymeric membranes (usually in force and/or pressure measurements) doped with appropriate lipophilic ion-exchangers can be also used to conveniently detect low levels of polyion species by simple potentiometry, based on a classical ion-selective electrode (ISE) configuration.

A transducer consisting of multiple layers of ionic polymer material is developed for applications in sensing, actuation and control [16.4]. A multilayer transducer is fabricated by layering individual transducers on top of one another. Each multilayer transducer consists of two to four individual layers of approx. 200 μm thickness. The electrical characteristics of the transducers can be varied by connecting the layers in either a parallel arrangement or a series one. The tradeoff in deflection and force is obtained by controlling the mechanical constraint at the interface. Packaging the transducer in an outer coating produces a hard constraint between layers and reduces the deflection with a force that increases linearly with the number of layers. This configuration also increases the bandwidth of the transducer. Removing the outer packaging produces an actuator that maintains the deflection of a single layer with an increased force output. This is obtained by allowing the layers to slide relative to one another during bending.

A model based on a linearly coupled, two ports, electrical equivalent circuit, to allow the design and evaluation of encapsulated ionic polymer transducers, is developed in [16.5]. Modal expansion is used to extend the applicability of the mechanical impedance terms through multiple resonances of the transducer. Charge sensing and blocked force {the maximum force an actuator can generate if blocked by an infinitely rigid restraint} were found to increase for a transducer after encapsulation, due to the higher coherence.

Solid-state actuators based on piezoelectric and magnetostrictive materials are characterized by forces reaching the range of kilonewton and reaction times in the range of microseconds [16.6]. Their multi-valued statical characteristics can be solved by driving in a closed loop control. The actual values, e.g. forces or displacements, are measured and fed to a controller, which generates suitable corrective signals in accordance with the intended values.

A force transducer with a silicon vacuum microcavity [16.7] has a cold field-emission cathode and a movable diaphragm anode (Fig. 16.2).



After J.C. Jiang et al.
Solid-State Sensors and Actuators
 IEEE Conference, New York, 1991

Fig. 16.2 Schematic of a vacuum diode force sensor (adapted from [16.8])

The cathode is a sharp silicon tip. When a positive potential difference is applied between the tip and the anode, an electric field is generated, which allows electrons to tunnel from inside the cathode to the vacuum, if the field exceeds 5×10^7 V/cm. The field strength at the tip and the quantity of electrons emitted (emission current) are controlled by the anode potential. When an external force is applied, the anode deflects downward, thus changing the field and the emission current I_e , expressed through the anode voltage V_a as

$$I_e = V_a^2 \cdot a \cdot \exp\left(-\frac{b}{\beta \cdot V_a}\right) \tag{16.1}$$

where a and b are specific constants and β is the tip geometry factor, which depends on the distance between the anode and cathode. To achieve a better sensitivity, the tip is fabricated with a radius of curvature of about $0.02 \mu\text{m}$.

Mechanical pressure applied directly to the thin-film transistors (TFTs) results in changes in carrier mobility, threshold voltage, and contact resistances [16.9]. The pressure dependence of pentacene transistors with solution-processed polyvinylphenol gate dielectric on glass substrates is investigated by applying uniaxial mechanical pressure with a needle. The force-induced change in drain and source currents is due to the distribution and activity of trap states at or near the semiconductor/dielectric interface. A force sensor could be considered as a field effect transistor [16.10], which additionally is contacted at both sides of its channel. The force measurement is based on the piezoresistive effect, mechanical stress onto the sensor rendering the channel resistance of the transistor anisotropic.

The fabrication of carbon nanotube field-effect transistors with semiconductors as the source and drain contact materials is depicted in [16.11]. A piezoelectric FET for nanoscale force and pressure measurements has been shown in Figure 6.4.

The restoration force of a radio-frequency microelectromechanical system (RF MEMS) switch has been improved by adopting a nonlinear spring [16.12]. When the electrostatic actuator, with 1.4 mm^2 movable electrode area, was driven at a voltage of 24 V, analysis showed a restoration force three-fold greater than that of conventional linear spring systems and a stable signal on-off control action, exceeding the characteristics of positive intrinsic negative (PIN) diodes or GaAs metal-semiconductor field-effect transistors (MESFETs).

CMOS (complementary metal-oxide-semiconductor), the most widely used integrated electronic circuit, appears in various force measurement principles, e.g.:

- 24-bit Sigma-Delta strain gauged bridge transducer for load cells,
- micromachined magnetic ultrasound transducer,
- amplified transducer for single photon read-out of photodetectors and integrated optical transducer assembly (US Patent 6963119).

Strain techniques, such as incorporating SiGe, should boost performance in future generations of CMOS silicon transistors without the need to radically miniaturize them [16.13]. A tensile layer improves the n-channel MOS devices while a compressive layer improves the pMOS ones. Other options: nonplanar multiple-gates (MuG) FET devices, high-conductive materials and metal gates.

Ion channels are mentioned like tools for monitoring lipid bilayer-membrane protein interactions as molecular force transducers {P. Michael Conn, *Ion Channels*, Part C, p. 294, Academic Press, 1999}.

A novel phenomenon of focused ion beam (FIB) induced bending of carbon nanopillars or cantilever beams is analyzed in [16.14]. The bending occurs during scanning due to temperature rise and gradients caused by the impinging ion beam. Its usefulness in the fabrication of nanosize mechanical components has been demonstrated by making a branch structure from a single cantilever.

Note: Do not confuse electronic ion beam with elastic cantilever beam!

16.2. CANTILEVER BEAMS FOR VARIOUS FORCE TRANSDUCERS

The majority of measurement principles can be applied to cantilever beams, the most widespread elastic elements [16.15]; among them are piezoresistivity, piezoelectricity, embedded transistor semiconductivity, optical beam deflection.

These cantilevers allow the sensitive detection of physical quantities such as forces and mass changes at submicron levels [16.16]. Two typical application examples are:

- *resonant cantilevers* for the mass-sensitive detection of volatile organic compounds. There is a spectacular combination of measurement principles: thin layer – ion beam – modal analysis – piezoresponse force microscopy.

Using the conventional actuation methods such as base excitation, the ratio of stiffness over the layer mass per unit length affects the resonant frequencies of the system as a single parameter [16.17].

- *force sensor arrays* for parallel scanning Atomic Force Microscopy of large areas. The first force sensors for application in AFM fabricated with industrial CMOS technology were presented in [16.18]. Sensing is based on two different detection schemes: a piezoresistive Wheatstone bridge and stress-sensing MOS transistors. The system combines on a single chip the following components:
 - two cantilevers for parallel scanning,
 - thermal actuators for independent deflection of the two cantilevers,
 - sensors to measure the deflection, and
 - offset compensation and signal conditioning circuitry.

The AFM probes were tested in contact and dynamic mode, recording images with a resolution of better than 20 nm.

Solid-state force transducers using folded cantilevers were made by chemical etching of a semiconductive wafer (US Patent 4783237).

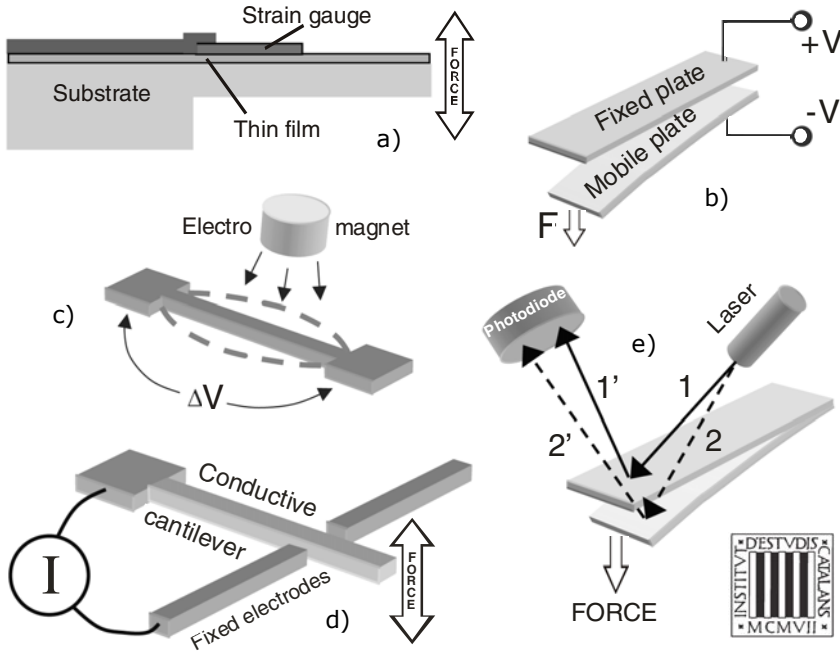


Fig. 16.3 Cantilever force transducer based on different measurement principles: a) piezoresistive thin film, b) capacitive plates, c) magnetomotive/electrodynamic sensing, d) electronic tunneling current, e) optical, i.e. laser emitter and photodiode detector

At the Institut d'Estudis Catalans, Barcelona, a few micro- and nano-mechanical structures fabricated by silicon micromachining technology are used as transducing elements in [bio]chemical sensors [16.19]. Cantilever beams with lengths in the tens of micrometers range and widths and thicknesses in the micrometer or sub-micrometer range are bent by forces in the range of intermolecular forces. Their deflection can be detected by optical or electrical methods and converted to an electrical output. There is a strong increase now in the use of mechanical transducers in chemical and biochemical sensors, as a result of the availability of microelectromechanical transducers which have better figures of merit, such as sensitivity, selectivity, linearity and drift. Five examples of cantilevers as basic tools for force transducers and using different measurement principles are shown in Figure 16.3.

The minimum measurable force value (6.94 pN) has been estimated by noise analysis [16.20] utilizing a strain gauged cantilever (See Figure 23.8).

Tellier and Leblois reported on GaAs microresonators with piezoelectric excitation and resistive detection using torsional vibration modes [16.21]. A piezoresistive four-terminal element is used to sense changes in frequency induced by a mechanical input. The geometries of (4 4 1) and (1 1 4) resonators are optimized for specific alignments of the {hhl} cantilever, fabricated by micromachining. A TENSOSIM simulator is used to predict etching shapes at the opening of the mechanical structure.

16.3. CNTs FOR MEASURING MECHANICAL QUANTITIES

A turning dynamometer measures static and dynamic cutting forces by using strain gauges bonded on octagonal rings and piezoelectric accelerometer respectively [16.22]. An innovative double-layer film force transducer is presented in [16.23]. It is based on a "sandwich" structure composed of two sensing elements glued together: one layer is a capacitive film and the other is a piezoelectric film. Both the layers are sensitive to compression loads, but they are suitable for working in different frequency ranges. In fact, while the capacitive element is capable of measuring from DC up to about 400 Hz, on the contrary the piezoelectric film works in the high frequency range. The output signals of both the sensors are acquired and then filtered and processed in order to achieve a single output signal, very useful for modal analysis. This piezo-capacitive sensor has been developed in order to synthesize, in a small, smart and cheap device, the capability to measure compression forces in a wide range of frequencies. Piezoelectric devices are basic sensors and actuators, strongly connected with other measurement principles and ensuring the ground for top technologies, such as bimorph and carbon nanotube.

The first direct observation of multi-walled CNTs was recorded in 1952 by Radushkevich and Lukyanovich [*Zurn. Fisic. Chim.* (1952) **26**, 88], while an image of a single- or possibly double-walled CNT was published in 1976 by Oberlin *et al.* [*J. Cryst. Growth* (1976) **32**, 335]. Aside from the controversy surrounding their discovery, the mechanical, electrical, and thermal properties of CNTs, combined with a low density, promise to revolutionize materials science and to realize exquisitely sensitive mechanical transducers [16.24]. Sumio Iijima reported the observation of multi-walled carbon nanotubes in 1991 [*Nature* **354**, 56-58]. Geim and Novoselov, Manchester University discovered graphene (a two-dimensional layer of carbon atoms that resembles “chicken wire”) in 2004 and won the Nobel Prize for Physics in 2010.

Single wall carbon nanotubes (SWCNTs) are hollow cylinders of graphene, composed of a single layer of carbon atoms that are densely packed in a honeycomb crystal lattice [16.25]. The length of the tubes can be several micrometers and the diameters are on the order of 1 nm, owing to very high aspect ratios. They reported gauge factors from -376 up to 856 for semi-conducting and small-gap semiconducting SWNTs, respectively.

CNTs can be connected in Wheatstone bridge (Fig. 16.4a), like piezo-resistors but can be also microresonators, piezoelectric or more complex electromechanical devices, integrated into MEMS-like structures. In the test stand shown in Figure 16.4b an individual SWCNT is connected to and fixed by electrodes being suspended from the substrate (electrodes: 1-2 nm Cr as adhesion layer, 30-50 nm Au as contact material). Force is applied to the tube via a precise mechanical interface (cantilever or bridge structure), actuated by an atomic force microscope.

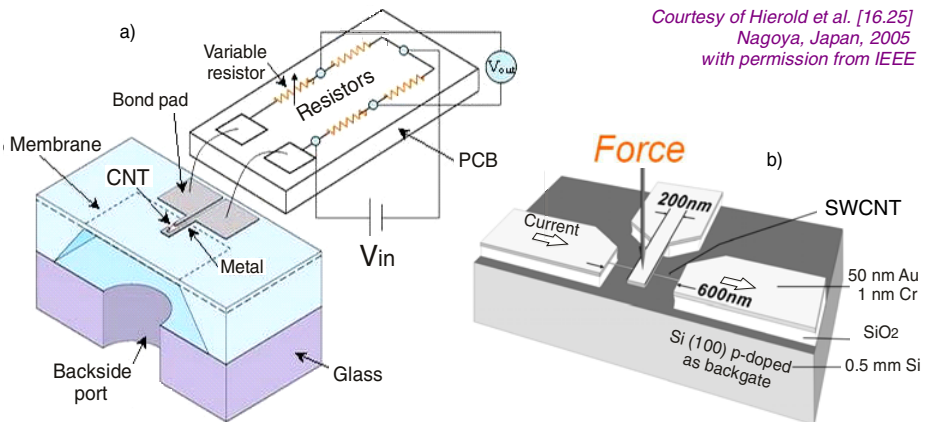


Fig. 16.4 a) Carbon nanotube on a pressure membrane, connected as an active arm of a Wheatstone bridge. b) Suspended single wall carbon nanotube force transducer.

A three-terminal memory cell based on cantilever CNT uses a conducting movable component, which could be a single- or multi-walled CNT, connected to a source electrode and suspended above a stepped Si substrate containing drain and gate electrodes [16.26]. In a nonconducting state '0', the nanotube is not in contact with the drain electrode (Table 16.1). When a voltage is applied between the source and the gate electrodes, charge is induced into the cantilever nanotube and it is deflected towards the substrate. At a certain, so-called "pull-in voltage", the nanotube comes into electric contact with the drain electrode, the device being now in a conducting state '1'.

Another form of electromechanical memories based on suspended CNTs has been developed and manufactured by the company Nantero, Inc. as a high-density, nanotube-based nonvolatile random access memory (NRAMTM). The project team at Mikroelektronik Centret in Denmark works on a new protocol to produce suspended nanostructures [16.27]. Three-dimensional pick-and-place assemblies of wire-like nanoscale components, such as carbon nanotubes and silicon nanowires, are examined inside a scanning electron microscope.

In Table 16.1 an insight is given into a new approach to storing memory bits based on carbon nanotubes. It employs a simple electromechanical switching rule, according to which the device is held together by a balance of three major forces: electrostatic, elastostatic, and van der Waals.

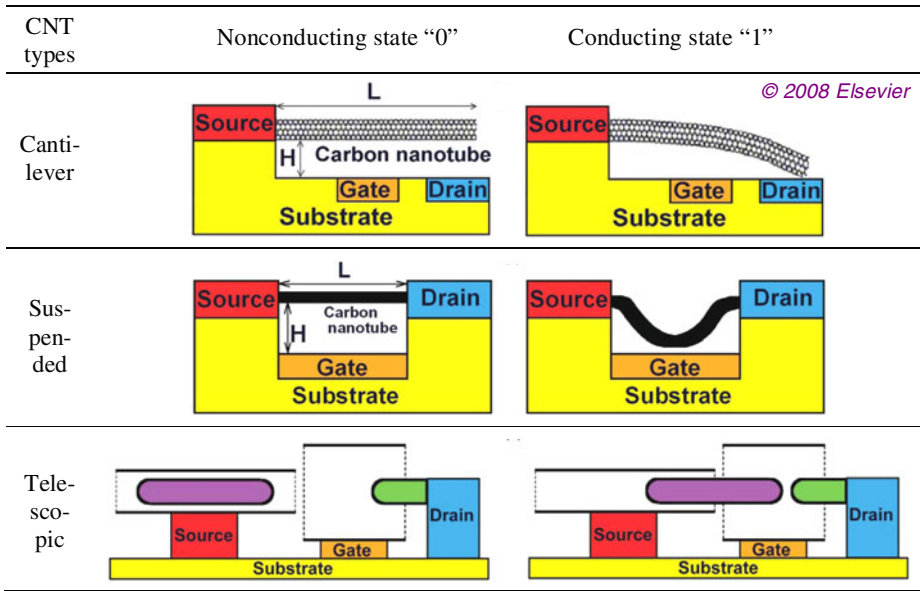
The achievement of the controlled and reversible telescopic extension of multi-walled carbon nanotubes (MWCNT) led to a suggestion for a route towards an electromechanical switch based on CNT telescopic extension (Copyright 2006 – American Chemical Society).

Low-friction, low-wear multiwall CNT bearings were demonstrated first by Cummings and Zettl [*Science* (2000) **289**, 602]. For example, if an inner tube from a doublewall nanotube is extruded with respect to the stationary outer tube, the inner tube can easily slide or rotate due to the intertube van der Waals interaction; their friction is at least two orders of magnitude smaller [16.28]. In Figure 16.1a there was a schematic configuration to monitor the inner nanotube oscillating motion for a profiling device.

Traditionally, a piezoelectric bimorph consists of two crystals or two thin strips cemented together e.g. a cantilever with two active layers which produce a displacement via electrical activation (electric field causes one layer to extend/expand and the other to contract). At NASA's Jet Propulsion Laboratory, Pasadena, California a proposal has been made to develop bimorph actuators and force transducers based on carbon nanotubes [16.29].

Because the electrical conductivity of a CNT perpendicular to its length is much lower than the electrical conductivity along its length, this configuration should make it possible to maintain a significant differential voltage across the two nanotubes, as needed to cause a differential length change in the pair.

Table 16.1 Three-terminal memory cells based on a cantilever CNT. A suspended structure is shown in Figure 16.4b and a telescopic profilometer in Figure 16.1a.



Conversely, the application of a lateral external force to the tip of the pair should give rise to a voltage between the electrodes so that this device can also function as a sensitive force detector.

The proposed bimorph device could be fabricated by growing two nanotubes by chemical vapor deposition (CVD) on closely spaced catalyst dots over prepatterned bias electrodes on a substrate (Fig. 16.1b). There are numerous potential variations on this basic fabrication scheme, including orienting the dots so that the nanotubes grow parallel (instead of perpendicular) to the substrate surface. These devices – proving a summum of qualities – would make possible novel microelectromechanical systems (MEMS), even microscopic robots.

A novel micrometer-sized mechanical force sensor that incorporates a polystyrene microsphere of 5 μm diameter attached to an individual MWCNT is presented in [16.30]. This simple device acts as a microcantilever beam whose deflection can be measured optically, since the sphere is large enough to be detected accurately with light (Fig. 16.5a). Calibration is made inside the scanning electron microscope (SEM). Once calibrated, it can measure forces as small as a few nanonewtons, e.g. the cell wall compliance in bio-chemistry. Force versus distance curves are shown (Fig. 16.5b) for six devices of varying nanotube lengths l [8 to 14.5 μm].

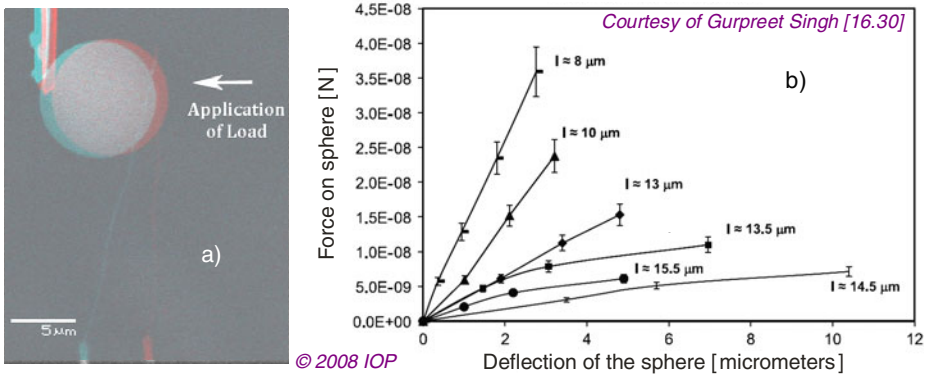


Fig. 16.5 a) A superimposed image from the first (dashed lines) and final load step from a CNT calibration test inside a scanning electron microscope. The tungsten probe is seen on the lower edge of the image. b) Force vs. distance curves for six CNT lengths.

16.4. COMBINED METHODS OF FORCE TRANSDUCTION

16.4.1. Force transducers in medical instruments

Optimal active compression and decompression (ACD) patterns have to be ensured during cardiopulmonary resuscitation (CPR). Two force transducers were integrated into the ACD device for continuously measure and display the required parameters [16.31]. Simple and safe in use, the modified CardioPump[®] with integrated electronics (Fig. 16.6a) provides an advanced solution for monitoring ACD-CPR on-line and accurately recording of compression and decompression forces and of compression frequency.

In addition to the mechanical force indicator, a cantilever beam (8 mm wide, 55 mm long) was mounted inside the handle of the CardioPump[®] as in Figure 16.6b). Onto the stainless steel cantilever beam HBM strain gauges (DK11G with nominal value 350 Ω) were glued 35 mm from the point of force transfer to the cantilever beam. This signal was amplified to yield 0.45 V/100 N covering a -300 N to +700 N force measurement range.

A force-sensitive resistor (FSR) element (8 mm in diameter, 0.5 mm thick) was fitted to the end of the central piston in such a way as not to restrict the removal or change of the silicon cup of the CardioPump[®] (Fig. 16.6c). When the device is pressed on to the casualty's chest, the silicon cup will deform. A force of about (110...130) N is necessary to deform the silicon cup to such an extent that its inner part is pushed by the piston against the casualty's chest. The FSR element senses this force and abruptly changes its electrical resistance at a loading force exceeding 120 N. Thus, both the beginning and the end of compression can be accurately determined.

Reprinted from [16.31] with permission from Elsevier

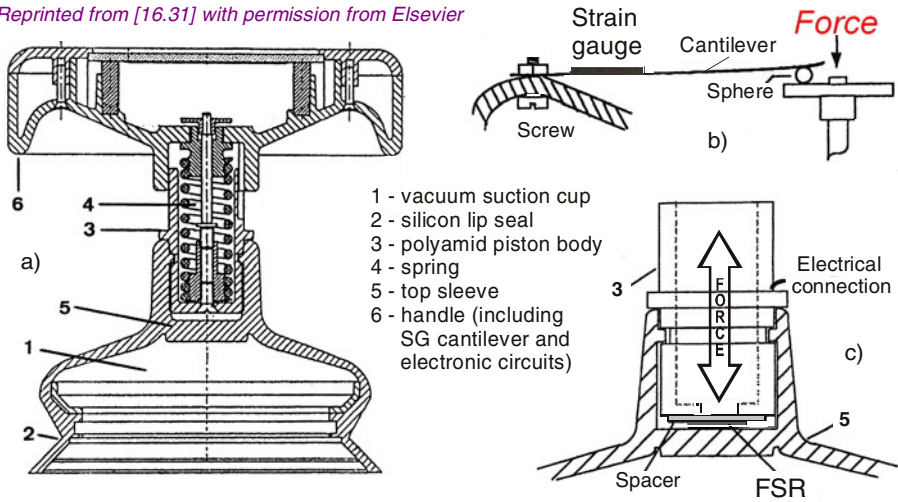


Fig. 16.6 Modified CardioPump® with integrated electronics (a). Cantilever beam with strain gauges (b) and force-sensitive resistor device (c) as force transducers.

Compression frequency was electronically determined by evaluating the force signal (Fig. 16.7): zero crossings were detected by software using the square FSR signals, their intervals were measured and, using the last 1.5 cycles, the mean value was computed. This value was converted into units of beats per minute and displayed on the monitor. For monitoring and recording all data a personal computer (Compact Concerto, INTEL) was available.

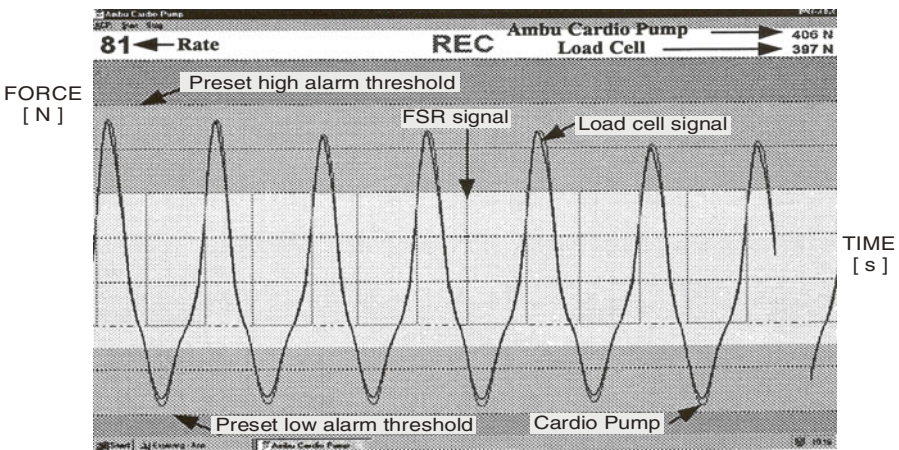


Fig. 16.7 The difference between the forces determined by CardioPump and calibration load cell is smaller than 2 % (406 N against 397 N). Copyright 1999 granted by Elsevier

Another model of CardioPump is based on a flat and thin, capacitive force transducer, pulse driven to realize low power consumption, when is used in the field [16.32]. The upper and lower parts on the capacitor plates are adapted to the rescuers hand and patient sternum, where the sensor is applied.

A strain gauge based transducer to measure isometric forces in parallel with magneto-encephalographic (MEG) recordings (i.e. without interference) is depicted in [16.33]. This device can be used in different geometries to measure forces in specific medical applications. Finally, on-line processing of the recorded forces, e.g., for the purpose of feedback, can be realized using standard MEG equipment.

16.4.2. EMAT (electro-magnetic acoustic transducer) and Lorentz force

An electromagnetic acoustic transducer is a non-contact NDT device that generates an ultrasonic pulse in the sample inspected instead of the transducer [16.34]. An EMAT induces ultrasonic waves into a test object with two interacting magnetic fields (Fig. 16.8a). A relatively high frequency (RF) field generated by electrical coils interacts with a low frequency or static field produced by magnets to generate a Lorentz force (Fig. 16.8b) in a manner similar to an electric motor. EMAT is capable of generating all wave modes used in ultrasonic testing (UT), including some modes that are very difficult or impractical with conventional piezoelectric transducers.

The main EMAT configurations are depicted in [16.35]: a tangential magnetic field makes forces normal to the surface (Fig. 16.8c) while a normal magnetic field makes tangential, shearing forces (Fig. 16.8d).

An active Lorentz force detuning compensation system is needed to reach high gradients in pulsed operation of superconducting cavities [16.36]. For this system a piezoelement or a magnetostrictive device can be used as an actuator. To guarantee the demanded lifetime of the active element, the proper preloading force adjustment is necessary. To determine this parameter an absolute force transducer is needed which will be able to operate at cryogenic temperatures. There is no calibrated commercial available transducer able to measure the static force in such an environment. The authors propose the testing of some effects caused by applied force: resistive, capacitive or resonance changes of the piezoelement. For complex evaluation during the design stages ANSYS Multiphysics is recommended, the most comprehensive coupled physics tool combining structural, thermal, computational fluid dynamics (CFD), acoustic and electromagnetic simulation capabilities into a single software product.

A calibration method for multicomponent microforce sensors using Lorentz forces is proposed in [16.37]. This method permits generation of six force and moment components in three orthogonal directions on 2D structures that can be fabricated using existing silicon micromachining technology.

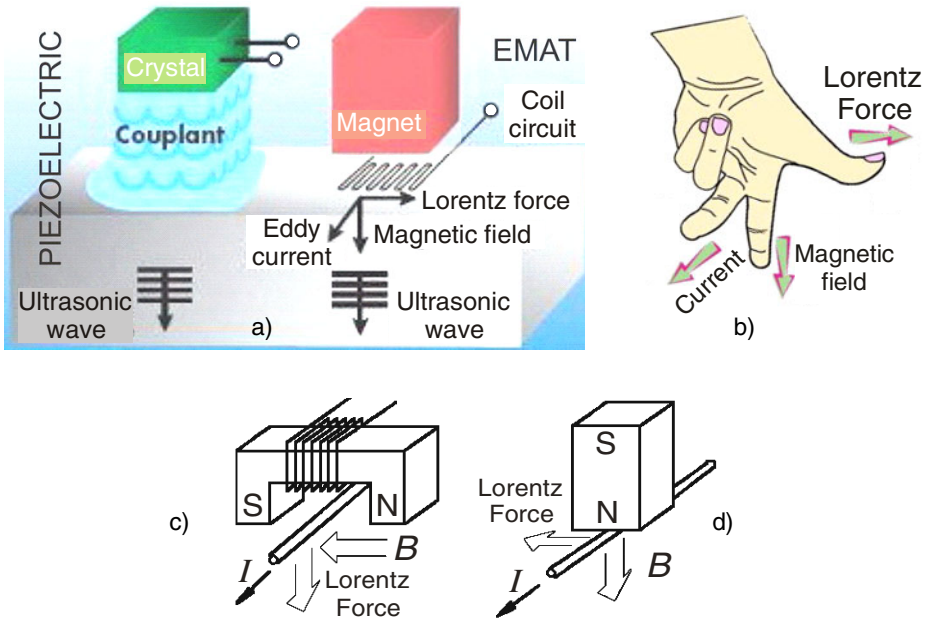


Fig. 16.8 Comparison of the piezoelectric and electromagnetic acoustic transducers (a); the Lorentz force sense as left thumb rule (b); normal (c) or tangential (d) Lorentz force

A Lorentz force based fusion magnetometer-accelerometer, which can detect simultaneously both geomagnetic field and acceleration is presented in [16.38]. A novel composite for magnetolectric transducers, presented in [16.39], shows a high DC magnetic field (H_{DC}) response when using the product of the Lorentz force effect from a metal ring in a DC magnetic field and the piezoelectric effect of a lead zirconate titanate (PZT) disc. The output voltage between the two faces of PZT shows a good linear response to the DC magnetic field ($< 1 \text{ kOe}$) under different AC electrical current inputs ($< 300 \text{ mA}$). The magnetolectric coefficient magnitude {about $33.2 \text{ mV}/(\text{T}\cdot\text{A})$ } can be manually controlled by the applied electrical current.

A Lorentz force flowmeter is a device originally proposed by Shercliff (1962) for the contactless measurement of flow rates in electrically conducting fluids [16.40]. Lorentz force velocimetry has a wide variety of potential applications in metallurgy, semiconductor crystal growth, and glassmaking.

Sandia National Laboratories, Defiant Technologies and the University of Louisville propose a smart preconcentrator (SPC) consisting of a pivot-plate resonator (PPR) based on Lorentz-force driving and electrical impedance measurements [16.41]. A free-standing paddle of silicon is

suspended from a silicon frame by two torsional beams. An AC current, I , passes through a metal transducer line encircling the paddle. This current interacts with a transverse, in plane magnetic field, B , generated by a pair of miniature permanent magnets situated along the die edges. The Lorentz force ($F \sim I \cdot B$) creates a torque on the paddle that changes direction with the phase of the AC current oscillation. Subsequent to microfabrication, the SPC was coated with an adsorbent for collection of chemical analytes. The frequency of operation of the SPC varies inversely with the mass of collected analyte.

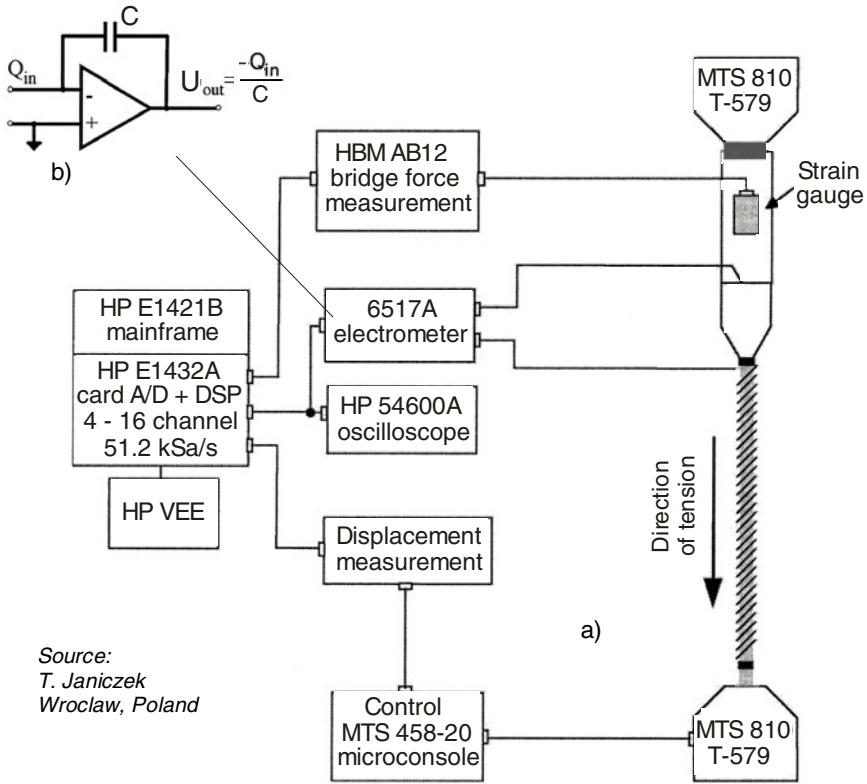
A semiconductor fabrication process has been applied to prepare resonant AlN and SiC beams operating at radio frequencies (between 0.1 and 2.1 MHz). The metallized beams were actuated in a permanent magnetic field of 0.5 T by the Lorentz force [16.42]. For systematic studies of the resonant frequencies and quality factors, the induced voltage was measured using time domain and frequency domain techniques. Resonator geometry, material and ambient pressure were varied to attain a generalized understanding of the RF performance. The dependence of the resonant frequency on tensile axial strain has been derived analytically and extended to include highly strained beams. Based on these formulas, accurate detection of the residual layer strain after fabrication is presented. To describe the quality factor a chain of beads model has been applied successfully. The influences of the beam width and the pressure-dependent viscosity on the model parameters are analyzed. MEMS resonators bear great potential for applications as RF sensors, filters and oscillators, e.g. in life sciences or information technology.

16.4.3. *Multitransducer equipment*

A complex installation for determining the elastic constants of rocks [16.43] uses inductive displacement transducers, combined with strain gauges bonded on a cage-shaped elastic element force transducer.

The analysis of PVDF transducer signals stimulated by mechanical tension is presented in [16.44]. The polyvinylidene fluoride cable was secured in special jaws to exclude any effects other than tension (Fig. 16.9a). The tensile force was measured using a manufacturer supplied strain gauged load cell, connected to an HBM AB12 bridge and the elongation was read out by a microconsole connected to the MTS 810 machine, utilizing internally mounted LVDTs. A Keithley 6571A electrometer (Fig. 16.9b) has measured the charge. All the measured signals: tensile force, elongation, charge were recorded via an HP workstation's analog-digital card in a HP VEE program.

The author is in course of preparing a second volume in order to explore the enormous field of force transducers applications, starting from the single-component force (and other mechanical quantities associated to force) transducers and finally developing multicomponent force-torque transducers for Robotics as well as sophisticated strain gauged balances for wind-tunnels.



Source:
T. Janiczek
Wroclaw, Poland

Fig. 16.9 Different measurement principles to evaluate a tensioned piezoelectric cable: a) strain gauges for force and LVDTs for displacement, b) electrometer for charge

16.4.4. Force transducers involving optical techniques

Ferroelectric thin films are important materials for integrated optical and piezoelectric principles in force measurement [16.45]. The piezoelectric coefficient of 100 nm thick polycrystalline films, measured by cantilever deflection with a Mach-Zehnder interferometer, was found: $d_{31} = -65 \text{ pC/N}$.

A cantilever-type silicon device for sensing pressure changes has been designed, fabricated and characterized in [16.46]. The cantilever with $9.5 \mu\text{m}$ thickness is surrounded by a thick and tight frame, since on the three free sides are only narrow, micrometer sized air gaps between the cantilever and frame. This design and excellent mechanical properties of single crystal silicon enable sensitive detection of time-dependent gas pressure variations, i.e. acoustic waves. The resonance frequency and the mechanical vibrational mode patterns of the cantilever have been determined using finite-element method (FEM) simulations and laser interferometry.

A miniaturized sensor capable of measuring high magnetic flux densities is presented in [16.47]. The magnetic flux density is converted into a movement of a micromachined U-shaped cantilever, which bears a thin film lead. The cantilever movement is accomplished by the Lorentz force. The cantilever acts as a deflecting mirror in an optical readout system. The ratio of the intensity of the light reflected by the front side of the cantilever to the intensity of the incident light is analyzed. The optical conversion principle was experimentally proven; it is well described by an optical near field model.

An indirect hanging pendulum thrust balance using a laser-optical-lever principle to provide micro- to millinewton force measurement for electric propulsion systems (e.g. hollow cathode microthruster) is presented in [16.48].

As the size of modern devices shrinks to micro- and nano-scales, the surface-to-volume ratio increases and the effects of body forces (gravity and inertia) become insignificant compared with those of surface forces (van der Waals, capillary, electrostatic, and chemical bonding). In micro-electro-mechanical systems, tribological and static interfacial forces are comparable with forces driving device motion. Atomic force microscopy is an ideal and powerful tool for studying nanoscale single asperity contact behaviors [16.49]. A typical AFM set-up is shown in Figure 16.10.

The end of the tip is typically modeled as a sphere with a characteristic radius of curvature, r_c (10...30 nm is typical for unused tips). The sharpness of this asperity provides new insights into a single asperity contact not observable at the macroscopic scale. The force acting at the tip deforms the cantilever vertically and/or laterally. A laser beam is reflected at the back of the cantilever and detected with a position-sensitive detector (PSD), which is then related to cantilever deformation. With various calibration methods, the normal (applied forces and adhesion) and lateral (frictional) forces acting on the cantilever can be determined with high resolution.

A new III-V cantilever-based atomic force sensor with piezoresistive detection and an integrated Hall probe for scanning Hall probe microscopy is reported in [16.50]. They propose a novel piezoresistive material based on the ternary alloy $n^+ \text{-Al}_{0.4}\text{Ga}_{0.6}\text{As}$ which allows the achievement of a cantilever deflection sensitivity $\Delta R/(R \cdot \Delta z) = 200 \mu\text{m}/\text{m}/\text{pm}$ at room temperature.

A batch fabricated scanning near-field optical microscope (SNOM) microprobe integrated with a piezoresistive cantilever beam with highly reproducible focused ion beam micromachined aperture is reported in [16.51]. In this way it is possible to produce cantilevers playing the role of a very sensitive AFM (atomic force microscopy) detector in special cases, e.g. vacuum and cryogenic temperatures. State-of-the art cantilever force transducers achieve quality factors between 10^4 and 10^7 , enabling the detection of forces less than a billionth of those needed to break a single chemical bond.

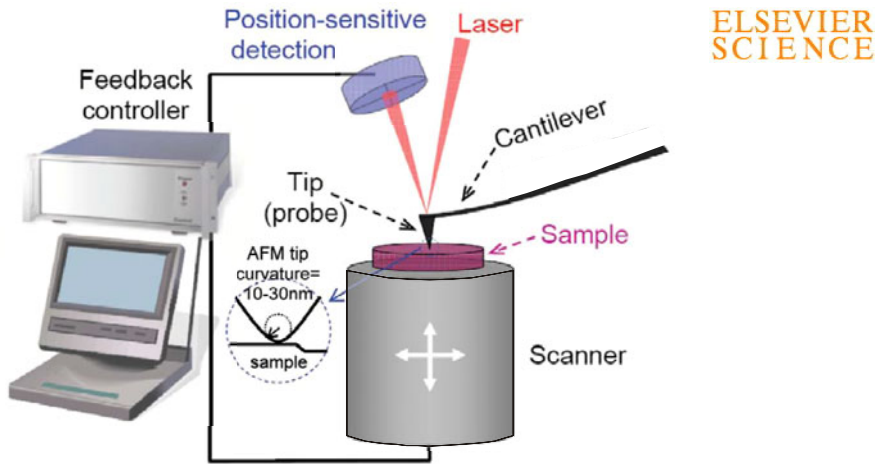


Fig. 16.10 Atomic Force Microscopy in nanotribology: probing cantilever deflection under load deviates the reflected laser beam position proportional with the applied force

Magnetic resonance force microscopy (MRFM) is a scanning probe technique that relies on the mechanical measurement of the weak magnetic force between a microscopic magnet and the magnetic moments in a sample. In MRFM, a nanomechanical cantilever is used to sense the tiny magnetic force arising between the electron or nuclear spins in the sample and a nearby magnetic particle. The advantage of force-detected over inductive techniques is that much smaller devices can be made [16.52]. An ultrasensitive mass-loaded Si cantilever, of 100 nm thickness and a spring constant under 100 $\mu\text{N/m}$, has been used as a force transducer in many of the latest MRFM experiments. Today it features a spin sensitivity that surpasses conventional, inductive nuclear magnetic resonance detectors by about eight orders of magnitude, having the potential to image matter with atomic resolution.

A team of Japanese researchers from Osaka University [16.53] proposes dynamic force microscopy (DFM), based on a frequency-modulation technique, that employs a high-stiffness quartz cantilever (performing at oscillation amplitudes as small as 0.1 nm) in combination with a low-noise interferometric deflection sensor, which exhibits a high sensitivity in force spectroscopy, even using a blunt tip.

By subtracting the huge van der Waals force contribution and minimizing the electrostatic force between the tip and the sample by means of a bias voltage, they obtained a short-range force curve that is in good agreement with the theoretical curve of the covalent bonding force between a Si atom from the tip apex and a Si adatom on the surface.

A readily available source of nanotube tips would further open up the AFM imaging world {materialstoday, 28 July 2009}, increasing tip longevity, reducing tip imaging artifacts, increasing resolution and decreasing tip–surface forces. It would also have a significant impact in key research areas such as structural biology, biotechnology, nanometrology and nanoelectronics.

The fabrication and characterization of carbon fiber tips for scanning probe microscopy (SPM) based on piezoelectric quartz tuning fork force transducers is presented in [16.54]. Their enlarged force sensitivity, in combination with high electrical conductivity and oxidation resistance, make them very convenient for combined STM / AFM imaging, i.e. simultaneous scanning tunnelling microscopy and atomic force microscopy measurements.

As professor Pertti Hakonen, Helsinki University of Technology said, *“A carbon nanotube is essentially an extremely thin but stiff piece of string and it can vibrate. As all guitar players know, heavy strings vibrate more slowly than the lighter ones, so if a suspended carbon nanotube is allowed to vibrate at its natural frequency, the frequency will fall if atoms or molecules become attached to the CNT”* [16.55].

Having in view the existing measurement techniques, the single electron transfer concept is more sensitive, while the field effect transistor concept is faster. Members of the consortium Cardeq have built a semiconducting nanotube into a transistor, so that the vibration modulates the current passing through it. The suspended nanotube is, at the same time, the vibrating string and the readout element of the transistor.

In November 2008 the partners reported in Barcelona that they had sensed the mass of single chromium atoms deposited on a CNT. If the resolution can be pared down to a single nucleon, then researchers can accurately weigh different types of molecules and atoms in real time. Afterwards, it may become possible to observe the radioactive decay of a single nucleus and to study other types of quantum mechanical phenomena.

REFERENCES

1. Eklund, P. (Chair): WTEC Panel Report on international assessment of research and development of carbon nanotube manufacturing and applications. PDF created by World Technology Evaluation Center, Baltimore, MD (September 1, 2007)
2. Landmann, W.: Solid state replacements for electro-mechanical potentiometer type pressure transducers. Kulite Semiconductor Products, Inc., Leonia, NJ, PDF created on February 21 (2004)
3. Lutze, O., Ravi, K., Meruva, R.K., Frielich, A., Ramamurthy, N., Brown, R.B., Hower, R., Meyerhoff, M.E.: Stabilized potentiometric solid-state polyion sensors using silver-calixarene complexes as additives within ion-exchanger-based polymeric films. *Fresenius J. Anal. Chem.* 364, 41–47 (1999)

4. Akle, B., Leo, D.J.: Electromechanical transduction in multilayer ionic transducers. *Smart Mater. Struct.* 13, 1081–1089 (2004)
5. Franklin, J.W.: Electromechanical modeling of encapsulated ionic polymer transducers. Master's Thesis, Virginia Polytechnic Institute and State University, VA (June 23, 2003)
6. Janocha, H., Kuhnen, K., Clepas, B.: Inherent sensory capabilities of solid state actuators. PDF SA98, Laboratory for Process Automation (LPA), University of Saarland, Germany (1998)
7. Fraden, J.: *Handbook of Modern Sensors – Physics, Design and Applications*, 3rd edn. Springer, New York (2004)
8. Jiang, J.C., White, R.C., Allen, P.K.: Microcavity vacuum tube pressure sensor for robotic tactile sensing. In: *Transducers 1991. Int'l Conf. Solid-State Sensors and Actuators. Digest of Technical Papers*, pp. 239–240. IEEE, New York (1991)
9. Darlinski, G., Böttger, U., Waser, R., Klauk, H., Halik, M., Zscheschang, U., Schmid, G.: Dehm Chr. Mechanical force sensors using organic thin-film transistors. *Journal of Applied Physics* 97, Paper 435702 (2005)
10. Intelligent force sensors using standard CMOS technologies, Fraunhofer Gesellschaft (2002)
<http://www.iis.fhg.de/asic/analog/microsystem/kraft/index.html>
11. Xiao, Z., Camino, F.E.: The fabrication of carbon nanotube field-effect transistors with semiconductors as the source and drain contact materials. *Nanotechnology* 20, Paper 135205 (2009)
12. Seki, T., Uno, Y., Narise, K., Masuda, T., Inoue, K., Sato, S., Sato, F., Imanaka, K., Sugiyama, S.: Development of a large-force low-loss metal-contact RF MEMS switch. *Sensors and Actuators A: Physical* 132(2), 683–688 (2006)
13. Parton, E., Verheyen, P.: Strained silicon – the key to sub-45 nm CMOS. III-Vs Review (The Advanced Semiconductor Magazine) 19(3), 28–32 (2006)
14. Tripathi, S.K., Shukla, N., Dhamodaran, S., Kulkarni, V.N.: Controlled manipulation of carbon nanopillars and cantilevers by focused ion beam. *Nanotechnology* 19, Paper 205302 (2008)
15. Boisen, A., Thundat, T.: Design & fabrication of cantilever array biosensors. *materialstoday* 12(9), 32–38 (2009)
16. Lange, D., Brand, O., Baltes, H.: *CMOS Cantilever Sensor Systems. Atomic-Force Microscopy and Gas Sensing Applications*. Springer, Berlin (2002)
17. Bashash, S., Salehi-Khojin, A., Jalili, N., Thompson, G.L., Vertegel, A., Muller, M., Berger, R.: Mass detection of elastically distributed ultrathin layers using piezoresponse force microscopy. *J. Micromech. Microeng.* 19, Paper 025016 (2009)
18. Lange, D., Akiyama, T., Hagleitner, C., Tonin, A., Hidber, H.R., Niedermann, P., Staufer, U., de Rooij, N.F., Brand, O., Baltes, H.: Parallel scanning AFM with on-chip circuitry in CMOS technology. In: *Proc 12th IEEE Int'l Conf. Micro Electro Mechanical Systems*, Nashville, TN, January 17-21, pp. 447–452 (1999)
19. Bausells, J.: Micro- and nano-electromechanical systems for [bio]molecular analysis. *Contributions to Science (Institut d'Estudis Catalans)* 3(1), 67–78 (2005)

20. Gel, M., Shimoyama, I.: Force sensing submicrometer thick cantilevers with ultra-thin piezoresistors by rapid thermal diffusion. *J. Micromech. Microeng.* 14, 423–428 (2004)
21. Tellier, C.R., Leblois, T.G.: On the design of GaAs (hhl) resonant cantilevers: Study of piezoelectric excitation, of piezoresistive sensing and of micromachined structure. *Sensors and Actuators A: Physical* 132(1), 224–235 (2006)
22. Yaldız, S., Ünsaçar, F.: A dynamometer design for measurement the cutting forces on turning. *Measurement* 39(1), 80–89 (2006)
23. Castellini, P., Montanini, R., Revel, G.M.: Development of a film sensor for static and dynamic force measurement. *Review of Scientific Instruments* 73(9), 3378–3385 (2002)
24. Wood, J. (ed.): The top ten advances in Materials Science. *Materials Today*, December 19 (2007)
25. Hierold, C., Stampfer, C., Helbling, T., Jungen, A., Tripp, M., Sarangi, D.: CNT based nano electro mechanical systems (NEMS). In: *Proc. IEEE Int'l Symp. Micro-NanoMechatronics and Human Science – MHS2005*, November 8-9, pp. 1–4. Nagoya Univ., Japan (2005); ISBN 0-7803-9482-8
26. Bichoutskaia, E., Popov, A.M., Lozovik, Y.E.: Nanotube-based data storage devices. *materialstoday* 11(6), 38–43 (2008)
27. Møllhave, K., Hansen, T.M., Madsen, D.N., Bøggild, P.: Towards pick-and-place assembly of nanostructures. *Journal of Nanoscience and Nanotechnology* 4(3), 1–4 (2004)
28. Popescu, A., Woods, L.M., Bondarev, I.V.: A carbon nanotube oscillator as a surface profiling device. *Nanotechnology* 19, Paper 435702 (2008)
29. Hunt, B., Noca, F., Hoenk, M.: Carbon nanotube bimorph actuators and force sensors. *NASA Tech Briefs NPO-21153*, Pasadena, CA, October 3 (2005)
30. Singh, G., Rice, P., Mahajan, R.L.: Fabrication and mechanical characterization of a force sensor based on an individual carbon nanotube. *Nanotechnology* 18, Paper 475501 (2007)
31. Baubin, M., Haid, C., Hamm, P., Gilly, H.: Measuring forces and frequency during active compression decompression cardiopulmonary resuscitation: a device for training, research and real CPR. *Resuscitation* 43(1), 17–24 (1999)
32. Šantić, A., Kovačić, D., Gilly, H.: Force measuring device applied in cardiopulmonary resuscitation. PDF on Internet, May 15 (2001)
33. Boonstra, T.W., Clairbois, H.E., Daffertshofer, A., Verbunt, J., van Dijk, B.W., Beek, P.J.: MEG-compatible force sensor. *Journal of Neuroscience Methods* 144(2), 193–196 (2005)
34. EMAT Technology from the R&D Lab to the Field. *Innerspec Technologies, Inc.*, Lynchburg, VA (2009)
35. Sonic Sensors – Your EMAT solutions provider, Wayne Pilkington, CA (August 2009), <http://sonicsensors.badlogic.net/img/whatis1.gif>
36. Sekalski, P., et al.: Static absolute force measurement for preloaded piezoelements used for active Lorentz force detuning system. In: *Proc. XXIIth Int'l Conf. LINAC (Linear Accelerator)*, Lübeck, Germany, pp. 486–488 (2004)

37. Jin, W., Mote Jr., C.D.: On the calibration of multicomponent microforce sensors. *J. Micromech. Microeng.* 7(2), 156–163 (1998)
38. Cho, J.-M., Lee, S.-Y., Kim, S.-W., Kim, K.S., An, S.: A Lorentz force based fusion magnetometer-accelerometer with dual functions for the electronic compass. *Applied Physics Letters* 91(20), Paper 203519 (2007)
39. Jia, Y.M., Zhou, D., Luo, L.H., Zhao, X.Y., Luo, H.S., Or, S.W., Chan, H.L.W.: Magnetolectric effect from the direct coupling of the Lorentz force from a brass ring with transverse piezoelectricity in a lead zirconate titanate (PZT) disk. *Applied Physics A [Springer-Verlag]* as Internet file (July 31, 2007)
40. Thess, A., Knaepen, B., Votyakov, E., Zikanov, O.: Sensitivity analysis of a Lorentz force flowmeter for laminar and turbulent flows in a circular pipe. In: *Proc. Summer Program 2006*, pp. 431–441. Center for Turbulence Research, University of Stanford, CA (2006)
41. Manginell, R.P., Adkins, D.R., Moorman, M.W., Hadizadeh, R., Copic, D., Porter, D., Anderson, J.M., Wheeler, D.R., Pfeifer, K.B., Rumpf, A.: Mass sensitive, Lorentz-force actuated, MEMS preconcentrator and chemical sensor. PDF from Internet, May 29 (2008)
42. Brückner, K., Cimalla, V., Niebelschütz, F., Stephan, R., Tonisch, K., Ambacher, O., Hein, M.A.: Strain- and pressure-dependent RF response of microelectromechanical resonators for sensing applications. *J. Micromech. Microeng.* 17, 2016–2023 (2007)
43. Bădescu, G., Ștefănescu, D.M.: Installation for determining the elastic constants of rocks (in Romanian). *Studii și cercetări de mecanică aplicată*, Tom 40(3), 451–466 (1981)
44. Janiczek, T.: Analysis of PVDF transducer signals stimulated by mechanical tension. *Journal of Electrostatics* 52, 167–172 (2001)
45. Larsen, P.K.: Ferroelectric films for optical and piezoelectric applications. Project number 4191. Katholieke Universiteit Nijmegen, The Netherlands (January 2007), <http://www.stw.nl/Projecten/N/nns/nns4191.htm>
46. Sievilä, P., Rytönen, V.-P., Hahtela, O., Chekurov, N., Kauppinen, J., Tittonen, I.: Fabrication and characterization of an ultrasensitive acousto-optical cantilever. *J. Micromech. Microeng.* 17, 852–859 (2007)
47. Keplinger, F., Kvasnica, S., Jachimowicz, A., Kohl, F., Steurer, J., Hauser, H.: Lorentz force based magnetic field sensor with optical readout. *Sensors and Actuators A: Physical* 110(1-3), 112–118 (2004)
48. Grubisic, A.N., Gabriel, S.B.: Development of an indirect counterbalanced pendulum optical-lever thrust balance for micro- to millinewton thrust measurement. *Meas. Sci. Technol.* 21, Paper 105101 (September 2010)
49. Kim, S.K., Asay, D.B., Dugger, M.T.: Nanotribology and MEMS. *Nanotoday* 2(5), 22–29 (2007); ISSN 1748 0132
50. Brook, A.J., Bending, S.J., Pinto, J., Oral, A., Ritchie, D., Beere, H., Springthorpe, A., Henini, M.: Micromachined III–V cantilevers for AFM-tracking scanning Hall probe microscopy. *J. Micromech. Microeng.* 13, 124–128 (2003)
51. Grabiec, P., Radojewski, J., Zaborowski, M., Domanski, K., Schenkel, T., Rangelow, I.W.: Microelectronics and nanometer structures. *Journal of Vacuum Science & Technology* 22(1), 16–21 (2004)

52. Poggio, M., Degen, C.L.: Force-detected nuclear magnetic resonance: recent advances and future challenges (Topical review). *Nanotechnology* 21, Paper 342001 (August 2010)
53. Morita, K., Sugimoto, Y., Sasagawa, Y., Abe, M., Morita, S.: Small-amplitude dynamic force microscopy using a quartz cantilever with an optical interferometer. *Nanotechnology* 21, Paper 305704 (July 2010)
54. Castellanos-Gomez, A., Agrait, N., Rubio-Bollinger, G.: Carbon fibre tips for scanning probe microscopy based on quartz tuning fork force sensors. *Nanotechnology* 21(14), Paper 145702 (2010)
55. Hakonen, P.: Nanotubes weigh the atom. *Research*eu results supplement* (17) 43 (2009),
[http://cordis.europa.eu/ictresults/
index.cfm?section=news&tpl=article&ID=90708](http://cordis.europa.eu/ictresults/index.cfm?section=news&tpl=article&ID=90708)

PART II

FORCE TRANSDUCERS COMPONENTS

Balzac: Man doesn't invent the force
but he only guides it.

Sophocles: There are all kind of forces in the world
but man is the strongest of all.

Stramusoli: Force is the first tool of men in high places.

Pascal: The force leads the world
but the ideas lead the force.

Chapter 17

THE FORCE MEASUREMENT CHAIN

17.1. FORCE MEASUREMENT CHAIN COMPONENTS

The purpose of a force measurement system is to provide an observer with a numerical value corresponding to the variable being measured which, in general, equals the true value of that variable only in the ideal case.

The measurement chain consists of several elements or blocks [17.1]. Four principal categories of functions or functional elements may be identified in Figure 17.1, and these will give the titles of the following four subchapters: strain gauges as sensing elements, signal conditioning, signal processing and output data presentation.

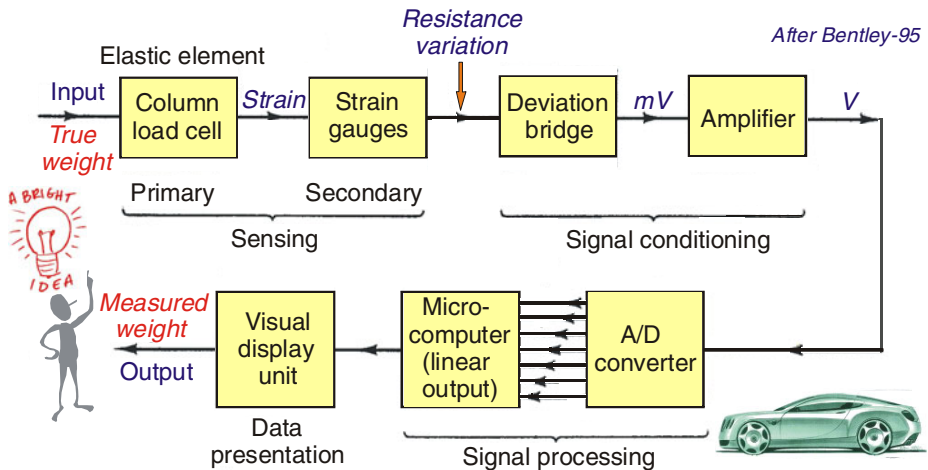


Fig. 17.1 General structure of a force measurement chain, reflecting the succession of physical quantities transformations, from the load application to the visual display unit

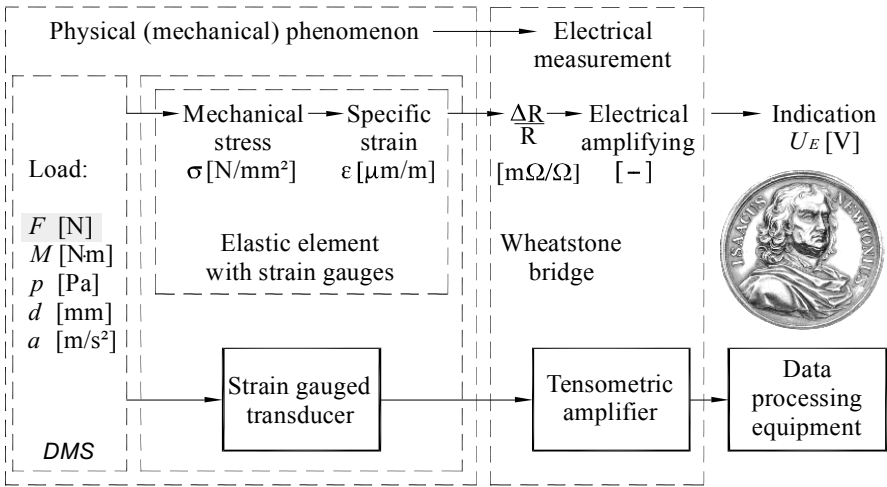


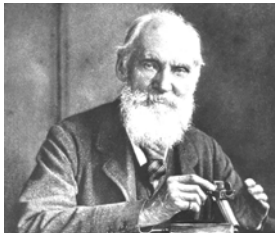
Fig. 17.2 Conversion steps for mechanical measurands into electrical quantities

Referring to the structural configuration of an electric force measuring system [17.2], the input mechanic quantity is force F , which, by successive changes, is converted into the output electric quantity, usually a voltage U_E . The succession of conversions of the physical quantities (Fig. 17.2), from the input force (the measurand) to the system output quantity (the measuring instrument), is the following:

- Force $F \rightarrow$ mechanical stress σ , conforming to the equations from Strength of Material science;
- Stress $\sigma \rightarrow$ specific deformation (strain) ε , following the Hooke’s law of elasticity (1678): *Ut tensio, sic vis*, meaning: *As the extension, so the force*;
- Elongation $\varepsilon \rightarrow$ variation of relative resistance ΔR (W. Thomson, Lord Kelvin discovered the piezoresistive effect in 1856);



Robert Hooke
1635 – 1703



William Thomson, Lord Kelvin
1824 – 1907



Sir Charles Wheatstone
1802 – 1875

Fig. 17.3 A triad of famous predecessors in the field of measurement science

- $\Delta R/R$ ratio \rightarrow variation of output voltage ΔU_E , using the Wheatstone bridge, as invented in 1843.

These great contributors in the field of electrical measurement of mechanical quantities are presented in Figure 17.3.

A global transfer function is evident, where the force transducer sensitivity has an important role. This structural model expresses the complexity of the force measuring system, based on the above-mentioned chain of changes:

$$F \rightarrow \sigma \rightarrow \epsilon \rightarrow \Delta R \rightarrow \Delta U_E$$

Another representation of the force measurement process is given in Figure 17.4. John Venn (1834 - 1923), an English priest and professor of logic and probability theory at Cambridge University, has been the father of the “Venn diagrams”. In this case, they symbolically show sets of elements, together with intersections and unions of component sets.

The two inserts in the upper corners suggest the spectacular evolution from the renowned scientist Isaac Newton's time, with the studying of the old prints and manuscripts, to the wide scale computerized activity, culminating with the automated tracing of the specific diagrams for strain gauged force transducers.

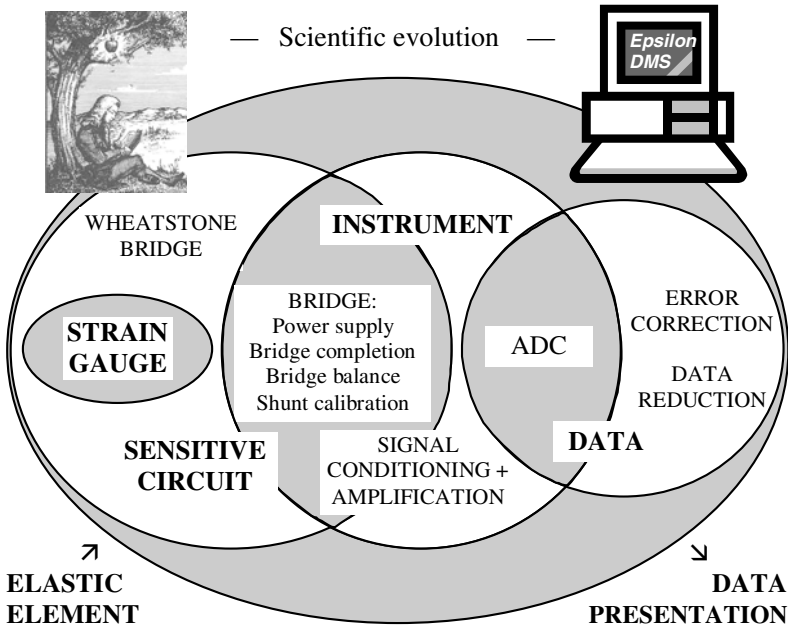


Fig. 17.4 Venn diagram illustrating the complexity of the force measurement chain

17.2. STRAIN GAUGE SENSING

The strain gauge is a device for measuring the changes in distances between (two) points in solid bodies that occur when the body is deformed [Britannica Concise Encyclopedia]. Note: The correct spelling is *gauge*, but prolonged grammatical assaults, especially in the United States, assassinated the “*u*”.

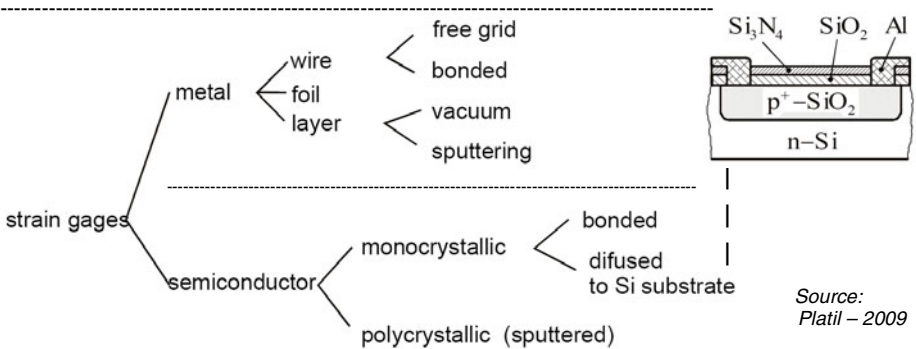
Strain gauges act as sensing elements on devices for measuring force and related physical quantities. By other words, strain gauges are:

- devices that respond to mechanical strain (unit deformation),
- sensors whose resistance is a function of the applied force,
- detectors which experience a change in resistance when they are stretched or strained, being indestructibly located on special flexible elements. If the conducting material is bonded to an elastic element under the strain, the resistance change can be measured, and utilized to determine the force from the calibrated transducer [17.3].

Strain gauges are not only resistive sensors [17.4], here are other measurement principles “connectable” with this category:

- A *capacitive strain gauge* contains two tiny electrode plates with minuscule space between them. Strain causes the plates to shift slightly closer together or further apart, affecting the measurable electric field between them.
- A *resonant strain gauge* is based on tuning fork-like tines not much longer than a human hair thickness. The tines are mechanically vibrated and the frequency of that vibration is detected by onboard electronics. As force is applied to the steel that it’s mounted on, the device stretches and the frequency changes.
- Other measurement principles are: *inductive SGs*, *TVSGs* (transverse voltage based on the *Hall effect*), *vibrating wires*, *SAWs* (*surface acoustic waves*), *CNTs* (*carbon nanotubes*) [17.5] or *optical SGs* (e.g. *fiber Bragg gratings*), the latter being compared with the resistive strain gauges in [17.6].

Table 17.1 Classification of strain gauges obtained by using different technologies



Source:
Platil – 2009

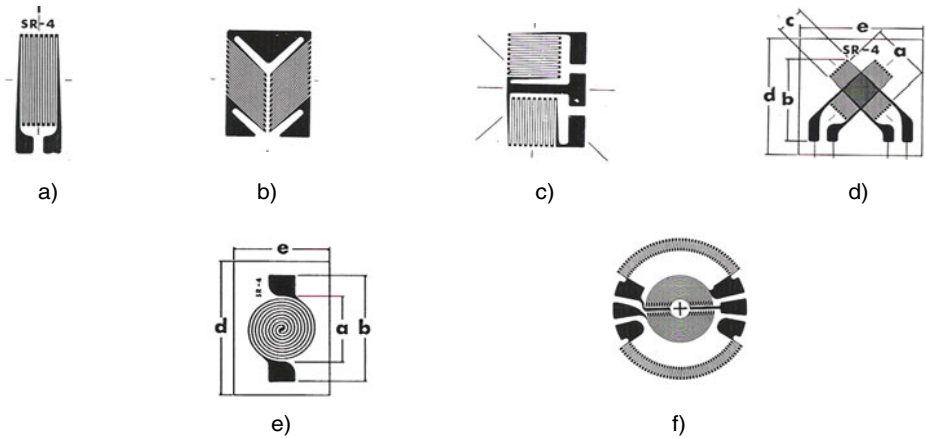


Fig. 17.5 Various types of strain gauges: a) single; b) “fish skeleton” rosette; c) T-type rosette; d) X-type rosette; e) spiral single; f) full bridge for pressure diaphragm

However, the most popular and extremely effective remain the electrical resistance strain gauges as depicted in Table 17.1: metallic wire, foil, thin film, semiconducting silicon, but also magnetoresistors or MEMS made by today solid state technology and integrated circuit manufacturing.

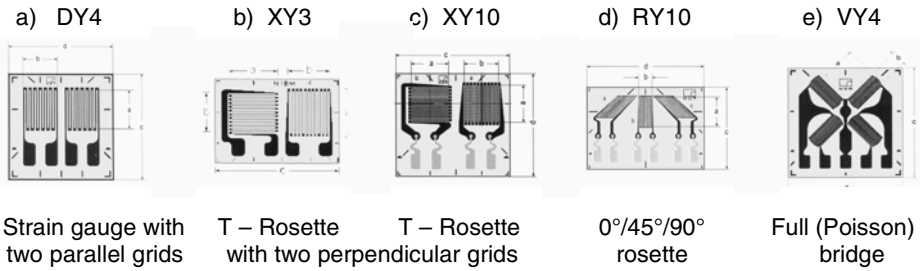
There are a variety of shapes for resistance strain gauges in various applications. Each model is designed to determine the strain along a precisely defined axis in order to be properly aligned with the strain field within the associated elastic body. Long longitudinal and short transverse segments are recommended to obtain the best strain sensitivity [17.7]. Typical resistance values vary from $100\ \Omega$ to several thousands ohms.

Fig. 17.5 shows some strain gauges manufactured by BLH for precision force transducers [17.8]. The models *b*, *c* and *d* are half-bridges with two perpendicular elements, the last having superposed grids.

Fig. 17.6 presents a series of strain gauges made by Hottinger: the models *a*, *b* and *c* have two SGs on the same pattern, the version *d* is a three-component rosette, useful in Experimental Stress Analysis, while the type *e* depicts a full bridged version for shear-, torsion- or stretching measurements [17.9].

Worth to be mentioned are the stick-on (self-adhesive) strain gauges for transducer manufacturers [17.10]. These special SGs are supplied with a dry adhesive precoated on the backing, facilitating the easy handling and accurate positioning on the associated elastic structure.

For performing high quality strain and, implicitly, force measurements, strain gauges must be selected and installed with the utmost care on the elastic elements of force transducers [17.11].



Strain gauge with two parallel grids

T – Rosette with two perpendicular grids

T – Rosette with two perpendicular grids

0°/45°/90° rosette

Full (Poisson) bridge

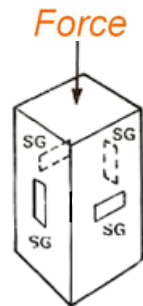
a), b) and e) – integrated solder tabs, c) and d) – big, integrated strain relieves (HBM)

Fig. 17.6 Various types of rosettes manufactured by Hottinger company in Darmstadt

At this point it is necessary to underline the indestructible connection between the elastic elements (primary sensing) and the strain gauges (secondary sensing) within the force transducers; a dozen of flexible bodies is summarized in Table 17.2 together with their measurement ranges. Their classification will be detailed in Chapter 20, and each of the twelve types of elastic elements for strain gauged force transducers will be analyzed in the next chapters (C21...32).

Table 17.2 Twelve principal types of elastic elements for SGTs

EE	Type	Force range [N]			
		10 ⁻²	10 ¹	10 ⁴	10 ⁷
I	Stretched/compressed column				
II	Stretched/compressed tube				
III	Bent lamella (cantilever beam)				
IV	Bent and/or torsioned shaft				
V	Middle bent bar with fixed ends				
VI	Shearing strained profile				
VII	Bent yoke				
VIII	Bent ring				
IX	Bent membrane				
X	Compressed torus				
XI	Axisymmetrical element				
XII	Sphere/volumetric element				



SG – Strain gauges
EE – Elastic elements



17.3. STRAIN GAUGES SIGNAL CONDITIONING

When a force is applied to an elastic structure, the length of that structure is modified. Strain gauges are sensitive to this change of dimension, so, being glued on the distorted structure, their resistance is changing under the applied load. By measuring this resistive change one can measure the strain. The best method to measure these small changes of resistance is generally through a Wheatstone bridge arrangement. With computerized systems the change in the bridge output voltage is usually measured, rather than the current. You do not need a computer to measure strain, but, while using it, you can speed up measurements, measure continuously, increase accuracy, eliminate transcription errors, automate testing, generate health and safety records, minimize human error and so on [17.12].

Wheatstone bridge circuits will be detailed in Chapter 18 while signal conditioning and other electronic circuits for strain gauged force transducers will be presented in Chapter 19. Here are some general considerations on deviation (unbalanced) bridges connected with instrumentation amplifiers.

Figure 17.7 illustrates the large variety of transducers connectable to the modern measurement systems, including those with resistive or inductive (half) bridges. In the actual instrumentation, the Wheatstone bridge, as analogical conditioning unit for resistive parametric transducers, is closely connected with amplification and processing circuits of the tensometric signals, ensuring wide possibilities to make up tensometric “chains” both for rough industrial processing and for high accuracy determinations in laboratories.

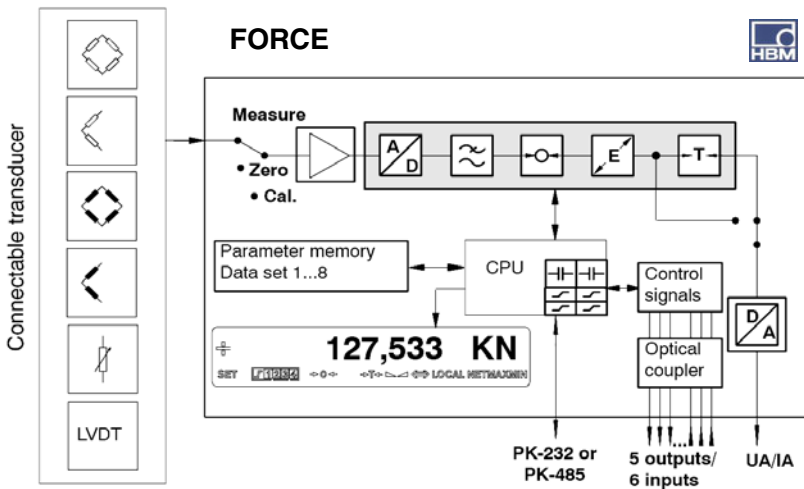


Fig. 17.7 Functional diagram of a digitalized force measurement chain

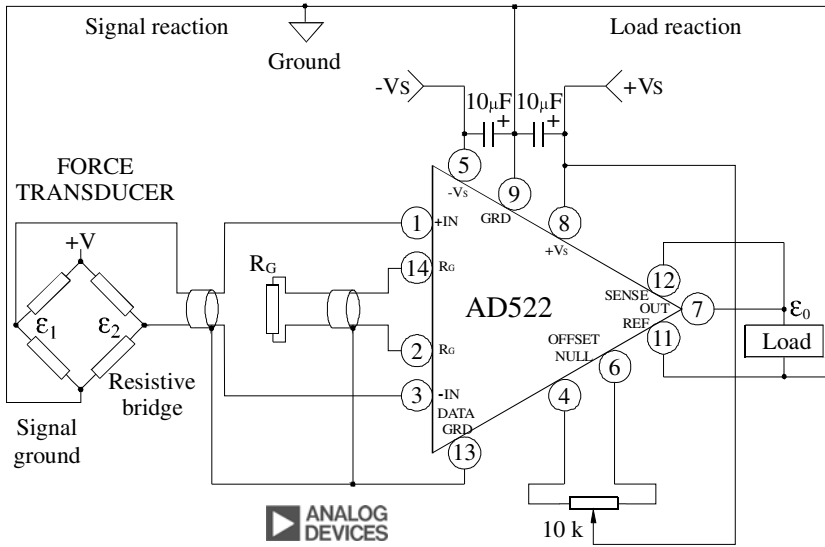


Fig. 17.8 AD 522 instrumentation amplifier connected with strain gauge bridge

Force transducers with incorporated electronics [17.13] are small sized measurement devices comprising both elastic bodies and related electronics: thermal compensation, linearization and computation. The coupling is so tight that the connecting and transmission elements, which are important with classical transducers, are no longer applied. The new expression “*electronic transducer*” [17.14] reflects this evolution. The microcomputer technology has changed the course of the industrial development by eliminating a great number of electronic components and including their functions in one single chip resulting in lower costs, flexibility and safety.

AD 522 instrumentation amplifier (Fig. 17.8) is a perfect combination of linearity and high CMR, with low noise and drift, very adequate for most data acquisition systems of 12 bits. In a connection diagram for a typical tensometric application one can notice that the ground terminal (9) is used both for the input connection (the transducer ground point) and for the connection of remote amplification setting resistor [17.15]. The adjustable amplification is also useful for the sensitivity settlement of interchangeable force transducers (FTs).

TLV 2262 is a specialized integrated circuit (Fig. 17.9), with a resistive network for amplification adjustment, all in a heatproof enclosure [17.16].

The MBSTC-02 (Fig. 17.10), made by Microbridge Technologies, Inc. [17.17], incorporates low-noise operational amplifiers with rejustors to provide precise signal conditioning with integrated temperature correction for use with sensors with a negative temperature coefficient (NTC).

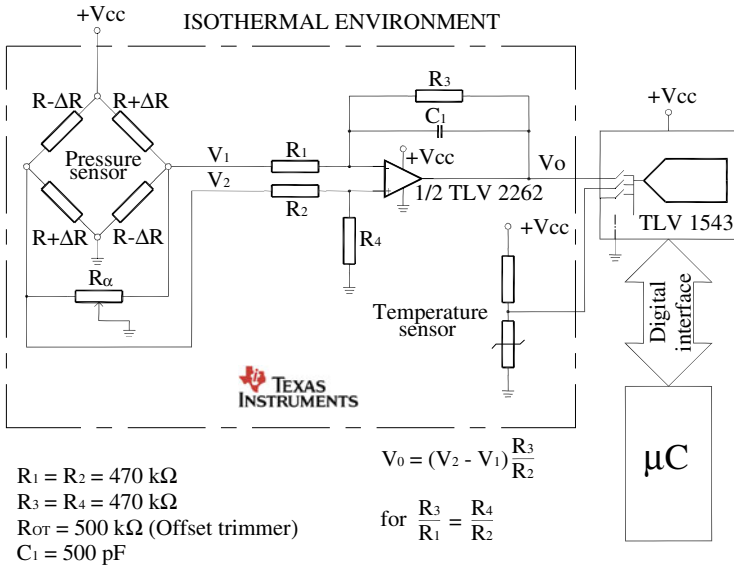


Fig. 17.9 Strain gauged transducer for measuring pressure in isothermal environment

Rejusters (as illustrated in Figure 3.7) are adjustable resistors whose ohmic values can be settled to better than 0.1 % tolerances, perfect for Wheatstone bridge sensor-based applications. This high-precision differential instrumentation amplifier provides complete analog calibration, compensation and amplification for any strain gauge bridge type transducers.

As technology evolves, classical (metallic) strain gauges tend to be replaced by semiconductor ones. Microfabricated silicon carbide sensor elements are combined with advanced packaging and signal conditioning electronics to create complete transducer solutions of unique performance and value [17.18].

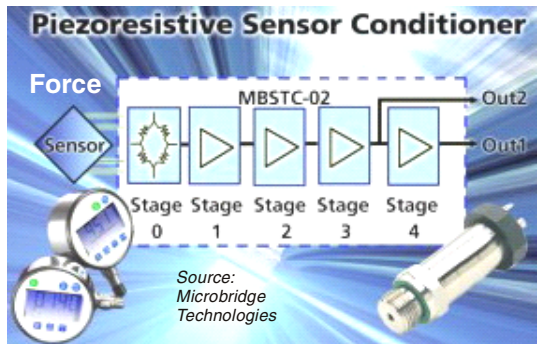


Fig. 17.10 Signal conditioning chip for piezoresistive force and pressure transducers

17.4. STRAIN GAUGES SIGNAL PROCESSING

The voltage changes due to the strain are tiny; they are measured in microvolts. Monitoring such small signal changes can often produce jitter in the readings from noise. For slow sampling one can counteract this with an integrating analog-to-digital converter (ADC), following the evolution from the classical transducers (Fig. 17.11a) to the intelligent ones (Fig. 17.11b and Chapter 35).

In the development of tensometrical instrumentation emphasis is laid on the digital measurement and computer support. The analog-to-digital conversion is more rapidly performed nearer to the input of the measuring system. The analogic part is reduced to the minimum and the signal conditioning becomes the PC task which, based on specific algorithms and using special application programs, performs a long listing of DSP functions (Fig. 17.12).

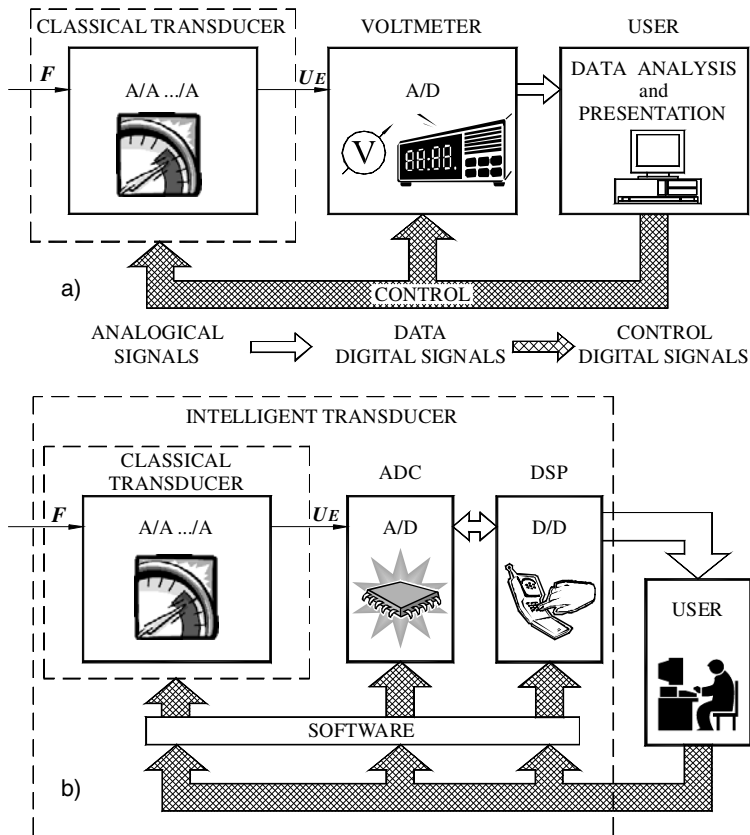


Fig. 17.11 The evolution from classical (a) to intelligent (b) transducers emphasizes the software role in the force measurement chain.

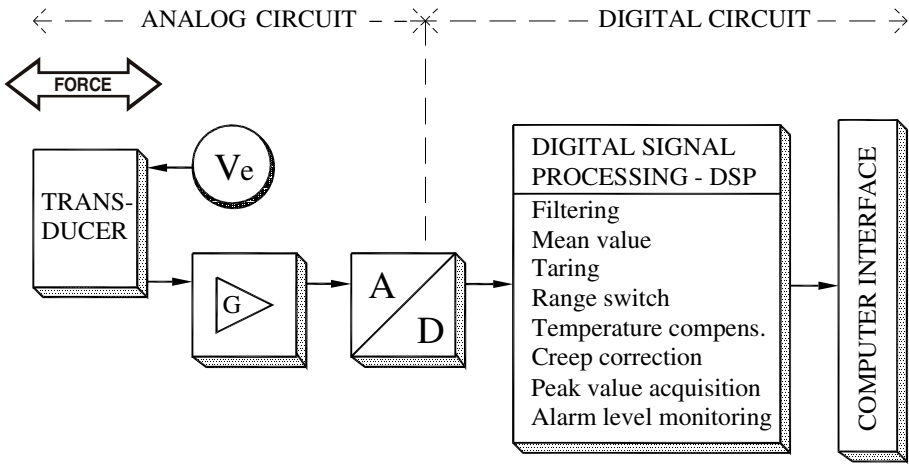


Fig. 17.12 Digital signal processing functions within the force measurement chain

Electro Standards Laboratories, Cranston, RI announced a new addition to the CellMite product line, model 4325A [17.19], which connects directly to a standard strain gauge, such as a load cell, extensometer or pressure transducer, simultaneously generating a serial output for connection to a PC with 24-bit internal resolution and ± 10 V analog output. The sample rate is 60 samples per second. Functions include tare, peak and valley (maximum and minimum), and user-defined units for force, mass and other physical quantities.

A transducer converts a physical quantity (e.g. force) to an electrical signal (e.g. mV/V), which is submitted to an A/D conversion in order to obtain a digital value. When setting up a measurement system, the measurement engineer used to manually enter the parameters that were necessary to express the digital value in physical units (called in practice scaling or setting sensitivity). This important step is sometimes a possible source of error, which can lead to corruption of the measurement results.

The intelligent transducer provides not only the analog measurement signal but also a digital identification interface, via which the transducer data can be read directly from the transducer (Fig. 17.13a). HBM has developed and applied patented solutions to use both the analog and the digital identification interface without additional wiring:

- T-ID™ (Transducer Identification): a unique identification number is stored in the transducer that is used as a reference for a central PC database with transducer settings.
- TEDS (Transducer Electronic Datasheet): allows the amplifier to be set up automatically and locally via an electronic datasheet in the transducer.

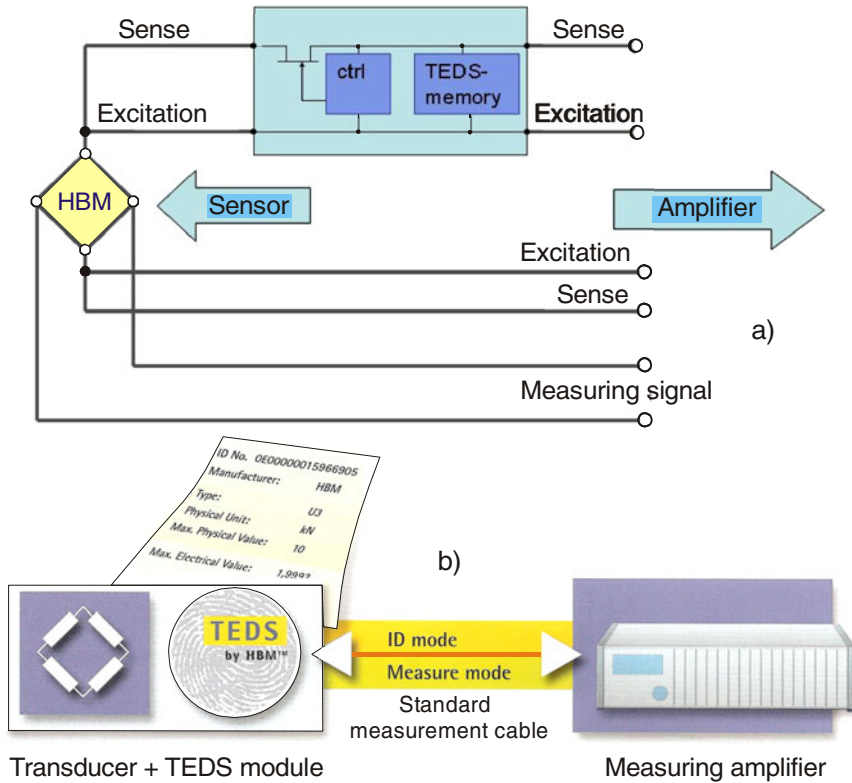


Fig. 17.13 TEDS connection to the strain gauged transducer (a) and its specific “fingerprint” for the force measuring chain (b)

These devices for transducer identification and electronic datasheet presentation increase the measurement system confidence due to:

- fast and fully-automatic transducer parameter setting,
- full traceability and automatic calibration validity checking,
- automatic channel assignment and wiring checking,
- shorter downtimes when replacing the transducers,
- simplified company-wide transducer management via specialized databases (Fig. 17.13b).

Verification measurements with the TEDS chip built into a force transducer checked for the technical specifications, e.g. temperature behavior of the sensitivity. Additional investigations focus on different linearization methods checked with force and voltage ratio calibrations. With force calibration according to ISO 376 a 3rd degree polynomial equation is calculated online from the calibration results [17.20].

17.5. DATA PRESENTATION FOR FORCE TRANSDUCERS

As mentioned at the beginning of this chapter, the four principal blocks of the force measurement chain are: sensing (elastic element + strain gauges), signal conditioning, signal processing and data presentation. The most complete instrumentation combination [17.3] is shown in Figure 17.14a, followed by the classification of data presentation possibilities (Fig. 17.14b) [17.1].

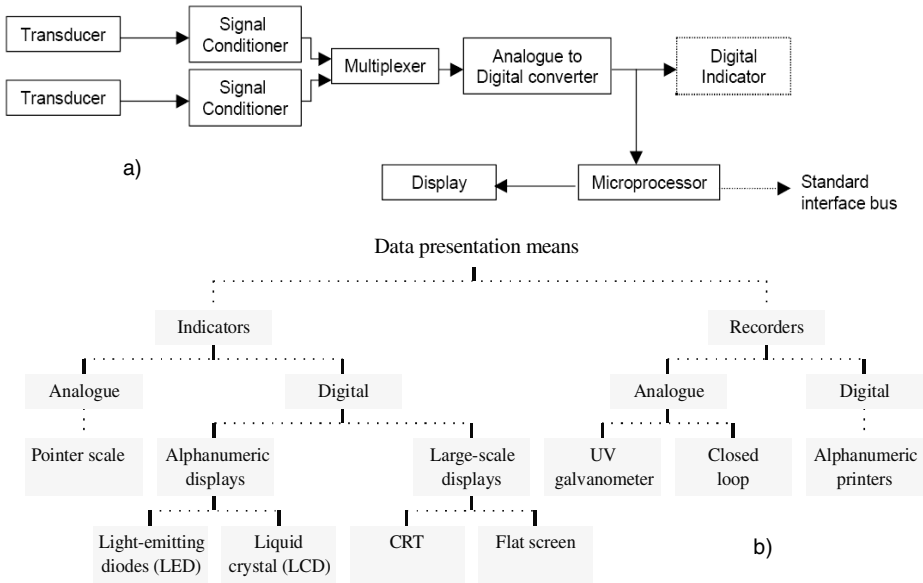


Fig. 17.14 Complete scheme of measurement chain (a) + means of data presentation (b)



Fig. 17.15 Digital displays in kilograms for weighing at the crane hooks

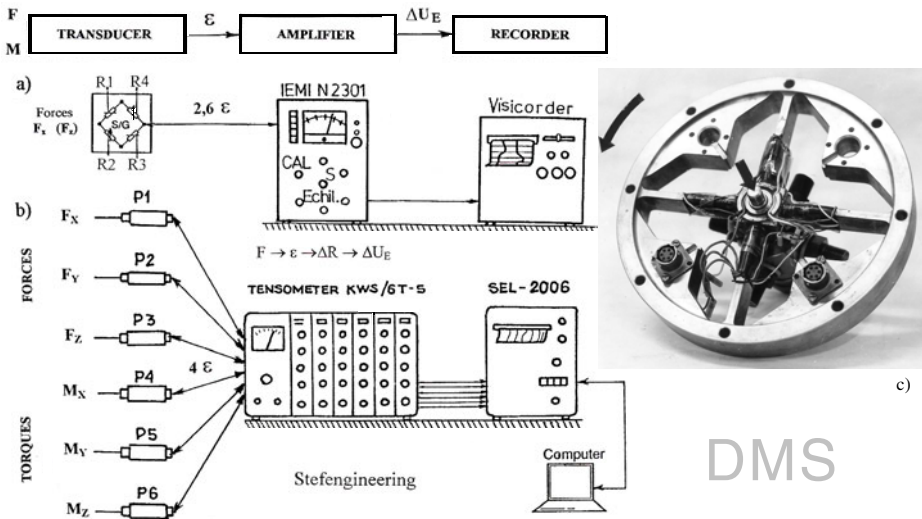


Fig. 17.16 Single (a) and multicomponent (b) force and torque measurement chains; c) strain gauged spoked-wheel for high axial force and low torque measurements

The classical force transducers can be connected to digital indicators specialized for electronic weighing systems [17.21], [17.22]. Special indicators for crane hooks are also produced [17.23]. Latest achievements include built-in digital displays (in engineering units) for strain gauged force transducers [17.24]. Figure 17.15 presents two digital indicators for crane hooks.

The same importance with data presentation has the force measurement scheme representation, inspired by the images of component apparatus [17.25]. Some configurations of Romanian achievements in the field of single- or multi-component force measurements [17.26], [17.27] are shown in Figure 17. 16.

Loadstar Sensors Inc. of Mountain View has launched a wireless weight measurement kit that enables product designers and end users to easily build an accurate and reliable weight measurement system [17.28]. The kit contains four Loadstar’s patent-protected CS Series capacitive sensors, one DS-2100 WiFi display and summing device with wireless connection capability, as well as the LoadVUE software for simplifying measurement and calibration tasks using a PC. All the components of the kit are designed to work well with each other, making the creation of a weight measurement system effortless. Another wireless application, for torque measurement telemetry, is presented in [17.29].

As described in a recent invention abstract: A radiotelephone with weighing means (Fig. 17.17) includes facilities for supporting an object to be weighed, including a microprocessor for determining the weight [17.30].

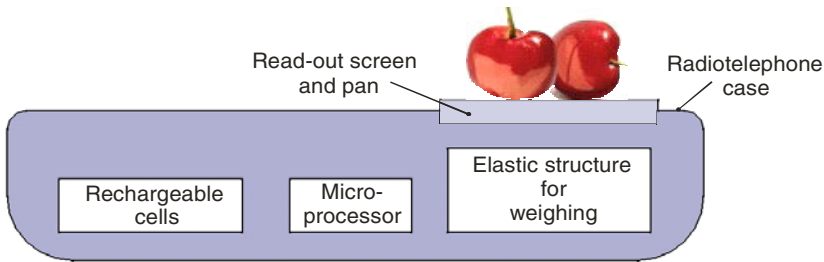


Fig. 17.17 Schematic of a patented radiotelephone with weighing means

REFERENCES

1. Bentley, J.P.: Principles of Measurement Systems, 3rd edn. Longman Singapore Publishers, Singapore (1995)
2. Ștefănescu, D.M.: Methods for increasing the sensitivity of strain gauge force transducers (in Romanian). PhD dissertation, Universitatea "Politehnica" București, Romania, September 10 (1999)
3. Hunt, A.(Coord.): Guide to the Measurement of Force. The Institute of Measurement and Control, London (Published 1998); ISBN 0-904457-28-1
4. Pescovitz, D.: Autosensing for autos, July 26 (2008), <http://www.coe.berkeley.edu/labnotes/0205/strain.html>
5. Li, X., Levy, C.: A novel strain gauge with damping capability. Sensors & Transducers Journal 7(Special Issue), 5–14 (2009)
6. Kleckers, T.: Fibre Bragg sensors compared with electrical strain gauges for use in force measurement – prospects and potentials. In: Proc. XIX IMEKO World Congress, Lisbon, Portugal, September 6–11, pp. 226–229 (2009)
7. Fraden, J.: Handbook of Modern Sensors – Physics, Designs, and Applications, 3rd edn. Springer-Verlag New York, Inc. (2004)
8. Precision force and weight measurement technologies. BLH Electronics, Inc., Canton, MA, Catalog 4M-95
9. High-quality strain gauge technology. In: Short form catalogue for economical sensors. Megatron Bauelemente, Putzbrunn, Germany (2002)
10. Strain gages for transducer manufacturers. Technical data, pp. 12–13, May 8 (2005), <http://www.hbm.com>
11. Strain Gage Based Transducers – Their Design and Construction, February 15 (2001), <http://www.measurementsgroup.com/guide/ta/sgbt/sgbtindex.htm>
12. How to use a PC to measure strain. Monitor Newsletter Archive (17), June 26 (2007), <http://www.windmill.co.uk/monitor17.html>
13. Ștefănescu, D.M.: Resistive Kraftaufnehmer mit integrierter Elektronik. In: Schanz, G.W. (Hrsg.) VFI, vol. 11(4), pp. 46–49. Baltz Verlag- und Werbung GmbH, München (1984)
14. Load cells and instrumentation. Ametek Controls Div., Feasterville, PA, Bulletin GCF-1-80

15. Sheingold, D.H. (ed.): *Transducer Interfacing Handbook. A Guide to Analog Signal Conditioning*. Analog Devices, Norwood (1980)
16. Beckemeyer, H.-P.: *Signal acquisition and conditioning with low supply voltages*. Texas Instruments Inc., Staples Printers, Rochester, England (June 1996)
17. Arts, S.: *CMOS and Rejutor based application-specific analog signal conditioning chip*. *Sensors & Transducers* (2008)
18. Zin Technologies and FLX Micro join forces to develop sensors for harsh environments. *Sensors & Transducers e-Digest* 63(1) (January 2006)
19. Gouin, J.: *Intelligent digital signal conditioner hassle free – strain gage direct to PC*. On-line Magazine “*Sensors & Transducers*” 59(6) (June 2005)
20. Schneider, J., Stenner, L., Wegener, G.: *Investigation of the influence of transducer electronic data sheets (TEDS) on calibration results*. In: *CD Proc. XVIII IMEKO World Congress on Metrology for a Sustainable Development, Rio de Janeiro, Brazil, September 17-22, Paper 372* (2006)
21. *Wizard – a programmable force indicator*. Dillon – Force Measurement Products & Systems (a division of Weigh-Tronix Inc.), Fairmont, MN, Prospectus 65-98
22. *Load cell accessories, electronic weighing*. Philips Wägetechnik GmbH, Hamburg, Germany, 9498-93
23. *Digital hanging scale legal for trade made in U.S.A.* John Chatillon & Sons Inc., Kew Gardens, NY (1989)
24. *Handheld digital force gauge model DFG 0.2 K*. Shimpo Industrial Co., Ltd., Kyoto, Japan, Catalog 72740A-88
25. Fricke, H.W.: *Measuring chains for non-electrical parameters*. *Philips in Science and Industry* 15(3), 14–15 (1970)
26. Ștefănescu, D.M.: *Strain gauge transducers for measurements in electrotechnics and energetics*. *Revue Roumaine de Sciences Techniques – série Électrotechnique et Énergétique*, Tome 32(4), 413–418 (1987)
27. Ștefănescu, D.M., Niculescu, A.: *Force and torque dynamometer for roll processing*. In: *Tehnologii – Calitate – Mașini – Materiale* (Selected papers, International Conference on Manufacturing Systems), vol. 33, pp. 123–126. Editura Tehnică, București (1998)
28. Harish, D., Patel, J.: *Wireless weight measurement kit*. Product News Loadstar Sensors, Inc., Mountain View, CA. *Sensors & Transducers e-Digest* 92(4) (May 2008)
29. *Wireless telemetry torque measurement*. Within “Sensing and Control” educational series, Honeywell, Golden Valley, MN, webcast, June 28 (2006)
30. Holland, P.: *A radiotelephone with weighing means*. Abstract of GB 2427979 invention. Data supplied from the esp@cenet database – Worldwide, January 10 (2007)

Chapter 18

WHEATSTONE BRIDGE – THE BASIC CIRCUIT FOR STRAIN GAUGE FORCE TRANSDUCERS

18.1. WHEATSTONE BRIDGE – GENERAL PRESENTATION

The strain gauge bonded on the elastic element is a secondary sensor which converts the strain produced by the force applied on the primary element into a resistance change. The classic configuration associated to the strain gauges is the low-power, Wheatstone bridge [18.1] – [18.4].

Bridge circuits are among the most elemental and powerful electrical tools. They are found in measurement, switching, oscillator and transducer circuits, serving from DC to bandwidths well into the GHz range. The electrical analogs of the mechanical beam balance, they are also the progenitors of many electrical differential techniques [18.5]. This circuit is usually credited to Charles Wheatstone, although Hunter Christie demonstrated it for the first time in 1833. But Wheatstone had a better public relations agency, namely himself, and his name became a common substantive in this respect.

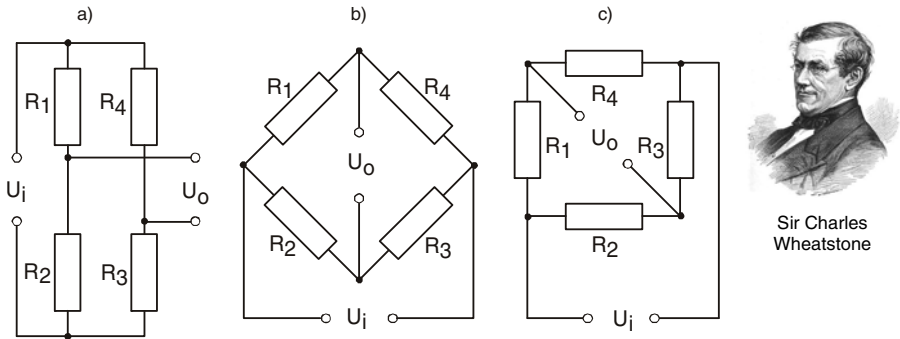


Fig. 18.1 Wheatstone bridge representations: a) rectangular, b) rhomboidal, c) square

A Wheatstone bridge is normally formed by four strain gauges, although it is possible to use only two SGs for a half-bridge or multiples of four on complex-shaped flexible bodies.

The classical Wheatstone bridge may be represented as an input-output device (two-port element), in several graphic formats, three of them being illustrated in Figure 18.1:

- rectangle – when the bridge is inserted into a complex measurement chain,
- rhomb – most useful and suggestive for strain gauges applications,
- square – rarely used, especially by American authors [18.6].

Due to the perfect symmetry, the input (power supply or excitation) and output (measuring signal or sensing) diagonals are interchangeable.

18.2. WHEATSTONE BRIDGE – FUNDAMENTAL PROPERTIES

The simple bridge (Fig. 18.2) is a complete network made of four sides (in which the usual strain gauge values are: 120 Ω , 350 Ω or 1 k Ω), four nodes (A, B, C, D) and two diagonals (U_A – supply, U_E – signal).

Our representation is in accordance with the Romanian tensometric standard and corresponds to the one of the German School. The initials DMS mean *DehnungsMeßStreifen*, i.e. *resistive strain gauges*.

Considering that the gauge is supplied from a constant voltage source of negligible internal resistance and its load is an amplifier having practically infinite input impedance and applying Kirchhoff's laws, the following is resulting:

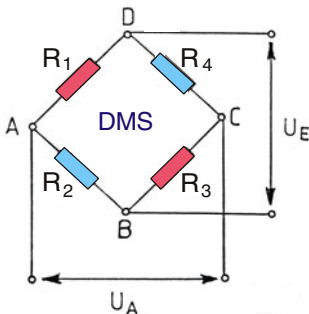


Fig. 18.2 Wheatstone bridge

$$\frac{U_E}{U_A} = \frac{R_1}{R_1 + R_2} - \frac{R_4}{R_3 + R_4} \quad (18.1)$$

The initial balance condition is:

$$R_1 \cdot R_3 = R_2 \cdot R_4 \quad (18.2)$$

meaning that the products of the resistances in the opposed arms should be equal and confirming the so-called

GOLDEN RULE OF STRAIN MEASUREMENT BY WHEATSTONE BRIDGE:

- the effects from two opposite arms are added,
- the effects from two adjacent arms are subtracted.

If $R_1 = R_2 = R_3 = R_4 = R$ (the usual case in the resistive electrical tensometry) and the resistance variations are considered much lower than the proper resistance values, then one may write the relation [18.7]:

$$\Delta U_E = \frac{U_A}{4} \left(\frac{\Delta R_1}{R_1} - \frac{\Delta R_2}{R_2} + \frac{\Delta R_3}{R_3} - \frac{\Delta R_4}{R_4} \right) \quad (18.3)$$

One may notice that in unloaded state ($\Delta R_i = 0$, where $i = 1, 2, 3, 4$) the balance $\Delta U_E = 0$ is found again. In case of a mechanical load ($\Delta R_i \neq 0$) one may write synthetically:

$$\Delta U_E = U_A \cdot \left| \frac{\Delta R}{R} \right| \quad (18.4)$$

which, expressed in words, means that:

The output voltage variation in the signal diagonal is proportional to the relative resistance variation of the Wheatstone bridge.

As a ratiometric device the bridge is extremely sensitive, its tensometrical sensitivity – obtained by correlating the formulas (3.2, for *gauge factor* k), (18.3) and (18.4) – being well approximated by the relation

$$S = \frac{\Delta U_E}{U_A} = \frac{n}{4} \cdot k \cdot \varepsilon \quad (18.5)$$

where n is the number of active arms, also called the *bridge factor* [18.8]:

- $n = 1$ quarter bridge;
- $n = 2$ half bridge;
- $n = 4$ complete (Wheatstone) bridge, made of four strain gauges, all of them being fully sensitive to the applied principal strain.

There are cases where the parameter n in the formula (18.5) is considered as an “equivalent number” of the bridge active arms and can have fractionary values. If two of the four strain gauges sense only the transverse effect of the axial loading, being “partially” active (Poisson’s coefficient $\nu = 0.3$), one can consider $n = 2.6$ (namely: $2 \times 1 + 2 \times 0.3$).

With the tensometrical transducers the Wheatstone bridge works in unbalanced mode (deviation method) [18.9]; the variation diagram of its relative sensitivity dependent on the amplitude and phase ratio between the adjacent arms impedances is shown in Figure 18.3a.

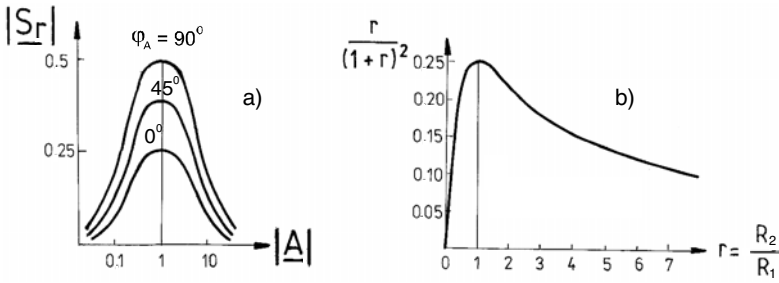


Fig. 18.3 Sensitivity diagrams for Wheatstone bridge (a) and bridge efficiency (b)

In other configuration [18.10] the circuit sensitivity variation (the bridge efficiency), shown in Figure 18.3b, leads to the same conclusion that the optimum value (0.25) is obtained when the resistances ratio R_2/R_1 is 1, namely when the resistances of the Wheatstone bridge are equal.

For the very sensitive sensors, as strain gauge like, the Wheatstone configuration is the best for the ideal conditioner. The complete bridge (with four equal and tensometrically active resistive arms), in combination with the differential nature of the electronic amplifier configuration, ensures a good rejection of the noise, thermal compensation and a linear transfer characteristic in a wide frequency bandwidth. It observes with respect to both diagonals (of excitation and response) the symmetry law, frequently encountered in nature.

18.3. BRIDGE COMPENSATION AND ADJUSTING RESISTORS

The following resistors are necessary for Wheatstone bridge’s compensation and adjusting (Fig. 18.4):

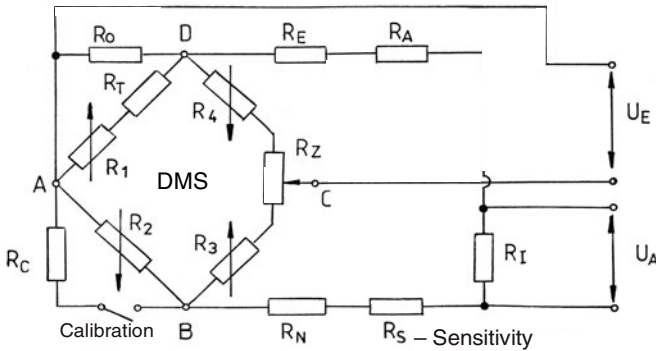


Fig. 18.4 Several correction, compensation and adjusting resistances needed to realize the full capability of strain gauged force transducers

- R_1, R_2, R_3, R_4 – strain gauges, for which the arrows offer a more suggestive representation of $\pm \epsilon$. We propose a code of colors (red = increases; yellow = dummy or constant; blue = decreases), with color nuances (pink or light blue) for strain gauges that are transversally strained where the increases or decreases are partial (Poisson’s coefficient: $\nu = 0.3$);
- R_T – compensation for the different thermal coefficient of the strain gauges by using some resistors with a low thermal coefficient, connected in series or in parallel with the strain gauges;
- R_Z – zero fine adjustment;
- R_E – compensation of the elasticity modulus variation due to the temperature, if the strain gauges and the elastic structure are not of similar alloys;
- R_A – compensation of the cross section variation during the loading;
- R_N – compensation of the unsymmetrical loading, if the structure is more sensible to the elongation than to the compression;
- R_S – sensitivity control when interchangeable transducers are to be used;
- R_I – the adjustment of the input resistance to the necessary value;
- R_O – initial balancing in case of the prestressed bonding of the strain gauges;
- R_C – calibration resistance (this adjustment is possible within the instrument that follows in the measuring chain too).

This shunt calibration resistor R_C is often fitted in the signal conditioner to be switched across one arm of the bridge when required [18.11]. For a 350Ω bridge, typical shunt calibration resistor values are $40 \text{ k}\Omega$ and $80 \text{ k}\Omega$, corresponding to approximately 90 % and 45 % of full load for a standardized value of 2 mV/V (2 millivolts output per volt applied at input).

Thanks to a special compensation procedure, crosstalk from parasitic stresses can be minimized [18.12]. To achieve this, each force transducer is individually subjected to a certain bending moment. By rotating the force transducer, this bending moment test is repeated in order to determine the influence on the output signal in multiple circumferential locations.

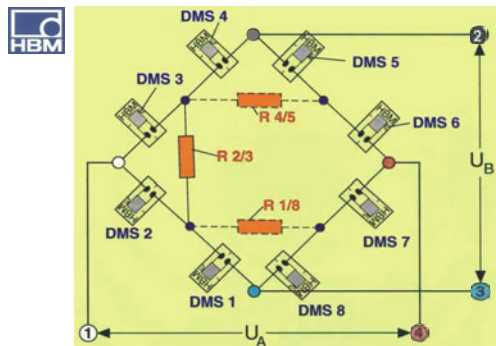


Fig. 18.5 Compensation resistors for reduced bending moment sensitivity

By means of a special algorithm that describes the interrelationship between moment stressing and its influence on strain in the measuring elements of the force transducer, the magnitude and location of compensation resistors – shown inside the Wheatstone bridge (Fig. 18.5) – can be specified. In this way, sensitivity to bending moment can be reduced by up to a factor of five.

In industrial applications, the distance between the force transducer and the measuring instrument may be considerable (hundreds of meters). The voltage drop along the connecting cable and its thermal dependence contribute to the system error; this can be avoided by using the six-wire technique: a couple of wires for excitation (sometimes called the “supply” or “drive” leads), another couple for output and two additional wires for “sense” leads.

Captain Ed Murphy Jr., a development engineer, frustrated with a strap transducer which was malfunctioning due to an error in wiring the strain gauge bridges, had a memorable remark – *“If there is any way to do it wrong, he will”* – referring to the technician who had wired the bridges. Nowadays, we assign Murphy’s law as a statement with a lot of associated variations.

18.4. SUPPLY POSSIBILITIES FOR WHEATSTONE BRIDGES

The Wheatstone bridge as a circuit for parametric transducers (resistive variation) arouses the interest especially in unbalanced mode, in which dynamic phenomena can be also measured, the DC supply being chosen from this latest point of view. The tensometrical sensitivity is not different in constant current or constant voltage supply versions [18.13]; however the first is to be preferred because it ensures a better “resources control” especially in the technique of the “dual current” [18.14], as well as high stability and convenient performance/cost ratio. A DC tensometric amplifier with a constant current generator and six measurement channels, achieved with integrated circuits, is depicted in [18.15].

This Handbook considers DC supplied tensometric bridges. A great part of the described properties and conclusions are also applicable to the AC bridge transducers or impulses supplied. As an alternative to DC excitation, the AC system excites the force transducers with sine waves (carrier frequency), square waves or other periodically varying inputs. The application of harmonic excitation is similar to the impulse excitation [18.16]. If two or more frequency carriers are used, it is possible to achieve a higher amplitude signal while maintaining the same effective value; the total signal is modulated and the procedure is similar to the single frequency carrier technique but multiplied.

To increase the SG signal output during the noise period, pulsed power supplies are sometimes used (Fig. 18.6). Considerable design effort ensures the pulse reaches its proper amplitude quickly and the voltage is maintained with minimum drop so as to prevent errors due to SG sensitivity decreasing [18.17].

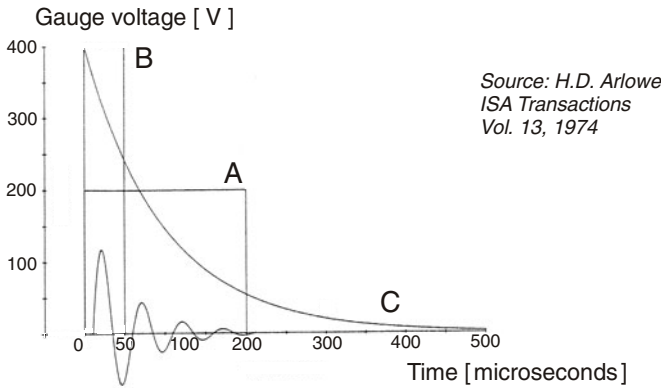
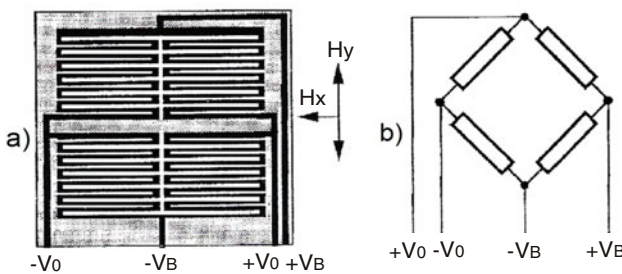


Fig. 18.6 Comparison between A and B pulses: to increase the signal amplitude A by a factor of 2, the pulse B must be increased by a factor of 4. The exponential pulse C is the real one for supplying the strain gauged force transducer.

In some force transducer arrangements various AC bridges intervene, which are not always exact equivalents of the Wheatstone bridge. For example, the four-arm capacitor bridge behaves like a resistive Wheatstone bridge only in balanced condition, while the unbalanced output is in a higher degree dependent on the load. Another frequently employed AC bridge is the inductive ratio/arm (or transformer-arm) one, which is an ideal differential device that can operate in both balanced and unbalanced conditions.

18.5. DIFFERENT APPLICATIONS WITH MEASURING BRIDGES

A magnetoresistive sensor is fabricated of permalloy strip positioned on a silicon substrate [18.18]. Each strip is arranged in a meander topology (Fig. 18.7) and form an arm of a Wheatstone bridge. The degree of bridge imbalance constitutes an indication of the magnetic field strength.



*Courtesy of Jacob Fraden
from [18.18]*

Fig. 18.7 Four magnetoresistors in Wheatstone bridge (a) and its equivalent circuit (b)

Electro Standards Laboratories (Cranston, RI) has announced the model 4336 CellMite Quad AC/DC four-channel digital signal conditioner with 24-bit internal resolution [18.19]. It connects directly to two AC (sine wave) linear variable differential transformer transducers and two DC strain-gauged force transducers and provides digital data input into the serial port of a standard PC and 16-bit analog outputs. The unit independently compensates each channel's transducer nonlinearities using its integrated six-point calibration capability. Optional CellView multi-unit graphical user interface software is available.

A new transducer concept for combined force and torque measurement proposes a surface micromachined chip, stiffly mounted, instead of resistive strain gauges, on a rod under load or a torsionally deformed shaft [18.20]. For the automotive customers the measuring device consists of a freestanding interdigitated electrode which forms a variable capacitor, changing its capacitance in accordance with the applied break force or powertrain torque. The fabrication process allows the sensor integration with a CMOS-ASIC on one chip.

Fig. 18.8a shows interdigitated, freestanding combfingers made of $4\ \mu\text{m}$ thick polycrystalline silicon, structured with 1:4 aspect ratio. The connected side of the combs is anchored to the substrate and thus a shear-deformation of the substrate causes the fingers to change their relative position to the substrate (Fig. 18.8b). The individual combs are electrically arranged to form a capacitive full-bridge (Fig. 18.8c). For shear deformation between 0.035 % and 0.1 % the measuring sensitivity is about $0.43\ \text{nF/MPa}$.

So, the best method to measure small changes of resistance, inductance or capacity is generally through a bridge arrangement. Figure 18.9a shows the measurement scheme used by Gel *et al.* [18.21] to establish a record in force measurement threshold ($6.94\ \text{pN}$). Figure 18.9b presents an inductive half-bridge completed with an internal resistive half-bridge of measuring amplifier.

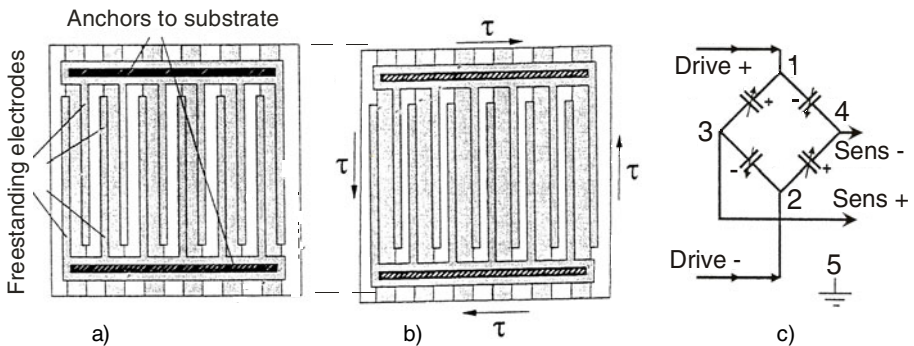


Fig. 18.8 Interdigitated combfingers (a), their shear-deformation (b) and capacitive bridge connection with driving and, respectively, sensing diagonals

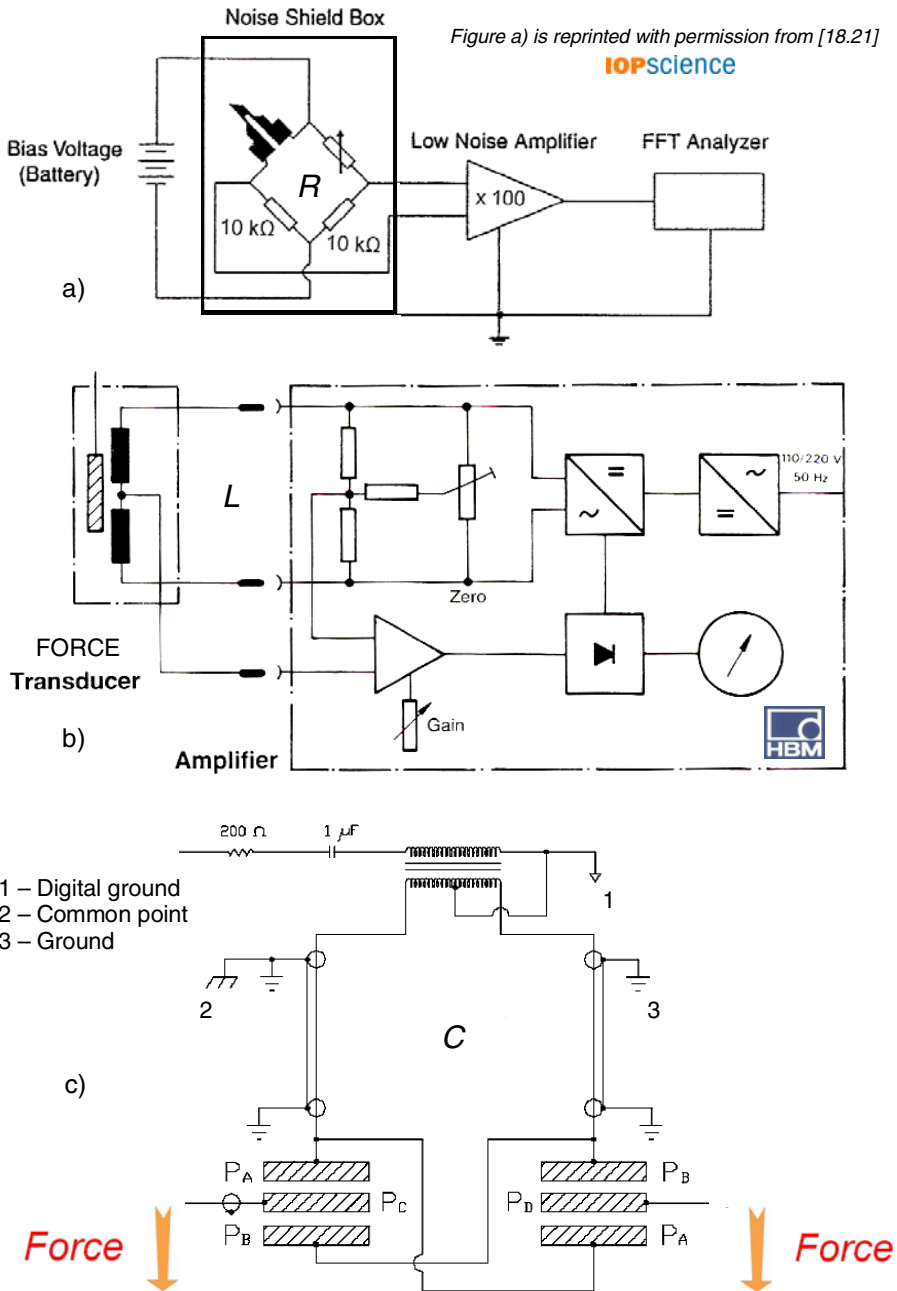


Fig. 18.9 Full resistive (a), half inductive (b) and half capacitive bridges (c). Different grounding representations: 1 – digital, 2 – common, 3 – classic.

Most professional seismometers and accelerometers appear to use a variable capacitance displacement transducer in a half-bridge configuration. Wanting to ensure decent performances from a crude homemade instrument [18.22], a full bridge, or symmetric differential capacitive (SDC) transducer was selected (Fig. 18.9c). SDC transducers consist of two separate sensing devices rigidly coupled together to move as a single unit. Each transducer forms a branch of the bridge circuit.

Compared to a half-bridge, an SDC transducer has double the sensitivity, a well defined null position and does not require a very precise symmetric oscillator. Its main drawback is the need for two variable capacitors and a precise method for differentiating their output signals. A three-plate transducer design balanced out the electrostatic forces acting between the plates. Finally, a performant vertical component seismometer with a broadband response, flat between frequencies 0.05 Hz and 10 Hz, resulted.

After seeing in the same Figure 18.9 (a, b and c) three parametric sensing elements (R, L, and C) connected into their associated bridges, one can think about a direct sensor-to-microcontroller interface for resistive, inductive and capacitive bridges.

18.6. FURTHER CONNECTIONS FOR WHEATSTONE BRIDGES

The Wheatstone bridge, comprising, for example, four strain gauges bonded on the elastic element of a force transducer, is the “heart” of the complex measurement chain. As part of an electrical “cascade” (Fig.18.1a), the Wheatstone bridge requires an excitation voltage to be supplied as well as conditioning and amplification of the output signal before its displaying or including in an automatic control system.

The Wheatstone bridge can be also connected to an analog-to-digital converter [18.23], the frequency conversion amplifying appreciably the small resistive variations. Fig. 18.10 shows a configuration with an AD 537 voltage-to-frequency converter. The bridge is supplied by means of a repeater to the U_r voltage of the integrated circuit. The sensitivity can be adjusted to 1 Hz/ $\mu\text{m}/\text{m}$. Such a system proves a higher immunity to thermal effects, improved noise rejection, good zero force stability and proper isolation between the output signal and the load cell. In case of deposited strain gauge technology, the high resistive values (11 k Ω) allow the work at high frequencies (1 MHz), having a rectangular wave on excitation with a space factor of 50 % and a sensibility value of about 1 Hz/ $\mu\Omega/\Omega$ [18.24].

The American patent [18.25] proposes the changing of the transducer sensitivity by selecting the corresponding phases of different amplitudes of a cyclical excitation.

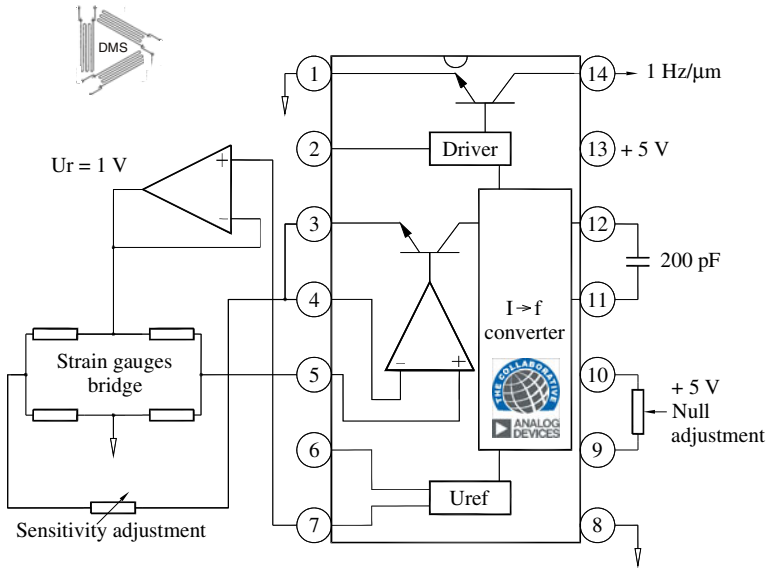


Fig. 18.10 Strain gauge Wheatstone bridge and voltage-to-frequency converter AD 537

At the picostrain level, a special Wheatstone bridge with small resistances (10Ω), connected to a DAQ system for recognizing the unique force signature of a moving vehicle at Idaho Transportation Department, is shown in [18.26].

Setting up a *Wheatstone bridge based transducer* requires several inputs from the data sheet, such as *gauge resistance* and *strain sensitivity*, in order to allow the instrumentation and software to properly convert the output voltage into engineering units. For example, the NI 9237 bridge-based measurement module, combining signal conditioning, analog-to-digital converters (ADCs) and signal connectivity into a single compact device, is a part of the C Series family of hardware and has several options for system development [18.27]:

- *Single-module carriers* are available for USB, Ethernet, or wireless communication back to a PC.
- For *larger systems*, National Instruments CompactDAQ offers two USB chassis which support the NI 9237 module.
- For *deployment without a PC*, the NI CompactRIO chassis support up to eight modules and have a built-in processor, memory and storage space designed to run a LabVIEW program locally in order to create rugged test, monitoring, and control systems.

With this modular, flexible hardware system, one can use the comprehensive lines of Honeywell load cells, and force, torque or pressure transducers in a wide variety of smart applications and over various buses for communication.

PCB Piezotronics, Inc. has introduced a broad range of Strain Gage Dual Bridge Load Cells for airframe structural test applications. PCB® Series 1200 includes a dual output feature to provide control feedback from one bridge while the other is used for data acquisition (DAQ). Other connection possibilities for Wheatstone bridges – today common substantives in strain gauge measuring – are shown in the next chapter.

In conclusion, a basic idea in the field of tensometric bridges used in force transducers is the strong “synergy” between the mechanic aspects (elastic elements to which the strain gauges are attached) and the electric ones (associated electrical techniques). Figure 18.11 shows an ingenious combination of nine complex elastic elements, each of them including seven Wheatstone bridges, for determining the weighing-in-motion load distribution for heavy trucks [18.28].

REFERENCES

1. Hoffmann, K.: An Introduction to Measurements using Strain Gages. Hottinger Baldwin Messtechnik GmbH, Darmstadt (1989)
2. Kautsch, R.: Elektrische Brückenschaltungen für nichtelektrische Meßgrößen. VFI – Der Versuchs- und Forschungsingenieur 10(3), 48–50, (4), 48–54, (5), 51–58 (1983)
3. Peiter, A., Keil, S., Rockschie, J., Fischer, W.: Spannungsanalyse mit Dehungsmeßstreifen. Grundlagen, Anwendung, Auswertung. VDI-Verlag, Düsseldorf (1981)
4. Rohrbach, C.: Handbuch für experimentelle Spannungsanalyse. VDI-Verlag, Düsseldorf (1989)
5. Williams, J.: Bridge circuits. Marrying gain and balance. Linear Technology, Application Note 43-90
6. Northrop, R.B.: Introduction to Instrumentation and Measurements. CRC Press, Boca Raton, FL (1997)
7. Pople, J.: Strain Measurement Reference Book. The British Society of Strain Measurement, Newcastle upon Tyne, England (1979)
8. Száva, I., Ciofoaia, V., Luca–Motoc, D., Curtu, I.: Experimental Methods in Mechanical Structures Dynamics, vol. 1. Editura Universităţii Transilvania, Braşov (2000) (in Romanian)
9. Ionescu, G., Dobrescu, R., Droaşcă, B., Guţu, A.: Transducers for Industrial Automatization, vol. I. Editura Tehnică, Bucureşti (1988) (in Romanian)
10. Dally, J.W., Riley, W.F., McConnell, K.G.: Instrumentation for Engineering Measurements. John Wiley & Sons, Inc., New York (1993)
11. Hunt, A. (Coord.): Guide to the Measurement of Force. The Institute of Measurement and Control, London (Published 1998); ISBN 0-904457-28-1
12. Reduced bending moment sensitivity. Hotline Hottinger – Informationen aus der industriellen Messtechnik (2), 22–23 (2004)

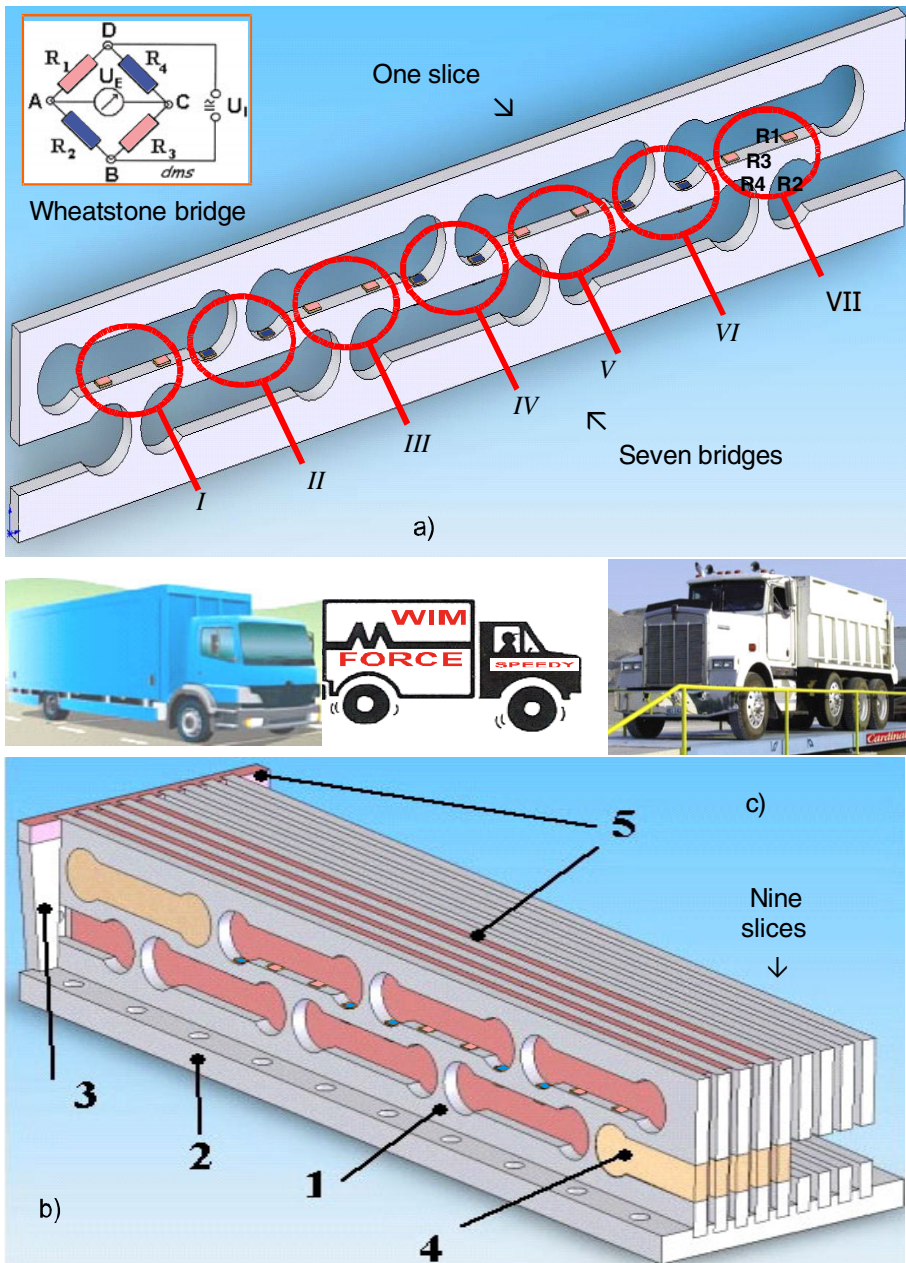


Fig. 18.11 Weigh-in-motion (WIM) system: a) strain gauged complex elastic element, b) general assembly: 1 – spring element, 2 – basic plate, 3 – lateral plate, 4 – soft foam, 5 – rubber, and c) weighing platform for heavy trucks

13. Low level digital data acquisition. Takeda Riken Co. Ltd., Japan, Appl. Note 1F-89
14. Pearce, J.R.: Logging with strain gauges using the dual current technique. Instrumentation Group Solartron-Schlumberger, Farnborough (1982)
15. Ștefănescu, D.M.: DC tensometric amplifier with integrated circuits. In: Proc. 2nd Romanian Symp. on Tensometry, Cluj-Napoca, June 11-14, vol. I, pp. 423–430 (1980) (in Romanian)
16. Kuhinek, D., Zorić, I., Butorac, J.: Increase of strain gage output voltage signals accuracy using virtual instrument with harmonic excitation. In: Proc. XIX IMEKO World Congress, Lisbon, Portugal, September 6-11, pp. 797–801 (2009)
17. Arlowe, H.D.: A new pulsed power strain-gage system. ISA Transactions 13, 269–273 (1974)
18. Fraden, J.: AIP Handbook of Modern Sensors – Physics, Design and Applications. American Institute of Physics, New York (1993)
19. Rubin, L.G.: Focus on sensors. Physics Today 59(6), 72 (2006), <http://www.physicstoday.org/vol-59/iss-6/p72.html>
20. Meckes, A., Aigner, R., Dorfinger, G., Wachutka, G.: Capacitive silicon microsensor for force and torque measurement. In: Int'l Conf. Transducers XI and Eurosensors XV, Munich, Germany, June 10-14, Paper 2A3.05 (2001)
21. Gel, M., Shimoyama, I.: Force sensing submicrometer thick cantilevers with ultra-thin piezoresistors by rapid thermal diffusion. J. Micromech. Microeng. 14, 423–428 (2004)
22. Coleman, A.: An amateur, vertical component, broadband seismometer (model MkXVIII), May 15 (2006) <http://www.physics.mercer.edu/petepag/mkxx.pdf>
23. Iliescu, C., Pantelimon, B., Cepișcă, C., Vlaicu, C.: Metrology. Measurement Systems. Actual Concerns. Editura ICPE, București (1994) (in Romanian)
24. Ferrari, V., Ghidini, C., Marioli, D., Taroni, A.: A conditioning circuit for resistive sensors combining frequency and duty-cycle modulation of the same output signal (design note). Measurement Science Technology 8, 827–829 (1997)
25. Talmage, P.C.: Method and apparatus for changing the sensitivity of a transducer. US Patent 5287748-94
26. Latta, B.M.: Picostrain engineering data acquisition system. US Patent 6556927-2003
27. Burger, B.: Pressure, load, and torque measurements made smarter and easier. National Instruments News (June 10, 2010)
28. Bârsănescu, P., Cârlescu, P., Ștefănescu, D.M.: A new weigh-in-motion and traffic monitoring system. In: CD IMEKO Int'l Conf. Cultivating Metrological Knowledge, Merida, Mexico, November 27-30, Paper 5 (2007)

Chapter 19

STRAIN GAUGES ELECTRONIC CIRCUITS

19.1. SIGNAL CONDITIONING FOR FORCE TRANSDUCERS

Transducers have an outstanding position within the force measurement chain (Fig. 19.1). Accurate measurement of low-level analog signals with a DAQ system requires more than simply wiring the output of the transducer to the signal conditioning circuitry and then to the analog-to-digital converter [19.1].

Most transducer-based measurement requirements are well served by the resistive strain-gauged transducers and signal conditioning techniques based on the Wheatstone bridge [19.2]. But strain gauges are not only the resistive sensors, here are other measurement principles “connectable” with this general category: inductive, capacitive, “transverse voltage” (Hall effect), vibrating wires, microresonant, surface acoustic waves and optical (fiber Bragg gratings).

Parametric sensing elements (R–L–C) have a wide range of applications. Interdigitated combfingers can be electrically arranged to form a capacitive full bridge. The operating principles of the inductive LVDTs are applied in the force-balanced pendulous accelerometer and in the rate gyroscope. Therefore, almost the whole dozen of measurement principles, presented in the first part of this Handbook, is “covered” by similar measuring techniques.

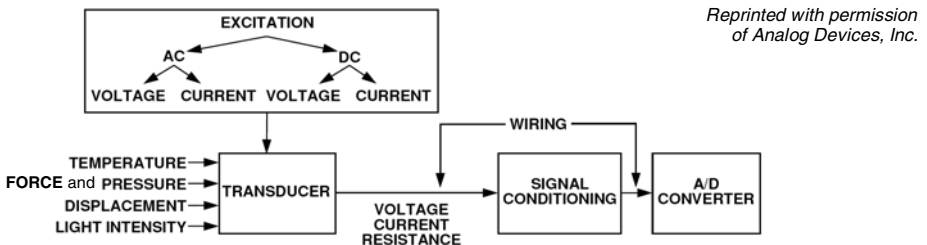


Fig. 19.1 A generalized block diagram of a transducer-based data acquisition system

In this chapter a short review is sketched of the main electronic circuit types that are frequently encountered in force measuring systems. Due to the multiple interdependencies of measurement principles and sensing devices and, on the other side, the high degree of integration of modern electronic circuits, it is difficult to achieve a systematic description as well as strict delimitations of the circuit categories involved [19.3]. In the following subchapters, the most important classes of such circuits are illustrated: conditioners, convertors, oscillators, pulse generators and other electronic circuits connected with PC.

19.2. SIGNAL CONDITIONERS

19.2.1. Pre- and post-conditioning

Warsza *et al.* [19.4] propose a double current supply for a four-terminal bridge as a valuable supplement for well-known conditioning techniques of analog signals (Fig. 19.2). This is an unconventional supply of four-arm bridge circuit by two current sources (with LM317) connected in parallel to opposite arms.

The output voltages from both diagonals, U_{AB} and U_{CD} , are applied to the inputs of the post-conditioning module which consists of an instrumentation amplifier (AD620AN) and a 24-bit sigma-delta A/D converter (AD7718). A microcontroller performs the data processing of the output signals, yielding a linear function related to the strain gauged cantilever beam deflection.

The advantages of this solution are the following:

- simultaneous measurement of mechanical strain and temperature;
- temperature reading and compensation without special sensors;
- no need for additional hardware or software linearization;
- custom designed elastic elements for measuring force, pressure, etc.

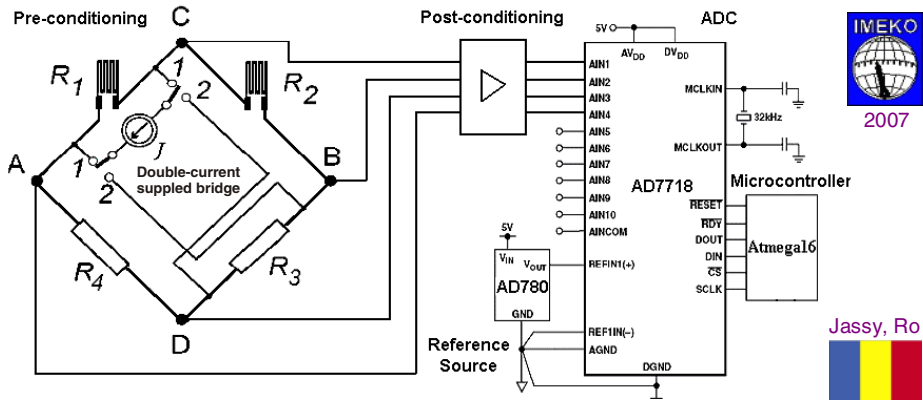


Fig. 19.2 Double-current supplied bridge circuit for strain gauged force transducers

19.2.2. High-gain signal conditioning

A high-gain signal conditioning circuit made by Maxim – Dallas Semiconductor is shown in Figure 19.3 [19.5]. Using the MAX4196 instrumentation amplifier as a pre-amp circuit adds a factor of 10 V/V gain to the signal path enabling sensor calibration and temperature compensation with the MAX1452. There are 16 gain settings that range from 39 to 234 in increments of 13.

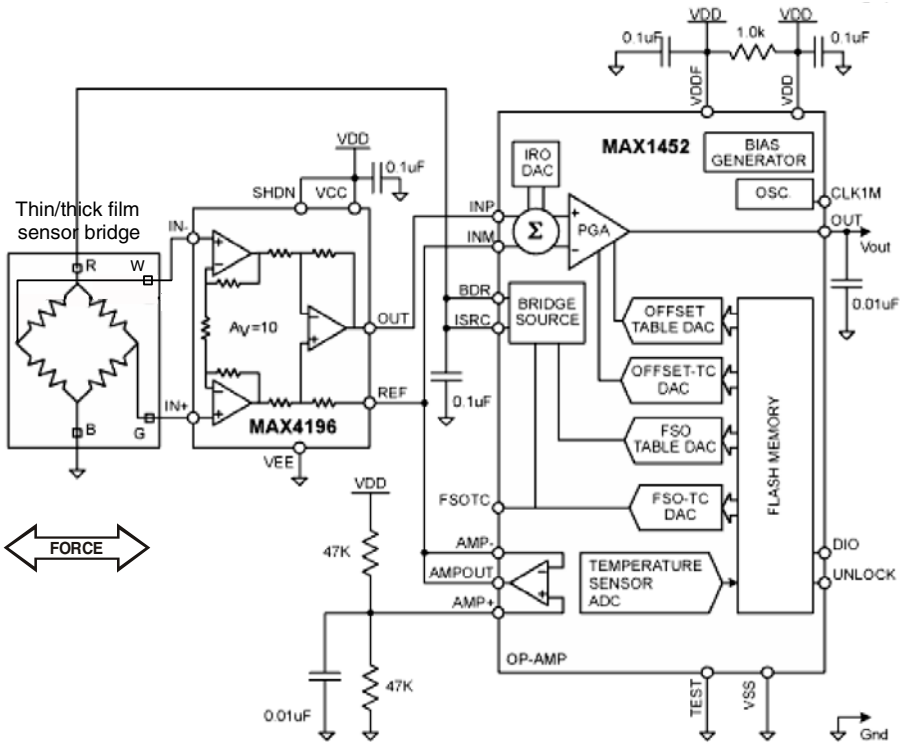


Fig. 19.3 High-gain signal conditioning circuit for thin and thick film transducers

19.2.3. “QuantumX” universal conditioner

QuantumX [19.6] is a “multi-talented” performer for numerous transducers having different measuring principles (Fig. 19.4a). A single MX840 amplifier module has eight universal connectors that suit all common transducer technologies, whatever the combination. One may simply connect the transducer and measure at 24-bit resolution with Advanced Plug & Measure! Its TEDS (unique identifier tag) ensures that transducer details are quickly, conveniently and safely transmitted to QuantumX, so that measurement can immediately start.

Here are four examples of different transducers to be connected with QuantumX, the universal conditioner:

- cubic unit cell with antisymmetric slots as an elastic element for strain gauged force transducers (Fig. 19.4b) [19.7];
- high-resolution, magnetic speed measuring system HBM, based on the non-contact sampling of a magnetized rotor by means of GMR sensors [19.8];
- PACEline CMC – piezoelectric force measurement chain HBM;
- optical strain sensors based on Bragg gratings [19.9].

The QuantumX Assistant sets new standards for functionality and ease of operation having the following features:

- fast and easy setup and parametrization;
- automatic sensor detection via TEDS;
- comprehensive sensor database;
- measurement data visualized as graphs.

Professional data acquisition with catman®AP bundles together highly efficient modules for a wide variety of different measurement tasks. Together they make up a flexible, powerful and networked high-performance package.

QuantumX can be conveniently integrated into LabVIEW® or other applications and programs via the API (application program interface).

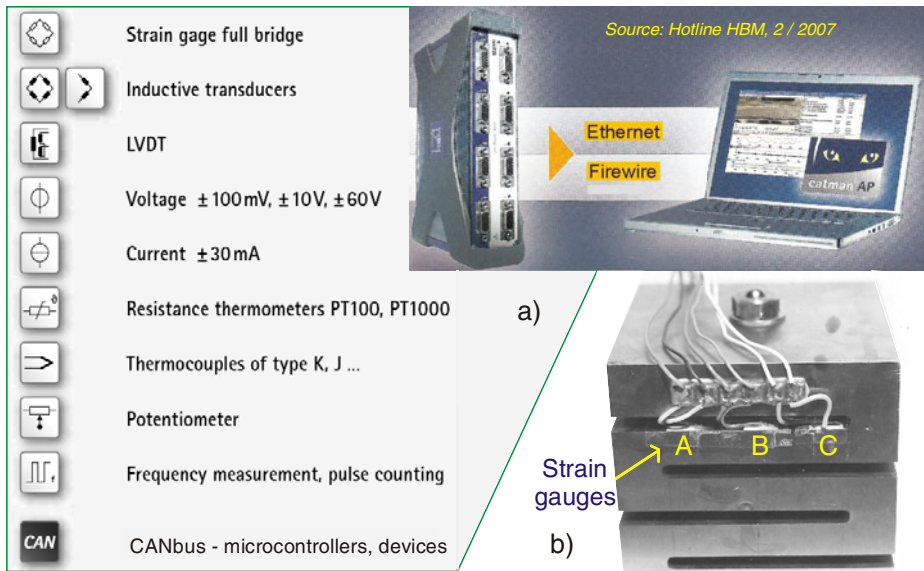


Fig. 19.4 a) Universal module that “embeds” a wide range of different techniques for measuring mechanical quantities [HBM]; b) Strain gauged parallelepipedic elastic element with antisymmetric slots [Găvan & Ștefănescu].

19.3. ANALOG-TO-DIGITAL CONVERTERS

19.3.1. Different conversions to frequency

Modern instrumentation uses the digital measurement and computer support. The analog-to-digital conversion is more rapidly performed nearer to the measuring system input. Voltage-to-frequency ADCs convert an analogical input voltage to an output pulse train having the frequency proportional to the input signal. Output frequency is determined by counting pulses over a fixed time interval. Voltage-to-frequency conversion, commonly used to convert slow and often noisy signals, has a high degree of noise rejection, because the input signal is effectively integrated over the counting interval.

Fig. 18.10 presented a strain gauge Wheatstone bridge connected to a voltage-to-frequency converter AD 537. Other configurations are based on current-to-frequency [19.10] or resistance-to-frequency [19.11] converters, some of them having programmable sensitivity and resolution [19.12].

Analog Devices, Inc. has introduced a series of high-precision, fully integrated converters that address the complex and difficult task of direct capacitance-to-digital conversion [19.13]. Combining advanced signal processing techniques with high levels of integration, ADI's capacitance-to-digital converters attain a level of precision previously only possible with conventional analog voltage-to-digital converters including a large number of discrete components. These devices provide designers significant advantages over existing discrete solutions for capacitance- and impedance-sensing applications that have historically lacked precision, and difficult design.

AD7745/6/7 integrates all stages of capacitance-to-digital conversion on one chip reducing costs associated with traditional multi-chip solutions by 65 percent. With 24-bit resolution, the AD7745 is the industry's highest-precision solution for interfacing with capacitive transducers.

Specifications include an operating range from 2.7 to 5.25 V, an error limit of 2×10^{-15} F, a speed of 5 to 90 Hz, and a power consumption of 1 mA maximum.

19.3.2. Resistance-to-time converter

It is often desirable to convert the resistance change of the resistive sensors into a proportional frequency or time interval, so that a digital output signal can be directly obtained. The converter presented in Figure 19.5 is essentially a relaxation oscillator, consisting of a bridge amplifier and a comparator [19.14].

The three resistors R_1 , R_2 and R_X and the series combination of R_3 and C are the four arms of a bridge which, together with OA_1 , forms a bridge amplifier. Assuming the op-amps to be ideal, it can be shown that the circuit will function as an oscillator when R_X takes a value greater than $R_1 \cdot R_3 / R_2$.

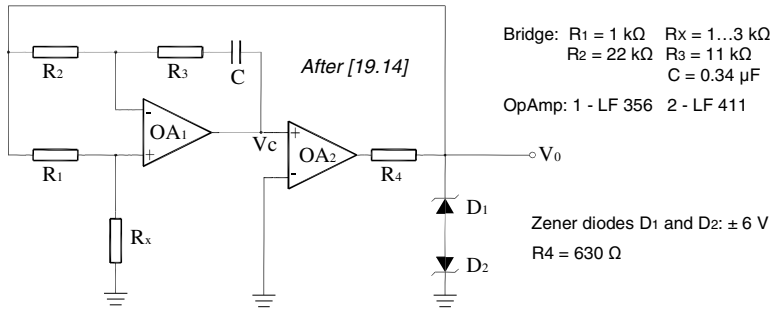
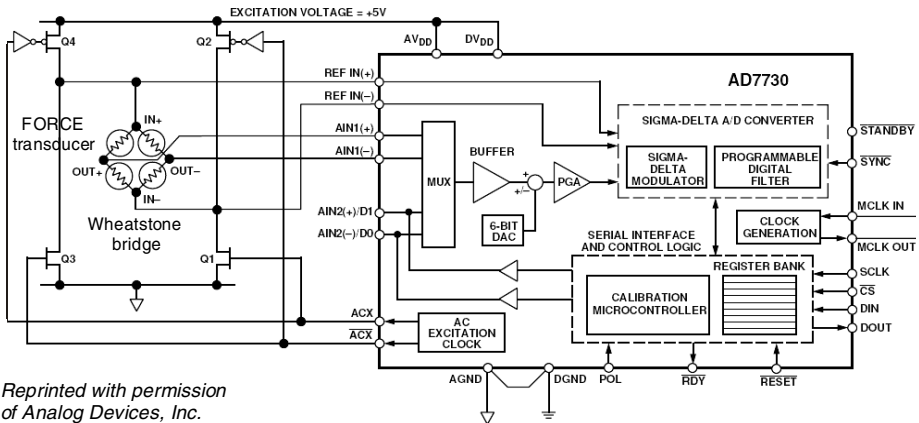


Fig. 19.5
Resistance-
to-time
converter

This simple circuit provides a time period output proportional to an input change in resistance. Besides a high order of resolution, the circuit offers an excellent linearity, over a wide resistance range. These features, together with its easily adjustable sensitivity and easy adjustment of the offset period by varying a single resistance, should favor wide application of the proposed circuit for resistive transducers signal conditioning.

19.3.3. Sigma-Delta converter

Fig. 19.6 shows a bridge-transducer application using the AD7730 ADC, which includes on-chip all the necessary circuitry to implement AC excitation and produce the computed output result following the switching of the excitation [19.1]. The AD7730 Sigma-Delta ADC is a complete analog front-end for weigh-scale and pressure-measurement applications. Ratiometric is preferred because it permits measurement and control with accuracy greater than the stability of voltage references or excitation supplies.



*Reprinted with permission
of Analog Devices, Inc.*

Fig. 19.6 Sigma-Delta converter for bridge-transducer applications

Operating from a single $\pm 5\text{ V}$ supply, it accepts low-level signals directly from a transducer and outputs a serial digital word. The input signal is applied to a proprietary programmable gain front end, based on an analog modulator. A low-pass programmable digital filter with adjustable filter cutoff, output rate, and settling time processes the modulator output. There are two buffered differential programmable-gain analog inputs and a differential reference input. It accepts four unipolar and bipolar analog input ranges from 10 mV to 80 mV full-scale.

19.4. BRIDGE OSCILLATORS

19.4.1. Wien bridge based oscillator

Another possibility of tensometrical signals discrete processing is represented by a Wien bridge RC oscillator (Fig. 19.7), with low frequency output (up to 100 kHz). It may be considered as a two reaction-loop amplifier and therefore the stability increases while the amplification and the nonlinear distortions decrease. In his British patent 1223810 A.J. Yerman proposes the measurement of forces or accelerations by means of a cantilever lamella having two pairs of opposite-type semiconductors: the bar is n-type and the strain gauges are p-type.

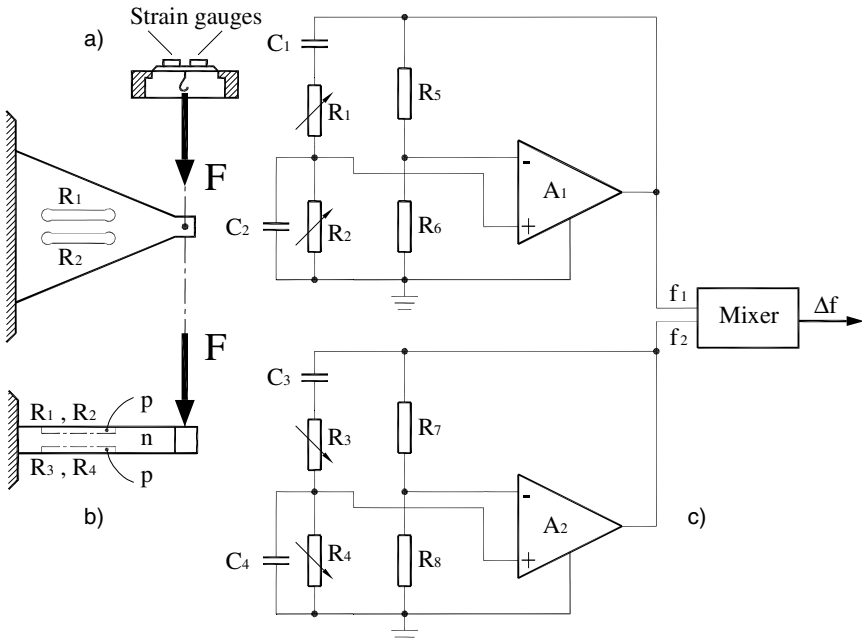


Fig. 19.7 Two of the most widely used SG elastic elements: circular membrane (a) and equal resistance lamella (b), working with a Wien bridge based oscillator (c)

The strain gauge pairs are located and cristallographically oriented in such a way as to produce equal and opposite signs resistance changes; so the frequency of an oscillator increases while that of the other decreases according to the applied force. Finally, one can obtain additive Δf , the tensometrical oscillator sensitivity being doubled. The frequency modulation allows the digital signal integration (acceleration \rightarrow speed \rightarrow distance) as for rockets guidance systems.

The silicon technology [19.15] allows to develop some integrated sensors which represent both the proper elastic element like the circular membrane (Fig. 19.7a) or the lamella of equal resistance (Fig. 19.7b), and the pairs of semiconductor strain gauges, having the sensitivity of two orders of magnitude over that of classical metallic strain gauges, to which the miniature amplification part and the microprocessor are added, making all an harmonious and efficient assembly of strain gauged force transducer [19.16].

The p-n semiconductor strain gauge pairs are actually resistive half-bridges which can be connected as variable resistances to the Wien bridge oscillator (Fig. 19.7c).

19.4.2. Wheatstone bridge based oscillator

The p-n semiconductor strain gauge pairs as resistive half-bridges can be included in the Wheatstone bridge based oscillators too. They are useful for mechanical quantities tensometry, as for a deflection sensor “cartridge” type [19.17] or for other applications found in a number of corporate documents [19.18] – [19.21].

The integration of cantilever arrays in a single chip along with signal processing electronic circuits, achieved by the Biofinger project, open new ways for miniaturized sensing systems [19.22]. An array-based approach was adopted by researchers at the Swiss Federal Institute of Technology to allow parallel screening of different analytes and increase the overall analysis speed. The resonant cantilever system has four equally-spaced cantilevers with read-out scheme integrated for their fully autonomous operation. The resonant cantilevers are actuated by electromagnetic forces generated by a permanent magnet and an alternating current flowing into a metal loop.

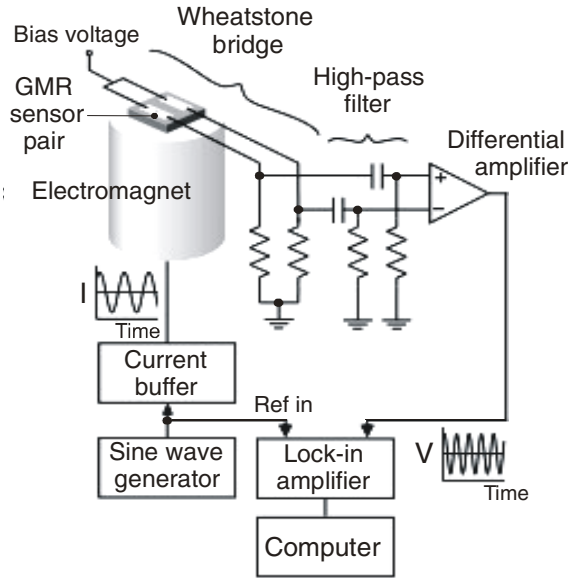
The binding of the analytes changes the mechanical properties of the cantilevers, which can be detected by piezoresistors (or stress-sensitive transistors), arranged in a Wheatstone bridge configuration. The cantilevers act as frequency-determining elements in a feedback oscillation circuit, with a counter.

A highly sensitive force/mass detection method and device using phase synchronization within an oscillation circuit of a mechanical vibrator is presented in [19.23].

19.5. AC GENERATORS

19.5.1. Sine wave generator

The sine wave generator, depicted in Figure 19.8, is a basic component inside the block diagram of a biosensor based on GMR (giant magnetoresistance) technology [19.24].



Reprinted from [19.24]
copyright 1998, with
permission from Elsevier

Source: Baselt et al.
Biosensors & Bioelectronics,
No. 13, pp. 731-739, 1998.



Fig. 19.8 Biosensor based on magnetoresistance technology and Wheatstone bridge

Up-to-date electronics is used to detect and manipulate magnetic beads. Two giant magnetoresistive elements (signal and reference) are incorporated in a Wheatstone bridge. The magnetizing-field electromagnet is modulated at 200 Hz and the resulting 400 Hz signal of the bridge is detected with a lock-in amplifier. High-pass filters eliminate the need to manually balance the resistance of the signal and reference.

19.5.2. Saw-tooth wave generator

A saw-tooth wave generator is included in the block diagram of a so-called “smart” pressure transducer [19.25] made by Honeywell (Fig. 19.9a). The skilful arrangement of discrete resistor combinations on the chip (Fig. 19.9b) and microprocessor-controlled generation of the pulse-width modulated signal gives noteworthy characteristics, the most important being the wide measuring range, with a ratio of 1:400.

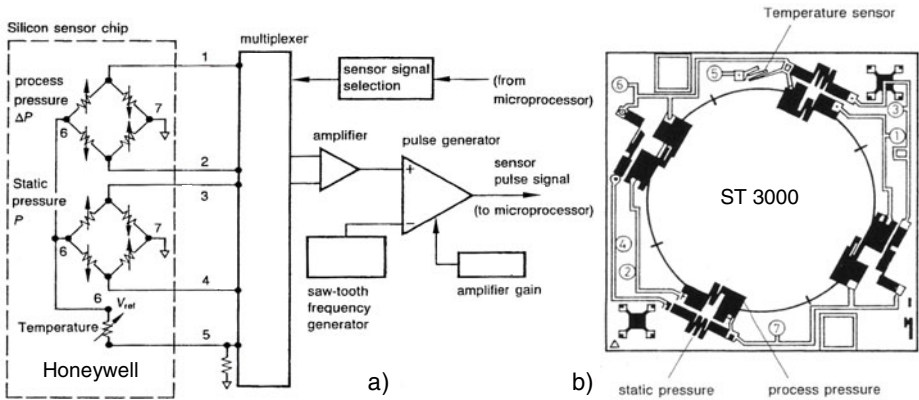


Fig. 19.9 Block diagram of a pulse-width modulated digital signal generator (a) and pressure sensor ST 3000 – Honeywell (b) (Carl Hanser Verlag Munich permission)

19.5.3. Rectangular wave generator

An application specific integrated circuit (ASIC) front-end interface in 0.7- μm CMOS for resistive-bridge sensors is proposed in [19.26]. The circuit is based on a relaxation oscillator where the frequency of the rectangular-wave output is related to the fractional bridge unbalance, and the duty cycle depends on the overall bridge resistance, typically related to temperature. In this way, two independent pieces of information are simultaneously and cost-effectively carried on the same output signal. The bridge is driven at constant current; this avoids accuracy degradation with remotely placed sensors and enables a first-order thermal compensation for piezoresistive semiconductor sensors.

The circuit has been characterized by means of a 1-k Ω reference bridge showing frequency and duty cycle sensitivities of 60.4 Hz/(1000 ppm) and 0.276 %/(m Ω / Ω), respectively, at a central frequency of about 6.4 kHz. The circuit has also been tested with a piezoresistive SiC sensor operated at temperatures up to 150 $^{\circ}\text{C}$, showing results in agreement with theoretical predictions.

An application specific paper [19.27] describes a design approach for intelligent pressure sensors and transducers. Direct interfacing is based on the universal frequency-to-digital converter (UFDC-1). By eliminating the need for ADC, the frequency (duty-cycle or PWM)-to-digital conversion schemes reduce the systems complexity.

The results of such a design approach are high-performance single-chip pressure sensors with truly digital output (RS-232 interface) or bus output (SPI or I²C) with significant reduction of production cost, time-to-market and simplification of the design process.

19.6. STRAIN GAUGED FORCE TRANSDUCERS CONNECTED TO PC

During the evolution of the force measurement chain, while the analog part is reduced to the minimum, the signal conditioning tends to become the PC task, based on specific algorithms and using specific digital signal processing functions. In this respect two directions were developed: direct resistance change measurement and strain gauge bridge signal processing.

19.6.1. Direct resistance change measurement

A simple, low-cost electronic interface, suitable for use with piezoresistive microcantilever-based sensors, utilizes the USB bus of any computer or laptop to communicate with the sensor via SPI commands [19.28].

Embedded piezoresistive microcantilever (EPM) sensors provide a simple, low-cost platform for the sensing of a wide variety of analytes. In the basic design, a tiny piezoresistive microcantilever (100...200 μm in length) is (partially) embedded in a “sensing material”, which is chosen to volumetrically react when exposed to the analyte. The reaction of the analyte molecules with the sensing material may be a chemical reaction, mechanical (partitioning or diffusion), absorption, or adsorption, or other reaction as long as some sort of movement of sensing layer takes place. The volumetric change in the sensing layer subsequently results in a strain in the EPM, which is measured as a resistance change by the associated sensor electronics.

The above-mentioned interface is based on LabVIEW and utilizes two primary integrated circuits. The first IC is used to translate commands from LabVIEW through the computer’s USB port into SPI commands, while the second IC serves as a 24-bit A-D converter (AD7793) and precision current supply for the EPM sensors. The AD7793 provides two programmable current sources, which are set at 100 μA to excite the two resistive elements (piezoresistive microcantilever and thermistor). Commands to the AD7793, and USB communication with the host computer are facilitated by a single U421 IC.

19.6.2. Strain gauge bridge signal processing

The increasing role of the digitization can be followed by examining the signal processing for strain gauge bridge force transducer presented in Figure 19.10.

Here are the characteristics for the principal module of a DC amplifier made by HBM:

AD 101B – DC amplifier for resistive transducers:

- recommended both for static and dynamic applications,
- direct computer connection via RS-232 interface,
- test certificate for 6000d class III available,
- high transmission rate and resolution, and memory for users setting.

Windmill Software Ltd announced their 751 SBox which lets a PC monitor four strain gauge bridges [19.29]. It connects to the computer over a USB cable and comes with the Windmill data acquisition and control software suite. When the Windmill software takes a reading from a strain gauge bridge, it automatically monitors excitation voltage and calculates the measurement in microstrain (i.e. 10^{-6}). This eliminates errors due to changes in excitation voltage. Users can also set a zero reference level and monitor changes relative to that level. An integrating analog-to-digital converter reduces noise and the system automatically recalibrates itself.

The 751 SBox accepts four easily-connected bridges in quarter- or half-bridge configuration. The modular Windmill software runs under Windows and offers data logging, charting, alarm indication and output control. Data can also be exported in real-time as spreadsheets to other applications like Excel.

The paper [19.30] presents a generic conditioning system based on a programmable chip adaptable to a wide range of strain gauge transducers. In order to obtain a high flexibility and reconfigurability, digital hardware and software modules are implemented on a field programmable gate array (FPGA).

Industrial machine manufacturers usually need to measure forces and weights that sometimes are misaligned along the load cells measuring axis and also need to transmit the measured data to a PLC (programmable logic controller) or computer without electrical noise and with high resolution. DS Europe [19.31] proposes off-center load cells series 500QD that reduce the errors due to force misalignments and can optionally have a built-in analog (outputs: ± 5 V, ± 10 V and 4...20 mA) or digital (outputs: CANopen, RS485 and RS422 – protocolli Modbus, DSEnet) electronics.

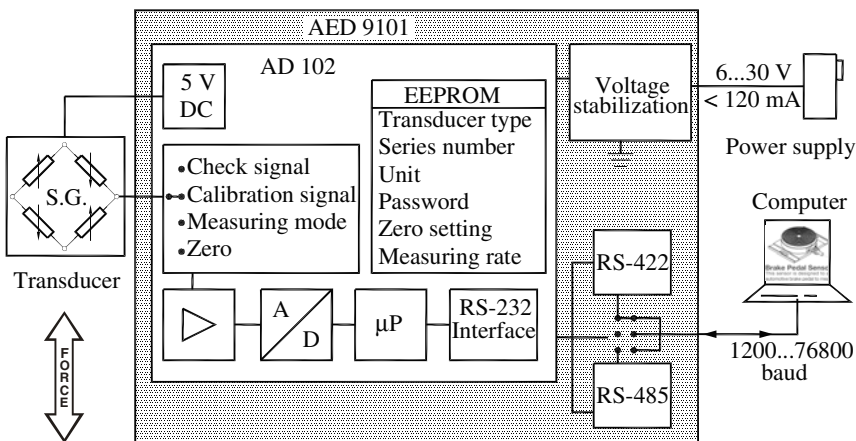


Fig. 19.10 AED 9101 digital amplifier adapted for strain gauged force transducers

Loadstar Sensors, Inc. of Mountain View announced the iLoad Series of digital load or force transducers based on its patented capacitive sensing technology [19.32]. These load sensors are designed to plug directly into the USB port of a PC and enable users to measure loads, forces or weights without need for any additional signal conditioning, data acquisition or special software. The sensor appears as a virtual COM port on a PC enabling a user to directly read data using simple ASCII commands with any terminal emulator such as HyperTerminal. In order to make this process even simpler, Loadstar offers LoadVUE Lite software that takes care of all communication functions and displays loads in lbs, kgs or newtons.

For users who need an analog output, they furnish the iLoad Analog sensor which is built on the same digital platform as the digital USB version but is designed to interface directly to a PLC or DAQ system.

REFERENCES

1. O'Grady, A.: Transducer / sensor excitation and measurement techniques. *Analog Dialogue* 34(5), 1–6 (2000)
2. Signal conditioning for sophisticated transducers. Application Note AN-005641, National Semiconductor Corporation (2002)
3. Ștefănescu, D.M.: Methods and means for electronic processing of tensometric signals. Second doctoral report, "Politehnica" Bucharest (June 1996) (in Romanian)
4. Warsza, Z.L., Idźkowski, A., Makal, J.: Experimental verification of the double-current supplied bridge circuit in 2D measurements of strain and temperature. In: *Proc. 15th IMEKO TC-4 Symposium on Novelties in Electrical Measurements and Instrumentation, Jassy, Romania, September 19-21, vol. I, pp. 127–131* (2007)
5. High-gain signal conditioning circuit for thin and thick film sensors. Application Note 1069, Maxim Integrated Products (2005)
6. Boersch, J.: QuantumX – the new, multi-functional amplifier system. *Hotline Hottinger – News from the World of Test and Measurement* (2), 4–5 (2007)
7. Ștefănescu, D.M., Găvan, M., Stoica, M., Ștefănescu, V.: Experimental stress analysis of an elastic element for force transducer. In: *Proc. 5th Romanian Symposium of Tensometry, Galați, September 20-23, vol. I, pp. 171–178* (1989) (in Romanian)
8. Schicker, R.: Master of the rings – a robust, magnetic speed measuring system with high resolution. *Hotline Hottinger* (2), 14–16 (2003)
9. Haase, K.: Strain sensors based on Bragg gratings. In: *CD Proc. IMEKO Int'l Conf. Cultivating Metrological Knowledge, Merida, Mexico, November 27-30, Paper 3* (2007)
10. Igarashi, I.: Semiconductor dynamic sensors. *Sensors and Actuators* 13, 53–62 (1988)
11. Zamfirescu, A., Bodea, M.: Tensometric oscillator with high linearity. *AMC (Automatică – Management – Calculatoare)* 23, 315–332 (1976) (in Romanian)

12. Rizzi, S.A., Doyle, J.F.: A simple high-frequency force transducer. *Experimental Techniques* 14, 45–48 (1990)
13. Martenson, S.: Capacitance-to-digital converter simplifies instrumentation and sensor design. *S & T e-Digest* 59(9) (September 2005)
14. Kaliyugavaradan, S.: Design note: A simple resistance-to-time converter for signal conditioning of resistive transducers. *Meas. Sci. Tech.* 11, N73–N75 (2000)
15. Middelhoek, S., Audet, S.A.: Silicon sensors: full of promises and pitfalls. *J. Phys. E: Sci. Instrum.* 20, 1080–1086 (1987)
16. Weighing load cells – a complete range from 30 grams to 300 tons. Scaime, Annemasse, France (1994)
17. Bolt-on microcell bulk weighing systems for industry (US Patent 4064744). Kistler-Morse Corporation, Bellevue, WA, Revue 5-81
18. Arshak, K.I., Ansari, F., McDonagh, D., Collins, D.: Development of a novel thick-film strain gauge sensor system. *Meas. Sci. Technol.* 8, 58–70 (1997)
19. Neues über elektrisches Messen mechanischer Größen. Kistler Instrumente AG, Winterthur, Schweiz, Info 44-91
20. Load cells, weighing equipment & systems. Kubota Corporation, Osaka, Japan, Catalog 1102-99
21. Wall, W.E.: Applications of piezoresistance to externally excited transducers. Technical Paper – 239, Endevco, San Juan Capistrano, CA, Revue 10-75
22. Microsensors integrated on a chip. In: *Research*EU Results Supplement* (2), 34. European Communities Office for Official Publications, Luxembourg (February 2008)
23. Kawai, S., Kawakatsu, H.: Highly sensitive force/mass detection method and device using phase synchronization circuit. European Patent EP-1746398 (January 2007)
24. Baselt, D.R., Lee, G.U., Natesan, M., Metzger, S.W., Sheehan, P.E., Colton, J.: A biosensor based on magnetoresistance technology. *Biosensors & Bioelectronics* (13), 731–739 (1998)
25. Hauptmann, P.: *Sensors: Principles and Applications*. Carl Hanser, Munich (1991)
26. Ferrari, V., Ghisla, A., Kovács Vajna, Z.S., Marioli, D., Taroni, A.: ASIC front-end interface with frequency and duty cycle output for resistive-bridge sensors. *Sensors and Actuators A: Physical* 138(1), 112–119 (2007)
27. Yurish, S.Y.: Intelligent digital pressure sensors and transducers based on Universal Frequency-to-Digital Converter (UFDC-1). *S & T e-Digest* 60(10), 432–438 (2005)
28. Porter, T.L., Delinger, W.: Electronics for LabView based piezoresistive micro-cantilever sensor system. *Sensors & Transducers Magazine* 68(6), 568–574 (2006), <http://www.sensorsportal.com>
29. Strain gauges monitoring over USB. *Sensors & Transducers e-Digest* 78(4) (April 2007)
30. Rabah, H., Poussier, S., Weber, S.: Toward a generic on chip conditioning system for strain gage sensors. *Measurement* 39(4), 320–327 (2006)
31. Piardi, D.: Load cells with built-in analog and digital electronics. *Sensors & Transducers e-Digest* 78(4) (April 2007)
32. Harish, D.: Digital load sensors with USB output. *Sensors & Transducers e-Digest* 80(6) (2007)

Chapter 20

CLASSIFICATION OF ELASTIC ELEMENTS

20.1. ELASTIC ELEMENTS LOADING MODES

Force causes stresses and displacements of the objects upon it acts (Fig. 20.1). If displacements are blocked, only stresses occur when a force vector is applied on a deformable body. By measuring these stresses, one can obtain the necessary information to determine the acting force. Direct stress measurements are difficult to proceed, they must be evaluated using measurable parameters, such as strain, that vary in response to loading. Many force transducers employ simple elastic elements (monoblock) or combination of elements (e.g. pillars, beams, rings) in assembled constructions [20.1]. Force application on such a flexible element produces a deflection in this first transducer, which is then sensed by a secondary transducer (e.g. strain gauge or LVDT) and converted into a measurable output (i.e. electronic unbalance of a Wheatstone bridge).

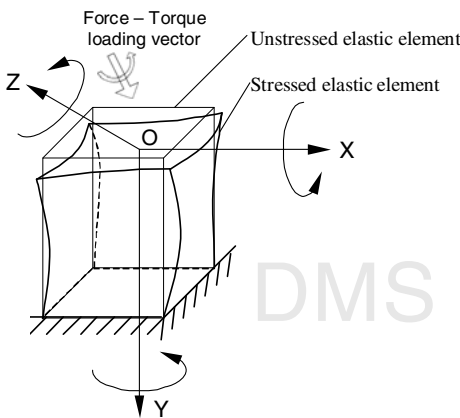


Fig. 20.1 Elastic element (EE) before and after loading

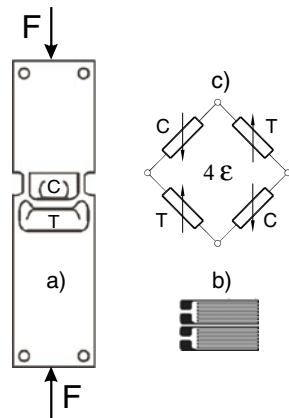


Fig. 20.2 Strain gauged EE

A spring element of known configuration is normally machined from a single billet of high tensile or precipitation hardening stainless steel, beryllium copper or other suitable material and heat treated to optimize its thermal and mechanical properties [20.2]. The strain gauges are indestructibly bonded to the element and connected into a four-arm Wheatstone bridge.

There are some elastic elements difficult to match a certain category, like that depicted in Figure 20.2a: an unconventional frame, “cartridge” or “cassette” included in an axially-loaded strip.

The “double” strain gauge (Fig. 20.2b) from the upper side is compressed (C) while that from the lower side is tensioned (T), both “double” SGs being connected in a Wheatstone bridge (Fig. 20.2c).

There are many criteria for classifying the transducers elastic elements. The most general criterion is the *shape*: 1D – bar, 2D – plate, 3D – block. More specifically, the main stress (or strain, due to their connection according to the Hooke’s law) can differentiate them: stretching and/or compression, bending, shearing, torsion, complex or combined stress. The Anglo-American technical literature uses the term of *strain sensitivity* according to which the elastic elements could be arranged in their increasing order:

- a) *Tension-compression or direct* (Fig. 20.3a). A columnar element may be in the form of a solid or hollow cross section having circular or square shape. To achieve a four-arm bridge circuit two gauges are aligned parallel to the load axis and two gauges aligned at 90° to measure Poisson strain ν (representing approximately the third part of the principal strain). The cross sectional area of the column increases in compression and decreases in tension. This is a typical dual sensing elastic element.
- b) *Bending* (Fig. 20.3b). A simple cantilever is an example of a bending load cell. When a force F or a torque M is applied to the free end, it deflects the beam so producing opposite strains at the top and bottom faces. Strain gauges may be installed near the root of the beam to sense tensile and compressive strains.
- c) *Shearing* (Fig. 20.3c). Shear elements are based on the fact that shear stresses are proportional to the applied force and are independent of loading position. The shear stresses themselves cannot be measured so pairs of gauge with their grid lines aligned at $\pm 45^\circ$ to the neutral axis are installed on both sides of the central portion of the beam to measure principal strains and connected into a full bridge circuit [20.2].
- d) *Complex* (Fig. 20.3d) is added to describe the multicomponent transducers in Robotics and wind tunnels (to be thoroughly treated in a second volume).

Tovey [20.3] has compared some characteristics of these flexible elements types (linearity, hysteresis, end effects, symmetry, uniformity of the specific field of deformations) evaluating them in a range between “very good” and “poor”.

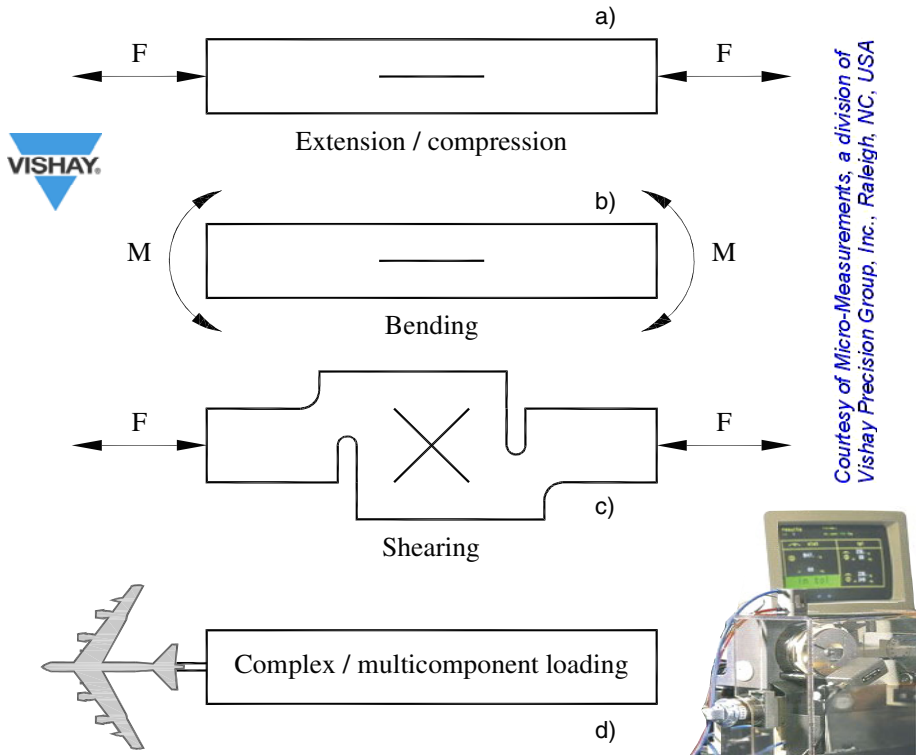


Fig. 20.3 Schematic division for elastic elements according to the type of strain field used: a) direct (tension/compression), b) bending of the upper and lower faces of the beam and c) shearing (adapted from [20.4]). Plus d) complex state of stress and strain.

Finally, Tovey has quantitatively estimated the sensitivity: 2.6 in the first case (a) and 4 in the others (b, c, d).

The strain gauge is considered as a single-use sensor, i.e. it can not be separated from the sensible body of the force transducer, but it can be utilized together with it in a lot of further applications.

A special solution is represented by the “champagne cork” [20.5], a kind of intermediate and reusable elastic element which is inserted with a close tolerance (up to 0.05 mm) into more ample elastic structures (Fig. 20.4). The transducer has a rectangular reference point (for the screw driver head) which can be located along the main axis (elongation), perpendicularly on it (compression) or at $\pm 45^\circ$ to the axis (shearing or torsion); besides these simple strains, it can measure also elongation or compression with bending combinations. The sensitivity of this multifunctional tensometrical “tablet” is variable, depending on the size and the loading of the incorporated structure.

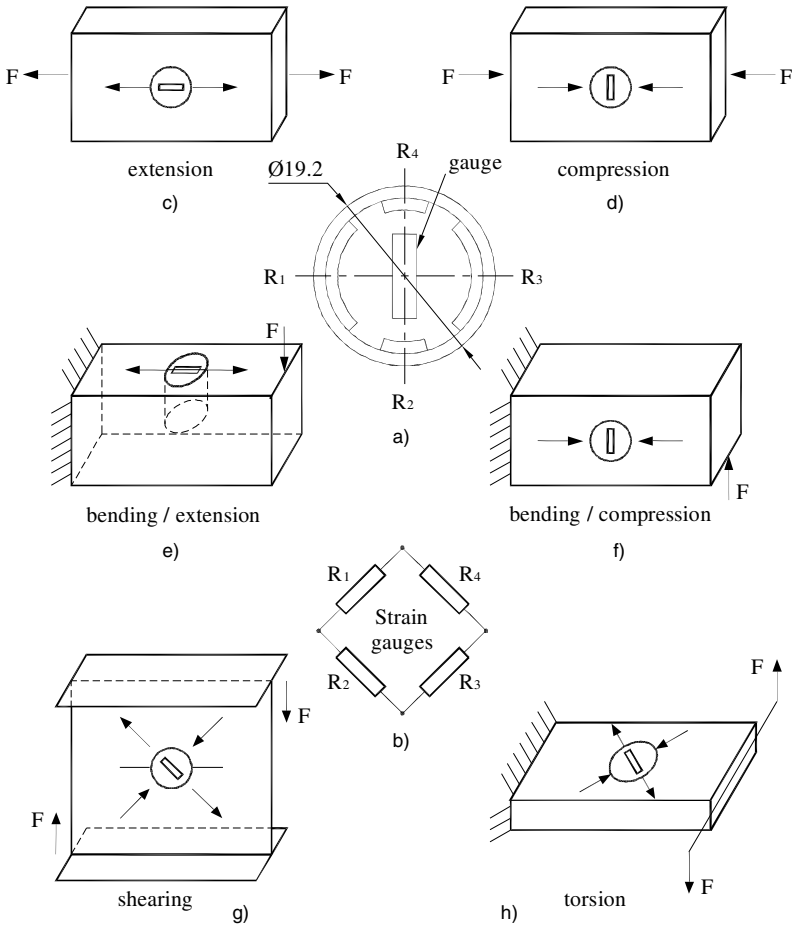


Fig. 20.4 The “champagne cork” Gozinta [20.5] with two circumferential (R_1, R_3) and two transversal (R_2, R_4) strain gauges (a) and their Wheatstone bridge connection (b). This prefabricated “gauge” can be placed longitudinally, for measuring extension (c) and/or bending (e), or transversally, for measuring compression (d) and/or bending (f). Placed in position with $\pm 45^\circ$ to the principal axes of the elastic body, this strain gauged cork can also measure shearing (g) or torsion (h) as elemental loading.

20.2. EXAMPLES OF ELASTIC ELEMENTS CLASSIFICATIONS

There are a number of different flexible elements presented in [20.6], but generally they consist of cantilever beams, pillars (columns), proving rings and diaphragms. More or less complete researches of some types of elastic structures of general interest can be found in the works [20.7] – [20.16].

Remarkable attempts were made by the German engineering school (Verband Deutscher Elektrotechniker) to quantify and classify the elastic elements types using the tight connection between the Materials Science and the strain gauge measurement methodology. A suggestive example is given in Table 20.1, containing three from the nine flexible structures described by Albert Haug, professor at the Fachhochschule für Technik Ulm, in [20.17].

Worth to be mentioned is The Institute of Measurement and Control, London, which has appointed an independent panel of force specialists to classify the huge variety of flexible elements for strain gauged force transducers in their valuable “*Guide to the Measurement of Force*” [20.18]. Ten types of elastic structures are correlated in Table 20.2 and Figure 20.5.

Table 20.1 Strains ε and sags f for some most usual bent elastic elements (equal strength lamella, circular membrane and ring) loaded by force F or pressure p

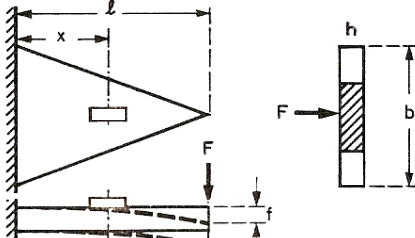
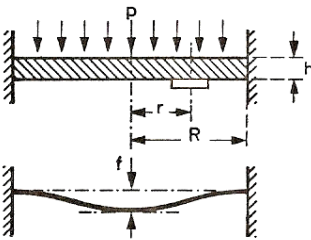
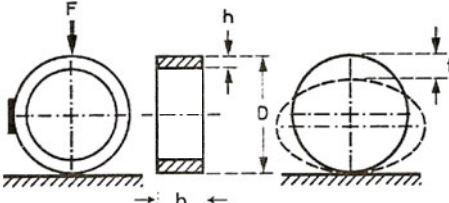
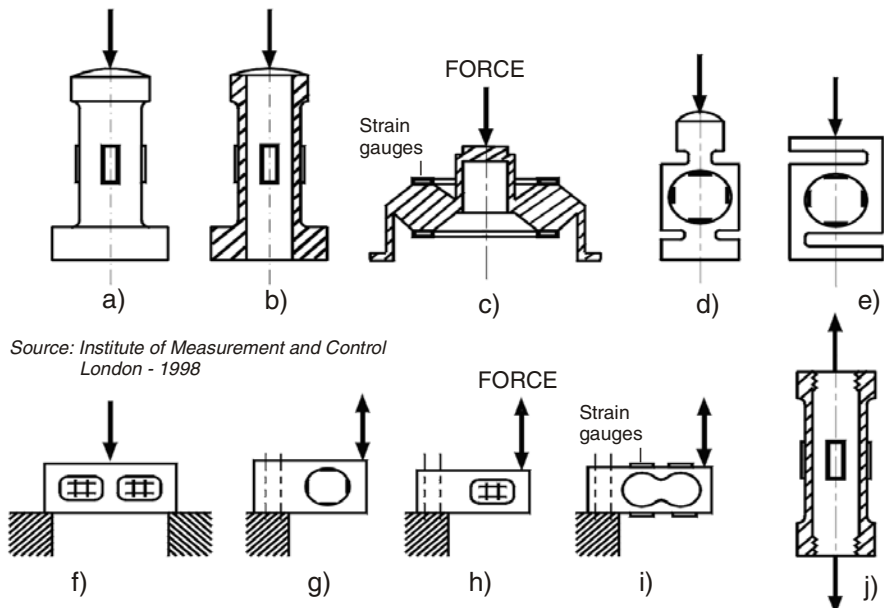
HBM	Übersicht über die Dehnung verschiedener Körperformen bei Belastung <small>Zusammengestellt von Albert Haug, Staatliche Ingenieurschule Ulm/Donau</small>	2-68
	$\varepsilon = 6 \cdot l \cdot F / (b \cdot h^2 \cdot E)$ $f = 6 \cdot l^3 \cdot F / (b \cdot h^3 \cdot E)$ <p>Ausführung der Spitze wie oben</p>	
	<p>tangentiale Dehnung</p> $\varepsilon_t = \frac{3}{8} \cdot \frac{1-\mu^2}{E} \cdot \frac{R^2}{b^2} \cdot (1-r^2/R^2) \cdot p$ <p>radiale Dehnung</p> $\varepsilon_r = \frac{3}{8} \cdot \frac{1-\mu^2}{E} \cdot \frac{R^2}{b^2} \cdot (1-3r^2/R^2) \cdot p$ $f = \frac{3}{16} \cdot \frac{1-\mu^2}{E} \cdot \frac{R^4}{b^3} \cdot p \quad \text{Linear für } f/b \leq 0,2$	
	$\varepsilon = 3 \cdot D \cdot F / (\pi \cdot b \cdot h^2 \cdot E)$ $f = \frac{3}{2} \left(\frac{\pi}{4} - \frac{2}{\pi} \right) \cdot D^3 \cdot F / (b \cdot h^3 \cdot E)$ <p>Gültig für dünnen Ring: $h \ll D$</p>	

Table 20.2 Ten types of elastic elements and their load ranges

Type	Elastic element	Range
a)	Compression cylinder	50 kN to 50 MN
b)	Hollow compression cylinder	10 kN to 50 MN
c)	Toroidal ring	1 kN to 5 MN
d)	Ring	1 kN to 1 MN
e)	S-beam (bending or shear)	200 N to 50 kN
f)	Double-ended shear beam	20 kN to 2 MN
g)	(Simplified) double-bending beam	500 N to 50 kN
h)	Shear beam	1 kN to 500 kN
i)	Double-bending beam	100 N to 10 kN
j)	Tension cylinder	50 kN to 50 MN

The rated capacities of strain gauge load cells range from 5 N to more than 50 MN and they are the most widespread of all force measurement systems, as stated by the Institute of Measurement and Control London [20.18].



Source: Institute of Measurement and Control London - 1998

Fig. 20.5 Ten models of strain gauged elastic elements for force transducers. Seven types (a, b, d, e, g, i and j) have normal strain gauges while special SGs are used for model c) – circumferential, and models f) and h) $\pm 45^\circ$ rosettes.

20.3. COMPREHENSIVE CLASSIFICATION OF ELASTIC ELEMENTS

An attempt for elastic elements systematization of force, torque and pressure transducers fabricated in Romania has been made in [20.19]. Nine types of flexible structures for aeronautical force transducers were presented in [20.20]. In the Romanian standard concerning the metrological verification of the load cells with tensoresistors for force or mass measuring ten variants are passed in review while in WELMEC guide [20.21] 11 types of flexible bodies are shown.

Finally, 12 main types of elastic elements for force transducers were chosen [20.22], and they will be detailed in the next chapters. This dozen of elastic bodies is synthesized in tables comparable to those of the most representative works in the field [20.23] – [20.27].

Table 20.3 shows, for each of the twelve sensitive elements:

- their name (in short);
- the draft of the elastic elements with uniform / standardized notations;
- the mechanical sensitivity (following the Strength of Materials formulas);
- the electric sensitivity (as a multiple of ε under one strain gauge);
- the load ranges, expressed in N (newtons).

The “extreme” values are outside the borders of this table:

- minimum level: 6.94 pN for cantilever beam (type III). The displacement sensitivity of the fabricated cantilever, measured by SEM (scanning electron microscopy), is equivalent to 10 pN, and its stiffness is in the range of $0.001 \text{ N}\cdot\text{m}^{-1}$ [20.28].
- maximum level > 20 MN (type I). A multiple plate system of elastic elements [20.29] contains 48 units combined in parallel and in series into one assembled block, resulting a compact structure with lower profile and smaller weight as compared with a classical load cell for 20 MN.

The next chapters will expand the description of the 12 relevant elastic elements together with a comparative study of their features and performances. A simplified model – principle illustration of the current stage along with a personal improved version, conceived and/or developed by the author, are shown for each type of strain gauge force transducer (SGFT): stretched / compressed column, stretched / compressed tube, bent lamella or cantilever beam, bent and/or torsion shaft (‘T’ or ‘X’ rosettes), middle bent bar with fixed ends, shearing strained profile, bent yoke, bent ring, bent membrane, compressed torus, axisymmetrical and sphere / volumetric elastic elements. To put it differently, each of the twelve “standard figures” has on the upper part the classical configuration of the flexible structure for force measurement and below the developed version, based on our tensometrical experience, by means of experimental stress analysis (strain gauges, photoelasticity, holography) and / or structural optimization using the numerical methods.

Table. 20.3 – first part. Strain gauged elastic elements for force transducers, their mechanical and electrical sensitivities and force ranges

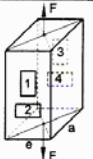
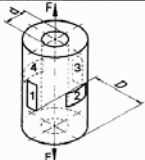

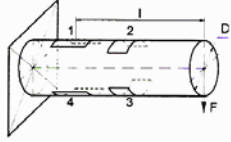
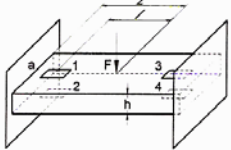
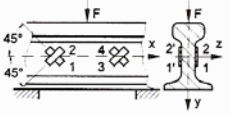
Type, Name	Elastic element's representation	Sensitivity		Force range [N]			
		Mechanical [$\mu\text{m/m}$]	Electrical [ϵ]	10^{-2}	10^1	10^4	10^7
I Stretched/ compressed column		$\frac{F}{Eac}$	2.6				
II Stretched/ compressed tube		$\frac{4F}{\pi E(D^2 - d^2)}$	2.6				
III Bent lamella (cantilever beam)		$\frac{6Fl}{Eah^2}$	4				
IV Bent and/or torsioned shaft		$\frac{32Fl}{\pi ED^2}$	2.6				
V Middle bent bar with embedded ends		$\frac{1.5F(2l - L)}{Eah^2}$	4				
VI Shearing strained profile		It depends upon F, E and the profile's dimensions	4				

Table. 20.3 – second part. Strain gauged elastic elements for force transducers, their mechanical and electrical sensitivities and force ranges

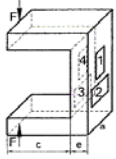

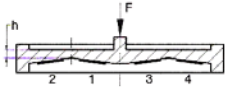
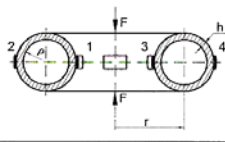
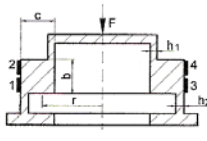

Type, Name	Elastic element's representation	Sensitivity		Force range [N]			
		Mechanical [$\mu\text{m/m}$]	Electrical [ϵ]	10^{-2}	10^1	10^4	10^7
VII Bent yoke		$\frac{F(6\frac{c}{e}-1)}{Eae}$	2.6				
VIII Bent ring		$\frac{3FD}{\pi Eac^2}$	3.7				
IX Bent membrane		$\frac{1.24F}{\pi E h_{med}^2}$	4				
X Compressed torus		$\frac{2(1-\nu^2)(1-\frac{\rho}{r})F}{\pi^2 Ehp(1+\frac{3}{2}\frac{h^2 r^2}{\rho^4})}$	3.7				
XI Axis symmetrical element		It depends upon F, E, b, c, h ₁ , h ₂ , r	4				
XII Sphere/volumetric element		It depends upon F, E, D	2.6				

Table 20.4 A basic dozen of elastic elements for SGFTs

Chapter	Type	Elastic element (EE) denomination
C.21	E-1	Stretched / compressed column
C.22	E-2	Stretched / compressed tube
C.23	E-3	Bent lamella (cantilever beam)
C.24	E-4	Bent and/or torsion shaft
C.25	E-5	Middle bent bar with fixed ends
C.26	E-6	Shearing strained EEs
C.27	E-7	Bent yoke or frame
C.28	E-8	Bent ring and “glasses”
C.29	E-9	Bent membrane (diaphragm)
C.30	E-10	Complex loaded torus
C.31	E-11	Axisymmetrical EEs
C.32	E-12	Volumetric EEs (cube, sphere)

The twelve types of elastic elements for strain gauged force transducers (SGFTs) are presented in the next chapters, as detailed in Table 20.4.

A typical configuration of elastic body (the most frequently used: cantilever beam), equipped with four piezoresistive elements connected in Wheatstone bridge, is presented in Figure 20.6. The twelve strain gauged elastic elements representations are grouped in Figure 20.7.

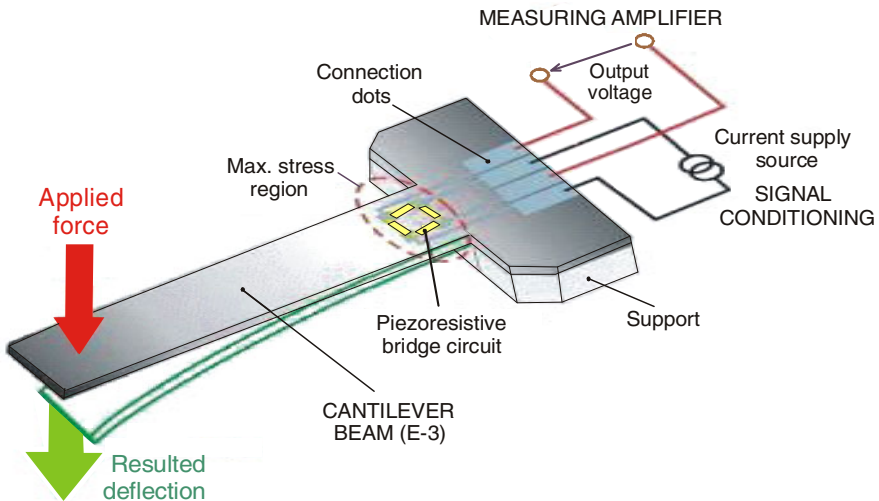
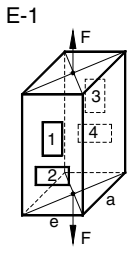
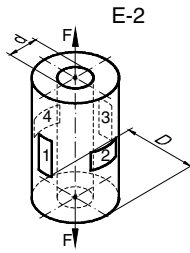


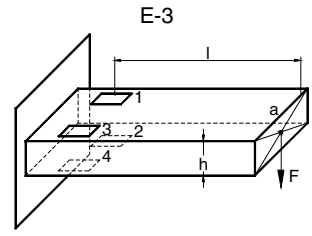
Fig. 20.6 Strain gauged cantilever beam (“trampoline”-shaped) with symbolization of associated circuitry (signal conditioning and bridge amplifier)



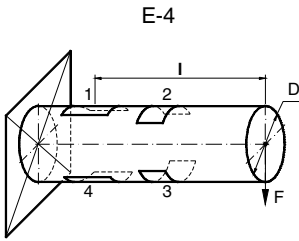
Chapter 21



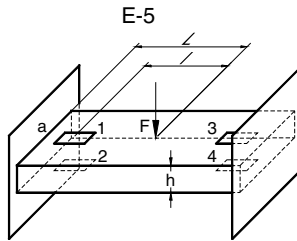
Chapter 22



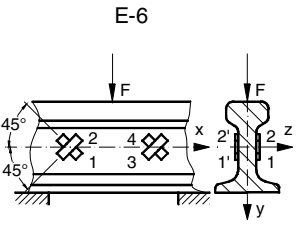
Chapter 23



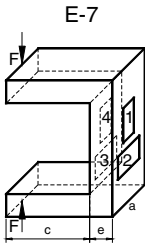
Chapter 24



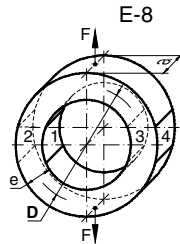
Chapter 25



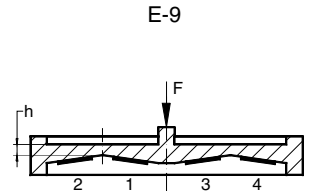
Chapter 26



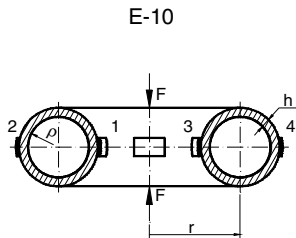
Chapter 27



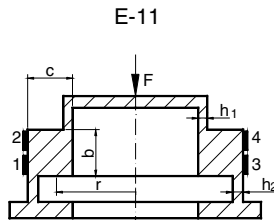
Chapter 28



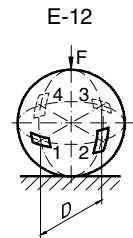
Chapter 29



Chapter 30



Chapter 31



Chapter 32

Fig. 20.7 A general picture of the twelve typical elastic elements for SGFTs

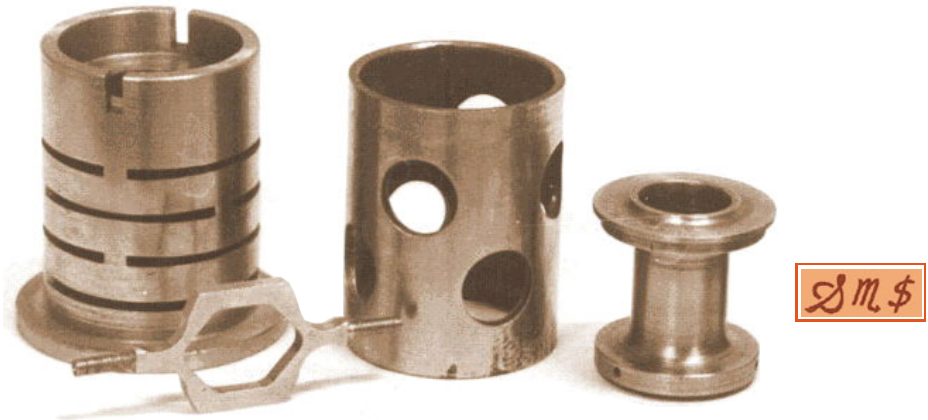


Fig. 20.8 Slitted, perforated and simple tubes (E-2), and a hexagonal ring (E-8)

Several customized elastic elements for strain gauge force transducers are presented in Figures 20.8 and 20.9.

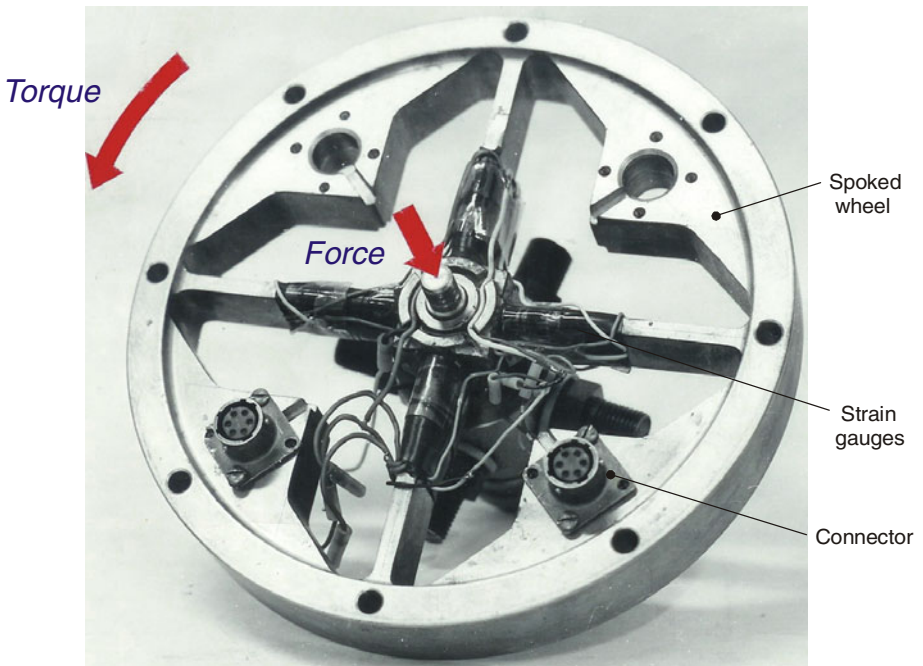


Fig. 20.9 A strain gauge spoked wheel for force and torque measurements using two perpendicular middle bent bar with fixed ends (E-5)

REFERENCES

1. Dolga, L., Ştefănescu, D.M.: About the parametric and feature-based design models for the elastic elements of force transducers. In: 3rd Int'l Conf. Research and Development in Mechanical Industry RaDMI 2003, Herceg Novi, Serbia, Montenegro, September 19-23, pp. 1253–1257 (2003)
2. Bahra, C.S., Evans, J.W.: Strain gauge load cell design and use. In: Proc. TEMPCON Transducers Conf., June 14-16, pp. 1–22 (1983)
3. Tovey, F.M.: Material properties in the design of transducer flexures. Authorized reprint from Laboratory for Measurement Systems Engineering, Publication no. 70, Phoenix, AZ (1994)
4. Strain Gage Based Transducers – Their Design and Construction, February 2 (2001), <http://www.measurementsgroup.com/guide/ta/sGBT/sgbtindex.htm>
5. Model GZ-10 Gozinta® sensor. Betriebs- Mess- Computertechnik Ingenieurgesellschaft mbH, Puchheim-München, Federal Republic of Germany (1986)
6. Usher, M.J., Keating, D.A.: Sensors and Transducers – Characteristics, Applications, Instrumentation, Interfacing, 2nd edn. MacMillan, Houndmills (1996)
7. Stoicoviciu, C.: Automatic Weighing in Industry. Editura Tehnică, Bucureşti (1971) (in Romanian)
8. The installation of load cells. Catalog G 21.03.1-e. Hottinger Baldwin Measurements, Inc., Framingham (1988)
9. Precision force and weight measurement technologies. Catalog 4M, BLH Electronics, Inc., Canton (October 1995)
10. Sensoren: Kraft- und Miniaturaufnehmer, Wägezellen, Mehrkomponenten, Dehnung, Drucksensoren. Qualität und Leistung. Lorenz Meßtechnik GmbH, Alfdorf (D) (1995)
11. Horn, K.: Design of sensors with very high stiffness. In: Proc. 15th Int'l Conf. on Accuracy Assurance in Force, Torque and Mass Measurements, Madrid, October 7-11, pp. 285–294 (1996)
12. Comprehensive weighing solutions for a profitable business. Industry Catalog, Mettler-Toledo AG, Greifensee, Switzerland (1997)
13. Systems engineering – SIWAREX weighing and batching systems. Catalog KT 30. Siemens AG Automation Group, Fürth (1997)
14. Méröcellák – Load Cells – Kraftmessdosen – Tenzodatciki. Kaliber Instrument and Measuring Technology (Founded 1924), Metrimex Budapest (1997)
15. Cioară, T.G.: Experimental Techniques in Mechanical Engineering. Sensors and Transducers. Editura Politehnica, Timișoara (1999) (in Romanian)
16. Sandu, M.A., Sandu, A.: Strain Gauge Transducers. Design and Applications. Editura Printech, Bucureşti (1999) (in Romanian)
17. Haug, A.: Übersicht über die Dehnung verschiedener Körperformen bei Belastung. Reprint Hottinger Baldwin Messtechnik GmbH, Darmstadt, 2-68
18. Hunt, A. (Coord.): Guide to the Measurement of Force. The Institute of Measurement and Control, London (published 1998); ISBN 0-904457-28-1

19. Ștefănescu, D.M., Sandu, M.A.: Strength of Materials calculus for elastic elements of force, torque and pressure transducers fabricated by I.A.U.C. Universitatea "Politehnica" București, Internal Document 264-82 (in Romanian)
20. Ștefănescu, D.M.: Strain gauge load cells for aeronautical testing. *Revista Transporturilor și Telecomunicațiilor* (2), 26–31 (1986) (in Romanian)
21. Guide for Load Cells. West-European Legal Metrology Cooperation – WELMEC 2.4 (Issue 1), Teddington, Middlesex (1997)
22. Ștefănescu, D.M.: Methods for increasing the sensitivity of strain gauge force transducers. PhD dissertation (160 pages, 26 tables, 86 figures, 336 references), Universitatea "Politehnica" București, Romania, September 10 (1999) (in Romanian)
23. La réalisation des capteurs a jauges électriques. Budd S.A., Neully sur Seine, N.I.T. 12-72
24. Malikov, G.F., Șneiderman, A.I., Șulemovici, A.M.: Strain gauged elastic elements computation. Izdat Mașinostroenie, Moskva (1964) (in Russian)
25. Complete Pressure, Strain and Force Measurement Handbook and Encyclopedia. Omega Engineering, Inc, Stamford, CT (1988), <http://www.omega.com>; Your one-stop source for process measurement and control, Stamford, CT, March 19 (2009)
26. DMS Messtechnologie, Formeln & Tabellen. Measurements Group – Vishay Meßtechnik GmbH, Lochham bei München (1991)
27. Young, W.C.: Roark's Formulas for Stress and Strain, 6th edn. Society for Experimental Mechanics, Bethel (1996); ISBN 0-07-072541-1
28. Gel, M., Shimoyama, I.: Force sensing submicrometer thick cantilevers with ultra-thin piezoresistors by rapid thermal diffusion. *J. Micromech. Microeng.* 14, 423–428 (2004)
29. Zhang, S., Chen, W.: Development of the integrated multiple plate-ring type load cell with large capacity. In: Shi, C., Zhang, Y. (eds.) *Acta APMF 1996 – Present Situation and Progress of Measurement on Mass and Force*, Beijing, China, August 20-22, pp. 151–153 (1996)

Chapter 21

STRETCHED / COMPRESSED COLUMNS

21.1. CLASSICAL COLUMNS

The typical image of a columnar elastic element, equipped with four T-type rosettes on its central circumference, is shown in Figure 21.1.

Another column or straight beam, axially and bidirectionally stressed (having different signs: + for stretching and – for compression, respectively), is shown in Figure 21.2 (top). The elastic element can have various shaped sections, ranging the rectangle to the most diverse profiles (H, I, L, U) and being easy to made by modern machining technologies. Because of the relative height of the column it is difficult to apply axially a perfect compression load and to eliminate the influence of other loads. That is why the use of more than four strain gauges is needed, and KIS model could be considered a prototype in this respect [21.1].

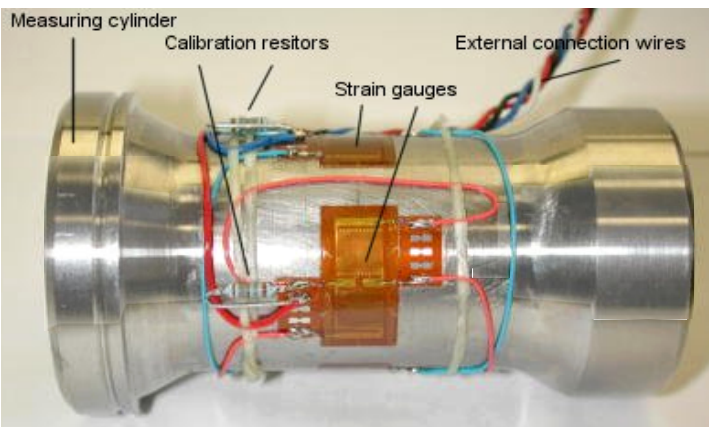


Fig. 21.1 Strain gauged cylinder for measuring tension and/or compression forces

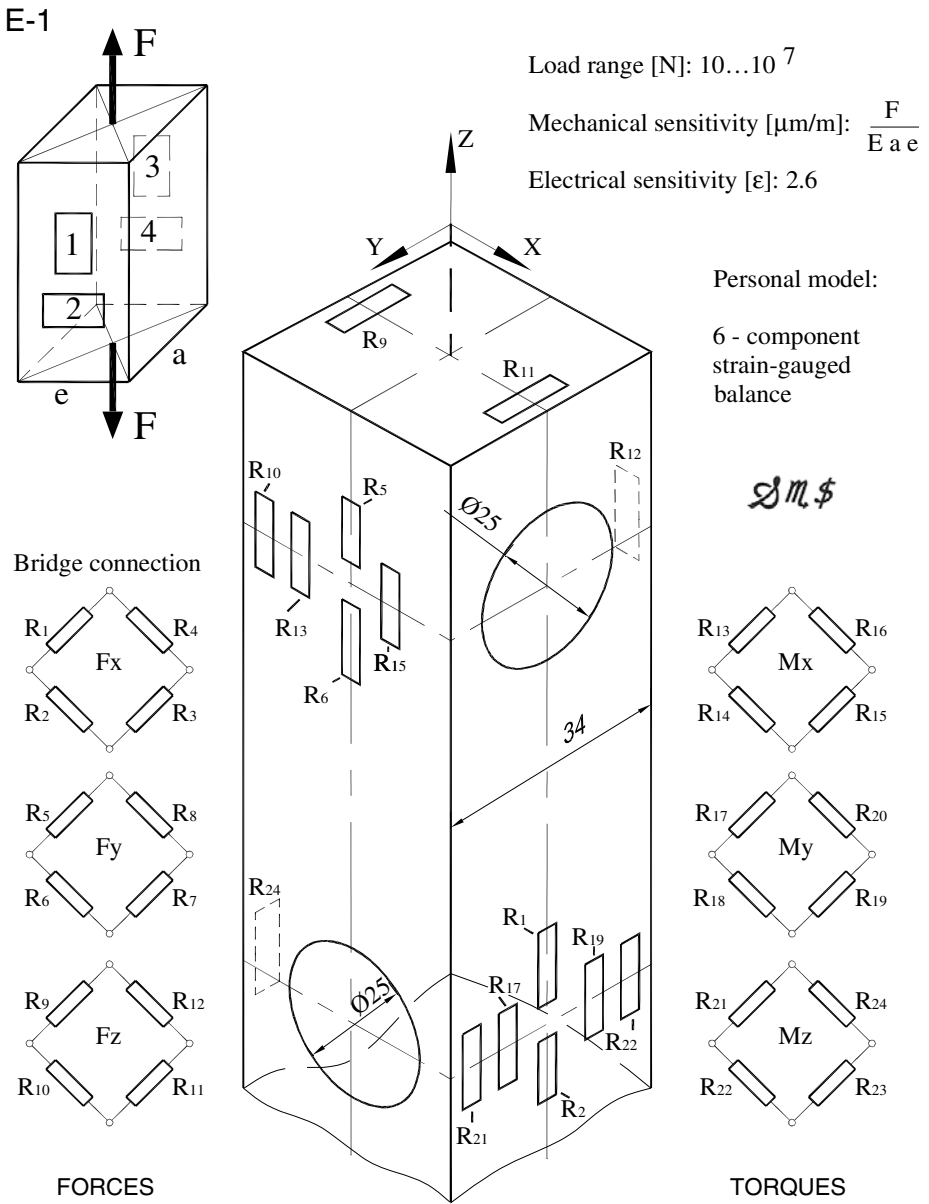


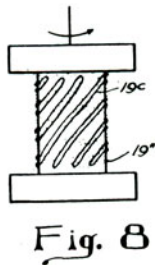
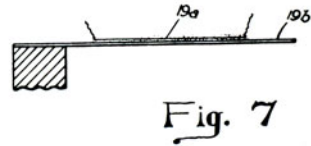
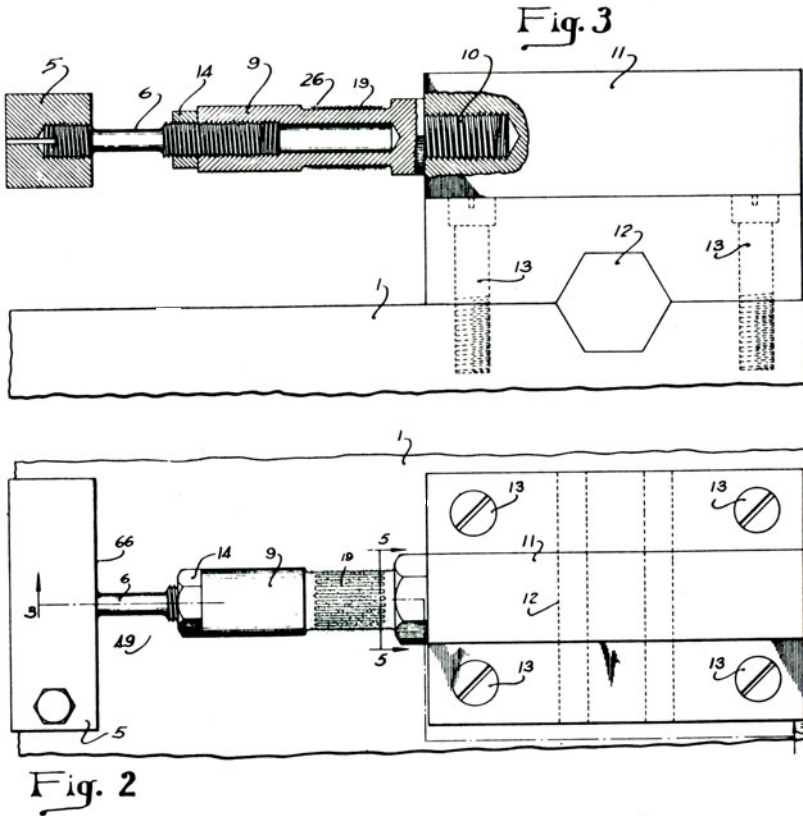
Fig. 21.2 Strain gauged elastic elements of type I for force transducers

Dr. Edward Simmons, a representative of Caltech, surnamed the “Strain Gauge Guy”, has defined the role of these tensometric devices to measure the

amount of deformation that occurs when a force is applied to an elastic body, such as rectangular plate, cylinder, tube and cantilever beam, which are presented in his invention drawings (see Figure 21.3).

Filed Feb. 23, 1940

2 Sheets-Sheet 2



INVENTOR
 EDWARD E. SIMMONS, JR.
 BY
Edward E. Simmons
 ATTORNEY

Fig. 21.3 Document attesting the strain gauges invention by Dr. Edward Simmons

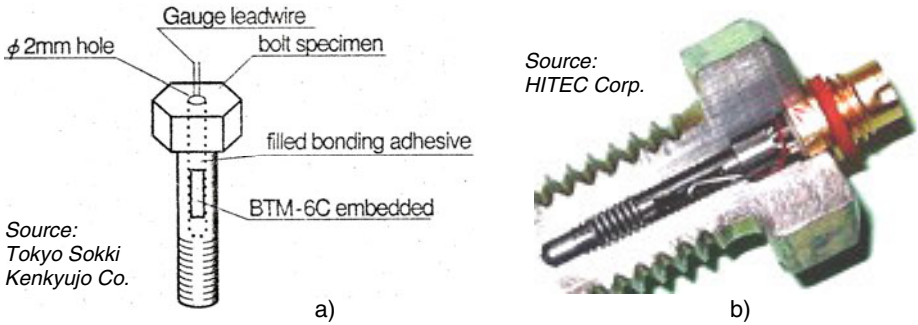


Fig. 21.4 Strain gauged bolts for measuring tensile forces in technological assemblings

A simple gauge is designed to measure the tensile force of bolts [21.2]. In order to install, simply insert the gauge together with A-2 bonding adhesive into a predrilled hole (diameter: $\varnothing 2$ mm, depth: 13 mm) in the bolt head (Fig. 21.4a).

The MMTTM [21.3] uses foil strain gauges configured as a full Wheatstone bridge to provide maximum sensitivity to axial loads while minimizing the parasitic effects of bending, torque, and shear forces. This special force transducer, shown in Figure 21.4b, uses a four wire connection for the full bridge that is compatible with most data acquisition units having a resistance of 120 Ω or 350 Ω . HITEC Corporation provides five points of NIST traceable calibration as part of the “strainsert” installation procedure, having accuracy better than 2 %.

Figure 21.5 shows the most intuitive representation for positioning strain gauges on a cylinder, top (a) and side view (b), and their connection in Wheatstone bridge (c). The perpendicularity between the active (1, 3) and transverse (2, 4) strain gauges is perfectly suggested by Dr. Dae-Im Kang [21.4], vice-president of the Korean Research Institute of Standards and Science and president elect of IMEKO (Fig. 21.5d).

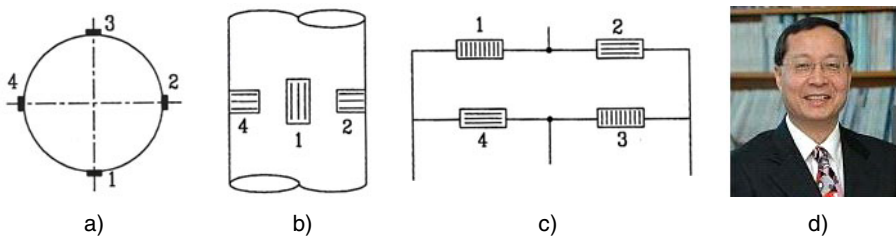


Fig. 21.5 Strain gauges emplacement on a classical cylinder and their Wheatstone bridge connection [according to Korean representation]

The calibration of testing machines designed for measuring the compressive strength of concrete is currently made under the European standard EN 12390-4. Strain cylinders, which are used to measure force distribution, shall be inter-changeable so that the calibration results of the machine do not depend on the cylinder. The procedure developed and implemented in the Force Department of the Laboratoire National d'Essais, France is described in [21.5]. This standard defines a set of characteristics concerning the strain cylinder dimensions (diameter: 100 mm and height: 200 mm), geometric shape and associated tolerances (flatness, cylindricity, squareness, parallelism). The choice for materials is limited to nickel-chrome steel.

The strain-gauge combination is specified: sixteen SGs are assembled to form four complete Wheatstone bridges (in which two SGs are vertical and two horizontal), each centered at one of the ends of a pair of orthogonal diameters half-way up the cylinder. A layout of the practical embodiment of a Wheatstone bridge is shown in Figure 21.6.

The European standard specifies that the response of the cylinder is measured by the strain ratio of the gauge bridges. The mean value e_m of the four bridge outputs (e_1, e_2, e_3 and e_4) is used to calculate the strain ratio $(e_i - e_m) / e_m$ for each bridge, where e_i is the strain at the bridge position under consideration.

An interesting application can be found in the patent [21.6]: a circular flange with four included semiconductor strain gauges each, in the vertical and horizontal wall respectively, in accordance with two perpendicular diameters. They are used to measure the ground pressure in different directions.

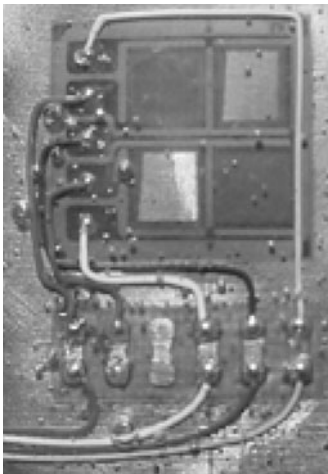


Fig. 21.6 Four strain gauges group on a cylinder

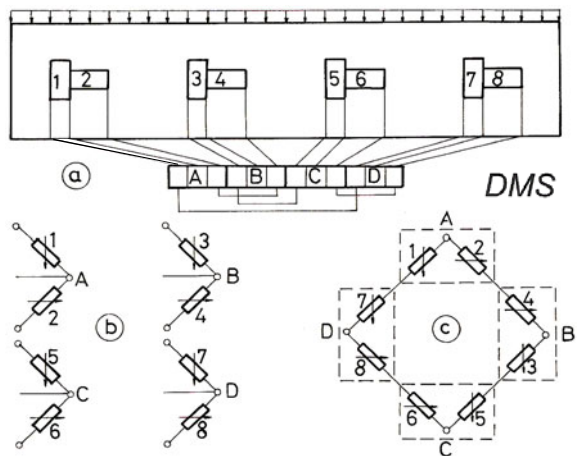


Fig. 21.7 Measurement variants for the tightening force on a compressor valve

Out of the many tensometric applications with stretched or compressed column type elastic element, we mention the following applications from the Romanian Symposia of Tensometry, organized by ARTENS:

- a coupling for engine thrust measuring;
- the strain inspection of the thermal power station boiler supports;
- force transducers for analyzing the effects of the compressor valves tightening, as presented in [21.7] and in Figure 21.7.

On the deployed representation of the cylinder (Fig. 21.7a) there are four T-type rosettes positioned at the ends of a pair of orthogonal diameters, just on the middle circumference. It is possible to evaluate the tightening force distribution in four points using four half-bridges (Fig. 21.7b) or to measure the global tightening force connecting all strain gauges into a single Wheatstone bridge, like in Figure 21.7c.

21.2. OPTIMIZED COLUMNS

A special case is represented by the cylindrical columns having variable sections in order to minimize their end-loading sensitivity. There are bars of an equal strength to stretching ($\sigma_n = \text{constant}$) with variable section in compliance with an exponential law as well as bars of an equal strength to compression with a hyperboloid profile (BLH) or close to Bezier's curve [21.8].

E.L. Wilson was the first one to introduce in 1963 the application of the finite element analysis to two-dimensional structures, the simplest one being the cylindrical column. In 1971 R.A. Mitchell has utilized the axisymmetrical finite elements to study the influence of concentrators (portions where efforts are concentrated) and of distribution variations of applied load [21.9].

The influence of the length to diameter ratio, of the curve radius variation and of the geometric nonlinearity, studied with nonlinear finite element analysis contributes to increase the accuracy by 0.052 % as compared to linear FEM [21.10]. This figure seems not so great but it is essential to the high accuracy force transducers.

The optimization of a column from the point of view of minimum weight and buckling risk avoidance is presented in [21.11].

21.3. INCREASING SENSITIVITY FOR COLUMNAR TRANSDUCERS

There are two directions to increase the sensitivity of the columnar force transducers:

- **Classical:** Multicolumn transducers can be designed [21.12], for instance eight longitudinal (active) strain gauges and eight transversal (compensating) ones can be located on the elastic structure made up of four prismatic bars.

- **Modern:** A simple parallelepiped (a column with a rectangular section) allows the measurement of the six components of a load torsor (three forces and three moments) but with a reduced sensitivity. The drilling of one hole brings out more sensible tensometric layouts, a solution used for the determination of the longitudinal force in the rail [21.13].

Continuing the evolution of the tensometric sensitivity enhancement, two parallel holes into a parallelepiped allow the tensometric equipping of a hammer to determine the vertical and horizontal reaction at their impact with concrete beams [21.14]. Finally, there are two perpendicular holes in an alloyed steel one-piece block, optimized by FEA, that contribute to a tensometric balance with six components (Fig. 21.2, bottom). This complex strain gauged device has been presented by the author at the Romanian Railway Authority and at KoREMA (Croatian Society for Communication, Computing, Electronics, Measurement and Control) [21.15].

21.4. COMPLEX STRUCTURES COMPOSED BY BARS / COLUMNS

The researchers from the Mechanical and Nuclear Engineering Department of Pennsylvania State University achieved a novel MEMS force transducer that exploits the post-buckling phenomenon of slender silicon columns [21.16]. The design philosophy and fabrication process are discussed and analytical expressions for the force-displacement characteristics are developed. This transducer can be used to perform quantitative and qualitative measurements *in situ* in SEM, TEM or STM, where the small chamber size makes it challenging to integrate conventional force-displacement transducers. Potential applications are characterization of carbon nanotube-polymer interfaces, nanoscale thin film testing and mechanical testing of single biological cells.

Geogrid is a macroscaled network of cylindrical bars used for reinforcing the body of a sloped fill subjected to loading from a footing located near the crest [21.17]. These pseudo-transducers made by bonding strain gauges direct on the cylindrical elastic elements need an appropriate calibration. The accurate estimating of the stabilizing force in the structure reinforcement is enhanced by calibrating each pair of strain gauges as installed in position on the top and bottom faces of the geogrid.

A complex force transducer has been designed like a network with six independent load cells (four placed vertically and two emplaced diagonally), in order to measure axial load (35 kN), shear (4 kN) and bending moment (3 kN·m) for a reinforced concrete structure, having in view the improvement of the buildings design against earthquakes in Turkey [21.18]. Eight calibration tests were conducted to form a calibration matrix for converting the six load cell readings into three reaction components at the base of a structural column.

21.5. DYNAMIC TESTING FOR CYLINDRICAL TRANSDUCERS

Once widely applied, the classical column is still utilized especially in dynamic applications due to its rigidity. An example is the cylindrical bar system for determining complex hydrodynamic forces, another one is the impact bar for studying of the impact wave propagation [21.19].

A team of researchers from KRISS and PTB describes the static and dynamic evaluation of multicomponent force-moment transducers using a calibrating machine developed by the Physikalisch-Technische Bundesanstalt in Germany [21.20]. Two types of these transducers, which can measure three force components, F_x , F_y and F_z , and three moment components, M_x , M_y and M_z , were developed. One has a *solid cylindrical* sensing element and the other has a *hollow cylindrical* shape, both being made by a special NiCrMo alloy.

Figure 21.8, reprinted with permission from IOP, shows the two types of columnar sensing elements, differentiated by an axial hole of $\text{Ø}11.2$ mm. Both force transducers measure three forces [F_x , F_y and F_z] and three moments [M_x , M_y and M_z] using strain gauges technique.

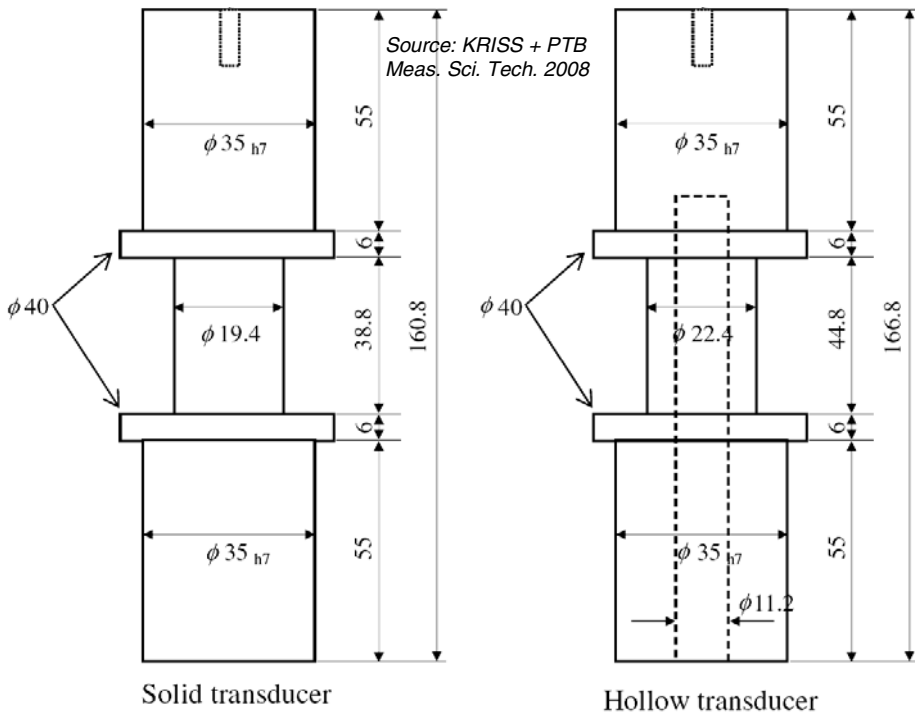


Fig. 21.8 Cylindrical and tubular elastic bodies for strain gauged force transducers

Source: Park & Kang (KRISS), Kumme & Roeske (PTB), Meas. Sci. Technol. 2008

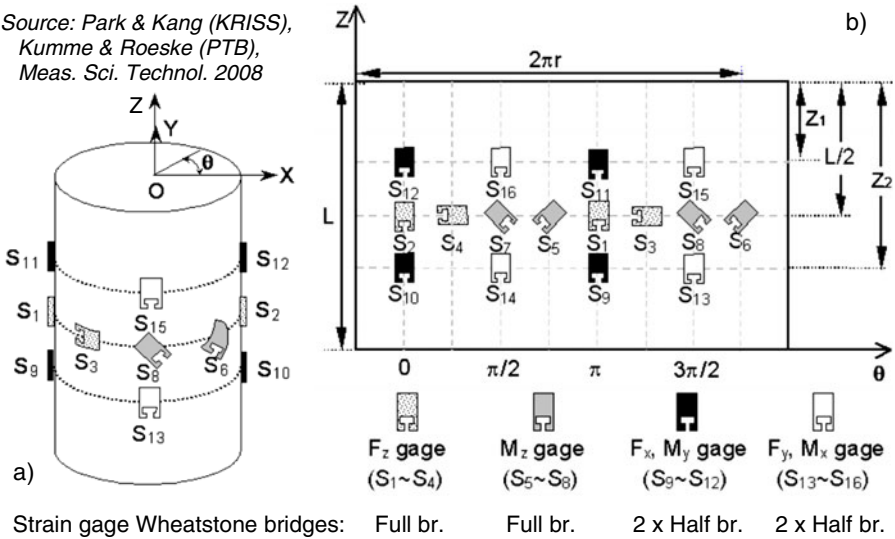


Fig. 21.9 a) Strain gauges emplacement to determine the load distribution on a cylinder and b) their deployed representation (reprinted with permission from IOP Publishing)

Figure 21.9a shows the positions of strain gauges to measure these six components. It is an intelligent distribution for only 16 strain gauges [type J2A, Micro-Measurements] to measure six components of the load torsor, using two full Wheatstone bridges and four half-bridges (Fig. 21.9b).

Another variant of multicomponent tensorresistive dynamometer for three forces and three moments, made up by Istituto di Metrologia “G. Colonnetti” from Turin, Italy is presented by Bray, Barbato and Levi in [21.21].

REFERENCES

1. Überall einbaubar dank der genialen Bauform. Die revolutionäre Kraftmessdose KIS. Bofors Elektronik, Schweden, EMG 1010 (1990)
2. Bolt strain gauge series BTM. TML Tokyo Sokki Kenkyujo Co., December 13 (2008), <http://www.hoskin-instrumentation.ca/sites/hoskin/im>
3. http://www.globalspec.com/FeaturedProducts/Detail/HITEC/MMT_Bolt_Insert_Strain_Gage_Transducer_Assembly/42329 December 13 (2008)
4. Kang, D.-I.: Design and application of force measuring system using build-up technique. PhD dissertation, KAIST, Korea (1994)
5. Averlant, P.: Strain cylinders for compression testing machines. In: CD Proceedings 19th IMEKO TC-3 Int’l Conf. Force, Mass & Torque Measurements: Theory and Application in Laboratory and Industry, Cairo, Egypt, February 19-23, Paper 10 (2005)

6. Welch, C.R.: Column-based stress gauge. US Patent 5361642-94
7. Ștefănescu, D.M.: Force transducer for analyzing the effects of the compressor valves tightening. In: Proc. 3rd National Symp. of Tensometry, Timișoara, September 28 - October 1, vol. I, pp. 155–158 (1983)
8. Robinson, G.M.: Genetic algorithm optimization of load cell geometry by Finite Element Analysis. PhD dissertation, City University of London (1995)
9. Mitchell, R.A., Woolley, R.M., Fisher, C.R.: Formulation and experimental verification of an axisymmetric finite-element structural analysis. Journal of Research of the National Bureau of Standards (U.S.A.) – Series C: Engineering and Instrumentation 75C(3,4), 155–163 (1971)
10. Lee, C.Y., Kang, D.-I.: Nonlinear finite element analysis according to design parameters of a column type load cell. In: Proc. IMEKO TC3/APMF 1998, KRIS, Korea, September 14-18, 1998, pp. 436–441 (1998)
11. Vanderplaats, G.N.: Numerical Optimization Techniques for Engineering Design with Applications. McGraw-Hill Book Company, New York (1984)
12. Buzdugan, G., Blumenfeld, M.: Tensometria electrică rezistivă. Editura Tehnică, București, Romania (1966)
13. Burada, C., Buga, M., Năilescu, L., Rogoz, T.: Schemes with strain gauges for measuring the longitudinal forces within continuous rail. In: Proceedings 2nd National Symposium of Tensometry, Cluj-Napoca, June 11-14, vol. III, pp. 185–194 (1980)
14. Bantia, N., Mindess, S., Bentur, A., Pigeon, M.: Impact testing of concrete using a drop-weight impact machine. Experimental Mechanics 29(1), 63–69 (1989)
15. Ștefănescu, D.M., Mănescu, T.: Vertical strain gauge multicomponent balances for vehicle models tested in wind tunnels. In: Proc. KoREMA 1996 41st Annual Conference, Opatija, Croatia, September 18-20, vol. 1, pp. 81–84 (1996); ISBN 953-6037-149
16. Samuel, B.A., Desai, A.V., Haque, M.A.: Design and modeling of a MEMS pico-Newton loading/sensing device. Sensors and Actuators A: Physical 27(1), 155–162 (2006)
17. Gnanendran, C.T., Selvadurai, A.P.S.: Strain measurement and interpretation of stabilising force in geogrid reinforcement. Geotextiles & Geomembranes 19, 177–194 (2001)
18. Canbay, E., Ersoy, U., Tankut, T.: A three component force transducer for reinforced concrete structural testing. Engineering Structures 26, 257–265 (2004)
19. Rizzi, S.A., Doyle, J.F.: A simple high-frequency force transducer. Experimental Techniques (Society for Experimental Mechanics, Bethel, CT) 14, 45–48 (1990)
20. Park, Y.-K., Kumme, R., Roeske, D., Kang, D.-I.: Column-type multi-component force transducers and their evaluation for dynamic measurement. Meas. Sci. Technol. 19, Paper 115205 (2008)
21. Bray, A., Barbato, G., Levi, R.: Theory and Practice of Force Measurement, p. 327. Academic Press, London (1989)

Chapter 22

STRETCHED / COMPRESSED TUBES

22.1. CLASSICAL TUBES

This elastic element allows a wide range of dimensions depending on the available materials and it is easy to process (Fig. 22.1). The tube is less sensitive to bending, twisting and buckling than the column and allows more installation possibilities in the tested equipment. The tube having the internal diameter $d = 0$ is just the full cylinder.

The tube is actually a hollow cylinder column, a pipe section or a thin wall elastic bar (Fig. 22.2, top); such elastic items are called “sleeve” or “barrel” and their prototype can be considered RA [22.1]. The caisson can be also included in this class having a square or rectangular contour [22.2].

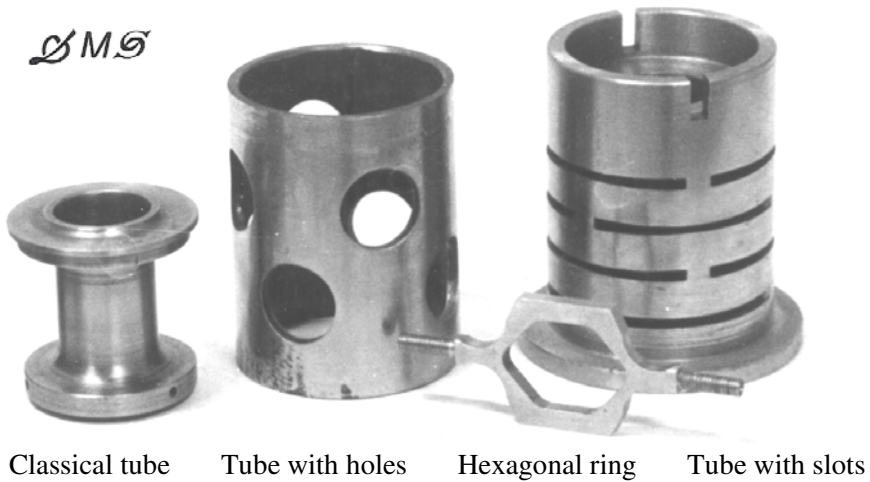
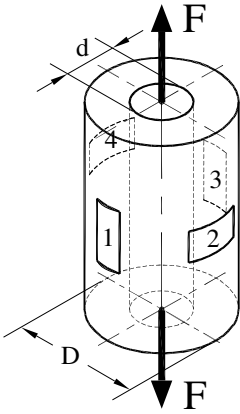


Fig. 22.1 Various elastic elements for customized strain gauged force transducers

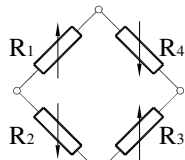
E-2



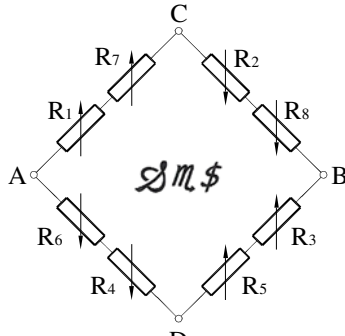
Load range [N]: $10 \dots 10^6$

Mechanical sensitivity [$\mu\text{m/m}$]: $\frac{4F}{\pi E (D^2 - d^2)}$

Electrical sensitivity [ϵ]: 2.6



Four strain gauges bridge connection



Eight strain gauges bridge connection

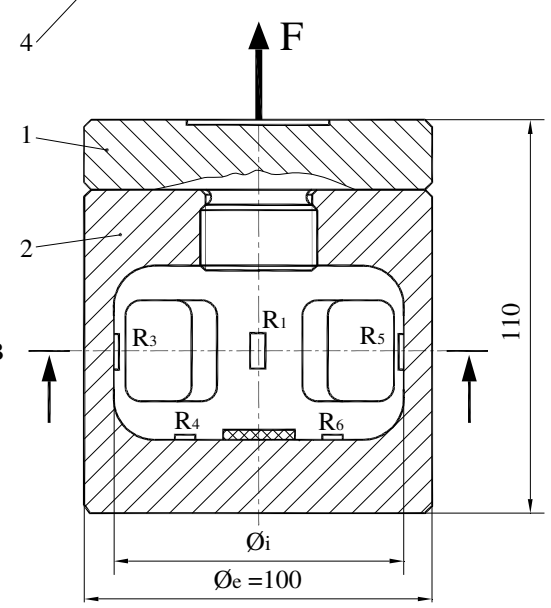
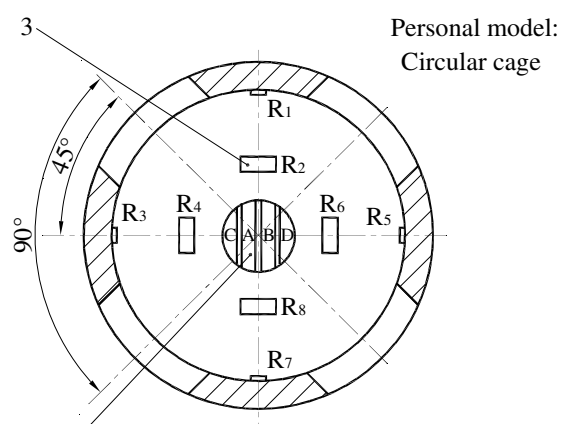


Fig. 22.2 Strain gauged elastic elements of type II for force transducers. Their tensometric sensitivity can be increased introducing stress concentrators (holes or slots).

A more advanced form is the one of the “champagne cork” named Gozinta, presented in Figure 20.4. A similar elastic structure but made of aluminum is shown in [22.3]. Tensometric bolts that is axial cylindrical groove screws are presented in [22.4].

H-shaped longitudinal section tubing (namely undrilled axial holes cylinder), shown in [22.5], suggests analogy with some biological abnormalities in trees [22.6]. An H-element with barometric compensation is shown in [22.7]. Other tube-shaped structures with variable section can also be studied, for instance a torus between two thin shells [22.8], described in Chapter 30.

A piezoresistive, three-axis, hollow micro-force and -torque transducer for mass production is mounted in the Smartpen™ [22.9]. This is a common tool that enables writing on usual surfaces, measuring normal and tangential contact forces as well as the inertial forces like an accelerometer; all signal are transmitted wirelessly to the computer system. The geometrical restrictions, marked in Figure 22.3, are the outer and inner diameter and the total length. A Romanian model of a strain gauged pen for the determination of handwriting characteristics is presented in [22.10].

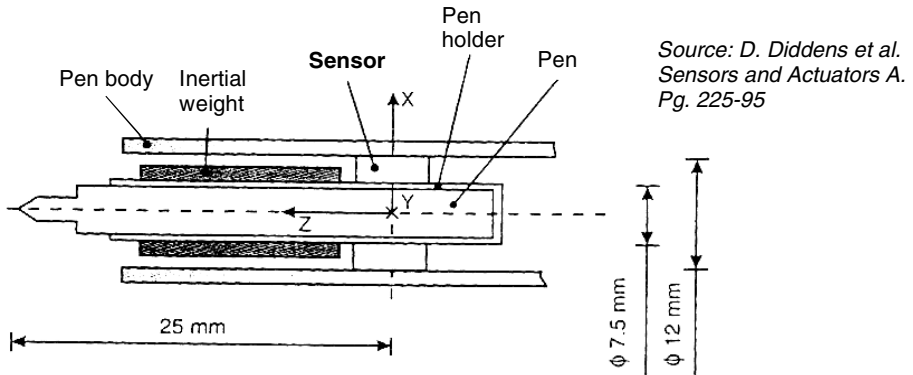


Fig. 22.3 Piezoresistive triaxial force and torque transducer for determining the normal, tangential and inertial forces during the writing process (© 1995 Elsevier)

Specific tubular applications at macro level are the scales for metallurgical bars and the structures for mining equipment. The stress study in the landing gear of an aircraft can be made either by means of directly bonded transducers or by means of strain gauged tension-compression force transducers, the latter being reused electromechanical devices [22.11]. As they are multifunctional, these sensing devices solve rapidly a lot of problems for the researches, design and maintenance of aircraft. The tubular elastic element equipped with strain gauges is presented in Figure 22.4.

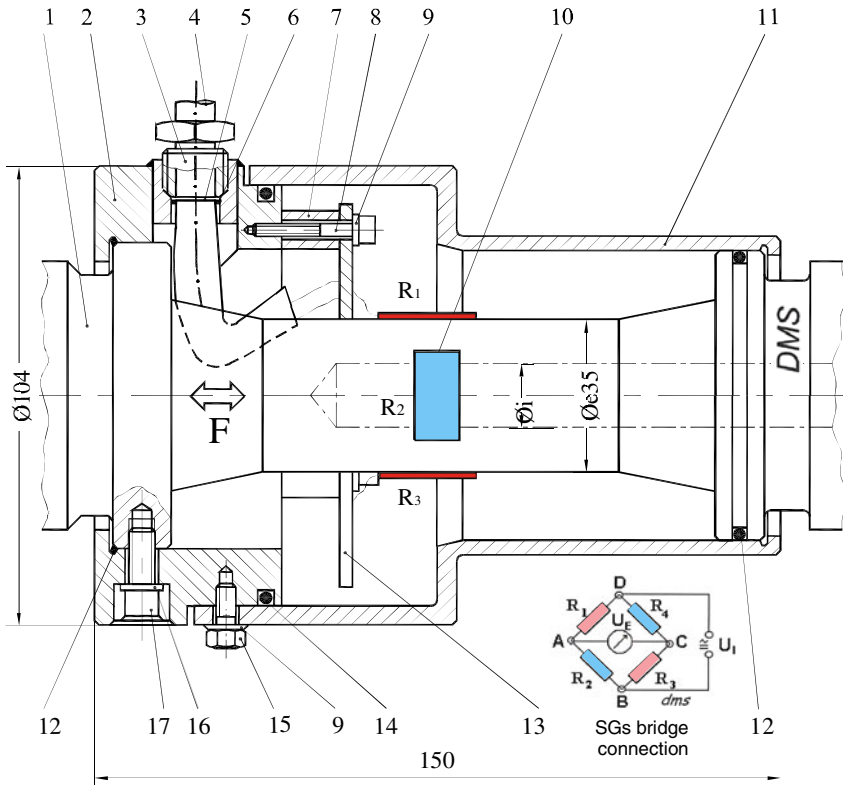


Fig. 22.4 A strain gauged transducer used for dynamic testing of a landing gear

The elastic element is tubular with the inner diameter chosen in accordance with the nominal load while the total length is that of the specific bar in the fitting system of the landing gear on the testing stand. The components of the force sensing device are: 1 – elastic body of improved OLC 45, 2 – link piece, 3 – stuffing box, 4 – four-wire shielded measuring cable, 5 – washer, 6 – ‘O’ ring 8×1.5, 7 – bushing, 8 – cylinder head screw for M5×25 hexagonal spanner, 9 and 16 – Grower washers, 10 – strain gauges (SGs), 11 – housing, 12 – ‘O’ ring 60×3, 13 – “horse shoe”-shaped connector, 14 – ‘O’ ring 85×4, 15 – hexagonal head screw M4×15, 17 – cylinder head screw M6×20.

A tubular transducer to measure the stress field in the debris piggish bone is depicted in [22.12]. The outer diameter of the transducer elastic body is 2.5 mm, wall thickness 0.2 mm and total length, according to medical demand, is 6 mm. Due to the space restriction, semiconductive strain gauges are axially orientated, the measuring half-bridge being completed with a dummy resistor for thermal compensation.



Fig. 22.5 Tubular Hexapod

Gradual distraction osteogenesis of a broken bone stimulates the body's self-healing capacities to form new tissue. To improve the treatment, a mechatronic actuator was developed integrating into a single device such components as: the motor-drive, transducer for longitudinal force, analog signal conditioning and embedded computing tool [22.13]. The Hexapod external fixator (Fig. 22.5), which is based upon the Stewart platform kinematics, allows six independent degrees of freedom for measurement of fracture loads and for spatial movement. The mechatronic actuator was designed to replace the manual elements of the hexapod external fixator. Its *telescopic bar* consists out of three threaded tubes

made from stainless steel with a length of 86 mm for the outmost and 75 mm for the inner tubes. Ball joints are attached to the ends of the bar. The length measured between the centers of the joints is 110 mm at the minimum and extends up to 234 mm when fully extracted. A spur gear is mounted slidable at the middle tube; one turn results in a lengthening of 2 mm. Two resistive strain gauge half-bridges (FSET-A6208P-100 from BLH) are bonded to a thinned area of the outmost tube and form the longitudinal force transducer. The resulting Wheatstone bridge is connected to the motor and electronics unit with a small connector. The actuator is controlled by a microcontroller that administers the movement and shows the results on a display. The integrated longitudinal force transducer was calibrated at a Zwick 1455 testing machine, the maximum output voltage being 440 nV/V/N.

22.2. CONCENTRIC TUBES

Interesting combinations of two concentric tubes are described in several works:

- double tubes having slightly different heights, making up a compression force transducer with two sensitivities [22.14],
- tube-shaped tandem with one stretched elastic element and another compressed one for increasing the tensometric sensitivity [22.15],
- “folded” tubing (as a rolled up sleeve) recommended for the study of the thermoelastic effects due to the stored energy at the load application [22.16].

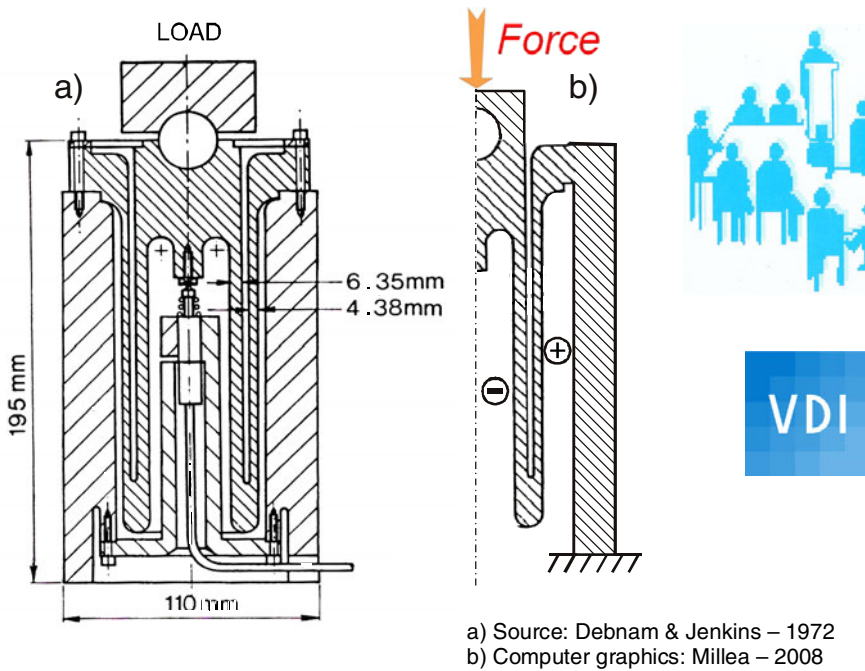


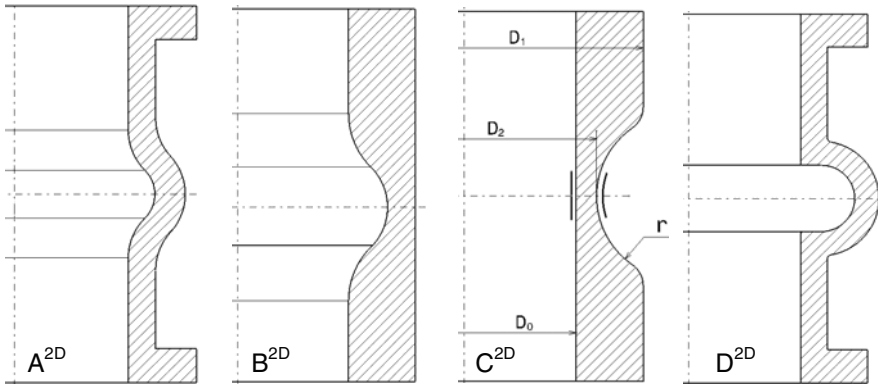
Fig. 22.6 Dual-element (“differential”) load column consisting of two concentric tubes with opposed deformations. Note the electro-mechanical analogy with the differential VWFT (vibrating-wire force transducer) as presented in Figure 11.10a!

The strain gauged dual form presented in Figure 22.6a has the advantage of considerably increasing the measurable deflection for a load of 500 kN. One could observe that, under loading, the internal tube is shortened while the external tube is extended practically in the same proportion (Fig. 22.6b).

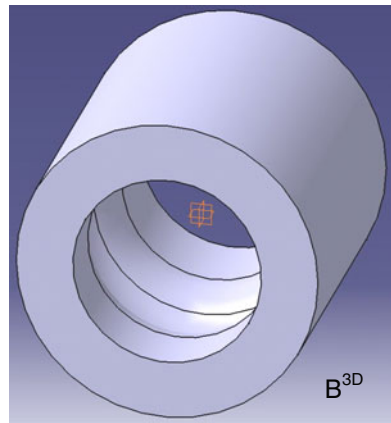
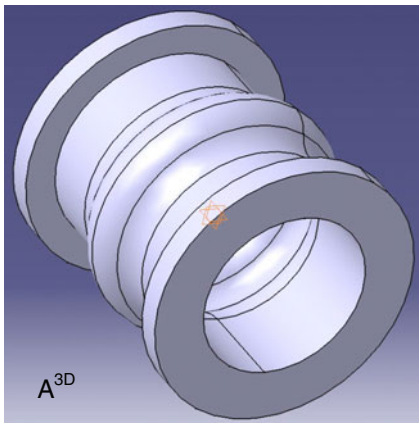
22.3. PROFILED TUBES

Depending on antagonistic demands of structural rigidity and tensometric sensitivity, various tubular shapes could be designed. For example, two tubes having different diameters are connected by circular matching or by rotation sections, like the truncated cone and other axisymmetric elastic elements to be presented in Chapter 31.

Figure 22.7 presents four complex tubular forms with diameters changing happening in the median region, through an axisymmetric structure. Another example was shown in Figure 10.12. There can be realized through technology with numeric command a diversity of radius profiling variants.



Source: Dr. Marin Sandu, Politehnica University of Bucharest, Romania



Catia design: Florian Stefanescu

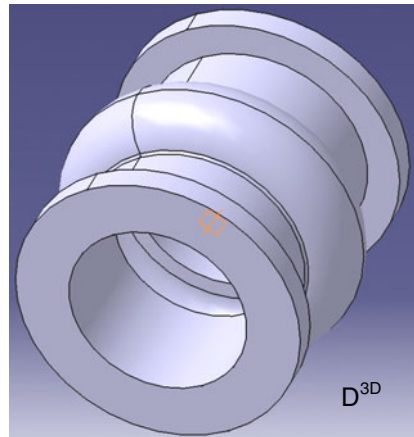
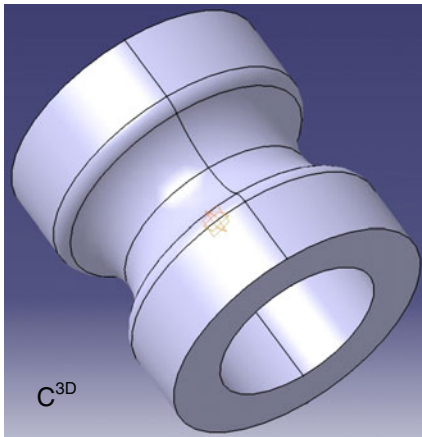


Fig. 22.7 2D and 3D visions for four models of profiled tubes using Catia software

Classical tubular structures are monolithic, one-piece of metal designed for easy manufacturing, but having reduced strain gauge sensitivity. In the well-known Wheatstone bridge only two strain gauges are active, the other two, mainly used for temperature compensation, have only transverse sensitivity (Poisson's coefficient: $\nu = 0.3$). To improve the sensitivity, it is possible to make holes or slots in the tube walls, but these are expensive technologies and they affect the assembly functionality. The best way is to profile the axisymmetric section of the tube by milling. The test piece can be obtained through machining on lathe to required dimensions and profiled with appropriate depth. After machining, the sample will be hardened to a yield strength of 1500 MPa or higher.

For these new elastic structures [22.17] do not exist analytical formulae, so the finite element analysis (FEA) and computer-aided design (CAD) are worthily indicated. These flexible bodies have high bending sensitivities and natural decoupling of torsion, if designing by finite elements a symmetric transducer geometry and placing strain gauges properly.

Let's study by finite element analysis a profiled tube as a strain gauged elastic element for high force measuring! The axisymmetric section (length = 169 mm and external diameter = 140 mm) depicted in Figure 22.8 is subjected to compression with 1 MN and analyzed by ANSYS Finite Element Program. The structure is automatically meshed by 1318 nodes in 1153 Quadrilateral42 axisymmetric finite elements and supported on its base. A special attention is necessary to obtain proper strain diagrams on the candidate elastic element measuring sections, because it is essential to compare these diagrams in order to establish the best strain gauges positioning.

The most important FEA observations and results are the following:

- Greater the fillet radius, smaller stress concentrators.
- Longitudinal strains are greater than the circumferential ones, but too unbalanced.
- Circumferential strains ε_z are greater inside than outside the tube, ensuring a better protection for the appropriate strain gauges.

The ε_z diagrams along three interior paths (superior, middle and inferior) indicate the following significant values:

- maximum strain in the superior portion, – 885 $\mu\text{m/m}$, appears at the distance 35.7 mm, very closed to the middle of that path (length: 64.5 mm);
- maximum strain in the middle portion, + 1436 $\mu\text{m/m}$, appears at the distance 9.1 mm, just in the middle of that path (length: 18.2 mm) and of the whole elastic structure;
- maximum strain in the inferior portion, – 484 $\mu\text{m/m}$, is reduced and displaced from the middle, comparatively with the superior portion, as an effect of supporting on its base in ANSYS program.

The best positions for emplacing the strain gauges are clearly resulting. Minimum strain ($- 885 \mu\text{m/m}$) represents 0.62 comparatively with the positive one ($+ 1436 \mu\text{m/m}$) and is more than double reported to the classical tube where transversal contribution is only 0.3 (Poisson’s coefficient), so the profiled tube is more sensitive, about 25 percent.

Figure 22.8 is a half-expanded representation of the profiled tube concerning the circumferential strains, i.e. specific deformations on the Z direction (as nodal solution). The four strain gauges, corresponding to the four indicated strains, are connected in full bridge, ensuring a sensitivity factor of 3.24 related to 2.6 for classical tube, maximum being 4. This is a very suggestive and complex mechatronic image, simultaneously representing the elastic deformations (superior and middle portions are opposite curved reporting to the central axis of the profiled tube), the best strain gauges position estimation (by means of finite element analysis) and the “differential” measurement using the Wheatstone bridge, represented as an electronic “locket” on a mechanical structure (like a special barrel).

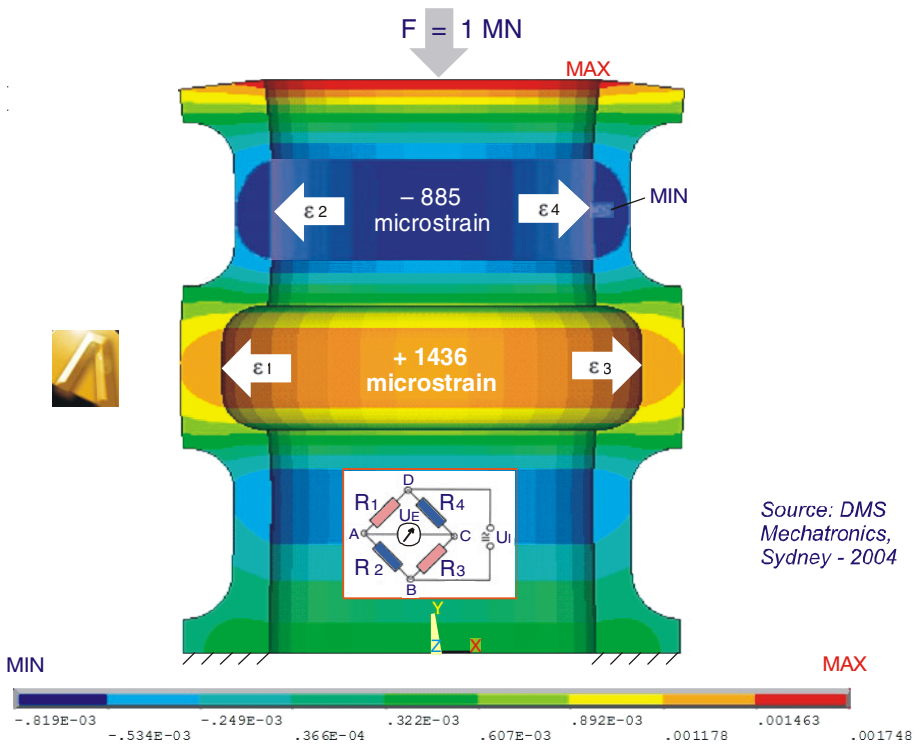


Fig. 22.8 Mechatronic image: profiled tube (mechanical structure) designed by FEM (computer program) and sensed by strain gauges (electrical measurement)

Using of this profiled tube as a complex mechatronic tool ensures a lot of advantages:

- wide load ranges due to various shapes and dimensions of the axisymmetric section,
- relatively easy to design by FEM and low cost manufacturing,
- compact, fully integrated into the structure or mounted by flanges as independent force transducer, mix mechanical and electronic component of the measuring system,
- easy reconfigurable or standardized for a large range of applications;
- strain gauges and the associated circuits bonded inside the tube and properly protected, like in a case,
- reduced size and weight and increased tensometric sensitivity (strain gauges are more “active”) comparing with classical tube/column,
- without affecting the installation functionality in different heavy-load and high precision applications.

Concluding, the best way to improve the tensometrical sensitivity of classical tubes up to 25 % is to “transform” tension / compression in bending after “profiling” the axisymmetrical section of the tube (by machining on lathe), knowing that greater the fillet radius smaller stress concentrators.

22.4. TUBES WITH HOLES OR SLOTS

Different solutions to increase the sensitivity can be also achieved by introducing concentrators (holes and slots of different forms and sizes):

- sleeve with 24 side holes, which is a multi-component force and torque transducer [22.18];
- our contributions to optimization of such elastic structures are the circular orifice tube (with two spaced rows of four equally away holes each) [22.19] and the horizontally slotted tube [22.20];
- tube with two rows of interlaid rectangular slots, named Octoplus [22.21];
- L-shaped cut-out tube utilized in Robotics [22.22] or within force transfer standards [22.23];
- tube with vertical slots, as presented in Figure 22.9.

A helical load cell [22.24] includes a first pair of transducers disposed along a neutral axis of a helical coil (Fig. 22.10). A second pair of transducers is disposed in diametrically opposed relation to the first pair. Sensitivity to side loading is eliminated by “splitting” the second pair of transducers. In another embodiment, each of the transducers in each pair are respectively oriented parallel and perpendicular to a neutral axis of the coil. This new configuration provides a measure of torsional forces.

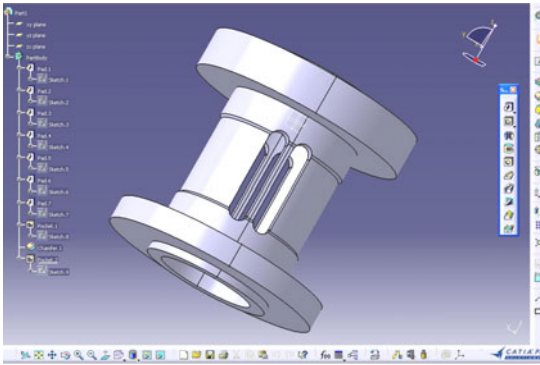


Fig. 22.9 Tube with vertical slots analyzed in Catia by Florian Ștefănescu

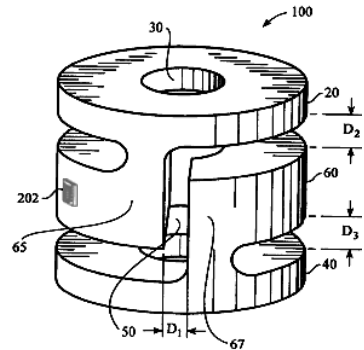


Fig. 22.10 Helical load cell

Another proposed elastic element (Fig. 22.11) was manufactured from a tube in which four windows were cut. As a result, three rings connected by four beams (two in horizontal plane and the other two in the vertical plane of the representation) were obtained [22.25]. Three full (Wheatstone) bridges were constituted for measuring the components F_x , F_y , F_z . The effects of the loads are theoretically uncoupled because of the symmetry or antisymmetry of bending moment diagrams; the cross influences of the measured components are less than 2 %. Also, the measuring sensitivities are satisfactory because are bigger than the imposed value which was of 0.75 mV/V.

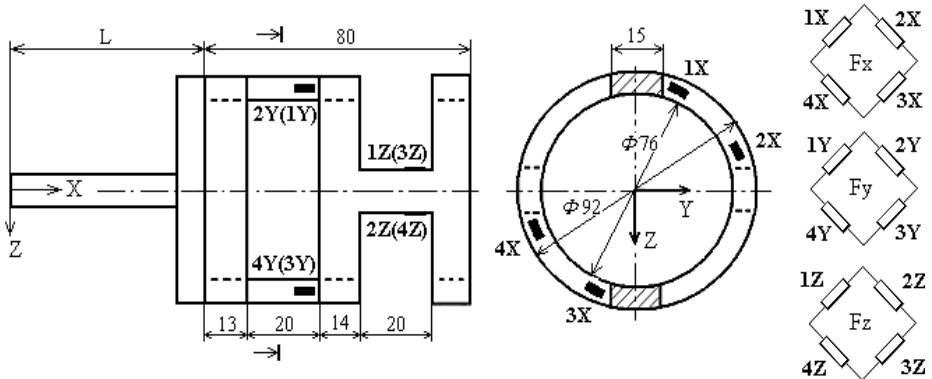


Fig. 22.11 Slotted tube, axially loaded in tension and/or compression [Cf. Marin Sandu]

The structural optimization of some complex loaded tubes, used in aviation or sea platforms, has been achieved by Eschenauer [22.26]. A force transducer with cage-shaped elastic element, a 4-rectangular window tube is

presented in Figure 22.2 (bottom). Strain gauges located on the generators are active, while the ones in the circumferential disposition are strained by means Poisson's coefficient. For doubling the sensitivity and averaging on two perpendicular diameters the eight strain gauges bridge scheme is used.

22.5. TUBULAR STRUCTURES UNDER COMPLEX LOADING

A high sensitivity combination of a cylindrical rod for vertical force measuring and a tube for determining the two forces in the horizontal plane of a complex structure is presented in [22.27].

The HBM collection of application notes includes a lot of measurement examples based on tubular structures:

- “*Messtechnische Briefe H.B.M.*” 1-67 shows that the perfect vertical location of the Surveyor mooncraft was achieved by considering the weight distribution of the mobile supports on which 24 strain gauges were bonded on the moon module legs.
- “*Reports in Applied Measurement*” 1-95 describes how C6 force transducers with central hole have been used with loading rods for measuring tensile loads when constructing a road bridge over the Main-Danube Canal.
- “*Hotline Hottinger*” presents the following two examples.

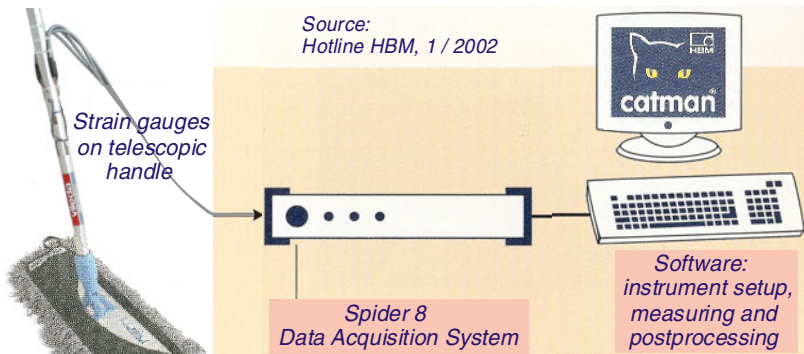


Fig. 22.12 Measurement system for forces during floor cleaning

In an EU research program, ergonomics and medical experts have investigated how manual floor cleaning affects the health of working team, recommending the using of less water and lighter cleaning implements with less friction [22.28]. The mop is under load throughout the entire cleaning process in the forward direction but also to both side forces when the mop is directed in a left-hand or right-hand curve, and when a new loop starts. This

method allows the axial forces and bending moments to be measured synchronously. Strain gauges were installed on the telescopic tubular handle and connected by cables to a Spider 8 DAQ system (Fig. 22.12).

Formula Student is organized by an Institute of Mechanical Engineers in UK [22.29]. Their task is to better design and build a single seat racing car, avoiding over-engineering and, as a consequence, the exaggerated weight. To understand the complex loading case, the team installed strain gauges at critical points on the bars of the wheel suspension, building such “embedded” force transducers, and used an MGCsplit to acquire racing load data with a sampling rate of 2.4 kHz. Data are imported into catman[®] software for analysis.

REFERENCES

1. Load Cells and Force Transducers Survey. Catalog G 21.04.9 e, Hottinger Baldwin Messtechnik GmbH, Darmstadt (1992)
2. Angrilli, F., Basso, R.: Monitoring and diagnostics of stresses in reciprocating machines. *Measurement* 12, 345–356 (1994)
3. Dixon, M.J.: A traceable dynamic force transducer. *Experimental Mechanics* 30(2), 152–157 (1990)
4. The Story of A.L. Design – the “customizers”. *Sensors, Transducers and Instrumentation*. A.L. Design, Inc., Buffalo, N.Y., Revue 06 (1994)
5. Theiß, D.: Die Wägezelle: Von Wägegut zum Meßsignal. Auszug aus: ‘Industrielle Wägetechnik’ von A. Schuster, Eigenverlag Schenck, pp. 21–36, Darmstadt (1983)
6. Mattheck, C., Burkhardt, S.: A new method of structural shape optimization based on biological growth. *International Journal of Fatigue* 12(3), 185–190 (1990)
7. Sava, J.: Loadcells 200 N – 1 kN with H-type spring elements. In: Kemény, T., Havrilla, K. (eds.) *Force Measurement and Weighing in the 90s*. IMEKO TC Event Series, vol. 29, pp. 243–250 (1104/1991)
8. Pressure Transducers, Load Cells, Torque Transducers, Accelerometers, LVDTs, Instrumentation. Catalog 119710, Sensotec, Columbus, OH (1997)
9. Diddens, D., Reynaerts, D., van Brussel, H.: Design of a ring-shaped three-axis micro force/torque sensor. *Sensors and Actuators A* 46–47, 225–232 (1995)
10. Ştefănescu, D.M., Sandu, M.: Strain gauged force transducer for measurement some writing characteristics. In: *National Symposium on Achievements and Perspectives in the Field of Transducers for Measurement Equipment*, Cluj-Napoca, Romania, October 23–24, pp. 62–67 (1986)
11. Ştefănescu, D.M.: Deformation and force transducers for testing in aeronautical industry. In: *MOCM-7 (Modelare și Optimizare în Construcția de Mașini)*, Methods and Techniques for Deformation Measurements, Bacău, Romania, vol. 2, pp. 126–131 (2001); ISSN 1224-7480

12. Volf, J., et al.: Special miniature transducer for in vivo of bone measurement. In: CD Proceedings XVII IMEKO World Congress Metrology in the 3rd Millenium, Cavtat - Dubrovnik, Croatia, June 22-27, pp. 2080–2082 (2003)
13. Wendlandt, R., Wackenhut, F., Schümann, U., Capanni, H., Seide, K., Müller, J.: Mechatronic actuator with integrated longitudinal force sensor for medical applications. In: Proc. 13th Int'l Conf. SENSOR 2007, Nuremberg, May 22-24, vol. I, pp. 87–90 (2007)
14. Alămoreanu, M., Zevedei, N.: Capteur dynamométrique de compression à deux sensibilités. In: Proc. 4th National Symposium of Tensometry, Braşov, September 24-27, vol. I, pp. 3–8 (1986)
15. Loghinov, V.N.: Elektriceskie izmerenia mehaniceskih velicin [Electrical measurement of mechanical quantities]. Izdat Energia, Moskva (1976)
16. Debnam, R.C., Jenkins, R.F.: An investigation of the performance of force measuring devices of very high precision. VDI-Berichte No. 176, 31–41 (1972)
17. Ştefănescu, D.M., Marinescu, A.: Strain gauged elastic elements for measuring large forces in Mechatronics. In: Proceedings of the 3rd IFAC Symposium on Mechatronic Systems, Sydney, Australia, September 6-8, pp. 439-444 (2004)
18. Grant, A.P. (Spar Aerospace Canada): Force moment sensor. US Pat. 5295399-94
19. Ştefănescu, D.M.: The study of a tubular elastic element with holes by the finite elements method. In: Proc. 3rd National Symp. of Tensometry, Timişoara, September 28 - October 1, vol. IV, pp. 205–210 (1983) (in Romanian)
20. Ştefănescu, D.M.: Untersuchung der Verformungszustands eines elastischen Rohrelements mit Spalten, anwendbar beim Bau der Kraftaufnehmer mit Dehnungsmeßstreifen. In: Revue Roumaine des Sciences Techniques – série de Mécanique Appliquée, Bucarest, vol. 29(5), pp. 519–533 (1984)
21. Mast, J.P., Wieringa, H.: Multidirectional Force and Moment Transducer. Report 5211901, Institute of Mechanical Constructions – TNO (Toegepast Natuurwetenschappelijk Onderzoek), Delft (NL) (March 1983)
22. Cornut, A.: Simplified computation method for force transducer. In: Proc. IVth Conf. Vibration in Machine Building, Timişoara, November 26-27, vol. III, pp. 95–99 (1982) (in Romanian)
23. Dubois, M.: Multicomponent force transfer standard of 300 kN. Conférence IMEKO sur les Pesées Industrielles, Odessa (U.R.S.S.), ONERA, Chatillon, T.P. 58-1977 (September 1977)
24. Bruns, R.W., Schindler, G.E.: Helical load cell. Abstract of WO 9848253, European Patent Office (October 1998)
25. Sandu, M., Sandu, A., Găvan, M.: Design and calibration of a 3-components force sensor. In: Abstracts of the 22nd Danubia-Adria Symposium on Experimental Methods in Solid Mechanics, Monticelli Terme, Italy, September 28 - October 1, pp. 30–31 (2005)
26. Eschenauer, H.A.: Multicriteria structural optimization as a technique for quality improvement in the design process. Microcomputers in Civil Engineering 10, 257–267 (1995)

27. Lucio, V.J.G., Regan, P.E.: Triaxial load cells for the tests of a waffle slab supported by 16 columns. In: Proc. 9th Int'l Conf. Experimental Mechanics, Copenhagen, Denmark, August 20-24, vol. I, pp. 292–300 (1990)
28. Schilling, R.: Mopping with SG – Measuring forces during floor cleaning. Hotline Hottinger – News from the World of Test and Measurement (1), 10–11 (2002)
29. Gittins, N.: HBM supports the racing team of the University of Hertfordshire. Hotline Hottinger (2), 10–11 (2004)

Chapter 23

BENT LAMELLA (CANTILEVER BEAMS)

23.1. VARIOUS APPLICATIONS WITH CANTILEVER BEAMS

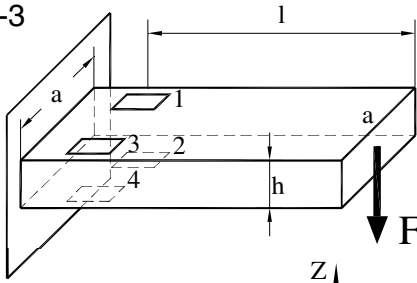
The cantilever beam (Fig. 23.1 top) has low rigidity, high deflection and it is recommended for low forces. Also called bent prismatic bar (with a constant rectangular cross section) [23.1a] or wide lamella (with width to thickness ratio higher than 1) [23.1b], the classic cantilever lamella has been described for the first time by Galileo, 360 years ago, and has a detailed presentation in an educational article by A.L. Window (Strain, 1/1970, pp. 29-33).

This bent lamella is mainly used to the force measuring but is also useful for investigating of other mechanical quantities:

- Position and orientation variations due to structural deformation and contact force detection of an end-effector [23.2] when a manipulator (a self-sensory robot arm based on a strain gauged cantilever) interacts with its environment (Canadian Space Agency).
- Pressure: two S-shape beams support on each side a square membrane [23.3].
- Two perpendicular components of the grinding force (normal and tangential) are measured mounting the workpiece for cylindrical grinding between two strain gauged support beams with square section [23.4].
- Tightening torque: a dynamometric wrench based upon a bent bar [23.5].
- Acceleration: a thin section lamella [23.6] or a frame with two lamellae supporting a mobile table [23.7].
- Vibration control by minisensors [23.8], and so on.

The bent lamellae are the best for accurate weighing in laboratory [23.9] or in industrial environment, ranging from pico- to kilo-newtons. A semi-fabricated, planar strain gauge assembly (Eurospäische Patentschrift 235329) was achieved by W. Ort [23.10]. Starting from the single point configuration [23.11] the transition is made to a parallelogram (Brüel & Kjaer) as a double (guided) cantilever beam.

E-3

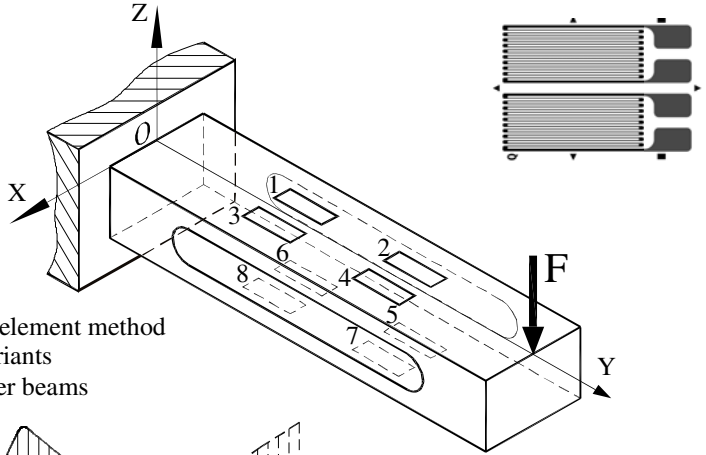


Load range [N]: $10^{-2} \dots 5 \times 10^4$

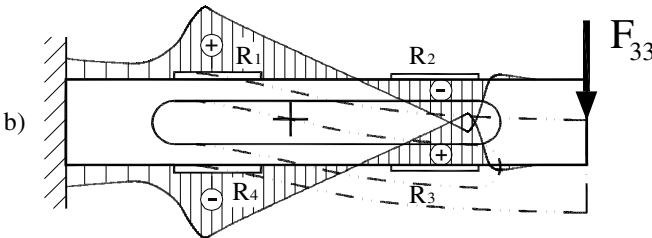
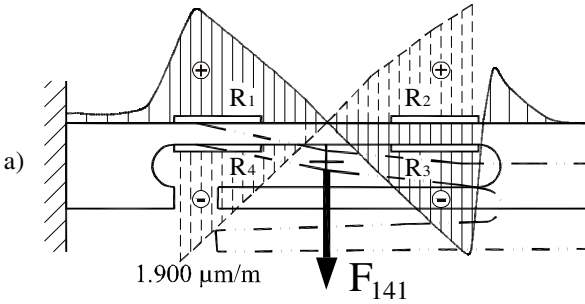
Mechanical sensitivity [$\mu\text{m/m}$]: $\frac{6Fl}{E a h^2}$

Electrical sensitivity [ϵ]: 4

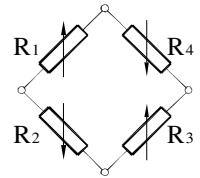
Personal model:



Strain diagrams obtained by finite element method applied on two variants of slotted cantilever beams



Bridge connection



S.M.S

Fig. 23.1 Strain gauged elastic elements of type III for force transducers. The upper and the bottom side of the double cantilever beam (b) become of a kind of S shape.

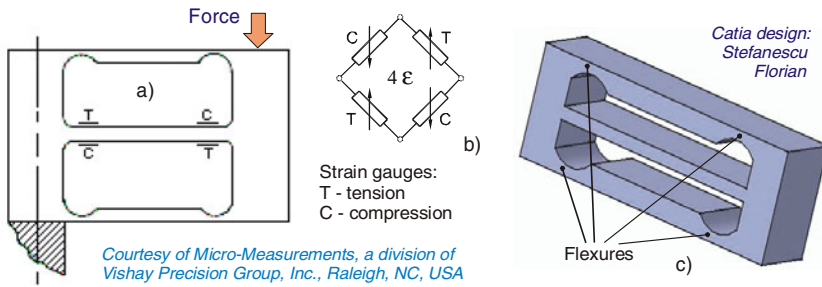
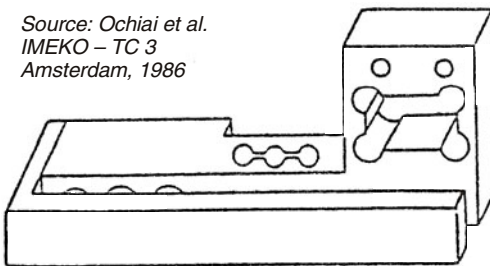


Fig. 23.2 Triple-beam design for isolation of sensing element from parasitic couples: a) 2D representation with strain gauges positioned on the central beam, b) the SGs connection in Wheatstone bridge, and c) 3D representation of the triple-beam

The multiple bended elastic elements constitute an extended category of cantilever beams. For example, double bending beam transducers PW-15 are load cells for platform scales [23.12]. Such flexible structures can be achieved by electroerosion (complex slotted one-piece item) or combining two lamellae and paying special attention to hysteresis [23.13]. A triple-beam design [23.14] is presented in Fig. 23.2a; in this case, the upper and lower members serve both as flexures and reactions for externally applied couples. Bending moments due to the vertical component of load are sensed in the central measuring beam, the four strain gauges being connected in a Wheatstone bridge like in Figure 23.2b. The flexures are locally thinned (Fig. 23.2c) to minimize bending resistance while retaining sufficient cross section to carry the axial forces.

Circular or rectangular slotted configurations [23.15] can be achieved by profiling the holes to provide increased sensitivity and internal strain uniformity. A more complex configuration is the embedded bar with a lever for load application [23.16]. A sophisticated force and tactile transducer composed by three cantilevers, each having series of holes connected through slots [23.17], is presented in Figure 23.3.

Source: Ochiai et al.
 IMEKO – TC 3
 Amsterdam, 1986



Permission granted by Koninklijke Brill NV
 for editor Helmer Wieringa in 1986 with
 Martinus Nijhoff Publishers, Dordrecht, NL

Fig. 23.3 Multiple slotted cantilever beam with loading lever

Photo-electro-chemical microprocessing of the silicon (Massachusetts Institute of Technology) allows the achievement of some miniature cantilever lamellae with sensitivity up to nano-newton level [23.18]. The research team of Limerick (Ireland) brings out a mixture based on ruthenium, bismuth and indium oxides used for the thick coats/layers in the sensor technology [23.19]. Standard half- and full-bridges were used in thick film resistors layouts having in view to “couple” or have pairs of longitudinal and transverse strain gauges.

Starting from the simple triangular lamella with an equal bending resistance [23.20] or from the “clutch” made up of four triangular plates in a compensated installation (SIEMENS), the optimization imposes the parabolic shape [23.21] as in Pareto's classical solution. An embedded lamella [23.22] is used as force pseudo-transducer to a medicine capsule machine. Shape factors for bent beams are to be found in [23.23]. The study of a cantilever bar with varying width and height is achieved by Rozvany in [23.24]. A combination of three circular section types varying in accordance with three different laws (linear – taper, constant – cylindrical and polynomial) is to be found in [23.25].

In Figure 23.1 (bottom) a comparison between the double cantilever lamella and the one fitted with a lever for load application was made [23.26]. If Lund tried an optimization with finite isoparametric elements [23.27], we have achieved an analysis with two-dimensional finite elements for the plane status of strain. By comparing the specific deformation diagrams in the two personal versions, a more balanced ϵ configuration can be noticed (“butterfly” type) in the cantilever lamella with lever for non-linearity compensation.

The applications presented at the Romanian Symposia of Tensometry are: classical bent bars, lamellae for torque moment measuring [23.28] and a set of three cantilever lamellae for the determination of loads in agricultural machinery [23.29]. The draught and the side force exerted on each working component of the model spot plough are measured [23.30]. The vertical supporting beam was converted into a so-called force transducer. Two pairs of strain gauges were bonded at the front and respectively back of the beam.

Details about the strain gauged cantilever lamella are also to be found in the other chapters of the handbook. This concept is basic throughout the work and its using is limited only by the experimenter's imagination. Among all the elastic elements, the cantilever beam covers the greatest load range, reaching the inferior extreme, at the atto-newton level. Some of the measurement principles presented in the Part One have a good connection with the cantilever beams; the best suited are piezoresistive ones (including strain gauges), (micro)resonators and optical devices (e.g. within atomic force microscopy).

Piezoresistive cantilevers, as compared to the optical read-out type, show several advantages:

- time-consuming laser alignment is not needed,

- read-out electronics can be integrated on the same silicon chip,
- temperature control can be easily implemented,
- piezoresistive detection can work in non-transparent solutions,
- compatibility with miniaturization and array fabrication.

A dual-frequency patch antenna was designed and fabricated by conventional photolithography techniques. Its application for strain measurement was evaluated by bonding the patch antenna to an aluminum cantilever beam and applying loads at its free end. The resulting strain changes the dimensions of the metallic patch, resulting in a shift in the antenna resonant frequency [23.31]. The shifts of the return loss S_{11} curves under loads were perfectly correlated to the strains experienced by the patch antenna. So, the applied loads can be measured from the changes in antenna resonant frequency.

23.2. CANTILEVER BEAMS FOR LOWER FORCES

After describing cantilever applications in the high forces range (up to 50 kN), this subchapter presents some interesting examples of cantilever beams in the field of micro- and nano-newton. An example is shown in Figure 23.4.

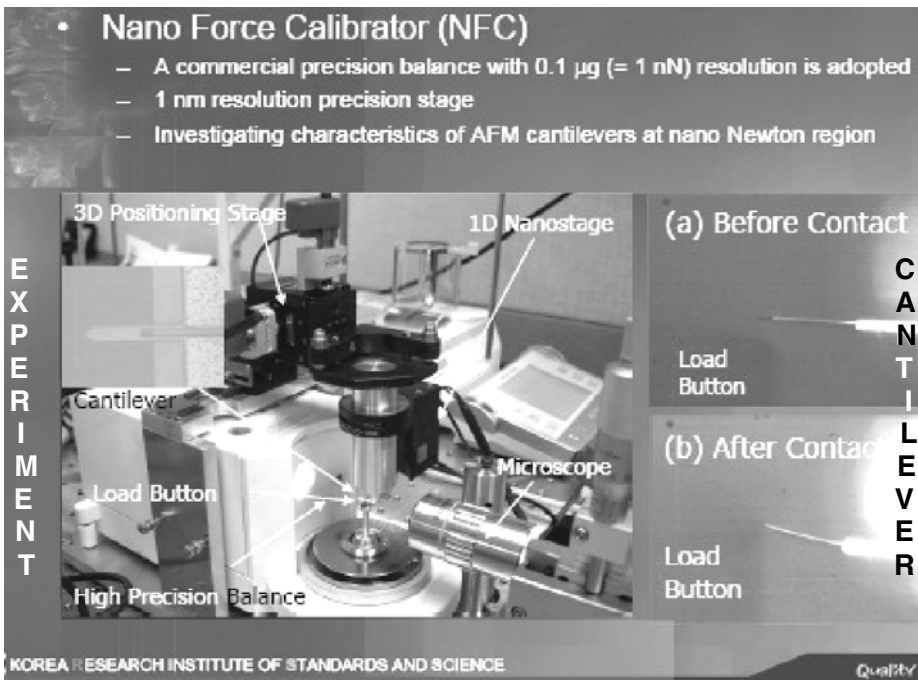
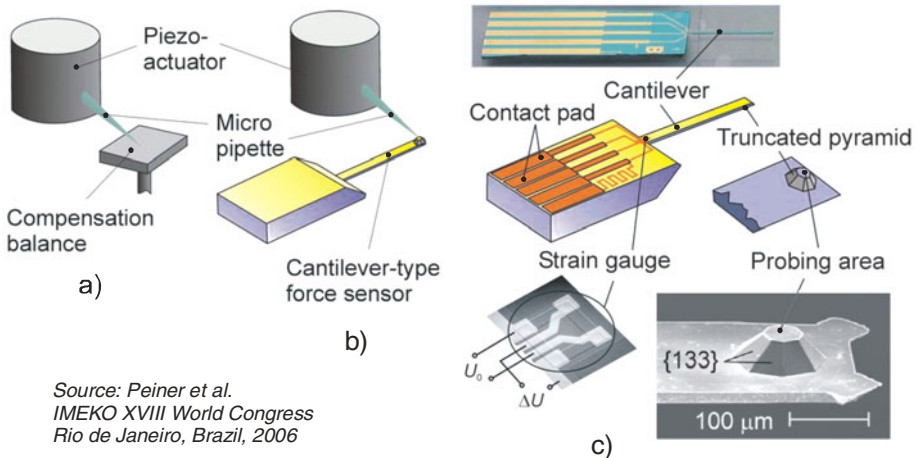


Fig. 23.4 Piezoresistive Nano Force Calibrator used within Korean Metrology

Needs for micro- and nano-force measurements are permanently increasing in the fields of nanotechnology, biology, chemistry and so on. Specially, a cantilever can be used as an important tool to measure and analyze interaction characteristics between a sharp tip and molecules on a sample surface. It can be also used for nanoindenting, scratching, wearing to measure hardness, adhesion, durability, etc [23.32].

The force lithography by precision force control can make a mechanical pattern on a disc which is not changeable chemically or optically. In this field, the cantilever is considered as an effective tool since it can measure even small interaction force between biomolecules such as DNA, virus, bacteria, etc. For example, the binding force measurement between biomolecules can be used to identify antigen/antibody characteristics and to investigate protein. The sensitive cantilever can be used in many application fields, but the exact value of its spring constant must be given for the accurate measurement and control.

Force calibration of micropipettes (Fig. 23.5) is used for application of mechanical stress to isolated ventricular cardiomyocytes which are immobilized on glass substrates. For this purpose two methods have been developed at Physikalisch-Technische Bundesanstalt in Germany [23.33], using nano-newton compensation balance or cantilever-type silicon sensors as transferable force standards. Cell elongation or contraction upon movement of the attached micro- pipette can be visualized by confocal laser scanning microscopy with the cell membranes stained with a marker substance.



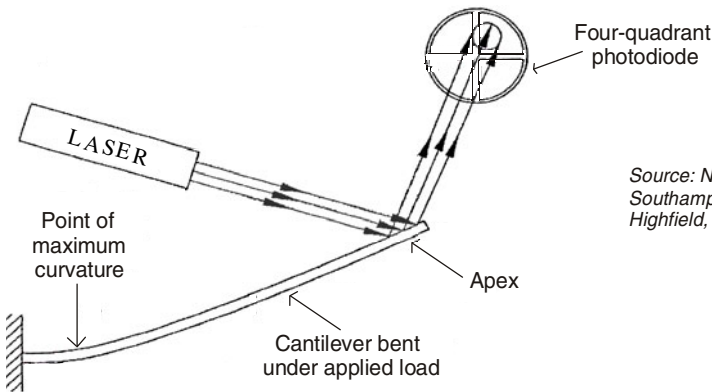
Source: Peiner et al.
IMEKO XVIII World Congress
Rio de Janeiro, Brazil, 2006

Fig. 23.5 Force calibration of micropipettes at PTB: a) Micropipette calibration using a nanobalance; b) transferable cantilever-type force standard; c) silicon cantilever with integrated strain gauges and probing tip.

For calibration procedure the sensor is mounted into a connector designed for simultaneous load-deflection and load-strain gauge output voltage measurement. The bridge output voltage is measured at a supply voltage of 1 V by means of a low-noise bridge amplifier (ML10B, Hottinger). Based on the nanobalance, calibration was performed in the sub- μN range at a resolution of several nN. In the alternate method, the cantilever sensor, which can be directly transferred to the cell probing setup, enables calibration immediately before and after a cell probing experiment. Resolution is better than 0.1 μN in a range of (1...50) μN . The reproducibility of both methods is between 5 and 7 %.

The development of the atomic force microscopy as an imaging tool has led to two main cantilever types: contact and non-contact. In “contact mode AFM” [23.34], the tip of a microcantilever is raster scanned across a surface. As the surface undulates, the cantilever bends as the tip rides the undulations. The cantilever deflection is sensed and used to form the image variable. The most popular method of deflection sensing is to reflect a laser beam off the upper surface of the cantilever onto a four-quadrant photodiode (Fig. 23.6).

The beam is centered onto the diode to maximize the output. PID (proportional, integral and derivative) control is used to maintain this signal while the tip is scanned across a sample by adjusting the height of the stage on which the cantilever is mounted. For optimum performance of this system, the relationship between the atomic forces acting on the tip and the resulting rotation at the apex of the cantilever (which reflects the beam) needs maximizing. This cannot be achieved by reducing the stiffness of the beam in the direction normal to the surface, as beam would become too supple in the scanning direction. Optimal performance can be gained by maintaining stiffness while increasing curvature at the cantilever apex (point of load).



Source: Niblock et al.
Southampton University,
Highfield, England, 1999

Fig. 23.6 Cantilever beam used in contact mode within Atomic Force Microscopy

A novel methodology to measure the pull-off force of rigid bodies by recording force curves with an atomic force microscope is described in detail [23.35]. Large sample arrays can be inspected using the AFM as a sensing element (Fig. 23.7). The inspected structures in this study are rigid silicon discs with a diameter of 200 μm , supported by soft silicon oxide springs. The discs are pushed down by the AFM tip on a bottom substrate. When retracting the AFM tip and the disc, a discontinuity in the force curve of the AFM occurs due to the pull-off. The surface interaction of silicon oxide surfaces provided with hemispherical tips and flat silicon surfaces is determined. Therefore, various surface configurations are inspected, with varying tip radii and varying number of tips.

The most prevailing surface interactions in silicon micromechanical systems are capillary forces, forces due to hydrogen bridging and van der Waals forces. The lowest adhesion force measured for a single device has the value of 240 nN. In terms of total work of adhesion per area this value equals $9 \times 10^{-7} \text{ mJ} \cdot \text{m}^{-2}$. This method features a relative error of 0.26, comparable to the corresponding value of cantilever beam detachment measurements from the literature. The resolution of the presented method is only limited by the force resolution of the AFM which in this work is 20 nN.

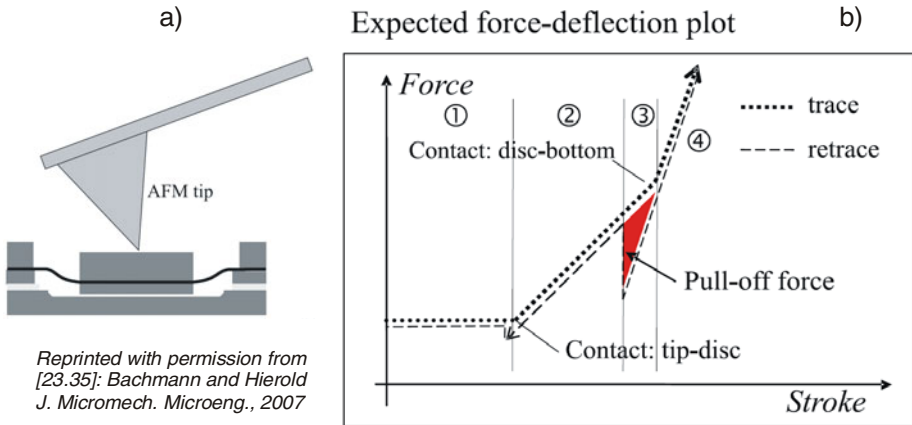


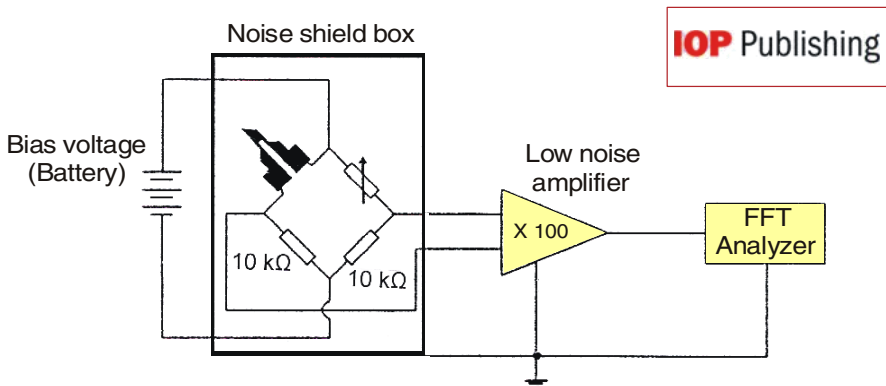
Fig. 23.7 Principle of the AFM measurement: a) The AFM tip pushes directly on the backside of the suspended silicon disc. b) Theoretical force curve: the adhesion force is determined with the discontinuity in the retrace curve.

One of the most important requirements for a cantilever-type transducer to obtain high force sensitivity is small thickness [23.36]. Where self-sensing piezoresistive cantilevers with sub-micrometer thickness are concerned, it is necessary to use a technology which can create ultra-thin ($< 100 \text{ nm}$) piezoresistors on a cantilever surface. The research team from Department of

Mechano-Informatics within University of Tokyo demonstrates a relatively simple, rapid thermal diffusion method by using spin-on glass film to fabricate sub-100 nm piezoresistors on a ultra-thin single-crystal silicon cantilever.

A lot of experiments were made on this thin cantilever, illustrating its close connection with different measurement methods as well as its great versatility:

- The *displacement sensitivity* of the fabricated cantilever is measured by SEM (scanning electron microscopy), moving the cantilever chip with a piezoelectric actuator against a sharp tip; this displacement is equivalent to 10 pN, and their stiffness is in the range of $0.001 \text{ N}\cdot\text{m}^{-1}$.
- The thermomechanical noise of the cantilever is used to measure *resonance frequency* by means of a laser Doppler vibrometer.
- In order to estimate the *minimum measurable force*, noise analysis is performed using the setup seen in Figure 23.8. A low noise amplifier (NF Electronic Instruments LI-75A) is connected to the output of a special Wheatstone bridge, which is driven by bias voltage. In order to prevent external noise sources, the cantilever and Wheatstone bridge are put together inside a shielding box which is connected to the same ground terminal with an amplifier and fast Fourier transform (FFT) analyzer (Agilent 35670A). After measuring the noise power spectral density and integrating the total noise for a bias voltage of 1.5 V, the minimum measurable fractional change in resistance is found to be 2.8×10^{-6} , and this gives a minimum measurable force value of 6.94 pN.



Reprinted with permission from [23.36]

Fig. 23.8 Electrical schematics for noise measuring in order to determine the value of the force measurement threshold (6.94 pN)

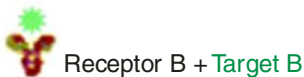
23.3. (BIO)CHEMICAL CANTILEVERS

Merging of silicon microfabrication techniques and surface functionalization biochemistry, together with the development of multi-cantilever transduction methods, offers new opportunities in (bio)chemical sensing [23.37].

Biosensors based on microcantilevers have become a promising tool for directly detecting biomolecular interactions with great accuracy. Microcantilevers translate molecular recognition of biomolecules into nano-mechanical motion that is commonly coupled to an optical or piezoresistive read-out detector system. High-throughput platforms using arrays of cantilevers have been developed for simultaneous measurement and read-out of hundreds of samples. The review [23.38] covers the basic working principles and types of sensors, examples of commercial instrumentation, applications reported in chemical and biological analysis, and future developments for bio- and/or chemical cantilevers.

The key to using microcantilevers for selective detection of molecules is their ability to biofunctionalize one surface of the silicon microcantilever in such a way that a given target molecule will be preferentially bound to that surface upon its exposure (Fig. 23.9).

Microcantilevers can transduce a number of different phenomena, such as changes of mass (and “connected” force), temperature or stress, into bending (static mode) or a change in resonant frequency (dynamic mode), which can be monitored. Adsorption of molecules, when they are restricted to one of the cantilever surfaces, produces differential surface stress that bends the cantilever.



Source: Carrascosa, Moreno, Alvarez & Lechuga, *Nanomechanical biosensors: a new sensing tool*, *Trends in Analytical Chemistry* – 2006

Reprinted with permission from Elsevier

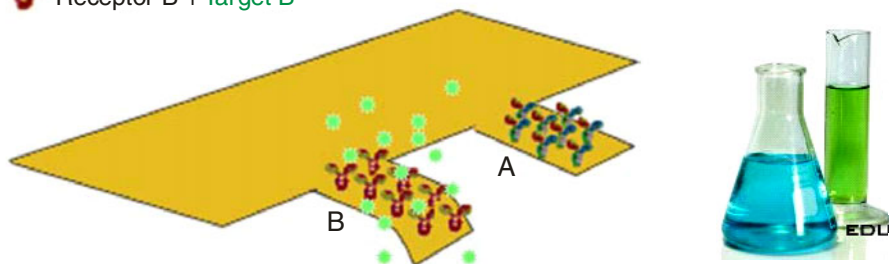


Fig. 23.9 Scheme of the cantilever bending due to a biomolecular interaction between an immobilized receptor and its target. Only the specific recognition causes a change on the surface stress, driving to the bending of the “chemiresistive” cantilever (Target B).

At the same time, the resonant frequency of the cantilever also varies due to mass loading. The bending and the changes in resonant frequency can be monitored by several techniques: optical beam deflection, piezoresistivity, piezoelectricity, interferometry, capacitance, electron tunneling. Changes in resonant frequency can be detected by measuring the thermal noise of the cantilever. However, to achieve great sensitivity, especially when working in liquids, it is necessary to pre-energize the cantilevers by using alternating electric, magnetic, or acoustic fields.

To measure the change in the resistance, silicon cantilevers must be included in a DC-biased Wheatstone bridge. This configuration is very suitable for further integration into arrays of cantilevers. Optical read-out is another common scheme for detecting the movement of microcantilevers, as derived from standard Atomic Force Microscopy. The displacement of the free end of the cantilever is measured using the optical deflection of an incident laser beam on a position-sensitive photodetector, which allows the absolute value of the cantilever displacement to be calculated. This method provides sub-angstrom resolution (i.e. 0.1 nm) and can be implemented easily. The main disadvantages of this read-out technique are that it requires external devices for deflection measurements, so that their continuous alignment and calibration are very time consuming. Both techniques of chemical sensing for different compounds and their detection limits are compared in Table 23.1 [23.38].

Table 23.1 Analytical comparison of different chemical sensing applications

Compound	Detection limits	Technique
Mercaptoethanol	50 ppb	Optical read-out
Mercury	10^{-11} M	Optical read-out
2,4-dinitrotoluene (DNT)	300 ppt	Optical read-out
Trinitrotoluene (TNT)	70 pg	Piezoresistive
pH detector	30 nm deflection / pH unit	Optical read-out
Cs ²⁺ / K ⁺	10^{-11} / 10^{-4} M	Optical read-out
DNA hybridization:		
Mismatch	10 nM	Optical read-out
8 cantilevers array	75 nM	Optical read-out
Nanoparticle labeling	0.05 nM	Piezoresistive
Proteins and pathogens:		
Two isoforms (PSA)	6 mg/ml (20 nm signal)	Optical read-out
C-reactive proteins	10 ng/ml	Piezoresistive
Salmonella enterica	25 bacteria	Piezoresistive
Vaccinia virus	20 mg/ml	Piezoresistive
Environmental control field:		
DDT	10 nM	Optical read-out

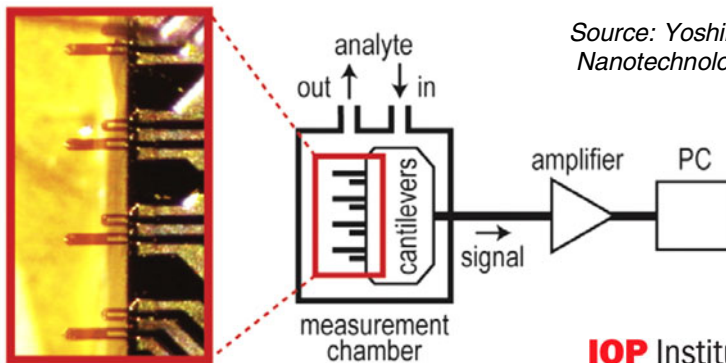
The experimental studies described in [23.39] reveals that:

- *high aspect ratio cantilevers*, that are much longer than wider, are optimal for point-loading applications such as microscopy and force measurements;
- *low aspect ratio cantilevers*, that are short and wide, are optimal for surface stress-loading scenarios such as those that occur in biological and chemical sensor applications.

Changes in the surface properties of the microcantilever through binding or hybridization of analytes to receptor molecules directly influence its surface stress. This causes a proportional deflection to the analyte concentration. Finite elements simulations are made using elliptical holes located in the piezoresistor area in order to maximize the integrated stress differences [23.40].

Piezoresistive microcantilever array sensors (Figure 23.10) have the selectivity of discriminating various vapors of volatile organic compounds including alkanes with different chain length, from 5 (n-pentane) to 14 (n-tetradecane), according to principal component analysis [23.41]. Piezoresistive microcantilever array sensors do not require bulky and expensive instrumentation. They have a lot of advantages, such as low cost, simple operation, and miniaturization of the whole system into a match-box sized device. Moreover, cantilevers in two- or even three-dimensional arrays can be integrated into the piezoresistive read-out system.

A group of researchers from Center for Materials Nanoarchitectonics, Ibaraki, Japan, and Research in Nanoscience, Basel, Switzerland, developed a new method to evaluate the sensitivity, taking advantage of the low vapor pressures of alkanes with longer chains under saturated vapor conditions. This method reveals sub-ppm sensitivity and the cantilever response is found to follow the mass of evaporated analytes as calculated using a quantitative model based on the Langmuir evaporation model.



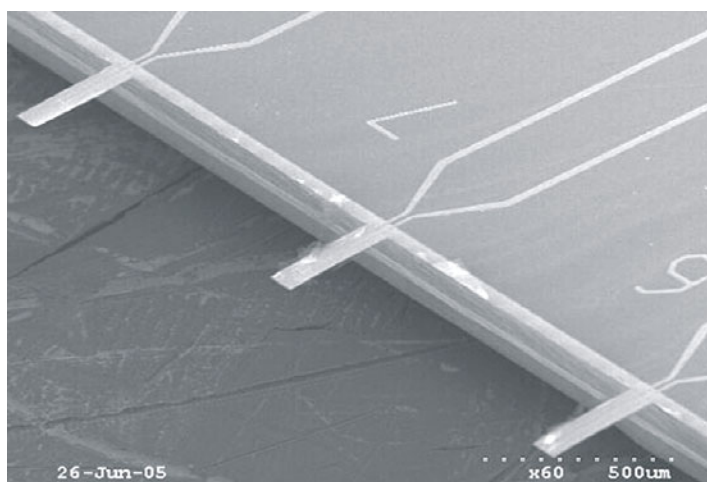
Source: Yoshikawa G. et al.
Nanotechnology 1 – 2009

IOP Institute of Physics

Fig. 23.10 Sub-ppm vapors detection by piezoresistive microcantilever array sensors

Nanomechanical effects offer unprecedented opportunities for trace explosive detection [23.42]. If molecular adsorption is restricted to one side of the cantilever, the beam undergoes bending because of adsorption forces. The force causing the cantilever to bend is independent of the adsorbed mass and depends solely on the binding energy of the adsorbate surface interaction. Cantilevers with very low spring constants (low resonance frequency) show high sensitivity for bending mode operation.

In piezoresistive cantilevers, any change in deflection results in a variation of the cantilever resistance. Boisen's group produces cantilevers with high sensitivity, low electronic noise, and very small drift. Fig. 23.11 shows a scanning electron micrograph of a piezoresistive cantilever array. The readout technique is miniatural and compatible with electronic packaging.



Reprinted from [23.42]
copyright 2008
with permission from
ELSEVIER

Fig. 23.11 Piezoresistive cantilever array for trace explosive detection

A simple, low-cost electronic interface for piezoresistive microcantilever-based transducers [23.43] uses the USB bus of any computer or laptop to communicate with the sensor via SPI commands. Embedded piezoresistive material is chosen to react volumetrically when exposed to the chosen analyte. The reaction of the analyte molecules with the sensing material may be a chemical reaction, mechanical (partitioning or diffusion) reaction, absorption, or adsorption, or other reaction as long as some sort of movement of sensing layer takes place. The volumetric change in the sensing layer subsequently results in a strain in the piezoresistive microcantilever, which is measured as a resistance change by the sensor electronics. This interface is based on LabVIEW and utilizes primary integrated circuits AD7793.

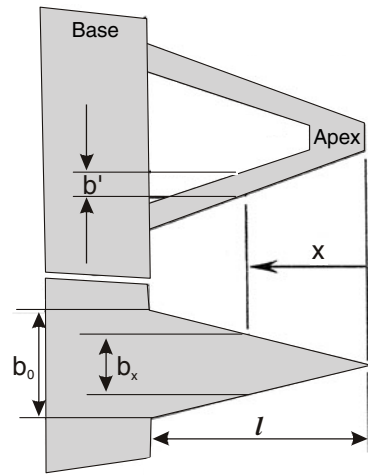
23.4. SEVERAL SHAPES OF CANTILEVER BEAMS

Various shapes of cantilever beams are designed and experimented to enhance the measuring sensitivity and to solve specific tasks of very different application types.

The conventional design of the contact mode AFM cantilever can be modified to improve sensitivity [23.34]. Frictional forces acting on the tip apply torsional loads on the cantilever and give misrepresentation of the surface topography. To counteract this effect, cantilever geometry is designed to be far more rigid in the scanned direction than that normal to the surface that is under scanning. This has led to two favored designs: the 'A' and 'V' frames, as depicted in Figure 23.12.

*Adapted by Millea from Niblock et al.
13th Euroconf. Solid-State Transducers
The Hague, The Netherlands, 1999*

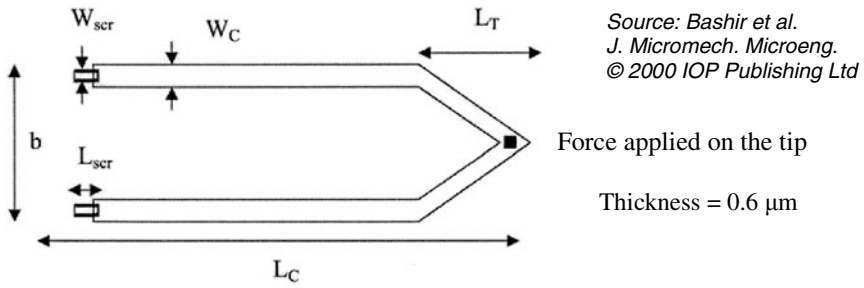
Fig. 23.12 Optimization of atomic force cantilever geometry by A and V frame designs. The rigidity provided by these optimized frames prevents the torsional bending and also increases the rigidity of the cantilever at its apex. The laser beam is reflected from this point, hence all the rotation is due to pivoting at the base of the improved cantilever.



Reflected laser beam type cantilevers can be designed to give greater deflection per unit force (stiffness). Non-uniform etch profiles offer the greatest improvement in performance but processing difficulties make them currently unfeasible. The solid V-frame design can increase the gradient of the apex of the cantilever by 50 % for the same stiffness as a conventional A- or V-frame.

ANSYS software has been used as a tool design to create stress concentrations regions [23.44] with smaller thickness in order to enhance the piezoresistive displacement as well as force and torque sensitivity. The piezoresistive effect in silicon results in a resistance change with applied stress, as a function of crystal orientation, dopant type and doping concentration.

Comparing with the classical rectangular cantilever, U-shaped cantilever with thickness and width smaller than the rest of the cantilever (Fig. 23.13) is about 5 times more sensitive in force measurement.



Cantilever dimensions: $L_C = 150 \mu\text{m}$, $W_C = 20 \mu\text{m}$, $L_T = 40 \mu\text{m}$, $b = 80 \mu\text{m}$
 Stress concentration region: $L_{scr} = 10 \mu\text{m}$, $W_{scr} = 12 \mu\text{m}$
 Resistor dimensions: $L_R = 14 \mu\text{m}$, $W_R = 4 \mu\text{m}$

Fig. 23.13 Sensitive piezoresistive silicon cantilever with stress concentration regions

Source: Melväs et al.
EuroSensors XV
Solid-State Sensors
and Actuators
Munich, June 2001

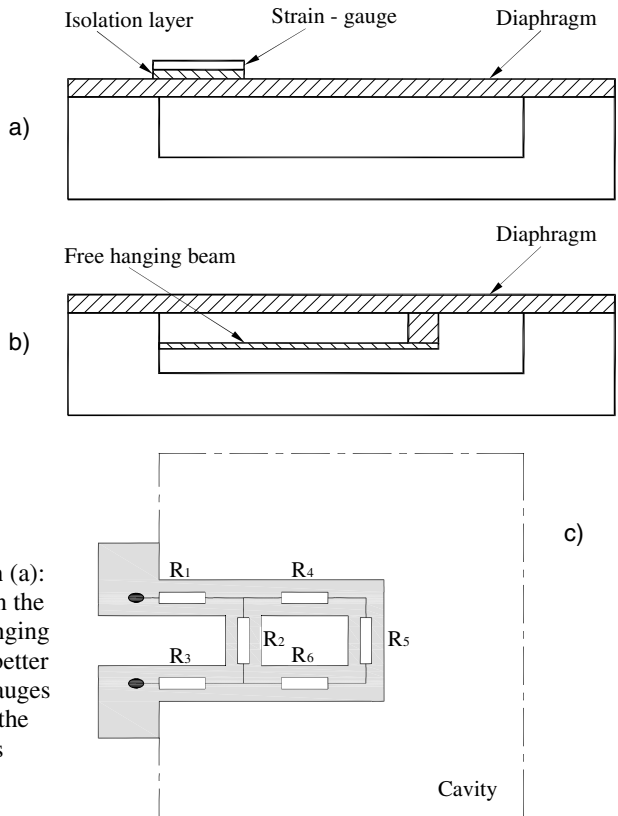


Fig. 23.14 Traditional design (a): Piezoresistor encapsulated on the diaphragm top. (b) New “hanging cantilever” design enabling better encapsulation of the strain gauges and less stiffening effect for the diaphragm. (c) Piezoresistors positioning on the A-shaped hanging beam.

An interesting leverage effect for increased sensitivity is presented in Figure 23.14, adapted from [23.45]. Free hanging flexible element has an ‘A’ or ‘H’ shape in its horizontal plane, which is parallel to the diaphragm. The sensing element consists of an A-shaped double ended supported force transducing beam having 80 μm long, 30 μm width and 0.4 μm thick. The beam is located beneath and at one end attached to a square polysilicon diaphragm.

Complex transducers based on multilayer piezoresistive microcantilevers have been proposed to measure the surface stress change by molecule adsorption from biochemical reaction on an immobilized surface [23.46].

The adopted design is that of a double-microcantilever: an immobilized one connected in series with the sensing cantilever by a transmitter based on a torsion bar or a “zigzag” elastic element (Fig. 23.15a).

When a flow sample injected from the PDMS (polydimethylsiloxane) inlet makes contact with the immobilized microcantilever, the bioanalytes induce surface stress, which is converted into uniaxial strain and measured by the piezoresistive layer integrated in the sensing microcantilever (Fig. 23.15b). In other words, the big cantilever, obstructed from its axial deformation, forces the small (and smart) one to bend.

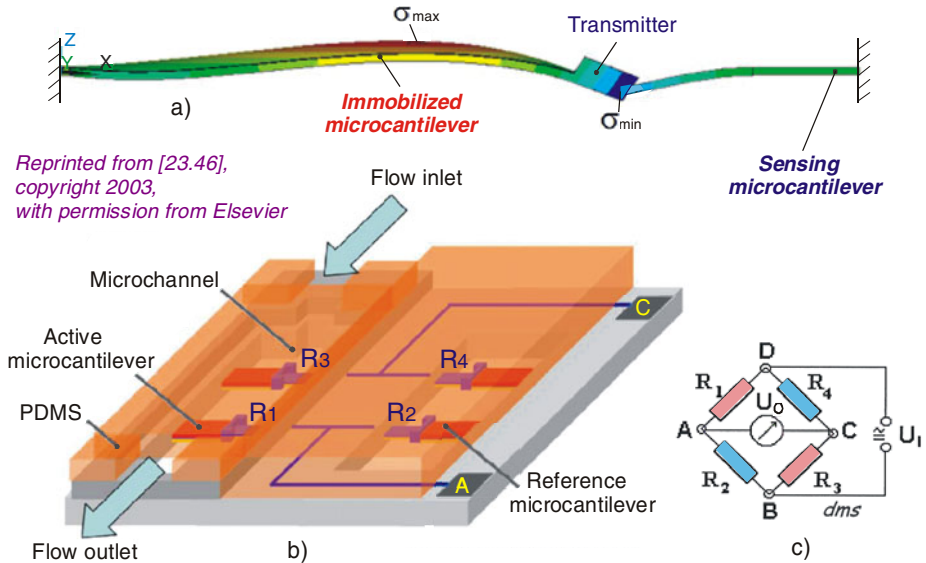


Fig. 23.15 Finite elements simulation of a double (i.e. immobilized and sensing) microcantilever with length ratio 2.7 (a), schematical diagram of the four-layer biosensor chip containing two active and two reference piezoresistive double-microcantilevers (b) and full bridge connection with two active and two compensating piezoresistors (c)

The measurement sensitivity can be increased by the design parameters of the length ratio of the two bent cantilevers and the transmitter rigidity between them. An effective way to alleviate the thermal noise is by using the “parallel” microcantilever configuration: an active one for biosensing and a reference one, unstressed by the input flow.

The perfect compensation of disturbing effects is achieved by four such microcantilevers: two of them are active, placed in the microchannel, whose piezoresistors are connected in opposite arms of the Wheatstone bridge, while the other two piezoresistors are on the reference microcantilevers (Fig. 23.15c).

23.5. CANTILEVER BEAMS IN MULTICOMPONENT FTs

By multiplying the number of cantilever beams one could obtain a multi-component force transducer as well as the increasing of strain gauge sensitivity for each measured component. A typical application is the surface forces apparatus (SFA), its evolution and recent advances being presented in [23.47].

The basic unit for normal and adhesion force measurements, SFA 2000 has one central single-cantilever spring used for generating both coarse and fine motions over a total range of seven orders of magnitude below millimeters. This bistable device allows for two kinds of pivoting motions (Fig. 23.16a):

Source:
Israelachvili et al.
Rep. Prog. Phys. - 2010

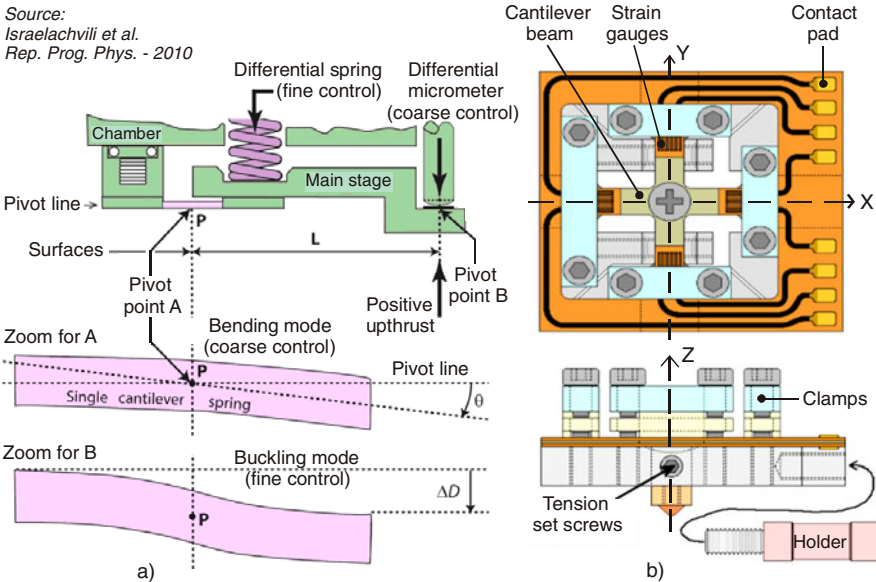


Fig. 23.16 The evolution from single- (a) to four-cantilever (b) elastic elements in surface force measurements (Reprinted with permission from IOP Publishing, © 2010)

- When a *normal force* is applied by the coarse control micrometer, the pivot point A is just at the center P of the cantilever, which is in the *bending mode*.
- When the force is applied by the fine control on a helical spring, due to the resulting *side effect* of the spring the pivoting is at point B and the cantilever is in the *buckling mode*, a rare case when buckling is a useful / stable situation!

A significant improvement in the SFA area is constituted by the miniature 3D attachment (Fig. 23.16b), designed to measure forces in any spatial direction. The probe is held in the middle of a four-cantilever foil, that is like a cross spring made of a single 25 μm thick titanium foil. Deflections of the probe in the X, Y and Z directions are detected by eight strain gauges, bonded on both sides of each cantilever. This complex elastic element is placed on a tension adjustable base by clamping the cantilevers down outside the strain gauges. The sensitivity of the four-cantilever spring can be readily varied by *in situ* adjustment of the tensions on the foils. Three strain gauged Wheatstone bridges are measuring the three components of the applied force. In principle, it is possible to scale this sensing device from macro- (tribometer, indenter) to meso- (SFA) and nanoscale (atomic force microscopy).

A tactile transducer for simultaneous detection of normal and shear stresses is presented in [23.48]. Four microcantilever beams, on which the strain gauge layers (Pt/Ti) are deposited on silicon and covered with high bio-compatible elastomer, are allocated in such a manner that adjacent beams are perpendicular to each other in order to decouple any potential discrepancy due to non-ideal orthogonality. These piezoresistive beams are curled beforehand so that they can concurrently measure, with increased sensitivity, normal stress up to 250 kPa and shear stress up to 35 kPa. Finally, the tactile transducer efficacy has been verified by experiments *via* a micromanipulator, a calibration device and a high-resolution microscope.

Turning back to the macroscale level, in the field of accurate weighing, there are a lot of applications based on different cantilever beams. In order to solve the dilemma “*weighing on a single load cell or on a platform supported by four strain-gauged elastic elements*” a thorough decision is necessary, referring to technical, metrological, economic, and even political aspects.

Figure 23.17 shows an original dynamometric platform for the perfect disconnected measurement of the six loads components (three forces and three torques) from an aircraft mock-up in the trisonic wind tunnel [23.49]. Its elastic elements are the four coplanar L-shaped beams with equal arms and constant rectangular cross sections. Their pre-dimensioning was made by means of the computational relations from the Strength of Materials. Then, the structural optimization was possible by using the finite element method and the pre- and post-processing facilities existent in the program COSMOS/M (Finite Element System, User's Guide, 1995).

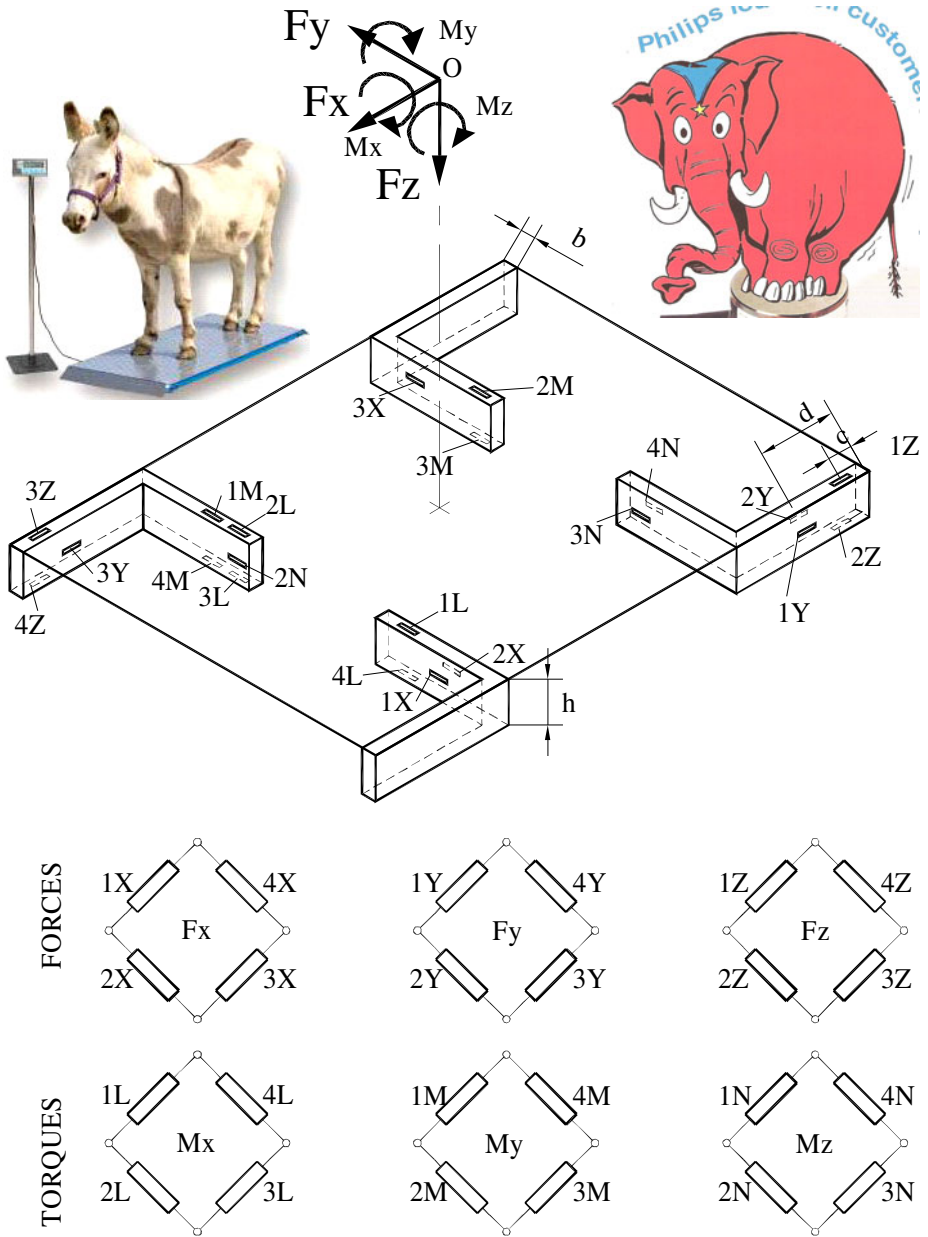


Fig. 23.17 Six-component strain-gauged balance based on four coplanar L-shaped beams for aerodynamic models tested in wind tunnel (adapted from Sandu [23.49])

REFERENCES

1. Lineback, D.: Experimental Stress Analysis Notebook – a newsletter for our friends in the educational community edited by Measurements Group, Inc., Raleigh, NC: a) Stress & strain in beams, Issue 27, pp. 3-14 (July 1996); b) Wide beams, Issue 28, pp. 3-11 (November 1997)
2. Gu, M., Piedboeuf, J.-C.: A flexible-arm as manipulator position and force detection unit. *Control Engineering Practice* 11, 1433–1448 (2003)
3. Tödt-Harten, W., Germer, W.: Low Cost Sensor zum Messen kleiner Drücke und Kräfte. 2. Fachtagung Konferenz Sensoren – Technologie und Anwendung, Session P. 1, Bad Nauheim, Deutschland, März (1984)
4. Li, Z.C., Lin, B., Xu, Y.S., Hu, J.: Experimental studies on grinding forces and force ratio of the unsteady-state grinding technique. In: *Journal of Materials Processing Technology*, vol. 129, pp. 76–80. Elsevier Science B.V, Amsterdam (2002)
5. Constantinescu, I.N., Ștefănescu, D.M., Sandu, M.Al.: Mechanical Quantities Measurement by Tensometry (in Romanian). Editura Tehnică, București (1989)
6. Wall, W.E.: Applications of piezoresistance to externally excited transducers. Technical Paper – 239, Endevco, San Juan Capistrano, CA, Revue 10-75.
7. Hoffmann, G.: Aktive Dämpfung der Gier- und Nickschwingung an einem Roboterarm mit Dehnungs- und Beschleunigungssensoren. at – Automatisierungstechnik, vol. 39, pp. 101–104. R. Oldenbourg Verlag, München (1991)
8. Jenkins, D.F.L., Cunningham, M.J., Clegg, W.W.: Sensors and actuators for active vibration control of small cantilevers. In: *Proceedings VIIth Int'l Conf. Sensors & their Applications*, Dublin, Ireland, September 10-13, pp. 401–405 (1995)
9. Schulze, W., Hirche, S., Eger, M.: Flat electronic scales (Sartorius). US Patent No. 6211472-2001
10. Ort, W.: Sensoren mit Metallfolien-Dehnungsmeßstreifen. *Mestechische Briefe (Hottinger Baldwin Messtechnik)* 16(1), 11–16 (1982)
11. Green, D.: How to get the best out of single point load cells. Reprinted by Huntleigh Technology from *Weighing and Measuring* 3(2), 1–4 (1985)
12. Knöll, B.: Wägezellen für Plattformwaagen / Load cells for platform scales. *Hotline HBM* (2), 24–25 (2002)
13. Škundrić, S., Kovačević, D.: *Electromehaničke vage (Merenje mase mernim pretvaračima sile na basi tenzometarskih traka)*, Štampa BMG, Beograd (1995)
14. *Strain Gage Based Transducers – Their Design and Construction [2/15/2001]*, <http://www.measurementsgroup.com/guide/ta/sGBT/sGBTindex.htm>
15. Baumgartner, A., Harzheim, L., Mattheck, C.: SKO (soft kill option): biological way to find an optimum structure topology. *International Journal of Fatigue* 14(6), 387–393 (1992)
16. Malikov, G.F., Šneiderman, A.I., Šulemovici, A.M.: Strain gauged elastic elements computation (in Russian). Izdat Mašinostroenie, Moskva (1964)
17. Ochiai, Y., Kameoka, K., Sugisako, T., Ono, T.: Application of a new beam type load-cell to mechanical hand. In: Wieringa, H. (ed.) *Mechanical Problems in Measuring Force and Mass*, Martinus Nijhoff Publishers, Dordrecht (1986)

18. Inuzuka, H., et al.: Semiconductor strain sensor. United States Patent 5329271-94
19. Arshak, K.I., Ansari, F., McDonagh, D., Collins, D.: Development of a novel thick-film strain gauge sensor system. *Meas. Sci. Technol.* 8, 58–70 (1997)
20. Peiter, A.: Messen mechanischer Beanspruchung und Messwertkorrekturen mit Dehnungsmeßstreifen. In: *GESA Symposium*, VDI-Verlag, Düsseldorf (1985)
21. Rodriguez, J., Seireg, A.A.: Algorithmic rule-based methodology for shape synthesis: 2D cases. In: *CAD (Computer-Aided Design)*, Butterworth - Heinemann, Oxford (August 1992)
22. Überall einbaubar dank der genialen Bauform – Die revolutionäre Kraftmessdose KIS. Bofors Elektronik, Schweden, EMG 1010-90.
23. Young, W.C.: *Roark's Formulas for Stress and Strain: Sixth Edition* (ISBN 0-07-072541-1). Society for Experimental Mechanics, Bethel, CT (1996)
24. Rozvany, G.I.N., Zhou, M., Gollub, W.: Continuum-type optimality criteria methods for large finite element systems with a displacement constraint, Part II. In: *Structural Optimization (Computer-Aided Optimal Design of Stressed Systems and Components)* 2(2), 77–104. Springer International, Berlin (1990)
25. Mou, Y., Han, P.S., Shah, A.H.: Exact dynamic stiffness matrix. *International Journal of Numerical Methods in Engineering* 40, 235–247 (1997)
26. Ștefănescu, D.M.: Untersuchungen der elastischen Biegebalken bei Aufnehmern mit Dehnungsmeßstreifen durch die Finitelement-Methode. *Rev. Roum. Sci. Techn. – Méc. Appl.* 31(4), 429–441 (1986)
27. Lund, E.: Finite Element based design sensitivity analysis and optimization. PhD Dissertation, Aalborg University (DK), Special Report No. 23 (April 1994)
28. Vasiloaica, C., Curtu, I.: Strain gauge transducers for cylinders pretensioned by winding (in Romanian). In: *Proc. 6th National Symp. Tensometry*, Craiova, September 24-25, vol. I, pp. 289–296 (1992)
29. Müller, Z.: Messungen mit Dehnungsmeßstreifen an den Land- und Fördermaschinen. In: *Proceedings 2nd National Symp. of Tensometry*, Cluj-Napoca, June 11-14, vol. V, pp. 42–49 (1980)
30. Shoji, K.: Forces on a model 'Spot Plough'. *Biosystems Engineering – PM (Power and Machinery)* 87(1), 39–45 (2004)
31. Tata, U., Huang, H., Carter, R.L., Chiao, J.C.: Exploiting a patch antenna for strain measurements. *Meas. Sci. Technol.*, Vol. 20, Paper 015201 (2009)
32. Choi, I.-M., Kim, J.-H., Lee, H.-J., Kim, M.-S., Park, Y.-K., Woo, S.-Y., Kang, D.-I.: Development of electromagnetic probe for micro force measurement. In: *CD Proc. 19th IMEKO TC-3 Int'l Conf. Force, Mass & Torque Measurements: Theory and Application in Laboratories & Industries*, Paper 46, Cairo, Egypt, February 19-23 (2005)
33. Peiner, E., Doering, L., Brand, U., Christ, A., Isenberg, G., Balke, M.: Force calibration of micro pipettes for single-cell probing. In: *CD Proceedings XVIIIth IMEKO World Congress*, Paper 178, Rio de Janeiro, Brazil, September 17–22 (2006)
34. Niblock, T.E.G., Brunnschweiler, A., Evans, A.G.R.: Optimisation of atomic force cantilever geometry. In: *Proc. 13th European Conference on Solid-State Transducers*, The Hague, The Netherlands, September 12-15, pp. 271–272 (1999)

35. Bachmann, D., Hierold, C.: Determination of pull-off forces of textured silicon surfaces by AFM force curve analysis. *J. Micromech. Microeng.* 17, 1326–1333 (2007)
36. Gel, M., Shimoyama, I.: Force sensing submicrometer thick cantilevers with ultra-thin piezoresistors by rapid thermal diffusion. *J. Micromech. Microeng.* 14, 423–428 (2004)
37. Raiteri, R., Grattarola, M., Berger, R.: Micromechanics senses biomolecules. *materialstoday*, pp. 22–29 (January 2002); [Reprinted from “Sensors and Actuators B: Chemical”, Vol. 79, pp. 115–126]
38. Carrascosa, L.G., Moreno, M., Alvarez, M., Lechuga, L.M.: Nanomechanical biosensors: a new sensing tool. *Trends in Analytical Chemistry* 25(3), 196–206 (2006)
39. Loui, A., Goerick, F.T., Ratto, T.V., Lee, J., Hart, B.R., King, W.P.: The effect of piezoresistive microcantilever geometry on cantilever sensitivity during surface stress chemical sensing. *Sensors and Actuators A: Physical* 147(2), 516–521 (2008)
40. Yang, M., Zhang, X., Vafai, K., Ozcan, C.: High sensitivity piezoresistive cantilever design and optimization for analyte-receptor binding. *J. Micromech. Microeng.* 13, 864–872 (2003)
41. Yoshikawa, G., Lang, H.-P., Akiyama, T., Aeschmann, L., Stauffer, U., Vettiger, P., Aono, M., Sakurai, T., Gerber, C.: Sub-ppm detection of vapors using piezoresistive microcantilever array sensors. *Nanotechnology*, 20, Paper 015501 (2009)
42. Senesac, L., Thundat, T.G.: Nanosensors for trace explosive detection. *materialstoday* [ISSN:1369 7021] 11(3), 28–36 (2008)
43. Porter, T.L., Delinger, W.: Electronics for LabView based piezoresistive microcantilever sensor system. *Sensors & Transducers Magazine* 68(6), 568–574 (2006)
44. Bashir, R., Gupta, A., Neudeck, G.W., McElfresh, M., Gomez, R.: On the design of piezoresistive silicon cantilevers with stress concentration regions for scanning probe microscopy applications. *J. Micromech. Microeng.* 10, 483–491 (2000)
45. Melväs, P., Kälvesten, E., Enoksson, P., Stemme, G.: Miniaturized pressure sensor using a free hanging strain-gauge with leverage effect for increased sensitivity. In: *Proc. 11th International Conf. Solid-State Sensors and Actuators – Eurosensors XV*, Munich, Germany, June 10–14, pp. 494–497 (2001)
46. Yang, S.M., Chang, C.: A piezoresistive bridge-microcantilever biosensor by CMOS process for surface stress measurement. *Sensors and Actuators B: Chemical* 145, 405–410 (2010)
47. Israelachvili, J., Min, Y., Akbulut, M., Alig, A., Carver, G., Greene, W., Kristiansen, K., Meyer, E., Pesika, N., Rosenberg, K., Zeng, H.: Recent advances in the surface forces apparatus (SFA) technique. *Reports on Progress in Physics*, 73(3), Paper 036601 (2010)
48. Huang, Y.-M., Tsai, N.-C., Lai, J.-Y.: Development of tactile sensors for simultaneous detection of normal and shear stresses. *Sensors and Actuators A: Physical* 159(2), 189–195 (2010)
49. Sandu, M., Sandu, A., Găvan, M.: Strain gauged aerodynamic balance for models tested in wind tunnel (in Romanian). In: *National Conference Aerospațial 1998*, Session II.1, INCAS, București, November 11–13 (1998)

Chapter 24

BENT AND/OR TORSION SHAFTS

24.1. BENDING OF CANTILEVER TUBE OR CYLINDER

It is very difficult to obtain a “pure” torsion (Fig. 24.1). On the other hand, a bent shaft (Fig. 24.2, top), i.e. a tubular or circular cross section bar, is more rarely used for force measuring because it is mainly intended as an industrial rotating shaft torque transducer [24.1]. So, in this chapter we try to analyze the complex loading of the static and rotating shafts.

The cantilever tube is described in the works of Klaus Horn, Technical University of Braunschweig, but he made use of force (“amplified” with the lever arm) for torque measuring and also calls the torque a “force transformer.” We have determined the force on the measuring bench of the aircraft engine torque at our flight company TAROM. In the electric, hydraulic and pneumatic engines there are 15 types of standard dynamometers [24.2] allowing combined measurements of torque, speed and power.

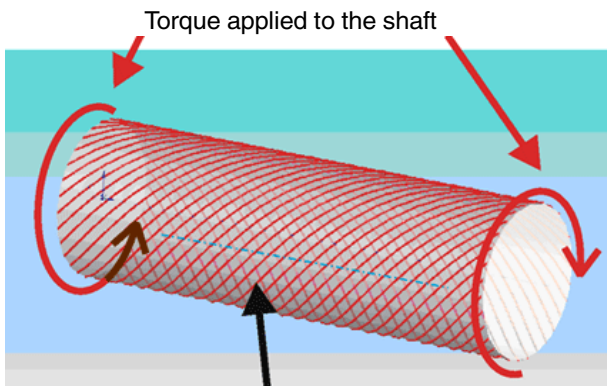
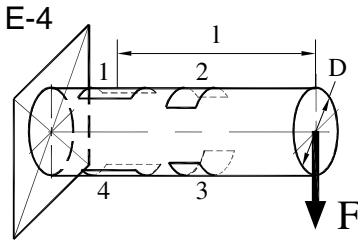


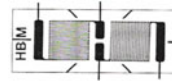
Fig. 24.1 The “infinite” number of strain paths ($\pm 45^\circ$) on a torsioned shaft



Load range [N]: $1 \dots 10^5$

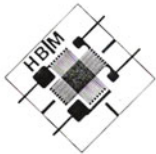
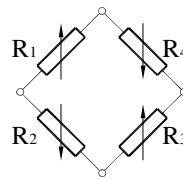
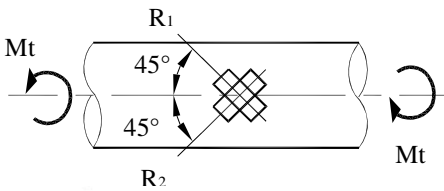
Mechanical sensitivity [$\mu\text{m/m}$]: $\frac{32 F l}{\pi E D^3}$

Electrical sensitivity [ϵ]: 2.6



Twisted circular shaft for measuring couples and forces

Bridge connection



Personal model:

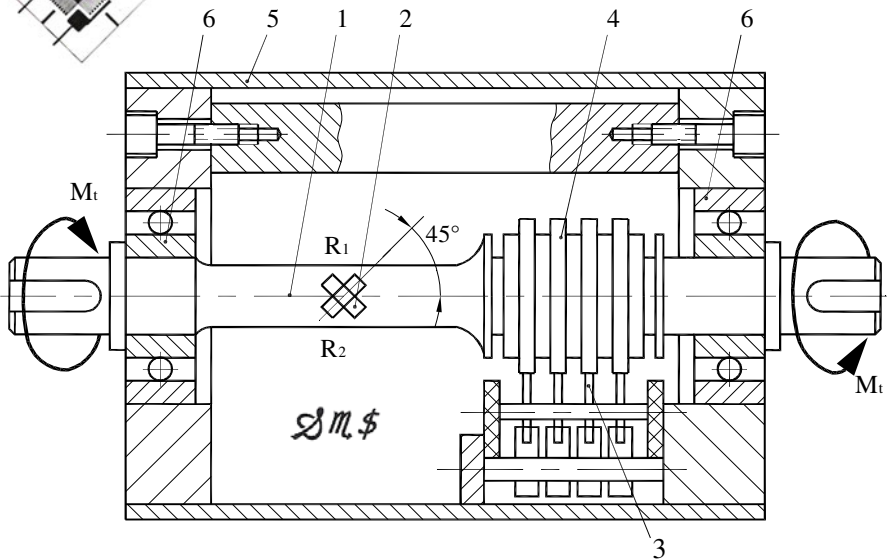


Fig. 24.2 Strain gauged elastic elements of type IV for force transducers loaded in bending or/and torsion

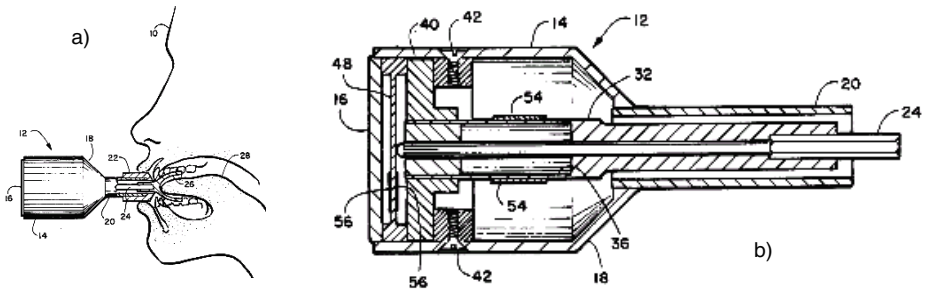


Fig. 24.3 Strain gauged device for measuring the forces of the tongue muscle

A special strain gauged device for measuring three-directional forces exerted by tongue muscle [24.3] is presented in Figure 24.3a. Strain gauges 54 are mounted on the hollow portion of the cylindrical beam 36 to measure deflection of the free beam end 24 in X (lateral) and Y (vertical) directions (Fig. 24.3b). A movably pin is positioned into the beam's axial bore contacting the diaphragm 48, strain gauges 56 bonded on the diaphragm detecting the movement in the Z direction. A tongue cup is mounted on the free end of the pin to receive a patient's tongue when the cup is inserted between the teeth. Signals generated by the strain gauges, expressing the three components of the applied force, are monitored on a meter, oscilloscope or computer display as the patient moves his tongue while pronouncing different words for evaluating, diagnosing and treating the speech disorders.

24.2. ROTATING SHAFTS

Fig. 24.2 (bottom) shows a cylindrical tensometric transducer (with strain gauges having directions at $\pm 45^\circ$) for the bench of measuring the friction moment in ball screws made in the Laboratory for Material Testing of the "Politehnica" University of Bucharest [24.4]. A twisted cross-shaped structure is depicted in [24.5] and by some authors from the Korean Research Institute of Standards and Science as well.

The first transfer of the analog signals of a strain gauged bridge applied on a rotating shaft was carried out with slip rings in 1952. In 1971, while electronics became smaller, it was possible to integrate an amplifier onto the rotating shaft, which was used for supplying the strain gauge bridge and processing the measurement signal [24.6].

A rotating transformer was used for the supply of the sensor; the second one for the frequency-modulated transfer of the measurement signal. Nowadays, the integrated electronics has microcontrollers (μC), both in the stator and in the rotor with an appropriate memory (Fig. 24.4).

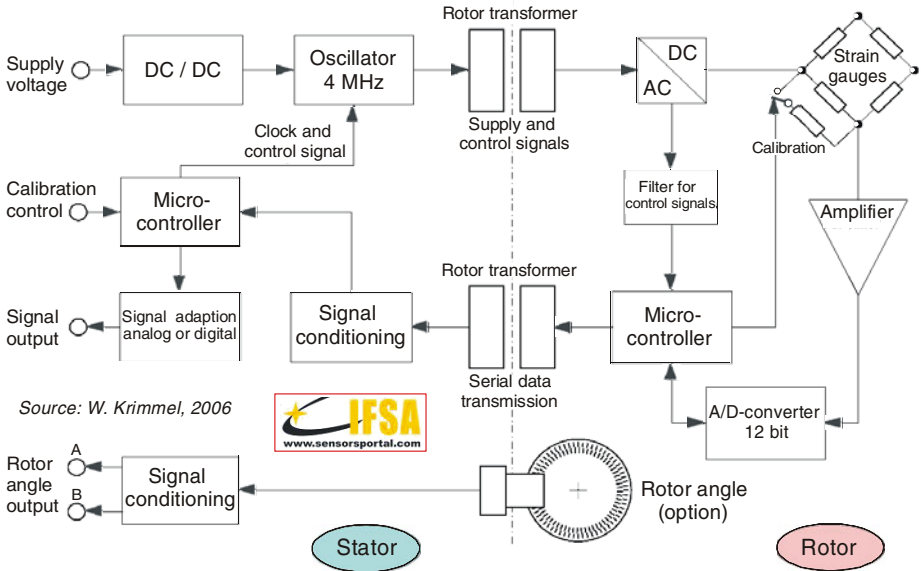


Fig. 24.4 Functional scheme of rotary torque transducers fabricated by Lorenz Measurement Technology GmbH, Alfdorf, Germany (IFSA copyright 2006)

The supply of the sensor takes place by a power supply unit, monitored by the μC , which can switch to a calibration control for the check-up of the sensor as well. A very high reliability of the measuring device is achieved by storing and read-out of the sensor data and the direct digitalization of the measurement signal at the point of origin.

The measured value occurs on the rotor by means of strain gauges, and the signal is immediately amplified and digitalized there. After this digital signal proceeds into a μC , which prepares it for the transfer to the stator in the form of a serial word with checksum. The data signal gets conditioned in the stator and then converted for a serial RS 485 interface in a μC .

TorqSense is the world first low cost non-contact rotary torque transducer suitable for OEM applications [24.7]. The patented method uses a surface acoustic wave (SAW) or Rayleigh wave device as a frequency dependent strain gauge, measuring the resonant frequency change caused by the applied strain in the shaft (Fig. 24.5a). The signal from the rotating shaft is transmitted via a RF couple to a fixed pick-up and its bandwidth is increased using a frequency-based device, eliminating the electronic interference common with analog signals. The TorqueVIEW software allows complete data handling in conjunction with a standard PC operating under Windows[®] (Fig. 24.5b).

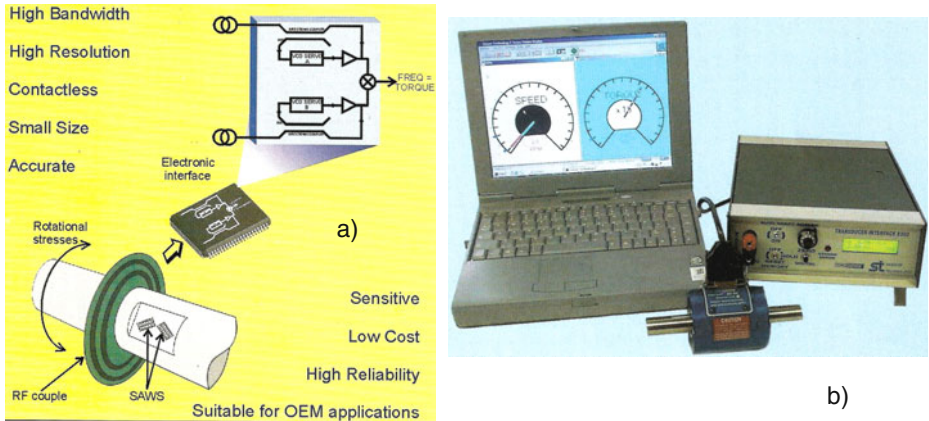


Fig. 24.5 Rotary torque sensing by SAW strain gauges (a) and associated virtual instrumentation display (b). Reprinted with permission of Sensor Technology Ltd., UK.

24.3. COMPLEX LOADED SHAFTS

In the Romanian Symposia of Tensometry and Experimental Stress Analysis, a series of torque transducers for screwing control were presented [24.8] along with devices for the strains in the wheels of agricultural machine Motocultor [24.9]. For determining the load components in the vehicles wheels the devices developed by Negruş (Transport Faculty, “Politehnica” University of Bucharest), Ghita (“Politehnica” University of Timișoara) and Pandrea (Dacia-Renault Center) are well-known [24.10].

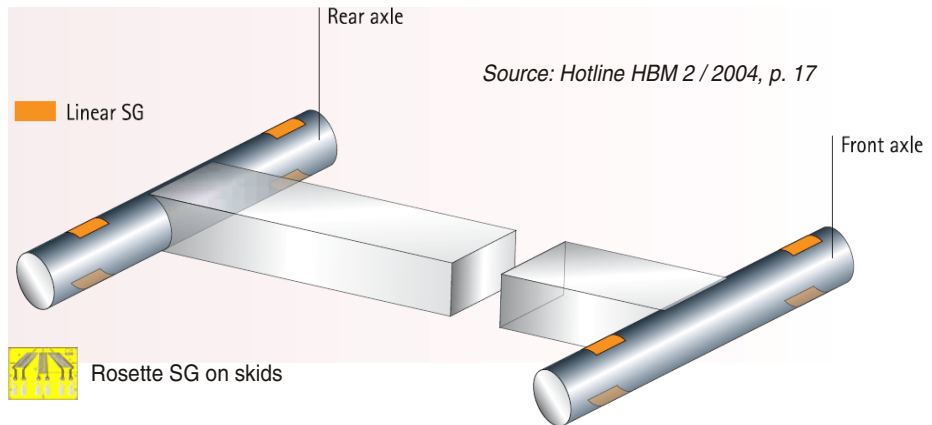


Fig. 24.6 Strain gauges locations for measuring dynamic loads on the bob axles and skids with HBM equipment

In “Messtechnische Briefe HBM” one could find two tensometric applications with bent tubes: [24.11], [24.12]; in the last one there are some force / torque transducers as components of a bicycle frame. Continuing its valuable traditions in force and torque measurements, Hotline HBM presents another interesting application: dynamic loads measurements in the Formula 1 of winter sports [24.13].

Forces acting on a racing bobsleigh in the ice channel at Königssee, Germany were systematically measured using a complete HBM measurement chain by the Material Tribology group at the Zentralinstitut für Medizintechnik, Technical University of München. Linear strain gauges were used to determine the axle bending while rosette strain gauges were bonded on the associated skids (Fig. 24.6), constituting special force transducers for measuring the principal stresses and their directions.

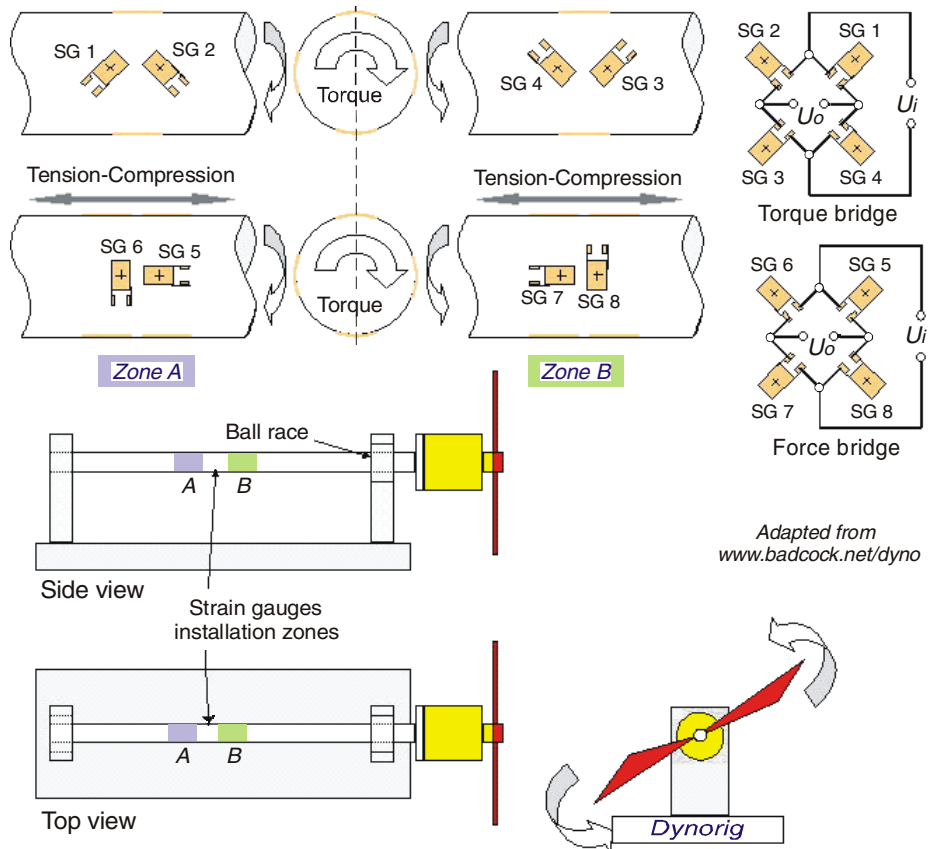


Fig. 24.7 Measurement schemes for torque and tension/compression in rotating shafts

“Pure” torsion is rarely encountered in industrial practice. In a rotating shaft, besides the twisting moment, bending forces and, sometimes, tension or compression components are present; the resulting complex loading has to be assessed using the basic Strength of Materials rules.

A strain gauge test rig, called Load and Torque Cell [24.14], is shown in Figure 24.7. It presents the strain gauges location on the shaft and their connection in Wheatstone bridge in order to separate torque (SG1 ... SG4) and tension / compression (SG5 ... SG8) during the measuring process.

REFERENCES

1. Measuring and controlling forces and torque. Product Overview 03.98, Haehne Elektronische Messgeräte GmbH, Erkrath, Germany (1998)
2. Motor Testing Equipment. Product Overview MT-10, Magtrol, Inc., Buffalo, NY (1997)
3. Durkee, D.L., Manning, F.E.: Tongue force measuring device. United States Patent 4697601-87
4. Ștefănescu, D.M., Buga, M., Mocanu, D.R.: Stand for determining the stiffness and the friction moment at the ball screws. In: Proceedings of the 2nd Conference Testing equipment for experimental investigation of mechanical properties of materials and structures, Moscow, October 9-14, pp. 519–526 (1989)
5. Tovey, F.M.: Material properties in the design of transducer flexures. Authorized reprint from the Laboratory for Measurement Systems Engineering, Phoenix, AZ, Publication 70-94
6. Krimmel, W.: Evolution and future of torque measurement technology. *Sensors & Transducers Magazine* 65(3), 500–508 (2006)
7. E-series torque transducers, instrumentation & software. New product release data sheet TSE2094R. Sensor Technology Ltd., Banbury, August 6 (2000)
8. Gheorghiadă, G., Lung, T.: Screwing control by moment transducers. In: Proceedings 4th National Symposium of Tensometry, Brașov, September 24-27, vol. I, pp. 105–112 (1986) (in Romanian)
9. Sperchez, F., Mocanu, V., Cilinghir, S.: Load cells for measuring forces from the Motocultor wheels. In: Proc. 7th National Symposium of Tensometry, Suceava, October 17-19, vol. II, pp. 243–250 (1996) (in Romanian)
10. Pandrea, N., Pandrea, M.: Load cell computation for measuring wheel forces. In: Seminar on Tensometry Utilization for Car Building, pp. 98–105. University of Pitești, May 24-25 (1991) (in Romanian)
11. Funke, P., Jain, A.: Elektrisches Messen der Ziehkräfte zur Beurteilung von Trockenziehmitteln beim betrieblichen Ziehen von Stahldrähten. *Messtechnische Briefe H.B.M.* 12(3), 45–47 (1976)

12. Barski, M., Groß, E., Rieck, D.: Anwendung von Dehnungsmeßstreifen zur Belastungsermittlung an Mountainbikes. *Messtechnische Briefe H.B.M.* 31(2), 39–43 (1995)
13. Hainzmaier, C., Kleemann, R., Wintermantel, E.: With 5 g in the precipice – HBM measurement technology in the Formula 1 of winter sports. *Hotline Hottinger* (2), 16–18 (2004)
14. <http://www.badcock.net/dyno/dynorig> (July 26, 2008)

Chapter 25

MIDDLE BENT BARS WITH FIXED ENDS

Using the straight bar or beam with both ends fixed and loaded in the middle with a concentrated load as an elastic element, a plane stress state is produced on the surface where the strain gauges are located in order to measure low and, respectively, high forces, namely:

- **bending** – with strain gauges longitudinally located, the spoked wheel being a prototype (Fig. 25.1, top) as designed by the author [25.1];
- **shearing** – with strain gauges at $\pm 45^\circ$ directions to the bar axis, having as a prototype a hollow disc to be analyzed in the next chapter (C.26.3).

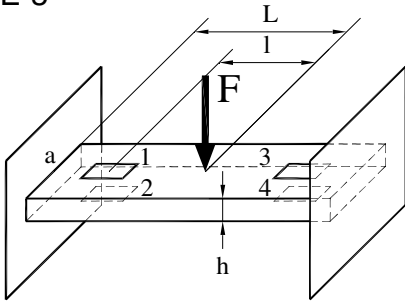
Generally speaking, the bending stress sensitivity is higher than the shearing stress one, on the assumption of an equal strength beam used in both cases. The tensometric indication depends on the strain gauges position on the bar, and their correct location is necessary for obtaining a symmetric measuring bridge and, implicitly, a maximum sensitivity.

25.1. EXAMPLES OF MIDDLE BENT BARS WITH FIXED ENDS

The beam with end supports and middle loaded can also be used [25.2]. Professor Albert Haug from Fachhochschule für Technik Ulm has compared this case (Fig. 25.2a) with the one where the beam (with rectangular or tubular cross section) is strained by concentrated end forces, the two supports being slightly moved inwards (Fig. 25.2b); in the last case, the bending moments diagram has a portion which allows a better location of strain gauges. A reversed solution with two symmetrical loads located round the center of the end supported beam is applied in the strain gauged tactile sensors for finger-mounted applications [25.3] and for high precision microweighing scales [25.4].

In Figure 25.3a a scale pan is supported at points B and D with a span of $n \cdot \ell$ on a lever supported at the both ends, in the points A and E, with a span of $(n + 2) \cdot \ell$. See a “reversed” solution (loaded in A + E against B + D) in [25.5]!

E-5

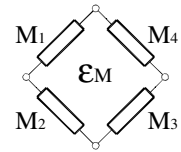
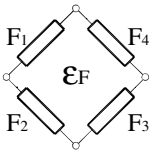
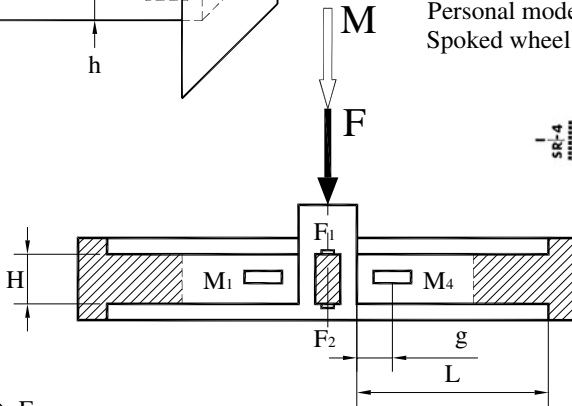


Load range [N]: $10 \dots 10^4$

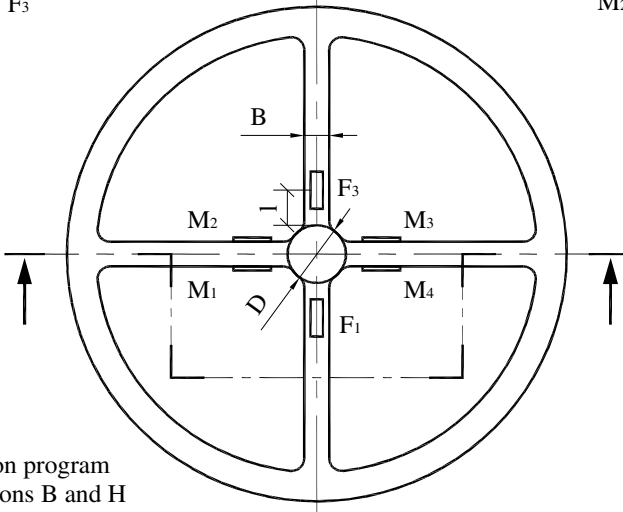
Mechanical sensitivity [$\mu\text{m/m}$]: $\frac{1.5 F (2l - L)}{E a h^2}$

Electrical sensitivity [ϵ]: 4

Personal model:
Spoked wheel



Bridge connection



Optimization program
for dimensions B and H

Sm\$

Fig. 25.1 Strain gauged elastic elements of type V for force transducers. Starting from the “linear” bar with fixed ends, one could develop various “plane” spoked-wheels and then “spatial”, three-directional “Maltese cross” elastic structures.

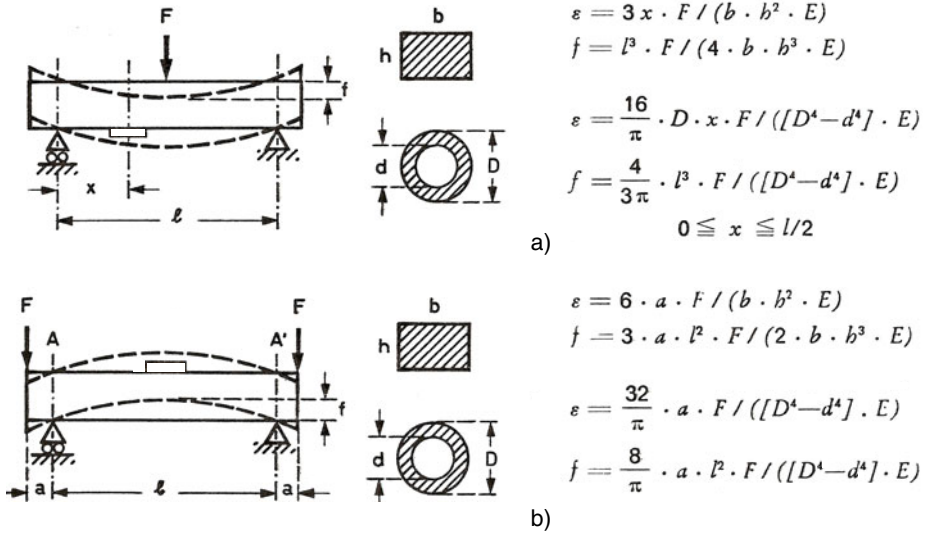
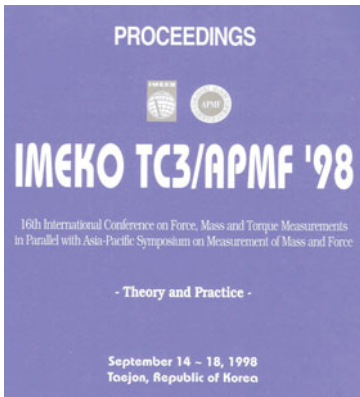


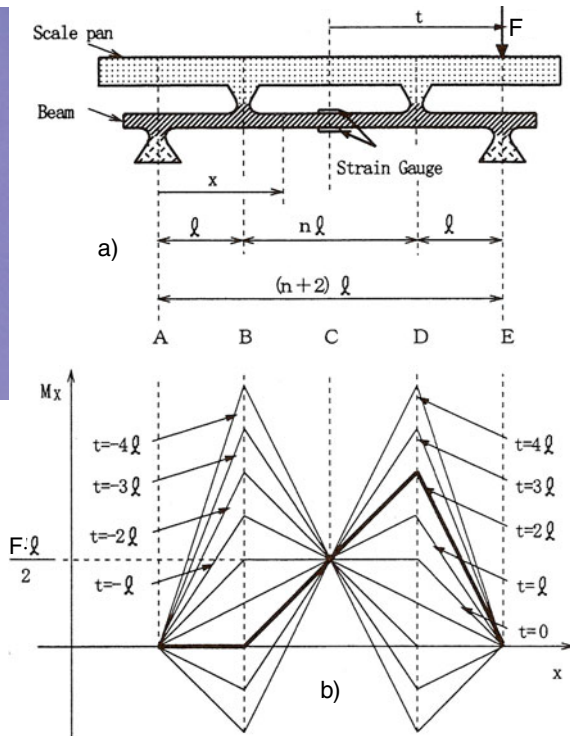
Fig. 25.2 Supported rectangular or tubular beams loaded in various positions



See page 411 ⇒



Fig. 25.3 a) Thin strain gauge elastic element for special weighing scales and b) bending-moments diagrams (like a butterfly)



A double strain gauge (T-type) is bonded on each lever side at the center C. Fig. 25.3b shows some bending-moment diagrams of the lever with $n = 2$, for different t parameters.

The “fixed” solutions provide better strength to the transducer assembly and are mainly used in the measuring of different mechanical quantities:

- *forces* – the lamellar elastic element, immersed in a U-shaped tube, allows the study of oscillatory flow at the Empire College for Science and Technology of London [25.6];
- *pressures* – overtaken from a diaphragm by a rod that strains the middle of the elastic lamella [25.7];
- *accelerations* – detected by a one-piece elastic structure microprocessed in quartz (French patent no. 273190-97, ONERA).

In the Romanian Symposia of Tensometry the following applications of the beams fixed at ends and mid-stressed have been resolved:

- the testing of a classic structure in Geomechanics,
- mobile crane with two wheel rows on the rolling track,
- lamella for the measuring of the axial force for pencil sharpening,
- device for the study of prestressed cylinders by winding.

25.2. SLOTTED STRUCTURES FOR MIDDLE BENT BARS WITH FIXED ENDS

The sensitivity can be increased by developing slotted elastic lamellae (“spectacles” type) and building flexors which would eliminate the effects of the unfavorable loads, an essential aspect for the tensometrical multicomponent balances [25.8].

The conceptual structure of the six-component force transducer [25.9] is presented in Figure 25.4a. The six hatched squares are elastic elements where forces are detected through the strains. Each elastic element is a parallel plate structure (PPS).

The measuring principle is the following:

- the pair of PPS on the X axis detects the force F_z and the moment M_y ,
 - the pair of PPS on the Y axis detects the force F_x and the moment M_z ,
 - the pair of PPS on the Z axis detects the force F_y and the moment M_x .
- {The general rule is that of the circular permutation of the indices x, y and z!}

Fig. 25.4b explains the model of a PPS pair. It is assumed that the central and the end blocks are not deformed under the applied load (force F and/or moment M) while the plate parts can be modeled as cantilevers (type E-3 of elastic elements). We could imagine three stages for constructing such a complex elastic structure, like a spatial, three-directional “Maltese cross”:

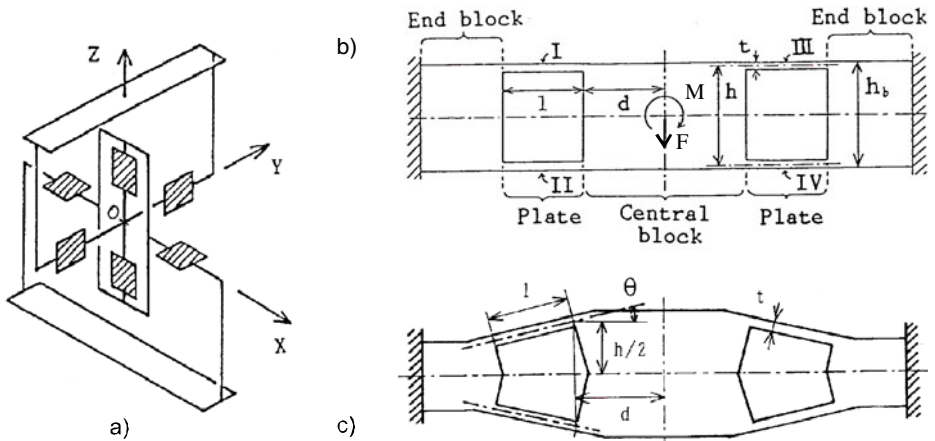


Fig. 25.4 Six-component force transducer with three-dimensional cross-shaped structure like a spatial combination of “spectacles”

- the single cantilever I from the left top is “doubled” to bottom cantilever II;
- the left structure I + II is “symmetrized” to the right structure III + IV;
- this assembled structure is “repeated” along the three axes (X, Y, Z) and “centered” in the system origin O.

Because the maximum measurable moment M is too small when compared with the maximum measurable force F , a better solution is shown in Figure 25.4c, where the pairs of thin plates are not parallel.

Three parallel plate structures for measuring mechanical properties of small organic elements in human ear are presented in [25.10]. There are two force transducers specialized for eardrum penetrating and tensile strength of an inner ear membrane, having the technical characteristics shown in Table 25.1.

Table 25.1 Specialized force transducers for mechanical properties of human ears

Characteristics →	Rated load [mN]	Resolution [μN]	Natural frequency [Hz]
Force transducer application			
Eardrum penetrating force	678	339	340
Tensile strength of inner ear membrane	944	472	485

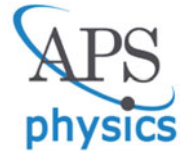
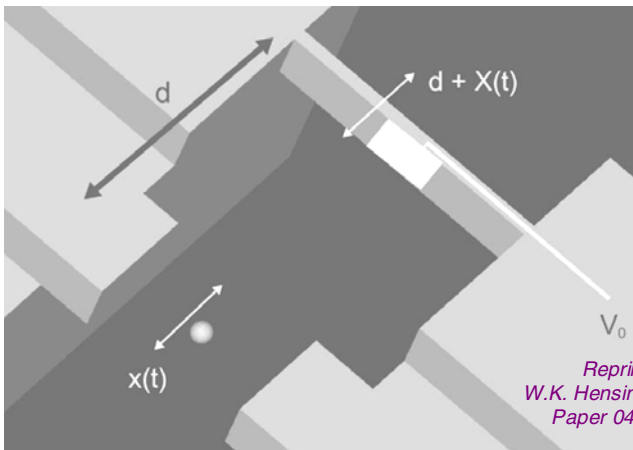
A third transducer, more complex, has a radial plate structure for measuring torque (19.1 N·mm with 9.53 mN·mm resolution) and a parallel plate structure for measuring pressure (244 kPa with 122 Pa resolution).

The optimization of this type 5 elastic element by hybrid methods (Moiré interferometry with a network of 600 lines/mm, with a fringe corresponding to $0.833 \mu\text{m}$, and finite element analysis with a matching within 5 % respectively) is presented in work [25.11]. The structural optimization of a rolling band drum (mid-loaded circular shaft) is found in [25.12] while the one of the gap beams under the aircraft floor is presented in [25.13].

25.3. DYNAMIC APPLICATIONS OF DOUBLE ENDED BEAMS

If a weak classical force is continuously applied to the cantilever after it has been prepared close to the ground state e.g., via sympathetic cooling the ion, its equilibrium phonon distribution will shift by an amount proportional to the square of the ratio of applied force to the energy damping rate. Thus we should be able to infer the size of a classical force so weak as to shift the mean phonon number of the oscillator by one quanta [25.14].

A quantum model of a single trapped atomic ion is electrostatically coupled to a very small doubly-clamped cantilever (Fig. 25.5). This coupling can be switched on and off using an external bias voltage at an electrode on the nanoelectromechanical oscillator.

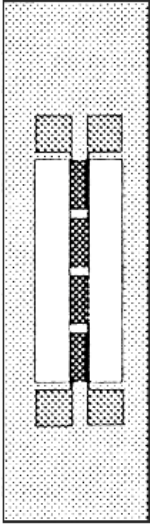
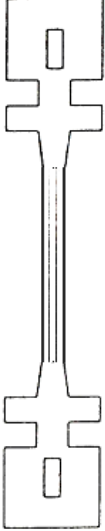
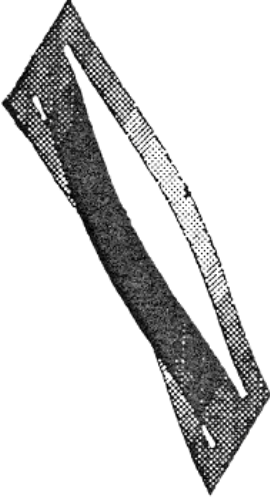


*Reprinted figure with permission from
W.K. Hensinger et al., Physical Review A72,
Paper 041405(R). Copyright 2005 by the
American Physical Society.*

Fig. 25.5 Ion trap transducer for quantum micromechanical oscillators

Table 25.2 gives a summary of resonant force microsensors which have been developed in the framework of a joint project entitled “*Application of Micromechanics of Sensors with Frequency Output*” and conducted by the Institut für Mikrotechnik der Technischen Universität Braunschweig, Germany. Their original images were presented at SENSOR’95 in Nuremberg [25.15].

Table 25.2. Resonant force transducers with double-ended beams

Type	Layout	Technology	Vibration mode	Frequency f_0 [kHz]	Sensitivity [Hz/N]
Single		ZnO on silicon	Out-of-plane fundamental	29	180
Double		Quartz micro-machining	In-plane fundamental antisymmetric	47	70
Triple		ZnO on silicon	Out-of-plane fundamental antisymmetric	8	8 600

25.4. VARIOUS MODELS OF FOUR-SPOKE WHEELS

The most important application of this chapter is the four-spoke wheel, represented in Figure 25.1, bottom. We can consider it as an ensemble composed by two perpendicular structures of the beams fixed at ends and mid-stressed, each spoke being a kind of bent lamella (type 3).

The SRM training system [25.16] is a state of the art device for displaying, collecting and analyzing performance data during cycling. As depicted in Figure 25.6a, the main component of the measuring system is a custom-made, strain-gauge instrumented crankset (the Powermeter) that enables pedal rate, effective torque and power output to be measured on all forms of bicycles and ergometers. Strain gauge strips are attached to the metal inside the powermeter, and measure the stretch of this metal as force is applied to the pedals throughout the pedal stroke. Strain gauges are connected in a Wheatstone bridge (Fig. 25.6b), which is the “universal” scheme in the field of electronic measurement of force and the related mechanical quantities.

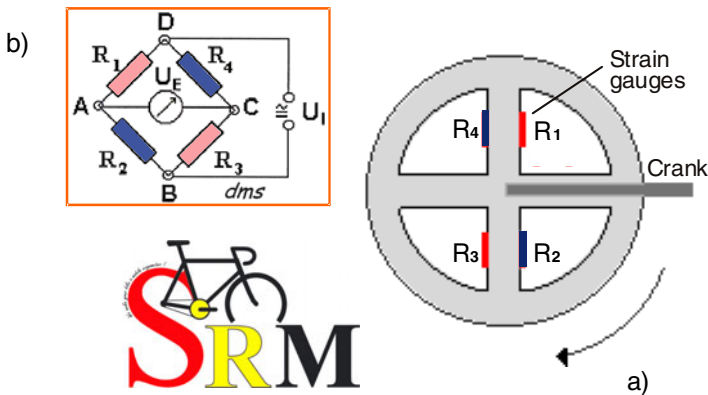


Fig. 25.6 Vertical spoked wheel with strain gauges as Powermeter during cycling

The work [25.17] presents the “square” version of the spoked wheel: a 3D silicon accelerometer with a truncated shape inertial mass, suspended by four spring beams, $\langle 110 \rangle$ -oriented and placed on the symmetry axes of the inertial mass. The top- and cross-sectional views of the modified structure are shown in Figures 25.7a and 25.7b, respectively. This elastic structure can be 3D configured by silicon micromachining (bulk anisotropic silicon etching through the complete wafer on the back side), using the piezoresistive effect that occurs in a diffused or implanted silicon resistor. The normal and shear stresses applied to the sensor can be determined by combining responses from eight piezoresistors located on appropriate positions on silicon spring beams.

Courtesy of Ioan Pavelescu,
 Institute of Microtechnology,
 Bucharest, Romania, 2002

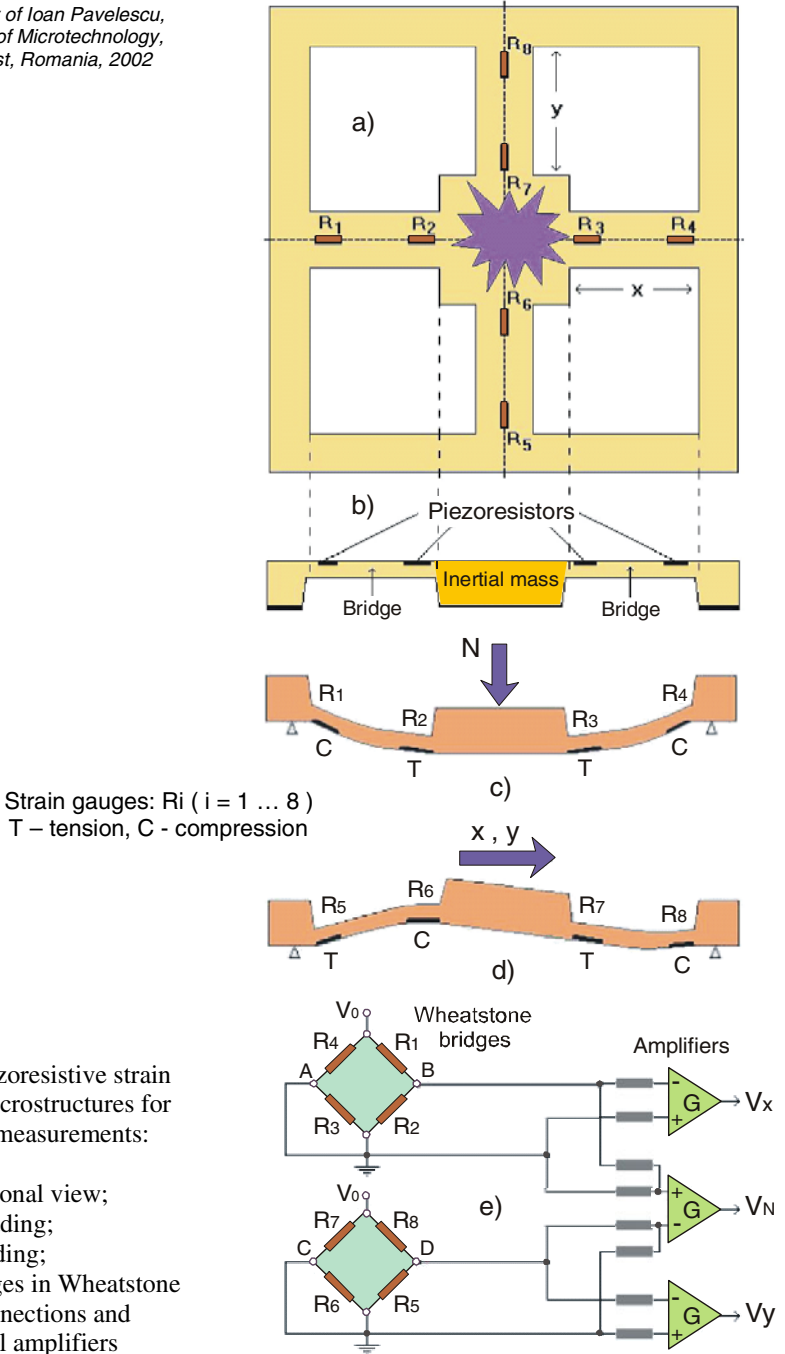


Fig. 25.7 Piezoresistive strain gauges on microstructures for acceleration measurements:
 a) top view;
 b) cross-sectional view;
 c) normal loading;
 d) lateral loading;
 e) strain gauges in Wheatstone bridge connections and operational amplifiers

When the device is subjected to acceleration, the mass is obeyed to a normal and/or shear force, thereby resulting in a stress-profile in the beam suspensions, causing the resistors' value to change. When a normal force N is applied (Fig. 25.7c), the resistors located close to the inertial mass (R_2, R_3, R_6 and R_7) will present a tensile stress and the values of resistance will increase; a reverse situation takes place for resistors located close to the rim (R_1, R_4, R_5 and R_8). When a lateral (x or y) acceleration is applied (Fig. 25.7d), the resistors R_1, R_3, R_5 and R_7 will present a tensile stress and the values of resistance will increase, and the resistors R_2, R_4, R_6 and R_8 will present a compressive stress and the resistive values will decrease, and *vice versa*.

By connecting the four piezoresistors located in the beams on the same symmetry axis in a Wheatstone configuration in such a way that two resistors experience tensile stress and two other resistors experience compressive stress and with an appropriate circuitry for signal processing (Fig. 25.7e), the acceleration vector can be determinate. Because the masses available for the acceleration to force conversion are relative large, very sensitive devices can be fabricated, to measure $40 \mu\text{V}/\text{V}/\text{g}$.

The spoked wheel allows the simultaneous measurement of the axial force and of the torque. If in [25.18] this goal is attained by measuring the axial load by means of the wheel associated shaft, we suggest the measuring of both components only with a spoked wheel, whose dimensions are adequately optimized. We are also mentioning here the two-component transducer (high force and low torque) for honing [25.19].

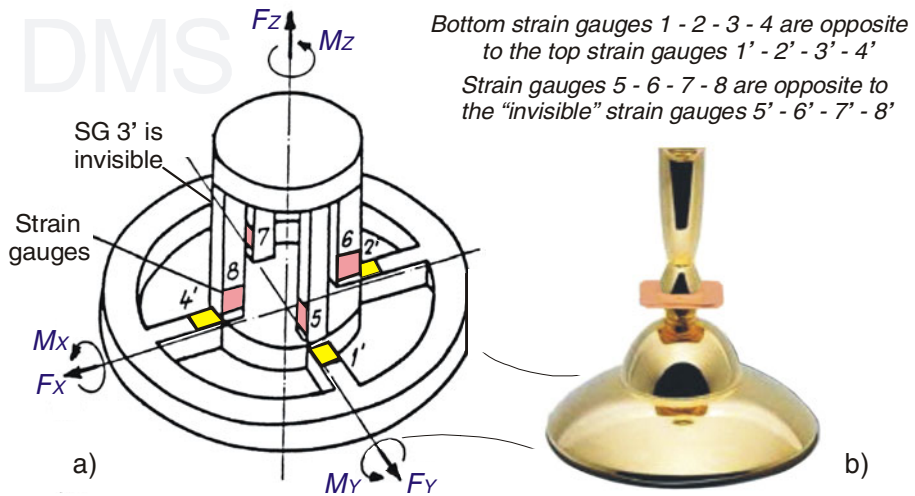


Fig. 25.8 Six-component robotic elastic element with strain gauges (a) and a joystick for entertainment (b)

If we extend the horizontal structure of the four-spoke wheel by four columns (Fig. 25.8a), we obtain a device that can measure all the components of the load torsor in Robotics after determining its influence matrix [25.20]. A commercial application of this smart sensing device is shown in Figure 25.8b.

Hottinger references for spoked wheels are: 2/84, p. 42 and 1/90 p. 13 in “Messtechnische Briefe”, and 2/90, p. 46 in “Reports in Applied Measurement.” A five-spoke wheel (a kind of steering wheel) is presented in [25.21]. A radial slotted wheel separating triangular spokes is to be found in the classical monograph [25.22]. The maximum sensitivity is assured by the spoked wheel shown in the patent [25.23] where each spoke is provided with complex slots (eye-glasses kind) ensuring its supremacy among the elastic elements.

REFERENCES

1. Ștefănescu, D.M.: Methods for increasing the sensitivity of strain gauge force transducers (in Romanian). PhD dissertation (160 pages, 26 tables, 86 figures, 336 references), Universitatea “Politehnica” București, Romania, September 10 (1999)
2. Haug, A.: Übersicht über die Dehnung verschiedener Körperformen bei Belastung. [Survey on the strain of different elastic elements under loading] Reprint Hottinger Baldwin Messtechnik GmbH, Darmstadt (February 1968)
3. Josivaldo, G.S., Aparecido, A.C., Doriedson, D.S.: A strain gauge tactile sensor for finger-mounted applications. *IEEE Trans. on Instrumentation and Measurement* 51(1), 18–22 (2002)
4. Maeda, C.: Thin load cell for weighing scales. In: Proc. 16th Int’l Conf. Force, Mass and Torque Measurements parallel with Asia-Pacific Symp. Measurement of Mass and Force, Taejon, Korea, September 14–18, pp. 408–414 (1998)
5. Tilmans, H.A.C.: Micro-mechanical sensors using encapsulated built-in resonant strain gauges. PhD dissertation, Twente University of Enschede, The Netherlands (1993)
6. Kühtz, S., Bearman, P.W., Graham, J.M.R.: Problems encountered in measuring forces on immersed bodies. In: Experimental Techniques, SEM, Bethel, CT, March/April 1997, vol. 21(2), pp. 20–23 (1997)
7. Stein, P.K.: Sensors / Transducers / Detectors: Basic Measuring System Components. Laboratory for Measurement Systems Engineering, Phoenix, AZ, Publication 60 (1972)
8. Ștefănescu, D.M.: Metrological check of deadweights for calibrating the multi-component strain gauge balances. In: Proc. Int’l Conf. Weighing and Measurement in the Year 2000, Sheffield, England, September 16–17, pp. 143–150 (1997)
9. Yoshikawa, T., Miyazaki, T.: A six-axis force sensor with three-dimensional cross-shape structure. In: Reprinted from “Memoirs of the Faculty of Engineering”, April 1993, vol. LV, Part 2, pp. 49–71. Kyoto University, Kyoto, Japan (1993)

10. Nakao, M., Okusa, T., Hatamura, Y.: Measurement of mechanical properties of eardrum, middle ear exudate and inner ear membranes. *Sensors and Actuators A: Physical* 83, 76–79 (2000)
11. Guo, Z.K., Oakes, B.R.: Optimizing load cell design using an experimental / numerical method. In: *Abstracts 8th Int'l Congr. Experimental Mechanics*, Nashville, TN, June 10-13, pp. 266–267 (1996)
12. Eschenauer, H.A.: Multicriteria structural optimization as a technique for quality improvement in the design process. In: *Microcomputers in Civil Engineering*, vol. 10, pp. 257–267. Blackwell Publishers, Cambridge (1995)
13. Rasmussen, J., Lund, E., Birker, T.: *Collection of Examples CAOS Optimization System*, 3rd edn. Report 13, Institute of Mechanical Engineering, Aalborg University, Denmark (April 1992)
14. Hensinger, W.K., Utami, D.W., Goan, H.-S., Schwab, K., Monroe, C., Milburn, G.J.: Ion trap transducers for quantum electromechanical oscillators. In: *Physical Review A* 72, Paper 041405(R). American Physical Society (2005)
15. Büttgenbach, S., Fabula, T., Schmidt, B., Wagner, H.-J.: Resonant force and pressure microsensors. In: *7. Intern. Fachmesse mit Kongress für Sensoren, Meßaufnehmern und Systeme – Sensor 1995*, Nürnberg, May 9-11, pp. 27–32 (1995)
16. SRM training system, July 26 (2008),
http://www.srm.de/.../SRM_English_Manual/HomeFrame.htm
17. Pavelescu, I.: Acceleration microstructures for industrial applications. Institute for Microtechnology (IMT), Bucharest, Romania, Research standing (December 2002)
18. Popescu, I., Tofan, M., Goia, I., Cosma, D.: Calculation and construction of axial force and torque moment measurement drilling devices. In: *Acta IMEKO XII*, vol. 2, pp. 385–389. International Academic Publishers, Beijing (1991)
19. Ștefănescu, D.M., Sandu, A., Găvan, M.: Transducer for high axial load and low torque. In: *2. Kongreßmesse für Industrielle Meßtechnik*, Session 6 B, No. 6, Wiesbaden, West Germany, September 27-29 (1988)
20. Ștefănescu, D.M.: Six component force transducer for robotics. In: *Proc. 5th Int'l Symp. Measurement and Control in Robotics (ISMCR 1995)*, Smolenice Castle, Slovakia, pp. 75-80, June 12-16 (1995)
21. What managers need to know about Finite Element Analysis: How do I know it's the right answer? NASTRAN, MacNeal-Schwendler Corporation, Los Angeles, CA (1994)
22. Dally, J.W., Riley, W.F., McConnell, K.G.: *Instrumentation for Engineering Measurements*. John Wiley & Sons, Inc., New York (1993)
23. Naganuma, M.: Device having improved load sensing ability. United States Patent 5349871-94

Chapter 26

SHEARING STRAINED ELASTIC ELEMENTS

Under the name of shearing strained elastic elements one can identify all the elastic elements where strain gauges are located at $\pm 45^\circ$ angles on the load application direction. There are bidirectional rosettes specially marked for these angles. Two layouts are presented in Figures 26.1a (“cross” type) and 26.1b (“square”). Within these shear-bridges the indicated shear strain exists along the bisector of any adjacent pair of gauge axes. The numbering of the four strain gauges as well as their measuring network orientation are coincident. Their Wheatstone bridge connections are graphically represented in two variants of rhombs: Vishay – Measurements Group (Fig. 26.1c) and Hottinger (Fig. 26.1d).

For an easy classification, the characteristics subgroups are the following:

- ‘I’-profile subjected to shearing,
- load measuring pin / bolt (at the crane hook),
- hollow disc (having holes with parallel axes with the generators),
- Z-shaped elastic element (or S “in mirror”),
- helix load cell.

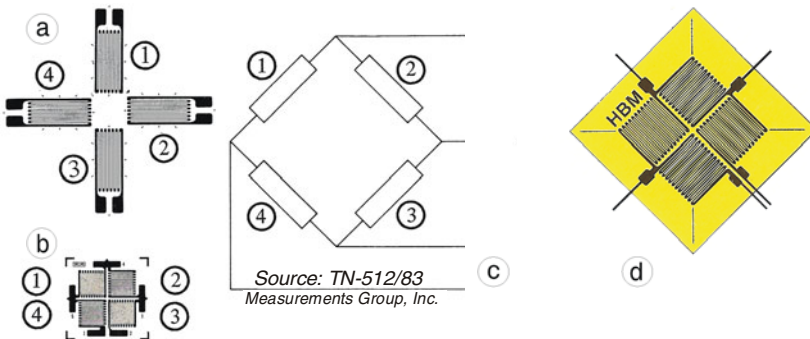
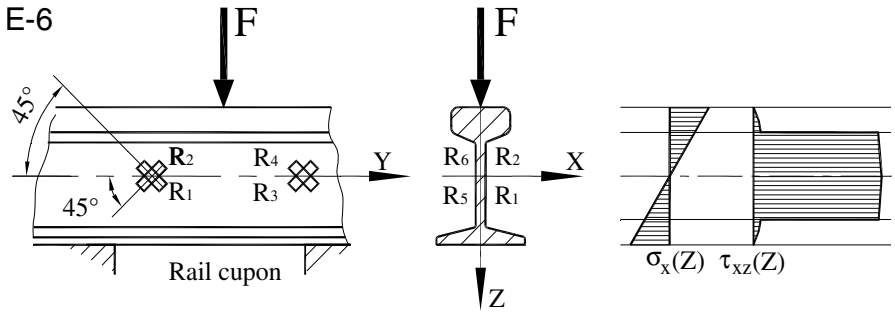


Fig. 26.1 Different full shear strain gauges and their appropriate Wheatstone bridges



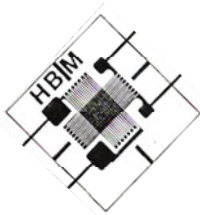
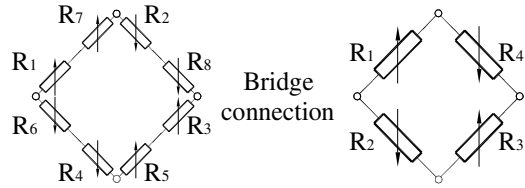
Load range [N]: $5 \times 10^2 \dots 5 \times 10^6$

Mechanical sensitivity [$\mu\text{m}/\text{m}$]:

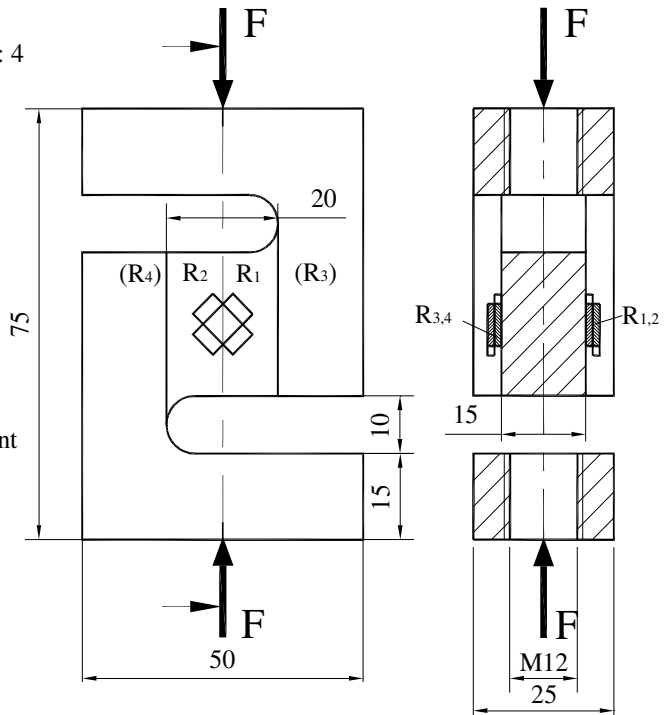
depending on: F, E and

the profile dimensions

Electrical sensitivity [ϵ]: 4



Personal model:
Z - shaped elastic element



SM\$

Fig. 26.2 Strain gauged elastic elements of type VI for force transducers: I-profile and Z-shaped. Other possibilities are: shearing bolt/pin, disc with holes and helix structure. They are presented in the following subchapters.

26.1. 'I'-PROFILES SUBJECTED TO SHEARING

An 'I'-profile subjected to shearing is wide spread as an elastic element for weighing. A tensometrically equipped rail section is a pseudo-transducer indicated for rolling stock weighing (Fig. 26.2, top).

The shear beam principle [26.1] is explained in Figure 26.3a: strain gauges are bonded to a reduced part of the cross section of the 'I'-beam in order to maximize the shear effect. They are bonded on principal strain directions, at 45 degree angles on each side of the beam, to measure the shearing.

Although the strain gauge must possess some finite physical dimensions, by equally straddling the neutral axis in bending, half of each strain gauge will experience some bending strain while the other half will experience the same strain in the opposite direction, thereby largely cancelling bending in the output of the sensor. Shear stresses by definition are equal only to the load carried by the area of the member, independent of the point of loading.

A better geometry induces the "double bending" (Fig. 26.3b) where the inflection point is centered on the shear web, thereby minimizing the bending that results at the strain gauge locations.

The classical configuration is the one in Haggstrom's patent: a cylinder with two lateral, coaxial and unpierced holes, resulting in a thin wall as an 'I', where two rosettes with strain gauges $\pm 45^\circ$ to the cylinder axis are placed on each side; the cylinder is embedded at one end and strained by a perpendicular force on it, at the other end [26.2]. In the axis of the bent cylinder, one can see that the bending stress is annulled while the shearing force is maximum, justifying the location for strain gauges at $\pm 45^\circ$.

There are a lot of achievements on this subject made by companies Measurements Group [26.3], PIAB [26.4] and Revere Transducers [26.5]. The modern technologies (Flintab) allow the welding of the tensometric cavity and the passing of the cable through "glass on metal" isolation, resulting explosion proof and sealed force transducers.

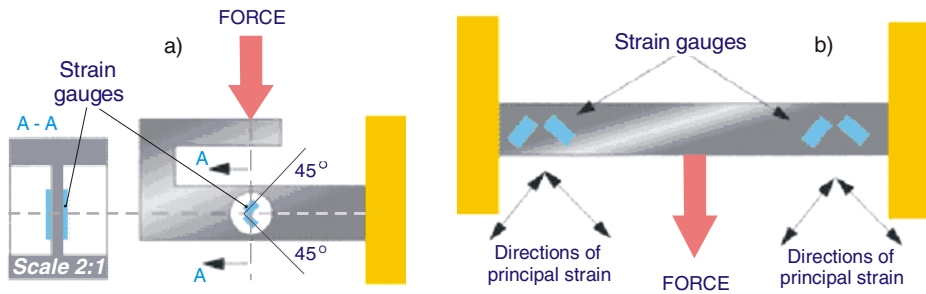


Fig. 26.3 Single- (a) and double-ended (b) shear beam principle applied on 'I'- profiles

An increased sensitivity is reported in [26.6] by a supplementary strain concentration stage: besides the thickness reduction (the central wall of the 'I'-profile) there is also a height reduction by means of two saddle-shaped cavities above and under the above-mentioned lateral holes. Such a pair with I-shaped thickness made in two perpendicular planes, suitably spaced is shown in "Messtechnische Briefe H.B.M." 2/95, page 35. Another sensitivity "doubling" can be obtained with two such extended mid-stressed cylindrical beams (a kind of type E-5 elastic element can be recognized).

In the same class of "I-profile subjected to shearing" the following modern applications can be included:

- a tactile sensor [26.7] with standing piezoresistive cantilevers embedded in an elastic material and detecting the shear stress (2.45 kPa) applied on its surface;
- a multicomponent dynamometer, made up of such sheared lamellae, joined in a cross in two perpendicular planes [26.8];
- a bearing force transducer [26.9] with twin shear beams made by wire cutting machining technique inside a metal block, capable of on-line measuring for bearing load simultaneously in three translational directions;
- a transversal slotted tube, which reveals by deployment a continuous succession of 'I'-beams stressed by shearing [26.10], [26.11].

26.2. LOAD MEASURING PINS / BOLTS

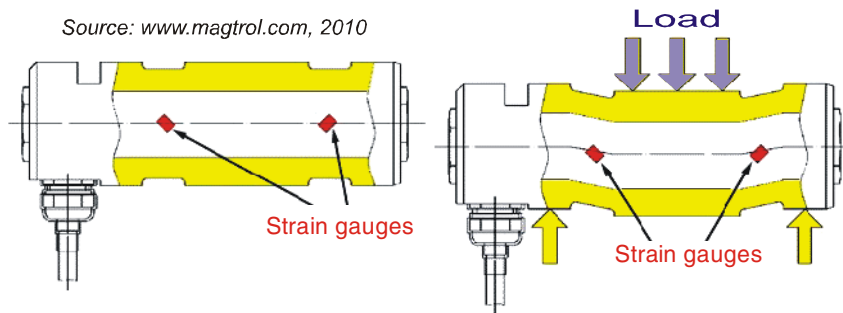
Load measuring pins or bolts are strain gauge based transducers which are used to measure load, overload, or tension conditions. Typically installed into machines in the place of normal shafts, load pins act as a direct component in an assembly, like in the crane hook.

This is an elastic structure to be found in the documentation of old companies in the field of force measurements and it is called *load measuring pin and shackle* [26.12] or *Lastmessbolzen* [26.13], the later having the European Patent 59295. A digital version that can have the weighing range between 100 kg and 2000 tons, electronically switched and having an adjustable input sensitivity between 0.1 mV/V and 4 mV/V towards a virtual instrument, can be found in [26.14].

The load measuring pin [26.15] offers an excellent solution since it acts as a direct element in the pulley or shackle assembly, replacing a non-instrumented pin or shaft and operating by shearing principle through a strain gauge bridge integrated into the pin (Fig. 26.4.). After the force is loaded on the measuring pin, the effect on the four independent strain gauges results in an output signal proportional to the applied load. An accuracy comparison between two types of usual Wheatstone bridges is given in Table 26.1.

Table 26.1 Load pins characteristics

Bridge type	Strain gauge number	Output impedance [Ω]	Mountings	Accuracy
Single	4	350	Simple, symmetrical	Standard
Double	8	700	Asymmetrical	High

**Fig. 26.4** Magtrol solution representation, before and after loading the pin

The bolt is actually a short tube with thick walls, with inner located strain gauges on each side of the center section, and having directions at $\pm 45^\circ$ to the tube axis. A similar solution, with strain gauges located inside a hole drilled into one of the teeth of a big excavator cup, is to be found in “Reports in Applied Measurement H.B.M.” 1/89, page 13.

Hottinger, the world leader in strain gauges based measurement and transducers, offers a large variety of load measuring pins, standard models or customized versions, covering a lot of applications [26.16]: cranes; winches; hoisting gears; cable laying equipment; marine, tankers, offshore platforms; rope, chain, and brake anchors; bearing blocks, pivots and shackles; elevators and floor conveyors; various applications in agricultural, aviation, and chemical industries.

Typical features for load measuring pins are:

- rated capacity from 5 to 1250 kN,
- overload: 150 % of rated capacity,
- ultimate breaking load: > 300 % of rated capacity,
- temperature compensated,
- pins made of high quality corrosion resistant stainless steel,
- maintenance-free, ideal for hostile environments,
- rugged construction,
- accuracy to ± 0.5 %,
- output signals: mV/V, (4 ... 20) mA, (0 ... 5) V.

26.3. HOLLOW DISCS / WHEELS

This is a kind of disc on whose middle circle, at half distance of its radius, are the centers of some holes having their axes parallel to the wheel generators. The separating walls of this circular row of holes are a kind of spokes that may have cavities at their upper and lower parts. Strain gauges are located inside these holes in the middle plan of the low profile wheel, on directions to $\pm 45^\circ$ to the loading axis.

By comparing these “spokes”, which are relatively high and sheared, with the wide bent spokes of the “flat” wheel shown in Figure 25.1, their sensitivities have similar values in the two cases, and both are higher than the sensitivities of the elastic elements stretched and/or compressed. A study on the sensitivity enhancing according to the increase of drilled holes number was developed by Erichsen consulting [26.17]. It is obvious that by increasing the number of holes the number of separating walls will increase as well. These walls are a kind of bent lamellas, namely elastic elements, on which can be bonded the strain gauges. A supplementary way to increase the tensometric sensitivity is the using of a “tandem” of such special spoked wheels, mounted in “opposition” on the same loading axis.

The National Research Laboratory of Metrology in Japan [26.18] had to develop an elastic element for a force transducer with improved characteristics:

- independent sensitivity at a certain degree of eccentric or side force,
- multiple sensing data provision with decentralized detection of the applied force,
- absence of error factors caused by the connection interface of the force transducer (load button or terminal) and by the loading machine,
- smaller overall dimensions ($\text{Ø}345 \text{ mm} \times 280 \text{ mm}$),
- reduced weight (118 kg for maximum capacity of 5 MN) as compared with conventional units,
- higher rated output, with smaller errors of nonlinearity (16×10^{-5}) and hysteresis (19×10^{-5}).

To develop a strain detection circuit able to offset parasitic force components, the finite element method has been used to analyze the inter-relationships between the load distribution mechanism, bending and twisting directions and stress distribution of the beam springs. 64 dual shear strain gauges were bonded on the sides of all beams radiating out from the spring elements A and B. The top view from Figure 26.5a indicates “double” strain gauges positioning on the spring elements.

Fig. 26.5b illustrates the position, direction and polarity of detected strains in relation with the beam springs in a cross section of two opposite “wheels.” Half of the strain gauges detects elongation and the other half

detects shrinkage, and their combination offsets the hardness differences between the central hub and the outer cylindrical flange.

The averaging of axial load and elimination of bending and twisting components is done by optimized combinations of strain gauges based on the symmetry of detection positions in shear web design (Fig. 26.5c).

This double wheel (A + B) solution, based on the perfect aligned built-in dual shear strain gauges (Fig. 26.5d), enables all strain discrepancies elimination from the assembled central hub and outer cylindrical flange.

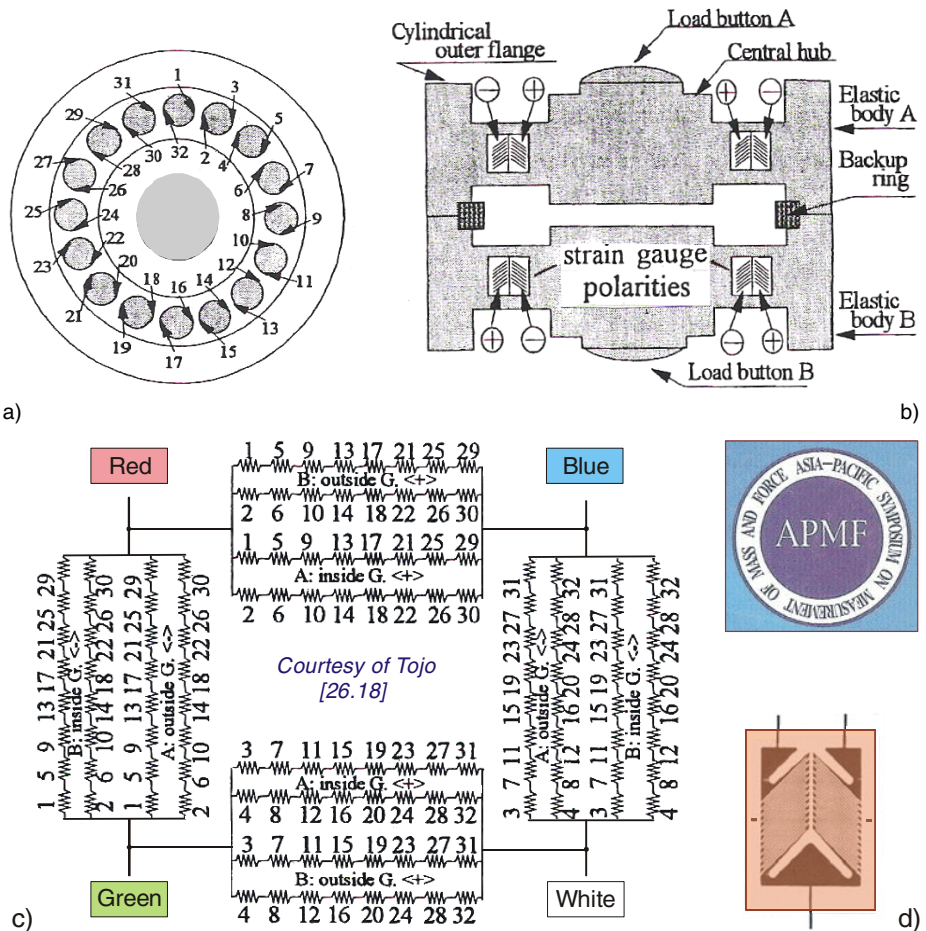


Fig. 26.5 Diagram of multiple sensing Wheatstone bridge circuit with 64 dual shear strain gauges (“fishbone” type) for a super-precision load cell made by TakuroTojo within the Japanese Metrology

26.4. S (Z) SHAPED ELASTIC ELEMENTS

S- or Z-shaped elastic element (Fig. 26.6a) allows a wide variety of structural solutions using rosettes with $\pm 45^\circ$ strain gauges of ‘X’ type, connected in Wheatstone bridge like in Figure 26.6b. It has a lot of advantages [26.19]: unexpensive, compact, one piece, easy to install in any testing equipment, can be both stretched and compressed, insensitive to side loads; it is characterized by linear dependence “*mechanical stress vs. specific deformation*” and output signal independent of the load position. ‘Z’ meets the installation requirements to provide optimum performances in overtaking the load [26.20]. The inventor Sandor Kovacs has made a “cage” with the walls composed of four Z's [26.21].

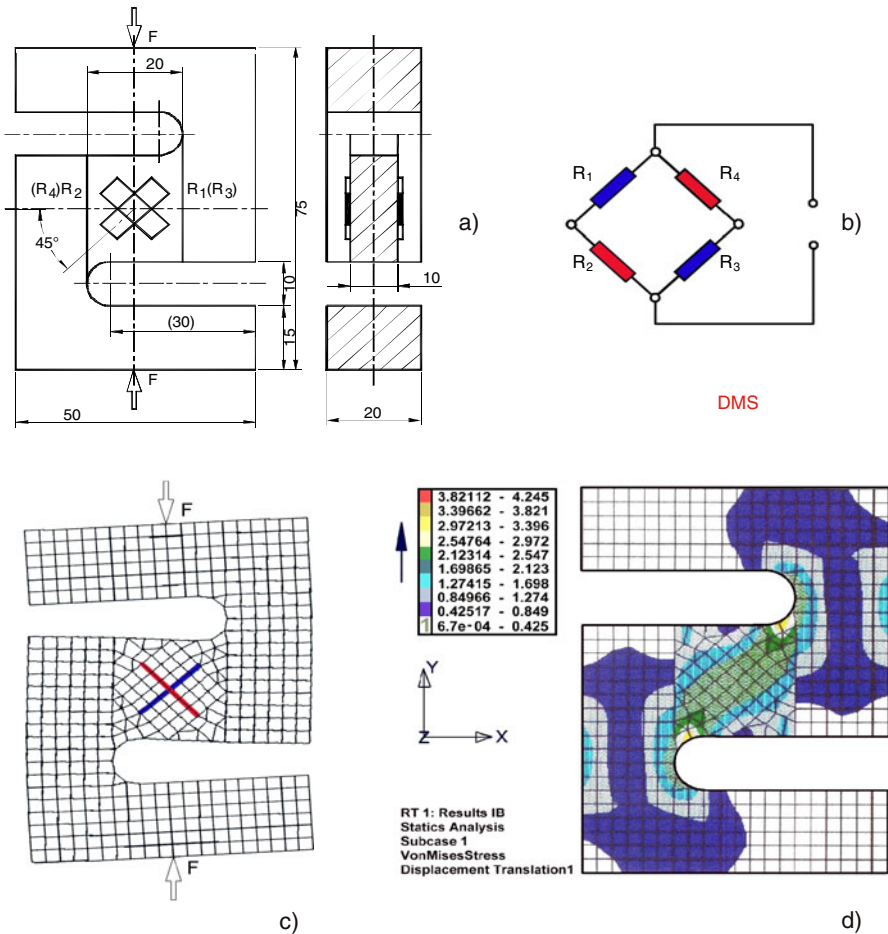


Fig. 26.6 Z-shaped flexible element optimized by FEM in Twente Enschede

The Z-shaped elastic element is ideal for the material testing equipment [26.22]. A training model made up of simple disc with two short parallel slots on each side of a diameter, plus three-directional tensometrical rosette, ensures the passage from an initially fundamental research to an experimental one in the field of surfaces roughness (Mechanics of Materials, 1/92, pp. 55-57).

The processing of a central hole or of a rectangular slot can change the 'Z' into an elastic element with multiple bending, having the sensitivities comparable to the sheared Z's. The author has made researches in many stages [26.23], [26.24], developing various applications for cutting devices fitted on agricultural equipment or to the bending of composite samples [26.25].

If in the past the shape optimization was made by graphic calculation and areas measuring (planimetry) with special equipment, today numerical methods and modern computation technique are available [26.26], [26.27]. An example is given in Figures 26.6c (FEM mesh deformation under the applied force F) and 26.6d (von Mises stress map for a 'Z' type force transducer).

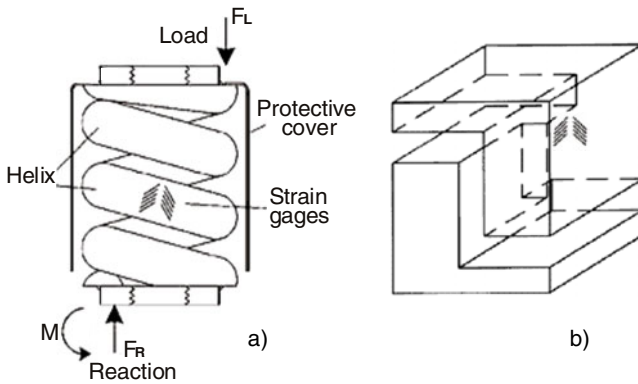
26.5. HELIX LOAD CELLS

The helical load cell [26.28] is based on the principle of the wirewound spring (Fig. 26.7a). A spring works by converting the vertical load force, F_L to a torsional moment in the wire. This torsional reaction travels through the wire from the top of the helix to the bottom, where it is again converted to a linear reaction force, F_R . The helical load cell is insensitive to off-axis loading because of the manner in which the torsional moment propagates around the helix. At any two points diametrically opposed across the helix, the sum of the torsional reactive moments is always a constant, proportional to the applied load, *regardless of where that load is applied*.

Refining the basic geometry of this torsional sensing load cells (TSLCs), a new type of elastic element, cut or casted from stainless steel could be created as a flat, circular sensing element in the center of the Helix load cell. The cube configuration (Fig. 26.7b) is also possible because the general formulas applicable to this type of force transducer are independent of shape. The configuration of the sensing element is unimportant, as long as it completes a 180° change in direction while propagating the loading force, and the gauges are set in diametric opposition to each other.

Gagetek Company has developed a load cell with a lot of remarkable properties:

- through hole for easy mounting,
- insensitivity to off-axis loading,
- rugged and tolerant of shock loading and overload,
- overload stops for up to 3 times loading,
- high sensitivity, infinite resolution, and low cost.



Courtesy of R.W. Bruns,
Gagetek Company



Copyright:
Melanie Martella
Executive Editor, *Sensors*
Questex Media Group LLC
Integrated Media Solutions for Business

Fig. 26.7 Dual shear strain gauged helix load cells with different geometry:
a) wirewound spring, b) cube configuration (like a “volumic S”)

Four load cells can be configured into a compact portable scale that can work with virtually any platform and perform equally well on concrete or dirt; the Sacramento Zoo uses this scale to weigh its collection of exotic animals.

REFERENCES

1. Pierson, J.: Load/Force Cells. How they work, July 21 (2008), <http://www.sensorland.com/How/Page005.html>
2. KIS – The logical choice of load cell. Document A2, Nobel Elektronik, Karlskoga, Sweden (October 1991)
3. Strain Gage Based Transducers – Their Design and Construction, February 15 (2001) <http://www.measurementsgroup.com/guide/ta/sGBT/sgbtindex.htm>
4. Force measurement, weight indication and overload protection. Info 9008-1, PIAB, Akersberga, Sweden (August 1990)
5. Product guide for load cells. Revere Transducers Europe, Breda, NL, GB/D/F-97
6. Grünbaum, P.: Measurement of forces in a rock-wool hardening oven at 230°C, Hottinger, Darmstadt. Reports in Applied Measurement, vol. 8(2), pp. 25–30 (1992)
7. Noda, K., Hoshino, K., Matsumoto, K., Shimoyama, I.: A shear stress sensor for tactile sensing with the piezoresistive cantilever standing in elastic material. *Sensors and Actuators A: Physical* 27(2), 295–301 (2006)
8. Quinn, T.P., Mote Jr., C.D.: Optimal design of an uncoupled six degree of freedom dynamometer. *Experimental Mechanics* 30(1), 40–48 (1990)

9. Yang, Z., Wang, S., Wang, Q., Xie, Y.: Three-dimensional bearing load sensor design and numerical investigations. *Sensors and Actuators A: Physical* 136(1), 304–312 (2007)
10. Ștefănescu, D.M.: Untersuchung der Verformungszustands eines elastischen Rohrelements mit Spalten, anwendbar beim Bau der Kraftaufnehmer mit Dehnungsmeßstreifen. In: *Revue Roumaine des Sciences Techniques – série de Mécanique Appliquée*, Bucarest, vol. 29(5), pp. 519–533 (1984)
11. Hara, R., Ban, K.: 6-axial force sensor using shearing strain gauges. Patent abstracts of Japan, JP 09318469 (December 1997)
12. Strength and sensitivity: electronic weighing and force measurement load cells. Veccer Limited, Reading, Berkshire, E 137/109-95
13. Lastmessbolzen (Europäisches Patent Nr. 0059295). Vibro-Meter AG, Fribourg, Schweiz (1987)
14. Digital load measuring system-patented, TÜV-approved for use in weighing systems. Preliminary issue, Müller Industrie-Elektronik GmbH, Neustadt (D) (August 1998)
15. Load pin operating principles, June 22 (2008), <http://www.magtrol.com/loadforceweight/principles.htm>
16. Load Measuring Pins. PDF S 1138, Hottinger Baldwin Messtechnik, Darmstadt (2008)
17. Kraftaufnehmer – Load cells – Capteurs de force. Katalog 1092, A.M. Erichsen Vertrieb GmbH, Wuppertal, Deutschland (1991)
18. Tojo, T.: The design and performance of super-precision load cell for high accuracy measurement of forces. In: Shi, C., Zhang, Y. (eds.) *Acta APMF 1996 – Present Situation and Progress of Measurement on Mass and Force*, Beijing, China, August 20-22, pp. 83–88 (1996)
19. Bahra, C.S., Evans, J.W.: Strain gauge load cell design and use. In: *Proc. TEMPCON Transducers Conference*, London, June 14-16, pp. 1–22 (1983)
20. van Wijk, E.: Aircraft weighing by REVERE and EVERGREEN. Revere Transducers, Inc., Tustin, CA (September 1998) (printed in USA)
21. Kemeny, T.: IMEKO activities in connection with force and mass measurement. IMEKO Technical Committees Event Series, vol. 29, pp. 3–17. MTESZ Házinyomda, Budapest 1104-91
22. Lohr, R.D.: Load cells for materials testing. Reprint INSTRON from *Measurement & Inspection Technology*, 37–40 (July 1980) (printed in England)
23. Ștefănescu, D.M.: Study of S-shaped flexible elements of force transducers instrumented with strain gages using the finite element method. In: *Proceedings IMEKO XI World Congress, Sensors*, Houston, Texas, October 16-21, vol. V, pp. 645–652 (1988)
24. Ștefănescu, D.M., Sandu, A., Mănescu, T.: Z-shaped strain gauge force transducers. In: *Proc. 14th IMEKO Int'l Conf. State of the Art in Force and Mass Measurement*, Warsaw, Poland, September 5-8, pp. 155–160 (1995)
25. Ștefănescu, D.M.: Stand for mechanical testing of composite materials. In: *Acta IMEKO XII, Measurement of Force, Mass, Pressure, Flow and Vibration*, Beijing, China, September 5-10, vol. II, pp. 431–435 (1991)

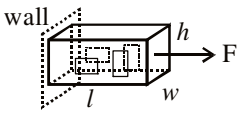
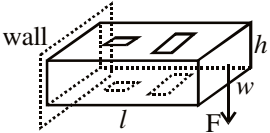
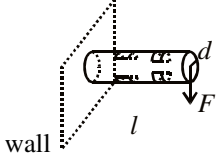
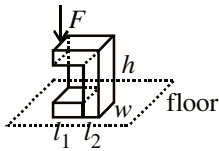
26. Rasmussen, J., Lund, E., Birker, T.: Collection of Examples – CAOS Optimization System, 3rd edn. Report 13, Institute of Mechanical Engineering. Aalborg University, Denmark (April 1992)
27. Ștefănescu, D.M.: Choosing and modeling criteria for elastic elements of transducers. Scientific Seminar, Measurement and Instrumentation Department, Twente University of Enschede, The Netherlands, October 16 (2002)
28. Bruns, R.W.: The helix load cell. Sensors Magazine (May 1998)

Chapter 27

BENT YOKES AND FRAMES

The bent yoke is a particular elastic structure, as compared with other elastic elements of simple shapes: stretched or compressed column (EE-1, presented in Chapter 21), bent lamella (EE-3, C.23) and bent or twisted shaft (EE-4, C.24). As one can see in the Table 27.1, the bent yoke (or open frame) is utilized in the middle range of forces, up to 50 kN [27.1].

Table 27.1 Force ranges and mechanical sensitivities for some elastic elements

Type	Force range [N]	Mechanical sensitivity [$\mu\text{m}/(\text{N}\cdot\text{m})$]	Sketch of the shape
Stretched or compressed column	$10^1 \dots 10^7$	$\frac{1}{E \cdot w \cdot h}$	
Bent lamella (cantilever beam)	$10^{-2} \dots 5 \cdot 10^4$	$\frac{6 l}{E \cdot a \cdot h^2}$	
Bent and/or twisted shaft	$10^0 \dots 10^5$	$\frac{32 l}{\pi E \cdot d^2}$	
Bent yoke	$5 \cdot 10^0 \dots 5 \cdot 10^4$	$\frac{6 l_1 / l_2 - 1}{E \cdot w \cdot l_2}$	

E-7

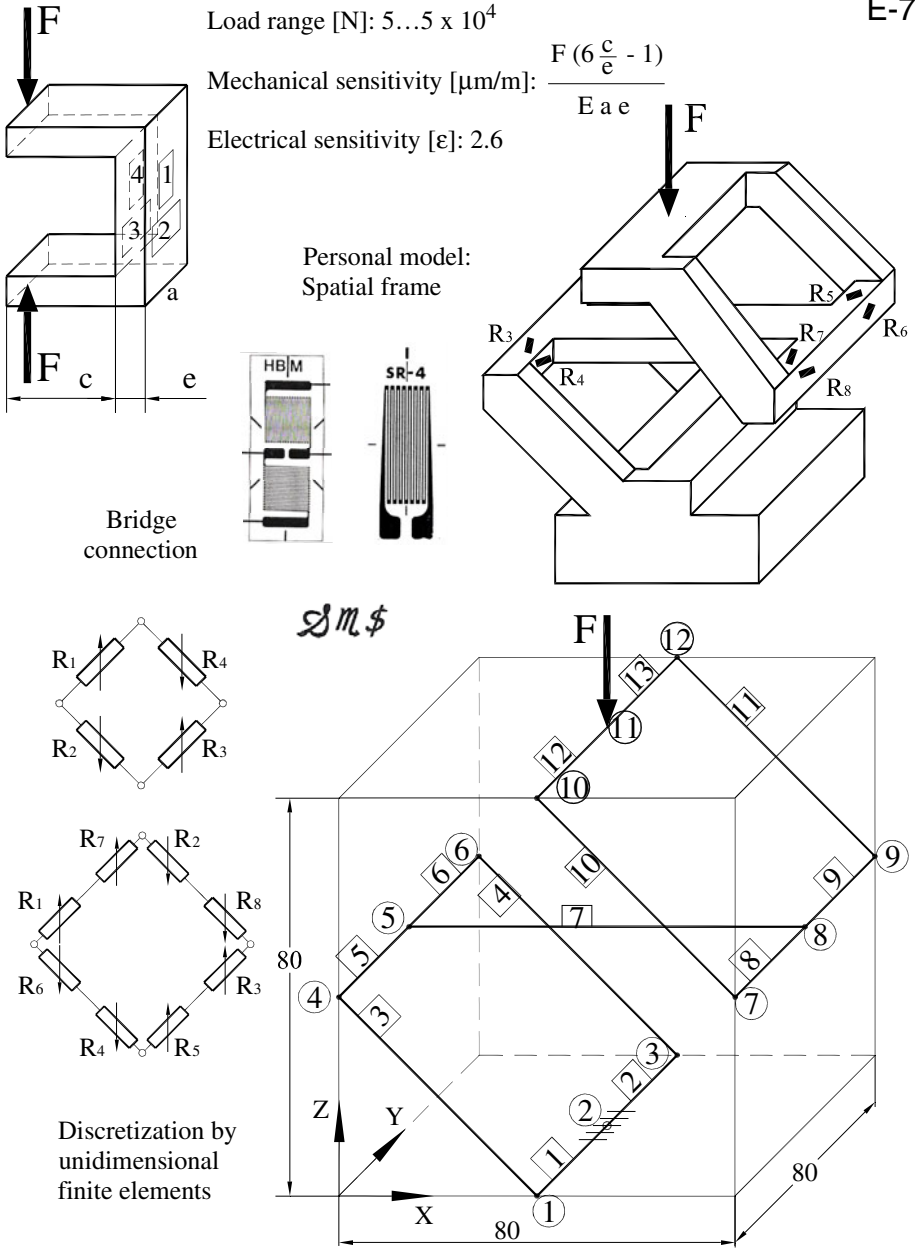


Fig. 27.1 Strain gauged elastic elements of type VII for force transducers. The evolution from 2D to 3D imposes the using of Finite Element Analysis.

27.1. VARIOUS SHAPES OF BENT YOKES AND FRAMES

The bent yoke has low rigidity, i.e. high deflection that can be used for the displacement measuring too, with the following “opposite” characteristics presented in Table 27.2.

Table 27.2 Different names for yokes used in force or displacement measurements

Measurand	Transducer name	Mounting	Deflection
Force F	Portal, porch	Series	Low
Displacement d	Clamp, collar	Parallel	High

There are transducer companies specialized in the measurement of the long displacements and small forces respectively: Measurements Group and Mikro-Epsilon. An elastic brace for the crack extension monitoring is described in [27.2]. The author achieved such tensometric devices for studying the cable stretching [27.3] and the wood deformations (quoted in [27.4]).

The squared ring, parallelogram flexure or rectangular spectacles can be considered plane frames with variable section and increased sensitivity. Other elastic structures showed in the present work in different chapters can be reduced to frames. The different sizing possibilities allow the covering of the whole range of necessary loads.

The yoke is a bent bar in plane (Fig. 27.1 top left) but could be used in complex combinations in space (Fig. 27.1 top right). One can obtain the maximum electrical sensibility (4ϵ) if all the four strain gauges are “active”, i.e. longitudinally positioned, in pairs on the interior and respectively exterior faces of the plane yoke.

Two such bidirectional yokes can make up a closed frame stressed to the symmetry axis. The closed frames are statically undetermined systems that in Strength of Materials are solved by force or displacement methods.

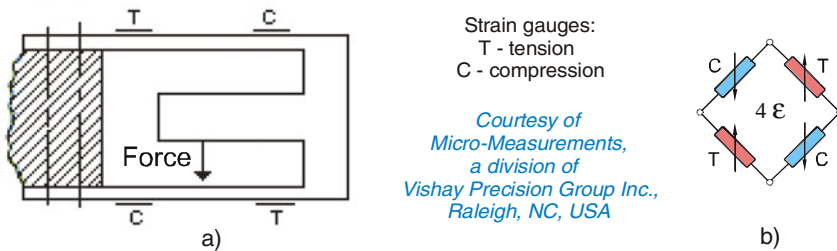


Fig. 27.2 Centrally loaded dual-beam arrangement: a) bending moments in the sensing beams are independent of the load application point; b) full Wheatstone bridge with two tensioned (T) strain gauges and two compressed (C) strain gauges.

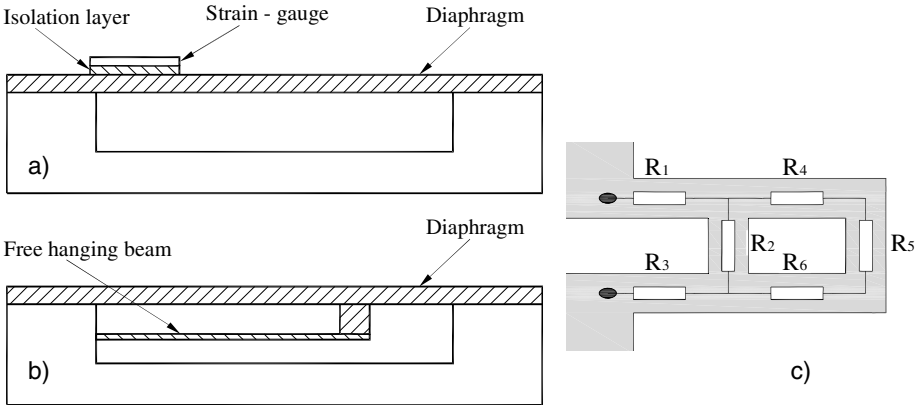
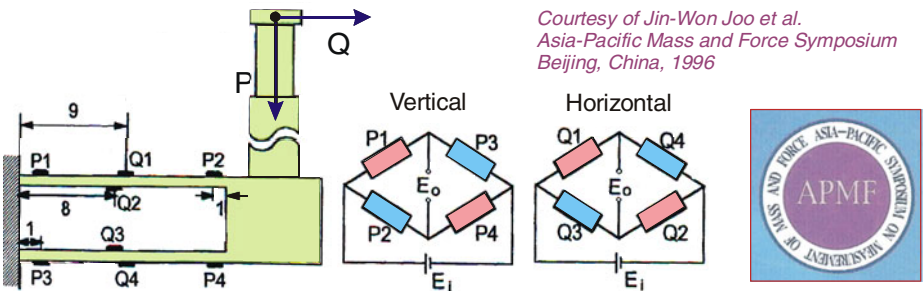


Fig. 27.3 Free hanging A-shaped piezoresistive cantilever (c), mounted beneath the pressure diaphragm (b), in order to replace the external strain gauge (a)

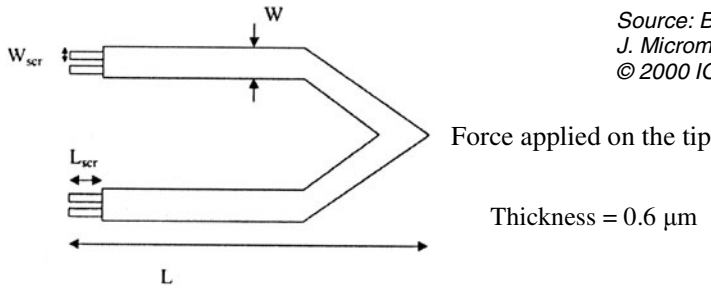
Here are several structures composed by various elastic frames from the point of view concerning dimensional proportions and mounting possibilities:

- E-shaped plane frame (Fig. 27.2), where the middle arm is bent stressed, avoiding buckling of the vertical portion [27.5]. Such an E-shaped elastic element is used to the weighing cells equipped with tensometric resistors made up of thin semiconductor layers [27.6].
- H-shaped plane frame, achieved by electrospark cut-out machine [27.7], or A-shaped frame (Fig. 27.3c), made by micromachining [27.8];
- Frame made up of two horizontal triangular plates, “joint” by two vertical bars, and resulting in a double cantilever lamella (Schenck);
- Tandem of two parallel frames, bent to two perpendicular directions (Messtechnische Briefe HBM, 1/73, p. 12);



*Courtesy of Jin-Won Joo et al.
Asia-Pacific Mass and Force Symposium
Beijing, China, 1996*

Fig. 27.4 Double-cantilever beam like a biaxial transducer (P - vertical, Q - horizontal) for measuring flange reaction forces of a digital video cassette recorder

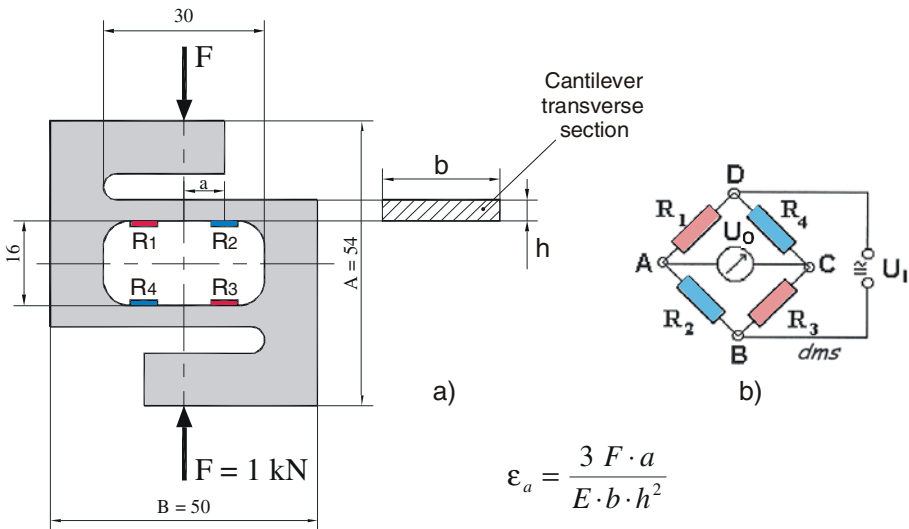


Source: Bashir et al.
 J. Micromech. Microeng.
 © 2000 IOP Publishing Ltd

Cantilever dimensions: $L = 150 \mu\text{m}$, $W = 20 \mu\text{m}$
 Stress concentration region: $L_{scr} = 10 \mu\text{m}$, $W_{scr} = 4 \mu\text{m}$
 Resistor dimensions: $L_R = 14 \mu\text{m}$, $W_R = 4 \mu\text{m}$

Fig. 27.5 Schematic diagram of U-shaped horizontal piezoresistive cantilever

- Double-cantilever beam elastic structure for two axis force transducer [27.9], shown in Figure 27.4.
- Double-cantilever beam (Fig. 27.5), made by a horizontal piezoresistive silicon cantilever with stress concentration regions, for scanning probe microscopy applications [27.10]. This U-shaped cantilever does not have the small losses in the first transverse part (R2), comparing with the A-shaped cantilever (Fig. 27.3c); here a low value of equivalent R5 is recommended.



$$\epsilon_a = \frac{3 F \cdot a}{E \cdot b \cdot h^2}$$

Fig. 27.6 Plane frame elastic element for strain gauged force transducers (a) and the SGs connection in Wheatstone bridge (b)

The author has achieved two rectangular plane frames for aeronautic applications [27.11]: one axially stressed (for aerodynamic force determination on the slat of a small unmanned vehicle for air surveillance); another is the “S-type folded cantilever” (Fig. 27.6a), subjected to multiple bendings during force measuring in the stick of a flight simulator. Equal tensile and compressive strains ε_a are produced at adjacent locations on the horizontal inner faces, having bridge connection shown in Figure 27.6b. These are independent force transducers, reusable and perfectly integrated into the assembly kinematics.

A complex spatial structure, made up of two rectangular frames jointed by a diagonal bar [27.12], was optimized by means of the one-dimensional finite elements (Fig. 27.1, bottom). The eight independent strain gauges are working in the shearing mode. This sensing device is also adequate for dynamic applications in the field of force and torque measurement.

27.2. FORCE–MEASURING CLAMPS

Vishay Company [27.13] achieved a small C-shaped elastic vice, which is, in fact, a pseudo-transducer used during the bonding of the strain gauges to achieve a pre-established pressing. This tensometric device can be considered as a small machine for compression testing (a yoke of a special shape, made up from a trapezoidal section bar), having a rare particularity: its compression sensitivity ($2.946 \mu\text{V}/\text{V}$) is greater than the sensitivity in traction ($2.182 \mu\text{V}/\text{V}$) accounted for by the C type elastic element nonlinearity.

Force-measuring clamps (Figure 27.7) have been invented to facilitate and simplify the task of measuring the forces or pressures applied to clamped parts, e.g. while bonding strain gauges to their substrates. One prior method of measuring clamping force involved the use of load washers or miniature load cells in combination with external power sources and load-indicating equipment. Calibrated spring clamps have been used too. Spring clamps can lose calibration quickly through weakening of the springs while load washers and miniature load cells constitute additional clamped parts in load paths and can add to the destabilizing effects of loading mechanisms.

The basic principle of a force-measuring clamp can be implemented on a clamp of almost any size and can enable measurement of a force of almost any magnitude. A force-measuring clamp is a complete force-application and force-measurement system all in one package.

This force-measuring clamp [27.14] contains strain gauges and exploits the well-known proportionality between strain and applied force or pressure. There are four strain gauges electrically connected in a Wheatstone bridge. The bridge output is fed to zero and span circuitry, the output of which is digitized and displayed.

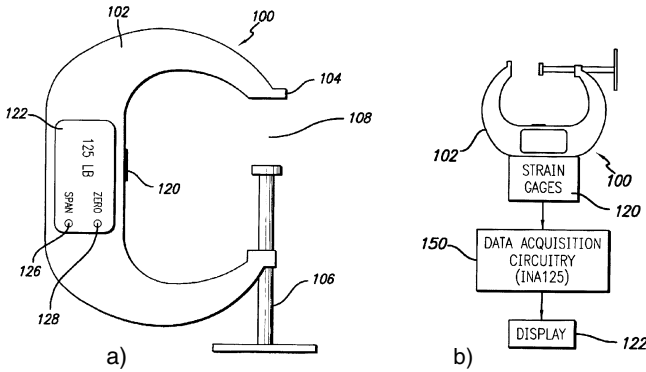


Fig. 27.7 Force-measuring clamp: a) C-shaped strain gauged elastic element; b) measurement circuitry

The printed-circuit board contains a voltage-regulation circuit, the span and zero circuits, two watch batteries, and a power switch. The final-stage output is fed to a digital-display device that is plugged into the printed-circuit board, and is controlled by the zero and span circuits. The associated circuitry makes possible the calibration of the bridge output in order to indicate force or pressure in any suitable unit of measure.

The functionality of a “breadboard” prototype force-measuring clamp was tested in one of the NASA laboratories [27.15] by use of the combination of certified weights, a load washer, a strain indicator, and a voltmeter. Force-measuring clamps have high versatility; they could be incorporated into other mechanisms to satisfy various functions.

C-shaped strain gauge force transducers were designed to enable dynamic measurements of the tension of the individual mitral valve chordae tendineae during the cardiac cycle under *in vitro* and *in vivo* experimental conditions [27.16]. The force transducers were constructed from a C-shaped brass ring with a diameter of 6 mm, width of 2 mm, thickness of 0.5 mm, and a mass smaller than 80 mg. Miniature strain gauges elements were cemented onto the inner and outer side of the ring and coupled in a Wheatstone half-bridge circuit to a signal conditioner and amplifier.

REFERENCES

1. Korsten, M., Ștefănescu, D.M., Regtien, P.P.L.: Sensor specification using the ISA and STEP standards for sensor selection. In: CD Proceedings XVIIth IMEKO World Congress Metrology in the 3rd Millenium, Cavtat-Dubrovnik, Croatia, June 22-27, pp. 393–396 (2003)
2. Keller, H.P., Munz, D.: Das J-Integral beim Einsetzen des stabilen Rißwachstums bei der Aluminium-legierung AlCuMg2. *Materialprüfung* 18(1), 8–12 (1976)

3. Ștefănescu, D.M.: Methods and means for measuring the extension of the cables. *Metrologia aplicată* XXXV(4), 146–151 (1985) (in Romanian)
4. Petrican, D., Curtu, I., Sperchez, F.: *Strain Gauge Technique Applications in the Wood Industry*. Editura Tehnică, București (1980) (in Romanian)
5. *Strain Gage Based Transducers – Their Design and Construction*. A Measurements Group Hypertext Publication, February 15 (2001)
6. Devenyi, A., Belu-Marian, A., Mitre, A., Mateescu, I., Korony, G.: Thin film load cell for small forces. In: *Proc. 4th National Symposium Tensometry, Brașov, September 24-27, vol. I*, pp. 85–90 (1986) (in Romanian)
7. Sava, J.: Loadcells 200 N – 1 kN with H-type spring elements. In: Tamas, K., Havrilla, K. (eds.) *Force Measurement and Weighing in the 90s, IMEKO TC Event Series, vol. 29*, pp. 243–250. MTE SZ Házinyomda, Budapest 1104-91
8. Melväs, P., Kälvesten, E., Enoksson, P., Stemme, G.: Miniaturized pressure sensor using a free hanging strain-gauge with leverage effect for increased sensitivity. In: *Proc. 11th International Conf. Solid-State Sensors and Actuators – Eurosensors, Munich, Germany, June 10-14, vol. XV*, pp. 494–497 (2001)
9. Joo, J.-W., Kim, G.-S., Lee, K.-W.: Two-axis force sensor for measuring flange reaction forces in digital VCR. In: Shi, C., Zhang, Y. (eds.) *Acta APMF 1996 – Present Situation and Progress of Measurement on Mass and Force, Beijing, China, August 20-22*, pp. 83–88 (1996)
10. Bashir, R., Gupta, A., Neudeck, G.W., McElfresh, M., Gomez, R.: On the design of piezoresistive silicon cantilevers with stress concentration regions for scanning probe microscopy applications. *J. Micromech. Microeng.* 10, 483–491 (2000)
11. Ștefănescu, D.M., Adam, C., Mănescu, T.: Force transducers with rectangular frames as elastic elements. In: *Proc. 7th National Symposium of Tensometry, Suceava, October 17-19, vol. II*, pp. 217–220 (1996) (in Romanian)
12. Constantinescu, I.N., Ștefănescu, D.M., Sandu, M.A.: *Mechanical Quantities Measurement by Tensometry*. Editura Tehnică, București (1989) (in Romanian)
13. Lineback, D.: *Clamps & Springs*. In: *Experimental Stress Analysis Notebook, vol. 26*, pp. 2–9. Measurements Group, Inc., Raleigh (1995)
14. Nunnelee, M.: Clamping forces can be measured easily and quickly. Scirus for scientific information DRC-99-37, Dryden Flight Research Center, Edwards, CA, July 21 (2007)
15. <http://www.nasatech.com/Briefs/Apr03/DRC9937.html> (2008)
16. Nielsen, S.L., Soerensen, D.D., Libergren, P., Yoganathan, A.P., Nygaard, H.: Miniature C-shaped transducers for chordae tendineae force measurements. *Annals of Biomedical Engineering (Springer Link)* 32(8), 1050–1057 (2004)

Chapter 28

BENT RINGS AND “GLASSES”

28.1. VARIOUS SHAPES OF BENT RINGS

The bent ring is an elastic element with high sensitivity, frequently used in the average force ranges. It has a large variety of shapes, the most important being represented by Jim Pierson [28.1]; in Figure 28.1 one can see three typical kinds of rings: a) circular, b) “modified” and c) “glasses”-shaped, as well as their strain gauges connection in Wheatstone bridge (d).

28.1.1. Circular rings

Classical ring is presented in Figure 28.2, top. The mechanical dynamometers used in the 80's at PTB Braunschweig and ASMW Berlin were more or less “expanded” rings according to one of their main axes [28.2]. Instrumentation for measuring the small deformations of the proving rings for testing machines has continuously evolved: comparing watch (M.F.L.), Zeiss microscope, electronic indicator, and laser system. Nowadays there are more accurate force transfer standards, so the simple mechanical rings are not in use.

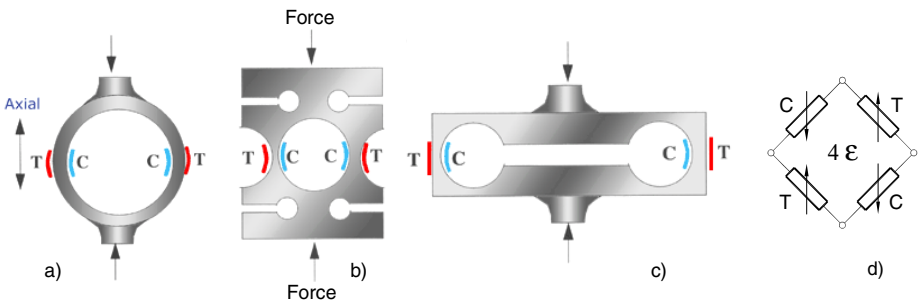
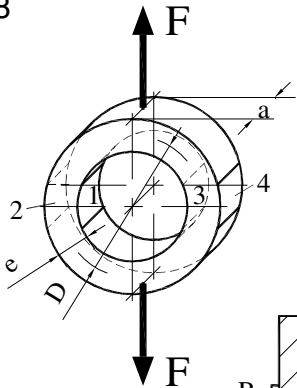


Fig. 28.1 Various shapes of bent rings and their strain gauges in Wheatstone bridge

E-8



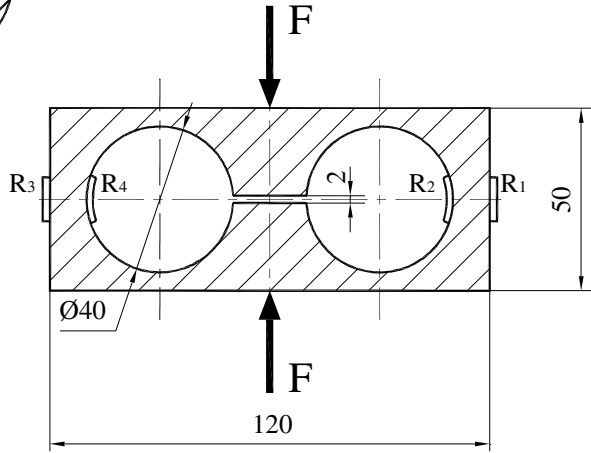
Load range [N]: $10 \dots 10^4$

Mechanical sensitivity [$\mu\text{m}/\text{m}$]: $\frac{3 F D}{\pi E a e^2}$

Electrical sensitivity [ε]: 3.7

Personal model:

Sm\$



Strain diagrams on four models of "glasses"

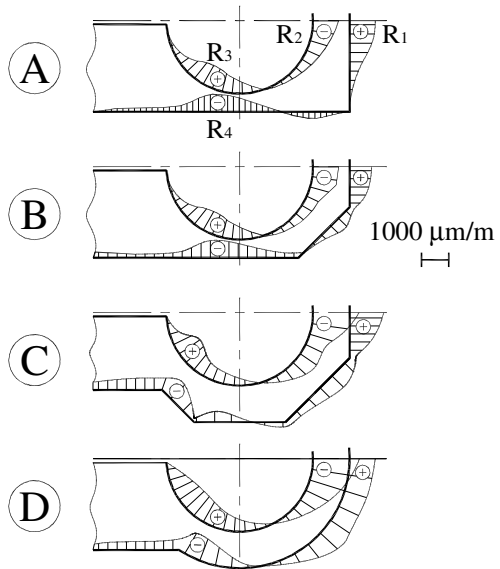
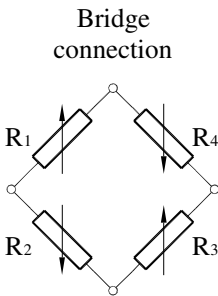


Fig. 28.2 Strain gauged elastic elements of type VIII for force transducers. Complicated shapes, like "binoculars", need analyses by Finite Element Method.

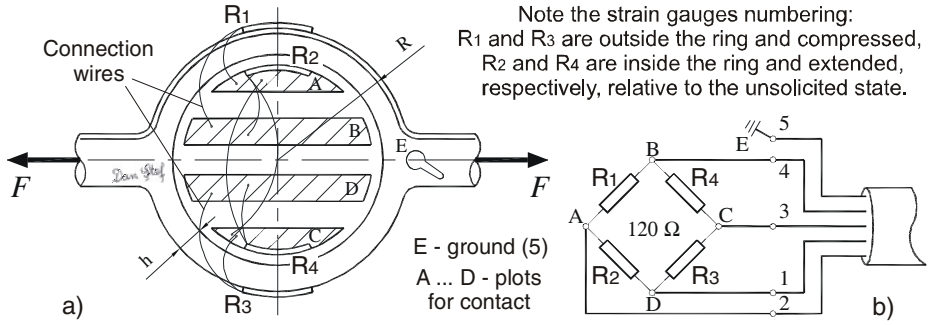


Fig. 28.3 Circular ring with four strain gauges (a) and their Wheatstone bridge (b)

The classical ring has a circular shape and it is diametrically and bi-directionally stressed [28.3]. This is a typical dual sensing elastic element. (In the compressed “washer” position, the loading mode and tensometric configuration are totally different). The industrial prototype of the ring can be considered the one in [28.4], and a specific application for weighing up to 10 kg is presented in Figure 28.3 [28.5]. An “amplified” elastic structure made up of two perpendicular rings and a shared axis can also be used.

A complete ring can be obtained by two half-rings. A suggestive example is presented in [28.6]. The length changes of the root between the two strain gauged clamps (Fig. 28.4) have resulted by calibrating their electrical resistance against the linear displacement measured by a vernier scale. This assembled force transducer functions as a “soft device” offering little opposition to the transfer of stresses within the root.

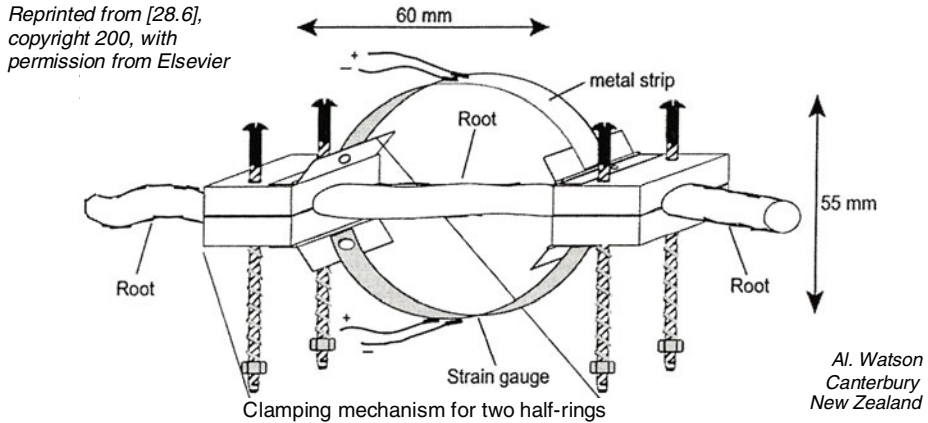


Fig. 28.4 A complete ring assembled by two half-rings to measure root stresses

Other (half)rings associated to this sensitive structure class are:

- half-rings for ship model testing [28.7] and half-ring or half-circular curved bar used in displacement measuring devices (extensometers) [28.8],
- a tubular ring extended from a “slice” to a loaded tube along a generator, but with difficulties in locating strain gauges inside (Norden),
- ring groupings in the dynamometric tables for the determination of the handwriting characteristics [28.9] or for the investigation of cutting force components [28.10],
- an “amplified” elastic structure made up of two perpendicular rings and a shared axis can also be used.

28.1.2. “Square” rings

The range of external “square” shapes having a central circular hole consists of:

- the Hottinger circularly matrixed parallelepiped,
- the rectangular box culvert subjected to modal analysis [28.11],
- “iron machine handle” shape (Peiter, T.U. Saarbrücken).

In ship building, civil engineering, metallurgical industry (especially rolling mills) it is necessary the measurement of very large forces, up to several tens meganewton. A force distribution upon much large area, based on a compact group of plate rings is proposed by the researchers from the Sensor Institute of Anshan, Liaoning province in China.

Multiple plate-ring system of elastic elements [28.12] contains 48 units combined in parallel and in series into one piece of measuring assembly, resulting a compact structure, with lower profile and smaller weight as compared with a classical load cell for 20 MN. It is a flexible and versatile solution than that to replace a 20 MN load cell with ten pieces of 2 MN mounted into a build-up system. The overall dimensions for measuring 20 MN are $(900 \times 200 \times 120) \text{ mm}^3$.

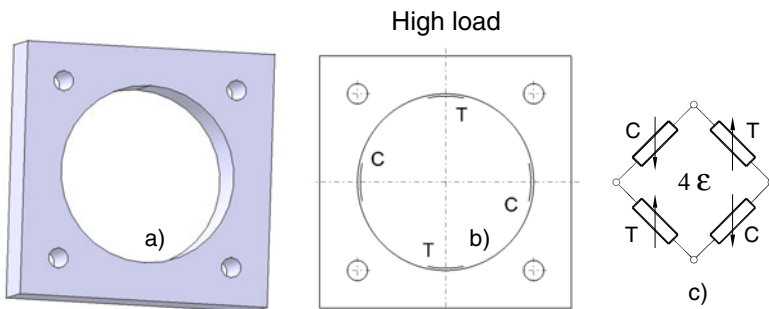


Fig. 28.5 A “square” ring with five holes: a) 3D representation, b) 2D representation with strain gauges positions (T – tension, C – compression), c) Wheatstone bridge

28.1.3. Hexagonal rings

Some typical hexagonal flexible structures are:

- hexagonal ring-dynamometer made of two half-rings and measuring two components of the applied force [28.13],
- hexagonal ring for measuring the car suspension loads [28.14],
- Rohrbach rings [28.15], formerly designed by means of nomograms, now using CAD programs (Fig. 28.6).

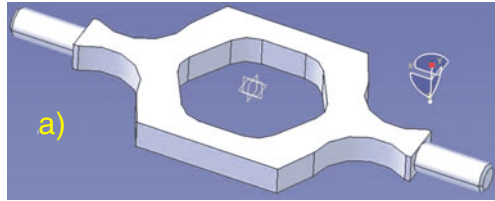
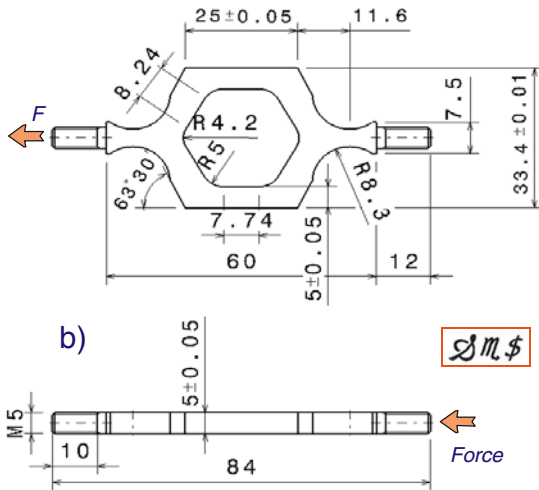


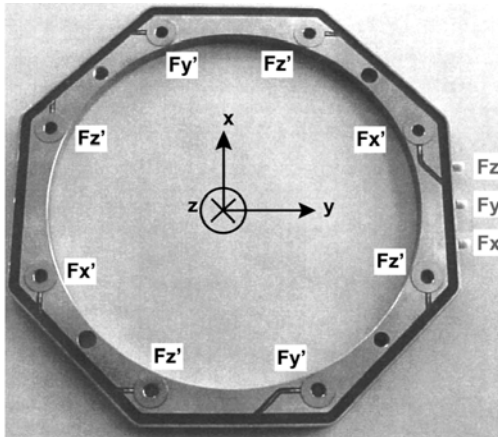
Fig. 28.6 Rohrbach ring designed by Catia program:
 a) 3D representation,
 b) 2D drawing together with technological indications.



This “dual sensing” elastic element may be axially loaded in tension and/or compression.

28.1.4. Octagonal rings

The octagonal shape is very useful for designing multiload component dynamometers [28.16]. The measurement of cutting forces in drilling and allied process is presented in [28.17]. The cutting forces generated in metal have a direct influence on generation heat, tool wear or failure, quality of machined surface and accuracy of the work piece. A milling dynamometer that can measure static and dynamic cutting forces, and torque by using strain gauge and piezoelectric accelerometer has been designed and constructed [28.18]. The orientation of octagonal rings and strain gauge locations has been determined to maximize sensitivity and to minimize cross-sensitivity.



Source: Martin Jun et al.
*International Journal of
 Machine Tools & Manufacture*,
 42 / 2002, p. 742

Reprinted from [28.21],
 copyright 2002,
 with permission from Elsevier

Fig. 28.7 Eight piezoelectric force transducers embedded in an octagonal ring for monitoring and fault diagnosis of machining operations

An extended octagonal ring force transducer mounted on a platform with two wheels for depth control as a real-time texture/compaction test for heavy agricultural machineries is described in [28.19]. An octagonal ring transducer, “glasses”-shaped [28.20], is used to measure both horizontal and vertical force while the agricultural tool is operated at oscillating frequency of (4.5...15.6) Hz and amplitude of (11...26) mm.

Kistler Instrumente AG [28.21] has developed a spindle-integrated piezoelectric force ring, which can provide a comprehensive force measurement based on an octagonal ring. As shown in Figure 28.7, the force ring is composed of eight uniaxial piezoelectric force sensors embedded in an octagonal ring-like frame with a special epoxy. Four of these sensors measure the axial (Z) force component while the other four measure the radial (X and Y) force components. Multiple sensors have been incorporated in each direction to enable the cancellation of the moment effects. The intended force measurement range is (10...3500) N.

28.1.5. Other shapes of bent rings

The bent rings have a lot of various geometrical shapes; after the “evolution” circle – square – hexagon – octagon, here are another examples:

- rhomboid cutting (Perry and Lissner, 1962),
- half-oval, investigated by Lineback by means of finite element and strain gauge methods (Notebook 11/89, pp. 11-15).
- a variety of shapes difficult to express by words, included in Bray's, Malikov's, Norton's and Rohrbach's works.

A special class is represented by the variable section and radial deformation elastic rings, used by the Philips and Elliot companies as well as in [28.22]. The rings having such unconventional outside surfaces ensure the deformation uniformity in the areas of strain gauges emplacement, at the highest level of sensitivity and linearity.

Other particular forms, possible after investigation by numerical methods [28.23], are the chain link, utilized in transportation [28.24] or within the mining equipment [28.25] and buckle (with equivalences at the “macro” level: the hydraulic press frame and the viaduct supporting structure) analyzed by CAOS (computer-aided optimization of shapes) in [28.26].

Starting from the rectangular plate, axially loaded (EE-1), a central hole transforms it in a “square ring” (No. 3 in Figure 28.8) or a “hexagonal ring” (No. 6). Two antisymmetrical slots conduct to an S-shaped frame (No. 5). Two connected holes on the horizontal axis represent a spectacular imagine of the binocular type (No. 4). These are only four of the six elastic models analyzed and compared by Macura and Fiala (Technical University Ostrava, Czech Republic) by photoelasticity and strain gauge methods in order to design high performances transducers [28.27].

Such extensometrical devices are utilized with good results for high force measurements, namely at rolling mills for heavy plates in Vitkovice or at the Ukrainian plant of Kommunarisk.

Axial loading for all these types of elastic elements

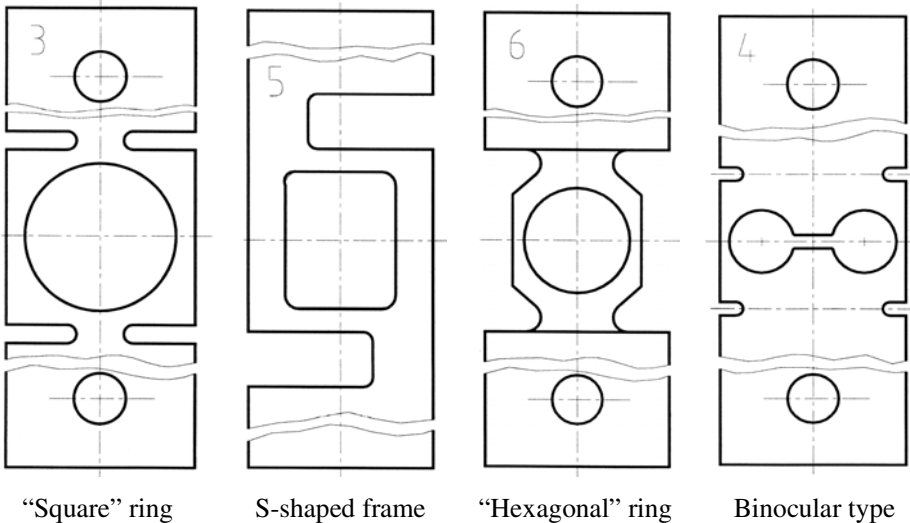


Fig. 28.8 Various “bent rings” to compare with other types of elastic elements (EE)

28.2. “GLASSES”-SHAPED ELASTIC STRUCTURES

A particular case of the axially stressed ring is represented by the elastic structure joining two identical rings to make up “glasses” or “binocular” shapes. In a metal parallelepiped even more holes/slots can be made along on axis, a triad (three elements) example is to be found in [28.28] but we shall restrict to two holes and try to use properly the metallic glasses flexibility as discovered by Douglas C. Hofmann from California Institute of Technology [28.29].

By use of high strength, high elastic strain limit and low Young's modulus of bulk metallic glasses [28.30], strain-sensing devices were practically prepared and the performances of the trial products using the devices were investigated. As a result, a Coriolis mass flowmeter constructed from Ti–Cu-based bulk metallic glass pipe exhibits 28.5 times higher sensitivity than conventional flowmeters made from SUS316 pipe. A pressure sensor using a Zr-based bulk metallic glass diaphragm also exhibits 3.8 times higher sensitivity than the conventional sensor using SUS630 diaphragm. These results for the industrial products made of bulk metallic glasses are promising for future developments as high performance materials and devices.

How to improve the “glasses” sensitivity in the field of force measurement? They can be installed in cantilever [28.31] or can be non-symmetrical, closer to the connecting rod [28.32], but it is more practical the symmetrical structure axially loaded (Fig. 28.2), as presented above.

“Glasses”-shaped elastic elements have the following advantages:

- ease of manufacturing (parallelepipedic block with two transverse holes connected by a slot, such as an “empty dumbbell”),
- high sensitivity due to the bending of elastic element,
- loading capability in both directions using adequate mountings,
- relatively small height,
- good cost / performance ratio.

Four “spectacles” (rectangular, half-octagonal, octagonal, and circular) were investigated in [28.33] by the finite element method. All these models can be coupled with resistive, inductive, capacitive or vibrating wire transducers, as schematically presented in Figure 28.9. Hence 16 possible combinations result.

Several fixed dimensions have been chosen for the “glasses” models: the holes have 40 mm diameter and 70 mm distance between centers, being connected by a 2 mm width slot, while the minimum frame width is 5 mm. The overall dimensions are $(120 \times 50 \times n) \text{ mm}^3$.

Due to the double symmetry, the FEM analysis is enough for one quarter of the elastic structure. Plane stress analysis is performed on n slices of unit thickness. Discretization (Fig. 28.10) contains 63 two-dimensional elements and 87 nodes. (For 3 times finer mesh, the calculation differences are less than 5 %.)

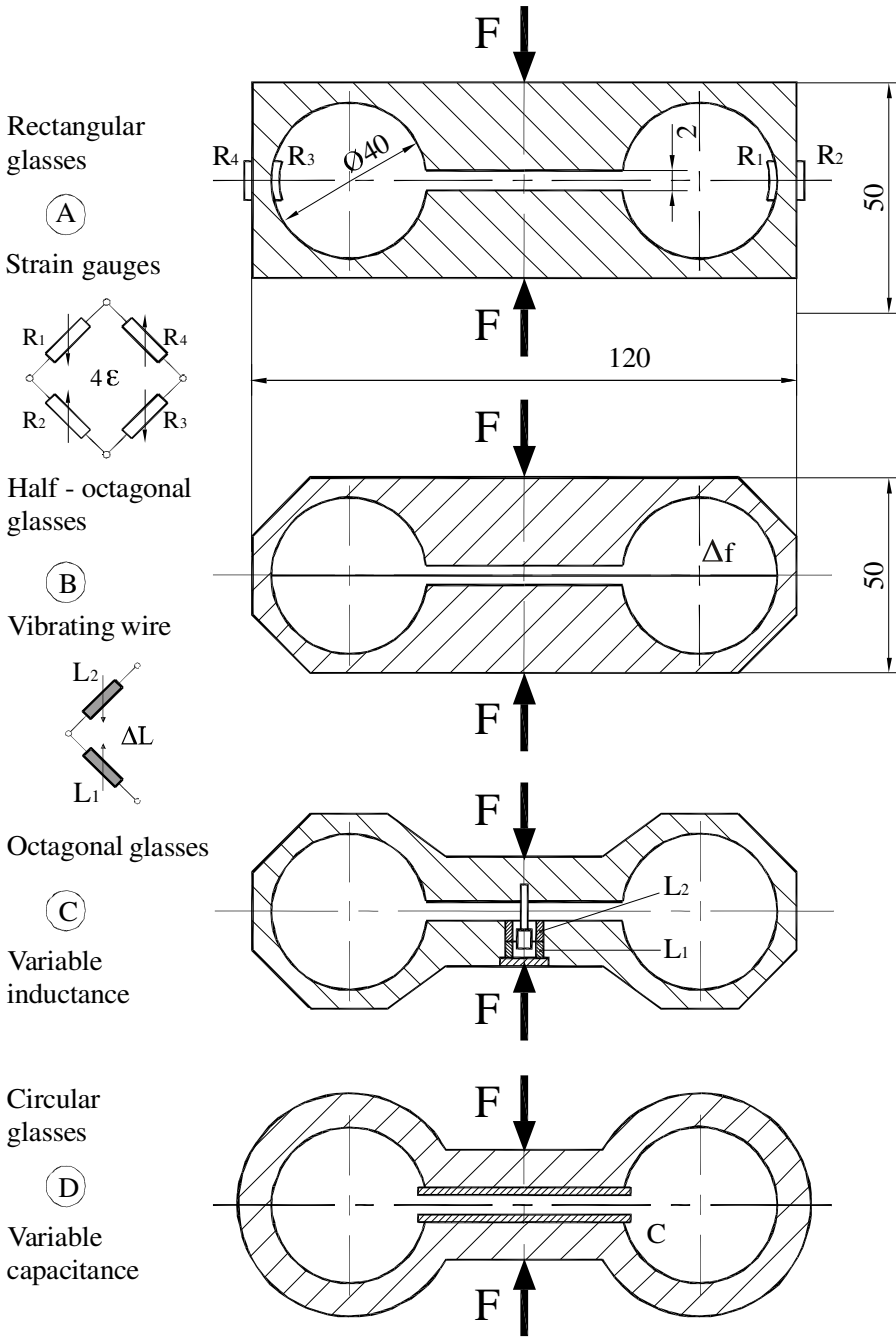


Fig. 28.9 Various types of "spectacles" with different measurement principles

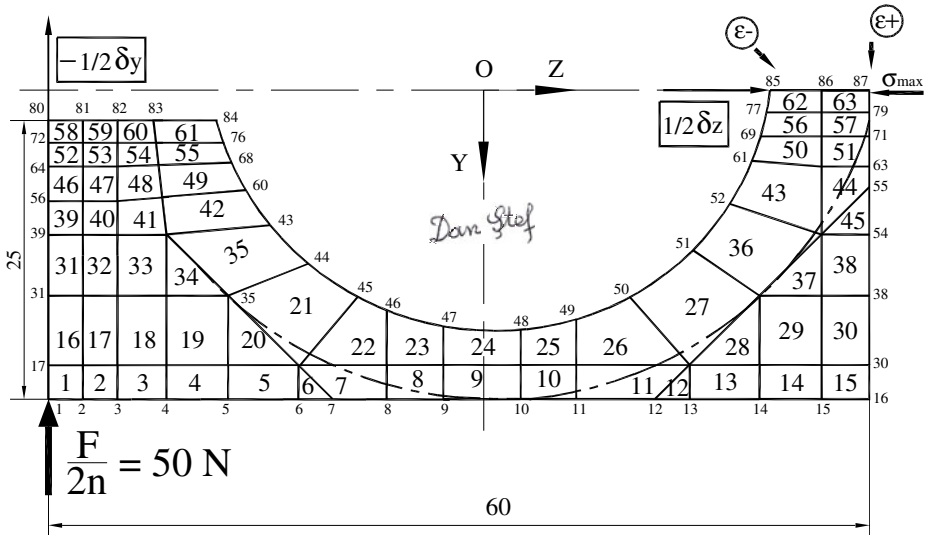


Fig. 28.10 Finite element quarter model for four variants of “spectacles”

A 50 N concentrated load is applied at the central node No. 1. Due to the symmetry of loading, nodes No. 1, 17, 31, 39, 56, 64, 72 and 80 are constrained on the vertical while nodes No. 85, 86, and 87 are guided on the horizontal.

The transition from one glasses model to another is done with minimum changes. Transition from rectangular to (half)octagonal glasses is accomplished by “elimination” of some elements, actually by replacing the steel by another material, with more elastic characteristics. Transition from half-octagonal to circular glasses is done by the slight “displacement” of some nodes.

The calculation was made using the computer program SAP IV which gives as results the node displacements and stresses from finite elements. Taking into account that, in order to convert mechanical strain into electrical signals, different transducers have to be mounted on these “glasses”, it is necessary to further process the data from the listing.

Thus, for inductive and capacitive transducers and, analogously, for mechanical measurement devices with gauges the vertical displacement of mode No. 80 is directly noted.

The effect of the vibrating wire is modeled by a truss or bound-type element E-1, the stiffness constant being calculated using formula (1.1):

$$K_s = \frac{F}{\Delta l} = \dots = \frac{E \cdot A}{l} \tag{28.1}$$

For a steel wire of 0.2 mm diameter and $l = 55$ mm one obtains $K_S = 120$ N/mm. The wire produces a decreasing of 25 % in the horizontal displacement of node No. 85 to which is fixed but, as this applies only to the central "slice", its overall effect on the elastic element can be neglected.

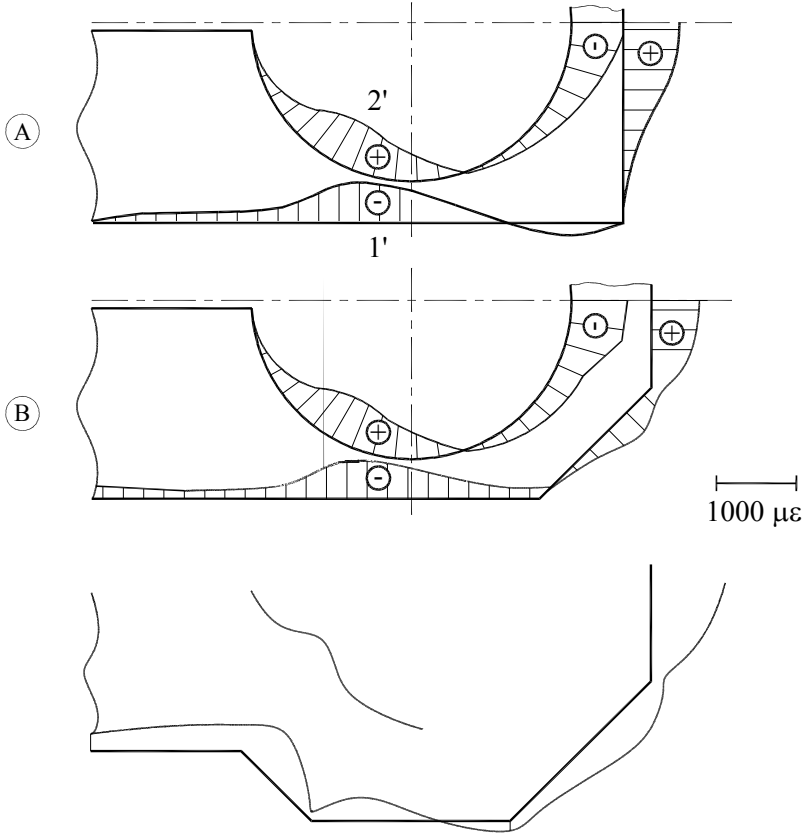
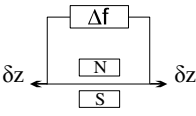
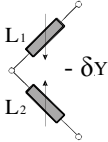
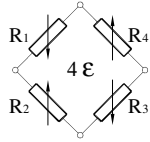


Table 28.1 Sensitivities for different measuring principles on four “glasses” models

Type	Vibrating wire 	Variable inductance 	Strain gauges: Bonded foils 		Check of σ_{max}
Model	δz [μm]	δy [μm]	ϵ_- [$\mu m/m$]	ϵ_+ [$\mu m/m$]	σ [N/mm^2]
A	90.7	170.5	- 923.9	780.2	103.3
B	96.8	197.2	- 784.0	645.7	88.3
C	67.1	486.9	- 1152.5	992.8	127.4
D	93.5	557.7	- 1199.4	984.8	125.1

Strain diagrams on inner and outer sides of the four “glasses” models are presented in Figure 28.11. It can be seen that, going from A to D, as elements are swept out, strains increase and rounding of the elastic element eliminates the discontinuities in the ϵ diagrams of octagonal “glasses”.

The traditional location of resistive strain gauges is in the zone 1-2 where maximum strains occur with relatively constant magnitudes and opposite signs. Another interesting zone (1'-2') also occurs which, passing from A to D, is displaced towards the slot.

Maximum sensitivity is ensured by circular “glasses” while rectangular ones are more easily machined. However, the sensitivity of rectangular “glasses” can be increased choosing the Wheatstone bridge connection with eight strain gauges, using also the zone 1'-2' and carefully locating the strain gauges in the optimal points.

Results of calculation carried out with FEM, for the four “glasses” types and in various measurement techniques, are summarized in Table 28.1. They demonstrate the accuracy and high resolution of the performed analysis.

The following are the conclusions of the comparative study:

- i) The vibrating wire transducer has maximum sensitivity in case B: 96.8 μm displacement of node No. 85, equivalent to a wire strain of 1500 $\mu m/m$.
- ii) The sensitivity of inductive and capacitive transducers increases from type A to type D. For both transducer types displacements should be limited within the linear operating range. At variable capacity type the nonlinearity error is less than 1 % if the plates’ relative displacement is not more than tenth of their initial distance, i.e. 200 μm . This condition is fulfilled for models A and B, while at models C and D the nominal load should be

correspondingly reduced. The differences between the displacements of the ends and the plate center do not exceed 3 % which does not affect the plane capacitor operating. At the variable inductance type (e.g. Enertec and Sangamo-Schlumberger), adoption of differential solution (two coils and plunger-type core) permits linear operation on the entire useful range of displacements (forces, respectively); from this point of view the most sensible is variant D.

- iii) In all four cases, the maximum strains necessary for strain gauges appear in zone 1-2, just at the symmetry axis. Table 28.1 contains the values ε_- (at node No. 85) and ε_+ (at node No. 87). Connection in full Wheatstone bridge ensures a reading of 4ε at the measuring amplifier. Maximum sensitivity is obtained in case D and is $4386.4 \mu\text{m/m}$. Semiconductor strain gauges provide a sensitivity at least one order of magnitude higher.
- iv) The sensitivities of these parametric transducers increase from the rectangular "glasses" to the circular ones, and the strain gauges location on the horizontal axis of every elastic element is confirmed by practice.

It follows that, taking advantage of the modern computer science, one can establish both the optimum shape of the transducer elastic element (circular "glasses") and the most adequate measurement technique (strain gauges or variable inductance). Nominal load on a "slice" of unit thickness is 100 N. Load cells can be obtained for a broad load range by increasing the number of slices n or by decreasing the diameter of the hole. Design can be based on an adequate computer program, establishing the necessary slot width so that it should play the role of an overload stop too. These results have been successfully utilized in the field of hydroelastic force measurements [28.34].

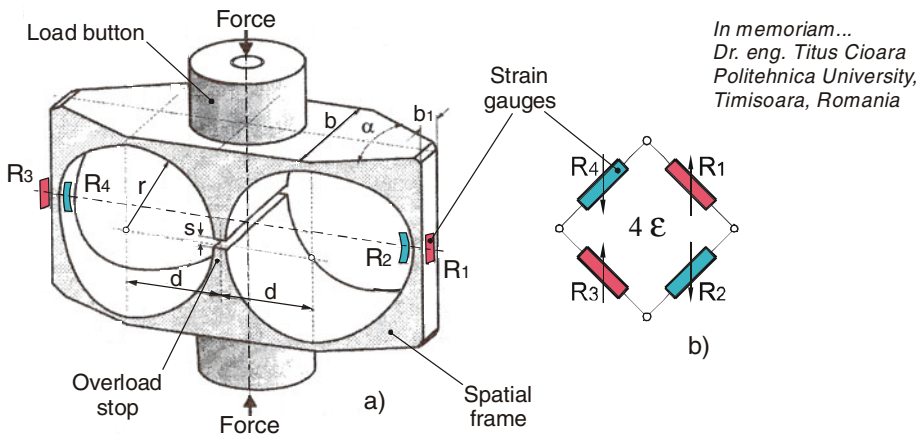


Fig. 28.12 a) "Binocular" weighing cell as an elastic frame with complex geometry and b) its strain gauges connection in full Wheatstone bridge

The plane elastic element of constant thickness (see Figures 28.2A and 28.11A) may be spatially modeled in order to ensure the structural stability of a weighing cell [28.35].

A new elastic frame, presented in Figure 28.12a, consists of a metallic plate in which two holes of the same diameter $2r$ and two symmetric lateral bevels are manufactured (angle α). In case of an accidental overload, the separation gap s between the two holes is cancelled, and the overload will be directly taken over, in this way the force transducer being protected. Four strain gauges are connected in Wheatstone bridge as illustrated in Figure 28.12b.

28.3. MULTIPLE “GLASSES”-SHAPED ELASTIC ELEMENTS

A multicomponent force transducer, consisting of multiple “glasses”-shaped sensing elements (Fig. 28.13a), is described in [28.36].

The rated capacity of the moment components over force components is significantly larger due to the higher rigidity of the binocular type structure compared with the parallel plate structure. The material used is Al 2024-T351, which has an elastic modulus of 68.6 GPa and a Poisson’s ratio of 0.3. The finite element mesh utilized the ANSYS program and an 8-node isoparametric plane stress element. The L16 orthogonal array was used and ANOVA (*analysis of variance*) was made in order to choose the best positions for strain gauges.

Strain gauges (model MM-N2A-13-T001N350, Micro-Measurements, a division of Vishay Precision Group, Inc., Raleigh, NC, USA) were attached on such positions of the cross-shaped beams (Fig. 28.13b) to give both maximum strain and offset coupling strain. The total number of selected strain gauges is 24 to comprise the six full Wheatstone bridge circuits for the three force and three moment components, as indicated in the associated table (Fig. 28.13c). Test results show that the fabricated sensor with maximum capacities of 196 N in forces and 19.6 N·m in moments has a coupling error less than 3 % full scale.

The finite element method, the most versatile technique of structural analysis, permits both the global approach of the problem and the detailed investigation in any point of the structure; it is a rapid computation technique allowing a graphical and/or tabular presentation of results. The method permits the parametric determination of design characteristics and the establishment of the optimal shape of the transducer elastic body. Moreover, since the design stage, simple or combined influences can be studied on sets of configurations, resulting from machining, transducer location, load application, etc. This multidisciplinary method can help to build new types of sensing elements, to build high sensitivity transducers for measuring of force and its associated mechanical quantities.

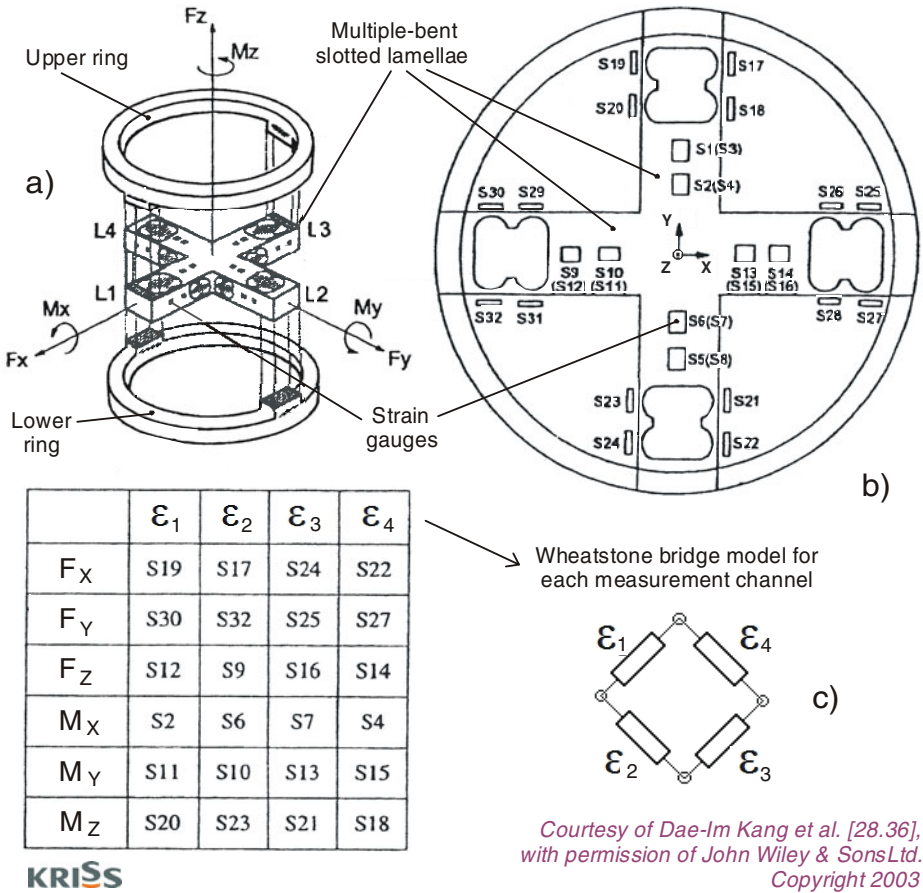


Fig. 28.13 a) General view of a cruciform elastic element made by four binoculars, b) strain gauges positioning on the cross-shaped slotted beams and c) their Wheatstone bridge connection for six force / torque components determination

REFERENCES

1. Pierson, J.: Load/Force Cells. How they work (July 21, 2008), <http://www.sensorland.com/How/Page005.html>
2. Chlumský, M., Šimonovský, V.: Force and mechanical testings of materials. Edice Základy Metrologie svazek 5, VÚNM, Prague (1984) (in Czech)
3. Nawwar, A.M., Godon, A., Roots, T., Howard, D.: Development of a measuring system for segmented ship models. *Experimental Mechanics* 29(2), 101–108 (1989)
4. Präzisions-Kraftaufnehmer zur statischen und dynamischen Messung von Zug- und Druckkräften. Vorläufiges Datenblatt, Elan-Schaltelemente – Kurt Maecker GmbH, Neuss (D) (1989)
5. Ștefănescu, D.M.: Electrotensometric transducer for measuring mass up to 10 kg. *Instrumentația (Măsurări – Automatizări – Acționări – Robotică)* 6(1), 6 (1996)

6. Watson, A.: Wind-induced forces in the near-surface lateral roots of radiata pine. *Forest Ecology and Management* (135), 133–142 (2000)
7. Pșegalinschi, A., Manolache, P., Marton, C.: Strain gauge transducers for studying the shock effects on the tug boat hook. In: *Proc. 4th National Symposium of Tensometry, Brașov, September 24-27, vol. I, pp. 191–194 (1986) (in Romanian)*
8. Ștefănescu, D.M.: Methods and means for measuring the extension of the cables. *Metrologia aplicată XXXV(4)*, 146–151 (1985)
9. Sandu, M., Ștefănescu, D.M., Sandu, A.: Table dynamométrique à sensibilité augmentée destinée à l'analyse de l'écriture en psychiatrie. In: *Proc. 4th National Symposium of Tensometry, Brașov, September 24-27, vol. III, pp. 323–328 (1986)*
10. Zgură, G., Ispas, C.: Design of a dynamometer for studying the three components of the turning forces. *Studii și cercetări de mecanică aplicată* 30(1), 237–250 (1971) (in Romanian)
11. Frederick, G.R., Tarhini, K.M.: Model analysis of box culverts subjected to highway loading. *Experimental Mechanics* 29(2), 183–187 (1989)
12. Zhang, S., Chen, W.: Development of the integrated multiple plate-ring type load cell with large capacity. In: Shi, C., Zhang, Y. (eds.) *Acta APMF 1996 – Present Situation and Progress of Measurement on Mass and Force, Beijing, China, August 20-22, pp. 151–153 (1996)*
13. Vermeyen, L.: Ringdynamometers. *Revue M Tijdschrift* 13(1), 37–45 (1967)
14. Chiriacescu, S., Balcu, I., Dancășiu, M., Lőx, A.: Force measurements for car suspensions identification. In: *Proc. 3rd National Symp. of Tensometry, Timișoara, September 28 - October 1, vol. I, pp. 35–40 (1983)*
15. Rohrbach, C.: *Handbuch für elektrisches Messen mechanischer Grössen. VDI-Verlag, Düsseldorf (1967)*
16. Kroencke, M., Hull, M.L.: A method for designing multiload component dynamometers incorporating octagonal strain rings. *Experimental Mechanics* 29(2), 195–204 (1989)
17. Karabay, S.: Analysis of drill dynamometer with octagonal ring type transducers for monitoring of cutting forces in drilling and allied process. *Materials & Design* 28(2), 673–685 (2007)
18. Yaldız, S., Ünsaçar, F., Sağlam, F., Işık, H.: Design, development and testing of a four-component milling dynamometer for the measurement of cutting force and torque. *Mechanical Systems and Signal Processing* 21(3), 1499–1511 (2007)
19. Mouazen, A.M., Durmont, K., Maertens, K., Ramon, H.: Two-dimensional prediction of spatial variation in top soil compaction of a sandy loam field-based on measured horizontal force of compaction sensor, cutting depth and moisture content. *Soil & Tillage Research* (74), 91–102 (2003)
20. Niyamapa, T., Salokhe, V.M.: Force and pressure distribution under vibratory tillage tool. *Journal of Terramechanics* (37), 139–150 (2000)
21. Jun, M.B., Ozdoganlar, O.B., de Vor, R.E., Kapoor, S.G., Kirchheim, A., Schaffner, G.: Evaluation of a spindle-based force sensor for monitoring and fault diagnosis of machining operations. *International Journal of Machine Tools & Manufacture* (42), 741–751 (2002)

22. Sandu, M., Mincă, I., Sandu, A.: Calculus of a ring with variable thickness for force transducers. *Construcția de mașini* 50(8), 36–38 (1998) (in Romanian)
23. Mattheck, C., Burkhardt, S.: A new method of structural shape optimization based on biological growth. *International Journal of Fatigue* 12(3), 185–190 (1990)
24. Boleanțu, L., Babeu, T.: Extensometers for machinery parts. In: Proc. 1st National Symposium of Tensometry, Iași, Romania, April 25-29, vol. III, pp. 17–21 (1977) (in Romanian)
25. Constantinescu, I., Elczner, G.: Strain gauge transducers for measurement in the field of mining equipments. In: Proc. 2nd National Symposium of Tensometry, Cluj-Napoca, June 11-14, vol. I, pp. 347–354 (1980) (in Romanian)
26. Rasmussen, J., Lund, E., Birker, T., Olhoff, N.: The CAOS (Computer-Aided Optimization of Shapes) System. In: *Int'l Series of Numerical Mathematics*, vol. 110 (Structures), pp. 75–96. Birkhäuser Verlag, Basel, CH (1993)
27. Macura, P., Fiala, A.: Design of extensometrical transducers. In: Proc. XVIth IMEKO World Congress Measurement Now and in the Future, Vienna, Austria, September 25-28, vol. 3, pp. 421–424 (2000)
28. Sensoren: Kraft- und Miniaturaufnehmer, Wägezellen, Mehrkomponenten, Dehnung, Drucksensoren. *Qualität und Leistung*. Lorenz Meßtechnik GmbH, Alfdorf (D) (1995)
29. Wood, J.: Adding a new flexibility to metallic glasses – Mechanical behavior. *Materials Today* (March 7, 2008)
30. Nishiyama, N., Amiya, K., Inoue, A.: Recent progress of bulk metallic glasses for strain-sensing devices. *Materials Science and Engineering: A* 449-451, 79–83 (2007)
31. Lineback, D.: A transducer-based stress analysis project. In: *Experimental Stress Analysis Notebook*, vol. 2, pp. 8–15. Measurements Group, Inc., Raleigh (1986)
32. Hwang, J.S., Choi, B.K., Chang, T.-C.: Shape design sensitivity and optimization. In: Haug, E.J. (ed.) *Mechanics of Structures and Machines*. Library of Congress Catalog 72-626950, vol. 11(2), pp. 111–129 (1997)
33. Ștefănescu, D.M.: Comparative study of the sensitivity of various measurement techniques on “glasses”-shaped elastic element models analysed by FEM. In: Wieringa, H. (ed.) *Experimental Stress Analysis*, pp. 291–300. Martinus Nijhoff Publishers, Dordrecht (1986)
34. Rusu, I.I.: On hydroelastic force measurement using a strain gauged transducer with ring elastic element. In: Proc. 7th National Symposium of Tensometry, Suceava, October 17-19, vol. I, pp. 99–104 (1996) (in Romanian)
35. Cioară, T.G.: *Experimental Techniques in Mechanical Engineering. Sensors and Transducers*. Editura Politehnica, Timișoara (1999) (in Romanian)
36. Kang, D.I., Kim, J.H., Park, Y.K.: Development of a binocular type six-component load cell. *Experimental Techniques*, 21–25 (January-February 2003)

Note for reference 36: Permission to use, together with usual acknowledgements, has been granted on August 16, 2010 by Verity Butler, Permissions Assistant, John Wiley & Sons Ltd. Thanks for this courtesy!

Chapter 29

BENT MEMBRANES

29.1. VARIOUS TYPES OF BENT MEMBRANES

Membranes, diaphragms or plates are multifunctional elastic elements suited for measuring both concentrated force and distributed pressure.

Figure 29.1 presents a generic load cell consisting of a “piston” (boss attached to the diaphragm center) under which the fluid is seated, the applied load producing a force-to-fluid transformation, measuring the pressure by a piezoresistive silicon “cork”.

Experimental results obtained at MESA Research Institute, University of Twente Enschede, The Netherlands [29.1], with loads up to 1000 kg (10 kN), show good repeatability and are in close agreement both with analytical and numerical calculations (fluid element 79 within ANSYS 5.3).

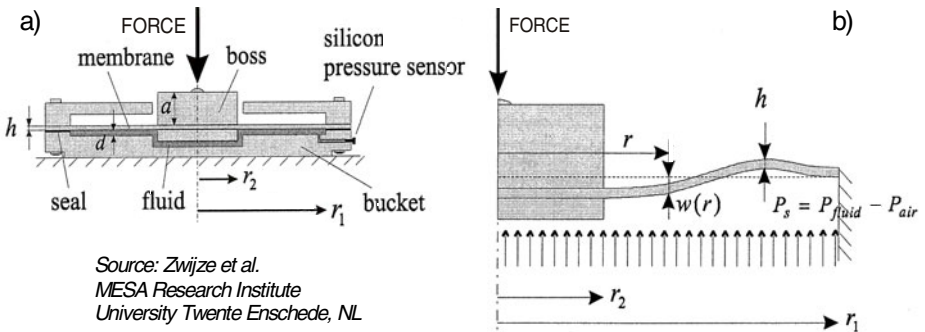
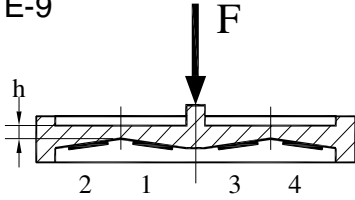


Fig. 29.1 a) Layout of the force-to-fluid pressure load cell. The force presses the boss downward and the membrane compresses the fluid in the bucket. b) One can see the so-called S-shaped deformation. Function $w(r)$ represents the membrane deflection at position r (radius near the “inflection” circle)

E-9



Load range [N]: $5 \times 10^{-2} \dots 10^6$

Mechanical sensitivity [$\mu\text{m}/\text{m}$]: $\frac{1.24 F}{\pi E h_{\text{med}}^2}$

Electrical sensitivity [ϵ]: 4

Personal model:
Diaphragm
Membrane

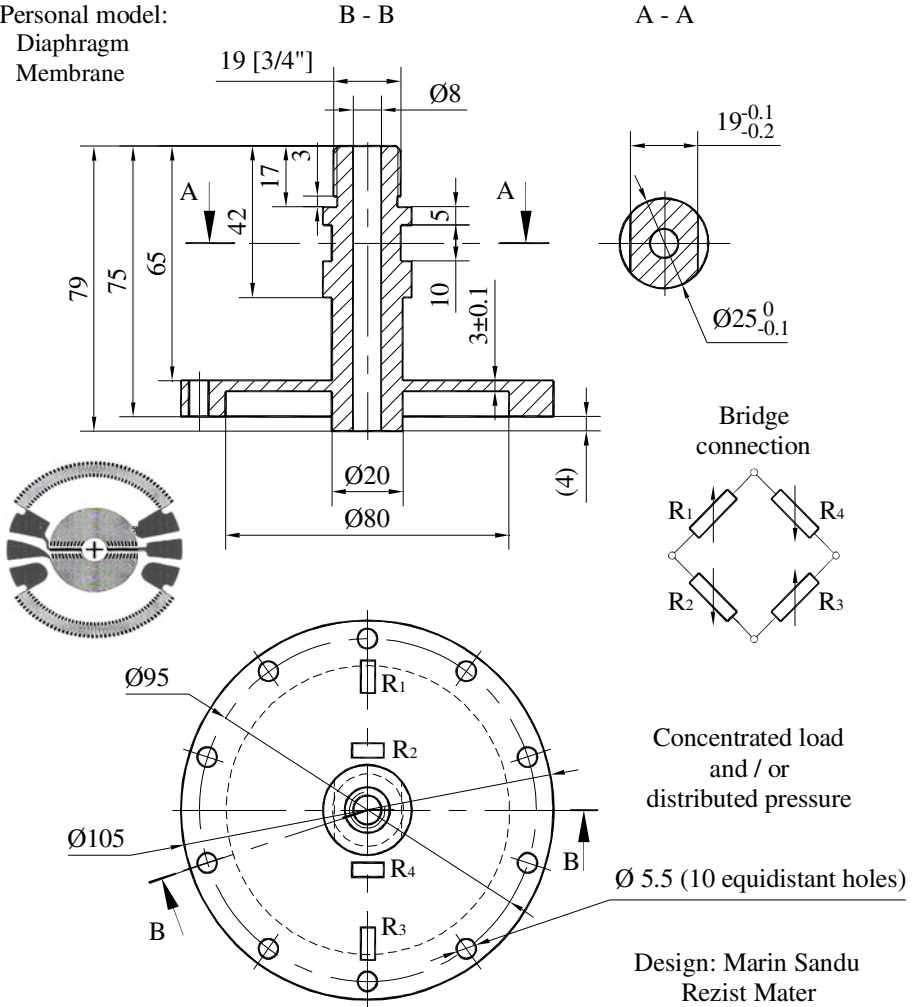


Fig. 29.2 Strain gauged elastic elements of type IX for concentrated force and/or distributed pressure – double functionality of membrane type transducers

The bent membrane is a usually circular elastic plate, with a constant or variable thickness, embedded on its contour (Fig. 29.2, top). The elastic element has a low height and can be easily made by lathing in the “metal period” or by silicon micromachining (Tuft, Chapman & Long, 1962). The membrane profiling / shaping enables the four strain gauges to be active: R1 and R3 are extended while R2 and R4 are shortened. The influence of the transversal stress is practically negligible, because all the strain gauges are radially located.

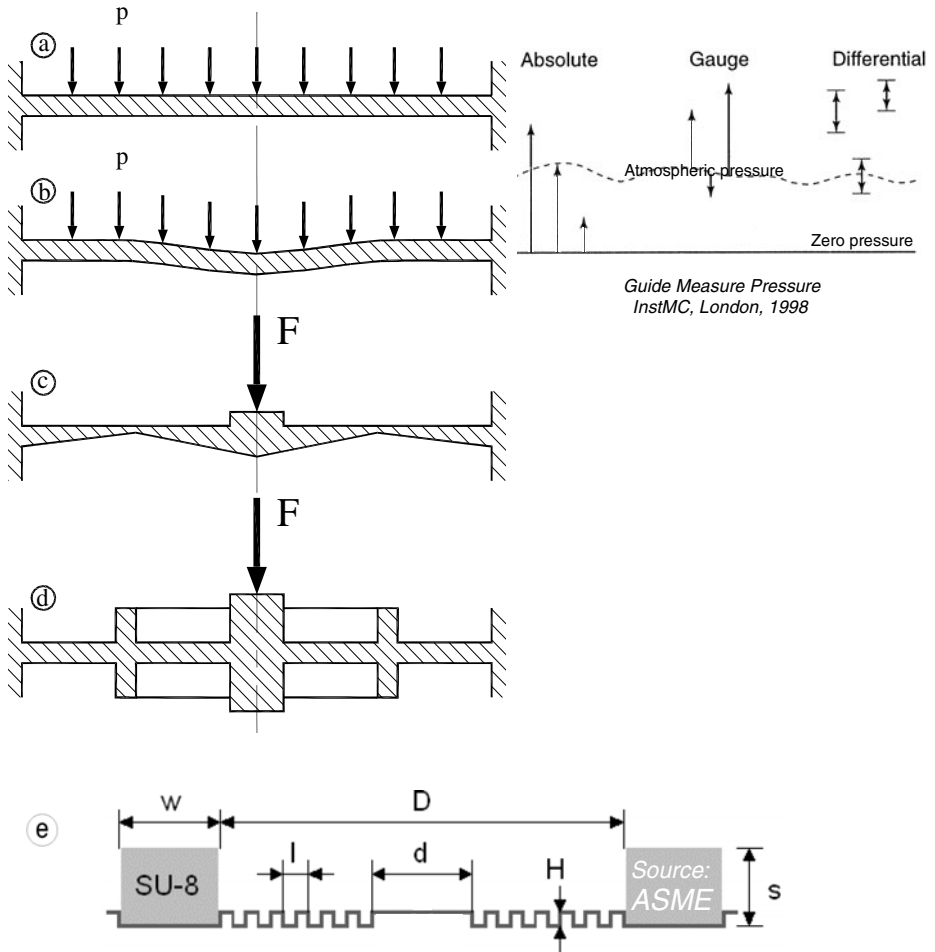


Fig. 29.3 Schematic cross-sectional views for various type of circular membranes for measuring concentrated force F and distributed pressure p : a) plane (constant thickness), b) shallow, c) profiled, d) ribbed, and e) corrugated

Due to the low height/diameter ratio, circular membrane gauges are the most adequate for civil engineering applications [29.2]. On one side, the surface of the pressure sensing membrane must be sufficient large so the local differences in the soil composition not to matter. On the other side, the gauge should not modify the pressure distribution within the soil. Gauges with the entire membrane sensible give larger errors than those sensible only at the center because of the nonuniform applied loading. Hence, as a function of the application envisaged, the membrane optimum diameter should be between 50 mm and 250 mm.

Five various membrane types utilized as flexible elements for pressure gauges are shown in Figure 29.3. They differ by the displacement at the center which can be calculated analytically and numerically or can be measured using inductive transducers or optical methods.

When strain gauges are utilized, they are bonded directly of the inner face of the simple, i.e. plane and with constant thickness (Fig. 29.3a), shallow (Fig. 29.3b) or profiled membranes (Fig. 29.3c), the latter giving the maximum measurement sensitivity.

A major interest presents the ribbed membranes (Fig. 29.3d) which are the stiffest from all. These special diaphragms can be used in three different types of force transducers, based on strain gauges, variable inductances or vibrating wires.

A research team from Georgia Institute of Technology, Atlanta, and BioTechPlex Corporation, San Diego, CA, developed a reusable silicon micro-mold based microfabrication process [29.3]. They manufactured a triple layer of Parylene-Chromium-Parylene, optically reflective, as a corrugated diaphragm (Fig. 29.3e) for fiber-optic-linked pressure sensing (FOLPS) in ultra-low pressure range (± 10 mm H₂O). The principal design parameters are the following: D – diaphragm diameter, d – diameter of the flat center, h – diaphragm thickness, H – corrugation depth, l – corrugation pitch, s – SU-8 thickness, and w – SU-8 width. The silicon micromolding is combined with a chip-level tube bonding method to mount the Parylene diaphragm on to the end of a tube before the releasing step. The sensors with 1.0 mm diameter deflect by up to 6 μ m at the maximum applied pressure.

Figure 29.4 presents three variants of Wheatstone bridges, using 4, 8 or 16 strain gauges, respectively. These progressive solutions for strain gauges emplacement are recommended for all axisymmetric elastic elements in order to improve their measurement sensivities.

Here is a membrane classification according to their shape elementariness (opposite to their complexity): circle – oval, square – rectangle, combined shapes. For clarification they will be separately presented in the following subchapters.

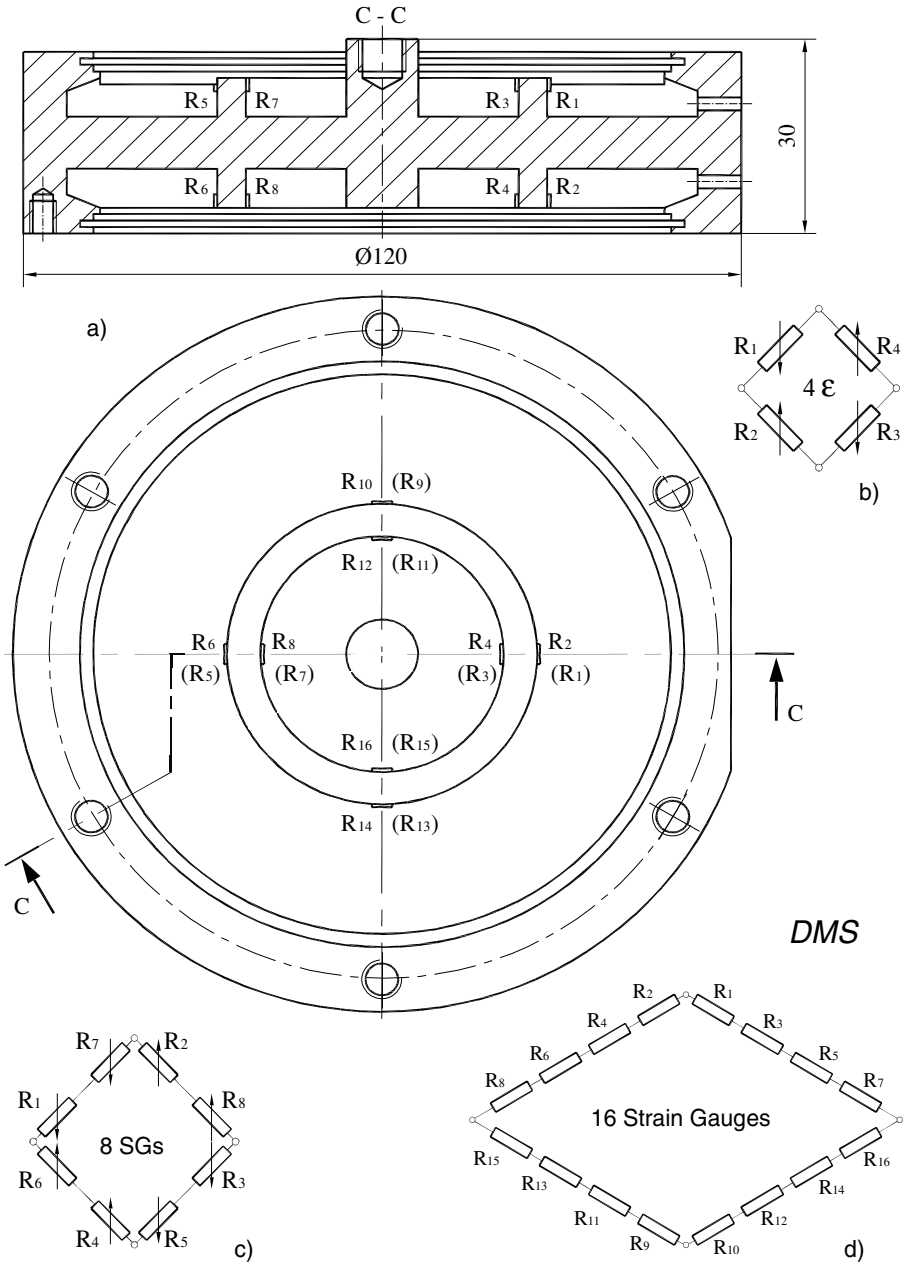


Fig. 29.4 Cross-sectional and bottom view for a circularly ribbed membrane (a). Wheatstone bridge connections for progressive increasing of the tensometric sensitivity: 4 strain gauges (b), 8 strain gauges (c) and 16 strain gauges (d).

29.2. CIRCULAR MEMBRANES

There are similarities between the bars embedded at both ends, stressed in the middle (EE-5) and circular membranes (Eurosensor) in the sense that by rotating such a bar round its short symmetry axis, a circular plate is obtained as axisymmetrical structure. The procedures for increasing sensitivity by geometrical optimization are the same in both situations [29.4].

A “parallel” application with that described in Chapter 25 [29.5] is the one depicted in [29.6]: a weighing installation where the load is transmitted through a horizontal ring pushing on a circular plate leaning against the contour (Fig. 29.5). The replacement of leaning with “flushing” leads to the deformation of the membrane radial section into an S shape.

Starting from the classical membrane (Fig. 29.6a), the intention is to obtain a way of a more advantageous elastic deformation in order to obtain as big as possible $\pm \varepsilon$ values.

The membrane with a central boss (Fig. 29.6b) produces a “narrow” bipolarity, implying a very precise positioning of the shortest strain gauges or piezoresistances.

The clearest “demarcation” of the sensitivity areas $\pm \varepsilon$, a kind of “step-functions” on each side of a zero/reference line, can be made by the membrane profiling (Fig. 29.6c), a brilliant idea belonging to Rohrbach and Andreae [29.7]. Bethe (T.U. Braunschweig) suggests the tandem use face to face of these profile membranes. C-20 load cell (Hottinger) carries on this profiling so that the tensometric force transducer assembly with built-in electronics has the shape of a classic weight [29.8].

Apart sections are to be found in some patents, as for instance D.P. 1252937. The optimization of a variable thickness plate with 128 and 3200, respectively, finite elements (closer to the “continuous environment”) is presented by Rozvany in [29.9]. The author’s contribution in the field of profiled membranes has been firstly presented in [29.10].

Comparing different elastic structures for pressure measurement, the deflection of a thin membrane is much larger than that of a thick diaphragm or a simply supported disc. For all these types of membranes the axial loading could be also in the opposite direction producing “reversing” deformations and “mirror” strain diagrams.

Gauge factors k are much less for metal than for semiconductors but the disadvantage of silicon strain gauges is their high sensitivity to temperature changes. Under the assumption that the membrane need to be much thicker than the metallic strain gauge, the detailed design is a function of the smallest critical dimensions and the thinnest homogenous metal microstructures that can be fabricated [29.11].

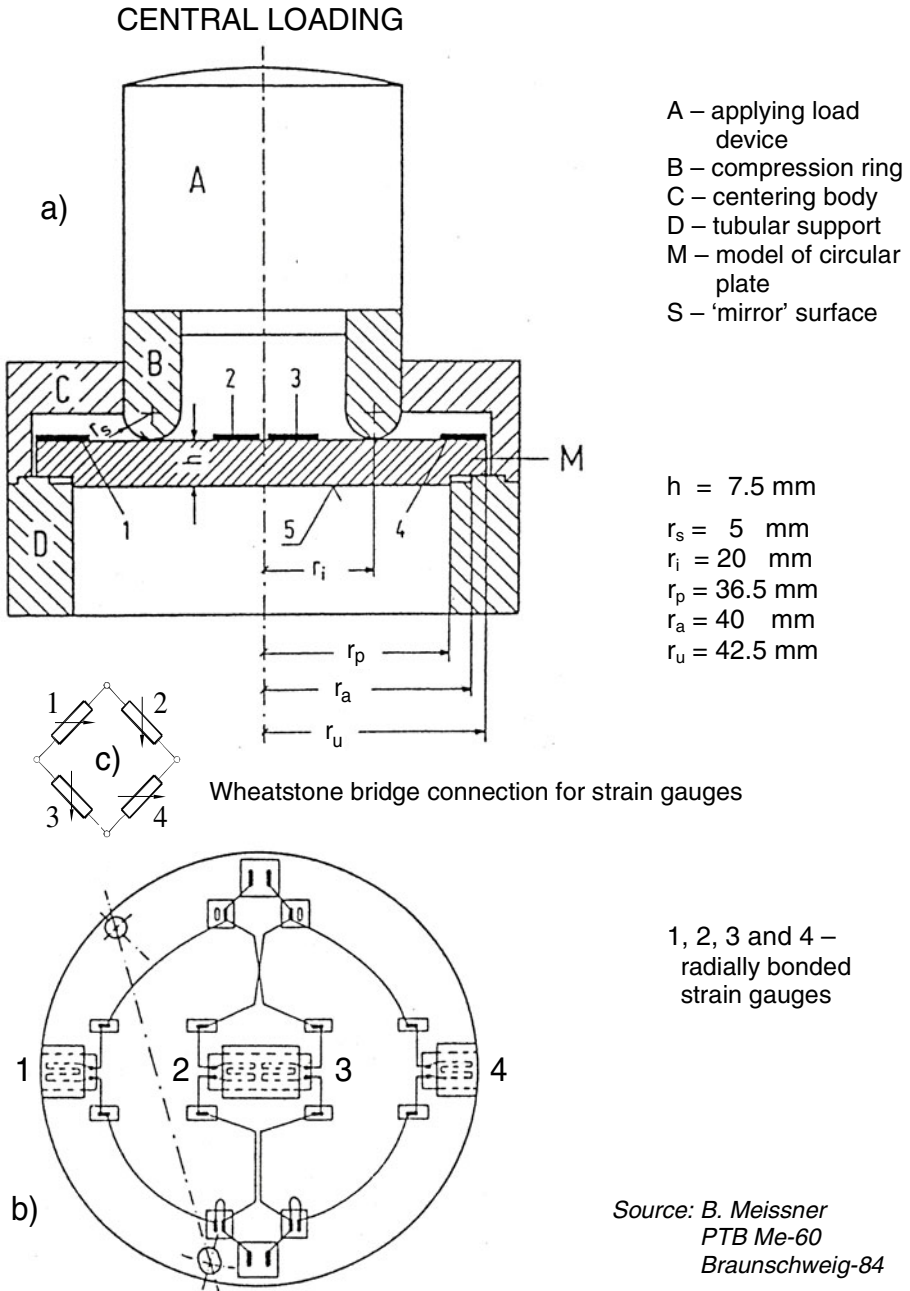


Fig. 29.5 a) Typical assembly of force transducer based on circular membrane. b) Top view of strain gauge positions. c) Wheatstone bridge connection for radial strain gauges

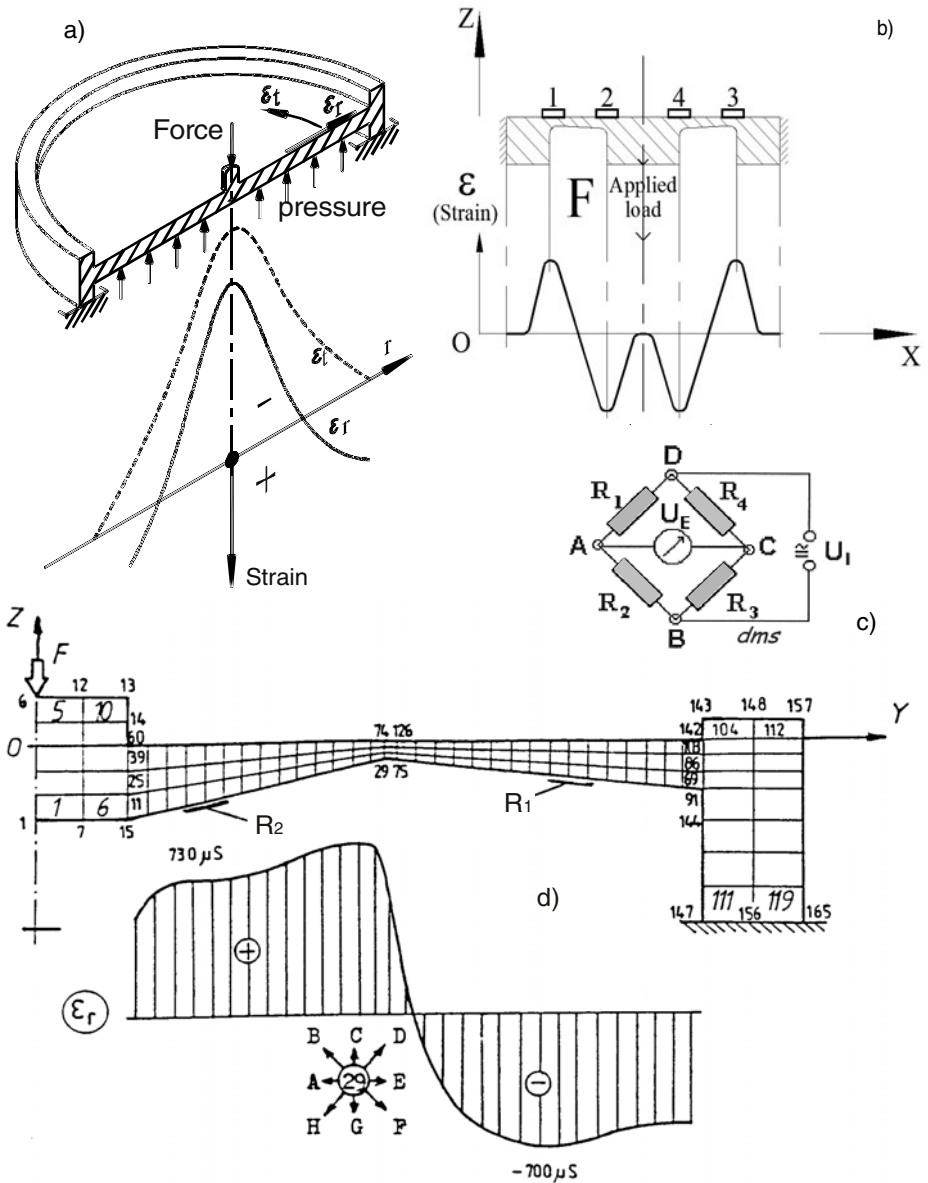


Fig. 29.6 Stages for increasing tensometric sensitivity of circular membranes: a) plane diaphragm with radial and tangential strain gauges (see Figure 29.2, bottom), b) central bossed plate, bipolar strain “pulses” ϵ_r for strain gauges in Wheatstone bridge (c), and d) membrane “profilation” and its “step-functions” for the best strain gauging procedure

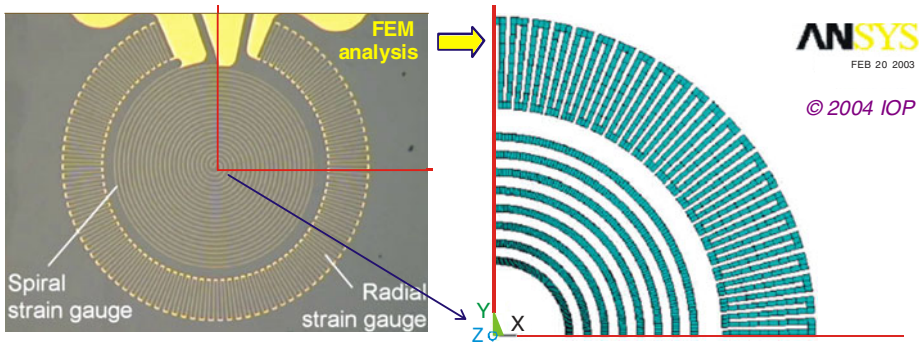
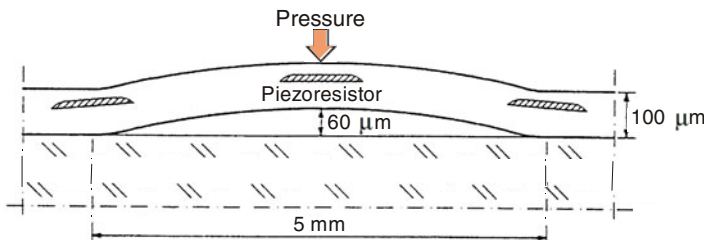


Fig. 29.7 An improved golden spiral and radial rosette made by Schomburg *et al*, Institut für Mikrostrukturtechnik, Forschungszentrum Karlsruhe [29.11]

The resistivity of a metal is small resulting in the need for long and narrow strain gauges. A perfect understanding of the strain distribution on the entire microdiaphragm ($\varnothing 2$) is necessary in order to cover a considerable area with piezoresistive SGs. An improved geometry is based on finite element analysis (Fig. 29.7); the new sensing grid (wire section: $3 \mu\text{m}$ wide and 200 nm thick) is much longer than that of the circular rosette presented in Figure 29.2.

An elegant approach for miniaturizing pressure diaphragm, developed by Robert Bosch GmbH, takes advantage of the nitrogen fireable dielectrics [29.12]. A print-and-fire sequence of pastes on alumina substrate conducts to a self-supporting dome-shaped diaphragm (5 mm diameter, $60 \dots 90 \mu\text{m}$ thick) having embedded four thick film piezoresistors (Fig. 29.8). The extra area of alumina substrate is available for the electronic integrated circuit.

Circular membranes with various concavities or convexities are realized through casting or cupping [29.13]. To the same purpose of the constant thickness circular membrane sensitivity increase, their curvature solution was applied with slight S-shaping in the sense of a more definite separation of the specific deformation areas $\pm \epsilon$. Thus $100 \mu\text{m}$ thick coating is achieved, with an initial center “displacement” of $60 \mu\text{m}$ [29.14].



Source:
Robert Bosch GmbH

Fig. 29.8 Integrated pressure transducer including a circular dome acting as diaphragm

The Hottinger Company delivers such “sensorized” elastic elements [29.15]. Various applications are presented in “Messtechnische Briefe HBM” [No. 1/82, p. 15 and No. 1/94, p.4] and in “Reports in Applied Measurement”: No. 1/87, p. 7 and No. 1/95, p. 2 (a tensometric device for the fetus extraction at delivery).

Combined (hybrid) techniques have been applied over these elastic elements: finite element analysis together with digital photoelasticity [29.16], and Moiré interferometry, respectively [29.17]. The circular membranes coupled with silicon strain gauges, have attained the apogee within the instrumentation for the Apollo space program. A first constructive optimization was made by Wall [29.18] giving up the constant thickness in the border areas to make the ε diagram uniform so that all the strain gauges be equally active.

For the circular plates there is a well established microelectronic technology for the development of radial and circumferential strain gauges, within a perfectly balanced and compensated Wheatstone bridge topology/configuration [29.19]. Considered flat structures, however they have a lid shape (with a role of protection housing), made by cupping or lathing with fine connections, where the accuracy of machining is essential for the transducer performances [29.20]. In a consulting study for Rohrbach it was demonstrated that the membrane thinning by 5 % results in a 10 % increase of the miniature transducer sensitivity [29.21].

Other axisymmetrical structures closer to the circular membranes and more or less utilized as elastic elements for force/pressure transducers are:

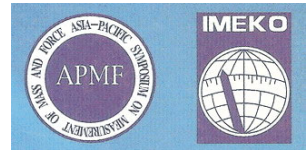
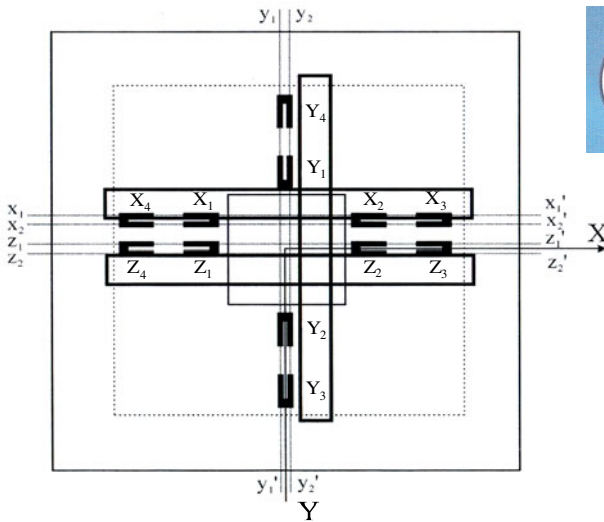
- flanged membrane, that is a flange ended curved membrane,
- two Belleville springs mounted as opposite plates,
- circularly (not radially) ribbed membranes, because the increasing of sensitivity not of rigidity is intended [29.22],
- curved triangular plate group in a compensated assembling, which is a “discrete” structure of clutching, different from the continuous disc with sophisticated cuttings.

An example from “Experimental Mechanics”: a sensitive plate for force and impact duration measuring in elasto-plastic bodies [29.23] with a tri-dimensional diagram of sensitivity. A personal achievement is the circular membrane that can be loaded with concentrated force and/or distributed pressure (Fig. 29.2, bottom). The planar plates have the property to sense both pressure p (force distributed on the whole surface) and concentrated force F (in the plate center). Therefore, a unique “dual” transducer design, easy to construct and based on a circular membrane with a central protuberance is possible, ensuring a “double” function: the four Wheatstone bridged strain gauges, emplaced on the opposite face to the pressure application, sensing the pressure and/or the compression force.

29.3. SQUARE MEMBRANES

A lot of production technologies, different measurement techniques, structural optimization methods and various applications for square membranes are presented in the next paragraphs.

A square membrane sized (2.4×2.4) mm² with a force range of ± 0.1 to ± 5 N for three components (one normal and two tangential and perpendicular on each other) is presented in [29.24]. An epoxy mesa (SU-8) was built-up on the silicon top to convert the applied force into distributed stress. Finally, the transducer membrane was fabricated by bulk-micromachining based on the anisotropic etching of the silicon. Optimal locations of piezoresistors (Fig. 29.9) were determined by the strain distribution obtained from finite element analysis. Piezoresistors were embedded in silicon using ion-implantation technique.



Source:
 Jong-Ho KIM
 KRISS – Korea
 APMF 2003
 Shanghai, China

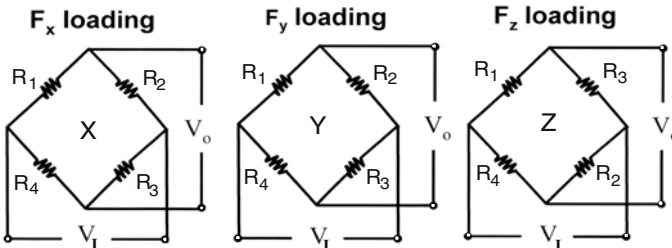


Fig. 29.9 Bulk-micromachined square membrane for three-component force transducer with optimal locations for strain gauges and associated Wheatstone bridge connections (using the American symbolization for piezoresistors)

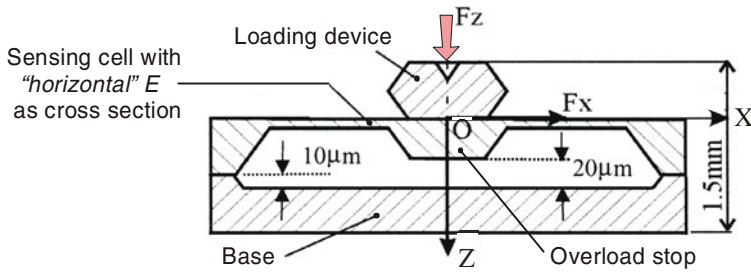


Fig. 29.10 E-shaped square membrane section of a piezoresistive tactile transducer

An integrated three-dimensional tactile sensor with robust MEMS structure and soft contact surface, suitable for robotic applications, has a maximum force range of 50 N in the vertical direction and 610 N in the X and Y horizontal directions [29.25]. The tactile sensor includes 4×8 sensing cells, each exhibiting an independent, linear response to the three components of applied forces. The sensing cell has an E-shaped square membrane cross section (Fig. 29.10), fabricated by silicon bulk-micromachining (Chinese Academy of Sciences from Hong Kong).

Two piezoresistive strain sensor membranes with improved sensitivity were successfully fabricated by using MEMS technology [29.26]. In the two sensor designs (single strip and multi-strip), the sensing element was patterned over a thin $3 \mu\text{m}$ $\text{Si}_3\text{N}_4 / \text{SiO}_2$ layer. Doped n-polysilicon was used to sense the strain changes. The silicon beneath the $\text{Si}_3\text{N}_4 / \text{SiO}_2$ layer was etched to form a membrane with an area of $(1000 \times 1000) \mu\text{m}^2$. The overall sensor area was $(10 \times 10) \text{mm}^2$. The values of nominal resistance of the single strip sensor and the multi-strip sensor were 4.6 and 8.6 k Ω , respectively. The gauge factor was as high as 15 (bending) and 13 (tension) for the single strip sensor, and 4 (bending) and 21 (tension) for the multi-strip sensor. The sensitivity of these MEMS sensors is much higher than the sensitivity of commercial metal foil strain gauges and strain gauge alloy.

A new type of micromachined tactile transducer that detects both the contact force and hardness of an object consists of a diaphragm with a central mesa structure (500 μm high), a piezoresistive strain gauge (920 Ω) at the diaphragm periphery and a chamber for pneumatic actuation [29.27]. The device measured $(11 \times 15 \times 0.4) \text{mm}^3$ and its diaphragm was $4 \text{mm} \times 4 \text{mm} \times 10 \mu\text{m}$. The fabricated tactile transducer detects differences in hardness in the range of $(10^3 \dots 10^5) \text{N/m}$.

In recent years polyimide layers have been successfully used as dielectric membranes in III-V semiconductors micromachining. GaAs is preferable to silicon, due to the easy integration of sensing elements with MMICs or

optoelectronic active devices [29.28]. The sensing element was a meander-like CrAu resistive structure of $1.35\ \mu\text{m}$ thickness, supported by a $2\ \mu\text{m}$ thick polyimide membrane (Pyralin PI 2555 from DuPont) on a GaAs substrate. The metallic structure had $42.8\ \text{mm}$ length and $40\ \mu\text{m}$ wide while the polyimide membrane area was $(3.5 \times 3.5)\ \text{mm}^2$. Once pressure is applied, the polyimide membrane bends and the change in the resistor value, due to the tensile effect, can be easily converted in a voltage output. For signal processing a DC coupled MESFET amplifier structure can be manufactured on the GaAs substrate.

At the Institute of Semiconductor Physics, National Academy of Sciences of Ukraine, Kyiv [29.29], the transducer sensitive element includes two parallel connected four-terminal piezotransducers with quasi-Hall topology (the transverse voltage strain gauges). The piezo-transducers are integrated in the planar side of the silicon square-shaped diaphragm with a center boss (the E-type diaphragm) near the two sides of the diaphragm thin part.

Standard silicon pressure transducers use a flat square diaphragm where a full Wheatstone bridge is integrated. Sensitivity can be increased acting on the square ratio $(a/h)^2$ where a is the side dimension and h is the diaphragm thickness, but nonlinearity error increases with the same ratio at a much faster rate. The nonlinearity of a full Wheatstone bridge operated with constant voltage has several sources:

- i) nonlinear dependence of the stresses with the applied pressure – to be compensated by local stiffening of the membrane while the resistors are kept in local concentration areas, the best alternative being the “double-island” diaphragm proposed by Wilner and further explored by Whittier *et al.* [29.30].
- ii) nonlinearity of the piezoresistive effect – can be minimized locating half of resistors under transversal stress; because of the different behaviors of non-linearity when the resistors are in tension or in compression, this “mixed” location produces a partial self-compensation of the piezoresistors nonlinearity contributions.
- iii) unbalance between the sensitivities of the different resistances which constitute the bridge – this term can be conveniently reduced by appropriate sensor design and proper selection of resistances.

Small size is necessary having in mind the biomedical applications: the pressure transducer has to be mounted in the front tip of a 7F standard catheter with outer diameter of $2.7\ \text{mm}$. The researchers from Centre Nacional de Microelectrònica, Universitat de Barcelona, used a single step micromachining, preserving a planar surface in the active side of the wafer. Because of the doping selectivity of the electrochemical etch stop (in four-electrode configuration), membranes with nonuniform thickness can be fabricated if n-diffusions with different junction depths are used. This technology gives a design freedom because the

bosses' geometry is defined by lithography from the active side of the wafer. The stress profile along the path going from the center of the diaphragm to the edge is obtained by FEM in order to establish a systematic procedure of structural optimization. This profile is significantly depending on the boss geometry.

The simulation work was carried out using ANSYS program running in a SPARC 20 computer and MEF/MOSAIC running in a Silicon Graphics (IRIS 4D/35). The basis was mainly to find an analytical representation (multivariate polynomials) of the FSO (full scale output) and NL (non-linearity) in the geometrical parameters which define the structure. This graphical method of two-dimensional plot optimization is very useful for analyzing the following "sequence" of miniature pressure diaphragms (Fig. 29.11):

- i) starting from flat square or rectangle,
- ii) adding two rectangular or trapezoidal "islands" and obtaining the double-bossed membrane structure,
- iii) adding the central beam between the two bosses, and, finally,
- iv) resulting the spectacular "butterfly" configuration.

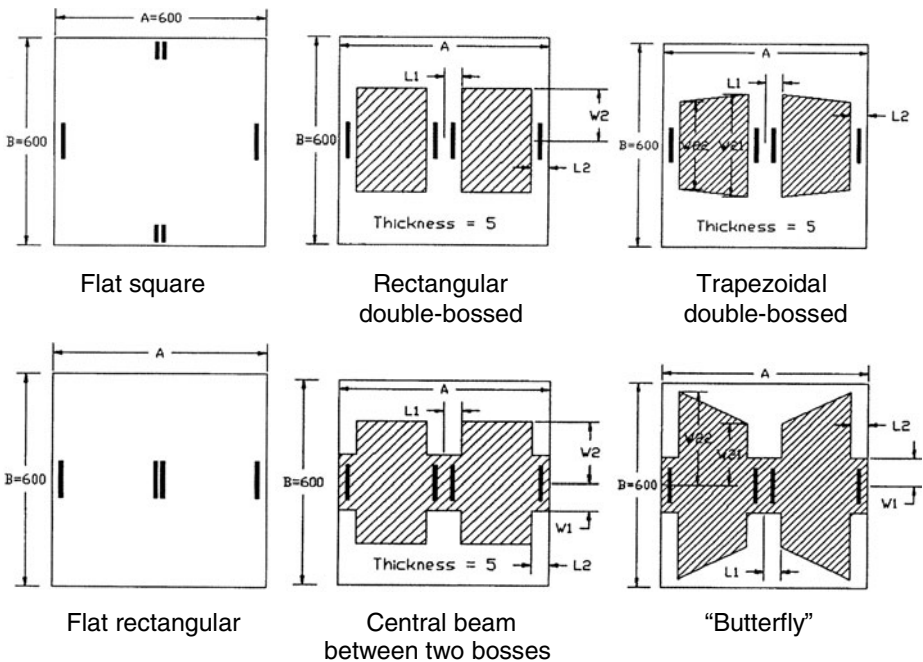


Fig. 29.11 Schematic of the six types of structures for miniature pressure transducers (dimensions in μm). Piezoresistors (thick traces) are $10 \mu\text{m}$ wide and $80 \mu\text{m}$ long. Thicker areas ($20 \mu\text{m}$) have diagonal hatches. Reprinted with permission from [29.30].

Here are other examples of structural optimization for quadratic membranes:

- Lund – square membrane, embedded on its contour and stressed by a center concentrated force, meshed with 100 Mindlin isoparametric elements [29.31];
- Zhang and Anderson – rectangular plate supported on corners, with a load distributed on the axes and contour, solved with 49 quadrilateral finite elements with 64 nodes [29.32];
- Stolarski – square membrane, studied by means of Serendip quadratic finite elements using three refined discretizing stages: each finite element is divided in another four and then in sixteen [29.33];
- Tibrewala . . . various square membranes, such as full or cross-shaped, having one or five bosses, were simulated using COSMOS software and then 16 p-type silicon piezoresistors were diffused on their surface [29.34].

29.4. MEMBRANES WITH VARIOUS SHAPES OF APERTURES

The technologic progress extends the possibilities of square or rectangular membranes use. Inspired by the adjacent fields (e.g. quartz microtechnology) apertures can be made (two longitudinal cuttings provide a triple lamella with embedded ends). The cross or L-shaped cuttings made by laser create optimum elastic structure for the force and acceleration transducers [29.35], [29.36].

For the strain-gauged pressure transducer [29.37] the pressure induced deflection of the rectangular diaphragm creates a torque, M , at the free hanging *H-shaped cut cantilever frame* to the diaphragm attachment (Fig. 29.12).

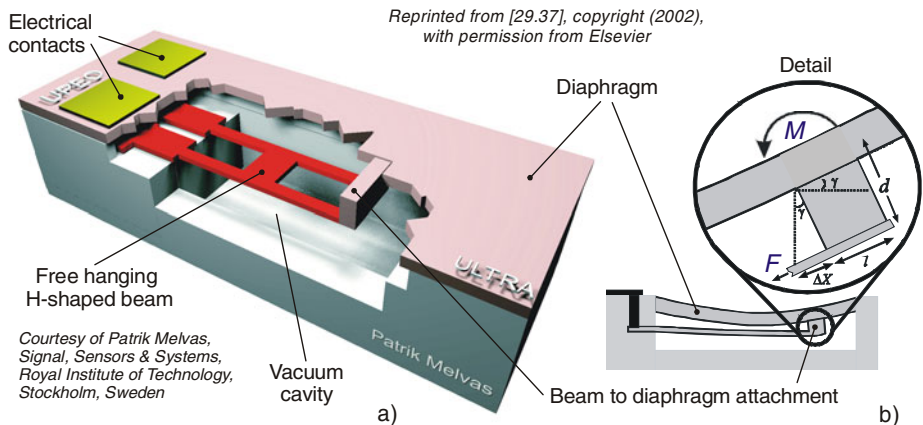


Fig. 29.12 A schematic view of the strain-gauged pressure transducer with free-hanging cantilever, illustrating the principle of operation (a) and the appropriate parameters: M – torque induced by pressure, γ – bending angle, F – reactive axial force, ΔX – beam lengthening, d – leverage attachment height and l – length (b)

This is a spectacular case when pressure is “transformed” into a (moment of) force while it is usual to “transform” the force applied on a membrane into a pressure in the associated enclosure.

“A thin plate-shaped six-axis force sensor chip (Fig. 29.13) comprising a semiconductor substrate formed by semiconductor film-forming processes, the sensor chip having through-holes formed therein and arranged so that the sensor chip is functionally divided by the through-holes into an action part to which an external force is applied, a support part to be fixed to an external structure, and a plurality of connecting parts each connecting together the action part and the support part and having a bridge portion of generally T-shaped configuration joined to the action part and an elastic portion joined to the support part” [29.38]. Each of the connecting parts has a plurality of strain resistance devices each comprising an active layer formed on at least one of front and rear faces thereof in an area where deformation strain effectively occurs, the strain resistance devices being electrically connected to corresponding electrodes disposed in the support part.

Table 29.1 gives a summary of resonant pressure microsensors which have been developed in the framework of a joint project entitled “Application of Micromechanics of Sensors with Frequency Output” and conducted by the Institut für Mikrotechnik der Technischen Universität Braunschweig [29.39].

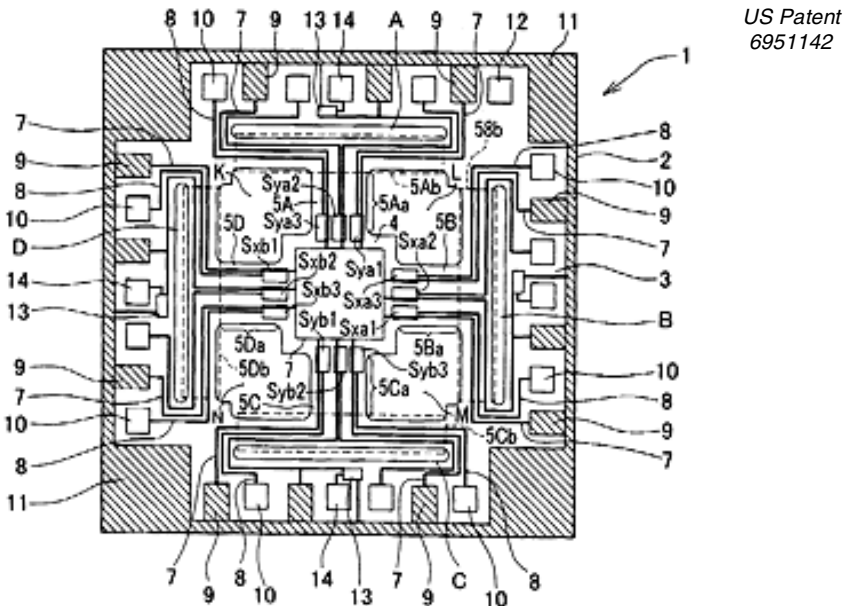
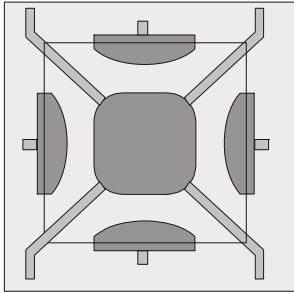
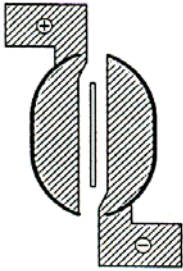


Fig. 29.13 Four T-shaped elastic bridges for a six-component force transducer

Table 29.1 Vibration modes and parameters for thin membranes with apertures

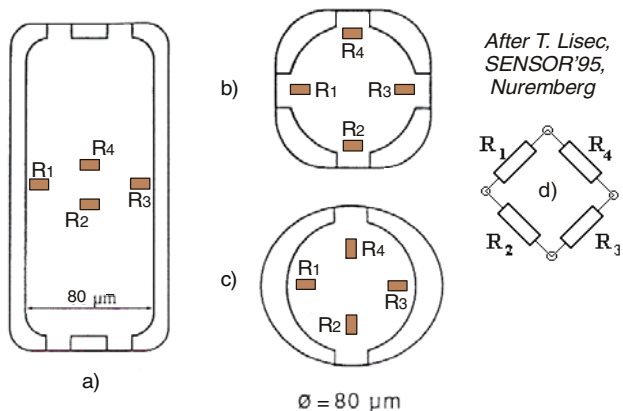
Type	Quadratic membrane	Oval-shaped membrane
Layout		
Technology	ZnO on silicon	Quartz micromachining
Vibration mode	Fundamental flexural	Low frequency bending
Frequency	8.5 kHz	35 kHz
Sensitivity	120 Hz/kPa	23 Hz/kPa

One can see the cuttings on the quadratic and oval-shaped membranes, respectively, defining the vibration modes.

29.5. OTHER SHAPES OF MEMBRANES

The noncircular elastic membranes of constant thickness, having square or rectangular (with or without rounded angles), elliptical/oval or more complex shapes, are difficult to calculate analytically, because in their formulas a lot of coefficients are required. By finite element analysis, optimal elastic structures and the best piezoresistors' positions have to be determined.

Fig. 29.14 Various shapes of membranes: a) rectangular, b) quadratic with rounded corners, c) circular, and d) strain gauges connected in Wheatstone bridge



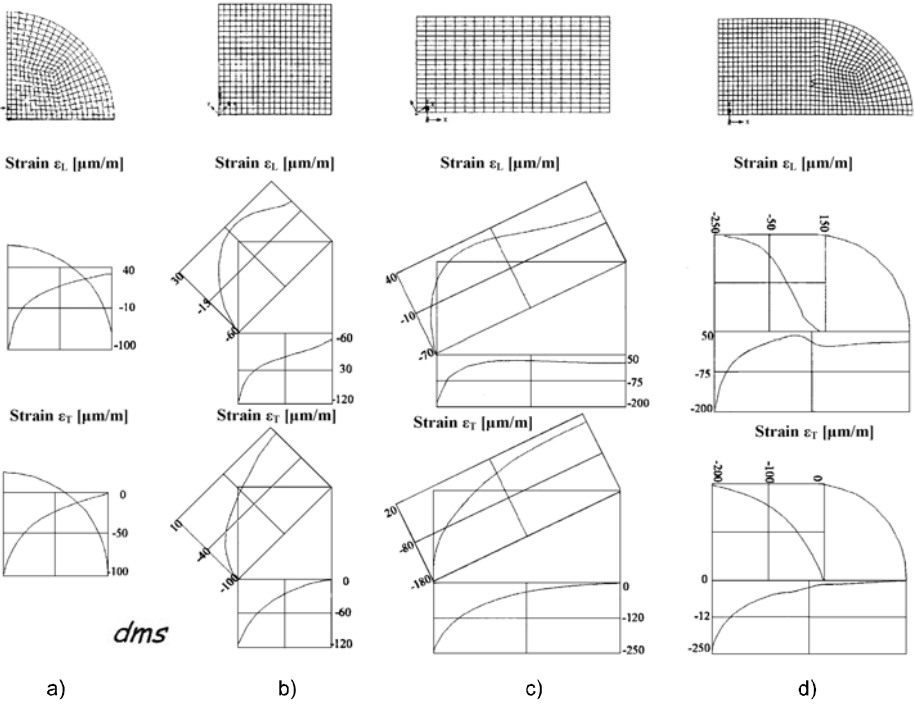


Fig. 29.15 FEA on circular (a), square (b), rectangular (c) and oval (d) membranes under the same concentrated force F at the membrane center

At the Fraunhofer Institute for Silicon Technology (ISiT), Berlin some membranes of various shapes and sizes have been designed, using finite element simulations by ANSYS software on a DECstation 5000 [29.40]. Assuming the same membrane thickness ($1.5 \mu\text{m}$) for three models: rectangular (Fig. 29.14a), quadratic (Fig. 29.14b) and circular (Fig. 29.14c), and applying a pressure of 1.3 bars, the resulting sensitivities ($\Delta U/U$ values) are: 0.015, 0.008 and 0.006 respectively. These miniaturized transducers (2.3 mm long, 0.4 mm wide and 0.5 mm thick), based on piezoresistive bridges (Fig. 29.14d), are useful for medical applications (e.g. catheter tip pressure measurements).

The paper [29.41] comparatively considers four types of membranes: circular ($\varnothing = 50 \text{ mm}$), quadratic ($50 \text{ mm} \times 50 \text{ mm}$), rectangular (two adjacent squares) and oval (like a combination of the circular and rectangular ones). The classical circular membranes are frequently used while the square membranes are useful for tactile sensors and the rectangular ones for surface-micromachined piezoresistive pressure sensors.

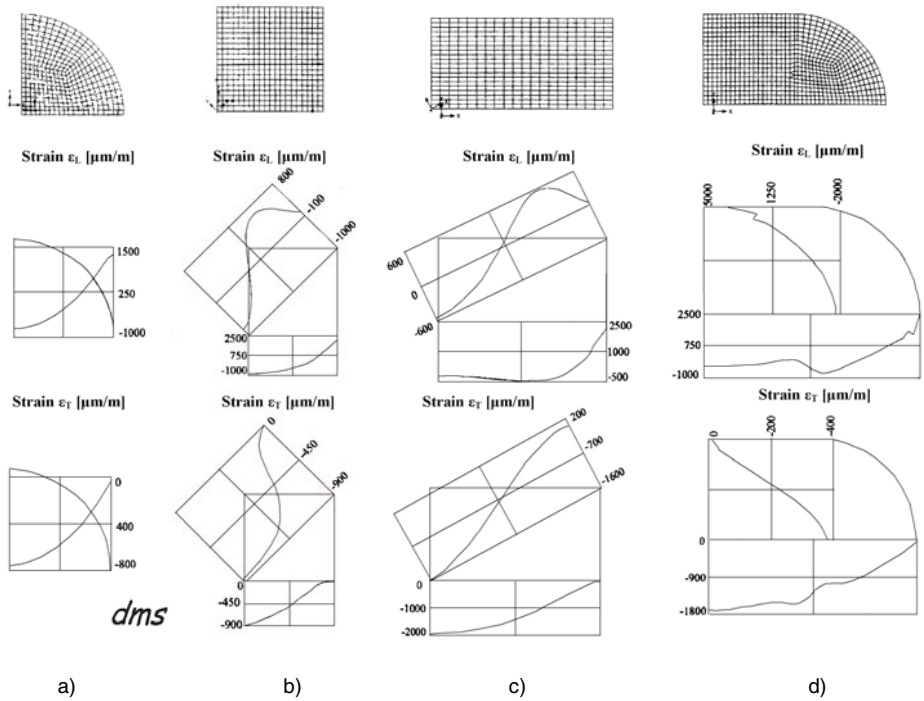


Fig. 29.16 FEA on circular (a), square (b), rectangular (c) and oval (d) membranes under distributed pressure p on the entire surface of the membrane (thickness = 1 mm)

Their analytical formulae being complicated, consequently FEM was used. Due to their structural symmetry, it is sufficient to analyze a quarter of the diaphragm. Mesh generation plots, together with longitudinal ϵ_L and tangential ϵ_T strain diagrams, are presented for two different loadings: concentrated force (Fig. 29.15) and distributed pressure (Fig. 29.16).

The following are the conclusions of this comparative study:

- i) The circular membrane is the preferred alternative, due to a more difficult manufacturing of the other shapes and to a more difficult fastening along the edges of those membranes, near the corners.
- ii) On the square membrane, one can outline a stress concentration at the middle of the edges when loading it with a concentrated force. This represents an inconvenient stress state.
- iii) The rectangular shape amplifies the strains in the central region, which corresponds to the initial square (about twice).
- iv) The oval-shaped membrane causes a better stress concentration, increasing the sensitivity, while avoiding the corner fastening.

A comparison between the concentrated force and the distributed pressure loading on the same membrane shape outlines the changing of the stress and strains distribution. This difference is higher on the square and rectangular membranes, where even the concavity of the strain curve visibly changes.

A patented elastic structure using a rectangular plate in order to improve the portable weighing truck scales is presented in [29.42].

REFERENCES

1. Zwijze, R.A.F., Wiegerink, R.J., Krijnen, G.J.M., Lammerink, T.S.J., Elwenspoek, M.: Low creep and hysteresis load cell based on a force-to-fluid pressure transformation. *Sensors and Actuators A: Physical* 78, 74–80 (1999)
2. Ștefănescu, D.M.: Comparative study of some force gauges with membrane-type flexible element utilized for measurements in civil engineering. In: *International Symposium on Geomechanics, Bridges and Structures*, Lanzhou, China, September 1–5, pp. 253–259 (1987)
3. Luharuka, R., Noh, H., Kim, S.K., Hesketh, P.J., Mao, H., Wong, L.: Improved manufacturability and characterization of corrugated Parylene diaphragm pressure transducer. IOP Publishing – Electronic Submissions Department, File Reference: RANL-6L8AEG (2006)
4. *Measuring and Controlling Forces and Torque. Product Overview 03.98*, Haehne Elektronische Messgeräte GmbH, Erkrath, Germany (1998)
5. Maeda, C.: Thin load cell for weighing scales. In: *16th Intl. Conf. on Force, Mass and Torque Measurements parallel with Asia - Pacific Symp. Measurement of Mass and Force*, Taejon, Republic of Korea, September 14–18, pp. 408–414 (1998)
6. Meissner, B.: Zum Verhalten von Dehnungsmeßstreifen-Wägezellen bei stoßartiger Lastaufbringung. In: Kochsiek, M. (Hrsg.) *Massebestimmung hoher Genauigkeit*, PTB Me-60, Braunschweig, Deutschland, pp. 157–166 (June 1984)
7. Rohrbach, C., Andreae, G.: Eine neuartige flache Präzisionskraftmeßdose einfacher Bauart mit DMS. *Materialprüfung* 3, 300–304 (1961)
8. Schlachter, W.: A new smart load and force transmitting system. In: *Proc. 13th Int'l Conf. on Force and Mass Measurement*, Helsinki, pp. 55–58 (May 1993)
9. Rozvany, G.I.N., Zhou, M., Gollub, W.: Continuum-type optimality criteria methods for large finite element systems with a displacement constraint. Part II. In: *Structural Optimization (Computer-Aided Optimal Design of Stressed Systems and Components)*, Berlin, vol. 2(2), pp. 77–104. Springer International (1990)
10. Ștefănescu, D.M.: Optimization of the shape of profiled membranes utilized at strain gauge instrumented transducers by FEM. In: *Proceedings 1st Conference IMEKO TC-15 on Experimental Stress Analysis*, Plzeň, ČSSR, May 25–28, pp. 513–518 (1987)
11. Schomburg, W.K., Rummler, Z., Shao, P., Wulff, K., Xie, L.: The design of metal strain gauges on diaphragms. *J. Micromech. Microeng.* 14, 1101–1108 (2004)
12. Prudenziati, M.: Thick Film Sensors. In: Middelhoek, S. (ed.) *Handbook of Sensors and Actuators*, vol. 1. Elsevier, Amsterdam (1994)

13. Bonfig, K.W., Bartz, W.J., Wolf, J.: Sensoren und Meßaufnehmer. Neue Verfahren und Produkte für die Praxis. Expert Verlag, Grafenau, Deutschland (1988)
14. White, N.M., Turner, J.D.: Thick-film sensors: past, present and future (review article). *Measurement Science Technology* 8, 1–20 (1997) (printed in the U.K.)
15. Ort, W.: Sensoren mit Metallfolien-Dehnungsmeßstreifen. *Mestechische Briefe (Hottinger Baldwin Messtechnik)* 16(1), 11–16 (1982)
16. Mahfuz, H., Case, R.O., Wong, T.-L.: Hybrid stress analysis by digitized photoelastic data and numerical methods. *Experimental Mechanics* 30(2), 190–194 (1990)
17. Morton, J., Post, D., Han, B., Tsai, M.Y.: A localized hybrid method of stress analysis: a combination of Moiré interferometry & FEM. *Experimental Mechanics* 30(2), 195–200 (1990)
18. Wall, W.E.: Applications of piezoresistance to externally excited transducers. Technical Paper 239, Endevco, San Juan Capistrano, CA, Revue 10-75
19. Henning, W.: Mikroelektronik – Sensoren. In: Sonderdruck eines Vortrages anlässlich des 3. Kolloquiums der Österreichischen Tribologischen Gesellschaft, pp. 3–15. SIEMENS, München, Deutschland (1981)
20. Ştefănescu, D.M.: Machining error influence estimation on the transducer performances using FEM. In: Workshop on Research and Design Supporting Fabrication, Session I.44, Arad, May 21-23 (1986) (in Romanian)
21. Hinweise zum Messen mit Wazau-Miniatur-Kraftaufnehmern. Dr.-Ing. G. Wazau, Berlin (1982)
22. Gassmann, H., Theiß, D., Baethke, K.: New bending ring force transducers as transfer-standards. In: Proc. 13th Int'l Conf. Force and Mass Measurement, Helsinki, Finland, May 11-14, pp. 48–54 (1993)
23. Daimaruya, M., Naitoh, M., Kobayashi, H., Tanimura, S.: A sensing-plate method for measuring force and duration of impact in elastic-plastic impact of bodies. *Experimental Mechanics* 29(3), 268–273 (1989)
24. Kim, J.-H., Lee, J.-I., Kim, M.-S., Kang, D.-I.: Development of a three-component force sensor using micromachining technology. In: Zhang, Y., et al. (eds.) Proc. 6th Asia-Pacific Symposium Measurement of Mass, Force and Torque, Shanghai, China, APMF 2003, November 3-6, pp. 195–198 (2003)
25. Mei, T., Li, W.J., Ge, Y., Chen, Y., Ni, L., Chan, M.H.: An integrated MEMS three-dimensional tactile sensor with large force range. *Sensors and Actuators A: Physical* 80, 155–162 (2000)
26. Cao, L., Kim, T.S., Mantell, S.C., Polla, D.L.: Simulation and fabrication of piezoresistive membrane type MEMS strain sensors. *Sensors and Actuators A: Physical* 80, 273–279 (2000)
27. Hasegawa, Y., Shikida, M., Shimizu, T., Miyaji, T., Sasaki, H., Sato, K., Itoigawa, K.: A micromachined active tactile sensor for hardness detection. *Sensors and Actuators A: Physical* 114, 141–146 (2004)
28. Petrini, I., Müller, A., Avramescu, V., Simion, G., Niţescu, N., Vasilache, D., Dascălu, D., Konstantinidis, G., Giacomozzi, F.: Resistive pressure sensing structures on polyimide membranes on GaAs substrate. *J. Micromech. Microeng.* 10, 218–222 (2000)

29. Zhadko, I.P., Babichev, G.G., Kozlovskiy, S.I., Romanov, V.A., Sharan, N.N., Zinchenko, E.A.: Silicon pressure transducer with differential sensitive element based on transverse electromotive force effect. *Sensors and Actuators A: Physical* 90, 89–95 (2001)
30. Marco, S., Samitier, J., Ruiz, O., Morante, J.R., Esteve, J.: High-performance piezoresistive pressure sensors for biomedical applications using very thin structured membranes. *Meas. Sci. Technol.* 7, 1195–1203 (1996)
31. Lund, E.: Finite element based design sensitivity analysis and optimization. PhD Dissertation. Aalborg University, Denmark, Special Report No. 23 (April 1994)
32. Zhang, J., Anderson, W.J.: Exploiting design length scales in structural optimization. *International Journal of Numerical Methods in Engineering* 40, 1465–1482 (1997)
33. Stolarski, H., Carpenter, N., Belytschko, T.: A Kirchhoff-mode method for C^0 bilinear and Serendipity plate elements. *Computer Methods in Applied Mechanics and Engineering* 50, 121–145 (1985)
34. Tibrewala, A., Hofmann, N., Phataralaotha, A., Jäger, G., Büttgenbach, S.: Development of 3D force sensors for nanopositioning and nanomeasuring machine. *Sensors* 9, 3228–3239 (2009); ISSN 1424-8220
35. Crescini, D., Ferrari, V., Marioli, D., Taroni, A.: Piezoresistive thick-film sensors for force and vibration measurements. In: *Proc. IMEKO XIIIth World Congress*, Torino, Italy, September 5-9, vol. I, pp. 271–276 (1994)
36. Pavelescu, I.: Acceleration microstructures for industrial applications. Institute for Microtechnology (IMT), Bucharest, Romania, Research standing (December 2002)
37. Melväs, P., Kälvesten, E., Enoksson, P., Stemme, G.: A free-hanging strain-gauge for ultraminiaturized pressure sensors. *Sensors and Actuators A: Physical* 97-98, 75–82 (2002)
38. Ohsato, T., Hirabayashi, Y.: (Honda) Six-axis force sensor chip and six-axis force sensor using the same. US Patent 6951142-2005
39. Büttgenbach, S., Fabula, T., Schmidt, B., Wagner, H.-J.: Resonant force and pressure microsensors. In: *7. Intern. Fachmesse mit Kongress für Sensoren, Meßaufnehmern und Systeme – Sensor 1995*, Nürnberg, May 9-11, pp. 27–32 (1995)
40. Lisec, T., Stauch, H., Wagner, B.: Surface-micromachined piezoresistive pressure sensor. In: *SENSOR 1995 Kongreßband*, Nuremberg, May 9-11, pp. 21–25 (1995)
41. Ştefănescu, D.M., Dolga, L., Marinescu, A.: Parametrical modeling of the strain gauged pressure and/or force transducers. In: *CD Proc. XVIIth IMEKO World Congress Metrology in the 3rd Millenium*, Cavtat-Dubrovnik, Croatia, June 22-27, pp. 1106–1110 (2003)
42. Ştefănescu, D.M., Chen, C.-T., Su, Y.-Y., Chang, C.-S.: Wheel scales. Taiwanese Patent I – 273219, February 11 (2007)

Note: Reference 34 is an open-access article distributed under the terms and conditions of <http://creativecommons.org/licenses/by/3.0/>.

Chapter 30

COMPLEX LOADED TORUS

30.1. TORUS AS ELASTIC ELEMENT FOR FORCE TRANSDUCERS

The shape of the torus (toroidal ring) is like that of the vacuum tight porcelain donut-shaped tube for the betatron (Fig. 30.1.). Torus type elastic element has low height and high rigidity; however, its manufacturing technology is rather sophisticated. It is a rotary toroid (Fig. 30.2, top), a circular ring that rotates perpendicularly on a circular guiding axis. Its main advantage as force transducer is the relative insensitiveness to the eccentricity of the applied load, concentrated or distributed on the platform over it.

Classical torus, compressed between two rigid plates, is described in Kautsch's [30.1] and Malikov's [30.2] works; the latter has given the formula of its mechanical sensitivity, bringing out that a too thin torus risks to "get screwed" [30.3]. To keep its elastic sensitivity a barrel type section is recommended. The SQAT (made by Newberry) or Davy models [30.4] can be considered as torus prototypes.

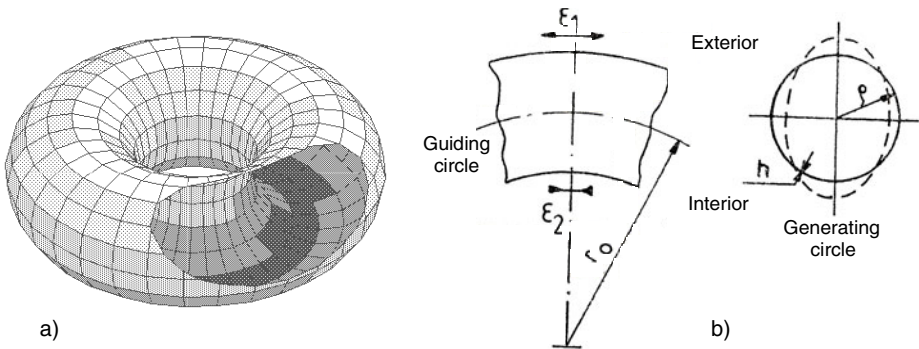


Fig. 30.1 Hollow torus as donut-shaped tube for the betatron (a) and its dimensions (b)

E-10

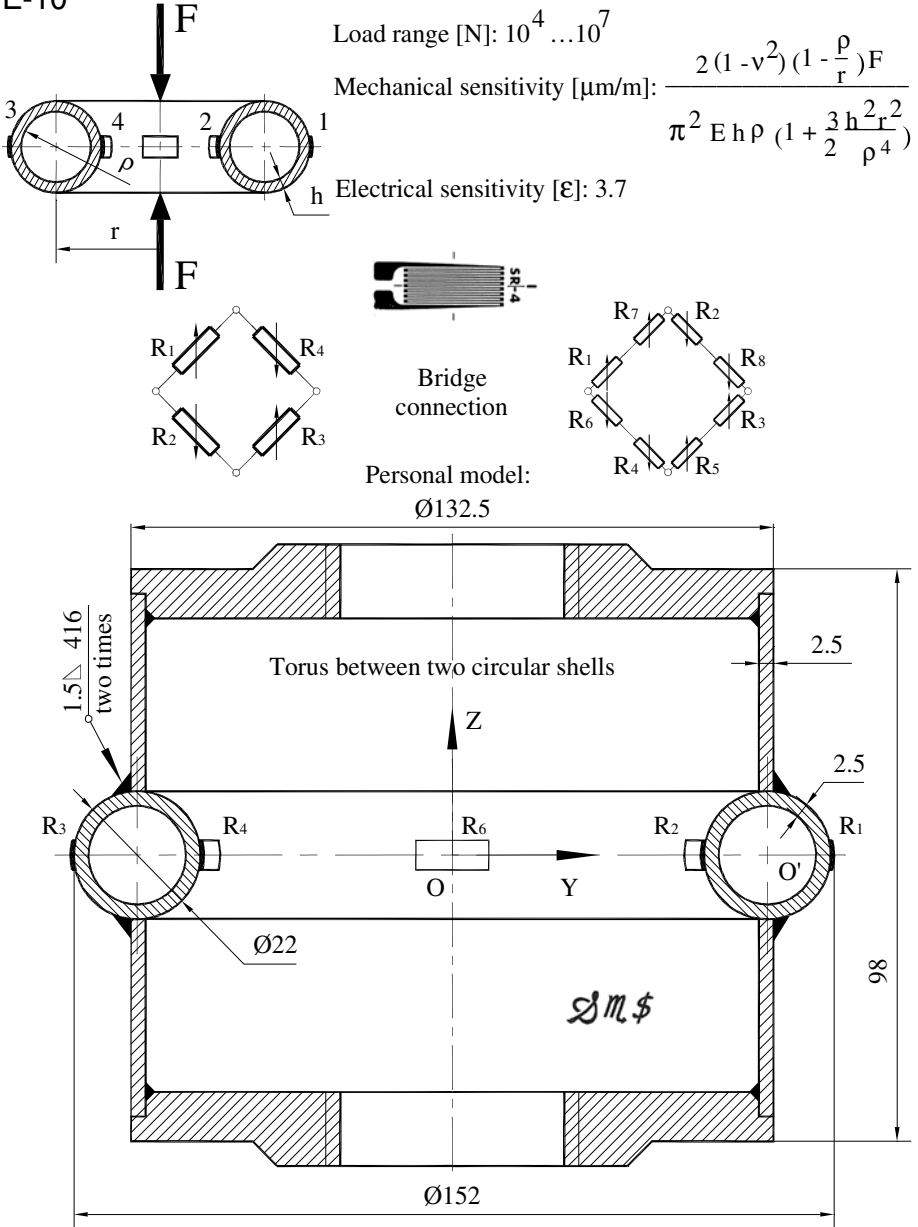


Fig. 30.2 Strain gauged elastic elements of type X for force transducers. Torus between two circular shells could become a multicomponent force and torque transducer.

Strain gauges on the outside surface are extended (ϵ_1), while the inside ones are shortened (ϵ_2). Ideally, the ratio ϵ_1/ϵ_2 should be of -1 , namely ϵ_1 and ϵ_2 should be equal in module and of adverse signs, this leading to the maximum sensitivity. They are located in symmetrical pairs, on opposite circular sections, in the median plane of the torus. Connecting schemes with 4, 8 or 16 strain gauges can be made up, their sensitivity being increased with the SGs number. Three similar Wheatstone bridges were represented for another complicated axisymmetric elastic element, the ribbed membrane shown in Figure 29.4.

An original contribution is presented in [30.5] referring specifically to the torus welded between two thin cylindrical tubes and becoming in every cross section a kind of bent ring. This version of torus fitted between two tube-shaped shells allows simultaneous measuring of the axial force (tension and/or compression) and torque moment by adding strain gauges to $\pm 45^\circ$ directions on the cylindrical sections.

Analytic computation of this elastic assembly is very difficult because of the complicated formulas, so the finite element analysis is indicated to solve this complex geometry. Numerical example starting from the dimensions shown in Figure 30.2: radius of the guiding circle: $r = 65$ mm; radius of the generating circle: $\rho = 11$ mm; thickness : $h = 2.5$ mm; axial load: $F = 50$ kN, modulus of elasticity: $E = 210$ GPa; Poisson's coefficient: $\nu = 0.3$. FEA program SAP IV is applied for 264 nodes and 198 finite elements of type 4 ("plane state" axisymmetric variant). Figure 30.3 shows the strain diagrams, at different scales, resulting the option (a) for circumferential strain gauges.

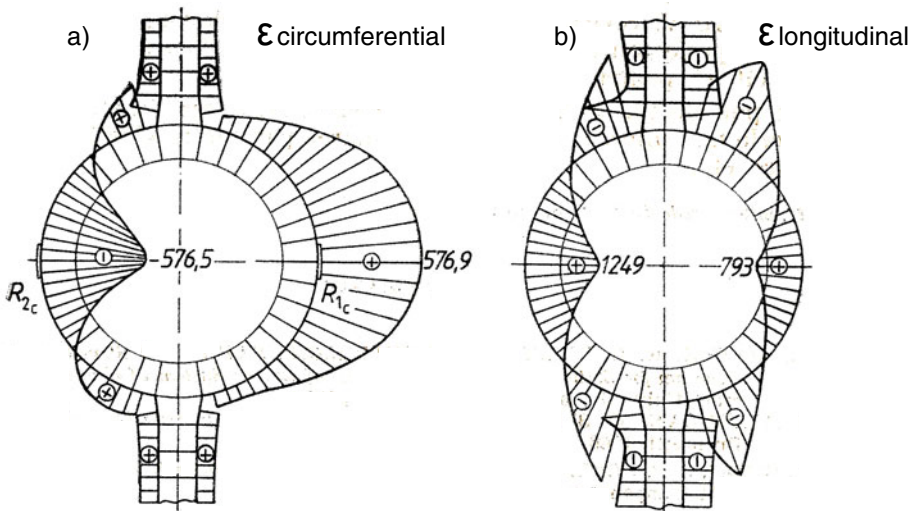


Fig. 30.3 Circumferential (a) and longitudinal (b) strain diagrams on compressed torus

Table 30.1 Comparative performances for three torus models

Torus model	Force [kN]	Dimensions [mm]			Ratio $\varepsilon_1 / \varepsilon_2$
		r	ρ	h	
Rohrbach	10	60	10	1.2	-0.7773
Davy Instruments	38	72	8	0.9	-0.8565
Ştefănescu & Sandu	50	65	11	2.5	-1.0007

In the Table 30.1 a torus designed at the “Politehnica” University of Bucharest is compared with other two models, as reported by Rohrbach [30.6] and Davy Instruments [30.7]. The Romanian model has better characteristics due to its special “architecture” adopted, being nearby the ideal ratio $\varepsilon_1/\varepsilon_2 = -1$.

30.2. TOROIDAL ELASTIC ELEMENTS IN SPECIAL APPLICATIONS

The concept of a sensitive and broadband resonant gravitational wave detector is presented in [30.8] with reference to a *dual torus* (Fig. 30.4). The detector is equipped with a readout which senses the quadrupolar vibrational modes created by gravitational forces while rejecting the contributions due to the other nongravitational wave sensitive modes.

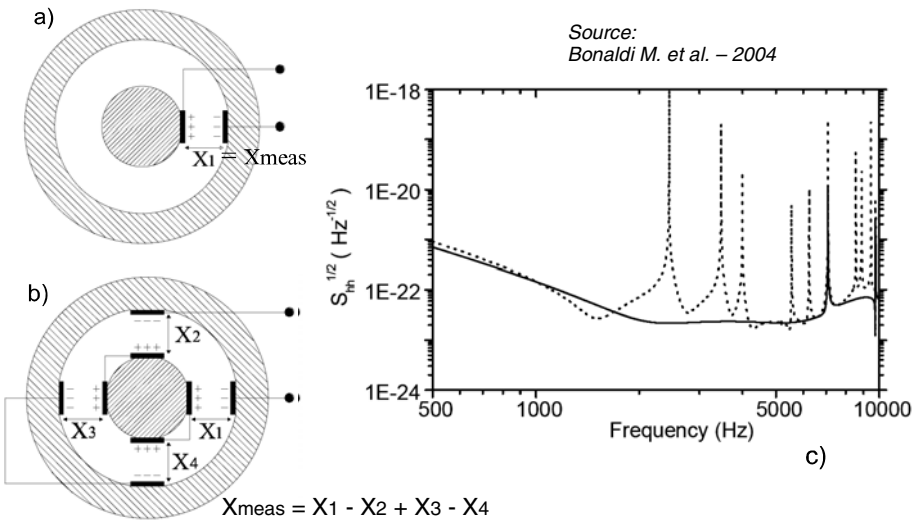


Fig. 30.4 Dual torus without (a) and with (b) selective readout. c) Equivalent strain power spectral density for both cases: the dotted line is for the nonselective readout while the continuous line is for the selective one.

For a Molybdenum dual detector, composed by an internal cylinder 0.5 m in diameter and an external torus with internal diameter of 0.52 m and external diameter of 0.94 m, the achievable sensitivity of $3 \times 10^{-23} \text{ Hz}^{-1/2}$ in the frequency window between 2 to 5 kHz is better than the expected sensitivity of the upgraded interferometers.

Inflated space-based devices have gained popularity over the past three decades due to their minimal launch-mass and volume [30.9]. A special torus was made of flat sheets of polyamide film Kapton (46 μm thick) and fabricated in the Emerging Techno Lab at Kentucky University (Fig. 30.5). Both sensor and actuator materials must be flexible enough to conform to the toroidal shape. Piezoelectric materials (PVDF sensors) or smart materials (macro-fiber composite) produce an electric field when a mechanical strain is applied, and *vice versa*. Connection between the shaker and the torus was made with the force transducer. Force, acceleration and strain data were collected through a DSPT SigLab multichannel dynamic signal analyzer.

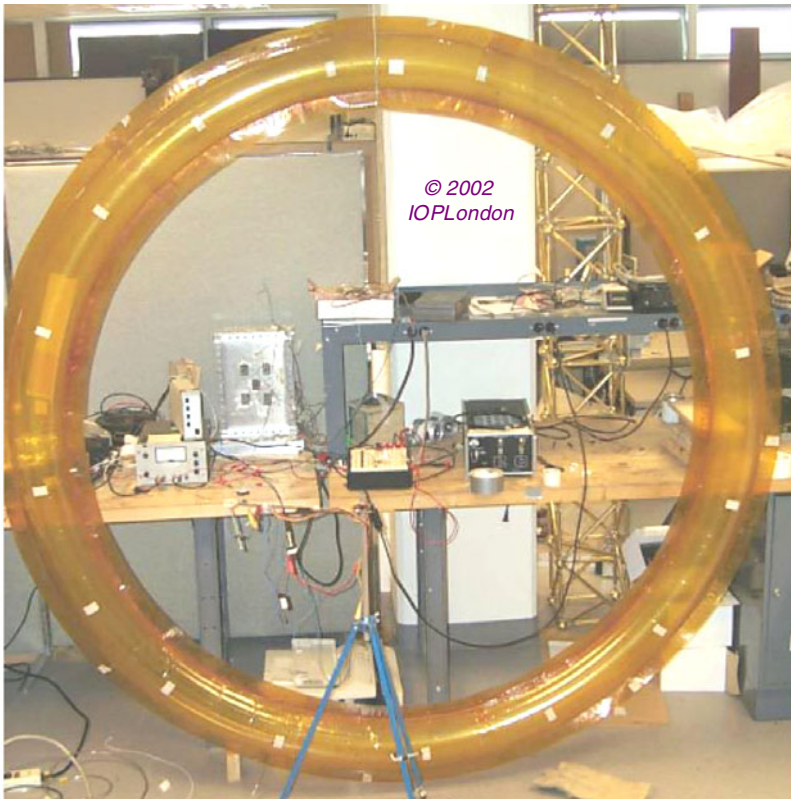


Fig. 30.5 Kapton torus for dynamic analysis of force, acceleration and strain [30.9]

United Applied Technologies (Huntsville, AL) has developed a novel, thin film casting approach to create a *self-rigidizing torus* [30.10]. Once inflated, the torus structure is able to support its own shape, thus eliminating the need for any internal pressure. The self-rigidizing torus is more flexible than its pressurized predecessors. Such compliancy makes modal testing extremely difficult. A stinger was attached to the head of the shaker through a force transducer to treat the input to the structure as a unidirectional force. The force and acceleration transducers measurements were fed back to the SigLab data acquisition board via the PCB Piezotronics signal conditioner. Through careful application of traditional modal testing techniques, the damped natural frequencies and mode shapes of the self-rigidizing torus can be discerned in the frequency bandwidth of interest, (1...12) Hz.

A microlevel application is presented in [30.11], promising for using the toroids with metallic inner surfaces as IR-frequency range resonators.

REFERENCES

1. Kautsch, R.: Messelektronik nichtelektrischer Größen. Teil 3: Messgrößen und Messeinrichtungen. Hans Holzmann Verlag, Bad Wörishofen, Deutschland (1981)
2. Malikov, G.F., Şneiderman, A.I., Şulemovici, A.M.: Strain gauged elastic elements computation. Izdat Maşinostroenie, Moskva (1964) (in Russian)
3. La réalisation des capteurs a jauges électriques. BUDD S.A., Neully sur Seine, N.I.T. 12-72
4. Force transducers and load cells. Short Catalog. Davy Instruments Ltd., Sheffield (1987)
5. Ştefănescu, D.M., Sandu, M.A.: The state of deformations analysis for an elastic element with thin shells. Studii şi cercetări de mecanică aplicată, Tom 45(2), 204–211 (1986) (in Romanian)
6. Rohrbach, C.: Handbuch für elektrisches Messen mechanischer Größen. VDI-Verlag, Düsseldorf (1967)
7. Weighing apparatus. Davy United Instruments Ltd. Patent Review GB19620042625-19621112
8. Bonaldi, M., Cerdonio, M., Conti, L., Pinard, M., Prodi, G.A., Taffarello, L., Zendri, J.P.: A broad band detector of gravitational waves: The dual torus (October 2004), http://www.lnl.infn.it/%7Eauriga/auriga/papers_src/repPS-2MB
9. Park, G., Ruggiero, E.J., Inman, D.J.: Dynamic testing of inflatable structures using smart materials. Smart Mater. Struct. 11, 147–155 (2002)
10. Ruggiero, E.J., Tarazaga, P.A., Inman, D.J.: Modal analysis of an ultra-flexible, self-rigidizing toroidal satellite component. In: Proc. International Mechanical Engineering Congress, Anaheim, CA, November 2004, pp. 1–7. ASME (2004)
11. Luchnikov, V., Kumar, K., Stamm, M.: Toroidal hollow-core microcavities produced by self-rolling of strained polymer bilayer films. J. Micromech. Microeng. 18, Paper 035041 (2008)

Chapter 31

AXISYMMETRIC ELASTIC ELEMENTS

31.1. VARIOUS AXISYMMETRIC EEs FOR FORCE TRANSDUCERS

The axisymmetrical elastic elements have a large variety of shapes, generically represented in Figure 31.1a, with strain gauges connected in Wheatstone bridge, as in Figure 31.1b. The axisymmetrical elastic body is made up of two short tubes with different diameters and the same wall thickness h , joined by a ring that gets a symmetrical deformation against its axis, a kind of a “single turn spring” (Fig. 31.2, top). This elastic structure is relatively easy to make just by lathing and is recommendable for great forces.

Tube (EE-2), membrane (EE-9) and torus (EE-10) are axisymmetrical structures, and have been presented in the previous chapters, but other rotational structures are more complicated and their analytic calculus is rather difficult.

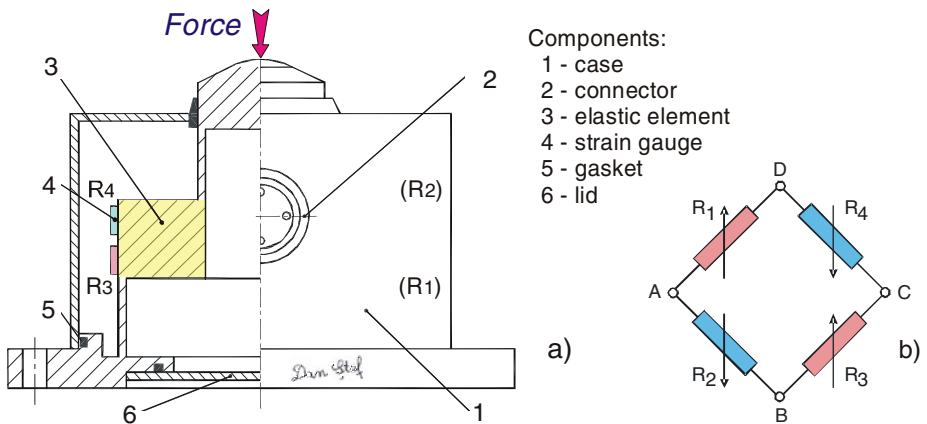


Fig. 31.1 Axisymmetric elastic element for strain gauged force transducers

The numerical calculus is advisable because it facilitates the structural optimization process which finally meets the requirements of the “golden rule” of the electro-resistive tensometry: to obtain specific deformations ε as great possible and of opposite signs in the adjacent arms of the Wheatstone bridge.

An original version of taper element has been firstly communicated to the Romanian Symposium of Tensometry in 1983 [31.1]. In Figure 31.2. (bottom) the longitudinal and tangential specific deformation diagrams are shown. These deformations on the outside and the inside taper suggest the “mixed” location of the strain gauges to achieve the maximum sensitivity: R₁ and R₃ – internal tangential, R₂ and R₄ – external longitudinal.

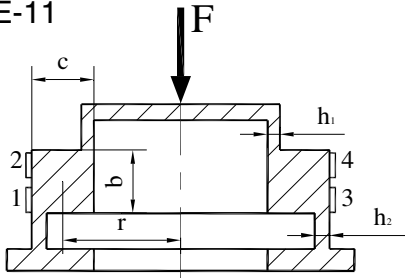
In accordance with the patents and documentation provided by certain companies the central ring has a great variety of sections (Fig. 31.3): square, rectangular, circular, toroid, hexagonal, rhomboid, triangular, N-shaped, taper (of extremely different shapes from “plate” to “cup”) and ribbed membrane (with a third tube in the middle, and the most sensitive) [31.2], [31.3], [31.4].

Trying for the first time in the world to systematize the wide range of the axisymmetrical elastic elements for the comparative analysis of the strain diagrams (ε), either longitudinal (l) or tangential (t) ones [31.5], a special computing programme, original and compatible with the NASTRAN {NAsa STRuctural ANalysis} soft [31.6] with a half-analytic approach has been utilized; it approximates the FEM rigidity matrix along with the force derivatives by the method of finite differences (the runnings have been effectuated by Laurențiu Niculcea on a Silicon Graphics workstation with a processor R-4000, using a simultaneous pre- and post-processing program XL).

For all cases the axial load is $F = 50$ kN. The results of the elastic deformation analysis on ten typical sections, discretized with hexahedral (cubical) finite elements, are shown in Figure 31.3, together with the best position for strain gauges emplacement. Here are some characteristics of the analyzed section-types; they look like “ostrichs”:

- a) *Square* – among the few with an analytical formula [31.7], with the strain gauges R₁ and R₂ tangentially located on the outside of the ring torsion, the other two strain gauges, which complete the Wheatstone bridge, being diametrically opposed.
- b) *Rectangular* (G. Birkholtz – Deutsche Patentschrift No. 1268878) – obtained by a minimum modification of the previous model, the strain gauges being located on the upper and the lower faces, respectively. There are different ratios between the two sides in [31.8]. The HBM ring torsion load cells [31.9] cover a large range, from 1 ton to 470 tons, using special strain gauges with resistance of 4.4 k Ω and ensuring a high output signal of 2.85 mV/V. Other compressive force transducer, C18, based on the ring torsion principle, has 11 models with different nominal forces ranging between 10 kN and 4.5 MN.

E-11



Load range [N]: $5 \times 10^2 \dots 10^7$

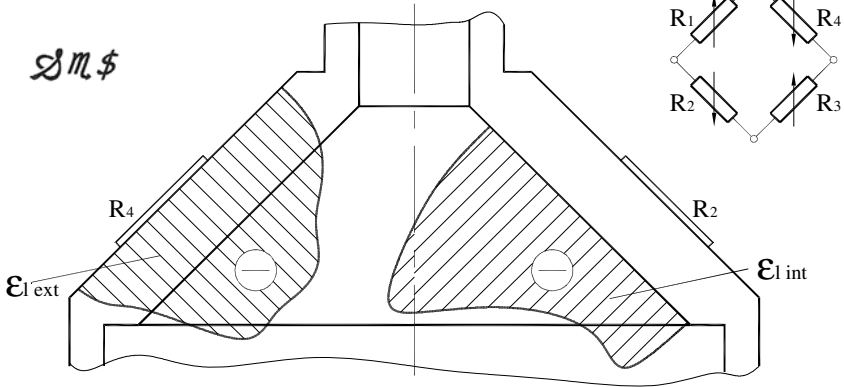
Mechanical sensitivity [$\mu\text{m/m}$]

depending on: F, E, b, c, h_1, h_2, r

Electrical sensitivity [ϵ]: 4

Personal model:

Truncated cone



Strain diagrams on inner and outer faces

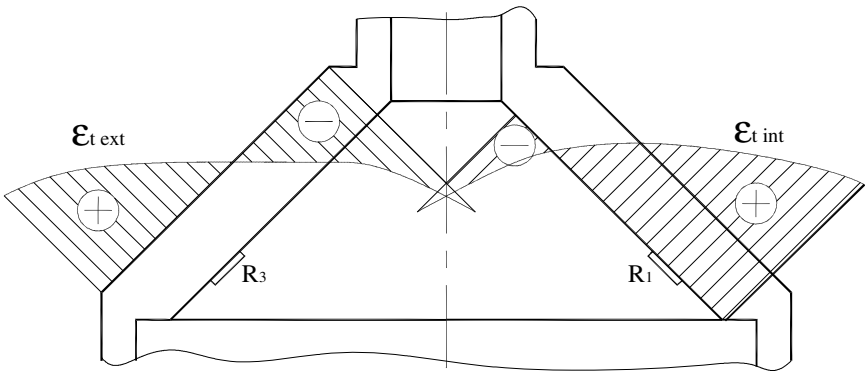


Fig. 31.2 Strain gauged elastic elements of type XI for force transducers. A special combination in strain gauge positioning is used to achieve the best sensitivity: R1 and R3 – internal tangential, R2 and R4 – external longitudinal.

- c) *Circular* – with the two slightly distanced half-circles (Deutsche Patentschrift 1268878), for which the numerical calculation permits a more precise location of the strain gauges, related to the complicated analytical methods existing in the Strength of Materials.
- d) *Toroidal* – resulted by “emptying” the previous section and having the diagrams ε_i and ε_t very much alike with the ones of the torus positioned between two thin cylindrical coatings, as mentioned in [31.10].
- e) *Hexagonal* – for which special circumferential strain gauges (4 k Ω) were made.
- f) *Rhomboidal* – with the strain gauges on the tangential direction as in case of all elastic elements until here.
- g) *Triangular* – with different positions of this section or even with a pair of triangles [31.11]; the strain gauges bonded on the obverse (external face), the other two sides of the triangle presenting ε diagrams with great discontinuities, improper for strain gauge emplacement.
- h) The *N-shaped* (G. Birkholtz – US Patent 3643502) – with different thickness of the diagonal arm and having the same way of tangential location of the strain gauges R_1 and R_2 . Besides, as in the case of the elastic elements *b*, *f* and *g*, the strain gauges may also be longitudinally bonded (R_3 and R_4), but the tensometric sensitivity is more reduced.
- i) *Truncated cone* (height = 64 mm; $\varnothing_{\text{ext}} = 70$ mm) – having tangential strain gauges, on the same face or on different faces (internal/external). The best variant is the “mixed” one: R_1 and R_3 , internal tangentially, R_2 and R_4 , external longitudinally, resulting thus a particular layout and connection way of the four strain gauges in the Wheatstone bridge [31.1].
- j) *Ribbed diaphragm* – with typical circumferential location for the strain gauges: R_1 and R_3 , prolonged, R_2 and R_4 , shortened. The longitudinal layout on the deformed S-shaped elastic element would be appropriate but the available space is small. A detailed study, containing FEM modeling, circumferential and longitudinal strain diagrams, and sensitivity comparison for different measurement techniques, is given in [31.12].

This work demonstrates a good agreement between the theoretical and the practical results obtained within the personal “repertoire” of axisymmetrical force transducers and sensor systems. The variation influence of each dimensional parameter has been studied, choosing the version with the maximum tensometrical sensitivity for each of the ten mentioned types.

As a further concern the multiparameter structural optimization, combining the computerized technology (for instance with Nastran optimizer for static analysis [31.13]) to the engineering research, which results in the developing of intelligent instruments in the force measuring field, is required.

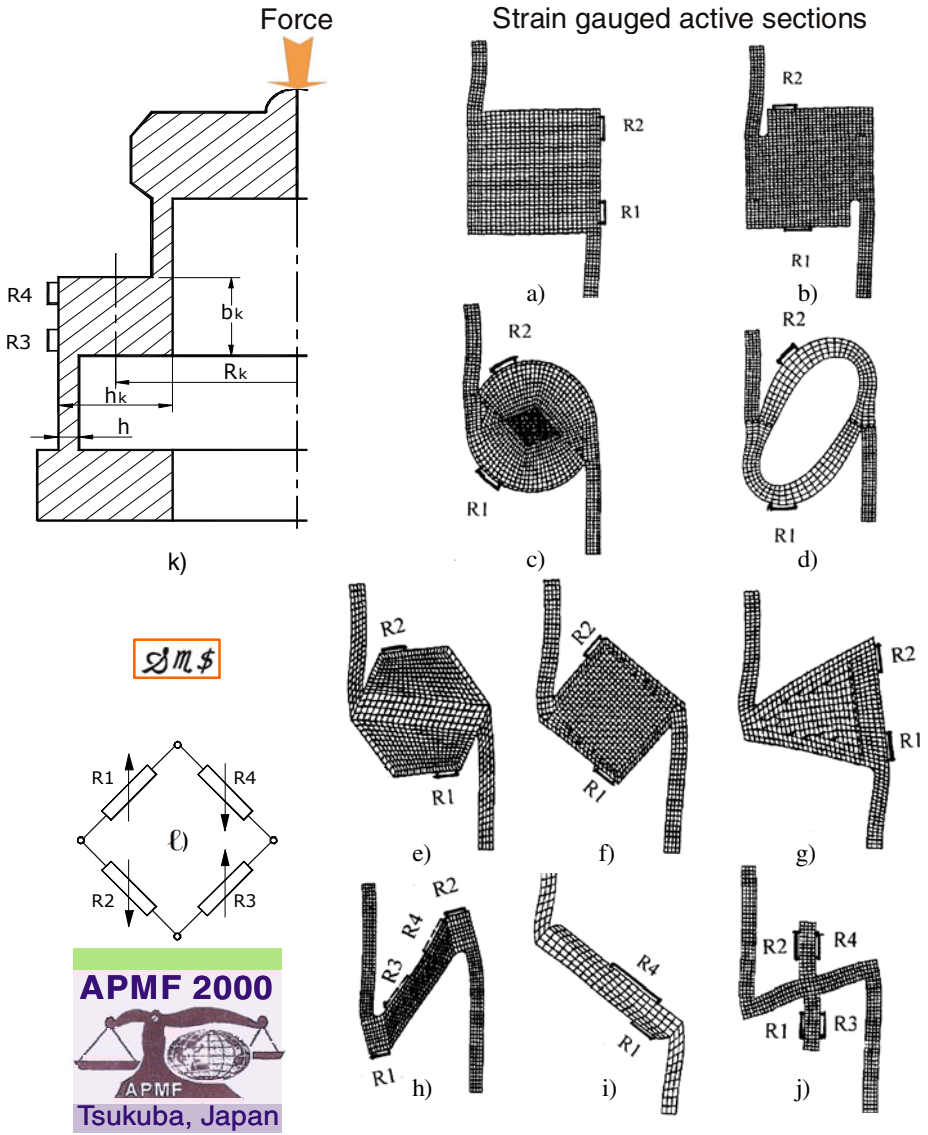


Fig. 31.3 Axisymmetric elastic elements with various types of active sections (*ostrichs*) a) square, b) rectangular, c) circular, d) toroidal, e) hexagonal, f) rhomboidal, g) triangular, h) N-shaped, i) truncated cone, j) ribbed membrane, all of them being generically loaded by a compressive force (k). Strain gauges positions are indicated for each sensing section, together with their electrical connection in Wheatstone bridge (l) (R_1 and R_3 are increased while R_2 and R_4 are decreased).

31.2. AXISYMMETRICAL EEs FOR VERY LARGE FORCE TRANSDUCERS

The challenge to measure greater forces, up to 10^7 N, constitutes a development trend together with the opposite one, that of the measuring methods for very small forces (micro- and nano-range). In different industries (ship or aerospace building, rolling mills, civil engineering) large forces measuring with high accuracy is a proper subject for harmoniously blending theory, practice and applications, with a special accent in the field of Metrology.

As visiting researcher in the Force Laboratory of KRISS, the author has developed a design technique for strain gauge type force transducers using the finite element method (FEM) having in view new transfer standards [31.14]. Design specifications of the present work are the following:

- capacities: 1 MN and 7 MN, overload: 200 %;
- average strain at nominal load under each strain gauge: $\varepsilon = \pm 1000 \mu\text{m/m}$ to $\pm 1500 \mu\text{m/m}$;
- maximum displacement under nominal load < 0.4 mm;
- height: as small as possible, not recommended column type sensing element;
- one-piece solution, maybe a new and aesthetic one.

Among the various flexible structures studied only few types are suited for measuring forces in the meganewtons range: tensioned/compressed column (cylinder – EE-1 or tube – EE-2), shearing structures (EE-6), membrane (EE-9), compressed torus (EE-10) or sphere (EE-12), and other axisymmetrical shapes. Their maximum strain gauge (tensometrical) sensitivity is ensured by loading in shearing or bending.

To generate complex shapes of monoblock elastic structures starting from simple shapes of the strain gauge measuring sections, the axisymmetrical ones are the best suited in this respect. The body of the force transducer is easy to design by 2D axisymmetric FEM and easy to manufacture.

Now, an increased measurement range, i.e. a possible extension up to 10 MN, is considered. We follow a unified approach of square (type A) and rectangular (type B) sections. Square section is among the few with an analytical but complicated formula, having the strain gauges R_1 and R_2 tangentially located on the outside of the ring torsion and the other two strain gauges, which complete the Wheatstone bridge, being diametrically opposed. The rectangular section (with different ratios between the two sides but without analytical formula), is obtained by a minimum modification of the previous one (adding two slots), the strain gauges being located on the upper and the lower faces of the measuring section, respectively, and has an industrial use.

Both above-mentioned strain gauged measuring sections belong to the generic category of *ring torsion*, also named *bending ring*, which is associated with special spiral strain gauges without end loops. So, the tangential or circumferential strain of the bending ring is transferred into such a spiral without any shear stress, since the spirals are, in this sense, endless. This elastic structure is insensitive to the interference effects by eccentric loading as well as to the side forces and torques.

For these axisymmetrical elastic elements with square (both equal sides) or rectangle section an analytical formula is given by Malikov *et al* [31.7]. It is a complicated, nonlinear relationship from the Strength of Materials field, referring only to the tangential / circumferential strains on the lateral side of the measuring section.

$$\varepsilon_{\max} = \frac{\varepsilon_0 \cdot (1-\nu^2) \cdot \beta_k^3 \cdot k^2}{(1-\nu^2) \cdot \beta_k^3 \cdot k^2 + 0,5 \cdot \sqrt[4]{[3(1-\nu^2)]^3} \cdot \beta_k^2 \cdot k_1 \sqrt{k_1} + \sqrt{3(1-\nu^2)} \cdot \beta_k \cdot k_1 \cdot k_2 + \sqrt[4]{3(1-\nu^2)} \sqrt{k_1} \cdot k_2^2}$$

where

$$\varepsilon_0 = \frac{3 \cdot F}{\pi \cdot E \cdot \beta_k^2 \cdot h_k^2} \quad \beta_k = \frac{b_k}{h_k} \quad k = \frac{h_k}{2R_k} \quad k_1 = \frac{h}{R_k} \quad k_2 = \frac{h}{h_k} \quad (31.1)$$

We choose, for $F = 7$ MN, a first model having the following geometrical parameters, considered as the design variables: $h = 25$ mm, $R_k = 120$ mm, $h_k = 90$ mm, $b_k = 54$ mm, resulting $\beta_k = 0.6$.

The influences of vertical dimensions (such as length of the two connection tubes, height of the cover or height of the base portion) or other shape factors (like the fillet / corner radius) are not estimated analytically but are best suited for FEM analysis! We can calculate only the maximum circumferential strain (1421 $\mu\text{m/m}$) on the lateral side of the measuring section, but predimensioning is very complicate because of the multiple cross-influences between the geometrical parameters as defined by Malikov. Substantial estimations and improvements are possible by using the finite element analysis and developments of new designs based on these, so that very little prototyping to be required.

We define a complete model representing the geometrical parameters from the Malikov's formulae (31.1) as well as other parameters not included in this analytical relation (Fig. 31.4). Material properties (elasticity moduli) are the same for all variants and are the classical ones for steel: Young's modulus $E = 210$ GPa (N/mm^2) and Poisson's ratio $\nu = 0.3$.

This starting model is very "flexible", so that, changing one by one different parameters (e.g. modifying the keypoints coordinates), a lot of variants could be studied. The strain gauges will be placed on areas with high

strain gradients, which make the gauge outputs very sensitive to placement errors. Therefore, it is important to generate high strain over a sufficiently large area. This objective is difficult to formulate analytically, but it can be achieved by finite element method.

A general procedure for finite element analysis of the force transducers elastic elements do not exist. Designers are working based on their experience and intuition in this multi- and inter-disciplinary field. We formulated at KRISS a standard FEA procedure for axisymmetrical elastic elements of strain gauged force transducers using ANSYS 6.1 – Mechanical program [31.15].

As finite element we choose QUAD42 which is a 2D quadratic and low order structural element. We create a bottom-up model, starting with keypoints, from which we build-up lines, areas and, by rotating the axisymmetrical section, the solid model. We may consider the model being fixed (UX and UY are constrained) or supported on its base (only UY is constrained), there are not significant differences in strain diagrams and the displacement on the base is negligible ($d_x = 0.05$ mm).

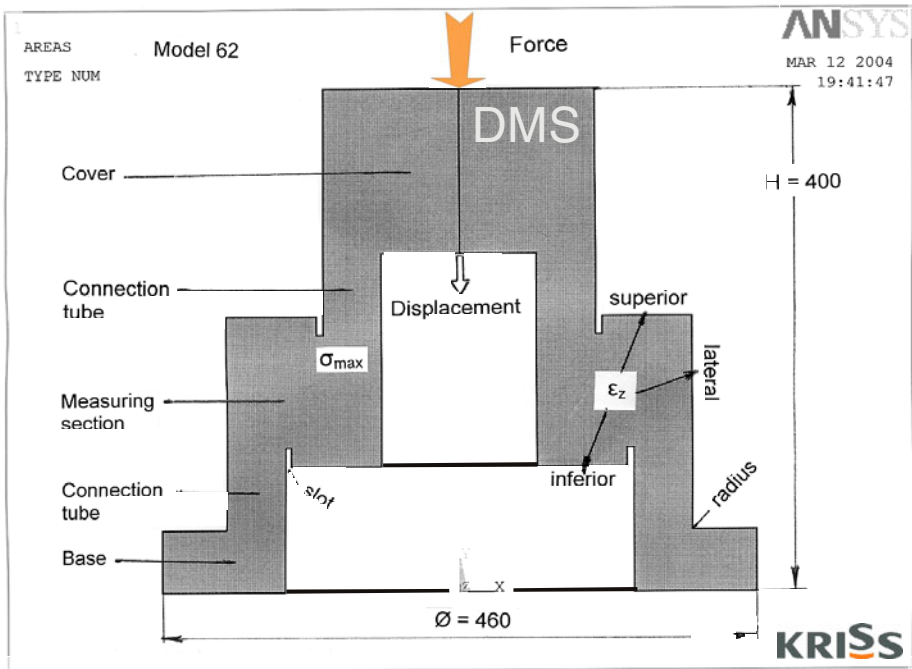


Fig. 31.4 Axisymmetric elastic element like a “hat”, illustrating the square (type A) and rectangular (type B) measuring sections. Applying compressive force F , it results: nodal displacements, stress map (σ_{max}), strain values on different sides (ANSYS program).

A special attention is necessary to obtain proper strain diagrams on the superior, lateral and inferior sides of the elastic element measuring section, because it is essential to compare these diagrams in order to establish the best strain gauges positioning. In this respect, appropriate paths for ε_z (STRAIN Z) were conceived and plotted each time on graph, more precise and suggestive than plotting on geometry! It is very important to define these paths in the same conditions for all variants of axisymmetrical elastic elements. A great importance has also the precise numerical computation of maximum stress and maximum displacement having in view the design criteria fulfillment.

The results obtained [31.16] conduct to the idea of a unified FEA approach of the rectangular axisymmetrical sections in order to investigate the influence of different parameters on strain gauge sensitivity, on all sides of the measuring section. A lot of interpretations are possible based on this multitude of data and having in view:

- the influence of the axisymmetrical elastic element shape (varying different parameters) on the strain gauge sensitivity; Figure 31.5 shows the influence of thickness h of the two connection tubes on the tensometric sensitivity.
- the best combination of conflicting design criteria: strain, stress (determining the overload) and displacement (determining the stiffness);
- the possible correlation between the nominal load and the dimensions of a particular variant, e.g. with square measuring section;
- the optimum strain gauge emplacement solution for a chosen model of axisymmetrical elastic element.

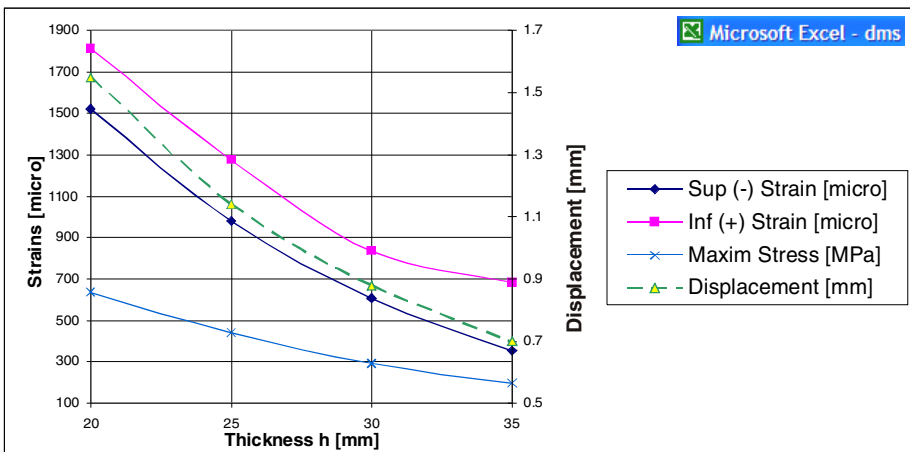


Fig. 31.5 The influence of the connecting tubes thickness h on the tensometric sensitivity of a rectangular axisymmetric elastic element for force transducers

“Active” data in Excel are Strain or Stress (connected by the Hooke’s law), represented on the left axis, and Displacement, shown on the right axis. Comparing their diagrams, strain and displacement have the same type of variation. So, it is necessary to establish clear priorities, like this concerning the shape factor:

- if a greater strain gauge sensitivity is preferred, the measuring section is placed horizontally;
- if a smaller displacement is preferred, the rectangular measuring section is placed vertically.

The square section is a particular case of the rectangle one and offers a multitude of dimensioning possibilities, because of its combined vertical and horizontal influences! Increasing progressively the dimensions is possible to increase the applied load.

We propose a unified FEA approach of the rectangular axisymmetrical sections, comparing a model without slots with a model with slots, the last being more sensitive from the tensometrical point of view (Fig. 31.6).

To resolve the classical dilemma “*sensitivity or stiffness*”, i.e. greater strains or smaller displacements, a careful negotiation of behavior restrictions is necessary. Of course, first priority is the maximum *strain* at the nominal load. For deciding between strength (maximum *stress*) and stiffness (minimum *displacement*) constraints, two new and very different research directions are envisaged, as follows:

- *Minimum displacement* (< 0.3 mm) for axisymmetrical elastic structures is ensured by tubes, but their strain gauge sensitivity is reduced, due to Poisson’s coefficient for two of them. The best way to improve their tensometrical sensitivity (up to 25 %) is to “transform” tension / compression in bending after profiling the tube section (by milling), knowing that *greater the fillet radius smaller stress concentrators*. Unfortunately, due to space restrictions, the overload is limited. The Saint Venant’s principle becomes invalid and the height of the tubular structure may be substantially reduced.
- *Maximum admissible stress* is supported by complex elastic structures subjected to very large forces (up to 10 MN) if they have pairs of deeper slots with larger radii, inspired by genetic algorithms. Such configurations are obtained starting from very flexible structures, like membranes (Fig. 31.3j) or N-shaped (Fig. 31.3h) elastic elements, and strengthening them by vertical ribs, respectively, thickening their sides, so that the displacement is also reduced. First example is, in fact, the GTM + PTB solution of ring torsion, having four symmetrical slots near the intermediate thick rib, while the second is a new one, based on an “oblique bending ring” resulted by cutting only two antisymmetric slots. Optimal design should be applied to satisfy reasonably strain, stress and displacement conditions.

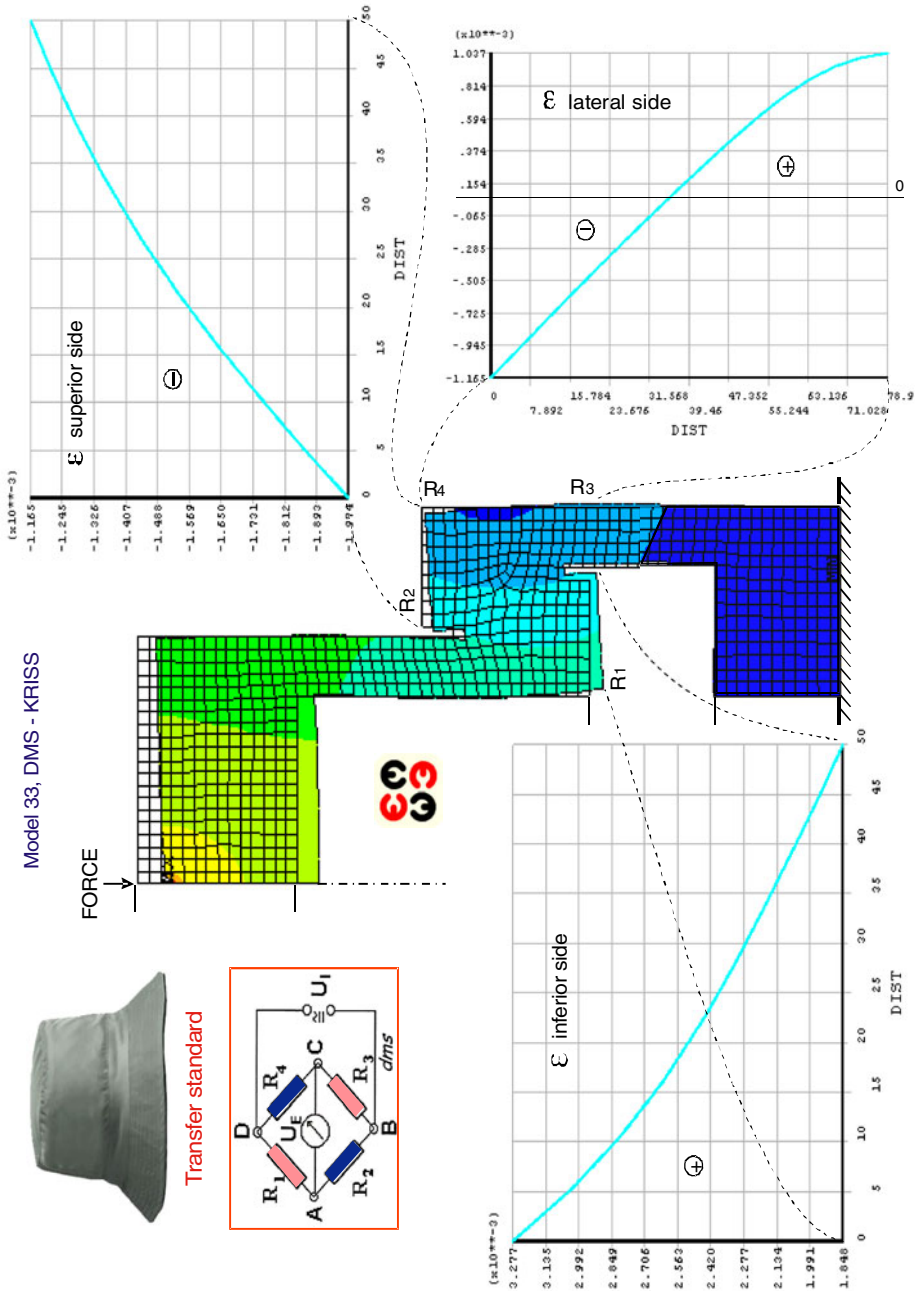


Fig. 31.6 Strain diagrams on the superior, lateral and inferior sides of a rectangular axisymmetric elastic element, strain gauges positions and Wheatstone bridge connection

31.3. N-SHAPED AXISYMMETRIC ELASTIC ELEMENTS

N-shaped elastic elements of strain gauged force transducers (SGFTs), have two cylindrical tubes of different diameters, concentrically telescoping one another, and a conical tube interconnecting their opposite ends (See Fig. 31.3h!). This right side of the N-shaped axial section is presented again in Figure 31.7a, together with the longitudinal (Fig. 31.7b) and tangential/circumferential strain diagrams (Fig. 31.7c). For the Wheatstone bridge connection (Fig. 31.7d) it is possible the “mixed” emplacement of strain gauges: R_1 and R_2 – circumferential while R_3 and R_4 – longitudinal. But having in view the golden rule of tensometry {Choose the zones with maximum strains and opposite signs!}, the best solution is: all strain gauges circumferentially located, R_1 and R_3 on the lower side of N-shaped section while R_2 and R_4 on the upper side of ‘N’ section (Fig. 31.8b). Other design and manufacturing aspects are presented in [31.17].

Continuing our initial research and extending 20 times the force range, from 50 kN to 1 MN [31.18], we envisage the following steps for N-shaped elastic elements design optimization:

- *mechanical* – establishing the optimum measuring range and overall dimensions for universal application of this new one-piece solution;

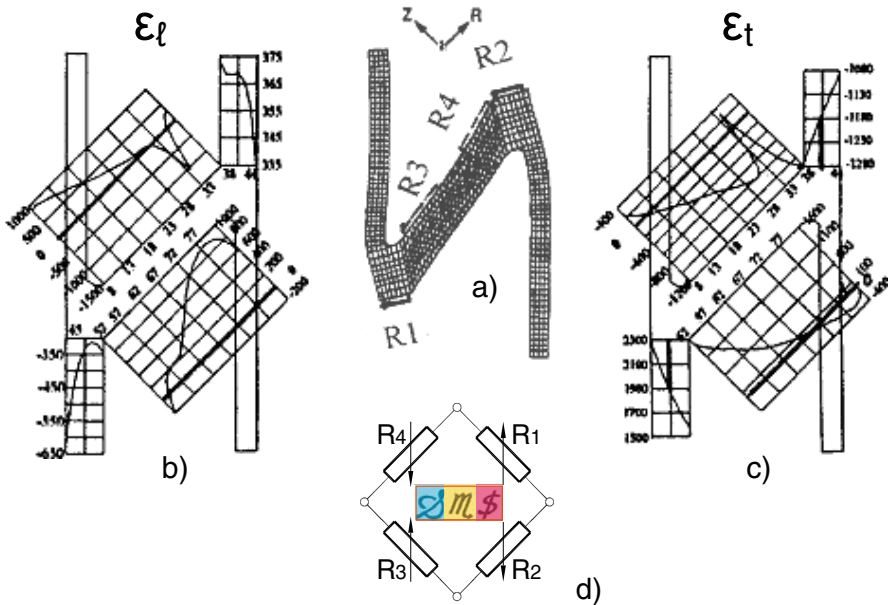


Fig. 31.7 N-shaped axisymmetric elastic element for strain gauged force transducer: a) FEM discretization & structural deformation, b) longitudinal and c) circumferential strain diagrams emplaced on the elastic element sides, d) Wheatstone bridge connection

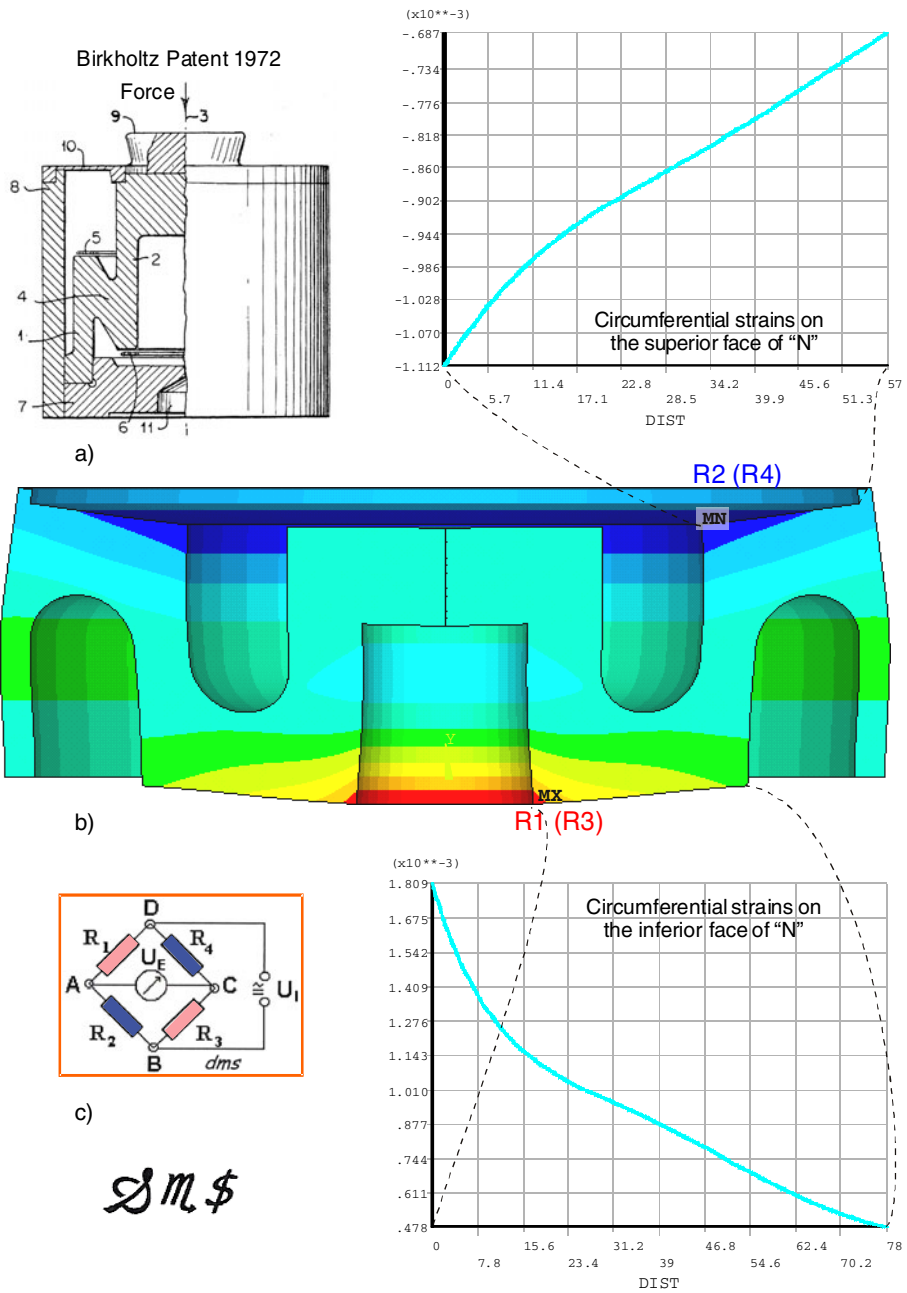


Fig. 31.8 N-shaped axisymmetric elastic element: a) initial patent, b) new model, FEM optimized, with associated strain diagrams, c) strain gauges in full Wheatstone bridge

- *numerical* – iterative FEM computation (2D analysis by ANSYS program based on Plane42 finite elements) for choosing the best axisymmetrical profile, to increase the measurement sensitivity;
- *electrical* – designing special strain gauges and choosing their optimal positions on the elastic body (tangential versus longitudinal) and Wheatstone bridge connections to improve the measurement accuracy and other metrological characteristics;
- *graphical* – representing, as a novelty, the longitudinal and circumferential strain diagrams directly located on the sensing sides of the N-shaped elastic element.

Figure 31.8 presents the final model of the N-shaped flexible element, which has been numerically modeled and simulated, reaching several important objectives during his evolution:

- decreasing of the elastic element height,
- embedded protection for 100 % overload,
- enhancing its tensometric sensitivity,
- obtaining of magnitudes ε_{max} and ε_{min} as close as possible in absolute values (nearly 2000 $\mu\text{m}/\text{m}$),
- optimal positions establishment for strain gauges.

We observe that the minimum height is obtained when realizing oblique slots, which allow connections with bigger radii, favorable for reduction the stress concentrators. It is derived, in fact, a new type of axisymmetrical elastic element, which has the sensible section like a horizontally placed ‘S’.

Comparing with Birkholtz’s patent (Fig. 31.8a), our solution has more advantages:

- one-piece, sturdy and easy-to-use construction,
- FEM optimized elastic element having in view the best tensibility, i.e. *tensometric sensibility*,
- more balanced $\pm \varepsilon$ values,
- specialized circumferential strain gauges, perfectly adapted to the chosen model of SGFT (We prefer the realization of customized strain gauges, as “doublets” of circumferential strain gauges, placed on the superior and respectively inferior side of the N-shaped elastic element),
- adapted models for different ranges of strain gauged force transducers,
- optimal positions establishment for strain gauges.

A complex and suggestive representation of the deformed N-shaped elastic element, together with the associated circumferential strain diagrams on the superior and, respectively, inferior sides of the axisymmetrical ‘N’, and the Wheatstone bridge connection, are shown (Fig. 31.8b and c). There are

two “circular” strain gauges on each side: R_2 and R_4 on the upper side, R_1 and R_3 on the lower one. A half sensitivity version could be performed by locating on each “active” side of a “double” strain gauge made by two half-circles completing an entire circle.

This new type of elastic structure for SGFT has all advantages of force transfer standards and, particularly, the following ones:

- minimum possible height and weight for strain gauge solution, the most popular and used technique for electrical measurement of mechanical quantities;
- special axisymmetrical shapes for the active sections – original design models, more sensitive than other uncustomized solutions;
- structural optimization of the force transducer elastic elements during the design stages using refined models in order to establish the best shape and the proper dimensions of the SGFT measuring section.

Here are some promising applications of the N-shaped axisymmetric elastic elements for strain gauged force transducers:

- on-site calibration of large testing machines in different industries (ship and aerospace building, rolling mills, civil engineering, etc);
- international comparison and technical expertise within sustainable development for countries without developed metrological infrastructure.

REFERENCES

1. Ștefănescu, D.M.: Truncated cone elastic element studied by Finite Element Method. In: Proc. 3rd National Symposium of Tensometry, Timișoara, September 28 - October 1, vol. IV, pp. 211–216 (1983) (in Romanian)
2. Kersten, J.: Innovative load cell technology. Application Note ISWM, Revere Transducers Europe, Breda, NL (1995)
3. Theiß, D.: Die Wägezelle: Von Wägegut zum Meßsignal. Auszug aus: A. Schuster. In: Industrielle Wägetechnik, Darmstadt, pp. 21–36. Eigenverlag, SCHENCK, Darmstadt (1983)
4. Allgeier, T., Gassmann, H., Sawla, A.: Load application and measuring behavior of a bending ring force transfer standard. In: Chung, M.S. (ed.) Proc. IMEKO 16th TC3 in Parallel with APMF 1998 Conf. Force, Mass and Torque Measurements – Theory and Practice, Taejon, Republic of Korea, pp. 112–117 (1998)
5. Ștefănescu, D.M.: FEM and strain gauge analyses for axisymmetric elastic elements of force transducers. In: Tojo, T., Ohgushi, K. (eds.) ACTA of the 5th Asia-Pacific Symposium on Measurement of Force, Mass and Torque, Tsukuba, Japan, November 7-10, pp. 85–90 (2000)
6. What managers need to know about Finite Element Analysis: How do I know it’s the right answer? Nastran-MacNeal-Schwendler Corporation, Los Angeles (1994)
7. Malikov, G.F., Șneiderman, A.I., Șulemovici, A.M.: Strain gauged elastic elements computation. Izdat Mașinostroenie, Moskva (1964) (in Russian)

8. Product guide for load cells. Revere Transducers Europe, Breda, NL, GB/D/F (1997)
9. Schrod, R.: RTN – the universal load cell – large performance but as small as a mouse. Hotline HBM, 12, November 20 (2002)
10. Ștefănescu, D.M., Sandu, M.A.: The state of deformations analysis for an elastic element with thin shells. Studii și cercetări de mecanică aplicată, Tom 45(2), 204–211 (1986) (in Romanian)
11. New generation diaphragmless ring-torsion load cells. Specification D 4133 e, SCHENCK Weighing – Handling – Testing, Darmstadt (1994)
12. Ștefănescu, D.M.: Strain gauge transducer with ribbed membrane. Buletinul Institutului Politehnic București – seria Construcții de Mașini, Tome L, pp. 91–95 (1988) (in Romanian)
13. Yang, R.J.: Shape sensitivity analysis and optimization using NASTRAN. Mechanical Structures and Machines 19(3), 281–300 (1991)
14. Ștefănescu, D.M.: Design technique development for strain gauge type force transducers using the finite element method. Final report, Brain Pool Program, KRIS, Division of Physical Metrology, Daejeon, Republic of Korea (2003–2004)
15. Introduction to ANSYS (UL registered ISO 9001:1994 Company). Training stage, Tae Sung Software & Engineering, Inc., Seoul, Republic of Korea, August 18-22 (2003)
16. Ștefănescu, D.M., Kang, D.-I.: Axisymmetrical elastic elements for very large force transducers. In: CD Proc. IMEKO TC-3 19th Int'l Conf. Force, Mass and Torque Measurements: Theory and Application in Laboratories and Industries, Cairo, Egypt, February 19-23, Paper 32 (2005)
17. Sandu, M.A., Sandu, A., Sorohan, Ș., Găvan, M.: Designing Manual for Strain Gauge Transducers. Editura Printech, București (2005) (in Romanian)
18. Ștefănescu, D.M.: N-shaped axisymmetric elastic elements for strain gauged force transducers. In: CD Proceedings XVIIIth IMEKO World Congress Metrology for a Sustainable Development, Rio de Janeiro, Brazil, September 17-22, Paper 141 (2006)

Chapter 32

VOLUMETRIC ELASTIC ELEMENTS

In the field of material strength and elasticity there are three ways for studying the massive bodies (blocks):

- the Euclid's solid – undeformable body from massive steel, slightly stressed,
- the perfectly elastic body – an idealization / simplification for calculus,
- the Hooke's solid – elastic element with a linear variation low $\sigma(\epsilon)$. The last concept is useful for transducer purposes but, generally, these massive volumetric bodies are not recommended for tensometric applications. For the sake of accurate presentation, the sphere is separated from the cube.

32.1. SPHERES

As an evolution of the passage from 2D (plane) to 3D (space), the work [32.1] analyzes the sensitivity for the following forms of elastic elements:

- drilled disc (washer) – a special case of thick tube;

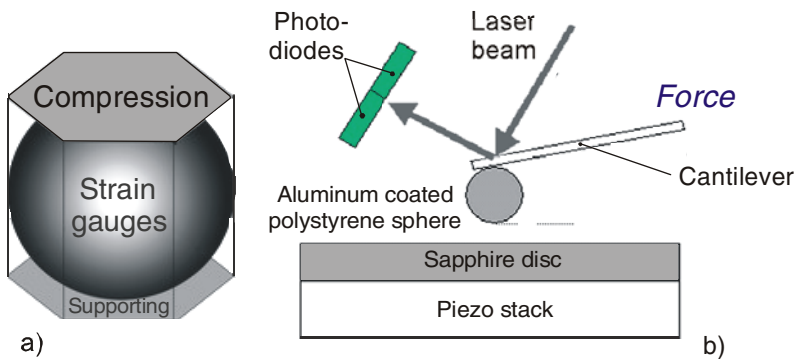


Fig. 32.1 Measurement principles on a spheric elastic element: a) strain gauges, b) atomic force microscopy

- thick wall tube, subjected to inner and/or outer pressure – differing of EE-2 type (stretched or compressed tube), presented in Chapter 22;
- spheric container (empty), the ultimate case of a full sphere (Fig. 32.1a).

The following measurement principles could be applied on the spherical elastic elements under variable loading: strain gauges, (micro)resonators, acoustic devices, and atomic force microscopy (AFM).

In the Mohideen and Roy's experiment (Fig. 32.1b) the force between an aluminum coated polystyrene sphere and an optically polished flat sapphire disc (also aluminum coated) is measured by the deflection of a laser beam. A piezo stack is used to bring the flat disc close to the sphere. The laser beam is reflected from the cantilever on which the sphere is mounted, and the position of the reflected beam is determined by the output of a pair of photodiodes. So, the elastic properties of the polystyrene sphere are essential during the force measuring by AFM.

While for the first two axisymmetrical shapes of this “progression” there are formulae for analytical calculus, the spheric shell can be approached by numerical methods: the finite differences method or the boundary elements one.

The sphere is a more rarely utilized elastic body, especially for high loads. It can not be deployed (as a map of the globe) because it does not have a ruled cylindric surface (where a line can be translated on a directory circle). Therefore, there are difficulties in the correct bonding of strain gauges on the spheric surface.

The spherical tensometric prototype can be found in [32.2], with an empirical sizing formula for the quotations given in Figure 32.2 (top):

$$\text{Diameter } D \text{ [mm]} = \text{one tenth of the force } F \text{ [N] square root} \quad (32.1)$$

In several interesting applications, Igarashi [32.3] makes use of chamfers to locate the semiconductor strain gauges. There are microsized ball load cells, fabricated by micromachining technique and having integrated the electronic circuitry.

An original solution is to be found in [32.4] where the elastic element of the force transducer type 7964 is a spheric dome (in other words the spherical portion over the “parallel 45°”), stressed in the middle as a beam supported at both ends (EE-5), with strain gauges located at $\pm 45^\circ$ directions (EE-6).

The model 7964 is a dual circuit load cell designed for those applications where the process can not be interrupted even in case of load cell failure. Based on dynamic piezoresistive effect of semiconductor silicon, two independent bridges are matched and interchangeable. The measuring element is a sphere portion, suitable for the direct measurement of compressive loads.

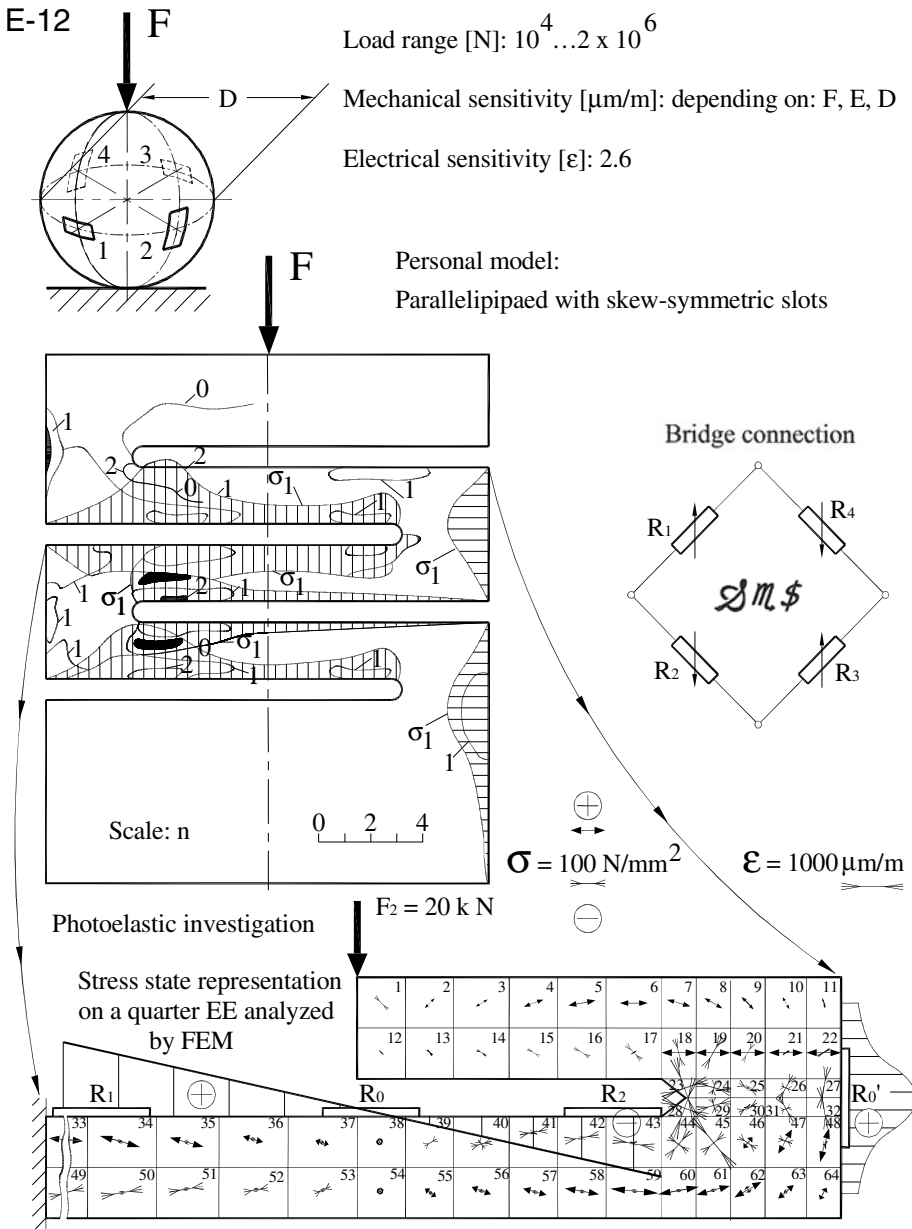


Fig. 32.2 Strain gauged elastic elements of type XII for force transducers. Investigations made by photoelasticity and tensometry are in good agreement with Finite Element Method determinations.

32.2. CUBES

32.2.1. Full cubes

Passing from the sphere to the cube, one could mention the 7928 product as a prototype in Kaliber Company, Hungary [32.4]: the cube is supported on the opposite corners of the square that represents the inner face, it is loaded with two forces applied on the ends of the perpendicular diagonal of the upper face, and $\pm 45^\circ$ strain gauges are located on the sides of the cube (Fig. 32.3).

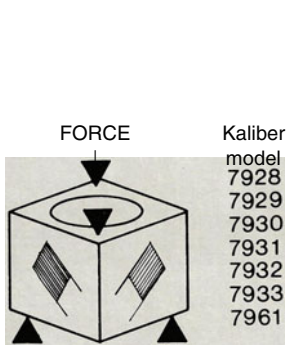


Fig. 32.3 Shearing force cube

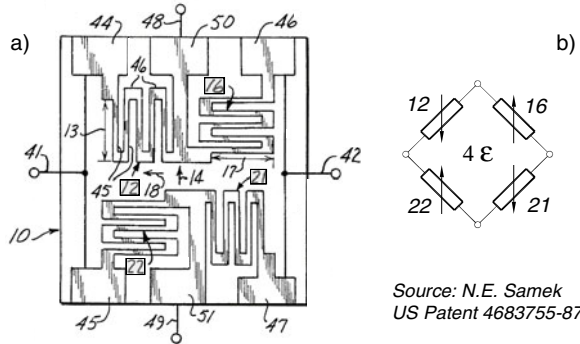


Fig. 32.4 Compressive force cube (a) and strain gauges connection in Wheatstone bridge (b)

A “force cube” sensor makes use of an elastic material in cube form with strain gauges emplaced to detect the longitudinal and transversal changes of dimensions caused by loading (not shearing components) [32.5]. This method is particularly suited to large forces, using a cube of metal rather than one made of more easily compressed materials.

Biaxial strain gauges and associated systems include or provide a substrate of semiconductor material having cubic unit cells. A first strain gauge has a dominant dimension oriented in the above mentioned first direction and is diffused into the substrate, having an absolute value of piezoresistive coefficient different from that in a second direction, transverse to said first direction [32.6].

For p-type gauges (with hole conductivity), tension will cause a positive resistance change, while compression will cause a negative change. For n-type gauges (with electron conductivity), tension will cause a negative resistance change, compression – a positive change. The highest longitudinal piezo-resistive coefficient is obtained if the gauges are oriented in the $\langle 1-1-1 \rangle$ crystallographic direction. This is the reason why many of the diffused silicon devices or also bulk silicon bar gauges are using (1-1-0) silicon wafers with gauges oriented in the $\langle 1-1-1 \rangle$ direction. In crystallographic terms, the first

and third gauges 12 and 21 are oriented with their dominant or longitudinal dimension (13) in the $\langle 1-1-0 \rangle$ direction of the (1-1-0) plane, while the second and fourth gauges 16 and 22 are oriented in the perpendicular direction on the cubic unit cell.

Properly mounted, this cubic unit cell could be used as an elastic element for strain gauged force transducers (Fig. 32.4). Its full Wheatstone bridge is positioned on the lateral side of the cubic unit.

Another model of cubical force transducer is presented in [32.7], comprising *“a force transmission block connected to the crystal face of the silicon semiconductor for transmitting a force perpendicularly to the crystal face; and a support bed supporting the silicon semiconductor and connected to the silicon semiconductor at a face opposite to the crystal face to which the force transmission block is connected, whereby a voltage corresponding to the force and to be measured is output from the input-output shared electrodes when the force is applied perpendicularly to the crystal face of the silicon semiconductor.”*

32.2.2. Cubic blocks with slots

The sensitivity increases greatly if the passage is made from the full cube to the empty one obtaining the following types of “cages”:

- structure with lateral walls represented by four S-shaped elastic elements, discovered by the American inventor Sandor Kovacs;
- cutting of the lateral walls resulting in bent or stretched/compressed lamellae for forces (and the measurement of moments with sheared “track-rails” located inside) for multipurpose multicomponent dynamometer [32.8]. One could also mention the “round cage” obtained from an “emptied” cylinder by cutting lateral windows [32.9].
- twin shear beams inside a cube in order to measure the bearing load simultaneously in three translational directions [32.10]. The custom designed sensor is manufactured from a metal block with wire cutting machining technique. Finite element analysis (FEA) have been carried out, with four load cases, to investigate the distribution of strain and stress within elastic structure, key measurement areas being identified. Full bridge electronic circuits, in three separate directions, are installed for strain measurements, ensuring on-line monitoring capabilities for the bearing force transducer.

An original contribution is represented by the parallelepiped with anti-symmetrical slots (Fig. 32.2, bottom), an elastic element fitted for resistive or inductive transducers. This tridimensional solid was theoretically studied (by means of the finite elements) and was investigated by comparative methods of experimental stress analysis (photoelasticity and tensometry), the results being in good agreement.

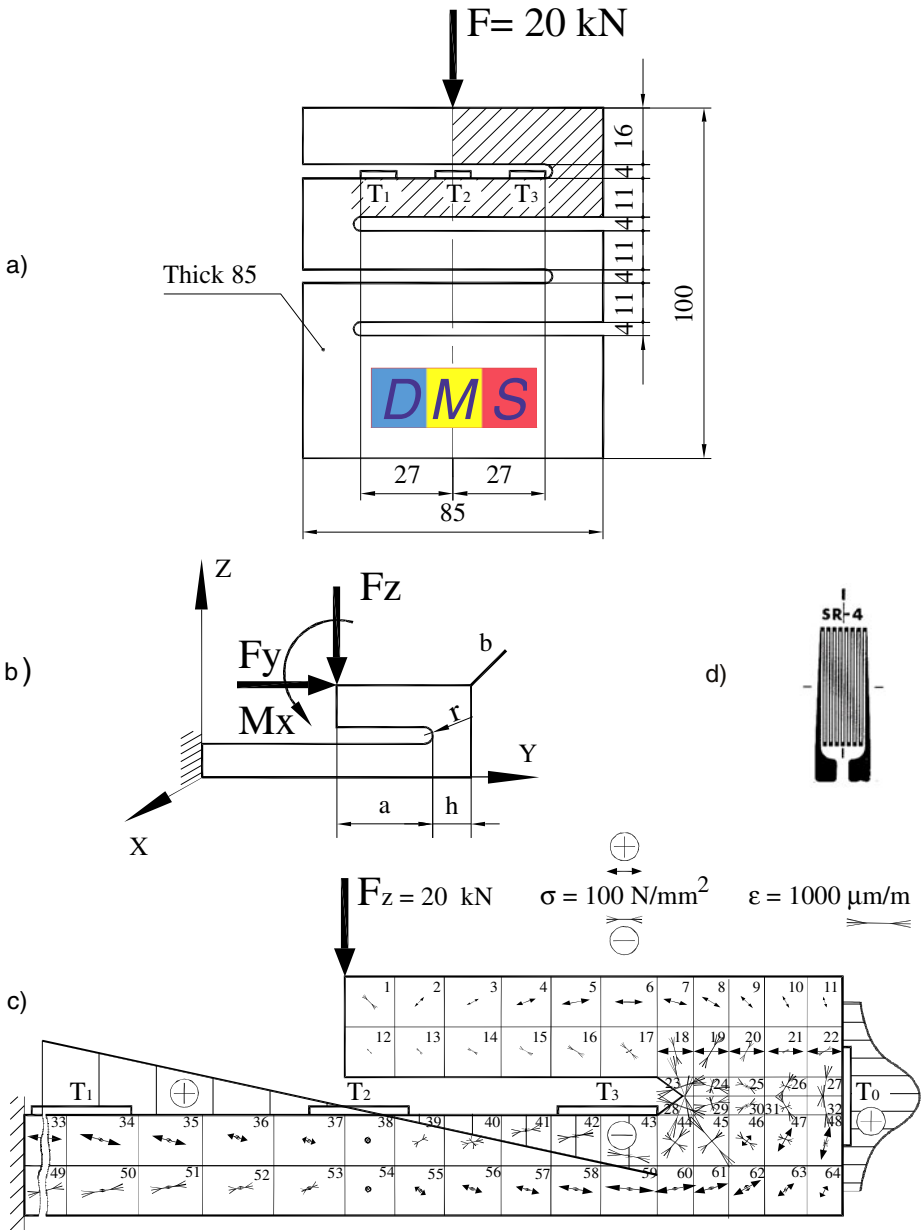


Fig. 32.5 Parallelepipedic elastic element with antisymmetric slots (a), computation model (b), finite element discretization, stress map and strain diagrams (c), and strain gauge pattern for the resistive force transducer (d)

Table 32.1 Strain measurements in three points for three force levels

Values	F [kN]	ε [$\mu\text{m}/\text{m}$]		
		T ₁	T ₂	T ₃
	0	0	0	0
Measured	10	636	12	-570
	20	1 274	25	-1 140
	0	0	0	0
Computed	10	650	12	-558
	20	1 300	24	-1 116

The paper [32.11] describes a parallelepipedic flexible element with horizontal slots (Fig. 32.5), suitable in the load cells prototyping. The simplest one, having only two antisymmetric slots, is the S-shaped elastic element. The analytic computation being complicated, the finite element method was used, studying an elastic structure quarter. Based on SAP IV and a proprietary post-processing program SV-01, the “map” of stresses and the strain diagrams were obtained, stimulating the comparative study for different measurement principles. Some typical effects are observed:

- applied load on element 1,
- encastree: elements 33 & 49,
- shear stress: elements 38 & 54,
- symmetry against axis 37-43,
- stress concentrator ($\sigma_{max} = 337 \text{ N}/\text{mm}^2$): elements 23 & 28.

To observe the full-field stress pattern and to determine accurately the stress concentration factors, a photoelastic sheet, having the shape of the elastic element from Figure 32.2 (middle), has been investigated by means of a reflection polariscope (Photoelastic Inc.). The test resolution is: band order $n_b = 2.35$ and $\sigma_{max} = 338 \text{ MPa}$. The photoelastic image is like an experimental “mirror” of the simulated loads on the model with finite elements.

Strain gauge measurements were performed using Hottinger equipment and P.T.B. recommendations. Some results are given in Table 32.1.

The conclusive point of view: owing to the “narrow” space for emplacing strain gauges, it is better to insert an inductive displacement transducer for maximum 1 mm in the sensitive body of the load cell [32.12], [32.13].

Fig. 32.6 presents the original elastic body prepared for the inductive load cell variant, more sensitive than the strain gauge instrumented one. The 20 kN inductive transducer prototype, made with indigenous parts, has the following components: 1 – applying force button, 2 – load cell body, 3 – nut M8, 4 – intermediate part, 5 – nut M2, 6 – LVDT transducer plunger, 7 – nut M12, 8 – displacement transducer, 9 – connection, 10 – overload stop.

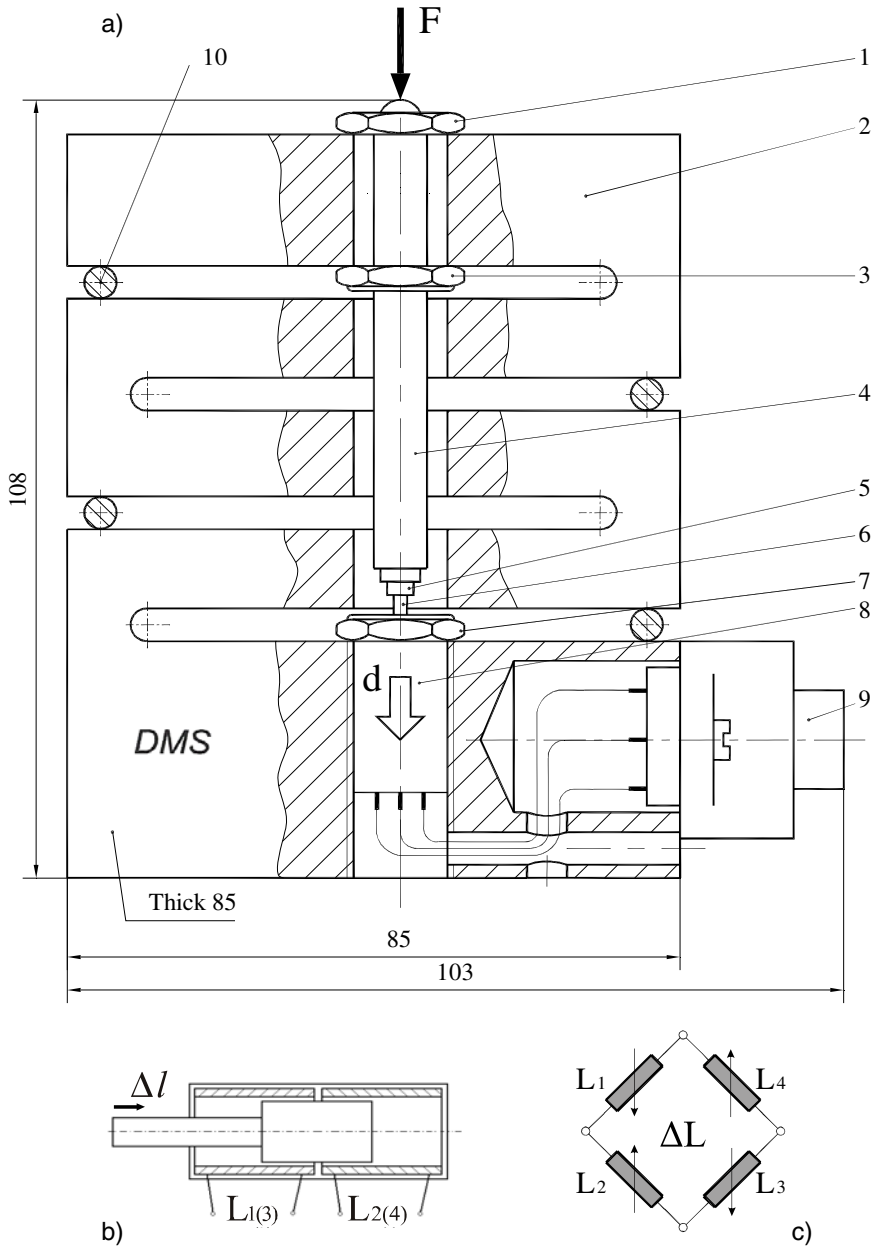


Fig. 32.6 Inductive variant for parallelepipedic elastic element (a), LVDT (linear variable differential transformer) displacement transducer (b), Wheatstone bridge connection for two LVDT devices (c)

The resulting deflection per slot is $314 \mu\text{m}$. The elastic element is practically insensitive to side force F_Y and bending moment M_X . Further research is necessary to optimize the shape of the slots (without notch stresses). Interactive structural optimization by the aid of a CAD system is very profitable.

The results of the numerical computation are in good agreement with those of photoelastic determinations and strain gauge measurement, stating this multidisciplinary research. Experimental stress analysis [32.14] has an important role to perform new elastic bodies for transducers. The homologated inductive load cell has a large practical utilization: testing machines for foundries, tension control in webs and strands, static or dynamic weighing.

32.3. COMPLEX BODIES WITH OBLIQUE SLOTS

Due to the great variety of cultivated plants, it is difficult to establish the optimum constructive and functional characteristics of the cutting devices in order to ensure the harvest with minimum energy and low losses [32.15]. In order to determine experimentally the cutting force, in static and dynamic regime, a special transducer, robust and sensitive in the same time, was necessary. It was designed as a “spatial Z” with two oblique slots and two positions for associated inductive transducers, mounted on a cutter device with alternating motion equipping the Romanian C.F.U. combine (Fig. 32.7).

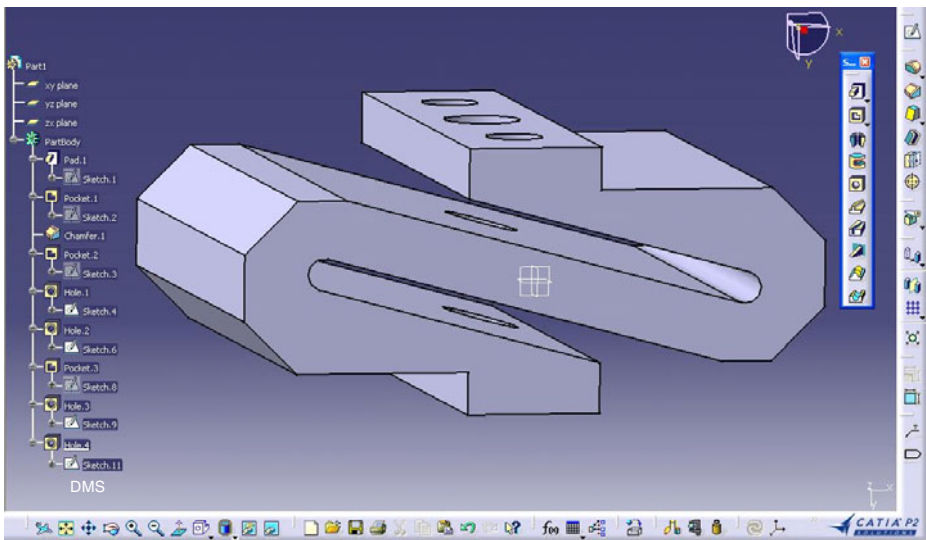


Fig. 32.7 Z-shaped spatial elastic element for measuring cutting force for thick plants

By connecting this elastic element, with two slots and two locations for the linear variable differential transformers (LVDT), to a process computer, it is possible to achieve a complete and modern data acquisition system. By these direct force measurements the working parameters of the cutter devices can be adjusted in order to maintain energy consumption during the work at optimal values. This applied research represents an important contribution to the structural optimization of the cutting devices for farm equipment.

REFERENCES

1. Lee, B.Y.: Direct differentiation formulation for boundary element shape sensitivity analysis of axisymmetric elastic solids. *International Journal of Solids and Structures* 34(1), 99–112 (1997)
2. Makarov, A.R., Renski, A.B., Borkunski, G.H., Etingof, M.I.: *Tensometry in machine construction*. Izdat Maşinostroenie, Moskva (1975) (in Russian)
3. Igarashi, I.: Semiconductor dynamic sensors. *Sensors and Actuators* 13, 53–62 (1988)
4. Méröcellák – Load Cells – Kraftmessdosen – Tenzodatciki. Kaliber Instrument and Measuring Technology (Founded 1924), METRIMPEX Budapest (1997)
5. Sinclair, I.R.: *Sensors and Transducers*, 3rd edn. Newnes – an imprint Butterworth-Heinemann, Oxford (2001)
6. Samek, N.E.: Biaxial strain gage systems. US Patent 4683755-87
7. Igarashi, I.: Force transducer and pressure detecting circuit using the same. US Patent 5349873-94
8. Millward, A., Rossiter, J.: The design of a multi-purpose multi-component strain gauge dynamometer (UDC 53.084). *Strain* 19, 27–30 (1983)
9. Bădescu, G., Ştefănescu, D.M.: Installation for determining the rocks elastic constants. *St. Cerc. Mec. Apl.*, Tom 40(3), 451–466 (1981) (in Romanian)
10. Yang, Z., Wang, S., Wang, Q., Xie, Y.: Three-dimensional bearing load sensor design and numerical investigations. *Sensors and Actuators A: Physical* 136(1), 304–312 (2007)
11. Ştefănescu, D.M., Găvan, M., Stoica, M., Ştefănescu, V.: Experimental stress analysis of an elastic element for force transducer. In: *Proc. 5th National Symposium of Tensometry, Galaţi, September 20-23, vol. I, pp. 171–178* (1989)
12. Kovacs, S.: Force measuring transducer. U.K. Patent 2139364 A, November 7 (1984)
13. Ştefănescu, D.M., Ştefănescu, V., Mănescu, T.: A new inductive force transducer. In: *Proc. 13th Int'l Conf. Force and Mass Measurement, Helsinki, Finland, May 11-14, pp. 145–149* (1993)
14. Mocanu, D.R., Buga, M., Iliescu, N., Atanasiu, C., Constantinescu, I., Pascariu, I.: *Experimental Stress Analysis*. Editura Tehnică, Bucureşti (1977) (in Romanian)
15. Ştefănescu, D.M., Ion, I.: Force and torque measurement at the farm equipment for thick plants cutting. In: *Proc. 12th IMEKO TC-3 Conf. Mass and Force Measurement for Improving the Efficiency, Szeged, Hungary, September 4-7, pp. 49–52* (1990)

Chapter 33

COMPLEX, COMPOSED AND COMBINED ELASTIC STRUCTURES

There are some elastic elements difficult to match a certain category. For example, here are two elastic elements with horizontal levers illustrating the classical dilemma concerning the best measurement sensitivity using strain gauges: bending (Fig. 33.1a) or shearing (Fig. 33.1b)?

The load cell type 7922 incorporates a classical measuring element of the “bent beam” type, suitable for directly measuring compression, tension and alternating tension-compression forces. This element is insensitive to lateral forces up to 50 % of the rated load.

The load cell type 7926 operates with a “screw”-shaped sensitive structure. It is sensitive to lateral forces and to force application disposed normally to its geometrical axis.

They cover a medium range of loads, having the following capacities: (1...5) kg for type 7926, (20...200) kg for type 7922, and (0.5...2) t for type 7923. These weights are also indicated in terms of (k)N in the producer’s catalog [33.1].

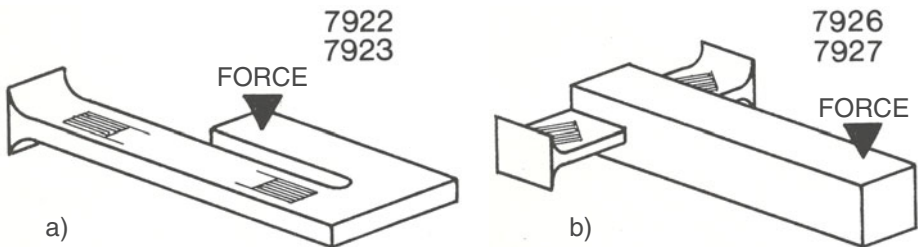


Fig. 33.1 Normal force is applied laterally, at a certain distance from the active elastic element. There are two different types of cantilever beams, *bender* vs. *twister*: simple, measuring longitudinal strain (a), and double ended, measuring shearing strain (b).

Among the unconventional elastic structures one can distinguish between three large categories, so-called “*three com*”:

- *complex* – made by cutting orifices with various shapes (holes and slots) into classical elastic elements (plates, prismatic bars, cylinders or tubes), sometimes resulting zoomorphic forms;
- *composed* – achieved by associating primary/elementary flexible elements nearly of the same kind, and obtaining complicate spatial structures;
- *combined* – assembled from different types of compatible elastic elements.

33.1. COMPLEX ELASTIC STRUCTURES

33.1.1. Plane complex structures

Starting from the circular or rectangular thick plates and machining holes and/or slots, some S-shaped elastic elements with zoomorphic forms are obtained: turtle (Fig. 33.2a) and duck (Fig. 33.2b).

Following the logical succession of the component drawings, Figure 33.3 has an interesting “story”, being appropriate for teaching applications:

- The spatial elastic element (3D) can be considered as being formed of 25 equally “slices” [usually thickness units, i.e. 1 mm] [33.2],
- easily to transform into a 2D representation by the design program Catia V5.

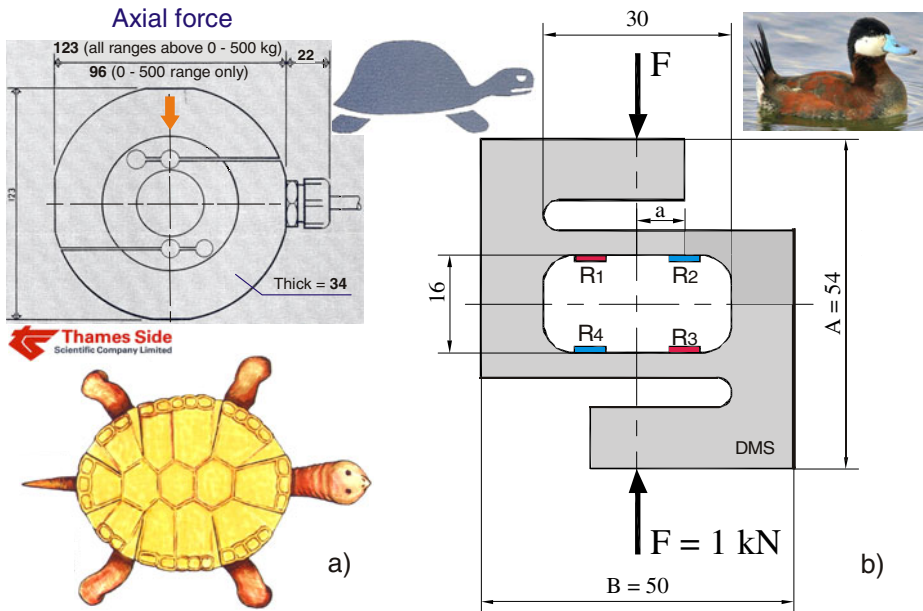


Fig. 33.2 S-shaped elastic elements with zoomorphic forms: a) turtle and b) duck

- c) Due to the structural antisymmetry, it is sufficient to analyze a half of the elastic element, in this case the upper part [33.3];
- d) the representation at an exaggerated scale of the elastic deformations of the discretized structure under the applied force (100 N) indicates the best places for strain gauges location and
- e) the associated electronic circuit connection, following the “golden rule” of the electroresistive tensometry: to obtain specific deformations ϵ as great possible and of opposite signs in the adjacent arms of the Wheatstone bridge.

Technological stages are the following:

- Cutting $(75 \times 55 \times 30) \text{ mm}^3$,
- Milling both ends $(50 \times 70) \text{ mm}^2$, $(25 \times 70) \text{ mm}^2$ and $(25 \times 50) \text{ mm}^2$,
- Boring $\text{Ø}30 \text{ mm}$,

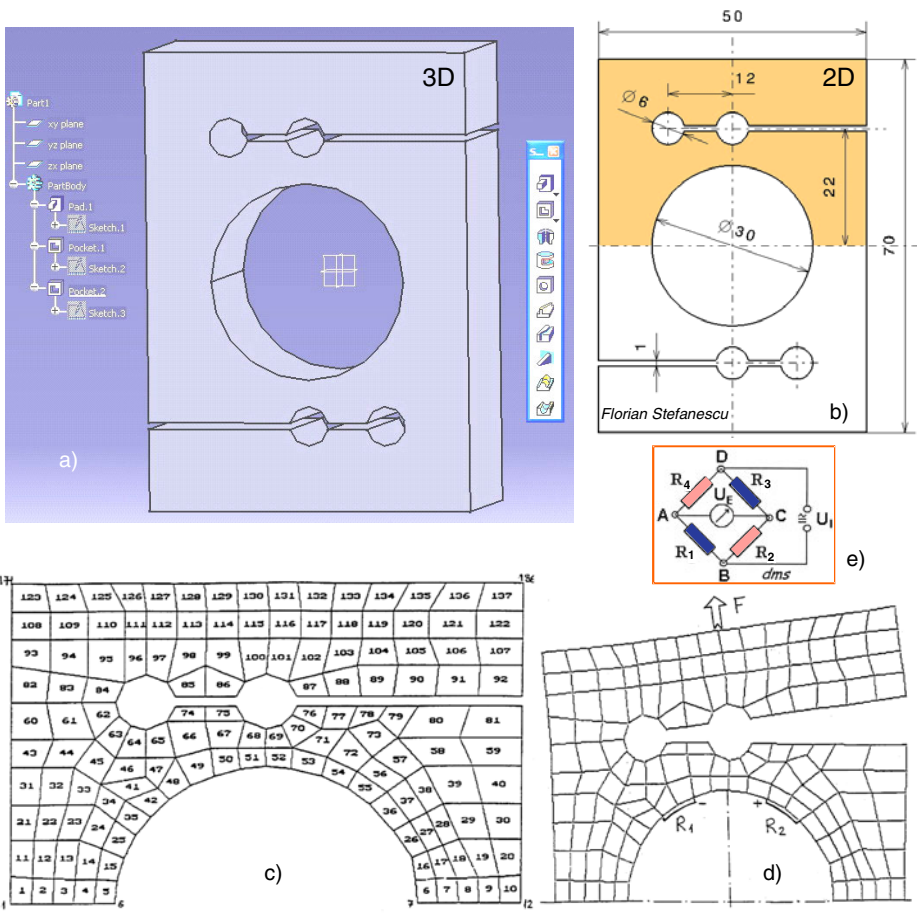


Fig. 33.3 ‘S’ element treated by Finite Element Method and Computer-Aided Design

- Drilling 4 holes $\varnothing 6$ mm,
- Cleaning,
- Electro-erosion metal working two channels $(1 \times 35) \text{ mm}^2$,
- Cleaning,
- Dimensional control.

33.1.2. Spatial complex structures

Figure 33.4 presents an internal strain gauged balance for aircraft models tested in wind tunnel [33.4]. It is a multicomponent force transducer made from a parallelepipedic block with a hole and a slot executed in two perpendicular planes. This complicated flexible element was calculated by FEM using the IMAGES (interactive microcomputer analysis of general elastic structures, Celestial Soft 1984) – 3D programme; about 600 eight-node three-dimensional solid finite elements were used.

An original balance for aircraft models tested in a supersonic wind tunnel [33.5] is shown in Figure 33.5 and detailed in Figure 15.10. The axial force is measured by four short lateral arms close to the middle of the balance interior. The other five components are measured in two symmetrical section, each consisting of a casing with three beams. This complex structure was developed by means of finite element analysis; the loads from 722 iso-parametric elements and the displacements for 1536 nodes were calculated by computer.

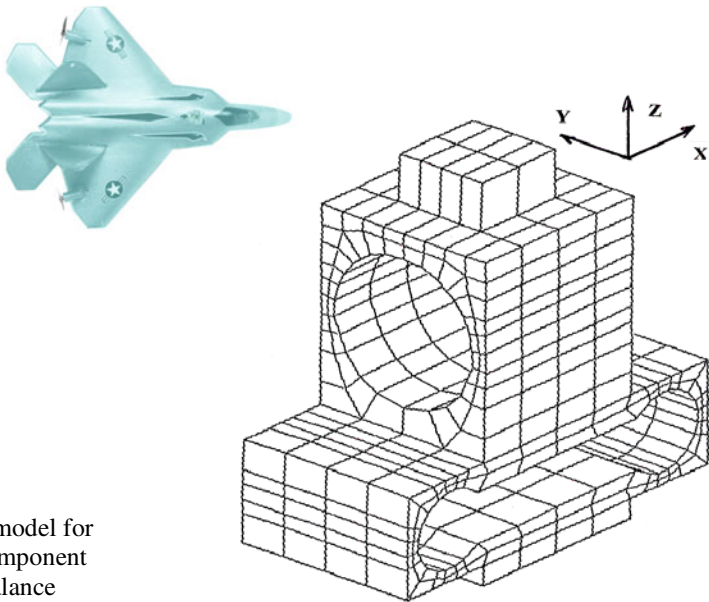


Fig. 33.4 FEM model for internal multicomponent strain gauged balance

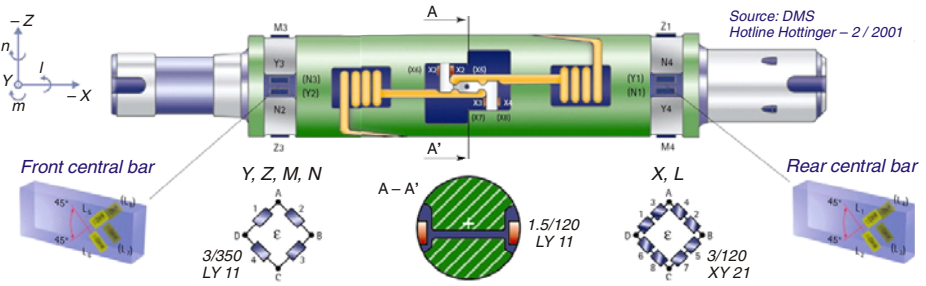


Fig. 33.5 Six-component strain gauged balance for aircraft models tested in the Romanian trisonic wind tunnel

The elastic tail of the balance was manufactured to the highest possible accuracy by electroerosion from a single piece of Armco 17-4 PH stainless steel and metallurgically treated to ensure a permissible tensile strength in excess of 400 MPa (N/mm²). It is 353 mm long and 50.8 mm in diameter.

In view of two conflicting requirements, the choice went to HBM’s Y series foil SGs with standard resistances as follows: 120 Ω – to satisfy the space restrictions; 350 Ω – in view of the total power supply (not exceeding 5 V) of the six Wheatstone bridges with four or eight active strain gauges.

Complex mechanical and electrical analysis was carried out in relation to the optimum method of attaching and connecting the SGs to the wind tunnel balance in order to increase sensitivity and compensate for disturbing influences. HBM’s transparent covering material SG 250 was used for additional protection.

This integral solution offers the best relation between capacity and volume, since the interplay between forces and/or moments is accurately specified by calibration.

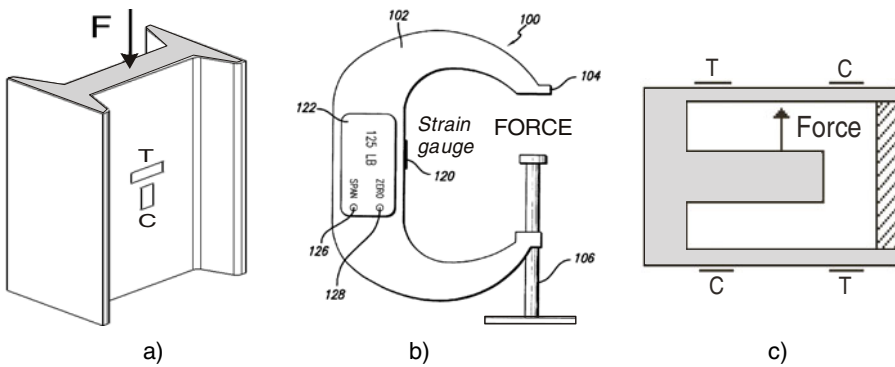


Fig. 33.6 Strain gauged elastic structures: a) I-profile, b) C-shaped and c) E-shaped

33.2. COMPOSED ELASTIC STRUCTURES

In the same way the words and sentences are made by letters, composed elastic structures can be achieved by simple shapes which could be letters too, like the I-profile presented in Figure 33.6a. Other “letters” are more complicated and might be classified as yokes (EE-7), e.g. ‘C’ (Fig. 33.6b), ‘E’ (Fig. 33.6c) and ‘U’ [33.6].

Elastic structures composed by rods with circular sections were presented in Chapter 22.5. Here are analyzed only configurations with rectangular sections. For example, ‘T’ and / or ‘L’ models, achieved by two perpendicular bars, are frequently used as composite elastic structures.

A special, optimized T-shaped transducer [33.7] was used for measuring the force of myofibrils with 1 μN in resolution and 100 Hz in frequency. Ca^{2+} activated force and recovery force during quick release of myofibrils have successfully measured by means of this microresonator.

In order to clarify characteristics of a new mechanism of movable lug, a model of single movable lug equipped with a L-shaped force transducer has been developed [33.8].

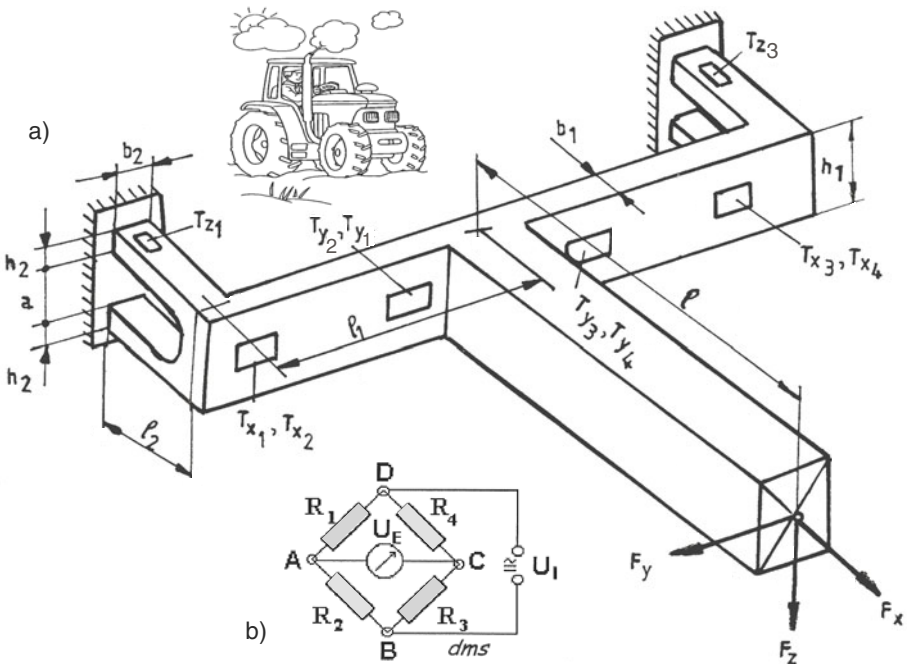


Fig. 33.7 Strain gauged force transducer for thick plants cutting (a), and general Wheatstone bridge connection for measuring three components: F_x , F_y and F_z (b)

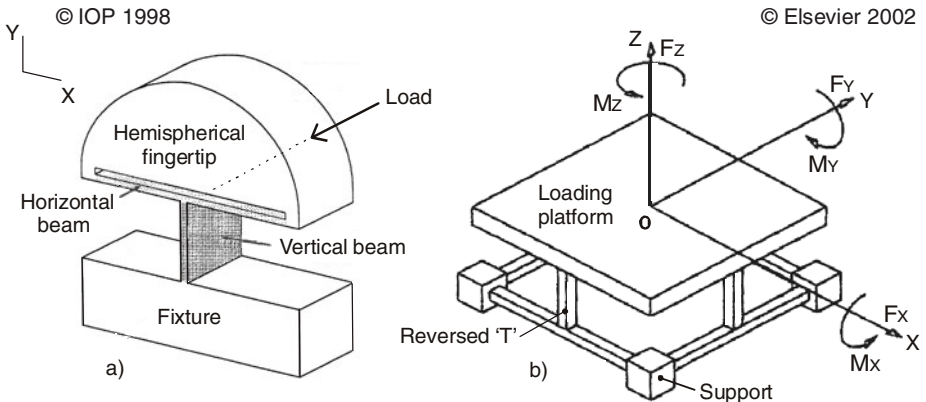


Fig. 33.8 Isotropic view of a T-shaped 3-component fingertip sensor (a) and isometric view (45°) of a 6-component force transducer based on four reversed T-shaped bars (b)

The soil reacting forces (normal and tangential) on a flat single movable lug, a curved single movable one and a fixed lug were measured on wet sandy loam soil in the laboratory soil bin test. Then these forces were converted into lug pull and lift forces. The forces obtained by the flat movable lug with 45° inclination angle and the curved movable lug were higher than those of the fixed one. In contrast to the flat movable lug with 45° slope angle, the curved movable lug produced bigger lift force, especially at high sinkage. The increase in lug slip from 5 % up to 50 % causes an increase in the peaks of pull and lift forces. The soil moisture content has affected the lug force significantly.

An elastic structure composed by two embedded yokes (EE-7) connected through a middle bent bar (EE-5) by means of a parallelepipedic lever (Fig. 33.7) is presented in [33.9]. At this stage, the analytical computation is still possible, but for the elastic structures presented below the finite element analysis (FEA) is more than necessary.

Some particular designs [33.10] use the deformation of the vertical and horizontal beams of the T-shaped bars. A structural design of a fingertip sensor for planar loading (forces F_X and F_Y , and torque M_Z) is shown in Figure 33.8a.

Four identical square-sectioned T-shaped bars (Fig. 33.8b) compose the sensitive part of a six-component force transducer in which a load transmitting thick plate sits on the four bars as a monolithic whole [33.11].

A wall balance for half-models (Fig. 33.9a), fitted into the Shlieren window ($\varnothing_{\max} = 750$ mm) of the Romanian trisonic wind tunnel is presented in [33.12]. A cross-sectional view is shown in Figure 33.9b. The elastic structure is made by two pairs of symmetrical arms (I and II), each arm being composed by cranked bars with rectangular sections (Fig. 33.9c).

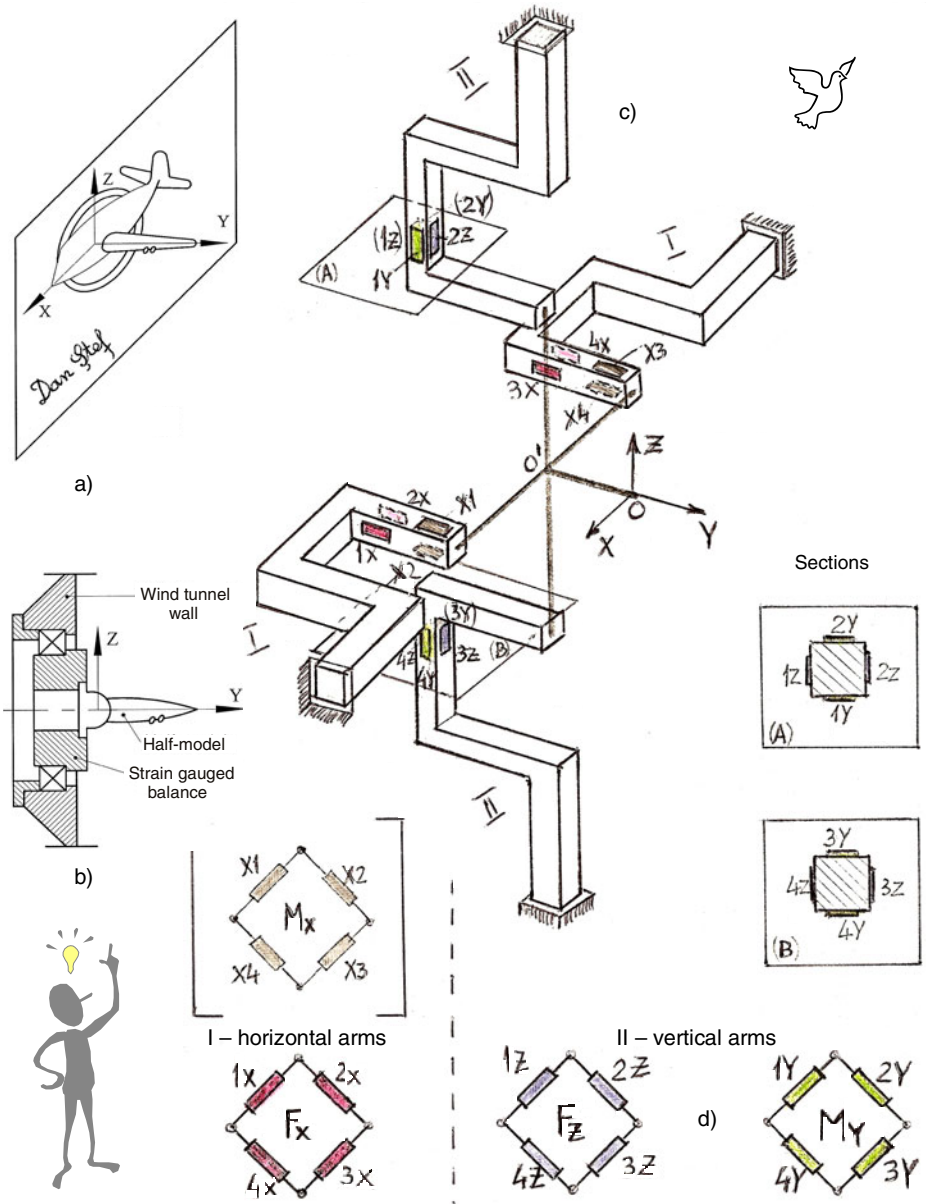


Fig. 33.9 a) Half-model fitted in the shlieren window of Romanian trisonic wind tunnel, and b) cross-sectional view of the assembly. c) The original drawing of a half-model balance with strain gauges positions. d) Wheatstone bridges for four components of the loading torsor, which is applied at the “central point” of the elastic structure.

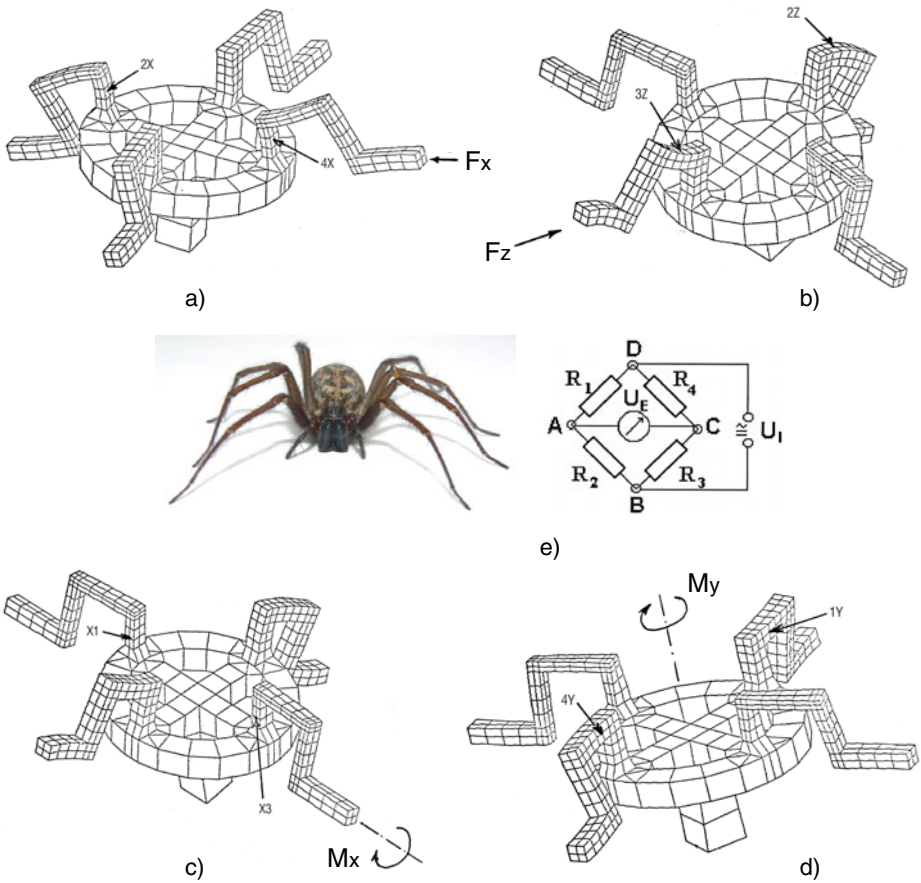


Fig. 33.10 Deformations for ‘spider’ (‘crab’) elastic element under different loading: a) drag, b) lift, c) roll, d) pitch, and e) Wheatstone bridge connection for strain gauges

All these elastic bars support compound loading (tension-compression, bending and/or torque), so FEA has been applied using 428 bricks (three-dimensional solid) and 980 nodes by means of structural analysis program IMAGES – 3D. The most favorable positions for strain gauges have been determined, and their Wheatstone bridge connection are shown in Figure 33.9d.

Figure 33.10 shows the deformation modes produced by the following group of loading components as zoomorphic-like images:

- a) Drag $F_x = 3 \text{ kN}$,
- b) Lift $F_z = 18 \text{ kN}$,
- c) Roll $M_x = 10 \text{ kN}\cdot\text{m}$,
- d) Pitch $M_y = 2.3 \text{ kN}\cdot\text{m}$.

33.3. COMBINED ELASTIC STRUCTURES

33.3.1. Plane combinations of elastic elements

The component parts of a microforce transducer (Fig. 33.11) are fabricated separately utilizing two different technologies [33.13]:

- four bulk-micromachined silicon sensing diaphragms, and
- two conventionally machined elastic structure (a inner silicon cross and an outer silicon frame).

These six elastic parts are assembled together using a Si-Au eutectic bonding technique.

On each of the four diaphragms (which are rectangular elastic bridges) two Wheatstone bridges are integrated, one for axial strains and other for shearing strains. This assembly of 8 bridges ensures the tensometric measurement of all the components (3 forces and 3 torques).

*Reprinted with permission from
Sensors & Actuators A: Physical
Vol. 65, page 110
Elsevier – 1998*

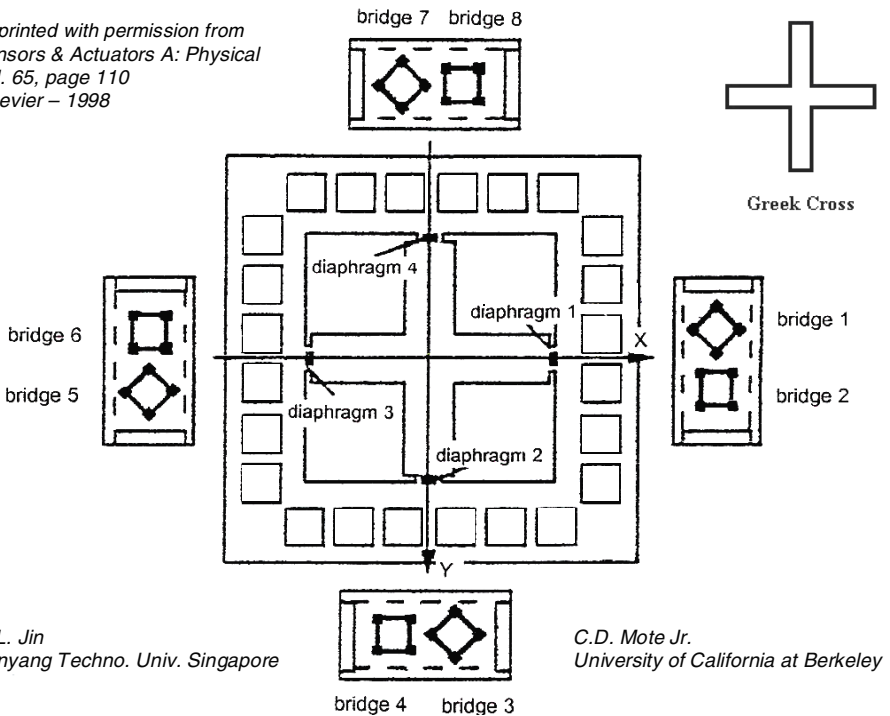


Fig. 33.11 Six-component microforce transducer based on four rectangular diaphragms connecting a inner cross and an outer frame.

Note the word “*bridge*” double meaning:

- elastic structure connecting the inner and outer parts of the transducer assembly;
- electrical connection of strain gauges using the Wheatstone circuit.

A strategy for the independent generation of the six components on the load plate during calibration uses the Lorentz force F generated on a conductor with length l carrying a current I in a magnetic field B to calibrate this multicomponent force transducer.

33.3.2. Axisymmetric combinations of elastic elements

Axisymmetric elastic elements {presented in Chapter 31 as EE-11} are made by various shapes of sections assembled between two tubes with different diameters [33.14]. The most of them could be fabricated as one-piece structures by computer numerical control (CNC) machining, but the torus (Fig. 33.12b) can be assembled between the inner and outer tubes only by welding (as shown in Figure 30.2, bottom!). These axisymmetric flexible structures are suitable both for static and for alternating tension-compression forces.

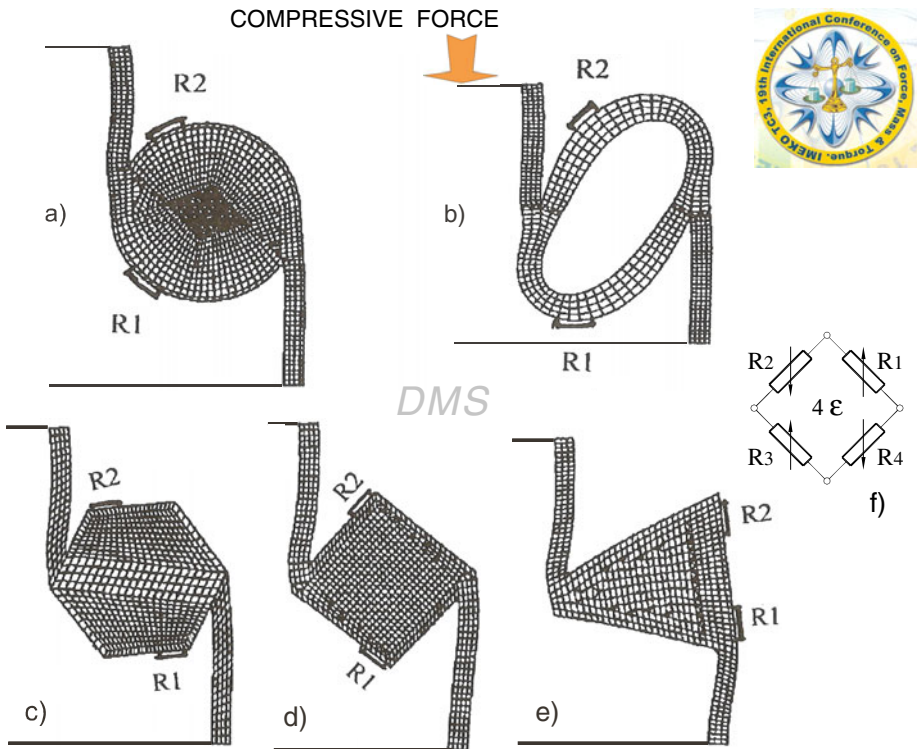


Fig. 33.12 Several ‘ostrichs’-like axisymmetric structures: a) circular, b) toroidal, c) hexagonal, d) rhomboidal, and e) triangular. One can notice the differences of flexibility (opposite to rigidity) under the compression force. f) Wheatstone bridge connection for strain gauges (R3, R4 are diametrically opposed to R1, R2).

33.3.3. Spatial combinations of elastic elements

A new type of force transducer [33.15] is mainly based on standard machine parts: two commercial spring discs (35.5 mm diameter), made by special stainless steel (DIN 1.4568), with known physical and mechanical properties (Christian Bauer GmbH). To realize such a force transducer two types of spring discs (Fig. 33.13), with the dimensions given in Table 33.1, are suitable.

The simple disc is an axisymmetric structure (Fig. 31.2, bottom), but it changes the feature of rotation composite structure by adding a central strap. Fig. 33.14 shows the new elastic assembly: a) sectional, and b) isometric view.

This force transducer is based on a tandem of plates (1, 2), positioned in mirror one to another. The sensitive element (3) is made by a sheet of steel from the same material, laser-cutted in rectangular shape, placed between the spring discs, and joined together by means of electron beam welding (4). Careful procedures are necessary to reduce the termic strain due to the welding process!

FEA was applied to simulate the mechanical strains and stresses within the force transducer and to improve its characteristics by optimal placing the strain gauges: (5) on the top and (6) on the bottom side of the sensitive strap.

The manufactured transducer was statically calibrated using a dead-weight testing machine with a maximum load of 125 kgf.

This is an ingenious mechanical converter of the compressive axial force (about 1 kN), which is vertically applied to the transducer assembly, into tensile horizontal force transmitted to its inner elastic element. The same kind of transformation is presented at the “resonanting” force transducer (Fig. 12.11b).

The main advantages of the new force transducer are:

- reduced height – important when it is introduced in testing machines,
- compact structure, easy to handle,
- low cost, using commercial spring discs.

The sensitivity is substantially increased by replacing the classical plane lamella (Fig. 33.14c) with a modified one, having a well-defined buckle with a certain radius and strain gauges sensing the “differential” bending (Fig. 33.14d).

This force transducer can be modified in such a way to permit the use of thin film strain gauges sputtered on ceramic plates.

Table 33.1 Models of spring discs for compressive force transducers

Spring discs	Dimensions [mm]			
	D_e	D_i	l_0	t
Thin	35.5	18.3	2.25	1.25
Thick	35.5	18.3	2.80	2

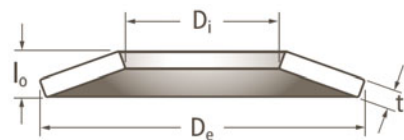


Fig. 33.13 Spring discs design parameters

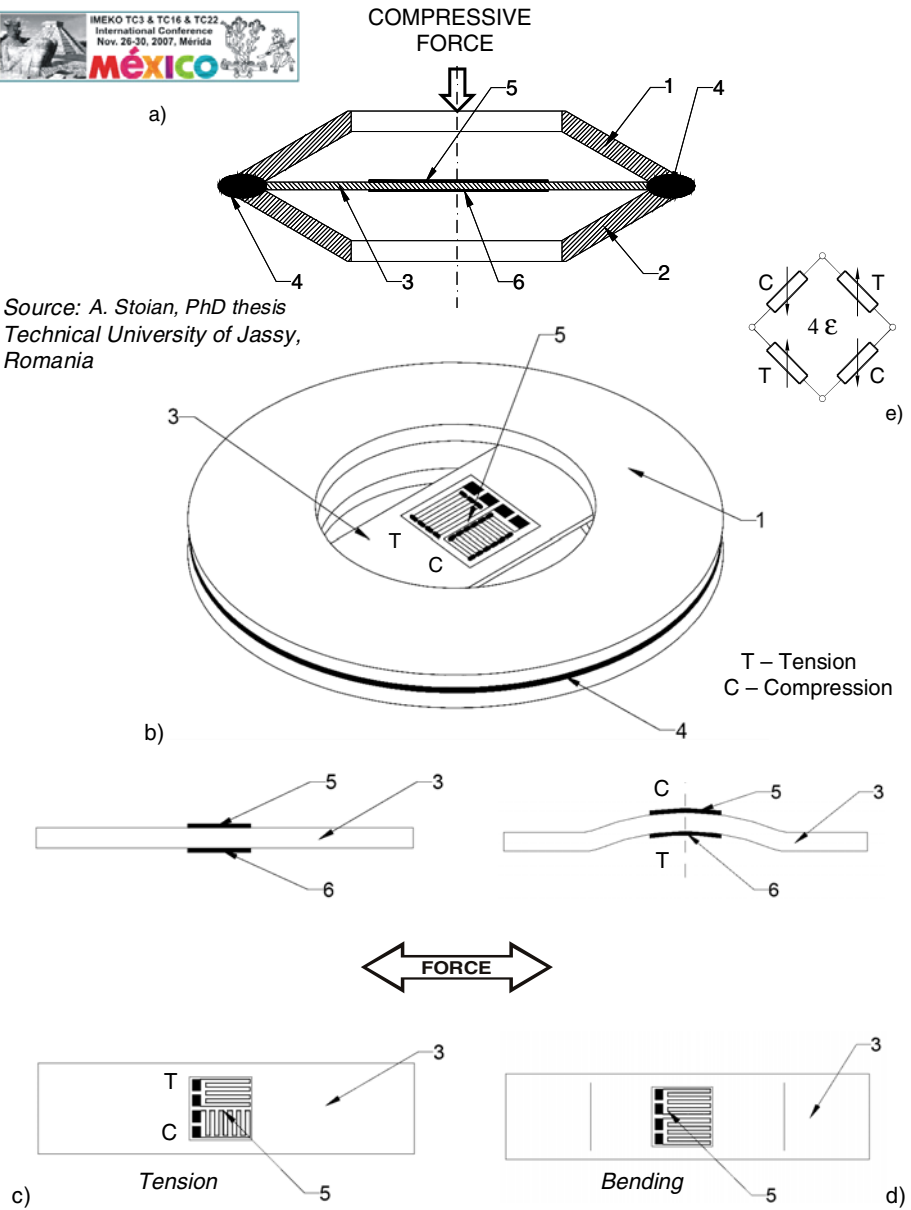


Fig. 33.14 Tandem of welded spring discs transforming the vertical compression into horizontal tension: a) section view and b) isometric view. Sensing strip with strain gauges subjected to tension (c) or bending (d). e) Wheatstone bridge for compressed (C) and tensioned (T) strain gauges.

REFERENCES

1. Méröcellák – Load Cells – Kraftmessdosen – Tenzodateci. Kaliber Instrument and Measuring Technology, Metrimpex – Budapest, Hungary (1997)
2. Ştefănescu, D.M.: Choosing and modeling criteria for elastic elements of transducers. Scientific seminar, Department of Measurements and Instrumentation, Twente University of Enschede, The Netherlands, October 16 (2002)
3. Ştefănescu, D.M., Sandu, A., Mănescu, T.: Z-shaped strain gauge force transducers. In: Proc. 14th IMEKO Int'l Conf. State of the Art in Force and Mass Measurement, Warszawa, Poland, September 5-8, pp. 155–160 (1995)
4. Ştefănescu, D.M., Mănescu, T.: Vertical strain gauge multicomponent balances for vehicle models tested in wind tunnels. In: Proc. KoREMA 1996 41st Annual Conf., Measurement Opatija, Croatia, September 18-20, vol.4, pp. 81–84 (1996)
5. Ştefănescu, D.M.: DMS in Windkanal - Rumanische Windkanalwaage mit Dehnungsmeßstreifen vom HBM. Hotline Hottinger – Informationen aus der industriellen Messtechnik (2), 12–13 (2001)
6. Schulze, W., Meyer, S., Hirche, S., Eger, M.: Flat electronic scales (Sartorius). US Patent 6211472-2001
7. Phan, K.N., Kobayashi, T.: Simple, effective and high sensitivity transducer for force measurement of myofibrils. *Sensors and Actuators A: Physical* 144(2), 389–393 (2008)
8. Hermawan, W., Yamazaki, M., Oida, A.: Theoretical analysis of soil reaction on a lug of the movable lug cage wheel. *Journal of Terramechanics* 37(2), 65–86 (2000)
9. Ştefănescu, D.M., Ion, I.: Force and torque measurement at the farm equipment for thick plants cutting. In: Proc. 12th IMEKO TC-3 Conf. Mass and Force Measurement for Improving the Efficiency, Szeged, Hungary, September 4-7, pp. 49–52 (1990)
10. Chang, Y.-H., Huang, Y.-C., Liu, Y.-P., Tsay, S.-M.: A novel structural design for force / torque fingertip sensors. *Measurement and Science Technology* 9, 1196–1203 (1998)
11. Liu, S.A., Tzo, H.L.: A novel six-component force sensor of good measurement isotropy and sensitivities. *Sensors & Actuators A: Physical* 100, 223–230 (2002)
12. Ştefănescu, D.M., Sandu, M.A., Sorohan, Ş.: Design and achievement of a strain gauged balance for half-models in wind tunnels. National Institute for Aerospace Research “Elie Carafoli”, Bucharest, Technical Report P-1491 (1994) (in Romanian)
13. Jin, W.L., Mote Jr., C.D.: A six-component silicon micro force sensor. *Sensors and Actuators A: Physical* 65, 109–115 (1998)
14. Ştefănescu, D.M., Kang, D.-I.: Axisymmetrical elastic elements for very large force transducers. In: CD Proc. IMEKO TC-3 19th Int'l Conf. Force, Mass and Torque Measurements: Theory and Application in Laboratories and Industries, Cairo, Egypt, February 19-23, Paper 32 (2005)
15. Stoian, A., Kuberczyk, T., Schultes, G.: A new type of force sensor. In: CD Proc. IMEKO Int'l Conf. Cultivating Metrological Knowledge, Merida, Mexico, November 27-30, Paper 2 (2007)

Chapter 34

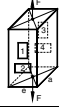
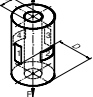
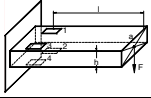
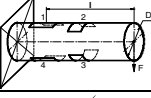
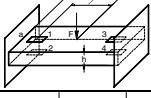
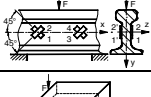
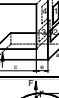

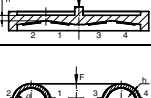
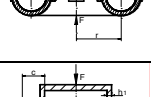
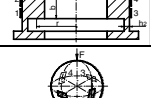
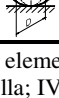
ELASTIC ELEMENTS SELECTION CRITERIA

Table 34.1 illustrates the “specific weight” of the twelve types of elastic elements which have been presented in the previous chapters. Figure 34.1 shows the first six positions classification. The cantilever beams (E-3) and elastic diaphragms (E-9) are most frequently employed, their basic Mechanics being deeply analyzed in the last volume of the series of “*Handbook of Sensors and Actuators*” [34.1]. The top triad is completed by the ring (E-8), and their positions are confirmed by the German classification (Table 20.1). Worth to be mentioned are the membranes (E-9), beams (E-3) and tubes (E-2) as the main elastic structures used to measure pressure, a physical quantity strongly connected with force.

Table 34.1 Twelve types of elastic elements and their “weight” according to this book. A supplementary category (Diverse elastic elements) reflects a “mean” specific weight.

ELASTIC ELEMENTS (EE)	Type	Ponderation	Chapter in this handbook
		0 5 10 15 20	
Column (pillar, tirant, rod)	1	10	C-21
Tube (hollow cylinder)	2	15	C-22
Cantilever beam	3	22	C-23
Shaft (bent or torsioned)	4	8	C-24
Middle bent bar	5	12	C-25
Shearing profiles	6	12	C-26
Yoke or frame	7	8	C-27
Ring (various shapes)	8	18	C-28
Membrane (diaphragm)	9	22	C-29
Torus (complex loaded)	10	6	C-30
Axisymmetrical	11	16	C-31
Block or sphere	12	10	C-32
Diverse elastic elements		15	<i>dms</i> C-33

Table 34.2

Type	Elastic element's representation	Sensitivity		Force range [N]			
		Mechanical [$\mu\text{m/m}$]	Electrical	10^{-2}	10^1	10^4	10^7
I		$\frac{F}{Eae}$	2.6				
II		$\frac{4F}{\pi E(D^2 - d^2)}$	2.6				
III		$\frac{6Fl}{Eah^2}$	4				
IV		$\frac{32Fl}{\pi ED^2}$	2.6				
V		$\frac{1.5F(2l - L)}{Eah^2}$	4				
VI		It depends upon F, E and the profile's dimensions	4				
VII		$\frac{F(6\frac{c}{e} - 1)}{Eae}$	2.6				
VIII		$\frac{3FD}{\pi Eae^2}$	3.7				
IX		$\frac{1.24F}{\pi Eh_{med}^2}$	4				
X		$\frac{2(1 - \nu^2)(1 - \frac{\rho}{r})F}{\pi^2 E h \rho (1 + \frac{3 h^2 r^2}{\rho^4})}$	3.7				
XI		It depends upon F, E, b, c, h1, h2, r	4				
XII		It depends upon F, E, D	2.6				

Types of elastic elements: I – Stretched - compressed column; II – Stretched - compressed tube; III - Bent lamella; IV - Bent and/or torsioned shaft; V - Middle bent bar with embedded ends; VI - Shearing strained profile; VII - Bent yoke; VIII - Bent ring; IX - Bent membrane; X - Compressed torus; XI - Axis symmetrical element; XII - Volumetric element.

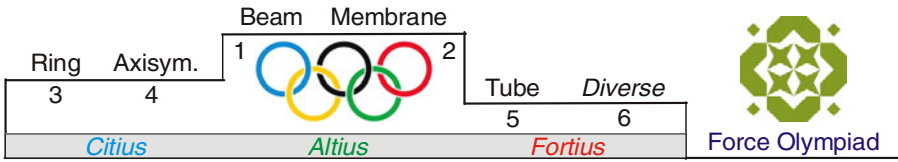


Fig. 34.1 Elastic elements classification in conformity with their weight in Table 34.1

34.1. ELASTIC ELEMENTS (EEs) EVALUATION CRITERIA

The most important selection criteria of force transducers are their load range and strain gauge sensitivity, the later influencing the measurement accuracy.

There are various ways of representing the load ranges [34.2] – [34.5]. Different catalogues [34.6], questionnaires [34.7], guides [34.8] or even flow charts [34.9] were made up; but, regarding the selection criteria of a certain tensometric force transducer type, the most important is the human decision. As Sophocles said, “*There are all kind of forces in the world but man is the strongest of all.*” Only for few industrial applications transducer accuracy between 0.5 and 2 % is acceptable; for the scientific applications a better accuracy, between 0.02 and 0.1 %, is required [34.10].

← Table 34.2 presents, like a universal poster, a global vision of the twelve types of force transducer flexible bodies, together with their measuring sensitivities and load ranges [34.11]. The following elastic element classification can be made according to their tensometric sensitivity, starting from the minimum value read for strain ϵ on the four strain gauges assembly making up a complete Wheatstone bridge (Table 34.3).

Some details regarding the fractionary values of the strain sensitivity are explained in Figure 34.2. There are three typical situations:

- a) *Tensioned/compressed strap.* The active strain gauge R₁ position coincides with the principal strain direction while the compensatory strain gauge R₂, transversally positioned on the elastic body E-1, senses approx. the third part (the Poisson’s coefficient) of the maximum strain. In this example, R₃ and R₄ are fixed resistors, without tensometric contribution in the Wheatstone bridge. In the full-bridge concept of a tensioned strap (rod, column or pillar), two strain gauges are active while other two SGs sense only the transverse effect of the axial loading, being “partially” active, so one can consider the “equivalent number” of the bridge active arms being 2.6, i.e. $2 \times 1 + 2 \times 0.3$.

Table 34.3 Strain sensitivity classification for 12 elastic elements presented in this book

ϵ_{read}	2.6					3.7		4				
EE type	I	II	IV	VII	XII	VIII	X	III	V	VI	IX	XI

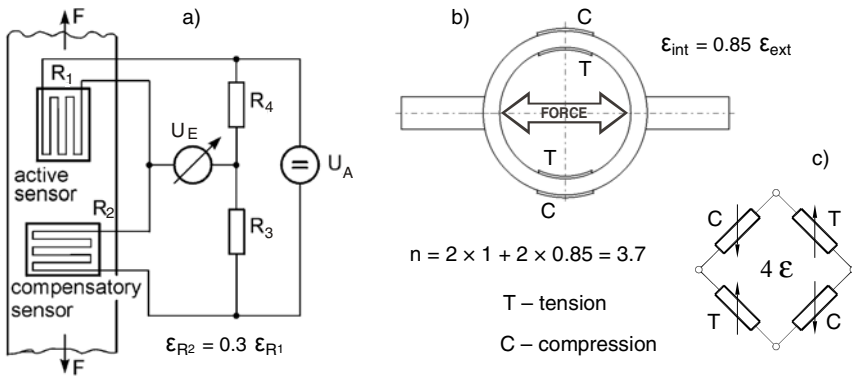


Fig. 34.2 Strain sensitivity for tensioned strap (a) and proving ring (b); general configuration for Wheatstone bridge (c)

- b) *Bent proof ring* (E-8) or *torus* (E-10). In the circular sections of the curve rods $\epsilon_{interior}$ is a little less than $\epsilon_{exterior}$, so that the global sensitivity of 3.7 is obtained (namely: $2 \times 1 + 2 \times 0.85$).
- c) *Shear* (E-4 and E-6) and *bent elastic elements* (E-3, E-5, E-9 and E-11) ensure the maximum value of strain sensitivity which is 4.

The sensitivity of the models E-1, E-2, E-7 and E-12 could be increased by carrying out appropriate slots or “profiling” their “active” sides.

In order to choose a certain elastic element other several criteria shall be considered, even if contradictory, that can make the option more difficult:

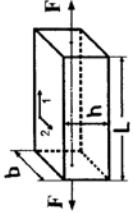
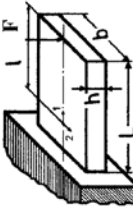
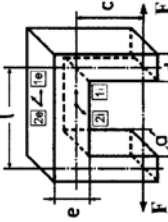

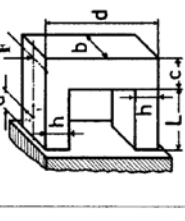
- the elastic properties of the material and heat treatment facilities,
- available space limitations determining the geometrical parameters [34.12],
- strain gauges emplacement possibilities in order to achieve proper mechanical and electronic symmetry of the force transducer [34.13],
- other specific characteristics: plane coefficient of compactness / compacity (circle versus square) or spatial coefficient of structural complexity [34.14].

ANNEX 1 shows the rules for strain gauges placement on the elastic elements.

34.2. ELASTIC ELEMENTS COMPARATIVE ANALYSIS

To evaluate the mechanical sensitivity of different elastic element types a unified notation is required, like in Table 34.4. Here are some elements (column, yoke, ring) at different loading modes (elongation, bending), suggesting valuable comparisons, such as model 1 (extended column) compared with 2 (bending beam), and 3 (clamp) compared with 5 (yoke, which differs from clamp by 90° rotation). The choice of a unique dimensional parameter, a , as comparison criterion, becomes necessary.

Table 34.4. Performance comparison for five elastic elements of strain gauged force transducers

Force Sensors Elastic Elements	1 - Column	2 - Bending beam	3 - Clamp	4 - Ring	5 - Yoke
Drawings → and Parameters ↓					
Calculus relations for strains ϵ_1	$\frac{F}{E \cdot b \cdot h}$	$\frac{6 \cdot F \cdot l}{E \cdot b \cdot h^2}$	$\frac{F}{E \cdot a \cdot c} \left(\frac{6 \cdot c}{c} + 1 \right)$	$\frac{F}{2 \cdot E \cdot a \cdot e} \left[1 + \frac{3 \cdot R}{e} \left(1 - \frac{2}{\pi} \right) \right]$	$\frac{3 \cdot F}{2 \cdot E \cdot b \cdot h^2} (L - 2 \cdot a)$
Calculus relations of the elastic constant k	$\frac{E \cdot b \cdot h}{L}$	$\frac{E \cdot b \cdot h^3}{4 \cdot L^3}$	$\frac{E \cdot a}{4 \cdot c^2 (2 \cdot c/d^3 + 3 \cdot l/e^3)}$	$\frac{E \cdot a \cdot e^3}{12 \cdot (\pi/4 - 2/\pi) \cdot R^3}$	$\frac{2 \cdot E \cdot b \cdot h^3}{L^3}$
Shape defined by the parameters	$b = h = a$ $L = 3a$	$h = a; b = 3h = 3a$ $L = 5b = 15a; l = 12a$	$d = e = a$ $c = 3a; l = 5a$	$e = a$ $R = 5a$	$h = a; b = 3a; c = 5a$ $d = 9a; L = 15a$
Maximum volume V	$3 \cdot a^3$	$45 \cdot a^3$	$21 \cdot a^3$	$121 \cdot a^3$	$540 \cdot a^3$
Maximum load $\frac{F}{\sigma_{max}}$	a^2	$\frac{a^2}{24}$	$\frac{a^2}{19}$	$\frac{a^2}{3.225}$	$\frac{a^2}{6.5}$
Sensitivity $\xi = \frac{\epsilon_1}{F}$	$\frac{1}{E \cdot a^2}$	$\frac{24}{E \cdot a^2}$	$\frac{19}{E \cdot a^2}$	$\frac{3.225}{E \cdot a^2}$	$\frac{6.5}{E \cdot a^2}$
Elastic constant k	$\frac{E \cdot a}{3}$	$\frac{E \cdot a}{4500}$	$\frac{E \cdot a}{756}$	$\frac{E \cdot a}{223.17}$	$\frac{E \cdot a}{562.5}$

Five elastic elements, made of the same material (elasticity modulus E , volume weight γ and maximum normal tension σ_{\max} being identical) can be compared according to five basic metrological and functional characteristics [34.15]:

- the maximum apparent volume, V (an overall size),
- mass: $m = \gamma \cdot V$ or force / weight ratio as a “quality factor”,
- the maximum relative load: P/σ_{\max} determining the applicability range,
- the sensitivity ξ defined as a ratio between the specific deformation under a single active strain gauge and the applied load,
- the elastic constant: k (the classical force/displacement ratio in mechanics) or the maximum deflection [34.16].

The hierarchy from the tensometrical sensitivity point of view is the expected one: cantilever beam (2), clamp (3), yoke (5), ring (4), and extended column (1). The elastic constant k has great variations (from 1 to 1500); it should have the smallest value for the displacement transducers and the greatest value for the force ones. The choice of an ideal shape for the transducer elastic element needs a complex multicriterial analysis based on a “decision matrix”; the relative variations of the characteristics considered as compared to the initially established reference version shall be introduced in this matrix [34.17].

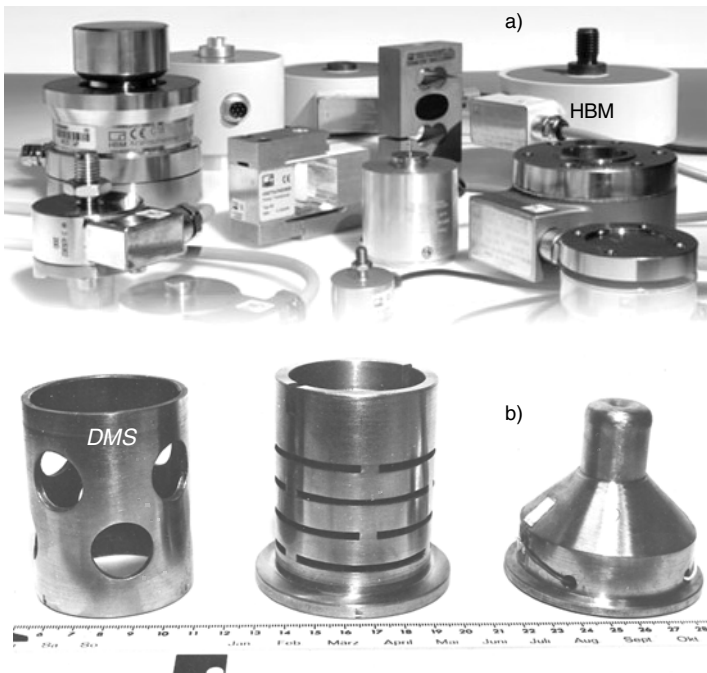


Fig. 34.3 Industrial (a) and custom-made (b) strain gauged force transducers

In the Hottinger catalogue [34.18] there are 17 force transducer and/or load cell types, which are included in 7 of the 12 categories established in this Handbook; part of this industrial production is depicted in Figure 34.3a. They have an attainable sensitivity between 1.8 and 2.2 mV/V (for Revere models it gets to 3 mV/V) with a tolerance in the range of ± 0.1 and ± 0.5 %; the associated amplifiers allow resistive bridges between 80 Ω and 5 k Ω , in measuring intervals between 0.1 and 2 mV/V for classical strain gauges, and between 20 and 500 mV/V for semiconductor strain gauges.

If there are particular requirements for force measurements, customized strain gauged transducers that optimally match every specific application are recommended, three examples being shown in Figure 34.3b.

34.3. EE SELECTION FOR SPECIFIC APPLICATIONS

34.3.1. From single- to multi-component force transducers

The force transducer functionality can be summarized as follows [34.19]: Virtually all force measurement transducers utilize a *spring-like structure*, which deforms under the application of a *force*, and a sensor to detect this *deflection* made by intimately bonded electrical conductors whose resistance changes with deformation. These *strain gauges* are normally applied in multiples of 4 and wired into a *Wheatstone bridge* configuration which allows measurement of the *change in resistance* of the gauges resulting from the force related deformation of the elastic structure. This Wheatstone bridge produces a variable *output voltage*, proportional to the applied force, when excited by a fixed voltage source. Typical outputs of a strain gauge transducer are on the order of 2 millivolts per volt of excitation when it is loaded to full scale, sensing correspondingly smaller voltages if lower forces are generated. Shortly expressed: the *elastic deflection* beneath the strain gauges is proportionally transformed into the Wheatstone bridge *electric indication*.

Source: Al. Brendel
Sensor Development Inc.
2001

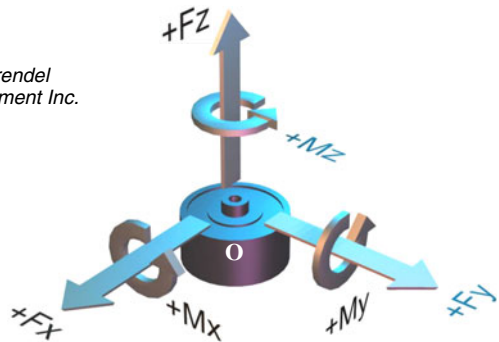


Fig. 34.4 Axes system for multicomponent force and torque transducers

A well designed transducer can be considered a force vector rezolver, and the obtained signal should be proportional to those force components which lie on, or parallel to, the force transducer sensitive axis. More complex elastic structures are necessary for measuring all the components of the force vector (Fig. 34.4) for specific applications in Robotics and for measuring aerodynamic loads on models tested in wind tunnels.

The usual types of force measuring applications in Robotics are [34.20]:

- gripping force measurement, correlated with the handled object items weight,
- robot action force determining in operating process,
- internal force measurement of the working gears (reactions in coupling, joggles, joints, etc),
- determining of forces generated by the robot mobile items displacement.

Special assemblings for the correct force overtaking are associated to the elastic elements. They are more rigid but also optimized by Experimental Stress Analysis and FEM (finite element method) procedures. Valuable presentations of these auxiliary structures are to be found in the references [34.21] – [34.23].

34.3.2. Force transducers in Mechatronics

Mechatronics today is more than the classical electromechanical engineering, including the information technology (Fig. 34.5a). The great majority of mechatronic devices used in the electronic measurements of force are based on strain gauges. Mechatronics imposes structural “concentration”: miniaturized SGs, piezoresistive thin films, nanodevices and microcontrollers (Fig. 34.5b). The author’s contribution consists in choosing a series of criteria for strain gauged elastic elements of force transducers in Mechatronics [34.24]. After all, like in holographic paradigm (Ken Wilber – the father of Integral Theory), one can notice in the same time the *unity-in-diversity* and the *diversity-in-unity*.

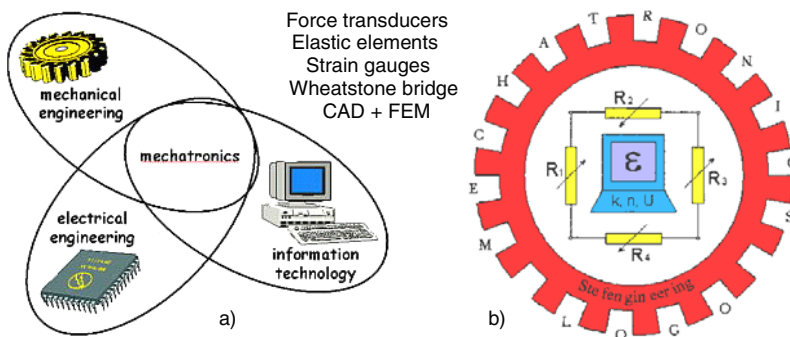
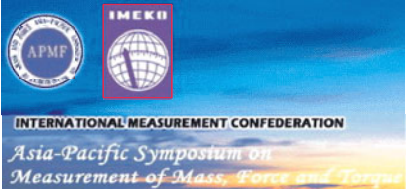
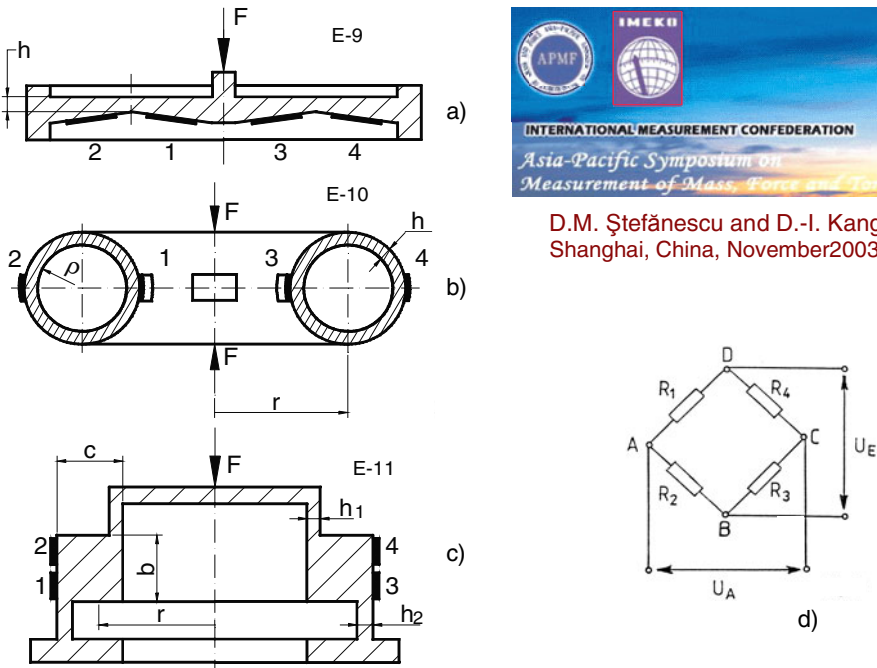


Fig. 34.5 Mechatronics evolution from Venn diagram, with overlapping surfaces (a), to concentric representation, “all-inclusive” style, suggested by DMS (b).

Addendum: In accordance with the international metrology nomenclature the item that measurand directly influences is called *sensor* (equivalent with detector or “capteur” in French) while *transducer* is the device that enables the correspondence between input and output, in compliance with a specific law. The *sensor* is, therefore, the sensitive element that enables a first conversion of the measured value applied at input (for instance, the strain gauge applied on the elastic element); the *transducer* is the assembly where the sensor is mechanically installed and electrically connected; a microprocessor for data processing can be also connected to it. The *transducer* always include a tensometric *sensor* (a resistive one, e.g. strain gauge), but also the associated electronic system. In Mechatronics, like in Robotics, the *sensor* detects the environment while the *transducer* is connected to the controls main operation, including sometimes the actuator. This joining of the two functions within the automatic force measurement system permits the simultaneous utilization of the two terms.

34.3.3. Elastic elements for very large forces (Fig. 34.6)

The challenge to measure greater forces ($> 10^7$ N) constitutes a development trend opposite to that of measuring small forces, within micro- and nano-range.



D.M. Ștefănescu and D.-I. Kang
Shanghai, China, November 2003

Fig. 34.6 Profiled diaphragm (a), torus (b), square axisymmetric elastic element (c) and their strain gauges connection in Wheatstone bridge (d)

Some of the most important selection criteria for the elastic elements as “hearts” of the very large force transducers are, after the load range:

- minimum volume, especially reduced height, due to the space limitations,
- high global (mechanical and electrical) sensitivity, but not to parasitic components,
- global price (including soft and hard accessories),
- other specific characteristics of force measurement particularized for industrial processes, research and development or for National Institutes of Metrology applications, e.g. force transfer standards for international inter-comparisons.

Among the various flexible elements studied only few types are suited for measuring forces in the meganewtons range: classical tensioned/compressed column (E-1) or tube (E-2), shearing structure (E-6), compressed torus (E-10) or sphere (E-12), and other axisymmetrical shapes (E-11).

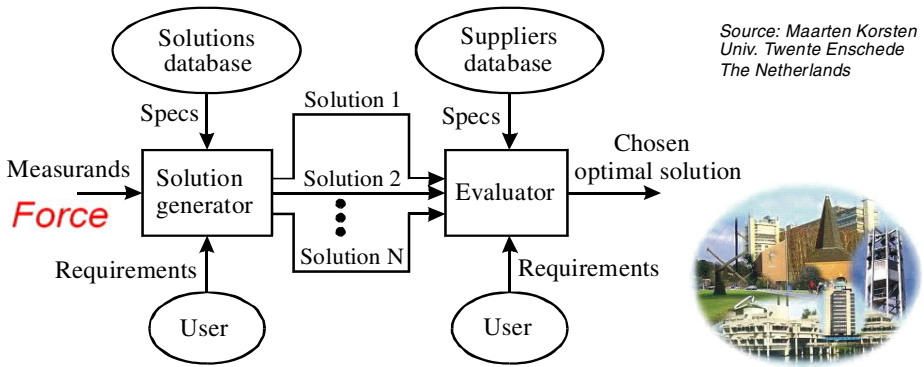
A lot of models have been compared within the Brain Pool program of the Korean Research Institute of Standards and Science [34.25]. In the ascending order of their height, the bent membrane (E-9) (Fig. 34.6a) is presented together with a compressed torus (Fig. 34.6b) and an axisymmetrical elastic element having a square sensitive section (Fig. 34.6c).

34.4. ELASTIC ELEMENTS AUTOMATIC SELECTION

There are a number of reasons for introducing computer support in the field of sensor selection to assist the design of automated systems. In the first place, these days no designer can have a complete overview of all available measurement principles used for existing transducers, so that computer support for finding one will be welcome. In the second place, the computer can assist in making an optimal choice based on criteria and requirements from the designer as well as on technical specifications provided by the sensor supplier.

Fig. 34.7 shows a scheme of a selection/design system, which has been worked out within KISSIS, namely a Knowledge-based Intelligent System for the Selection of Industrial Sensors [34.26], and has been applied on the four elastic elements presented in Table 27.1. According to this scheme, there are, in general, two stages: first, a measurement principle is selected (e.g. strain gauges) and then, during a second stage, one or more transducers are chosen from a supplier's guide (e.g. bent yoke, as type of elastic element inside the force transducer), using a program called *PLib Editor*.

Fig. 34.8a shows a tree reflecting a dictionary with a simplified concept of force transducer. The definitions of the properties of the Yoke-element are shown in Figure 34.8b. After finishing the description, the user can save it in the form of a PLib-compliant file.



Source: Maarten Korsten
 Univ. Twente Enschede
 The Netherlands

Fig. 34.7 Transducer selection system architecture at Twente University of Enschede

The choice between solutions means comparing specifications of different sensors, but also “weighing” various criteria, as accuracy and costs. Thus, the user should give requirements on different specification fields, including admissible ranges, and also indicate how important they are. A complication arises if not all sensor specifications are available.

Multi Criteria Decision Making (MCDM) is a useful tool, a discipline aimed at supporting specialists, who are faced with numerous and conflicting evaluations, in order to find the best compromise in a transparent process of decision.

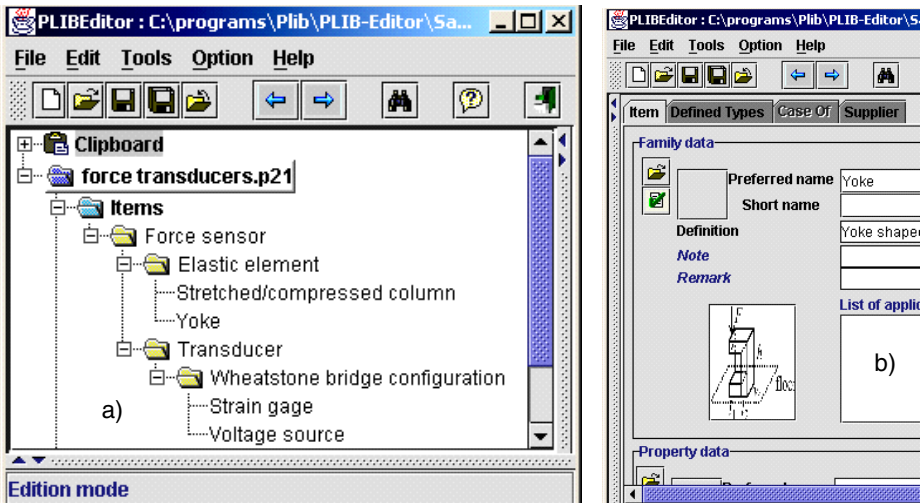


Fig. 34.8 Force transducers dictionary – tree structure (a); yoke element description (b)

The values and the importance of a requirement will have to be expressed in terms, linking up with the user's way of thinking. Thus, expressions like "not so important" or "absolutely necessary" may be more appropriate than numbers like 0.7. Therefore, the use of fuzzy criteria may be a good proposition [34.27].

Faster evolutions took place during the last two decades, from the first elastic elements of load cells evaluated by computer in the years '80 [34.28], [34.29], to the parametric modeling, design optimization [34.30], CAD-CAE and automatic selection of force transducers [34.31] in the new millenium.

Concluding the elastic elements selection: their *strain sensitivity* is the most important parameter of the force transducer within the tensometrical measurement chain. Strain is a complex measurand with a treble significance as:

- an elastic deformability coefficient, with listed values for the most used materials;
- a specific deformation expressed in $\mu\text{m}/\text{m}$ (ppm) or equated in mV/V as a reading (an indication) of the tensometrical Wheatstone bridge;
- a postprocessed mechatronic parameter on computer.

REFERENCES

1. Bao, M.-H., Middelhoek, S.: Pressure Sensors, Accelerometers and Gyroscopes. In: Handbook of Sensors and Actuators, vol. 8. Elsevier Science, Amsterdam (2000)
2. Messung von Bahnspannungen, Seilkräften, Fördermengen und davon abgeleiteten Größen. Technische Information 30 PM 103, Hartmann-Braun Meß-und Regeltechnik, Frankfurt/Main (1985)
3. Measuring ranges of Philips transducers for mechanical quantities. Philips in Science and Industry 14(1), 14 (1968)
4. Loadcell & force measurement. POWER (Professional Organization of Worldbest Engineering Resources), KAIST/Techno-Innovation Center, Taejon, Korea, 07-98
5. Weighing load cells – a complete range from 30 grams to 300 tons. SCAIME, Annemasse, France (1994)
6. Messen, Regeln, Automatisieren. Erzeugnisse, Firmen, Begriffe der Fachgebiete 2.04, pp. 40–42. Verlag Hoppenstedt, Darmstadt (1995)
7. Hinweise zum Messen mit WAZAU-Miniatur-Kraftaufnehmern. Dr.-Ing. G. Wazau, Berlin (1982)
8. Load cell product guide. Teda-Huntleigh World Leaders in Load Cell Technology, Cardiff, U.K., SFC - 1/12-94
9. Pressure transducers, load cells, torque transducers, accelerometers, LVDTs, instrumentation. Sensotec, Columbus, OH, Catalog 119710-97
10. Profos, P., Pfeifer, T.: Handbuch der industriellen Meßtechnik. R. Oldenbourg Verlag, München (1994)
11. Ştefănescu D.M.: Methods for increasing the sensitivity of strain gauge force transducers. PhD dissertation, Universitatea "Politehnica" Bucureşti, Romania, September 10 (1999) (in Romanian)

12. Dolga, L.: Contributions to force transducers design and optimization. PhD dissertation, Universitatea "Politehnica" Timișoara, Romania (1997) (in Romanian)
13. Ștefănescu, D.M., Mănescu, T., Ion, I.: Strain gauges emplacement possibilities for force/torque transducers in Robotics. In: Proceedings IMEKO-XV World Congress Measurement to Improve the Quality of Life in the 21st Century, Osaka, Japan, vol. 10, pp. 117–124 (1999)
14. Moulianitis, V.C., Aspragathos, N.A.: Integration of complexity in a Mechatronics index. In: Amerongen, J.v., Jonker, B., Regtien, P., Stramigioli, S. (eds.) Book of Abstracts Mechatronics 2002: 8th Mechatronics Forum Int'l Conf., University of Twente Enschede, The Netherlands, June 24-26, p. 162 (2002)
15. Constantinescu I.N., Ștefănescu D.M., Sandu M.A.: Măsurarea mărimilor mecanice cu ajutorul tensometriei (Romanian Academic Prize "Aurel Vlaicu"). Editura Tehnică, București (1989)
16. Dumitriu, A., Bucșan, C., Demian, T.: Robotic Sensorial Systems. Editura Medro, Brașov (1996)
17. Ștefănescu, D.M., Sandu, A., Sandu, M., Sorohan, Ș.: Computation particularities for the elastic elements of strain gauge transducers. In: Proc. 10th Int'l Conf. Experimental Mechanics, Lisbon, Portugal, July 18-22, vol. 2, pp. 983–986 (1994)
18. Load cells and force transducers survey. Catalog G21.04.9e, Hottinger Baldwin Messtechnik GmbH, Darmstadt (1992); www: HBM Measurement – Products – Transducers & Sensors – Force Transducers for Industrial Applications (2009)
19. Brendel, A.: Application and selection of force sensors. Sensors Web Portal – Sensors – Mechanical – Force – Literature, May 27 (2002)
20. Ștefănescu, D.M., Marinescu, A., Ștefănescu, A.: Romanian contributions for evaluating force sensors in Robotics. In: Fachtagung ROBOTIK 2002 – Leistungsstand – Anwendungen – Visionen – Trends, VDI-Berichte 1679, Ludwigsburg, Germany, June 19-20, pp. 455–460 (2002)
21. The instalation of load cells. Catalog G21.03.1e., Hottinger Baldwin Measurements, Inc., Framingham, MA (1988)
22. Stoicoviciu, C.: Automatic Weighing in Industry. Editura Tehnică, București (1971) (in Romanian)
23. Guide for Load Cells. West-European Legal Metrology Cooperation – WELMEC 2.4 (1), Teddington, Middlesex (1997)
24. Ștefănescu, D.M.: Criteria for choosing transducer elastic elements in Mechatronics. In: Amerongen, J.v., Jonker, B., Regtien, P., Stramigioli, S. (eds.) CD Proc. Mechatronics 2002: 8th Mechatronics Forum Int'l Conf., Enschede, The Netherlands, June 24-26, pp. 302–309 (2002)
25. Ștefănescu, D.M., Kang, D.-I.: Selection criteria for the elastic elements of very large force transducers. In: Zhang, Y., et al. (eds.) Proceedings 6th Asia-Pacific Symposium Measurement of Mass, Force and Torque, APMF 2003, Shanghai, China, November 3-6, pp. 95–100 (2003)
26. Korsten, M., Ștefănescu, D.M., Regtien, P.P.L.: Sensor specification using the ISA and STEP standards for sensor selection. In: CD Proceedings XVIIth IMEKO World Congress Metrology in the 3rd Millenium, Cavtat-Dubrovnik, Croatia, June 22-27, pp. 393–396 (2003)
27. Zimmerman, H.J.: Fuzzy sets, decision making and expert systems. Kluwer Academic Publishers, Dordrecht (1987)

28. Brendel, A.: Evaluation of strain gage force sensors by computer. In: Proc. SEM Fall Conf. Transducer Technology for Physical Measurements, Grenelefe, FL, November 17-20, pp. 1–6 (1985)
29. Constantinescu, I.N., Ștefănescu, D.M., Dăneț, G.: Le choix de la configuration optimale pour les elements elastiques des capteurs. In: Proc. 4th Romanian Symp. Tensometry, Brașov, September 24-27, vol. I, pp. 73–78 (1986)
30. Ștefănescu, D.M., Dolga, L., Korsten, M.: About the parametrical design of strain gauged pressure and/or force transducers. In: Proc. 7th Int'l Research / Expert Conf. Trends in the Development of Machinery and Associated Technology – TMT 2003, Lloret de Mar, Spain, September 15-17, pp. 617–620 (2003)
31. Korsten, M.J., Regtien, P.P.L.: Systematic and computer assisted design of measurement systems. *Measurement* 33(2), 145–156 (2003)

Chapter 35

DIGITAL AND INTELLIGENT FORCE TRANSDUCERS

At present there are two opposite progress ways in force measurement [35.1]:

- fitting the transducer with electronic and data processing components, as a “black box”, the force transducer, provided with three ports (input, interrogation and output), being capable to carry out a great part of the system functions;
- simplifying the transducer configuration, reduced to a Wheatstone bridge, and using the interfaces (data acquisition and control boards of high efficiency and performance) [35.2] in order to assure the digital connection to any PC as a friendly virtual instrument for force measuring [35.3].

The monograph [35.4] reviews all of the principal features relating to strain gauge load cells that incorporate signal conditioning electronics to provide measuring output signals in a digital form. A minimum configuration has an analog-to-digital converter (ADC) to convert the analog signal into a digital format for retransmission. It may incorporate additional electronic devices to store various load cell performance characteristics and optimize them by the use of software algorithms.

35.1. EVOLUTION FROM ANALOG TO DIGITAL

Here are some stages during the evolution from the classical Analog to the intelligent Digital, with their permanent interconnection [35.5]:

- 1983 – first intelligent pressure sensor made by Honeywell using DSSP (digital sensor signal processing);
- 1985 – a single-chip ASIC (with constant current source) made by Keller using ASSP (analog sensor signal processing);
- 1993 – a single-chip analog computer for simultaneous measurement of pressure and acceleration in automotive industry, achieved by MCA Electronics in Silicon Valley;

– 1994 – hardware independent communication standard for low-cost smart sensors designed by NIST (the National Institute of Standards and Technology in USA).

Following this series of discoveries, the MAX111 analog-to-digital converters use an internal auto-calibration technique to achieve 14-bit resolution plus overrange, with no external components. Operating supply current is only 550 μA and reduces to 4 μA in power-down mode, making these ADCs ideal for high-resolution battery-powered or remote-sensing applications (Fig. 35.1).

A fast serial interface simplifies signal routing and optoisolation, saves microcontroller pins, and offers compatibility with SPI™, QSPI™, and Microwire™.

Strictly referring to force transducers and load cells, the following are some outstanding performances:

- i) Mettler-Toledo Inc. has been patented a digital load cell including a rocker pin, a guided beam torsion ring or other counterforce, a circuit board with an ADC and a microcomputer; digital communication is provided with the circuit board through a connector mounted on the enclosure [35.6].
- ii) Tedeia has introduced the “Digital Load Cell Companion”, which is able to accommodate either single or multiple load cells. It converts the inherently low analog output into a digital signal of approximately 32000 counts, resolution being adjustable up to 1:40000. Ratiometrically operated, it requires power supply to serve both its own power needs and those of the strain gauged force transducers. Output is provided in two digital forms: pulsed stream serial and multiplexed BCD parallel. Tedeia DLCC exceeds OIML requirements for 3000-division scales, having maximum nonlinearity of 0.01 %.

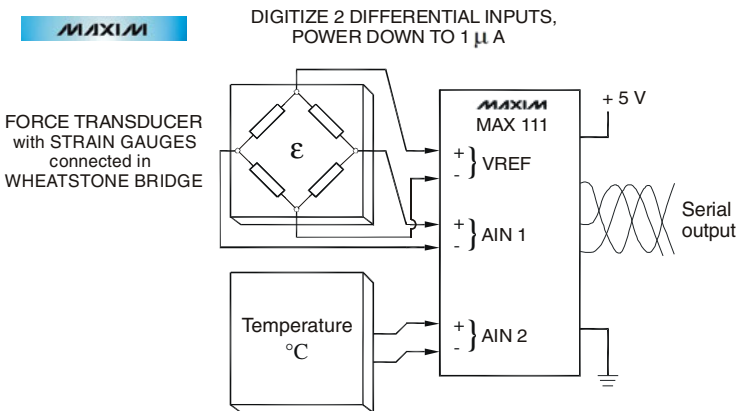


Fig. 35.1 Analog-to-digital converter for strain and temperature measurements

- iii) Sensy SA introduces what it claims to be the first digital standard reference force transducer according to the norm EN ISO 376. The transducer is available in the load range from 10 N to 30 MN, in tension, compression, and universal (tension + compression) together with a basic communication software or a dedicated "Sensy Soft 376" [IEN, No. 3, p. 28, April 2004].

35.2. AUTOMATIC RECOGNITION OF FORCE TRANSDUCERS

The IEEE TEDS 1451 specification provides an industry standard Transducer Electronic Data Sheet which contains the necessary gain factor and other characteristics in a memory location that can be automatically read by the instrument whenever a new transducer is attached [35.7].

This flexible document contains complicated template formats, interpretive language specifications, and very complex protocol on embedded instrumentation. The instrument must be able to handle the wide variety of electronic templates and each vendor must strictly adhere to the TEDS format, otherwise – as the document states – “the objective of *plug-and-play* becomes nothing more than *plug-and-pray*.”

Four principal variants are available in this respect (Fig. 35.2), all of them supporting the basic TEDS premise of plug-and-play operation and electronic data sheets, but differing in WHERE the electronic data is stored and HOW it is updated and retrieved:

- a) *Basic architecture*: data are stored inside the sensor. A tiny electronic chip (e.g. Dallas Semiconductor, part number DS2401) is included within the transducer housing; it contains the electronic identification tag and the programmable memory. A TEDS compatible computer or instrument is used to write the calibration data and related information into the memory chip in the electronic format specified by the TEDS 1451 standard. Transducer calibration data is automatically read from the memory and installed into the instrumentation, avoiding human errors. Both force transducer and instrument are separately calibrated.
- b) *Virtual architecture* is useful when transducers can not support the inclusion of the electronic chip into their housing. Using the virtual TEDS, the electronically stored data is saved in a computer database that is accessed via the Web and downloaded into a local machine. National Instruments, the main promoter of this system, uses a PC to retrieve the database information and to act as a host for the DAQ electronics. Although automatic transducer identification is not supported, the calibration data is available electronically.
- c) *German T-ID™* system, made by HBM, proposes a tiny electronic chip with only the electronic tag incorporated into the transducer housing, while the data is stored in a computer database. This allows for plug-and-play

operation but still requires the use of a PC to support the downloading of the transducer data, including calibration.

- d) *TEDS-Tag*TM is a plug-and-play system for independent instrumentation and embedded instruments (e.g. CellMite digital signal conditioners, Electro Standards Laboratories). The electrical interface and tag identifier are housed within the transducer or in a small in-line adapter, while the calibration data is stored inside the instrument. After the user enters the data, the unit can recognize the transducer and recall the calibration from its internal memory. No computer, large database or additional connectivity is required, and plug-and-play operation is achieved. A transducer could be paired with a particular instrument and precisely calibrated together as an accurate measurement system. The paper [35.8] presents a dedicated IEEE 1451.1 transducer block that enables connecting of plug & play transducers.

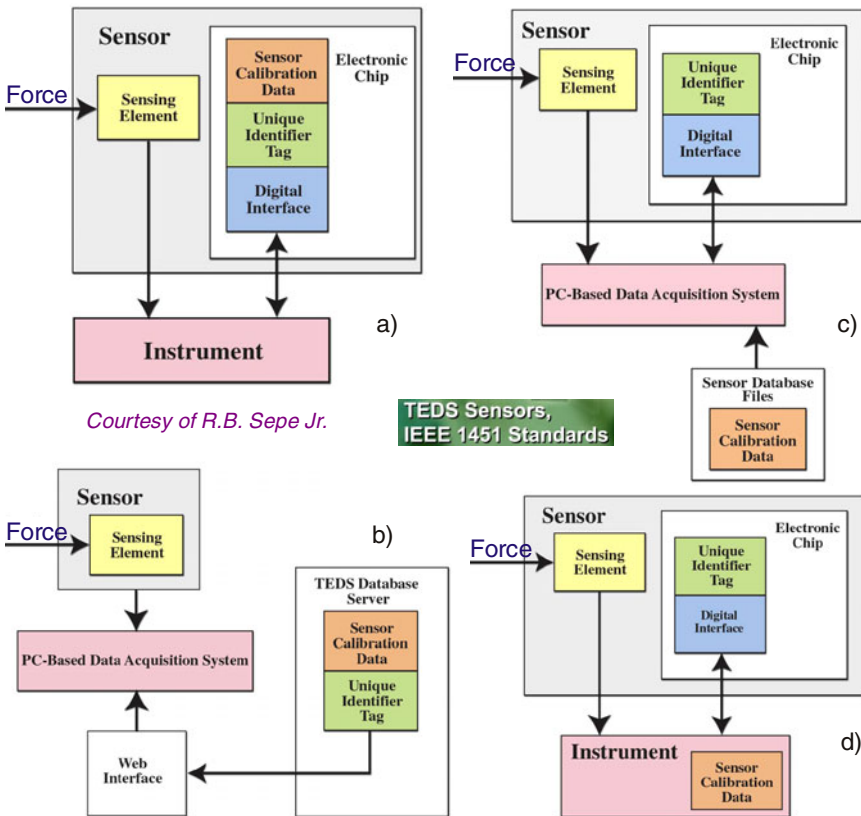


Fig. 35.2 Four TEDS variants for automatic recognition of force transducers [35.7]
 © IFSA (<http://www.sensorsportal.com>) and permission from Electro Standards Labs

35.3. FORCE TRANSDUCERS IN DYNAMIC REGIME

In most cases, the dynamic properties of the transducers are decisively involved in, i.e. measurements of time variable forces. The dynamic interaction between the transducer and the structure it is installed into may lead to unexpected results if specific requirements are not fulfilled. A valuable survey on dynamic measurement of force, achieved by the Swedish National Testing and Research Institute in Boras, can be found in [35.9].

Load cells were developed specifically for use in dynamic weighing processes by means of the fast intelligent transducer (FIT) [35.10]. Both in their mechanical construction and in the integrated electronics, they take into account the requirement for dynamic weighing, dosing and filling systems (Fig. 35.3). They include fast DSP, rapidly settling digital filters, and are also able to weigh with great accuracy in a dynamic regime. The load cells – used for weighing in the food industry – are able to register under hygienic conditions the weight, in the shortest possible measuring time.

The main properties of FIT[®] load cells specially developed for use in dynamic weighing processes are:

- highly rigid and resistant to overload,
- corrosion resistant stainless steel enclosure, laser welded, IP 66,
- built-in digital signal processing, rapid transient response digital filters,
- data output and parameter assignment via RS 485 or 232 serial interface,
- bus operation with up to 90 load cells,

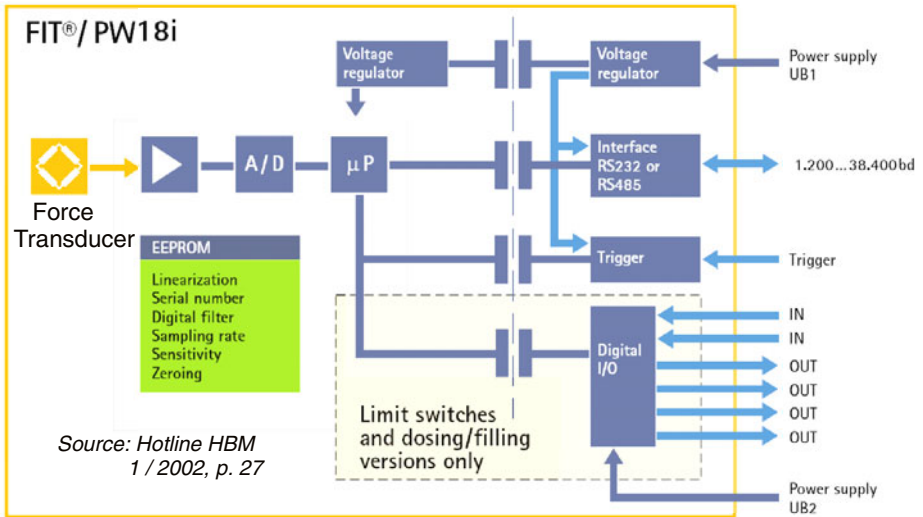


Fig. 35.3 Block diagram of a FIT[®] (fast intelligent transducer) load cell

A high-temperature pressure transducer interface (Fig. 35.4) has been realized by combining CMOS ASIC's with a thick-film packaging technology [35.13]. The well fluid, working up to (250...275) °C, compresses a pressure gauge, which changes the imbalance of a Wheatstone bridge. The voltage across the bridge is measured using the four-wire measurement technique. The bridge signals are converted into a period-modulated output signal by means of a smart signal processor (SSP) with 16 bits accuracy. Internal diagnostics continually verify the smart cell performances.

35.5. FURTHER PROSPECTS: MATERIALS, TECHNOLOGIES, IDEAS

35.5.1. *Smart materials and structures*

Some piezo- or strictor materials are naturally suited for force transduction since they undergo strain deformation in response to certain external stimuli such as an electric or magnetic field, or temperature change [35.14]. The inherent electromechanical response of such materials thus allows a single piece of material to replace a more complicated device previously needed to perform the same function. Smart materials exhibit bidirectional electro-mechanical responses, accepting and producing force.

This built-in functionality of smart materials enables the construction of force transducers that are simpler and cheaper than those of previous technology [35.15]. At present, the materials most attractive for electromechanical force transduction are piezo-ceramics, piezo-polymers, magnetostrictive materials, and shape memory alloys (SMAs). They have a fundamental multifield opto-magneto-piezo-electro-thermo-elastic behavior [35.16].

A recent invention of UT-Battelle [35.17] provides a multi-range force transducer comprising a load cell made of a shape memory alloy, a strain sensing system, a temperature modulating system, and a temperature monitoring system. The ability of this transducer to measure contact forces in multiple ranges is affected by the change in temperature of the shape memory alloy. The heating and cooling system functions to place the shape memory alloy of the load cell in either a low temperature, low strength phase for measuring small contact forces, or a high temperature, high strength phase for measuring large contact forces. Once the load cell is in the desired phase, the strain sensing system is utilized to obtain the applied contact force. The shape memory alloys are selected from a large group including CuAuZn, AgCd, TiNi, NiAl, FePt, etc.

Actuation strains greater than 3 % have been reported for IPMCs (ionic polymer-metal composites) under applied voltages smaller than 7 V [35.18]. Substantial bending in these cantilever type actuators (Fig. 35.5) is caused when one side of the material contracts [*here is the lower side*] and the other expands [*the upper side*]. Reported stresses of actuation are as high as 30 MPa.

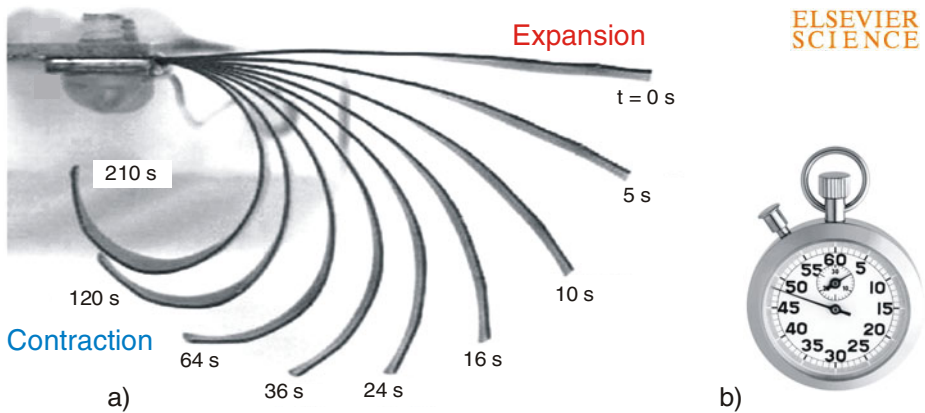


Fig. 35.5 Actuation of a Flemion-based IPMC strip (a) as a function of time (b)
(© 2003 American Institute of Physics)

Applications for IPMC actuators include mechanical grippers, contact force transducers, metering valves, diaphragm pumps, fins for robotic fish, and an IPMC-operated artificial eye developed by Eamex.

35.5.2. Intelligent design and smart technology

Brignell has formulated the intelligent principles of structural compensation by design symmetry in the electrical (strain gauges in Wheatstone bridge) and mechanical (elastic element of transducer) subsystems, both forming an indestructible monolith [35.19]:

- an elastic structure composed by multiple and symmetrical flexible elements reduces the load eccentricity influence;
- strain gauges connected in full Wheatstone bridge provide a maximum differential output with linearity.

The breakthrough technology of MEMS has the potential to revolutionize many transducers by realizing the complete-system-on-a-chip [35.20]. This technology may be used to develop “smarter” transducers by combining the ability of microelectronics with the control capabilities of microsensors.

New microelectromechanical systems have been designed on a cantilever beam or a diaphragm basis, where the substrate has been locally removed. The membranes contain alternating layers of different materials with the same structural orientation. Here the quantum-physical effects become important and provide advanced facilities, such as detecting signals in the low signal to noise ratio regime. The involved technology offers very high speed (GS/s), low power ($1 \mu\text{W}$), high resolution (9 bits) and fast analog-to-digital conversion.

A smart vision on smart sensor systems is developed in the book [35.21].

35.5.3. *Neuro-fuzzy concepts*

As professor Laurent Foulloy, Université de Savoie, France said, “*Due to its ability in representing gradual information, familiar to human beings, the fuzzy subset theory is one possible tool to integrate some kind of intelligence at the very basic level.*”

Mettler-Toledo employs sophisticated algorithms, many of which are patented, to digitally compensate for creep, hysteresis, linearity and temperature (static and dynamic). Using digital compensation, the fully compensated overall performance of a SG load cell can be an order of magnitude higher than its uncompensated analog performance. To make the load cell less susceptible to environmental influences, such as mechanical vibrations, M-T strain gauged sensing cells make extensive use of DSP to improve the quality of the output signal. A new approach of digital load cell compensation based on a function link neural network is presented in [35.22].

K.-C. Lee *et al.* from the National Huwei Institute of Technology, Taiwan, R.O.C. propose a method of accurate modeling of load cells using an adaptive neuro-fuzzy inference system to establish the relationship between the reading and the actual weight considering temperature-varying effect and nonlinearity.

35.6. UPDATED FORCE TRANSDUCERS + DATA COMMUNICATION

35.6.1. *Dual output force transducers*

A survey of traditional resistance-based sensor conditioning techniques, going from simple analog op amp solutions to sophisticated digital technology using digital signal processing is presented in [35.23].

A still actual alternative is the “hybrid approach”: use of the analog technology for the front end and of the DSP for compensation and error correction functionality.

Some manufacturers have started produce transducers with both analog and frequency output in the same device [35.24]. The dual output of both digital and analog signals allows for flexibility for the customer with force / torque measurement applications, where both conventional 0...5 V_{DC} is required and digital output directly into a PC is needed [35.25]. Digital output is available in both RS485 and RS232.

With less than 1 millisecond step response on the analog output and greater than 300 readings per second on the digital output, Honeywell Sensotec’s digital output load cells and torque cells provide dual solutions. These products feature very good thermal characteristics because the effects of temperature are automatically corrected internally. Their zero and span adjustments are made electronically, without need for manual adjustments.

The digital output is especially useful on the manufacturing shop floor because it alleviates the problems of data measurement caused by EMI and RFI.

Dual outputs are also visible in Figure 35.6. The PME (precision measurement equipment) range of HBM products offers different types of modules for the determining of all measured quantities, strongly “connected” and relevant to processing, such as force, torque, pressure, displacement, temperature, speed of rotation, frequency, voltage, and/or current.

The MP55DP intelligent module is a carrier-frequency amplifier, expanded to include a Profibus interface. The features on the CAN-interface remain the same; the object directory is expanded to include some parameters for the Profibus connection. This connection is made conforming to standard and using a 9-pin sub-D connector on the front panel next to the transducer port. DP protocol is used on the Profibus.

CAN in Automation, Nuremberg, has released the CiA 302 specification series of CANopen additional functions concerning the frequency-output transducers, useful for companies that use cascaded networks [35.26]. SDO (service data object) and Emergency Communication is routed, while PDOs (process data object) are forwarded with the bridge functionality. The following information is communicated:

- the measured values (gross, net, peak values) and the limit switches status;
- control bits for taring, zeroing, peak value store control and changing the parameter set, and optionally, the limit value levels.

Loadstar Sensors Inc., Fremont, CA, announced the availability of its DI-1000 digital load cell interface, designed to work with conventional resistive load cells [35.27].

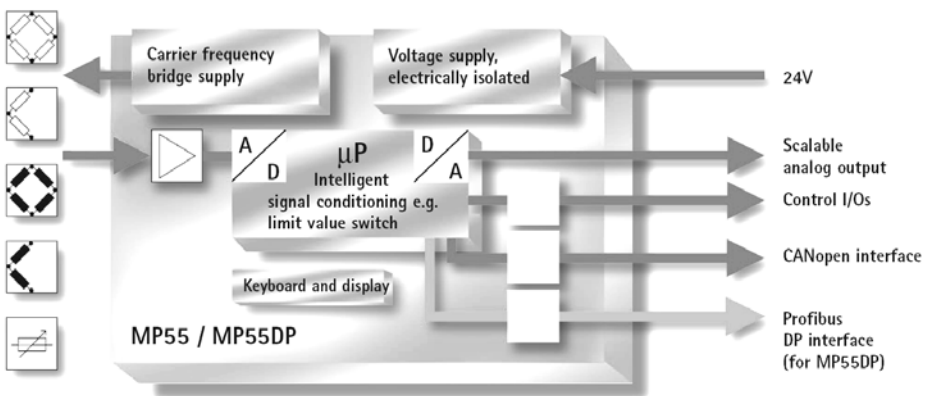


Fig. 35.6 MP55DP intelligent module amplifier with scalable analog output and digital interface for measuring mechanical quantities: force, torque, pressure, and so on

The DI-1000 provides a simple, convenient method to convert the millivolt output from a load cell into a PC friendly digital USB output. According to the company's slogan, “*Just plug in the force transducer into one end of the DI-1000 and plug the other end to a PC and you get a PC ready force measuring chain!*”

The DI-1000 has many key features in order to simplify the process of building a PC friendly load measurement system:

- compatible with any PC and most operating systems,
- calibrated output in simple ASCII format,
- view loads on demand or in streaming mod,
- command set for software integration,
- optional wireless: Bluetooth or Zigbee,
- optional LoadVUE software allows user to log and plot data.

35.6.2. Data display and communication

The latest achievements for the force measuring chains include the digital display (in engineering units) within the tensometric transducers (Fig. 35.7). The Aikoh 9800 series push pull force gauges use a precision force transducer to measure the compressive and tensile forces applied to the force probe [35.28]. They have a lot of applications in connection with high precision motorized testing machines. The unit displays real time force data on the LCD screen. The instruments can be set up to record a series of measurements and to tabulate and plot peak and average values. High and low limit values can be set up for quality control and inspection operators. Other handheld displays may have the form of a watch, called Digi-force [35.29].

Zentrum Mikroelektronik from Dresden, Germany has recently demonstrated the Multi-Sensor Interface Circuit (MUSic) series which offer multi-channel and multi-use sensor interfaces for microcontroller-based systems. Known for very high precision and ultra low power, these ICs are ideal for industrial systems executing multiple sensor-based measurements such as weighing scales and flow monitors. The first device in the MUSic family, the ZMD21013, is a highly integrated smart-power architecture that offers programmable interfaces for up to three resistive bridge sensors, and connects through a SPI interface to a microcontroller or a digital signal processor.

An important role has the further processing of the data resulting from the force measurement and their transmission to all concerned. There are two information exchange protocols conforming to the ISA-standard S37.8, entitled “*Strain gage as force sensor*”: STandard for the Exchange of Product model data (STEP) and PLib (Parts Library); they were achieved by international cooperation within the Twente University of Enschede, NI [35.30].

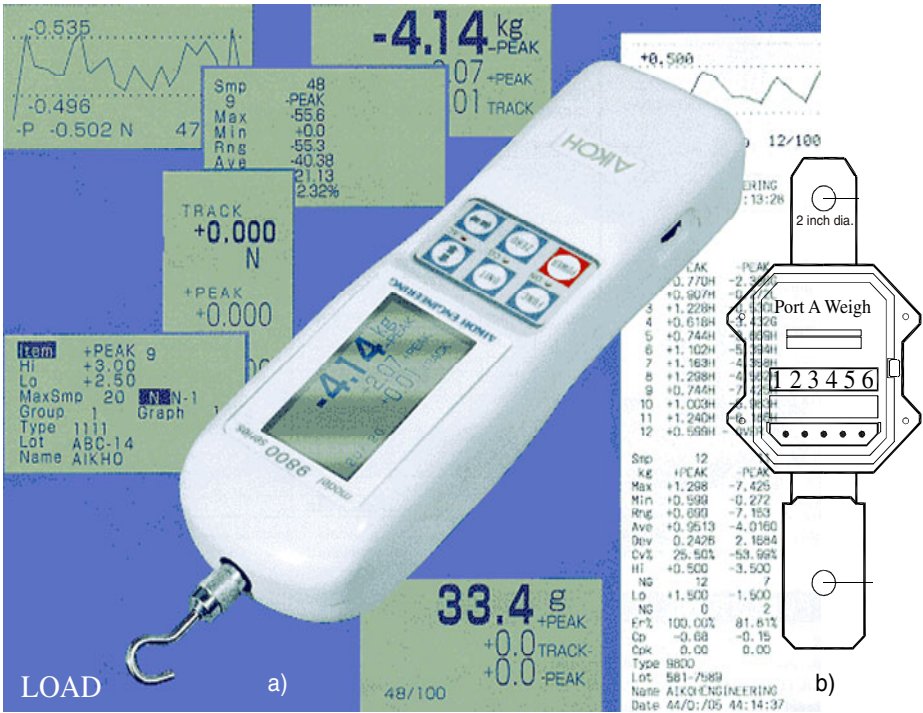


Fig. 35.7 Japanese (a) and American (b) push pull gauges for weighing applications. One can observe the wide variety of presentation for the weighing documents.

New sensor technologies and deployment concepts have pushed transducers into the net centric world and have simultaneously presented a requirement for joint standard digital communications capable of dynamic discovery of nodes on the network, runtime configurability of sensing devices, multi-connection support, and sensor to sensor direct communications.

In order to support the full range of force transducer data and capabilities, a highly flexible messaging format is required [35.31]. It was determined that the optimal path to meet the interface exchange requirements and ensure standard data representations for transducers was to develop the SDL as a subset of the Variable Message Format (VMF) standard for the Defense Department (Interface Standard: MIL-STD-6017, 2003). This vehicle established a framework of not only formatting and processing rules but also of review and acceptance with maximum interoperability across the Joint Services and NATO countries.

While the computer is the “brain” due to its “thinking” abilities, the force transducer is the “heart”, being the sensing element of the measurement chain.

Irrespective of the progress in instrumentation and computer science, SG force transducer stays the system's main component, defined as follows [35.32]:

- mathematically: as a “solving” element of the vectorial force;
- mechanically: a spring (elastic element);
- thermally: a resistive temperature sensor for the correction of thermal effects;
- electrically: transducer in the proper sense;
- metrologically: its own testing device (self-calibration) where accuracy is more important than sensitivity, both being very high.

REFERENCES

1. Ștefănescu, D.M.: Methods for increasing the sensitivity of strain gauge force transducers. PhD dissertation (160 pages, 26 tables, 86 figures, 336 references), Universitatea “Politehnica” București, Romania, September 10 (1999) (in Romanian)
2. Load cell product guide. Tedeo-Huntleigh, World Leaders in Load Cell Technology, Cardiff, UK, SFC, December 1 (1994)
3. Ilea, H., Istrate, M., Dudescu, M.C.: Virtual instrument for force detecting. Monografia Rezist Mater 75, 386–389 (1998) (in Romanian)
4. Zecchin, P. (Chair.): Digital Load Cells – A Comparative Review of Performance and Application. The Institute of Measurement and Control, London, Document WP0803 (2003)
5. Bryzek, J.: Evolution of smart transducer technology. In: SENSORS 1995 Kongressband, Nürnberg, May 9-11, pp. 45–50 (1995)
6. Dillon, B.N., Griffen, N.C., Weihs, M.E.: Load cell. US Patent 5076375-1991
7. Sepe Jr., R.B.: IEEE TEDS 1451: ‘Plug-and-Play’ or ‘Plug-and-Pray’? Sensors & Transducers Journal 71(9), 692–697 (2006)
8. Viegas, V., Dias Pereira, J.M., Silva Girão, P.: Smart transducer block enables plug & play transducers. In: Proc. XIX IMEKO World Congress on Fundamental and Applied Metrology, Lisbon, Portugal, September 6-11, pp. 1452–1455 (2009)
9. Hjelmgren, J.: Dynamic measurement of force – a literature survey. Swedish National Testing and Research Institute, Borås, Sweden, SP Report 27-2002
10. Milz, U.: Soybean oil and baby milk split-second bottling with FIT[®] fast intelligent transducers. Hotline Hottinger – News from the World of Test and Measurement (1), 27 (2002)
11. Hotline Hottinger: a) Bathe, K., Ruh, S.: Upgrade your mind – HBM in the digital age (1), 4–5 (2001); b) Schrod, R., Merz, H.: Weighing & batching with digital HBM technology (1), 24–25 (2002); c) Doughty, P.: NASA safety with HBM measurement technology (2), 19 (2004)
12. Beeby S., Ensell G., Kraft M., White N. MEMS Mechanical Sensors. PDF on Internet (created on March 12, 2004)
13. de Jong, P.C., Meijer, G.C.M.: A high-temperature electronic system for pressure-transducers. IEEE Transactions on Instrumentation and Measurement 49(2), 365–370 (2000)

14. Fletcher, R.: Force transduction materials for human technology interfaces. *IBM Systems Journal* 35(3&4), 630–638 (1996)
15. Jin, G., Zhang, J., Bao, N.K., Yu, M.: Smart force sensors and their applications. In: *SPIE Proceedings*, vol. 4235 (2001)
16. Tzou, H., Lee, H.-J., Arnold, S.: Smart materials, precision sensors/actuators, smart structures, and structronic systems. *Mechanics of Advanced Materials and Structures* [Taylor & Francis] 11(4-5), 367–393 (2004)
17. Varma, V.K.: Multi-range force sensors utilizing shape memory alloys. US Patent 6546806, April 15 (2003)
18. Mirfakhrai, T., Madden, J.D.W., Baughman, R.H.: Polymer artificial muscle. *materialstoday* 10(4), 30–38 (2007); ISSN: 1369 7021
19. Brignell, J.B., White, N.M.: *Intelligent Sensor Systems*. Institute of Physics Publishing, Bristol (1994)
20. Hartnagel, H.: “Smarter” electromechanical systems. *Cordis Focus – RTD Results* (38), 32 (November 2002)
21. Meijer, G.C.M. (ed.): *Smart Sensor Systems*. John Wiley & Sons, New York (2008)
22. Zhu, Z.: Researches on function-link artificial neural network based load cell compensation. In: *CD Proc. 19th IMEKO TC-3 Int’l Conf. Force, Mass & Torque Measurements: Theory and Application in Laboratories and Industries*, Cairo, Egypt, February 19-23, Paper 59 (2005)
23. Cheeke, D.: Sensor Signal Conditioning. *Sensors & Transducers Journal* 82(8), 1381–1388 (2007)
24. Yurish, S.Y.: Sensors and transducers: frequency output versus voltage output. *Sensors & Transducers Magazine (S&T e-Digest)* 49(11), 302–305 (2004)
25. Dual Output Load Cells and Torque Cells. Honeywell Sensotec, *www Bulletin* (April 2006)
26. Zeltwanger, H.: CANopen additional functions. *Sensors & Transducers e-Digest* 102(3) (March 2009)
27. Harish, D.: New digital load cell interface. *Sensors & Transducers e-Digest* 96(9) (September 2008); ISSN 1726-5479
28. Aikoh 9800 Digital Push/Pull Force Gauge (March 2009), <http://www.microphotonics.com>
29. Force measurement products: A complete line of force gauges, test stands & accessories. Ametek – Mansfield & Green Division, Largo, FL, *Bulletin J-90*
30. Korsten, M., Ștefănescu, D.M., Regtien, P.P.L.: Sensor specification using the ISA and STEP standards for sensor selection. In: *CD Proceedings XVIIth IMEKO World Congress Metrology in the 3rd Millenium*, Cavtat-Dubrovnik, Croatia, June 22-27, pp. 393–396 (2003)
31. Whitworth, R., Mayott, G., Meehan, J.R., McKerley, S.S., Patty, K.D.: *Sensor Data Link – Flexible and standard digital communications for current and future force sensors*. Report OMB 0704-0188 (December 2004)
32. Brendel, A.E.: Some comments on the evaluation of (force) transducer performance. In: *Strain-Gage and Transducer Techniques (Popular Articles from ‘Experimental Techniques’ and ‘Experimental Mechanics’)*, Society for Experimental Mechanics, Bethel, CT, Issue 1, pp. 18–19 (1994)

Annex 1. Rules for strain gauges placement on the elastic elements of force transducers

Case	Strain gauges placement and connection	Sensitivity								
1		$\varepsilon = \varepsilon_n + \varepsilon_b = \frac{4}{k} \cdot \frac{U_A}{U_E} - \varepsilon_t$ <table border="1"> <tr> <td>t</td> <td>P</td> <td>M_b</td> <td>M_d</td> </tr> <tr> <td>1</td> <td>1</td> <td>1</td> <td>0</td> </tr> </table>	t	P	M _b	M _d	1	1	1	0
t	P	M _b	M _d							
1	1	1	0							
2		$\varepsilon = \varepsilon_n + \varepsilon_b = \frac{4}{k} \cdot \frac{U_A}{U_E}$ <table border="1"> <tr> <td>t</td> <td>P</td> <td>M_b</td> <td>M_d</td> </tr> <tr> <td>0</td> <td>1</td> <td>1</td> <td>0</td> </tr> </table>	t	P	M _b	M _d	0	1	1	0
t	P	M _b	M _d							
0	1	1	0							
3		$\varepsilon = \varepsilon_n + \varepsilon_b = \frac{1}{1+\nu} \cdot \frac{4}{k} \cdot \frac{U_A}{U_E}$ <table border="1"> <tr> <td>t</td> <td>P</td> <td>M_b</td> <td>M_d</td> </tr> <tr> <td>0</td> <td>1+ν</td> <td>1+ν</td> <td>0</td> </tr> </table>	t	P	M _b	M _d	0	1+ν	1+ν	0
t	P	M _b	M _d							
0	1+ν	1+ν	0							
4		$\varepsilon = \varepsilon_b = \frac{1}{2} \cdot \frac{4}{k} \cdot \frac{U_A}{U_E}$ <table border="1"> <tr> <td>t</td> <td>P</td> <td>M_b</td> <td>M_d</td> </tr> <tr> <td>0</td> <td>0</td> <td>2</td> <td>0</td> </tr> </table>	t	P	M _b	M _d	0	0	2	0
t	P	M _b	M _d							
0	0	2	0							
5		$\varepsilon = \varepsilon_n = \frac{1}{2} \cdot \frac{4}{k} \cdot \frac{U_A}{U_E} - \varepsilon_t$ <table border="1"> <tr> <td>t</td> <td>P</td> <td>M_b</td> <td>M_d</td> </tr> <tr> <td>2</td> <td>2</td> <td>0</td> <td>0</td> </tr> </table>	t	P	M _b	M _d	2	2	0	0
t	P	M _b	M _d							
2	2	0	0							

Trilingual nomenclature for different loads and signals

Basic quantity	German index	Romanian index	English index
Bending moment M	b – Biegung	i – incovoiere	b – bending
Rolling moment M	d – Drehung	t – torsiune	r – rolling
Supply voltage U	E – Eingang	I – intrare	I – input
Output voltage U	A – Ausgang	E – iesire (exit)	O – output

Annex 1-2

Case	Strain gauges placement and connection	Sensitivity								
6		$\varepsilon = \varepsilon_n + \varepsilon_b = \frac{l}{2(1+\nu)} \cdot \frac{4}{k} \cdot \frac{U_A}{U_E}$ <table border="1"> <thead> <tr> <th>t</th> <th>P</th> <th>M_b</th> <th>M_d</th> </tr> </thead> <tbody> <tr> <td>0</td> <td>2(1+ν)</td> <td>2(1+ν)</td> <td>0</td> </tr> </tbody> </table>	t	P	M _b	M _d	0	2(1+ν)	2(1+ν)	0
t	P	M _b	M _d							
0	2(1+ν)	2(1+ν)	0							
7		$\varepsilon = \varepsilon_n = \frac{l}{2} \cdot \frac{4}{k} \cdot \frac{U_A}{U_E}$ <table border="1"> <thead> <tr> <th>t</th> <th>P</th> <th>M_b</th> <th>M_d</th> </tr> </thead> <tbody> <tr> <td>0</td> <td>2</td> <td>0</td> <td>0</td> </tr> </tbody> </table>	t	P	M _b	M _d	0	2	0	0
t	P	M _b	M _d							
0	2	0	0							
8		$\varepsilon = \varepsilon_b = \frac{l}{4} \cdot \frac{4}{k} \cdot \frac{U_A}{U_E}$ <table border="1"> <thead> <tr> <th>t</th> <th>P</th> <th>M_b</th> <th>M_d</th> </tr> </thead> <tbody> <tr> <td>0</td> <td>0</td> <td>4</td> <td>0</td> </tr> </tbody> </table>	t	P	M _b	M _d	0	0	4	0
t	P	M _b	M _d							
0	0	4	0							
9		$\varepsilon = \varepsilon_n = \frac{l}{2(1+\nu)} \cdot \frac{4}{k} \cdot \frac{U_A}{U_E}$ <table border="1"> <thead> <tr> <th>t</th> <th>P</th> <th>M_b</th> <th>M_d</th> </tr> </thead> <tbody> <tr> <td>0</td> <td>2(1+ν)</td> <td>0</td> <td>0</td> </tr> </tbody> </table>	t	P	M _b	M _d	0	2(1+ν)	0	0
t	P	M _b	M _d							
0	2(1+ν)	0	0							
10		$\varepsilon = \varepsilon_b = \frac{l}{2(1-\nu)} \cdot \frac{4}{k} \cdot \frac{U_A}{U_E}$ <table border="1"> <thead> <tr> <th>t</th> <th>P</th> <th>M_b</th> <th>M_d</th> </tr> </thead> <tbody> <tr> <td>0</td> <td>0</td> <td>2(1-ν)</td> <td>0</td> </tr> </tbody> </table>	t	P	M _b	M _d	0	0	2(1-ν)	0
t	P	M _b	M _d							
0	0	2(1-ν)	0							

Active SG
 Passive SG or resistor
 Thermal Compensation SG

Annex 1-3

Case	Strain gauges placement and connection	Sensitivity								
11		$\epsilon = \epsilon_b = \frac{l}{2(1+\nu)} \cdot \frac{4}{k} \cdot \frac{U_A}{U_E}$ <table border="1"> <thead> <tr> <th>t</th> <th>P</th> <th>M_b</th> <th>M_d</th> </tr> </thead> <tbody> <tr> <td>0</td> <td>0</td> <td>2(1+ν)</td> <td>0</td> </tr> </tbody> </table>	t	P	M _b	M _d	0	0	2(1+ν)	0
t	P	M _b	M _d							
0	0	2(1+ν)	0							
12		$\epsilon = \epsilon_b = \frac{l}{2} \cdot \frac{4}{k} \cdot \frac{U_A}{U_E}$ <table border="1"> <thead> <tr> <th>t</th> <th>P</th> <th>M_b</th> <th>M_d</th> </tr> </thead> <tbody> <tr> <td>0</td> <td>0</td> <td>2</td> <td>0</td> </tr> </tbody> </table>	t	P	M _b	M _d	0	0	2	0
t	P	M _b	M _d							
0	0	2	0							
13		$\epsilon = \epsilon_d = \frac{l}{4} \cdot \frac{4}{k} \cdot \frac{U_A}{U_E}$ <table border="1"> <thead> <tr> <th>t</th> <th>P</th> <th>M_b</th> <th>M_d</th> </tr> </thead> <tbody> <tr> <td>0</td> <td>0</td> <td>0</td> <td>4</td> </tr> </tbody> </table>	t	P	M _b	M _d	0	0	0	4
t	P	M _b	M _d							
0	0	0	4							
14		$\epsilon = \epsilon_d = \frac{l}{4} \cdot \frac{4}{k} \cdot \frac{U_A}{U_E}$ <table border="1"> <thead> <tr> <th>t</th> <th>P</th> <th>M_b</th> <th>M_d</th> </tr> </thead> <tbody> <tr> <td>0</td> <td>0</td> <td>0</td> <td>4</td> </tr> </tbody> </table>	t	P	M _b	M _d	0	0	0	4
t	P	M _b	M _d							
0	0	0	4							
15		$\epsilon = \epsilon_d = \frac{l}{4} \cdot \frac{4}{k} \cdot \frac{U_A}{U_E}$ <table border="1"> <thead> <tr> <th>t</th> <th>P</th> <th>M_b</th> <th>M_d</th> </tr> </thead> <tbody> <tr> <td>0</td> <td>0</td> <td>0</td> <td>4</td> </tr> </tbody> </table>	t	P	M _b	M _d	0	0	0	4
t	P	M _b	M _d							
0	0	0	4							

Active SG

Passive SG or resistor

Thermal Compensation SG

Annex 2. The Newton's Apple Tree in Korea

Sir Isaac Newton (1642-1727) discovered the notion of universal gravitation, when he saw an apple drop while sitting in his garden at Kensington in England in 1665. Today, a lot of Newton's Apple Trees are spread all over the world.

Here is the history of the Korean Newton's Apple Tree, the third descendant of the original English one:

- 1842 - 1942 A graft was taken from the Newton's original apple tree and transplanted in the Lord Brownlow's garden at Belton, and then was propagated to the East Malling Research Station.
- April 1943 Transferred to the Pennsylvania Historical Commission in U.S.A. through the Royal Society from U.K.
- March 1957 Transplanted to the National Bureau of Standards (NBS) in Washington, D.C.
- February 1977 Grafted in NBS to be transplanted to KSRI (The Korean Standards Research Institute) in Daejeon, as a cooperation symbol for science and technology
- October 1978 A sapling of the tree was transferred from NBS to KSRI
- April 1980 Planted, in the place shown below, by Dr. Zae-Quan Kim, the first president of KSRI, and Dr. Ernest Ambler, director of NBS



Dr. Dan Mihai Ștefănescu near the Korean Newton's Apple Tree, in May 2004

Index

<1-1-1> crystallographic direction, 542
 ϵ_z diagrams, 406
 $\pm 45^\circ$ strain gauges, 542
17-4 PH stainless steel, 244, 553
3D energy space diagram, 24
3D piezoelectric force sensor, 120
3D silicon accelerometer, 452
3D wheel Hall sensor, 198
III-V semiconductors micromachining, 506

A

‘A’ and ‘V’ frames, 428
acoustic emission, 254
acoustic force transducer, 251
acoustic impedances, 258
acoustic radiation force impulse, 261
acoustic rate gyroscope, 284
acoustic transducers, 209
“active” data in Excel, 532
active transducers, 103
actuation force of a brake pedal, 38
actuators, 14
adhesion force, 422
alternating tension-compression forces, 549
amorphous carbon, 59
analog potentiometer, 52
analog-to-digital conversion, 340, 365
analog-to-digital converter, 356, 577
angle between the two electrodes, 91
anisotropic magnetoresistive, 135
ANSYS Multiphysics, 243, 318
ANSYS program, 406, 490, 508, 530
application-specific integrated circuits, 582
array of resistive sensors, 66

A-shaped frame, 472
atomic force microscopy, 322, 539
atto-newton force detection, 41
automatic calibration procedure, 52
automatic dead load machine, 12
automatic force rebalancing control, 282
automatic recognition of force transducers, 579–80
auto-resonating, 209
axisymmetric combinations of elastic elements, 559
axisymmetrical elastic elements, 523
axisymmetrical structures, 500, 504, 523

B

“barber pole” structure, 135
barrel, 399
barrel type section, 517
bars of an equal strength to stretching, 394
Belleville springs mounted as opposite plates, 504
Belleville washers, 88
bender vs. twister, 549
bending, 376, 445
bending beam, 75
bending mode, 432
bending moments, 471
bending moments diagram, 445
bending ring, 529
bent beam, 549
bent lamella, 415
bent membrane, 497
bent proof ring, 566
bent ring, 477
bent yoke, 469
Beziers curve, 394
biased Hall-effect sensor, 196

- biaxial strain gauges, 542
 - bidirectional force transducer, 26
 - bidirectional rosettes, 457
 - bidirectional shear force transducer, 198
 - bimorph, 299, 312
 - binocular type, 483
 - binoculars, 491
 - (bio)chemical cantilevers, 424–27
 - biparameter, 31
 - biparameter frequency transducers, 82
 - biparametric force transducer, 83
 - bistable device, 431
 - black box, 577
 - blocked force, 308
 - boundary elements, 540
 - bridge amplifier, 365
 - bridge connection, 270
 - bridge efficiency, 350
 - bridge factor, 349
 - Brownian thermal noise, 281
 - buckling mode, 432
 - build-up system, 480
 - built-in intelligence, 582
 - “butterfly” configuration, 508
 - “butterfly” type, 418
- C**
- cage-shaped elastic element, 409
 - caisson, 399
 - cantilever beams, 92, 195, 200, 310, 316, 362, 378, 384, 415, 419
 - cantilever beam used in contact mode within atomic force microscopy, 421
 - cantilever CNT, 314
 - cantilever tube, 437
 - cantilever-based atomic force sensor, 322
 - cantilever-type silicon sensors, 420
 - capacitance-to-digital conversion, 365
 - capacitive force transducer, 318
 - capacitive force-balance, 299
 - capacitive full-bridge, 354
 - capacitive half-bridge, 301
 - capacitive sensing technology, 104
 - capacitive strain gauge, 334
 - capacitive transducer for combined force and elasticity modulus, 104
 - capacitive transducers, 488
 - capillary force balance, 297
 - carbon nanotubes, 42, 122, 252, 307, 314
 - carrier-frequency amplifier, 586
 - Casimir force, 148
 - catheter tip pressure measurements, 512
 - Catia software, 405
 - centrally loaded dual-beam arrangement, 471
 - ceramic ultrasound transducer, 260
 - CFT “joystick”, 93
 - champagne cork, 377
 - characteristic (force – frequency), 84
 - charge amplifier, 123, 282
 - choke-type transducer, 176
 - circular diaphragm, 267
 - circular elastic plate, 497
 - circular membrane, 368, 379, 513
 - circular membrane gauges, 498
 - circular ring, 479
 - circular rosette, 503
 - circumferential and longitudinal strain diagrams, 526
 - circumferential strain gauges, 519
 - classic strain gauges, 52
 - classification of Elastic Elements, 381–86
 - classification of Force Transducers, 40–44
 - closed-loop force feedback, 287
 - coercive force, 182
 - coil fiber gyroscope, 287
 - Colpitts or TTL customized oscillators, 232
 - column type elastic element, 394
 - columnar elastic element, 389
 - combfinger capacitors, 95
 - common mode rejection, 268
 - compensation and adjusting resistances, 350
 - complete-system-on-a-chip, 584
 - complex loaded shafts, 441–43
 - complex loading case, 411

composed elastic structures, 554
 compression frequency, 317
 compression test apparatus, 259
 computer numerical control, 559
 concentrators, 408
 concentric representation, “all-inclusive”
 style, 570
 concentric tubes, 403
 conflicting design criteria, 531
 contact force, 257
 contact force sensor, 88
 contact force transducer, 66
 continuum transducer, 34
 controlled permanent-magnet field, 139
 converters, 104
 coplanar L-shaped beams, 432
 Coriolis acceleration, 282
 Coriolis force, 276, 280, 285
 Coriolis mass flowmeter, 484
 Coriolis vibratory gyroscope, 284
 Corona discharge, 103
 Corona technique, 111
 corrugated diaphragm, 498
 Coulomb force, 103
 counterforce, 37
 Crookes radiometer, 37
 cruciform elastic element, 491
 C-shaped elastic vice, 474
 cubic blocks with slots, 543–47
 cubical force transducer, 543
 customized elastic elements, 386
 customized strain gauged transducers, 569
 customized strain gauges, 536
 cylinder, 392
 cylindrical capacitor, 97
 cylindrical rod, 410
 cylindrical tensometric transducer, 439

D

damped natural frequencies, 522
 data acquisition, 358
 data presentation, 343
 decision matrix, 568
 deflection per slot, 547

deflection sensor “cartridge” type, 368
 deflection type transducers, 293
 deformations for ‘spider’ (‘crab’) elastic
 element, 557
 delay line, 269
 design optimization, 534
 design symmetry, 584
 deviation (unbalanced) bridges, 337
 dial gauge, 8
 diamond-like carbon, 59
 diaphragms, 11, 32, 78, 90, 378, 495, 563
 dielectric, 89
 “differential” bending, 560
 differential capacitance, 31
 differential device, 353
 differential measurement of resonant
 frequency, 266
 differential solution for vibrating-wire
 force transducer, 217
 differential techniques, 347
 differential transducer with variable
 inductance, 73
 differential transformer, 73, 167
 differential variable reluctance transducer,
 79
 digital capacitive accelerometer, 301
 digital FTs, 42
 digital load cell, 578
 digital load cell interface, 586
 digital load or force transducers, 373
 digital photoelasticity, 504
 digital potentiometer, 52
 digital signal conditioners, 580
 digital signal processing, 585
 digital standard reference force transducer,
 579
 digital weighing, 211–12
 dilemma “sensitivity or stiffness”, 532
 direct resistance change measurement,
 371–73
 disc-pendulum, 100
 distributed forces, 3
 diverse elastic elements, 563
 dome-shaped diaphragm, 503
 donut-shaped tube, 517

doped n-polysilicon, 506
 double (guided) cantilever beam, 415
 double beam (micro)resonators, 240–44
 double bending, 459
 double bending beam transducers, 417
 double cantilever lamella, 418
 double current supply, 362
 double ended beams, 450–51
 double parallelogram structure, 212
 double SAW, 266
 “double” strain gauge, 376, 537
 double wall CNT, 307
 double wheel, 463
 double-cantilever beam, 472, 473
 double-ended tuning fork sensor, 241
 double-ended tuning forks, 228, 240–42
 double-parallelogram device, 204
 doubly-clamped beam nanoresonators, 234
 doubly-clamped cantilever, 450
 drilled disc (washer), 539
 dual circuit load cell, 540
 dual coil transducer, 78
 dual output, 358
 dual output force transducers, 585–87
 dual sensing elastic element, 79, 376, 479
 dual shear strain gauges, 462
 dual torus, 520
 “dual” transducer design, 504
 dual-axis gyroresonator, 283
 dual-axis gyroscope, 288
 dual-element (“differential”) load column, 404
 dual-frequency patch antenna, 419
 dummy resistor for thermal compensation, 402
 Dunnwald-like copper wire force transducer, 212
 dynamic force microscopy, 323
 dynamic measurement of force, 581
 dynamic signal analyzer, 521
 dynamic testing, 396–97
 dynamic weighing, 581
 dynamically force-balanced, 278
 dynamic-feedback amplifier, 582

dynamometers, 82
 dynamometric cell, 38
 dynamometric electrobalance, 159
 dynamometric platform, 432
 dynamometric wrench, 415

E

eddy-current sensor, 81
 eight strain gauges bridge scheme, 410
 elastic cantilever, 270
 elastic deflection, 569
 elastic element, 5, 203, 572, 584
 elastic elements, 44, 168, 375, 563
 elastic elements (primary sensing), 336
 elastic wave propagation, 270
 elasticity module, 207
 elastomagnetic effects, 165
 elastomer, 89
 elastomeric sensors, 62
 elasto-optical contact, 9
 electret film, 113
 electric and magnetic force vectors, 154
 electric indication, 569
 electric sensitivity, 381
 electrical measurement of mechanical quantities, 582
 electrical methods, 17
 electroacoustic transducer, 253
 electrodynamic, 153
 electrodynamic compensating balance, 158
 electrodynamic feedback, 156
 electrodynamic field generator, 154
 electrodynamic force cells, 156
 electrodynamic force compensation, 155
 electrodynamic force measuring apparatus, 160
 electrodynamic force transducers, 37, 157
 electrodynamic transducer, 34, 160
 electromagnetic, 153, 215
 electromagnetic acoustic transducer, 318
 electromagnetic force balance, 297
 electromagnetic force compensation, 34, 142, 144, 157

- electromagnetic force-assisted UV-imprint system, 138
 - electromagnetic force-feedback, 299
 - electromagnetic forces, 4
 - electromagnetic levitation, 289
 - electromagnetic measurement principles, 134
 - electromagnetic probes, 144–46
 - electromagnetic transducers, 37
 - electromagnetically compensated balance, 298
 - electromechanical film, 112
 - electrometer, 103
 - electrometer for charge, 321
 - electromotive force, 161, 308
 - electron charge, 147
 - electronic dynagraph, 82
 - electrostatic force, 102, 103, 252, 323
 - electrostatic force balance, 99, 301
 - electrostatic force compensated comb drive, 279
 - electrostatic force compensation, 299
 - electrostatic levitation, 289
 - elongation, 332
 - embedded piezoresistive microcantilever, 371
 - embedded yokes, 555
 - energetic balance, 264
 - environment interaction, 29
 - equal strength lamella, 379
 - “equivalent number” of the bridge active arms, 349
 - Esaki diode relaxation oscillator, 183
 - E-shaped elastic element, 472
 - E-shaped plane frame, 472
 - E-shaped square membrane section, 506
 - E-type diaphragm, 193
 - EU research program, 410
 - Euclid's solid, 539
 - experimental stress analysis, 381, 547
 - extensometers, 480
- F**
- fabric-based sensors, 67
 - Fabry-Perot cavity, 147
 - Fabry-Perot interferometer, 32
 - Faraday (or magnetic) balance, 297
 - Faraday pail sensors, 103
 - fast Fourier transform, 423
 - fast intelligent transducer, 581
 - FEM analysis, 484
 - fiber Bragg gratings, 334
 - fiber optic gyroscopes, 286–87
 - fiber-optic-linked pressure sensing, 498
 - field effect transistor, 324
 - finite differences method, 540
 - finite element analysis, 145, 470, 504, 519, 552
 - finite element discretization, 544
 - finite element method, 490, 528
 - “fish skeleton” rosette, 335
 - five-spoke wheel, 455
 - flexible elements, 378
 - FlexiForce sensors, 65
 - flux-quantum-based force facility, 147
 - footprint of a pressure, 68
 - force adapter, 32
 - force and tactile transducer, 417
 - force balance, 31, 35
 - force balance loop, 284
 - force balance techniques, 304
 - force based magnetometers, 82, 288, 297
 - force calibration of micropipettes, 420
 - force comparison standards, 8
 - “force cube” sensor, 542
 - “force cube” transducers, 117
 - force feedback weighing machine, 143
 - force footprint, 28
 - force inside the seat belt, 38
 - force joystick, 68
 - force measurand, 6
 - force measurement chain, 331–33, 361
 - force measurement SI unit, 41
 - force measurement terminology, 16
 - force sensing, 14
 - force sensing resistors, 49, 67
 - force sensitivity of an atomic force microscope, 302
 - force sensor arrays, 311

force standard machines, 298
 force transducers, 13, 14, 17, 589
 force transducer sensitivity, 208, 333
 force transducers in Mechatronics, 570
 force transduction, 3, 583
 force transfer standards, 477
 force transformer, 437
 force vector resolver, 570
 force versus distance curves, 315
 force-balanced accelerometer, 296
 force-balancing, 295
 force-displacement characteristics, 395
 force-measuring clamps, 474
 force-pressure transformer, 32
 force-sensitive resistor, 316
 force-to-displacement converter, 74
 force-to-fluid transformation, 495
 Foucault pendulum, 282
 four-coil triaxial transducer, 161
 four-quadrant photodiode, 421
 four-terminal bridge, 362
 four-terminal gauge, 193
 four-terminal piezotransducers with
 quasi-Hall topology, 507
 frame-shaped magnetoelastic sensing
 element, 174
 free hanging A-shaped piezoresistive
 cantilever, 472
 free-hanging cantilever, 509
 frequency domain, 233
 frequency scale, 252
 frequency-domain signal processing, 122
 frequency-output transducers, 213, 586
 friction force, 26
 friction stir welding, 27
 friction testing apparatus, 9
 friendly virtual instrument, 577
 full Wheatstone bridge, 392, 471,
 489, 584
 fundamental conversion process, 35
 fundamental frequency, 206, 229
 fundamental resonance frequency, 214
 fuzzy criteria, 574

G

galvanomagnetic effects, 187
 galvanomagnetic force transducers, 37–38
 gauge factors, 56, 96, 313, 349, 500
 generic conditioning system based on a
 programmable chip, 372
 giant magnetoresistance, 136, 369
 giant magnetoresistors, 196
 “glasses” or “binocular” shapes, 484
 “glasses”-shaped elastic elements, 484
 global tightening force, 394
 global transfer function, 333
 graphene, 313
 graphene-based resonators, 234
 gravimeter, 5
 gravimetric balances, 262, 297, 304
 gravitational forces, 4
 grid-based configurations, 64
 grinding force (normal and tangential),
 415
 grounding representations, 355
 gyroscopic force transducers, 34, 277
 gyroscopic load cells, 277

H

half-bridge configuration, 266
 half-bridge with two SAWs, 269
 half-bridges, 196, 394
 half-rings, 479
 Hall effect, 37–38, 185
 Hall generator, 191
 Hall voltage, 185
 Hall-effect force transducer, 197
 Hall-effect sensors, 38, 189
 Hall-effect strain transducer, 191
 Hall-effect tachometric transducer, 195
 hardness, 506
 HBM collection of application notes, 410
 height/diameter ratio, 498
 H-element with barometric compensation,
 401
 helical load cell, 408, 465

Helmholtz coils, 159
 hexagonal rings, 481
 high aspect ratio cantilevers, 426
 high-gain signal conditioning, 363
 hollow cylinder column, 399
 hollow cylindrical shape, 396
 hollow discs, 462–63
 hollow hat, 241
 holography, 381
 Hooke's law, 5, 74, 376, 532
 Hooke's law of elasticity, 191, 206, 332
 Hooke's solid, 539
 Hotline HBM, 442
 Hottinger references, 455
 H-shaped cut cantilever frame, 509
 H-shaped plane frame, 472
 hybrid gyroscope, 288
 hybrid position and force controller, 197
 hydraulic dynamometer, 12
 hydraulic force transducers, 12
 hydraulic load cell, 11
 hydrodynamic gravimetric balance, 157
 hydrostatic force transducer, 10
 hyperboloid profile, 394

I

IDT phase-locked vibratory gyroscope, 283
 impact bar, 396
 impedance analyzer, 81
 impedance head, 116
 induced charge, 124
 inductance, 134
 induction coil sensors, 73
 induction transducers (with moving coils), 37
 inductive half-bridge, 354
 inductive load cell, 545
 inductive ratio/arm (or transformer-arm), 353
 inductive transducers, 543
 inductor, 134
 inertial force detection, 38
 inertial gyroscopes, 279–81

input-output device (two-port element), 348
 instrumentation amplifier, 338, 362
 integrated Hall probe, 322
 integrated transducers (force and acoustic), 39
 intelligent transducer, 341
 interaction forces, 4
 interdigital electrode structure, 252
 interdigital transducers, 42, 252–54, 268, 284
 interdigitated combfingers, 354
 interdigitated electrodes, 62, 94
 interferometric micro-opto-electro-mechanical system, 40
 interferometric transducer, 105
 international comparison, 537
 inverse piezoelectric effect, 265
 inverse transducers, 294
 ion channels, 310
 ion-selective electrode, 308
 I-profile, 554
 'I'-profile subjected to shearing, 459
 IR-frequency range resonators, 522
 isotonic transducer based on the Hall effect, 190
 iterative FEM computation, 536

J

joystick, 454
 "joysticks" (masters), 303

K

Kirchhoff's laws, 348
 Knudsen numbers, 159

L

lamella of equal resistance, 368
 Langmuir evaporation model, 426
 Larmor precession frequency, 290
 laser Doppler vibrometer, 254, 423
 laser interferometry, 321
 LC tank circuit, 84
 LCR meter, 162

length to diameter ratio, 394
 lever for load application, 418
 leverage effect, 430
 levitated rotor gyroscope, 288
 levitational system, 148
 linear variable differential transformer,
 171, 296, 548
 liquid metal strain gauge, 55
 load and torque cell, 443
 load cell, 14
 load cells prototyping, 545
 load measuring pins, 460
 load ranges, 381, 565
 load torsor in Robotics, 455
 longitudinal and circumferential strain
 diagrams, 536
 longitudinal and tangential specific
 deformation diagrams, 524
 Lorentz force, 135, 139, 144, 186, 318,
 559
 Lorentz force based fusion magnetometer-
 accelerometer, 319
 Lorentz force flowmeter, 319
 low aspect ratio cantilevers, 426
 low frequency generator, 211
 LR relaxation oscillator, 81
 L-shaped cut-out tube, 408
 L-shaped force transducer, 554
 LVDT, 76, 197, 296
 LVDT force transducer, 74

M

Mach-Zehnder interferometer, 40, 321
 magnetic and electric force sensing, 140
 magnetic circuit, 134
 magnetic field gradient, 147
 magnetic field measuring methods, 131
 magnetic flux quantum, 146–48
 magnetic force microscopy, 82
 magnetic higher-order harmonic fields,
 141
 magnetic induction, 131
 magnetic permeability, 173
 magnetic resonance force microscopy, 323
 magnetic sensor principles, 133

magnetic speed measuring system, 196
 magnetizable material, 179
 magnetization curve, 168
 magnetoanisotropic devices, 166
 magnetoelastic force transducer, 34, 166
 magnetoelastic shaft, 180
 magnetoelastic strain gauge, 181
 magnetoelastic structures, 168
 magnetoelastic tape, 182
 magnetoelastic transducers, 319
 magneto-electro-elastic transducers, 168
 magnetoinductive magnetometers, 81
 magnetoresistive sensors, 137, 196, 353
 magnetoresistors, 335
 magnetostriction, 165
 magnetostriction sign, 178
 magnetostrictive amorphous wires, 172
 magnetostrictive delay line, 173
 magnetostrictive strips and bars, 170–72
 magnetovolume (Nagaoka-Honda) effect,
 166
 Maltese cross, 448
 “Maltese cross” elastic structures, 446
 manganin grid, 54
 mass balance, 293
 massive bodies (blocks), 539
 massive volumetric bodies, 539
 matrix of capacitive sensing elements, 96
 “matrix” type solutions, 123
 matrix-based pressure measurement, 65
 Matteucci pulses, 173
 meander-like strain gauge, 58
 measurand, 29, 332, 574
 measurement methods, 29, 44
 measurement principles, 6, 35, 307, 312,
 361, 572
 measurement principles or methods, 23
 measurement techniques, 488
 measuring amplifier, 354
 measuring displacement and force, 38
 measuring principles, 32, 182, 363
 measuring sensitivities, 565
 mechanical dynamometers, 8, 10, 477
 mechanical energy domain, 26
 mechanical oscillator, 5

mechanical sensitivity, 381
 mechanical stress vs. specific deformation, 464
 mechatronic image, 407
 membrane, 60, 103, 141
 membrane “profilation”, 502
 membrane deflection, 495
 mercury-in-rubber strain gauges, 55
 metallic digital strain gauges, 244
 metallic strain gauge, 500
 metallic triple-beam resonators, 244, 246–47
 method of finite differences, 524
 metrological and functional characteristics, 568
 (micro)resonators, 540
 microcantilever force sensor, 59
 microcantilevers, 424
 microcontrollers, 362, 439, 570
 microdiaphragm, 503
 microdynamometer, 146
 microelectronic technology, 504
 micromachining technology, 289
 micromechanical rate gyroscope, 289
 micromechanical resonators, 228, 243
 microoptical device with force feedback, 303
 microtubules, 102
 microvibrating electrode, 221
 middle bent bar, 555
 middle bent bars with fixed ends, 445–48
 miniature pressure diaphragms, 508
 minimum measurable force, 423
 “mixed” location of the strain gauges, 524
 modal testing techniques, 522
 modifiers, 15
 modulators, 15
 modulus of elasticity, 209
 Moiré interferometry, 450, 504
 molecular force transducers, 310
 monoblock elastic structures, 528
 moving-coil tester, 160
 multi criteria decision making, 573
 multicolumn transducers, 394

multicomponent force transducer, 163, 490
 multicomponent force-moment transducers, 396
 multicomponent force-torque transducers for Robotics, 320
 multicomponent piezoelectric force transducers, 118
 multicomponent tensometric balance, 304
 multicomponent tensoresistive dynamometer, 397
 multicomponent transducers, 376
 multicriterial analysis, 568
 multifunctional elastic elements, 495
 multifunctional transducers with moving coils, 161–63
 multilayer piezoresistive microcantilevers, 430
 multiloading component dynamometers, 481
 multiparameter structural optimization, 526
 multiple “glasses”-shaped elastic elements, 490–91
 multiple beams, 75
 multiple bended elastic elements, 417
 multiple bendings, 474
 multiple dynamometer, 92
 multiple plate-ring system of elastic elements, 480
 multitransducer equipment, 320–21
 multi-walled carbon nanotubes, 61, 313
 Murphy’s law, 352
 mutual inductance force sensor, 80
 mutual inductance variation, 79
 mutual induction, 182

N

nanodevices, 570
 NASTRAN, 524
 natural frequency, 230
 neuro-fuzzy concepts, 585
 newton, 6
 Newton’s 3rd law, 294
 Newton’s “cake”, 43

Nobel Prize for Physics, 136, 148, 313
 nonlinearity of a full Wheatstone bridge,
 507
 normal force, 432
 N-shaped elastic elements, 534
 n-type gauges, 542
 nuclear magnetic resonance, 290
 nuclear-spin gyroscope, 288
 numerical weighing system, 211

O

oblique bending ring, 532
 oblique slots, 536
 octagonal rings, 481–82
 odor sensors, 126
 one-piece solution, 534
 on-site calibration, 537
 optic fiber devices, 40
 optical beam deflection, 425
 optical gyroscopes, 288
 optical interferometer, 33
 optical interferometry, 147
 optimum shape of the transducer elastic
 element, 489
 optoelectronic active devices, 507
 oscillating quartz tuning forks, 232
 oscillator feedback loop, 266
 oscillators, 104, 123
 ‘ostrichs’-like axisymmetric structures,
 559
 oval-shaped membrane, 513

P

pair of bimorph cantilevers, 121
 pair of Hall sensors, 189
 parabolic shape, 418
 parallel plate structures, 449
 parallelepiped, 395
 parallelepiped with antisymmetrical slots,
 543
 parallelepipedic block with a hole and a
 slot, 552
 parallelepipedic elastic element, 544
 parallelepipedic lever, 555
 parallelogram, 415

parallelogram design, 212
 parallelogram flexure, 471
 parallel-plate acoustic wave-guide, 255
 parallel-plate capacitor, 90, 101
 parametric sensing elements (R–L–C), 361
 parametric transducers, 337, 352
 parametrical, 43
 parasitic factors, 30
 passive sensor elements (R, L, C), 110
 passive transducers, 103
 Paul-Straubel ring-type electrodynamic
 trap, 159
 PC ready force measuring chain, 587
 pendulous accelerometer, 296
 pendulous mass, 220
 pendulum thrust balance, 322
 perfectly elastic body, 539
 permanent magnet, 215
 photoelasticity, 381, 483, 541
 piano wire, 206
 piezo actuators, 116
 piezo sensors, 116
 piezoacoustic interdigital transducers, 251
 piezo-capacitive sensor, 312
 piezoceramic interdigital transducers, 256
 piezoelectric balance, 118
 piezoelectric bimorph, 120, 314
 piezoelectric ceramics, 239
 piezoelectric crystals, 115
 piezoelectric devices, 312
 piezoelectric disc resonator, 235
 piezoelectric effect, 111, 265
 piezoelectric FET, 114
 piezoelectric force measurement chain, 364
 piezoelectric force ring, 482
 piezoelectric force transducers, 110
 piezoelectric gyroscopes, 281
 piezoelectric materials, 521
 piezoelectric microbalances, 125
 piezoelectric multilayer cantilever, 117
 piezoelectric nanowire, 114
 piezoelectric quartz, 324
 piezoelectric quartz frequency, 109
 piezoelectric resonators, 124
 piezoelectric transducer, 211

piezoelectricity, 113
 piezometer, 219
 piezoresistive beams, 432
 piezoresistive cantilever beam, 322
 piezoresistive cantilever magnetometer, 140
 piezoresistive double-microcantilevers, 430
 piezoresistive microcantilever array sensors, 426
 piezoresistive sensors, 57
 piezoresistive silicon “cork”, 495
 piezoresistive strain gauges, 56
 piezoresistive thin films, 570
 piezoresistive Wheatstone bridge, 311
 piezoresistivity, 56
 piezoresistors, 454, 505
 piezoresponse force microscopy, 124
 piezo-transistor, 57
 pillars (columns), 378
 pipe section, 399
 plane combinations of elastic elements, 558–59
 plane complex structures, 550–52
 plane frames, 471
 plane-parallel capacitors, 93
 platform load cells, 582
 plug-and-play, 579
 p-n semiconductor strain gauge pairs, 368
 pneumatic force transducers, 12
 pneumatic load cell, 11
 Poisson strain, 376
 Poisson’s coefficient, 351, 406
 Poisson’s ratio, 529
 polar diagram force versus angle, 27
 polycrystalline diamond, 60
 polystyrene sphere, 540
 portable weighing truck scales, 514
 positive magnetostriction, 178
 post-buckling phenomenon, 395
 post-processing program SV-01, 545
 potentiometer, 51
 power spectral density, 520
 precession, 276
 precision force transducer, 335, 587

pressductor, 167, 178
 pressure balance, 36, 294
 pretensioned resistive wires, 51
 profiled diaphragm, 571
 profiled membranes, 498
 profiled tubes, 404–8
 programmable current sources, 371
 proving rings, 8, 75, 79, 378, 477
 pseudo-transducers, 395, 459, 474
 p-type gauges, 542
 p-type silicon piezoresistors, 509
 pull-off force, 422
 pulsar-receiver, 259
 pulsed power supplies, 352
 push pull force gauges, 587

Q

quadratic and oval-shaped membranes, 511
 quality factors, 231, 320, 322
 quantum micromechanical oscillators, 450
 quantum tunneling, 281
 quantum tunneling composite, 63
 “QuantumX” universal conditioner, 363–64
 quartz-crystal microbalance, 10, 126
 quartz crystals, 110–11
 quartz microbalances, 232
 quartz resonator, 231
 quasi-Hall topology, 193

R

“radar” signal processing, 269
 radial and tangential strain gauges, 502
 radiation force balance, 262, 297
 radiometric technique, 37
 radiotelephone with weighing means, 344
 range of forces, 7
 radiometric device, 349
 radiometrically operated, 578
 Rayleigh wave device, 440
 RC sensing principles, 87
 rectangular axisymmetrical sections, 531
 rectangular diaphragms, 558
 rectangular membranes, 509

rectangular plate, 514
 rectangular spectacles, 471
 rectangular wave generator, 370
 reflected laser beam type cantilevers, 428
 reflection polariscope, 545
 reflection ratio of acoustic pressure, 258
 rejustors, 58, 339
 relative permittivity, 88
 relaxation oscillator, 89, 365, 370
 reluctance force transducer, 78
 reluctance torque transducer, 79
 resistance-to-time converter, 365–66
 resistive electrical tensometry, 349
 resistive force transducer, 544
 resistive half-bridge, 354
 resistive load cells, 586
 resistive network, 51
 resistive strain gauges, 488
 resistive strain-gauged transducers, 361
 resonance frequency, 227, 230, 276, 423
 resonant cantilevers, 310, 368
 resonant force microsensors, 450
 resonant frequency, 126, 268, 320, 440
 resonant gravitational wave detector, 520
 resonant microsensor, 227
 resonant pressure microsensors, 510
 resonant strain gauge, 334
 resonant / vibrating wire, 31
 resonating beams for force transducers, 236
 resonating diaphragms, 237–38
 “resonating” force transducer, 560
 resonator force transducer, 265
 resonator microgyroscope, 283
 resonators, 203
 Reynolds number, 118
 ribbed diaphragm, 526
 ribbed membranes, 498
 ring, 563
 ring laser gyroscope, 288
 ring torsion, 529
 ring torsion load cells, 524
 ring-shaped sensing element, 176
 rocker pin, 578
 Rohrbach rings, 481

Romanian Symposia of Tensometry, 394,
 418, 441, 448, 524
 rosette strain gauges, 442
 rosettes, 336
 rotary toroid, 517
 rotary torque transducers, 440
 rotating shaft torque transducer, 437
 rotational structures, 523
 round cage, 543
 rules for strain gauges placement on the
 elastic elements, 566, 591

S

S- or Z-shaped elastic element, 464
 Saint Venant’s principle, 32, 532
 SAW fluidic transducers, 267–68
 SAW pressure transducers, 267
 SAW sensing element, 39
 SAW strain gauges, 441
 SAW torque transducer, 266
 SAW-based devices, 271
 SAW-based dispersion strain gauging
 resonator, 267
 saw-tooth wave generator, 369
 scaling or setting sensitivity, 341
 scanning electron micrograph, 427
 scanning electron microscope, 315
 scanning electron microscopy, 138, 381,
 423
 scanning Hall probe microscopy, 198,
 322
 scanning near-field optical microscope,
 322
 scanning probe microscopy, 324
 scanning tunnelling microscopy, 324
 “screw”-shaped sensitive structure, 549
 search coils, 131
 second law of Sir Isaac Newton, 6
 selection criteria of force transducers, 565
 self-adhesive strain gauges, 335
 self-calibration, 140, 589
 self-generators, 15
 self-inductances, 167
 self-resonance frequency, 213
 self-rigidizing torus, 522

- self-sensing piezoresistive cantilevers, 422
- semiconducting nanotube into a transistor, 324
- semiconductive strain gauges, 402
- semiconductor SGs, 56
- semiconductor strain gauges, 52, 393, 489
- sensing element, 14, 588
- sensing technologies, 20
- sensitivities for different measuring principles, 488
- sensor, 13, 571
- sensor and actuator materials, 521
- sensor database, 364
- servo-type pressure-transducer, 294
- shape, 376
- shape factor, 532
- shape memory alloy, 255, 583
- shear beam principle, 459
- shear-bridges, 457
- shear-deformation, 354
- shearing, 376, 445
- shearing strained elastic elements, 457
- shlieren window, 556
- shock transducer based on a Hall-effect sensor, 195
- shrinking force, 139
- shunt calibration resistor, 351
- side effect, 432
- Sigma-Delta converter, 366–67
- signal conditioner, 351, 354
- signal conditioning, 337–39
- signal conditioning circuitry, 361
- signal domains, 23
- signal integration (acceleration → speed → distance), 368
- signal processing, 340–42
- silicon beam, 232
- silicon resonator, 233
- silicon sensing diaphragms, 558
- silicon-on-sapphire, 58
- sine wave generator, 369
- single atom weighing, 42
- single beam (micro)resonators, 238–40
- single electron transfer, 324
- single load cell, 64
- single wall carbon nanotubes, 313
- single-crystal silicon cantilever, 423
- single-point force transducer, 3
- six-component force transducer, 448
- six-component robotic elastic element, 454
- six-component strain gauged balance, 553
- sleeve, 399
- slotted elastic lamellae, 448
- slotted tube, 409
- smart materials, 521
- smart signal processing, 582
- smart transducers, 582
- solid-state actuators, 308
- solid-state device, 139
- solid-state electronic devices, 32
- solid-state force transducers, 311
- solid-state piezoresistive potentiometers, 308
- spatial combinations of elastic elements, 560–61
- spatial complex structures, 552–53
- spatial S, 77
- “spatial Z” with two oblique slots, 547
- special force transducers, 442
- specific applications in Robotics, 570
- “spectacles” (rectangular, half-octagonal, octagonal, and circular), 484
- spectral power densities, 122
- spectrum analyzer, 238
- spheric container, 540
- spheric dome, 540
- spheric elastic element, 539
- spherical capacitive transducers, 88
- spin, 276
- spring (elastic element), 589
- spring deformation, 5
- spring discs, 560
- spring-like structure, 569
- square axisymmetric elastic element, 571
- square membrane, 505, 513
- square membrane / diaphragm, 200
- “square” ring, 480, 483
- “square” version of the spoked wheel, 452
- squared ring, 471
- S-shape beams, 415

S-shaped deformation, 495
 S-shaped elastic elements, 545, 550
 S-shaped frame, 483
 stacked piezoelectric plates, 114
 standard figures, 381
 standardized notations, 381
 “step-functions” for the best strain
 gauging procedure, 502
 Stewart platform, 403
 strain, 574
 strain cylinders, 393
 strain diagrams, 544
 strain diagrams on the superior, lateral and
 inferior sides, 531
 strain gauge half-bridges, 403
 strain gauge sensitivity, 565
 strain gauged balance for aircraft models,
 552
 strain gauged balances for wind-tunnels,
 320
 strain gauged force transducers, 157, 344,
 379, 534, 554
 strain gauged force transducers connected
 to PC, 371–73
 strain gauged pen, 401
 strain gauges, 31, 49, 316, 334, 350, 361,
 377, 397, 401, 432, 439, 445, 452, 459,
 471, 489, 490, 519, 523, 560, 565, 584
 strain gauges (“fishbone” type), 463
 strain gauges (secondary sensing), 336
 strain ratio, 393
 strain sensitivity, 357, 376, 574
 strain-gauge combination, 393
 strain-gauge force transducer, 149
 strain-gauged diaphragm, 198
 Strength of Materials rules, 443
 stress concentration regions, 429
 stress map, 544
 stress-sensitive transistors, 368
 stretched / compressed bar, 200
 structural antisymmetry, 551
 structural optimization, 381, 409
 structural optimization for quadratic
 membranes, 509
 S-type folded cantilever, 474

super carbon nanotubes, 61
 superconducting accelerator magnets, 139
 superconducting quantum interference
 device, 146, 290
 surface acoustic waves, 251, 264, 440
 surface acoustic waves force transducer,
 34
 surface-force apparatus, 104, 431
 surface-wave resonator, 265
 suspension balance with Hall sensors, 192
 symmetry law, 350

T

tandem of welded spring discs, 561
 tangential/circumferential strain diagrams,
 534
 taper element, 524
 telescopic bar, 403
 telescopic profilometer, 315
 telescopic tubular handle, 411
 tensibility, 536
 tensile force of bolts, 392
 tension-compression, 376
 tensometer for monitoring concrete
 structures, 215
 tensometric force transducer type, 565
 tensometric force transducers, 50
 tensometric sensitivity, 349, 395, 499,
 502, 568
 tensometric transducers, 587
 tensometrical instrumentation, 340
 tensometrical measurement chain, 574
 tensometry, 543
 tensoresistive pressure sensors, 58
 theoretical force curve, 422
 thermophoretic force, 159
 thick film piezoresistors, 503
 thick wall tube, 540
 thin wall elastic bar, 399
 thin-film transistors, 309
 three-terminal memory cells, 315
 thrust measurement for the Space Shuttle,
 42
 tiltmeter with pendulous mass, 219

time domain, 233
 time-domain analysis, 159
 torductors, 180
 toroidal shape, 521
 torque, 276
 torque transducers, 441
 torsion balance, 5
 torsion ring, 578
 torsional forces, 408
 torus (toroidal ring), 517, 571
 torus fitted between two tube-shaped shells, 519
 trace explosive detection, 427
 traceable calibration, 392
 transducer, 13, 25, 571
 transducer electronic datasheet, 341
 transducer identification, 341
 transducers based on mechanical deformation, 36
 transducers' cube, 15, 24
 transduction element, 14, 295
 transduction principles, 29, 31
 transduction process, 25
 transduction techniques, 20
 transferable force standards, 420
 "transform" tension / compression in bending, 408, 532
 transformer, 134
 transformer bridges, 104
 transformer-type transducer, 176
 transforming the vertical compression into horizontal tension, 241, 561
 transverse electromotive force, 185
 transverse piezoelectricity, 118
 transverse voltage strain gauge, 193
 triangular lamella with an equal bending resistance, 418
 triangular plates, 93
 triangular symmetry, 93
 triaxial galvanomagnetic force transducers, 198
 tri-axis accelerometer, 288
 tridimensional solid, 543
 tridirectional piezoelectric force transducers, 117–20

triple-beam resonators, 244
 truncated cone, 526
 T-shaped configuration, 510
 T-shaped transducer, 554
 T-type rosettes, 389
 tube, 399
 tube with vertical slots, 408
 tube-shaped tandem, 403
 tubular elastic element, 401
 tubular elastomagnetic elements, 176
 tuning fork, 276
 tuning-fork torque transducer, 246
 two pairs of opposite-type semiconductors, 367
 two-dimensional strain transducer, 270
 type of force transducer, 223
 typical elastic elements, 385

U

ultrasonic hammer, 259
 ultrasonic power, 263
 ultrasonic pulser-receiver, 259
 ultrasonic wave transmission, 256
 ultrasonographic probe, 261
 ultrasound Doppler transceiver, 262
 ultrasound imaging apparatus, 260
 ultrasound standing wave, 263
 unbalanced mode (deviation method), 349
 unbonded wires, 53
 unconventional elastic structures, 550
 unique dimensional parameter, 566
 unit of force, 6
 universal (tension + compression), 579
 universal conditioner, 364
 universal force transducers, 8
 universal frequency-to-digital converter, 370
 U-shaped cantilever, 428, 473
 U-shaped tube, 448

V

vacuum diode force sensor, 309
 van der Waals forces, 235, 307, 323, 422
 variable inductance, 31, 489

variable reluctance, 78
 variable transformer, 159
 variable-impedance transducer, 31
 vector signal analyzer, 246
 vector touch sensor, 240
 vectorial force, 278
 Venn diagram, 333, 570
 Vernier dual-range force transducers, 9
 vibrating carbon nanotube, 222
 vibrating dual-wire technique, 216
 vibrating elements, 247
 vibrating FTs, 42
 vibrating wire, 486
 vibrating-wire densimeter, 218
 vibrating-wire force transducer, 34, 206
 vibrating-wire load cell, 212
 vibrating-wire sensitivity, 207
 vibrating-wire strain gauges, 220
 vibrating-wire tiltmeters, 220
 vibrating-wire transducers, 203
 vibrating-wire viscometers, 217
 vibrating-wire weighing technology, 220
 vibration modes, 237, 282, 312, 511
 vibratory gyroscopes, 283
 Villari effect, 170
 virtual instrumentation display, 441
 “viscous friction” law, 10
 vision-based force measurement, 40
 voltage-controlled oscillator, 582
 voltage-force curve, 63
 voltage-to-force transducers, 254

voltage-to-frequency converter, 356, 365
 volumic S, 466
 von Mises stress map, 465

W

weighing based on Hall devices, 192
 weighing-in-motion, 12, 358
 Wheatstone bridge, 52, 54, 135, 137, 180,
 185, 211, 313, 333, 337, 347, 352, 356,
 361, 375, 384, 393, 406, 407, 425, 443,
 452, 457, 464, 498, 519, 523, 543, 553,
 556, 565, 577
 Wheatstone bridge based oscillator, 368
 Wheatstone bridge based transducer, 357
 Wheatstone bridge connection, 293
 Wheatstone configuration, 454
 Wheatstone half-bridge circuit, 475
 Wien bridge based oscillator, 367–68
 wireless transmission, 269
 word “bridge” double meaning, 558

Y

yarn-based sensors, 68
 yoke-element, 572
 Young’s modulus, 6, 484, 529

Z

zoomorphic forms, 550